RNA-based Therapeutics for Alzheimer's Disease

Caroline A. Woffindale

Thesis submitted for the degree of Doctor of Philosophy

Department of Physiology, Anatomy and Genetics, University of Oxford

Somerville College

Trinity 2015

Declaration

The work presented in this thesis was undertaken at the Department of Physiology, Anatomy and Genetics, University of Oxford, between 2011 and 2015 in the laboratory of Professor Matthew Wood. All work presented is my own with the following exceptions: (1) The multi-gene targeting LNA-ASO study (**Chapter 5**) was completed in collaboration with Dr. Miguel Varela, Wood Lab, University of Oxford. Dr. Varela conducted bioinformatics analyses to identify potential multi-gene LNA-ASO sequences while *in vitro* screening of candidate LNA-ASOs was undertaken by Caroline Woffindale. (2) Electron microscopy for the analysis of extracellular vesicle morphology was conducted in collaboration with Fiona Lee, Wood Lab, University of Oxford. This work has not been submitted for any other degree at this university or any other institution.

Acknowledgements

Firstly, I am incredibly grateful to the family of Margaret Pelly for their generosity in supporting the Margaret Pelly Scholarship, Somerville College. Without the Margaret Pelly Scholarship, this thesis would not have been possible.

I would like to thank my supervisors, Professor Matthew Wood and Dr. Imre Mäger, for all of their help, support and advice and for allowing me the freedom to pursue different projects and learn new techniques.

Thank you to all the members of the Wood Lab, both past and present, for making the last 3 ½ years so enjoyable. I would particularly like to thank Samir El Andaloussi and Pieter Vader for their brilliant input with exosome projects; Miguel Varela for the opportunity to develop the multi-gene LNA-ASO project; Tom Roberts and Graham McClorey for sharing qPCR wisdom; Corinne Betts for performing injections and providing Western advice and Fiona Lee for help with NTA, EM and Western blotting. Thank you also to my wonderful friends who have helped to make Oxford such an unforgettable experience.

I would like to thank my amazing family for all of your love and support, which has helped to keep me somewhat sane throughout this process! I appreciate all you do so very much. Thank you also to the lovely Booths who have been so supportive.

Finally, thank you so much to Matt for all you have done over the past 5 years. Thank you for always finding a way to make me laugh when things have not quite gone to plan and for doing everything possible to support me.

Abstract

Alzheimer's disease (AD) is a progressive neurodegenerative disorder characterised pathologically by the accumulation of amyloid-β plaques and neurofibrillary tangles within the brain. Currently, there are no disease-modifying therapeutic interventions available. This thesis describes the development and delivery of novel RNA-based therapeutics for AD.

Recently, significant advances have occurred in the field of RNA interference (RNAi)-based therapeutics, allowing targeted silencing of disease-relevant genes through the use of short interfering RNAs (siRNAs) or microRNAs (miRNAs). However, development has been impeded by poor penetrance of the blood-brain-barrier (BBB) *in vivo*. Exosomes, as secreted extracellular vesicles (EVs), may overcome this problem as they naturally deliver RNA between cells and cross the BBB. Furthermore, recent evidence suggests that they may be loaded with exogenous RNA and preferentially targeted to neuronal tissue. Thus, this study investigated EV-mediated delivery of RNAi-based therapeutics shown to regulate AD-relevant genes. A comparison of EV-loading methods revealed that electroporation was confounded by the formation of large siRNA aggregates and indicated that endogenous loading strategies may be preferable. Endogenous loading of RNAi molecules was shown to be enhanced by co-expression with RNA-binding proteins, particularly following inclusion of an acylation domain. These findings highlight the potential for EV-mediated delivery of RNAi-based therapeutics.

A combinatorial therapeutic approach is increasingly recognised to hold the most promise for the future of AD. Thus, this study also focused upon the development of novel multi-gene targeting locked nucleic acid-modified antisense oligonucleotides (LNA-ASOs) as a combinatorial approach towards AD therapy. Two multi-gene LNA-ASOs each produced potent silencing of two separate target genes simultaneously, resulting in a significant reduction in amyloid-β production *in vitro*. A murine-specific multi-gene LNA-ASO was also identified, paving the way for future *in vivo* studies. These findings suggest that multi-gene targeting LNA-ASOs may represent a promising novel therapeutic strategy for AD.

In summary, this thesis has investigated novel strategies for both RNA delivery and multi-gene targeting, demonstrating the potential of RNA-based therapeutics for the treatment of AD.

List of Abbreviations

A4	Anti-Amyloid Treatment in Asymptomatic Alzheimer's
AAVs	Adeno-Associated Viruses
Aβ42	Amyloid-beta (42)
ABC	ATP-Binding Cassette
ACh	Acetylcholine
AChE	Acetylcholinesterase
AChE-I	Acetylcholinesterase Inhibitor
AD	Alzheimer's Disease
AD-MSCs	Adipose-Derived Mesenchymal Stem Cells
Aex	Ascites-derived Exosomes
AGO2	Argonaute 2
AICD	Amyloid Precursor Protein Intracellular Domain
AIDS	Acquired Immune Deficiency Syndrome
ALS	Amyotrophic Lateral Sclerosis
Amyloid-β	Amyloid-beta
APH-1A/B	Anterior Pharynx Defective 1 Homolog A/B
API	Alzheimer's Prevention Initiative
APOE	Apolipoprotein E
APP	Amyloid Precursor Protein
APPswe	Swedish mutation of APP
AS	Antisense
ASO	Antisense Oligonucleotide
BACE1	Beta-Secretase
BBB	Blood-Brain-Barrier
BCL	B-Cell Lymphoma
BCR/ABL	Breakpoint Cluster Region/Abelson Murine Leukemia Viral Oncogene Homolog 1
BDNF	Brain-Derived Neurotrophic Factor
BM-DCs	Bone Marrow-derived Dendritic Cells
BSA	Bovine Serum Albumin
CDK5	Cell Division Protein Kinase 5
cDNA	Complementary DNA
CD-UPRT	Cytosine Deaminase Fused to Uracil Phosphoribosyltransferase
Chr.	Chromosome
CNS	Central Nervous System
CSF	Cerebrospinal Fluid
CTF	Carboxy-Terminal Fragment
DCs	Dendritic Cells
Dex	DC-derived Exosomes
DKK1	Dickkopf-Related Protein 1
DMD	Duchenne Muscular Dystrophy
DMEM	Dulbecco's Modified Eagle Medium
DNA	Deoxyribonucleic Acid
dsRNA	double stranded RNA
DUSP6	Dual Specificity Phosphatase 6

EGFR	Epidermal Growth Factor Receptor
ELISA	Enzyme-Linked Immunosorbent Assay
EM	Electron Microscopy
EP300	E1A Binding Protein p300
ER	Endoplasmic Reticulum
ESCRT	Endosomal Sorting Complex Required for Transport
ESCs	Embryonic Stem Cells
EV	Extracellular Vesicle
FBS	Fetal Bovine Serum
FGF20	Fibroblast Growth Factor 20
FOXO1	Forkhead Box Protein O1
GABA	Gamma-Aminobutyric Acid
GDNF	Glial Cell Line-Derived Neurotrophic Factor
GFP	Green Fluorescent Protein
GM	Grey Matter
GM-CSF	Granulocyte Macrophage-Colony Stimulating Factor
GRIN2A/B	Glutamate Receptor, Ionotropic, N-methyl D-aspartate 2A/B
GSCs	Glioma Stem Cells
GSK3	Glycogen Synthase Kinase 3
GSK3α	Glycogen Synthase Kinase 3 Alpha
GSK3β	Glycogen Synthase Kinase 3 Beta
GvHD	Graft-versus-Host Disease
GWASs	Genome-Wide Association Studies
HCV	Hepatitis C Virus
HD	Huntington's Disease
HEK293	Human Embryonic Kidney 293 Cell Line
hESC-MSCs	human Embryonic Stem Cell-derived Mesenchymal Stem Cells
HIV	Human Immunodeficiency Virus
HMC-1	Human Mast Cell Line 1
HMEC-1	Human Microvascular Endothelial Cell Line 1
HN1	Hematological and Neurological Expressed 1
HSC70	Heat Shock Cognate 70
ICAMs	Intracellular Adhesion Molecules
IDO	Indoleamine 2,3-dioxygenase
idSp	Int 1' 2'-Dideoxyribose Spacer (abasic site)
IL	Interleukin
ILVs	Intraluminal Vesicles
iNOS	inducible Nitric Oxide Synthase
iPSCs	induced Pluripotent Stem Cells
IU	International Unit
JNK	c-Jun N-Terminal Kinase
LB	Lysogeny Broth
LNA	Locked Nucleic Acid
LNA-ASO	Locked Nucleic Acid-Antisense Oligonucleotide
LPS	Lipopolysaccharide
LTD	Long-Term Depression
LTP	Long-Term Potentiation
MAPK	Mitogen-Activated Protein Kinase

MAPT	Microtubule-Associated Protein Tau
MCI	Mild Cognitive Impairment
miRNA	microRNA
MRI	Magnetic Resonance Imaging
mRNA	messenger RNA
MSCs	Mesenchymal Stem Cells
MSP	Muscle Specific Peptide
MT	Membrane-Tagged/Associated
mTOR	mammalian Target of Rapamycin
MVBs	Multivesicular Bodies
NADPH	Nicotinamide Adenine Dinucleotide Phosphate (Reduced)
NAV3	Neurone Navigator 3
NC	Negative Control
NCT	Nicastrin
NLRs	NOD-Like Receptors
NMDA	N-Methyl-D-Aspartate
NMDAR	NMDA Receptor
NOD	Nucleotide-Binding Oligomerization Domain
NOX2/4	NADPH Oxidase 2/4
NPCs	Neural Progenitor Cells
NR2A/B	N-methyl D-aspartate Receptor subtype 2A/B
NSAIDs	Non-Steroidal Anti-Inflammatory Drugs
nSMase	Neutral Sphingomyelinase
NTA	Nanoparticle Tracking Analysis
PBS	Phosphate Buffered Saline
PCP	Planar Cell Polarity
PCR	Polymerase Chain Reaction
PD	Parkinson’s Disease
PEI	Polyethylenimine
PEN2	Presenilin Enhancer 2
PET	Positron Emission Tomography
PFA	Paraformaldehyde
PI3K	Phosphoinositide 3-Kinase
PMO	Phosphorodiamidate Morpholino Oligomers
PNA	Peptide Nucleic Acid
PNS	Peripheral Nervous System
POL II/III	RNA Polymerase II/III
PPP1CA	Protein Phosphatase 1 Catalytic Subunit Alpha
PreADViSe	Prevention of AD by Vitamin E and Selenium
pre-miRNA	Precursor miRNA
pri-miRNA	Primary miRNA
PS1	Presenilin-1
PSD-95	Postsynaptic Density Protein 95
PSEN1	Presenilin-1
PSEN2	Presenilin-2
PTBP1/2	Polypyrimidine Tract Binding Protein 1/2
qPCR	Quantitative Real-Time PCR
RISC	RNA-induced Silencing Complex

RNA	Ribonucleic Acid
RNAi	RNA interference
RNS	Reactive Nitrogen Species
ROS	Reactive Oxygen Species
rRNA	Ribosomal RNA
RVG	Rabies Viral Glycoprotein
sAPPα	Soluble Amyloid Precursor Protein Alpha
sAPPβ	Soluble Amyloid Precursor Protein Beta
SDS	Sodium Dodecyl Sulfate
SEM	Standard Error of the Mean
Ser/Thr	Serine/Threonine
shRNA	short hairpin RNA
siRNA	small interfering RNA
SIRT1	Sirtuin-1
SMA	Spinal Muscular Atrophy
SMAD	Mothers Against Decapentaplegic
SN	Supernatant
SNPs	Single Nucleotide Polymorphisms
Stau1/2	Staufen 1/2
TβR II	TGF-β Receptor type II
TBS	Tris Buffered Saline
TBST	TBS with Tween
TE	Tris-EDTA
Tex	Tumour-derived Exosomes
TGF-β	Transforming Growth Factor Beta
TLRs	Toll-Like Receptors
TNF-α	Tumour Necrosis Factor Alpha
TNRC6A	Trinucleotide Repeat-Containing 6A
TREM2	Triggering Receptor Expressed on Myeloid Cells 2
TRIM2	Tripartite Motif Containing 2
TrkA	Tropomyosin Receptor Kinase A
UF-LC	Ultrafiltration paired with Liquid Chromatography
UT	Untreated
UTR	Untranslated Region
WM	White Matter
Wnt	Wingless-related
WT	Wild-Type

Table of Contents

List of Figures

List of Tables

1 Introduction

1.1 Alzheimer's Disease

Alzheimer's disease (AD) is a progressive neurodegenerative disorder primarily characterised by a loss of episodic memory. However, deficits become more encompassing as the disease progresses and there is a wide-ranging decline in both cognitive and physical capacities, ultimately resulting in death. Pathologically, AD is characterised by the accumulation of amyloid-beta (amyloid-β) plaques and neurofibrillary tangles, comprised of hyperphosphorylated tau protein. There is also progressive atrophy of the hippocampus and cortical areas with a particular loss of cholinergic neurons[1]. As the leading cause of dementia, AD is responsible for more than 60-80% of dementia cases worldwide[2]. The global prevalence of AD was estimated at 44.4 million sufferers in 2013 and is predicted to reach 135 million by 2050[3]. This is expected to cost the UK £50 billion/year by 2038[4]. Currently, the approved treatment options are limited and aimed solely at symptom management. There are no available therapeutic interventions that are capable of preventing, halting or reversing disease progression. Thus, AD represents an increasing social crisis, in terms of both the health and economic burden, for which finding an effective therapy is imperative. Significant advances in our understanding of the mechanisms underlying disease pathology and developments in drug design and delivery could be pivotal for the identification of novel disease-modifying therapeutics. Specifically, this thesis will focus upon the development of novel RNA-based therapies for AD.

1.2 Genetics of Alzheimer's Disease

AD may be divided into either familial or sporadic AD. Familial AD accounts for less than 5% of all AD cases and is caused by autosomal dominant mutations in the genes coding for Amyloid Precursor Protein (*APP*)[5,6], Presenilin-1 (*PSEN1*)[7] or Presenilin-2 (*PSEN2*)[8–10]. In contrast, the precise cause of sporadic AD, which accounts for the majority of cases, is unknown but is thought to result from a complex interaction of genetic, epigenetic and environmental risk factors[11]. Despite the different causal factors that trigger familial and sporadic AD, both forms are clinically indistinguishable. However, familial AD is more likely to be early-onset (< 65 years of age) while sporadic AD is typically late-onset (> 65 years of age).

1.2.1 Familial Alzheimer's Disease

The highly-penetrant autosomal dominant mutations in *APP*, *PSEN1* and *PSEN2* influence the processing of APP and subsequent formation of amyloid-β peptides. *APP* mutations are typically heterozygous missense mutations[12] although recessive missense mutations[13], whole gene duplications[14] and recessive deletions[15], all located in or near the coding region for amyloid-β, have been reported. Mutations in *APP* account for between 10-15% of familial AD[16] and are associated with increased production of either total amyloid-β or the longer species, amyloid-β (42), which is more prone to aggregation[5,12,17,18]. *PSEN1* and *PSEN2* code for proteins, which constitute part of the γ-secretase complex. Similar to *APP* mutations, *PSEN1* and *PSEN2* mutations alter the cleavage of APP by γ-secretase, resulting in either increased production of amyloid-β or modulation towards the amyloid-β (42) isoform[19]. Mutations in *PSEN1* account for

between 30-70% of familial AD cases while *PSEN2* mutations are estimated to cause ~5% of familial cases[16]. As a mutation in any of these genes is sufficient to cause disease, this has implicated *APP* gene-dosage and amyloid-β processing as causal to the pathogenesis underlying AD. Indeed, Down's syndrome patients, who possess a triplication of chromosome 21 on which the *APP* gene is located, also develop early-onset dementia with characteristic pathological hallmarks of amyloid-β plaques and neurofibrillary tangles[20]. Conversely, a mutation located adjacent to the β-secretase (BACE1) cleavage site in *APP*, which disrupts cleavage of APP by BACE1 and reduces amyloid-β production by ~40%, is protective against AD[21].

1.2.2 Sporadic Alzheimer's Disease

In contrast to familial AD, identifying the genetic variants that predispose an individual to sporadic AD has proved more challenging. The gene *APOE*, encoding the apolipoprotein E (APOE) protein, was identified by classic linkage-based and candidate-gene based association studies and remains the largest known genetic risk factor for sporadic AD[22,23]. Nonetheless, aside from *APOE*, these techniques often identified susceptibility factors that could not be independently replicated, likely due to a lack of power associated with inadequate sample sizes or sample heterogeneity. However, advances in genome technology have recently allowed for large collaborative genome-wide association studies (GWASs) that have proved more fruitful in the identification of disease-associated genetic variants.

APOE is a lipid-binding protein essential for the normal catabolism of triglyceride- and cholesterol-rich lipoproteins[24]. In recent years, APOE has been implicated in other

important roles including the clearance of amyloid-β[25], glutamate receptor function and synaptic plasticity[26] and neurite outgrowth[27,28]. In humans, *APOE* is expressed as three different isoforms encoded by three different alleles; *ε2*, *ε3* and *ε4*. Specifically, the *ε4* allele is associated with increased risk for AD while conversely the *ε2* and *ε3* alleles appear protective[29,30]. *APOE ε4* has a dose-dependent effect upon increasing the risk for AD and lowering the age-of onset[23,31–33]. One copy of *APOE ε4* increases the risk of developing AD three-fold while two copies confer a 7-15-fold increase in risk. Each APOE *ε4* copy lowers age-of-onset by 6-7 years[23,31–33].

Why *APOE ε4* contributes to an increased risk for AD while the *ε2*/*ε3* alleles are protective remains largely unknown. However, evidence suggests that there are isoform-specific effects upon diverse physiological processes including; amyloid-β clearance and aggregation[25,34–36], neurite outgrowth and APOE receptor recycling[26–28], mitochondrial function[37], entorhinal cortical thinning[38], GABA interneuron number[39,40] and disrupted brain activity both in resting-state connectivity and in response to specific memory tasks[41]. Many of these effects are evident in healthy young *APOE ε4* carriers, decades before symptoms are expected. The *APOE ε4* allele may therefore confer risk for AD through disruption of multiple pathways over many years. However, the *APOE ε4* allele is neither sufficient nor required for the development of AD. Hence, a significant research effort has focused upon identifying additional disease-related variants.

Following the advent of GWAS, over 20 novel risk loci for sporadic AD have been replicated across independent datasets[42–49]. These risk loci are common single nucleotide polymorphisms (SNPs) located in or near a number of different genes. The

first set of GWASs identified *CLU*, *CR1*, *PICALM*, *BIN1*, *EPHA1*, *ABCA7*, *CD2AP*, *CD33* and the *MS4A* cluster as novel susceptibility loci[42–46]. Subsequently, a meta-analysis of all these GWASs identified a further 11 loci including; *PTK2B*, *SORL1*, *SLC24A4*, *INPP5D*, *MEF2C*, *NME8*, *ZCWPW1*, *CELF1*, *FERMT2*, *CASS4* and *HLA-DRB5/HLA-DRB1*[48]. While the *APOE Ɛ4* allele confers a relatively large increase in risk of ~35%, the odds ratios for these loci are smaller, ranging from 1.08 to 1.29[50]. This meta-analysis therefore highlights the importance of large sample sizes when individual variants contribute only a modest increase in risk.

The identified loci all have functional relevance and cluster in pathways hypothesised to be important in AD. These will be discussed in more detail in **Section 1.3**. Briefly, these pathways include; APP processing (*CASS4* and *SORL1*), tau processing (*CASS4* and *FERMT2*), lipid processing (*ABCA7*, *CLU1* and *SORL1*), synaptic function (*MEF2C* and *PTK2B*), cytoskeletal function and axonal transport (*CASS4*, *CELF1* and *NME8*), immune response regulation (*ABCA7*, *CD33*, *CLU1*, *CR1*, *EPHA1*, *HLA-DRB5/DRB1*, *INPP5D*, *PTK2B* and *MEF2C*), synaptic function (*BIN1*, *CD33*, *CD2AP*, *MEF2C*, *PICALM* and *PTK2B*), cell migration and MAPK signalling (*PTK2B*) and microglial cell function (*INPP5D*)[48,51–65]. While each variant only contributes a small increase in risk alone, the combinatorial effect of many risk variants exposed to epigenetic and environmental influences may result in biochemical changes within these disease-relevant pathways. Over many decades, this may predispose towards the development of AD. Future large-scale GWASs are expected to identify further genetic variants associated with sporadic AD. The identification of novel variants, which link to established or novel disease pathways, will further extend our understanding of the underlying disease mechanisms predisposing towards AD.

1.3 Disease Mechanisms and Pathology

There are two key pathological hallmarks required for a confirmed AD diagnosis at post-mortem; extracellular amyloid-β plaques and intracellular neurofibrillary tangles comprised of hyperphosphorylated tau. In addition, increasing neuronal and synaptic loss is observed across hippocampal and cortical areas as the disease progresses. These core pathologies have prompted several theories concerning the causal pathogenic mechanisms responsible for AD and underpin current therapeutic development.

1.3.1 APP Processing and Function

APP processing is disrupted by mutations in *APP*, *PSEN1* and *PSEN2*. Furthermore, there is a gene-dosage effect of APP upon age-of-onset and disease severity. These observations prompted the "amyloid-cascade" hypothesis of AD which posits that amyloid-β plaques are the basis to AD and are responsible for the associated neurofibrillary tangles, cortical atrophy and cognitive deficits[66].

In humans, *APP* is expressed as three major isoforms, APP751, APP770 and APP695, via alternative splicing[67]. APP751 and APP770 are widely expressed while APP695 is primarily expressed in neurons[68]. All three isoforms are type 1 transmembrane proteins which undergo processing by several different secretases[69,70]. In the non-amyloidogenic pathway, APP is cleaved by α-secretase within the amyloid-β domain, which precludes formation of the amyloid-β peptide, instead generating soluble APPα (sAPPα) and a C-terminal fragment (C83). In the amyloidogenic pathway, APP is sequentially cleaved by BACE1 and γ-secretase. Processing by BACE1 generates soluble APPβ (sAPPβ) and a

C-terminal fragment (C99). The C-terminal fragment is further cleaved by the γ-secretase protease complex, comprised of PSEN1/PSEN2, APH-1A/APH-1B, NCT and PEN-2[71], to produce amyloid-β peptides and the APP intracellular domain (AICD), which may be cleaved by caspases to produce a C31 fragment[72] (**Fig. 1.1**).

Given the intensive research effort focused upon delineating the causal mechanisms of AD, it is perhaps surprising that the physiological function of APP remains unknown. However, in recent years APP has been implicated in a range of functions including neurite outgrowth, synaptogenesis, axonal transport, transmembrane signal transduction, cell adhesion, calcium metabolism, axonal pruning and neural cell death[72–77].

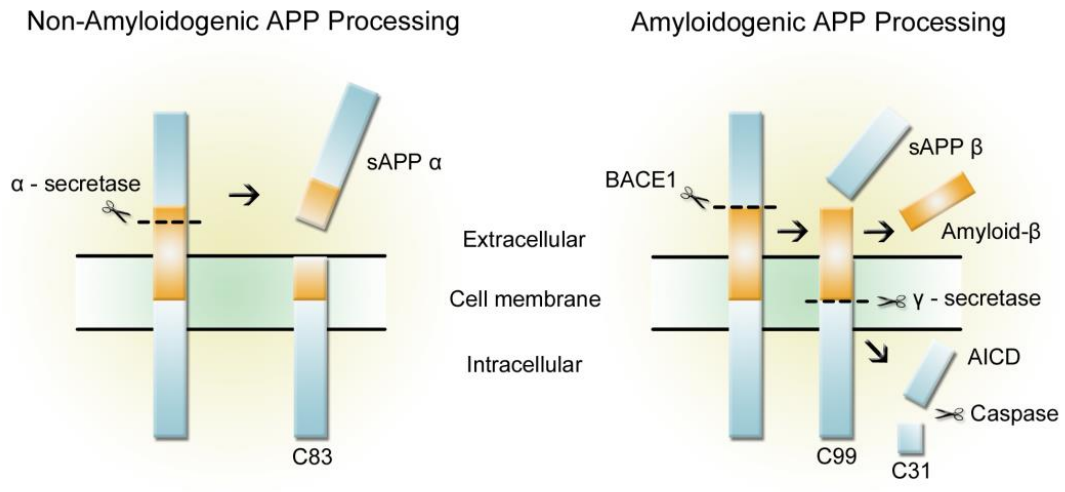

Figure 1.1 Non-amyloidogenic and Amyloidogenic Processing Pathways of APP. In the non-amyloidogenic pathway, APP is cleaved by α-secretase within the amyloid-β domain. This generates soluble APPα (sAPPα) and a C-terminal fragment (C83), preventing formation of amyloid-β peptides. By the amyloidogenic pathway, APP is sequentially cleaved by BACE1 and γ-secretase. Processing by BACE1 generates soluble APPβ (sAPPβ) and a C-terminal fragment (C99) which is further cleaved by γ-secretase to produce amyloid-β peptides of various lengths and the APP intracellular domain (AICD). AICD may be further cleaved by caspases to produce C31 fragments.

The original formulation of the amyloid-cascade hypothesis placed toxic amyloid-β plaques at the centre of neuronal dysfunction and death. However, recent findings have challenged this model. While amyloid-β plaques may be associated with onset of clinical symptoms, amyloid-β plaque density is not the best correlate of neuronal degeneration, synaptic loss or disease severity[78–80]. Amyloid-β plaques can be found in non-demented individuals and conversely, patients whose plaques were cleared by immunotherapy, discussed in **Section 1.4**, still suffered with dementia[81–83]. Instead, evidence suggests that small soluble oligomers of amyloid-β may represent the most toxic species as they correlate more strongly with pathophysiology and cognitive impairment[84–93]. Plaques might therefore represent a protective mechanism in a system overwhelmed by neurotoxic amyloid-β oligomers[94]. The amyloid-cascade hypothesis has therefore been updated to focus upon amyloid-β oligomers rather than plaques as initially suggested[87,93,95].

While accumulating evidence supports the toxicity of soluble amyloid-β oligomers, the biological structures of the most pathogenic oligomers remain to be identified. However, dimers and trimers are present in soluble fractions from patients and transgenic AD models and are associated with neurotoxic effects upon long-term potentiation (LTP), long-term depression (LTD), spine density and impaired learning and memory[96–98]. There appears to be a nonlinear relationship to oligomer order and toxicity as dimers and tetramers are three- and 13-fold more toxic than monomers respectively[99]. Another amyloid-β oligomer, Aβ*56, comprising ~12 amyloid-β peptides, also impairs cognitive function[100–102]. Amyloid-β dimers, trimers and Aβ*56 all increase with age in cognitively normal humans[103]. However, Aβ*56 was the only

species found to positively and negatively correlate with pathological tau and postsynaptic proteins, respectively[103].

Together, these findings highlight the importance of disrupted APP processing in the formation of small neurotoxic soluble amyloid-β oligomers and identify these oligomers as a target for novel therapeutics.

1.3.2 Tau Processing and Function

Amyloid-β clearly plays a pivotal role in AD. However, the importance of pathological tau cannot be discounted. Mutations in *MAPT*, encoding for microtubule-associated protein tau, are sufficient to cause a range of neurodegenerative diseases, collectively referred to as tauopathies, which are characterised pathologically by neurofibrillary tangles comprising hyperphosphorylated tau[104–107]. As neurofibrillary tangles form in the absence of amyloid-β pathology in these diseases, this highlights the importance of abnormal tau in neurodegenerative disease.

MAPT is located on chromosome 17q21 and primarily expressed within neurons of the central (CNS) and peripheral nervous systems (PNS)[108]. The *MAPT* locus comprises 16 exons which, in the adult human brain, undergo alternative splicing to produce six different tau isoforms[109,110]. Tau comprises three major domains; an amino-terminal projection domain, a carboxy-terminal domain of microtubule-binding repeats and a short tail sequence. Alternative splicing of exons 2 and 3 generates isoforms which contain either zero (0N), one (1N) or two (2N) amino-terminal inserts while alternative splicing of exon 10 generates isoforms containing either three (3R) or four (4R)

microtubule-binding domains[109,111]. During embryonic and early developmental stages 3R tau is the predominant isoform, while in the adult brain 3R:4R isoforms are present at an approximately equal ratio[109,112]. Perturbation of this ratio is linked to a number of tauopathies[105,111,113].

Two major genetic haplotypes, H1 and H2, define the *MAPT* locus. The haplotypes are under high linkage disequilibrium and include a 900 kb inversion in addition to numerous SNPs[114–116]. Both the H1 haplotype and specific H1 polymorphisms are associated with increased risk of tauopathy[114,117,118]. Indeed, the H1c haplotype has been associated with an increased risk of AD[119]. How the H1 haplotype confers susceptibility to neurodegeneration is unclear. However, haplotype-specific effects upon total tau expression or alternative splicing of disease-related isoforms may be important[117,119–121]. Thus, the H1 haplotype expresses a greater proportion of disease-associated 4R transcripts while the protective H2 haplotype expresses a greater proportion of 2N transcripts[119,122,123]. Polymorphisms between the H1 and H2 haplotypes may therefore have subtle consequences upon tau expression and function conferring vulnerability to neurodegenerative disease over time.

Tau is predominantly localised within axons and contributes towards neuronal morphology by promoting the stability and assembly of microtubules through interactions with tubulin[124]. Tau also regulates axonal transport through interactions of the N-terminal projection domains with the p150 subunit of the dynactin complex[125]. Tau may also localise, in lower levels, to dendrites where it interacts with the tyrosine protein kinase, Fyn, and may play a role in neurite outgrowth and cell signalling[126,127].

The impaired ability of pathological tau to perform these functional roles may interfere with key neuronal processes and therefore account for some of the impairments in AD.

Neurofibrillary tangles are comprised of hyperphosphorylated tau. Exactly how tau hyperphosphorylation contributes to disease is not fully understood. However, hyperphosphorylation of tau, particularly at serine/threonine epitopes near the tubulin microtubule-binding domains, prompts its dissociation from microtubules[128]. Abnormal hyperphosphorylation also promotes self-assembly into paired helical filaments which are a key component of the neurofibrillary tangles observed in AD and other tauopathies[128]. Given the important role that tau plays in maintaining neuronal stability and in promoting axonal transport via binding to microtubules, any disruption to its binding abilities is likely to comprise a range of cellular functions.

An important study by Ittner *et al.*[126] has also revealed a pathological dendritic function for hyperphosphorylated tau. Phosphorylation of tau strengthens the interaction with Fyn, both *in vitro* and *in vivo*[126,129]. Via this interaction, tau facilitates the targeting of Fyn to post-synaptic sites. Here, Fyn phosphorylates the NMDA receptor (NMDAR) subunit 2B, resulting in the formation of a complex between NMDARs and postsynaptic density protein 95 (PSD-95)[126]. As this complex is required for excitotoxic downstream signalling, the interaction between tau and Fyn may enhance the potential for the neurotoxic signalling observed in AD. Furthermore, while interest has focused upon hyperphosphorylation, other pathogenic post-translational modifications also disrupt function. Thus, tau acylation also impairs microtubule binding and promotes the pathological aggregation of tau[130].

Numerous studies have found that tau pathology is a better correlate of dementia severity than markers of amyloid-β pathology. Paired helical filaments and neurofibrillary tangles correlate well not only with the areas of the brain suffering from neurodegeneration but also with the extent of neuronal and synaptic loss and degree of cognitive impairment[131–135]. However, it is debated whether soluble tau oligomers or neurofibrillary tangles represent the most harmful species[136]. Growing evidence suggests that, as for amyloid-β, neurofibrillary tangles may be an adaptive response to toxic soluble tau species.

In vitro studies have confirmed that overexpression of tau or changes to its conformational state impairs a range of cellular processes in the absence of neurofibrillary tangles including synaptic signalling, calcium homeostasis, mitochondrial trafficking and function, loss of dendritic spines and impaired axonal transport[85,137–141]. These findings are strengthened by *in vivo* data showing a correlation between soluble tau species and neuronal or synaptic dysfunction, prior to the appearance of neurofibrillary tangles[142–145]. Perhaps most remarkably, regulatable transgenic mouse models of tauopathy have been developed[146,147]. Pro-aggregant mice develop synaptic loss, deficits in LTP and impaired memory. However, when pro-aggregant tau was switched off, both memory and LTP recovered although insoluble neurofibrillary tangles remained[146,147]. It has also been shown that tau oligomers but not fibrils, extracted directly from the cerebral cortex of AD patients, are sufficient to propagate abnormal tau conformation in the brains of wild-type mice, inducing synaptic deficits, mitochondrial dysfunction and memory impairments[145]. Together, these findings support the importance of hyperphosphorylated tau oligomers in the propagation of disease.

As such, research is now focusing upon the cause of hyperphosphorylation. This has led to the proposal of the GSK3 (glycogen synthase kinase 3) hypothesis of AD[148]. GSK3, which exists as two different isoforms, GSK3α and GSK3β, is a proline-directed serine/threonine kinase, which contributes to a range of cellular functions including cell signalling, growth metabolism and regulation of transcription factors. The GSK3 hypothesis posits that over-activity of GSK3 contributes towards tau hyperphosphorylation, increased amyloid-β production and memory impairment[148].

GSK3 directly regulates the hyperphosphorylation of tau at numerous sites[149–152]. GSK3β transgenic mice display neurodegeneration characterised by somatodendritic localization of hyperphosphorylated tau in addition to reactive astrocytosis and microgliosis[153]. GSK3 expression and activity is upregulated in the hippocampus and frontal cortex of AD patients, respectively[154,155]. GSK3 also co-localizes with pre-tangle neurons, neurofibrillary tangles and dystrophic neurites, appearing first in the entorhinal cortex before extending to other regions of the brain, coincident with the spread of neurofibrillary changes[152,156,157].

Pharmacological activation of GSK3, both *in vitro* and *in vivo*, induces tau hyperphosphorylation, increases amyloid-β production by regulating APP cleavage, suppresses acetylcholine (ACh) and induces memory deficits[158–161]. These findings are of interest given that a reduction in ACh is associated with the loss of cholinergic neurons in AD[1]. Why cholinergic neurons are susceptible in AD is unknown. However, growing evidence suggests GSK3β is also a key mediator of apoptosis[162,163]. Suppression of ACh in response to GSK3 activation could therefore be an early step in the loss of cholinergic neurons.

Conversely, treatment with lithium, a GSK3β inhibitor, *in vitro* and *in vivo*, has been shown to reverse levels of both soluble and aggregated hyperphosphorylated forms of tau and rescue memory impairments[164–168]. Treatment of transgenic AD mice prior to pathology onset not only reduced tau hyperphosphorylation but also reduced the size of amyloid-β plaques and prevented neuronal loss in the hippocampus and entorhinal cortex[169].

Why GSK3 expression and activity may be upregulated in AD is unknown. However, exposure to amyloid-β increases GSK3β activity through inhibition of PI3-kinase signalling[170]. Furthermore, a polymorphism within the GSK3 promoter is associated with increased risk of AD[171]. Interestingly, GSK3β may also regulate alternative splicing of tau exon 10 via phosphorylation of the key splicing factor, SC35[172,173]. This raises the possibility that GSK3β may contribute towards AD via aberrant splicing of exon 10, disturbing the normal ratio of 3R:4R tau isoforms in the adult brain.

Together, these findings suggest a role for both tau and GSK3 in the pathogenesis of AD and suggest how they may interact to drive disease progression. As such, both tau and GSK3 may represent valuable therapeutic targets.

1.3.3 Interaction between APP and Tau Pathologies

While the contributions of the respective APP and tau pathologies have largely been discussed separately above, it is important to consider how they may interact in AD. This becomes important for novel therapeutic design as it is increasingly likely that

targeting multiple components at early disease stages will be crucial for the identification of effective therapeutics.

Increasing evidence suggests that amyloid-β induces tau hyperphosphorylation. *In vitro* amyloid-β treatment of cortical, hippocampal and septal cultures activates GSK3β, resulting in increased tau phosphorylation, disturbed exon 10 splicing and decreased activity of choline acetyltransferase[170,172–175]. These findings are consistent with those *in vivo* which demonstrate amyloid-β-induced tau hyperphosphorylation and formation of neurofibrillary tangles in transgenic mice[92,176–179]. Conversely, genetic reduction of Bace1, the rate-limiting step in the production of amyloid-β, reduced somatodendritic localization and hyperphosphorylation of tau in a transgenic mouse model of AD, rescuing learning and memory deficits[178].

Killick and colleagues[180] have also identified a novel amyloid-β-induced clusterin/p53/DKK1/Wnt-planar cell polarity (PCP)-c-Jun N-terminal kinase (JNK) signalling pathway which drives the upregulation of several genes found to regulate amyloid-β-induced neurotoxicity and tau hyperphosphorylation. In response to amyloid-β, intracellular clusterin was rapidly upregulated resulting in the p53-dependent induction of DKK1 and activation of the JNK signalling pathway. This induced several genes including *EGR1*, *NAB2* and *KLF10* which protected against amyloid-β neurotoxicity and/or tau phosphorylation when individually silenced[180]. These findings complement previous reports of increased DKK1 expression in AD patients and transgenic mouse models[181–183]. The role of clusterin is particularly interesting given that it is the product of *CLU*, a susceptibility factor for sporadic AD[44], which is increased in mouse models of AD[184]. Not only do these findings identify novel

components linking amyloid-β to tau hyperphosphorylation but, in doing so, highlight novel therapeutic targets.

Tau phosphorylation may also mediate amyloid-β neurotoxicity. Silencing tau expression either *in vitro* or *in vivo* protects against amyloid-β-induced neurodegeneration[185,186]. Tau reduction also prevents amyloid-β-induced deficits in axonal transport of mitochondria and the neurotrophin receptor, TrkA, both vital for normal neuronal function[187]. How tau may mediate amyloid-β-induced neurotoxicity has been partly delineated by Ittner and colleagues[126]. Excitotoxicity, due to increased NMDAR activity, had previously been identified as a key pathway via which amyloid-β induces neuronal damage, with increased seizures reported in APP transgenic mice[96,186,188]. However, with no evidence for a direct interaction between amyloid-β and NMDARs, the mechanism remained unclear. Ittner *et al.*[126] showed that in transgenic mice either completely lacking tau ($Tau^{-/-}$) or in which only a truncated form was expressed, the postsynaptic localization of Fyn was reduced, destabilising the NMDAR-PSD-95 interaction and protecting against NMDAR-mediated excitotoxicity. This prevented memory deficits and protected against excitotoxic seizures and premature death. This was recapitulated following treatment with Tat-NR2B9c, a compound which destabilises the NMDAR-PSD-95 interaction. Thus, these findings identify a pathway via which tau may mediate amyloid-β-induced excitotoxicity.

Together, the findings above highlight how amyloid-β and tau-mediated pathologies may interact towards AD. A model may be envisaged in which increased amyloid-β elicits multiple toxic effects including the hyperphosphorylation of tau, resulting in its dissociation from microtubules and increased mislocalization to the somatodendritic

compartment. In this way, both tau and amyloid-β-based mechanisms may disturb key processes disrupted in AD either independently or in concert. This suggests that a combinatorial approach, targeting both amyloid-β and tau-based components of the disease mechanism, may represent a promising therapeutic strategy.

While research interest has focused upon unravelling the respective roles of amyloid-β and tau, emerging evidence increasingly implicates additional mechanisms in a causal role for AD pathogenesis. These include neuroinflammation, oxidative stress and deregulation of the microRNA (miRNA) network.

1.3.4 Neuroinflammation

Neuroinflammation occurs within the CNS in response to traumatic brain injury, infection and disease. Although neuroinflammation has long been recognised in AD as a response to neurodegeneration, in recent years it has been attributed a causal role in pathogenesis.

Microglia are specialised resident phagocytes of the CNS[189,190]. They are found ubiquitously within the brain and monitor for the presence of pathogens or cell debris via highly motile processes. Microglia are activated by pathological triggers which bind to specific receptors such as scavenger receptors, NOD-like receptors (NLRs) and pattern-recognition receptors, including Toll-like receptors (TLRs). Upon activation, microglia migrate to the injury site and initiate an immune response which involves the production of pro-inflammatory cytokines including interleukins (IL-1 and IL-6), tumour necrosis factor (TNF)-α and chemokines[191]. Astrocytes are also involved in the

innate immune response. They express a variety of receptors including NLRs, TLRs and scavenger receptors and release cytokines and chemokines in response to environmental challenges[192,193].

Evidence from several sources implicates a role for neuroinflammation in AD. Amyloid-β is a ligand for a number of microglial/astrocyte receptors which are upregulated in reactive microglia and astrocytes surrounding amyloid-β plaques[194–198]. Amyloid-β-receptor binding triggers the production of inflammatory cytokines and chemokines and the phagocytic clearance of amyloid-β[194–198]. Furthermore, genes encoding for the immune receptors, TREM2 and CD33, are susceptibility factors for AD[199,200]. TREM2 and CD33 are expressed on microglia and play key roles in regulating phagocytic clearance. Mutations in these genes appear to compromise microglial phagocytosis of amyloid-β, suggesting that inefficient clearance of amyloid-β may contribute to disease[199–202].

Exposure to pathological accumulations of amyloid-β is associated with increased levels of pro-inflammatory cytokines in AD patients and transgenic models which may impair neuronal function by suppression of LTP[203–206]. Indeed, an increase in the cerebrospinal fluid (CSF) concentration of TNF-α (pro-inflammatory) paired with a decrease in TGF-β (anti-inflammatory) is associated with an increased risk for converting from mild cognitive impairment (MCI) to dementia[207]. Furthermore, IL-1 increases the secretion of amyloid-β by regulating the synthesis and processing of APP[208,209]. Thus, amyloid-β may induce the secretion of pro-inflammatory cytokines and chemokines which further increase amyloid-β production.

Amyloid-β is an important trigger for the neuroinflammatory response in AD. However, environmental risk factors associated with AD including traumatic brain injury, obesity and systemic inflammation may also modulate the neuroinflammatory response. Traumatic brain injury is associated with increased microglial activation[210] while the release of pro-inflammatory cytokines from human adipose tissue is enhanced in obesity[211]. Systemic inflammation may also exacerbate neuroinflammation and studies have revealed that both acute and chronic systemic inflammation are associated with increased cognitive decline in AD patients[212].

Thus, under normal circumstances, the innate immune reaction represents an acute protective response to clear pathogens and cell debris. However, in the face of prolonged exposure to amyloid-β, a multitude of factors may combine to produce a chronic long-term neuroinflammatory response, which may have significant detrimental consequences.

1.3.5 Oxidative Stress and Mitochondrial Dysfunction

Oxidative stress, arising from mitochondrial dysfunction, is an imbalance between the production and ability to process ROS/RNS (reactive oxygen/nitrogen species). Oxidative stress is a normal part of ageing. However, increasing evidence is firmly placing it as an early contributing factor to AD.

Mitochondria are the main source of ROS although activated microglia and astrocytes and reactions catalysed by redox active metals also generate ROS/RNS[213]. The neurotoxicity of ROS/RNS is conferred by their oxidation of a range of cellular

macromolecules including DNA, RNA, lipids and proteins[214–216]. The detrimental effects are wide-ranging but include disruption to gene expression, cell membrane integrity and misfolding and loss of protein activity[214–216].

Amyloid-β damages mitochondria and increases the production of ROS resulting in increased lipid oxidation in transgenic mouse models[217]. The interaction between amyloid-β and mitochondria appears to be mediated by Aβ-binding alcohol dehydrogenase resulting in increased ROS production, mitochondrial dysfunction and apoptosis[218,219]. Oxidative stress may also increase amyloid-β production, potentially resulting in a neurodegenerative feedback cycle[220].

Markers of oxidative stress, 4-hydroxyhexenal, F2-isoprostane, F4-isoprostane and DNA/RNA oxidation, are increased at the earliest stages of disease in AD patients[221–224]. However, F2-isoprostane was not increased in Parkinson's disease (PD) or schizophrenia patients suggesting this may not reflect a general disease mechanism[225]. Furthermore, the relationship between oxidative stress and pathological hallmarks is modulated by *APOE* genotype[224]. This is consistent with other reports that *APOE ε4* is linked to higher levels of oxidative stress and reduced anti-oxidant enzyme activity in patients and healthy controls, which may relate to isoform-specific anti-oxidant properties[213,226–228]. Finally, the effects of neuroinflammation and oxidative stress may converge given that cytokines stimulate the production of ROS via increased expression of inducible nitric oxide synthase (iNOS), which is upregulated in the brains of AD patients[229]. These results suggest that compounds aimed at reducing neuroinflammation and oxidative stress may have therapeutic utility.

1.3.6 Deregulation of the miRNA Network

miRNAs are an endogenous species of small non-coding RNA that act as post-transcriptional regulators of gene expression. The miRNA biogenesis pathway will be discussed in more detail in **Section 1.5**. Briefly, miRNAs regulate gene expression by binding to partially complementary sites, predominantly in the 3' UTR of target mRNAs[230–232]. Depending on the extent of complementarity, miRNA binding induces translational repression or mRNA degradation[233–236]. A single miRNA regulates the expression of multiple genes, often within one biological pathway, while one gene may be regulated by multiple miRNA species[237,238]. Thus, miRNAs are powerful regulators of highly complex cellular networks.

miRNAs regulate a wide range of processes including proliferation, differentiation, immune function, neuronal development, apoptosis, plasticity and survival[239,240]. As such, any change to miRNA expression can have profound effects upon neuronal function. Indeed, miRNA dysfunction is implicated in a range of diseases including cancer, schizophrenia and neurodegenerative diseases such as AD and PD[241–246]. Deregulation of miRNAs may involve upregulation or downregulation of specific miRNAs. Disruption to the highly regulated miRNA network may predispose to disease in two ways; directly, via a gene-dosage effect in which miRNA-mediated silencing of a disease-associated gene is alleviated or enhanced, or more indirectly by affecting genes involved in important processes such as cell signalling or apoptosis.

A number of studies have now identified deregulation of the miRNA network in AD (**Table 1.1**). Importantly, several of these miRNAs regulate genes important to AD

pathogenesis (**Fig. 1.2**). The miR-20a cluster (miR-20a, miR-17-5p and miR-106b) negatively regulates APP expression and miR-106b expression is significantly decreased in sporadic AD patients[247]. APP expression is also negatively regulated by miR-106a, miR-520c and miR-101[248,249]. miR-101 may specifically contribute to the regulation of APP in response to the pro-inflammatory cytokine IL-1β, providing a link between miRNAs and neuroinflammatory pathologies[249].

miRNAs also regulate BACE1 expression. The miR-29a/b-1 cluster negatively regulates BACE1 expression *in vitro* and is significantly downregulated in a subset of AD patients displaying elevated BACE1 expression[250,251]. miR-29a also negatively regulates the expression of neurone navigator 3 (*NAV3*), a key regulator of axon guidance. NAV3 expression is elevated in AD brains, particularly in degenerating cortical neurons[251]. This example demonstrates how downregulation of miRNA expression might contribute to multiple detrimental pathways.

BACE1 expression is also negatively regulated by miR-107, which is downregulated in the brains of AD patients at the earliest stages of pathology[252,253]. miR-107 also regulates the actin-binding protein, cofilin, a constituent of rod-like structures found in AD patients[254]. Reduced levels of miR-107 (and miR-103) were associated with elevated cofilin protein expression and the formation of rod-like structures in transgenic AD mice[254]. Downregulation of specific miRNAs might therefore contribute to increased BACE1 expression and elements of cytoskeletal pathology.

Alternative splicing of tau is associated with disease. It is therefore of note that several brain-expressed miRNAs including miR-9, miR-124, miR-132 and miR-137 appear to

regulate the 3R:4R ratio of tau isoforms in neuronal cells[255]. miR-132 was also negatively correlated with levels of the important neuronal splicing factor, PTBP2, in progressive supranuclear palsy, a 4R tauopathy model[255]. As miR-9, miR-124, and miR-132 appear downregulated in AD[256–258], it is conceivable that they could contribute to altered splicing of tau exon 10 in AD.

The splicing of APP may also be regulated by miRNAs[259]. A lack of miRNAs in post-mitotic neurons *in vivo* was associated with inclusion of exons 7/8 in APP. miR-124, an abundant neuronal-specific miRNA downregulated in AD, appeared to regulate PTBP1 expression. PTBP1 levels were correlated with the presence of APP exons 7/8 in post-mitotic neurons but with their skipping during neuronal differentiation. This therefore implicates miR-124 in the fine-tuning of APP alternative splicing. Together, these results suggest that miRNA deregulation may disrupt normal splicing of APP and tau.

Increased miRNA expression may also contribute to AD. miR-34a was more highly expressed in AD transgenic mice prior to amyloid-β plaque formation at three months of age[260]. Furthermore, miR-34a expression inversely correlated with BCL-2 expression, a key anti-apoptotic protein, while levels of caspase-3, an apoptotic effector caspase, were increased. This relationship was confirmed by experimental inhibition of miR-34a which increased levels of BCL-2, resulting in reduced active caspase-3[260]. Importantly, the levels of miR-34a and miR-34c are also both elevated in AD patients[261,262].

Phosphorylation of tau may also be under miRNA regulation. miR-26b is upregulated in the brains of early-stage AD patients and is associated with aberrant cell cycle entry and tau hyperphosphorylation[263]. miR-125b is also upregulated in AD and linked to tau

hyperphosphorylation via upregulation of CDK5/p35 and p44/42-MAPK signalling[264]. The phosphatases, DUSP6 and PPP1CA, and the anti-apoptotic factor, BCL-W, were downregulated in AD patients and identified as targets of miR-125b[264]. This was confirmed by direct hippocampal injections of miR-125b in mice which impaired associative learning and resulted in downregulation of BCL-W, DUSP6 and PPP1CA associated with tau hyperphosphorylation[264].

It is not only the expression of miRNAs that influences their regulatory effect upon target mRNAs. Genetic variability may also disrupt miRNA binding by the loss or creation of novel miRNA binding sites. In PD, a SNP in the 3' UTR of fibroblast growth factor 20 (FGF20) disrupts miR-433 binding, resulting in increased α-synuclein expression *in vitro* and *in vivo*[246]. A number of AD-specific polymorphisms which disrupt miRNA binding have now been identified in the 3' UTR of *APP* and *BACE1*[265]. Specifically, the T117C *APP* variant inhibits miR-147 binding while the A454G *APP* variant increases miR-20a binding, with inverse effects upon APP expression[265].

Whether deregulation of miRNA expression is a cause or consequence of disease remains to be determined. However, amyloid-β (42) appears to rapidly downregulate miRNA expression[257]. A feedback loop may therefore exist in which amyloid-β downregulates miRNA expression resulting in further elevation of APP, BACE1 and amyloid-β. Consequently, both elevated amyloid-β and genetic polymorphisms disrupting miRNA binding may perturb the regulatory capacity of miRNAs. As each miRNA potentially regulates many targets, disruption to this network may have significant detrimental effects. Restoration of specific miRNA function may therefore represent a powerful therapeutic strategy.

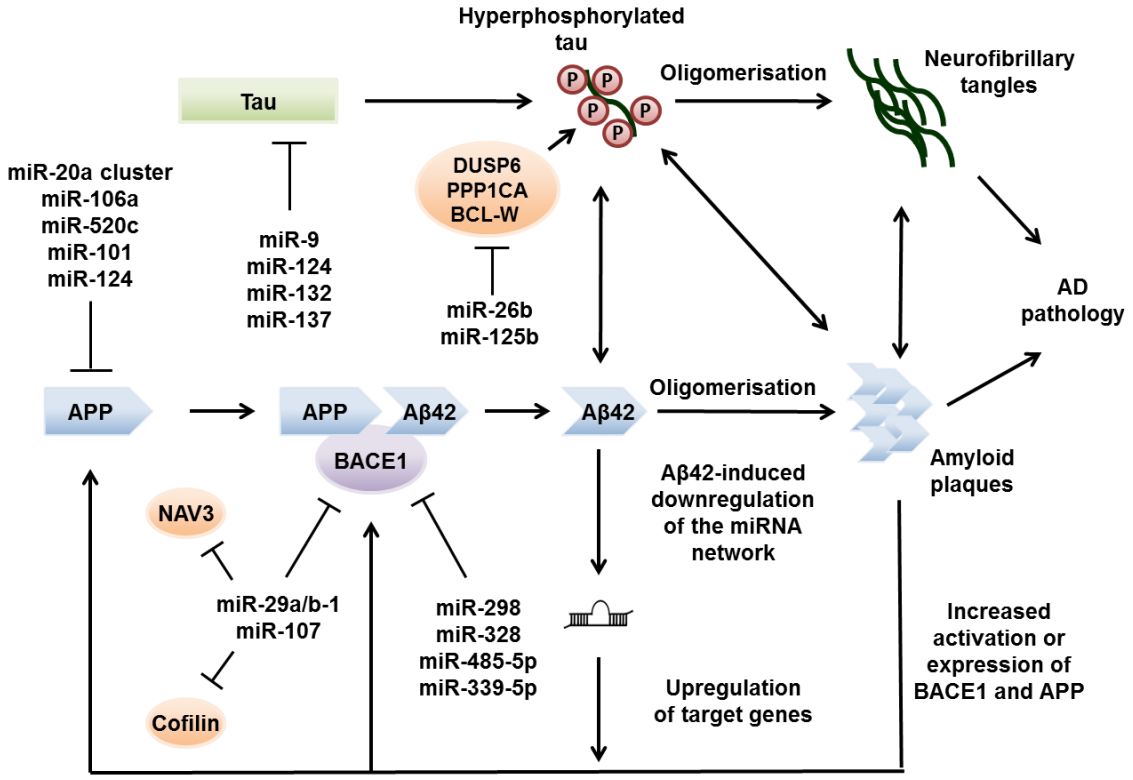

Figure 1.2 Schematic of AD-relevant miRNA and Protein Interactions. A number of miRNAs, which are deregulated in AD, have been shown to regulate the expression of key AD-associated proteins including APP, BACE1 and Tau. miRNAs may regulate protein expression of target mRNA transcripts via translational repression, mRNA degradation or modulation of exon splicing. miRNAs have also been shown to regulate the hyperphosphorylation of tau via their action upon intermediary signalling pathways. Deregulation of the miRNA network may either alleviate or increase repression of critical AD-relevant proteins resulting in increased amyloid-β (42) (Aβ42) production and tau hyperphosphorylation along with their associated downstream pathologies. A pathological feedback loop may also exist as amyloid-β (42) has been shown to induce downregulation of the miRNA network which in turn may result in the upregulation of disease-relevant proteins. Restoration of the miRNA network may therefore represent a viable therapeutic approach for AD.

Table 1.1 Key Studies Showing microRNA Deregulation in Alzheimer's Disease.

Ref.	Key Findings
266	• miR-9, miR-125b and miR-128 expression was elevated while miR-124a expression was reduced in moderate-severe AD patients compared to controls.
252	• miR-107 and miR-23b decreased in temporal cortex of mild AD patients. • miR-107 negatively regulated *BACE1* mRNA. *BACE1* mRNA levels increased in AD patients as miR-107 levels decreased during progression of AD.
256	• miR-9 and miR-132, regulators of neurogenesis and differentiation, downregulated in hippocampus and medial frontal gyrus of AD patients. • AD-specific miRNA changes in CSF, potential biomarker of AD.
250	• 13 miRNAs significantly downregulated in sporadic AD patients including miR-9, miR-29b, miR-181, miR-15a, miR-19b, let-7, miR-101 and miR-106b. • miR-29a/b-1 and miR-9 regulated BACE1 expression *in vitro.* • miR-29a/b-1 cluster significantly decreased in AD patients displaying abnormally elevated levels of BACE1 protein. • Inverse correlation observed between miRNA cluster and BACE1 during brain development and in primary neuronal culture. • APP β-CTFs and amyloid-β downregulated upon miR-29a/b-1 expression *in vitro.*
267	• Bace1 protein increased while *Bace1* mRNA decreased with age in APPswe/PS1 mice indicating loss of translational control. • miR-298 and miR-328 regulated Bace1 expression *in vitro* and were significantly decreased (≥ 50%) in brains of 13-month old APPswe/PS1 mice.
248	• miR-106a and miR-520c negatively regulated APP expression *in vitro*. • Overexpression of either miRNA repressed APP translation by ~50%.
247	• miR-20a family regulated APP expression *in vitro*. • Inverse correlation between miRNA family and APP during brain development and in differentiating neurons from C57BL/6 mice. • miR-106b expression significantly decreased in sporadic AD patients.
260	• 37 deregulated miRNAs in cerebral cortex of APPswe/PS1 mice prior to plaque formation at 3 months of age. • miR-20a, miR-29a, miR-125b, miR-128a and miR-106b downregulated while miR-34a, let-7, miR-28 and miR-98 upregulated. • miR-34a highly expressed and inversely correlated with BCL-2 protein expression in 3-6 month old transgenic mice. miR-34a inhibited BCL-2 translation *in vitro*. • Caspase-3 expression increased in APPswe/PS1 mice. • BCL-2 increased and caspase-3 decreased following *in vitro* inhibition of miR-34.
268	• miR-106b expression increased in 3-6 month old but reduced in 9 month old APPswe/PS1dE9 mice. TβR II reduced in 3-9 month old APPswe/PS1dE9 mice. • miR-106b inversely correlated with TβR II protein levels in APPswe/PS1dE9 mice. • miR-106b directly inhibited TβR II translation *in vitro.* • Reduced phospho-Smad2/3, increased Smad6/7 expression and significant neurodegeneration following stable transfection of miR-106b *in vitro*. • Amyloid-β (42) peptide increased then decreased miR-106b expression and reduced TβR II expression. Amyloid-β (42)-induced impairment of TGF-β signalling through reduced TβR II and inhibition of downstream Smad signalling.

Table 1.1 Continued.

Ref.	Key Findings
251	• miR-29a significantly downregulated in AD brains. • NAV3, regulator of axon guidance, negatively regulated by miR-29a *in vitro.* • NAV3 expression elevated, particularly in degenerating pyramidal neurons of cerebral cortex, in AD patients.
269	• miR-485-5p and *BACE1-AS* compete for binding in exon 6 of *BACE1* mRNA. • *BACE1-AS* prevents miR-485-5p repression of *BACE1* mRNA by masking binding site. • BACE1 and *BACE1-AS* expression upregulated and miR-485-5p expression downregulated in AD patient brain samples compared to controls.
253	• Validation of miR-107 expression in temporal cortex of a separate group of AD patients. • miR-107 expression decreased relative to other miRNAs as AD progressed. • miR-107 expression negatively correlated with BACE1 expression. • Correlation between decreased miR-107 expression and increased neuritic plaques and neurofibrillary tangles in adjacent brain tissues.
249	• Downregulation of AGO2 increased APP expression in rat hippocampal neurons. • miR-101 negatively regulated APP expression and miR-101 expression inversely related to amyloid-β levels. • miR-101 contributed to regulation of APP in response to pro-inflammatory cytokine IL-1β.
257	• 47% of tested miRNAs rapidly downregulated in response to amyloid-β (42) treatment in primary hippocampal neurons from C57BL/6 mice including miR-9, miR-181c, miR-30c, miR-20b, miR-148b and let-7i. • miRNA deregulation *in vivo* at onset of amyloid-β plaque deposition in APP23 AD mice. • Downregulated miRNAs predicted to target genes in key pathways including; axon guidance, MAPK signalling, ErbB signalling, TGF-β signalling, ubiquitin-mediated proteolysis, glutamate metabolism, LTP and regulation of actin cytoskeleton.
270	• Comparison of miRNA expression in GM and WM from superior and middle temporal cortex from female AD patients. • miRNA expression variability associated with early-AD pathology mostly found in GM. • Some miRNAs differentially expressed in WM including miR-212 (downregulated) and miR-424 (upregulated). • Downregulation of a set of miRNAs in GM including miR-15/107 and miR-29 paralogues correlated strongly with density of diffuse amyloid plaques in adjacent tissues.
265	• Analysis of *APP* 3' UTR genetic polymorphisms; T117C, A454G and A833C. • 12 putative miRNA binding sites located in or near *APP* 3' UTR variants. • 7 miRNAs including miR-20a, miR-17, miR-147, miR-655, miR-323-3p, miR-644 and miR-153 regulated APP expression *in vitro.* • T117C variant inhibited miR-147 binding while A454G increased miR-20a binding resulting in increased or decreased APP expression, respectively.

Table 1.1 Continued.

Ref.	Key Findings
259	• Lack of miRNAs associated with inclusion of APP exons 7/8 in post-mitotic neurons *in vivo*. • miR-124, abundant neuronal-specific miRNA, downregulated in AD patients. • Ectopic expression of miR-124 or depletion of PTBP1 (target of miR-124) reduced inclusion of exons 7/8. • PTBP1 correlated with presence of APP exons 7/8 in post-mitotic neurons but with their skipping during neuronal differentiation. • miR-124 regulates fine-tuning of APP alternative splicing in neurons.
271	• miR-9 and miR-181c downregulated by amyloid-β (42) treatment. • TGF-β, TRIM2, SIRT1 and BTBD3 repressed up to 12-fold by miR-9 and miR-181c, either alone or in combination, *in vitro*. • Genes involved in a number of roles/functions including; TGF-β signalling pathway (*TGFB1*), ubiquitin ligase (*TRIM2*), histone deacetylase (*SIRT1*) and transcription factor (*BTBD3*).
258	• Deregulation of 35 and 41 miRNAs in hippocampus and prefrontal cortex, respectively, in 2 large independent cohorts of late-onset AD patients. • miR-132-3p upregulated between Braak stages I-II then strongly downregulated by Braak stages III-IV, prior to loss of neuron-specific miRNAs. • Strong downregulation of miR-132-3p and 3 family-related miRNAs encoded by same cluster on chromosome 17 confirmed by next-generation sequencing and occurred mainly in neurons displaying tau hyperphosphorylation. • miR-132-3p regulated MAPT, EP300, SIRT1 and transcription factor, FOXO1a *in vitro*. • FOXO1a expression increased in hippocampal samples of AD patients with low miR-132-3p expression.
272	• Differential expression of miR-16, miR-34c, miR-107, miR-128a and miR-146a in hippocampus of AD patients. • miR-16 and miR-146a most significantly different; both increased at Braak stage III/IV but decreased by Braak VI. • miR-107 and miR-128a significantly decreased in Braak VI while miR-34c elevated in Braak III/IV samples. • miR-146a significantly decreased in CSF of AD patients; differentiated AD patients from controls with sensitivity of 60% and specificity of 90%.
273	• miR-339-5p downregulated (45%) in brain samples from advanced AD patients. • BACE1 expression significantly elevated (41%) in AD samples. • miR-339-5p regulated BACE1 expression *in vitro.* • miR-339-5p mimic reduced BACE1 and amyloid-β (40/42) expression in human glioblastoma and fetal primary brain cultures.

miR, microRNA; **AD**, Alzheimer's disease; **BACE1**, β-secretase; **CSF**, cerebrospinal fluid; **CTF**, carboxy-terminal fragment; **BCL-2**, B-cell lymphoma 2; **NAV3**, neurone navigator 3; **TβR II**, TGF-β receptor type II; **TGF-β**, transforming growth factor beta; **BACE1-AS**, BACE1 antisense; **AGO2**, argonaute 2; **IL**, interleukin; **MAPK**, mitogen-activated protein kinase; **LTP**, long-term potentiation; **GM**, grey matter; **WM**, white matter; **TRIM2**; tripartite motif containing 2; **SIRT1**, sirtuin-1; **BTBD3**, BTB (POZ) domain containing 3; **MAPT**, microtubule-associated protein tau; **EP300**, E1A binding protein p300; **FOX01**, forkhead box protein O1.

1.4 Current Therapeutic Approaches for Alzheimer's Disease

An increasing understanding of the underlying disease mechanisms has driven a substantial research effort to identify new therapeutic compounds. However, despite the promise offered by early pre-clinical/clinical trials, several high profile compounds have recently failed at phase III. Thus, there are currently no disease-modifying drugs for the treatment of AD. Given the predicted growth in patients over the following decades, a therapy capable of preventing, halting or even reversing the disease is urgently required.

1.4.1 Existing Treatments

There are currently two main treatment options for patients diagnosed with AD; acetylcholinesterase inhibitors and Memantine. However, these therapeutic interventions are aimed purely at symptom management with only modest effects upon cognition.

Acetylcholinesterase Inhibitors

AD is associated with a reduction of the neurotransmitter, ACh, following the severe loss of cholinergic neurons[1]. ACh is synthesised by choline acetyltransferase in cholinergic neurons and released into the synaptic cleft where acetylcholinesterase (AChE) is responsible for its metabolism[274]. One therapeutic strategy is therefore to inhibit the activity of AChE to prolong the action of ACh. Four reversible acetylcholinesterase inhibitors (AChE-I) are approved for the treatment of mild-to-moderate AD including Tacrine, Donepezil, Rivastigmine and Galantamine. However,

due to hepatotoxicity, Tacrine is generally no longer prescribed[275,276]. In clinical trials, Donepezil, Rivastigmine and Galantamine all demonstrated small significant beneficial effects upon cognition and daily function, with similar levels of efficacy[277–279]. There is also some evidence to suggest Donepezil may have efficacy for severe AD[280]. AChE-Is are generally well-tolerated with side-effects limited to gastrointestinal symptoms[281]. However, while the AChE-Is show modest beneficial effects upon the stabilisation of cognition and global function, these effects are temporary and have no effect upon long-term outcome[282].

Memantine

Memantine, a glutamate NMDA receptor antagonist, is approved for the treatment of moderate-to-severe AD. Memantine is a non-competitive low-affinity open channel blocker which preferentially inhibits excessive NMDA receptor activity without disrupting normal synaptic transmission, thus protecting against excessive excitotoxic signalling[283]. In clinical trials, Memantine significantly reduced rate of deterioration across a number of measures in moderate-to-severe AD although its efficacy for mild AD is debated[284–287]. Memantine appears to have fewer side-effects than the AChE-Is and is well-tolerated. However, similar to the AChE-Is, Memantine only delays clinical deterioration and does not improve long-term outcome. Several studies have investigated the combined use of Memantine with AChE-Is and meta-reviews suggest a small but significant benefit after six months of combinatorial treatment[288,289]. However, as individual variability was high, further studies are required to ascertain the efficacy of this approach.

1.4.2 Development of New Disease-modifying Treatments

There has been a concerted effort to identify new disease-modifying treatments based on the increased understanding of disease pathology. Recent drug development has therefore focused upon reducing the production and aggregation of amyloid-β and hyperphosphorylated tau and ameliorating neuroinflammation and oxidative stress.

Targeting Amyloid-β

A number of strategies have been employed to prevent either the initial formation of amyloid-β or its subsequent aggregation. Thus, one approach aims to reduce total amyloid-β production or modulate processing towards shorter less toxic species by targeting the secretases (BACE1 and γ-secretase) which mediate the proteolytic cleavage of APP. Alternative strategies focus upon preventing the aggregation of amyloid-β or enhancing its clearance.

BACE1 Inhibitors

A wealth of pre-clinical evidence suggests that reducing BACE1 expression has beneficial effects in reducing amyloid-β and improving cognition. McConlogue and colleagues[290] confirmed that Bace1 was required for production and deposition of amyloid-β as 13 month old Bace1$^{-/-}$ knockout mice lacked both plaques and dystrophic neurites. It was initially reported that Bace1$^{-/-}$ knockout mice were phenotypically normal[291]. However, recent reports have revealed subtle behavioural and electrophysiological abnormalities[292]. These likely relate to impaired processing of additional BACE1 substrates, which are increasingly being identified, such as

Neuregulin-1 and the β2-sodium channel subunit which suggest additional roles in myelination and cell signalling[293–295]. These findings indicate that complete silencing of BACE1 expression may be detrimental and suggest that partial inhibition is desirable.

Promisingly, McConlogue *et al*.[290] reported that partial (50%) reduction of Bace1 led to a 12% reduction in amyloid-β levels at 3 months which was associated with a dramatic 50% reduction in amyloid-β load at 18 months. This protected mice against synaptic deficits, dystrophic neurites and significantly delayed onset of pathology. Thus, even a modest reduction of amyloid-β following partial silencing of Bace1 appeared to have significant disease-modifying benefits. These findings have subsequently been confirmed by others who have shown that partial deletion of Bace1 reduces the production of soluble amyloid-β, decreases tau hyperphosphorylation and protects against learning and memory deficits[178,296–300]. As BACE1 expression may be elevated in AD patients[301–303], these findings suggest that partial inhibition of BACE1 may represent a viable therapeutic strategy.

BACE1 inhibitors must be selective and not interfere with the processing of other substrates. Furthermore, the active site of BACE1 is more open and less hydrophobic than other aspartyl proteases. Together, this has made the development of small inhibitory molecules more challenging given that inhibitors must also be capable of penetrating the blood-brain-barrier (BBB) and neuronal membrane. Despite this, a number of BACE1 inhibitors have progressed to clinical trials in recent years.

LY2886721, a small molecule BACE1 inhibitor, significantly lowered CSF levels of amyloid-β (40/42) and sAPPβ and appeared well-tolerated by controls and AD patients.

However, a phase I trial in MCI and mild AD patients was terminated as ~10% of patients developed hepatotoxicity. While the company identified hepatotoxicity as an off-target effect, this may relate to undesirable side-effects associated with reduced processing of other BACE1 substrates[304,305]. Merck have also developed a small molecule BACE1 inhibitor, MK-8931[305,306]. Results from phase I trials showed that MK-8931 reduced CSF amyloid-β levels by up to 84% in mild-to-moderate AD patients[306]. Two combined phase II/III trials to assess safety and efficacy in mild-to-moderate AD and MCI patients are underway and so far the drug appears well-tolerated (Clinical trial: NCT01739348 and NCT01953601). A number of other BACE1 inhibitors are under development including AZD3293 (AstraZeneca) and E2609 (Eisai)[305]. Phase 1 studies have been completed for both compounds where they appeared well-tolerated and reduced CSF amyloid-β levels. Phase II/III trials to assess safety and efficacy in patients with MCI or mild AD are now recruiting for AZD3293 (NCT02245737) and E2609 (NCT02322021).

In summary, a number of candidate BACE1 inhibitors are under development. While they seem capable of achieving up to ~90% reduction in CSF amyloid-β, how this impacts upon cognitive impairment, global function and survival remains to be seen. However, if they continue to be well-tolerated and the CSF amyloid-β reduction translates to meaningful alterations in disease processes, these compounds may represent a promising approach for the future.

γ-Secretase Inhibitors and Modulators

Inhibition of γ-secretase may also decrease amyloid-β production. However, γ-secretase also has a large number of substrates including insulin and neurotrophin receptors, Notch, the β4-sodium channel subunit and N-cadherin[307,308]. Consequently, side-effects are associated with γ-secretase inhibition including skin reactions and haematological and gastrointestinal toxicity[307,308]. Indeed, a lack of specificity may account for several compound failures at clinical trial.

For example, in phase I/II trials, Semagacestat, a small-molecule γ-secretase inhibitor, reduced the rate of amyloid-β synthesis[309,310]. Although side-effects including skin rashes were reported, two phase III trials were initiated. These were subsequently terminated following increased adverse events including skin cancers and infections. A significant worsening in cognition and functioning were also observed[311]. At least some of these deleterious effects are likely attributable to impaired processing of other substrates. As a result, research is now focused upon developing selective γ-secretase inhibitors which spare Notch processing. A number of compounds are under investigation and have entered clinical trial including; Begacestat/GSI-953 (phase I), BMS-708163 (phase II), NIC5-15 (phase II) and PF-3084014 (phase I)[312–316].

Given the inherent challenge of off-target effects associated with γ-secretase silencing, an alternative strategy is γ-secretase modulation where processing of APP is directed towards the production of less toxic forms of amyloid-β. A subset of non-steroidal anti-inflammatory drugs (NSAIDs) have been found to modulate γ-secretase processing and reduce amyloid-β (40/42) production in favour of amyloid-β (38)[317]. In a phase II study,

Tarenflurbil was well-tolerated for up to 24 months and appeared to have a beneficial dose-related effect upon global function in mild AD. However, a subsequent phase III clinical trial showed no significant clinical effect[318]. Second generation NSAID-derived and non-NSAID-derived compounds are now under development and appear to show improved *in vitro* potency and BBB penetration[319,320].

APP Aggregation

Perhaps the most intensely studied target for novel therapeutics has been amyloid-β aggregates themselves. A large number of compounds have aimed to remove insoluble amyloid-β plaques either through preventing their deposition or promoting their clearance.

Tramiprosate is a compound tested for its ability to bind soluble amyloid-β and prevent aggregation. In phase II trials, Tramiprosate was well-tolerated and reduced the concentration of CSF amyloid-β in patients with mild-to-moderate AD[321]. However, at phase III, Tramiprosate failed to demonstrate any significant benefit[322]. Subsequently, in a highly criticised move, the compound was renamed "Vivimind" and marketed as an over-the-counter supplement to protect memory function[323].

An alternative strategy to reduce amyloid-β aggregation is active or passive immunotherapy directed at amyloid-β plaques. Immunotherapy may clear plaques by antibody-mediated solubilisation of insoluble amyloid-β aggregates, by triggering microglial phagocytosis or by the peripheral sink hypothesis in which downregulation of amyloid-β in the periphery draws amyloid-β from the brain to the plasma. However,

while immunotherapy approaches appeared promising in transgenic AD models, this success has not yet translated into humans[324–327].

Active immunotherapy primes the immune system to recognize amyloid-β as foreign to trigger a response against it. The first clinical trial of amyloid-β active immunisation involved AN1792 in which amyloid-β (42) was combined with an adjuvant to prime the immune system. This trial was halted at phase IIa when 6% of patients developed meningoencephalitis[328]. Follow-up studies revealed that while immunisation did lower the load of amyloid-β and tau, there was no relationship between plaque removal and symptom severity. Pathological side effects were also observed including increases in microglial activation, cerebral amyloid angiopathy and soluble/oligomeric amyloid-β levels[81,82,329]. It was subsequently revealed that a T-cell response was initiated in response to the amyloid-β (25-35) epitope. Second generation active amyloid-β vaccines including ACC-001, CAD106 and Affitope AD02 are currently being tested in pre- or early-stage AD[330,331].

In contrast to active immunization, passive immunization involves the injection of antibodies that are generated *ex vivo* against the epitope of interest. Based on the T-cell response to AN1792, antibodies have largely been developed against the N-terminus of amyloid-β[331]. A number of anti-amyloid-β antibodies have been tested in clinical trials but with limited success. For example, Bapineuzumab, a monoclonal antibody binding both soluble and insoluble amyloid-β, reduced amyloid-β load in APP transgenic mice[327]. However, no significant improvement was observed in phase II/III trials in mild-to-moderate AD patients[332,333]. Several patients also suffered vasogenic cerebral

edema which increased with dose and *APOE Ɛ4* allele number and thus development of Bapineuzumab has been discontinued[333,334].

Solanezumab, a newer monoclonal anti-amyloid-β antibody, preferentially binds soluble amyloid-β oligomers. A promising phase II trial revealed a dose-dependent increase in plasma and CSF levels of amyloid-β following Solanezumab treatment[337]. While no significant benefit was observed in two Phase III trials in mild-to-moderate AD patients, pooling of results revealed a significant slowing of cognitive decline and a non-significant reduction in functional decline after 78 weeks in mild AD patients[335,336]. Thus, Solanezumab and Gantenerumab are currently being tested in another phase II/III trial aimed at carriers of a dominantly inherited familial AD gene who suffer from early-onset AD (Dominantly Inherited Alzheimer's Network, NCT01760005). A similar preventative approach is being taken in two other trials; The Alzheimer's Prevention Initiative (API) and the Anti-Amyloid Treatment in Asymptomatic Alzheimer's (A4). These aim to recruit asymptomatic participants carrying either known autosomal dominant gene mutations or individuals who show early signs of amyloid-β deposition by positron emission tomography (PET). Participants will be treated with Crenezumab (API) or Solanezumab (A4) to assess whether intervention prior to the emergence of clinical symptoms can slow or prevent AD[337–339].

The recent failure of a number of compounds aimed at amyloid-β has raised the question as to whether targeting amyloid-β represents the most effective approach. As a result, alternative therapeutic strategies are under development.

Targeting Tau Pathology

As discussed previously, reducing tau expression protects against amyloid-β-induced neurodegeneration *in vitro* and *in vivo*[185–187]. Consequently, strategies which reduce pathological tau may have disease-modifying outcomes. Two main strategies have been explored; inhibition of tau kinases to reduce tau phosphorylation and compounds to inhibit aggregation or promote the disassembly of tau aggregates.

Tau Phosphorylation

Inhibition of tau kinases may prove promising. However, tau-targeting kinases also regulate a wide range of different proteins and must be carefully assessed for their selectivity. GSK3β, CDK5 and ERK2 are the primary kinases currently targeted as they are involved in the phosphorylation of epitopes in and around the microtubule-binding domain[340,341]. Reducing the function of these kinases might help to prevent tau's dissociation from microtubules, reducing its potential to aggregate and mediate pathological pathways.

Lithium and valproate inhibit GSK3β and may also have neuroprotective properties via upregulation of neurotrophic factors and the anti-apoptotic factor, BCL-2[342]. Lithium was therefore assessed for its ability to modulate GSK3β activity and reduce CSF levels of phosphorylated tau in a short trial in mild AD patients. However, no significant effect of lithium treatment was observed upon biomarker measures, GSK3β activity or cognitive performance[343]. Valproate was also tested in phase III clinical trials to assess its ability to attenuate agitation and disease progression in moderate AD patients.

Valproate treatment did not delay the emergence of agitation or slow cognitive and functional decline. Furthermore, the valproate group showed a greater loss in hippocampal and whole brain volume accompanied by greater ventricular expansion[344].

Despite these results, several further GSK3β inhibitors are under development. Tideglusib/NP-031112 is a selective, irreversible, small molecule non-ATP competitive GSK3β inhibitor undergoing assessment in AD and paralysis supranuclear palsy[345–347]. Tideglusib was well-tolerated in a short-term pilot in mild-to-moderate AD patients and produced positive trends in several cognitive and functional measures[347]. A larger phase II clinical trial in mild-to-moderate AD found no significant benefit of Tideglusib treatment, although BACE1 expression was significantly decreased in a small subset of patients. Furthermore, patients with mild AD showed a significant response on three different measures of cognition[346]. Given the short trial duration and non-linear dose response, particularly in mild patients, longer dose-response studies may be warranted[346].

In summary, only a small number of compounds modulating tau phosphorylation have reached clinical trial. However, this is an area attracting growing interest and may yield more promising compounds in the future.

Tau Aggregation

Tau-based immunotherapy to target pathological aggregates of tau is under development. The first pre-clinical study assessed the effect of immunizing wild-type mice with full-length human tau[348]. Treatment resulted in the appearance of

histopathological correlates of AD including neurofibrillary tangle-like structures, axonal damage and gliosis and caused severe encephalomyelitis. This appeared to be triggered specifically by unphosphorylated tau protein and highlighted the need for caution when designing immunization protocols for humans[348]. Subsequent pre-clinical immunization studies utilised active and passive immunization against phosphorylated tau peptides and observed reduced tau pathology, improved cognitive performance and no obvious adverse effects[349–351]. Thus, pre-clinical data suggested that tau-immunization may represent a promising approach by targeting the toxic phosphorylated tau species strongly associated with progression of AD[85,137–145].

The first human phase I trial to test the tolerability and safety of a vaccine directed against pathologically modified tau (AADvac1) is currently ongoing in mild-to-moderate AD patients (NCT01850238). An 18-month follow-up phase I study will continue to assess the long-term safety of the immune response to AADvac1 (NCT02031198). The results of these early clinical trials will be of great importance in informing the development of future anti-tau vaccines.

Methylthioninium chloride (TRx0237, TauRx Therapeutics Ltd) represents an alternative anti-aggregate strategy. This involves the repurposing of an existing drug, which has both anti-tau-aggregant and anti-oxidant properties and reduces pathology in transgenic models[352]. An exploratory phase II study of methylthioninium chloride in mild-to-moderate AD patients demonstrated significant treatment benefits in two independent populations at 138 mg/day dose[353]. Phase III clinical trials in mild-to-moderate AD are underway to test the efficacy of a novel stabilised reduced form of methylthioninium (LMTX) that has better tolerability and absorption parameters[353].

Anti-inflammatory and Anti-oxidant Strategies

In addition to therapies targeting amyloid-β and tau-based pathologies, compounds are also under development to modulate more general AD pathology such as neuroinflammation and oxidative stress.

Trials with NSAIDs, which target neuroinflammation, have generated mixed findings. An early trial testing the efficacy of Indomethacin suggested beneficial effects upon cognitive decline[354] but this effect was not replicated[355]. A number of clinical trials testing a range of NSAIDs including aspirin, Simvastatin and Rosiglitazone all failed to show significant beneficial effects upon cognition[356–358]. However, more recent data suggest that NSAIDs may have therapeutic efficacy but this depends critically on the drug tested and timing of intervention[359].

Anti-oxidant-based treatments have also yielded inconsistent results. One clinical trial showed that Selegiline, a monoamine oxidase-β inhibitor, and vitamin E increased median survival by 215 and 230 days over placebo, respectively[360]. However, a later meta-analysis suggested that treatment with doses of vitamin E higher than 400 IU/day was associated with increased mortality. These findings were themselves challenged by a large-scale clinical trial which supported the use of vitamin E at doses of 2000 IU/day[361]. A number of other vitamins, anti-oxidants and supplements are also undergoing assessment including vitamin C, selenium, omega-3 fatty acids, mitochondrial co-factors (CoQ10), "nutraceutical formulations" and neurotrophins[362–370]. Finally, the large PreADViSe prevention trial (Prevention of AD by Vitamin E and

Selenium) is following the cognitive status of a large number of healthy participants exposed to supplements of vitamin E or selenium for 5 years[371].

In summary, a range of compounds has been developed based on the increasing knowledge of pathogenic mechanisms in AD. Although a number of compounds have reached phase III trials, several have recently failed. Thus, novel disease-modifying compounds able to alter the course of AD are still required.

1.4.3 Challenges to Clinical Trial Success

The recent failure of several phase III trials raises the question as to why they were not successful. Largely, this has been attributed to the therapeutic intervention being applied too late in the disease process when substantial synaptic and neuronal loss had already occurred. A number of preventative trials have now been initiated in which interventions will be administered prior to or very early in the disease process[337–339,371]. These studies will be instrumental in determining whether compounds have preventative utility which requires earlier intervention.

The success shown by many compounds in pre-clinical trials has not translated to humans. Transgenic mice expressing only mutant APP do not recapitulate all aspects of human pathology. Instead, multiple mutations in APP, tau and presenilin are required to elicit both amyloid-β and tau-based pathologies. Furthermore, there may also be species and isoform-specific effects of APOE on the clearance of amyloid-β[34,40]. Thus, a failure of transgenic models to accurately recapitulate human AD might contribute towards a failure to translate from pre-clinical to clinical settings.

The heterogeneity of patient samples might also preclude compound success. Sporadic AD is a complex disorder with multiple interacting components and it is not clear whether it should be considered the same disease as familial AD. Several trials have reported that subsets of patients responded differently to treatment, depending on disease stage or *APOE* genotype. Thus, potentially effective compounds may have failed if they were not applied to the most appropriate group of patients. In the past, this has been hampered by a lack of highly standardized disease biomarkers. This makes it difficult to identify a homogenous population of test patients and to evaluate a compound's disease-modifying efficacy. A recent revision to the diagnostic research criteria highlights the long prodromal phase occurring prior to symptom onset[372]. This revision places a greater emphasis on the inclusion of biomarkers which include structural MRI scans[373], PET with amyloid-β and tau-binding ligands such as PiB or Florbetapir[332,374] and CSF levels of amyloid-β and tau[375,376]. Increased efforts are therefore underway to identify more sensitive and less invasive biomarkers that will allow for earlier, more predictive diagnoses and aid in monitoring the effect of therapeutic interventions upon disease progression[377–379].

Determining whether a compound has the desired effect upon its disease target is important. A number of unsuccessful clinical trials have been criticised for their failure to assess the compound's impact upon the intended target[40,323]. A failure to assess the extent of disease target modulation makes it challenging to determine why a trial failed. A compound may be ineffective because it failed to modulate its target to the degree required to elicit a therapeutic effect or it may simply be that the target is not the most appropriate for achieving disease-modifying outcomes.

Indeed, whether compounds have targeted the most appropriate aspects of disease pathology has been questioned[323]. A large body of evidence has shown that soluble amyloid-β and tau oligomers likely represent the most toxic species and should be targeted for effective therapeutic strategies. However, most clinical trials have aimed to reduce the insoluble load of amyloid-β plaques. Furthermore, targeting aggregation by immunotherapy may actually increase soluble load following solubilisation of plaques. A more effective approach may therefore be a combinatorial one in which multiple aspects of pathology are targeted[380]. A number of tau-modifying therapies are now under development, paving the way for truly combinatorial therapies that target multiple aspects of disease pathogenesis. In combination with sensitive biomarkers which allow identification of prodromal patients, preventative combinatorial therapies may represent the most promising approach for future AD therapeutics.

1.5 RNA-based Treatment Strategies for Alzheimer's Disease

An alternative and potentially combinatorial approach to the strategies pursued above may be to exploit recent developments in RNA interference (RNAi) therapeutics. RNAi refers to the highly conserved cellular mechanism in which double stranded RNA (dsRNA), which may take the form of miRNA or small interfering RNA (siRNA), mediates the degradation or translational inhibition of target mRNA. In this way, the expression of virtually any disease-related gene may be silenced. As the development of BACE1 inhibitors has been hampered by its challenging protein structure, an RNAi-based approach in which mRNA is targeted may represent a powerful tool to silence the expression of deleterious disease-associated genes. Thus, this thesis will focus upon the development of novel RNA-based therapies for AD.

1.5.1 miRNAs

As outlined previously, miRNAs are an endogenous species of small non-coding RNA that act as post-transcriptional regulators of gene expression. miRNAs are transcribed by RNA polymerase II in the form of long pri-miRNAs. pri-miRNAs undergo processing in the nucleus by the Drosha/DGCRB complex to yield 60-80 nucleotide RNA hairpins called pre-miRNAs[381]. Pre-miRNA hairpins are exported to the cytoplasm via Exportin-5 where they undergo processing by Dicer to generate mature miRNAs[382]. Dicer incorporates one strand of the mature miRNA into Argonaute 2 (AGO2) which then guides RISC to target mRNA[381] (**Fig. 1.3**). Although AGO2 was identified as the catalytic component of RISC over a decade ago[383,384], recent studies have recognised an essential role for GW182, another RISC component, in mediating

gene silencing[385–389]. Typically, miRNAs bind within the 3' UTR of target mRNA with imperfect complementarity to elicit target degradation or translational repression[231,233,236]. However, studies have also reported miRNA binding within the 5' UTR and protein coding regions of target mRNA[230,269,390–393]. Furthermore, miRNA binding within promotor regions may increase target mRNA expression[394]. As mentioned previously, a single miRNA may regulate the expression of multiple mRNAs while one mRNA may be regulated by multiple miRNA species[238,395]. miRNAs are therefore powerfully placed to regulate complex networks and, as such, may represent valuable pharmacological targets.

1.5.2 siRNAs

The increased understanding of endogenous miRNA-mediated gene silencing has permitted the development of exogenous siRNA which exploit the endogenous miRNA regulatory machinery to repress target gene expression[396]. Exogenous siRNA can be delivered either in the form of short hairpin RNA (shRNA) expression plasmids or as chemically synthesised dsRNA duplexes. siRNA-mediated silencing by siRNA duplexes is typically transient as the intracellular concentration is diluted over successive cell divisions. In contrast, shRNA expression plasmids, driven by Pol II or III promoters, result in high constitutive levels of shRNA expression and may be used for longer-term silencing[397]. As for miRNA-mediated silencing, one strand of siRNA is loaded into AGO2 and guides RISC to target mRNA (**Fig. 1.3**). However, unlike miRNAs which tolerate mRNA:miRNA mismatches, siRNAs target fully complementary sequences for mRNA degradation. The requirement for fully complementary sequences bestows strong specificity upon siRNA-mediated silencing.

Thus, while miRNAs may target a number of genes, highly specific siRNAs may be designed to target a single disease-relevant gene. This is particularly valuable for the avoidance of off-target effects. siRNAs are also amenable to chemical modifications which may be used to improve the stability, binding strength or *in vivo* targeting and uptake of a specific siRNA. There are currently 39 listed clinical trials (www.clinicaltrials.gov) which aim to assess the efficacy of siRNA-mediated therapy in a range of different diseases.

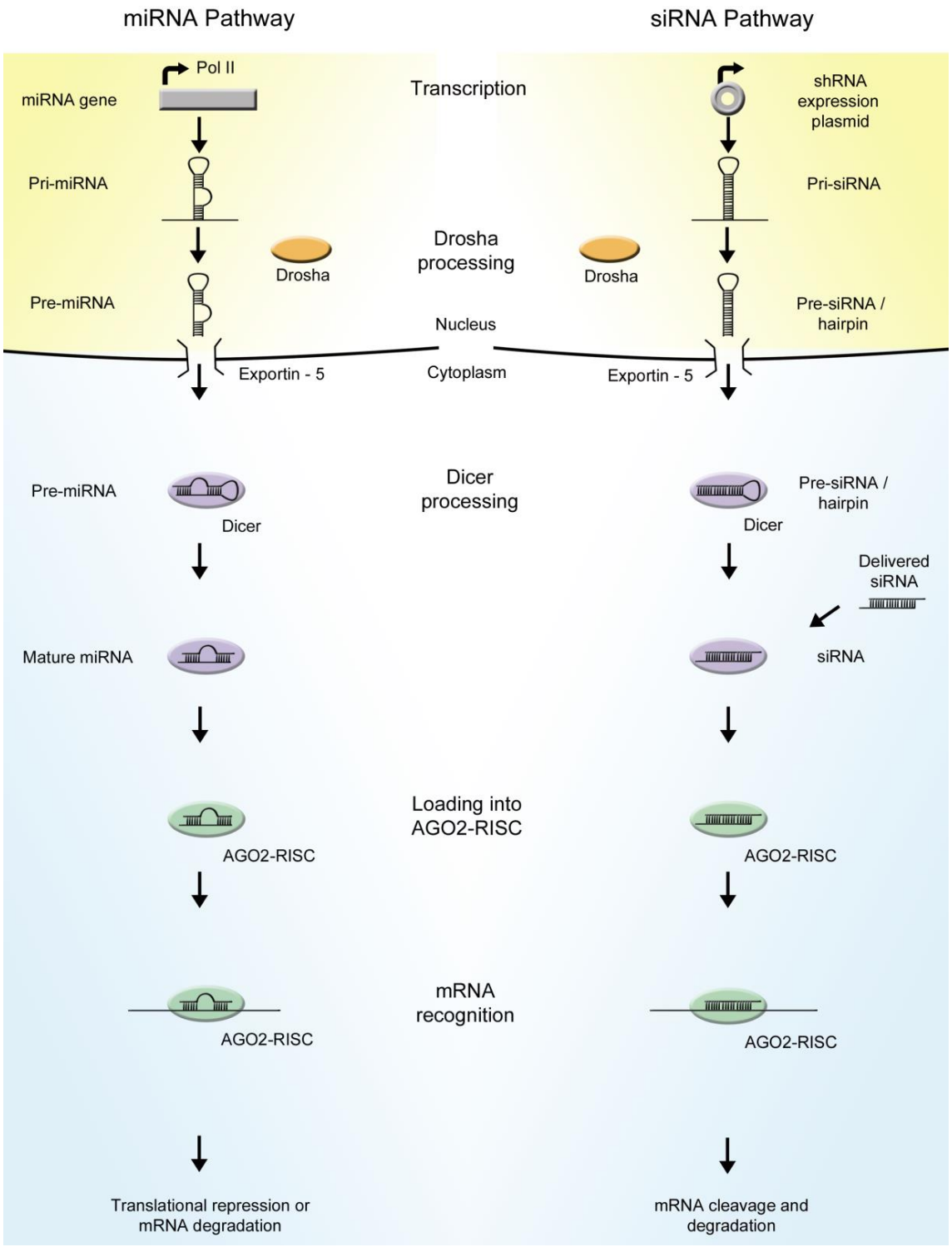
miRNA Pathway
siRNA Pathway
Pol II
miRNA gene
Transcription
shRNA expression plasmid
Pri-miRNA
Pri-siRNA
Drosha processing
Drosha
Drosha
Pre-miRNA
Pre-siRNA / hairpin
Nucleus
Exportin - 5
Cytoplasm
Exportin - 5
Pre-miRNA
Dicer processing
Pre-siRNA / hairpin
Dicer
Dicer
Delivered siRNA
Mature miRNA
siRNA
Loading into AGO2-RISC
AGO2-RISC
AGO2-RISC
mRNA recognition
AGO2-RISC
AGO2-RISC
Translational repression or mRNA degradation
mRNA cleavage and degradation

Figure 1.3 The RNAi Processing Pathways. RNAi can be achieved via two pathways; **(A)** the miRNA pathway and **(B)** the siRNA pathway. **(A)** Endogenous miRNA transcription, driven by polymerase II (Pol II), produces long primary miRNA transcripts (pri-miRNA). The pri-miRNA is cleaved by Drosha in the nucleus to produce preliminary miRNA structures (pre-miRNA), which are exported to the cytoplasm by Exportin-5. Here, pre-miRNAs are processed by Dicer to produce shorter double-stranded miRNAs. miRNAs are incorporated into AGO2 and the RNA-induced silencing complex (RISC) where the passenger strand is unwound leaving the remaining active mature miRNA to guide AGO2-RISC to target mRNAs. Typically, miRNAs bind to the 3' UTR region of target mRNA with imperfect complementarity resulting in translational repression or degradation of the target mRNA. **(B)** siRNA are introduced into the cell either by expression from an exogenous short hairpin (shRNA) plasmid in the nucleus or by direct transfection of synthetic double stranded RNA (dsRNA) in the cytoplasm. Primary siRNA transcripts (pri-siRNA) are produced following transcription driven by Pol II or III promoters and are processed by Drosha to produce pre-siRNA. pre-siRNA are exported from the nucleus via Exportin-5 where they are processed by Dicer to produce short double-stranded siRNA. siRNA are loaded into AGO2 and RISC where one strand is degraded and the remaining mature siRNA guides AGO2-RISC to target mRNA. siRNAs bind with full complementarity to target mRNA sequences which leads to cleavage and degradation of the mRNA transcript.

1.5.3 Antisense Oligonucleotides and Locked Nucleic Acids

Alternatively, gene expression may be regulated by antisense oligonucleotides (ASOs). Antisense oligonucleotides are synthetic single-stranded nucleic acids, 8-50 nucleotides in length, which bind to complementary sequences in target mRNA to modify gene expression. ASOs may repress total protein expression, selectively repress expression of a mutant allele or interfere with splicing to restore function of a mutant protein[398,399]. Repression of protein expression may occur either via RNase H-mediated degradation following recognition of RNA-DNA heteroplexes or by steric blocking leading to translational arrest. ASOs may also be chemically modified to improve their stability, binding strength and *in vivo* efficacy. These include backbone modifications (phosphate linkages), sugar group modifications (2'-O-methyl and 2'-O-methyl-ethyl group or locked nucleic acid (LNA) substitutions) or non-ribose modifications such as the addition of PMOs (phosphorodiamidate morpholino oligomers) or PNAs (peptide nucleic acids)[398].

Currently, two phosphorothioate-modified ASOs, Fomivirsen and Mipomersen, are approved for the treatment of acquired immune deficiency syndrome (AIDS) and familial hypercholesterolemia, respectively[400,401]. However, ASOs are now under development for a wide range of diseases including cancer, Duchenne muscular dystrophy (DMD), Hepatitis C Virus (HCV) and neurodegenerative diseases including spinal muscular atrophy (SMA), amyotrophic lateral sclerosis (ALS) and Huntington's Disease (HD)[398,399,401–405]. Importantly, studies have also highlighted the promise of ASO-based therapies for AD[406–411]. Together, these studies have demonstrated that intracerebroventricular and intravenous administration of ASOs directed at a range of

AD-relevant targets including APP, GSK3β and presenilin-1 not only reduces target gene expression but also markers of neuroinflammation and oxidative stress, reversing learning and memory deficits in AD mouse models[406–413]. Similar results have also been obtained using antisense PNAs in both rats and mice[414,415]. Thus, future chemical modifications which further improve compound efficacy should enhance the potential therapeutic utility of ASO-based therapeutics.

In particular, the therapeutic potential of LNA modifications has received increasing interest. LNA bases are ribonucleic acid analogues in which the ribose ring is locked by an additional methylene linkage between the 2' oxygen and 4' carbon (**Fig. 1.4**). This imposes a conformational constraint and confers a close structural resemblance between the LNA-modified ASO and target mRNA[416]. This increases binding affinity and specificity for the target mRNA and increases *in vivo* stability. The addition of LNA modifications can impede RNase H-mediated degradation. However, "gapmer" oligonucleotides have been designed in which a central region of DNA nucleotides is flanked by the desired modified bases[417]. The central region allows the activation of RNase H while a small number of modified bases at the 3' and 5' ends protect against exonuclease activity[398,417].

A number of studies have shown that LNA-modified ASOs elicit potent silencing of targets both *in vitro* and *in vivo* with minimal toxicity[404,418,419]. These findings have prompted the transition to clinical trials for several LNA-modified ASOs including SPC2996 (Santaris Pharma A/S), SPC4955 (Santaris Pharma A/S) and EZN-2968 (Enzon Pharmaceuticals) for the treatment of chronic lymphocytic leukaemia,

hypercholesterolemia and lymphoma, respectively. Promising results from preliminary phase I trials for EZN-2968[420] and SPC2996[421] highlight the potential of this approach.

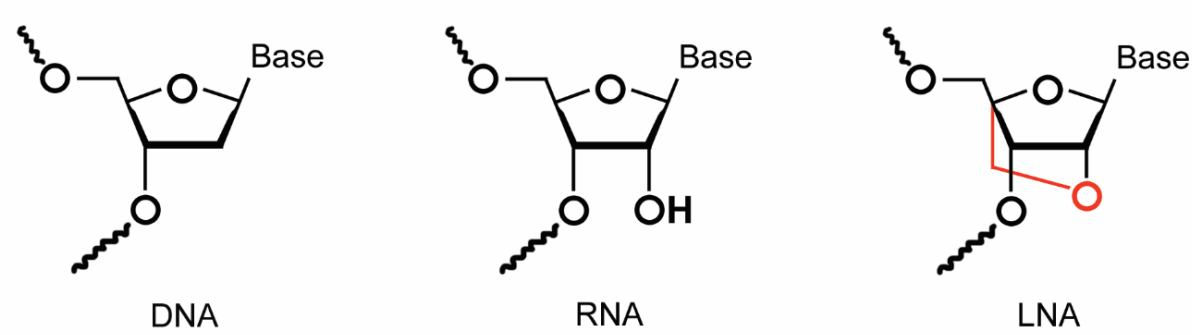

Figure 1.4 Structures of DNA, RNA and LNA. Locked nucleic acid (LNA) refers to a ribonucleic acid analogue structure in which the ribose ring is locked by an additional methylene linkage between the 2' oxygen and 4' carbon. This confers greater binding affinity and specificity for target mRNA and increases *in vivo* stability.

1.5.4 Potential for RNA-based Therapeutics in Alzheimer's Disease

Two different RNA-based approaches may hold therapeutic utility for the treatment of AD. Firstly, siRNAs or ASOs may be utilised to mediate a reduction in gene-dosage for AD-relevant genes, either to reduce total expression or to selectively target mutant alleles for familial cases. Alternatively, restoration of miRNA expression may be employed to re-establish appropriate regulation of gene expression.

Several studies have offered support for an RNAi-mediated approach to silencing disease-relevant genes. Kao and colleagues[422] showed that Bace1 siRNAs and shRNAs produced potent silencing of both mRNA and protein expression in primary cortical neurons, resulting in 40-60% reduction in amyloid-β (40/42). This effect has been replicated *in vivo* where lentiviral-mediated delivery of Bace1 siRNA silenced Bace1 mRNA and protein expression resulting in a significant reduction in amyloid-β burden, amelioration of dendritic and synaptic pathology and rescue of cognitive deficts[296]. More recently, a receptor-mediated delivery approach has been utilised to deliver opioid-conjugated BACE1 siRNA to human neuroblastoma cells, resulting in a significant reduction in BACE1 activity, although an accompanying increase in APP expression was noted[423].

Allele-specific RNAi-mediated silencing of AD-relevant genes has also been demonstrated. Mutant allele-specific silencing of presenilin-1 in human fibroblasts resulted in a 50% reduction in amyloid-β production[424]. The design of mutant allele-specific siRNA and shRNAs targeting tau and APP mutations has also been reported[425]. Subsequent *in vivo* testing revealed specific long-term silencing of mutant APP in the

hippocampus of transgenic APP mice which suppressed amyloid-β production (~62%) and protected against memory impairment[426]. These reports build on the studies discussed previously in which genetic deletion of key disease-relevant genes such as Bace1 and tau significantly reduced amyloid-β and tau pathology, preventing memory deficits[126,178,186,290]. Together, these findings offer evidence for siRNA or ASO-mediated gene silencing of AD-relevant genes as a promising therapeutic option.

As outlined above, a large number of miRNAs are deregulated in AD. There are two main approaches towards the normalisation of miRNA expression. Firstly, synthetic miRNA mimics may be utilised to restore downregulated miRNA function. Exogenous miRNAs may be introduced either through the use of synthetic mature miRNA mimics or pri-/pre-miRNA expression plasmids. This could prove fruitful where miRNAs have been shown to target AD-relevant genes and where their downregulation results in an upregulated gene-dosage effect. As a number of these miRNAs also target other genes involved in important neuronal functions such as exon splicing and axon guidance, restoration of miRNA expression may reinstate regulation of a wide number of affected genes.

The alternative approach is to reduce upregulated miRNA expression. This may primarily be achieved by two different strategies including miRNA-directed ASOs (antagomirs) or miRNA sponges. ASOs may be designed to target mature miRNA sequences resulting in either their degradation or sequestration[427,428]. Alternatively, miRNA sponges are competitive inhibitors, constitutively expressed from strong promoters, which contain multiple target miRNA binding sites. These serve to derepress miRNA targets by competing with the endogenous mRNA for miRNA binding[429]. Both

antagomir and miRNA sponge-based strategies reduce the number of miRNA molecules available and hence alleviate miRNA-mediated gene repression. This approach could hold promise for miR-34a which is upregulated in AD patients and transgenic models, resulting in reduced expression of the anti-apoptotic protein, BCL-2[260–262]. Indeed, ASOs against both miR-206 and miR-34c have been shown to rescue cognitive deficits in mouse models of AD[430,431].

In summary, RNA-based therapeutics may have potential in the treatment of AD. These techniques may be utilised to elicit partial silencing of disease-relevant genes or to restore the regulatory capacity of the miRNA network. RNA-based approaches are also amenable to combinatorial treatment by allowing the simultaneous targeting of multiple disease-relevant genes. However, although corrective RNA-based therapies hold substantial promise, their translation to clinic has been impeded by a number of challenges. These issues must be resolved before the promise of RNA-based therapeutics may be realised.

1.5.5 Current Limitations to the Development of RNA-based Therapeutics

Biological Stability, Targeting and Toxicity of Naked RNA

Unmodified naked RNA has a short half-life in serum as it is rapidly degraded by extracellular exonucleases and endonucleases[432,433]. Furthermore, systemically administered RNA accumulates in organs such as the liver and kidneys and is susceptible to rapid degradation and excretion[434,435]. Naked RNAs display a lack of specificity for target tissues and are unable to efficiently cross biological barriers or hydrophobic cell membranes due to their negative charge. Due to this lack of specificity, naked siRNAs risk off-target effects resulting in toxicity and the activation of immune responses[436,437]. Modifications to increase their stability or encapsulation/conjugation to a delivery vehicle are therefore required to prevent their rapid breakdown and enhance targeting[433].

Blood-Brain-Barrier

A significant challenge to the development of RNA-based therapeutics is delivery, due to the presence of biological barriers which prevent systemically applied RNAi molecules from reaching intended cell targets. In addition to the hydrophobic cell membrane, a number of other biological barriers impede the delivery of RNA to target tissues. The most important of these for neurodegenerative diseases is the BBB.

The BBB is a highly regulated and dynamic interface which encapsulates and separates the brain from the periphery. The BBB protects the brain against toxic insult and

maintains CNS homeostasis by tightly controlling the entry of peripheral molecules. The BBB is a complex multi-cellular system which comprises endothelial cells, the capillary basement membrane, pericytes, astrocytes, microglia and neurons, which all interact to form the neurovascular unit. The selective permeability of the BBB is controlled by a monolayer of endothelial cells which surround capillaries and are connected by tight junctions. Astrocytic end-feet and pericytes provide biochemical support to endothelial cells and are essential for the formation and integrity of endothelial tight junctions[438,439] (**Fig. 1.5**). Endothelial cells restrict the diffusion of large or hydrophilic molecules, allowing only small hydrophobic molecules (< 400 Da) to diffuse relatively freely across the plasma membrane. Larger molecules require specialised transport systems to cross the BBB. These include receptor-mediated transcytosis or passive and active solute carriers which maintain an influx of nutrients to the brain[440]. The presence of the BBB therefore prevents many therapeutics from reaching their target and has impeded the systemic delivery of RNAi molecules[441]. However, in AD the integrity of the BBB may be compromised in an *APOE ε4*-dependent manner[442,443]. While this may contribute to ongoing neurodegeneration by allowing the leakage of peripheral molecules toxic to neurons, it may also aid the delivery of systemically applied therapeutics.

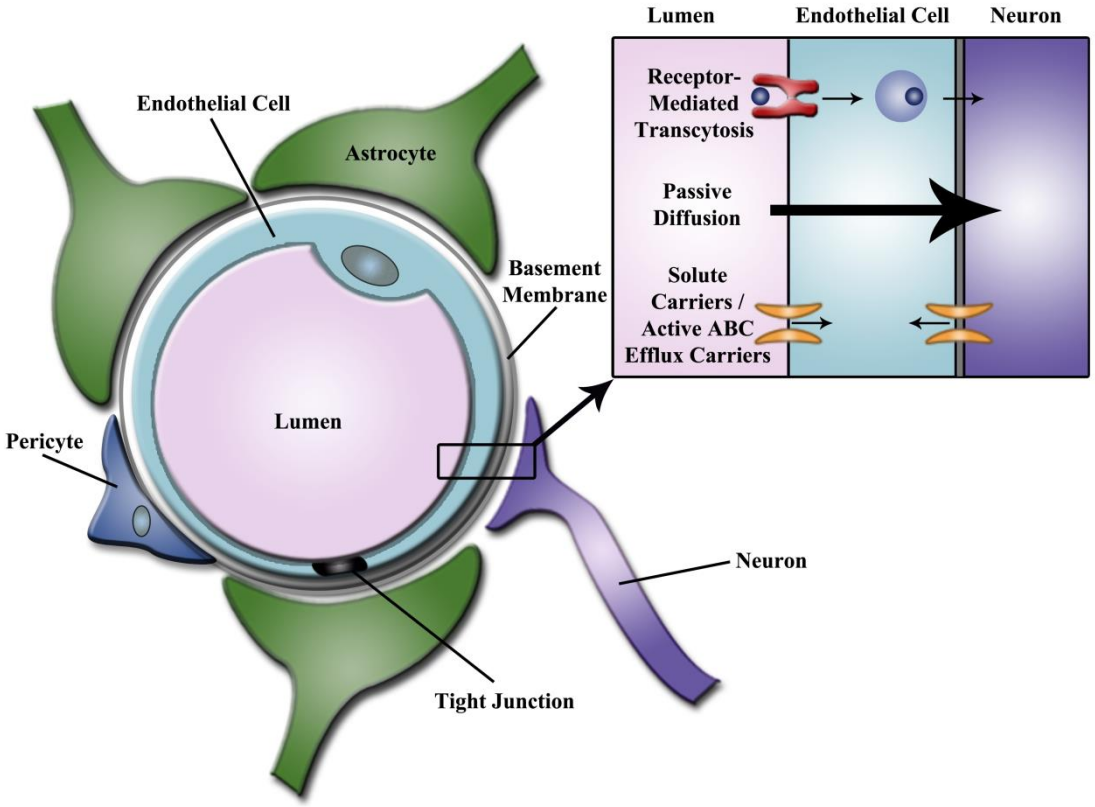

Figure 1.5 Components of the Blood-Brain-Barrier. The BBB is a multi-cellular dynamic interface tightly regulating the passage of molecules from the periphery to the central nervous system (CNS). The BBB is comprised of a sealed layer of endothelial cells, connected by tight junctions. Endothelial cells surround capillaries and interact with the capillary basement membrane, pericytes, astrocytes, microglia and neurons to form the neurovascular unit. The BBB restricts the diffusion of large or hydrophilic molecules, allowing only small hydrophobic molecules (< 400 Da) to diffuse across the plasma membrane. Larger molecules require specialised transport systems including receptor-mediated transcytosis and solute carriers. Conversely, active ATP-binding cassette transporters (ABC efflux carriers) actively export molecules from the CNS. The BBB impedes the systemic delivery of many classes of drug by preventing therapeutics from reaching their intended targets within the CNS.

Existing Delivery Vehicles

Given the challenges outlined above, RNA-based therapeutics require accessory delivery vehicles to promote their stability and ensure efficient delivery across the BBB. Effective delivery vehicles must also avoid immune activation and display cell-specific targeting to avoid off-target toxicity. To date, the development and clinical translation of RNA-based therapies has been greatly impeded due to the lack of an effective delivery vehicle that efficiently fulfils these roles. A wide range of delivery systems have been tested including viral vectors, bacterial vectors, bacteriophage vectors, lipid-based vectors, nanoparticles and peptide-conjugations[444–447]. However, each of these are associated with their own limitations including immunogenicity, risk of insertional mutagenesis, limited cargo choice and packaging size constraints, limited cell/tissue specificity, reduced efficacy with repeat administration, rapid clearance and *in vivo* toxicity[446–450]. Thus, the further development of RNA-based therapeutics depends upon a novel delivery system that is capable of fulfilling the above criteria. In recent years, exosomes, as natural nanocarriers, have attracted increasing attention as a potential solution to these issues.

1.6 Exosomes as Therapeutic Delivery Vehicles for Alzheimer's Disease*

Exosomes are small (40-100 nm) extracellular vesicles (EVs), secreted from the late endosomal compartment by most cells. They have been implicated in a wide range of biological processes; perhaps most notably in cell-to-cell communication by the transfer of material between source and recipient cells. Exosomes appear capable of crossing the BBB, may be immunologically inert depending on their cell of origin and act as endogenous delivery vehicles for functional nucleic acids. Thus, it may be possible to exploit these properties to deliver RNA-based therapeutic compounds in AD.

1.6.1 Exosome Biogenesis

The invagination and fusion of small vesicles from the plasma membrane results in the formation of early endosomes, which mature to produce late endosomes[451]. Inward budding of intraluminal vesicles (ILVs) from the late endosomal membrane results in the formation of multivesicular bodies (MVBs). MVBs are then directed either towards lysosomes for degradation or towards the plasma membrane where they fuse, resulting in the extracellular release of ILVs as exosomes[452]. The secretion of exosomes from the plasma membrane, which may be constitutive or induced, is thought to be driven by the activity of several Rab GTPase proteins, including RAB27A, RAB27B, RAB11 and RAB35, which are involved in the transport and docking of MVBs at the plasma membrane[453–456] (**Fig. 1.6**).

* Within this section some subsections have been updated and amended from[720].

Exosomes are able to travel to near and distant recipient cells where they may influence recipient cell activity either through direct release of their cargo following internalisation or by binding to target cell receptors to drive signal transduction. Internalisation and release of cargoes may be achieved by direct fusion with the plasma membrane of recipient cells, by endocytosis or following receptor-ligand mediated interactions. Although the mechanisms controlling recipient cell uptake are not fully understood, adhesion molecules including integrins, ICAMs (intracellular adhesion molecules) and tetraspanins may be important for exosome and recipient cell binding[457,458]. Tetraspanins may also be instrumental in conferring target cell specificity both *in vitro* and *in vivo* with minor differences in exosomal tetraspanin complexes strongly influencing target cell selction[458,459].

Throughout biogenesis, exosomes retain membrane topology from the source cell. Thus, cytoplasmic content is protected and membrane proteins retain their position within the exosomal membrane. Exosome membranes contain lipid raft microdomains which are enriched in glycosphingolipids, cholesterol, ceramide and phosphatidylserine. While exosome composition is dependent upon the identity and physiological condition of source cells, exosome-enriched proteins have also been identified. These include ALIX, TSG101, lysosomal proteins (Lamp2B), heat shock proteins (HSC70) and tetraspanins (CD9, CD63, CD81), which are commonly used as exosomal markers. Exosomes also carry a wide range of cargoes including mRNA, miRNA and proteins (discussed in **Section 1.6.2**). Comprehensive web-based databases of proteomic, transcriptomic and lipidomic exosomal content may be found at EVpedia[460] and Vesiclepedia[461].

Although exosome composition partly reflects source cell content, cargoes may be selectively enriched within exosomes in comparison to the proportions present within source cells. This suggests selective loading rather than simple enclosure during inward budding of ILVs. A number of mechanisms appear important for selective cargo loading. The endosomal sorting complex required for transport (ESCRT) plays a key role, not only in exosome biogenesis, but also in their loading and secretion. ESCRT consists of four major protein complexes, ESCRT-0-III and accessory proteins including TSG101 and ALIX. The four complexes and associated proteins appear to be involved in different stages of exosome biogenesis. Specifically, ESCRT-0 appears to direct sorting and sequestration of cargoes for exosomal loading in an ubiquitin-dependent manner[462].

ESCRT-independent mechanisms also exist and recent data suggest that members of the tetraspanin family are involved in selective cargo loading[463,464]. Lipid-raft microdomains also contribute towards selective loading in a ceramide-dependent manner[465]. The importance of ceramide-dependent mechanisms is confirmed by experimental inhibition of exosome secretion following treatment with GW4869, an inhibitor of neutral sphingomyelinase (nSMase) which is crucial for ceramide biosynthesis[465]. Heat shock proteins including HSC70 are also implicated in exosome loading. HSC70, in interaction with ALIX, was shown to bind with the transferrin receptor to direct its secretion within exosomes[466]. Furthermore, cytosolic proteins containing a KFERQ-motif were selectively sorted to ILVs in a chaperone-dependent manner following binding to HSC70[467].

With regard to RNA-based therapeutics, it is of particular interest that both AGO2 and GW182 (components of RISC) and Stau1 and Stau2 (RNA-binding proteins implicated in stability, localisation and transport of dsRNA) are found within exosomes[385,387,468–470]. Downregulation of either AGO2 or GW182 significantly reduces miRNA secretion within exosomes, suggesting members of RISC contribute to miRNA exosomal loading[385,471]. Specific sequence motifs (EXOmotifs) have also been identified within exosome-associated RNA which may function as cis-acting elements to selectively target mRNA and miRNA to exosomes[472–474]. Similarly, nontemplated nucleotide additions, and particularly 3' uridylation, may contribute to the enrichment of specific miRNA isoforms within exosomes[475], while target mRNA abundance also modulates miRNA loading[476].

Finally, it should be noted that other EV species have also been identified which may be distinguished from exosomes by their origin. These include microvesicles (50-1000 nm) and apoptotic bodies (800-5000 nm), which are heterogeneous populations of vesicles formed following outward budding/blebbing of the plasma membrane of healthy cells or those undergoing apoptosis, respectively.

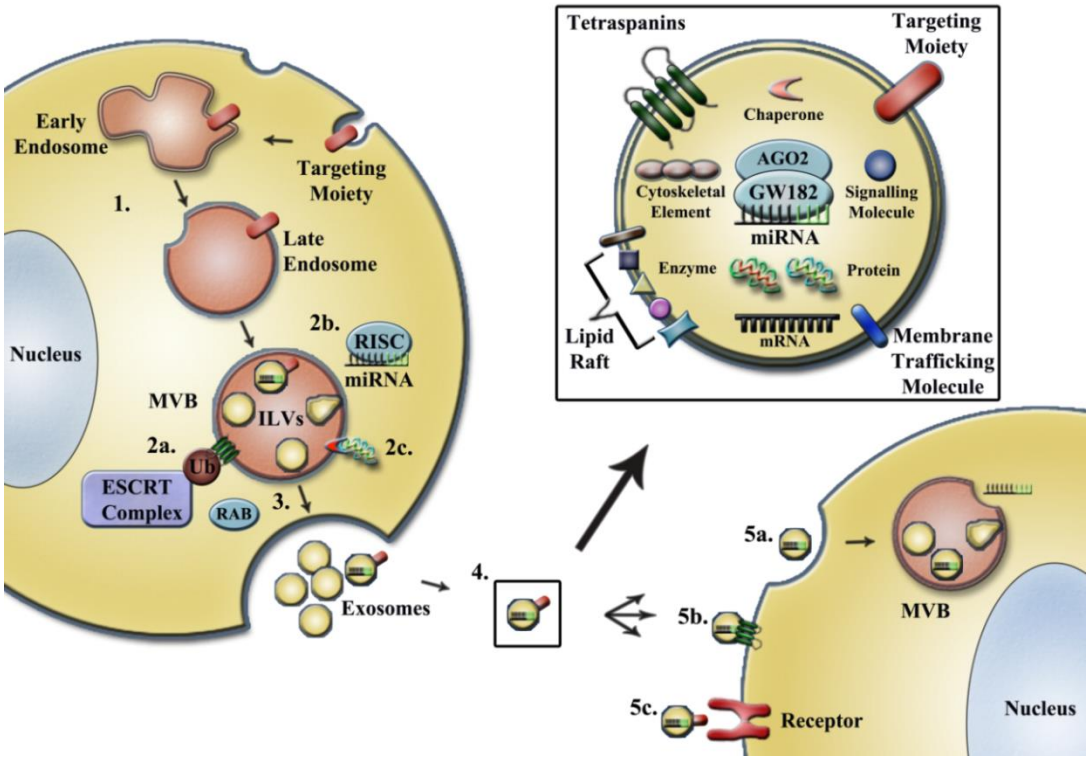

Figure 1.6 The Exosome Biogenesis Pathway. (1) Exosomes are formed within the endosomal pathway following inward budding of the plasma membrane to produce early endosomes, late endosomes and eventually multivesicular bodies (MVBs) containing intraluminal vesicles (ILVs). During this process, cargoes are selectively loaded into ILVs via different mechanisms. **(2a)** The endosomal sorting complex required for transport (ESCRT-0) directs cargoes for inclusion into ILVs in an ubiquitin-dependent manner. **(2b)** Components of RISC may contribute towards the incorporation of miRNAs into ILVs. mRNAs and miRNAs may be targeted into ILVs by specific sequence motifs and nontemplated nucleotide additions. **(2c)** Chaperone proteins, lipid-rafts and tetraspanins may also contribute towards selective exosome-loading. Chaperone proteins sort proteins via recognition of short sequences motifs while lipid-raft microdomains contribute towards loading in a ceramide-dependent manner. **(3)** ILVs are released as exosomes, constitutively or in response to stimuli, following fusion of MVBs with the plasma membrane. This may be driven by the activity of Rab GTPase proteins. **(4)** Exosomes may transport cargoes to near and distant cells. Lipid rafts, exosomal markers (e.g. tetraspanins) and plasma membrane proteins, retained from the cell of origin, are found within the exosomal membrane. Expression of targeting moieties on the exosomal membrane may selectively direct exosomes to specific cellular subtypes. Exosomes carry a range of cargoes including mRNA, miRNA, proteins, signalling molecules and components of RISC. Recipient cell uptake of exosomes may occur via several mechanisms including; **(5a)** exosome internalisation by endocytosis into MVBs, **(5b)** direct fusion of the exosome and plasma membranes or **(5c)** receptor-ligand mediated interactions driving signal transduction or exosome internalisation. Adhesion molecules such as integrins and tetraspanins appear important for exosome and recipient cell binding and may confer target cell specificity.

1.6.2 Exosomes as Mediators of Cell-to-Cell Communication

Exosomes are secreted by most, if not all, cell types and are abundant in many biological fluids[477–481]. Circulatory exosomes may therefore reflect a widespread natural delivery system by which near and distant cells communicate for a range of physiological purposes. As they are present in a variety of easily accessible biological fluids they may also represent a novel class of biomarker.

Exosomes have been implicated in a growing number of biological and pathological functions including immune regulation, antigen presentation, stem cell maintenance and plasticity, cell phenotype modulation, synaptic signalling, tumour progression and the spread of pathological proteins[482–491]. However, arguably the most important finding in relation to exosome-mediated delivery of RNA-based therapeutics is that exosomes are natural carriers of mRNAs and miRNAs between source and recipient cells.

Ratajczak *et al*.[487] provided early evidence that EVs carry functional mRNA and protein to recipient cells. Vesicles derived from mouse and human embryonic stem cells (ESCs) were enriched in Wnt-3 and Oct-4 proteins and mRNA encoding for several early pluripotent transcription factors. Vesicle treatment of recipient hematopoietic stem cells resulted in upregulation of early pluripotent protein markers, activation of MAPK and Akt signalling pathways and enhanced their survival and proliferation[487].

Similar results were reported by Baj-Krzyworzeka *et al*.[492] who showed that tumour-derived microvesicles carried both characteristic proteins (tumour surface determinants) and an array of growth factor mRNAs. Following uptake by recipient monocyte cells,

EVs provided protection from apoptosis *in vitro* and activated the Akt-PI3K signalling pathway. Endothelial progenitor cell-derived vesicles also enhance the survival of recipient endothelial cells *in vitro* and *in vivo* by exerting anti-apoptotic effects and promoting neoangiogenesis[493]. Interestingly, mesenchymal stem cell (MSC)-derived vesicles did not trigger the same recipient cell response, suggesting cell-type specific effects. Together, these results provided early evidence that EVs are involved in the shuttling of bioactive cargoes capable of producing distinct phenotypic changes in recipient cells.

Subsequently, two seminal papers ignited the interest of the field and raised the question as to whether exosomes could be exploited for the purpose of delivering exogenous RNAi molecules. In the first, Valadi and colleagues[494] reported that mouse and human mast cell-derived EVs contained large numbers of mRNAs and miRNAs. Over 1300 different vesicular mRNA and 121 miRNA transcripts were discovered, not always reflecting parent cell abundance, suggesting an element of selective loading. Furthermore, incubation of human mast cells with exosomes derived from murine cells resulted in the expression of mouse proteins in recipient human cells. As one of the first papers to demonstrate functional transfer of RNA and recognise the presence of RNAi effectors within exosomes, this work triggered a wealth of interest into the content and potential physiological roles of exosomes. In a follow-up to this work, Ekström *et al*.[495] further characterised the mRNA and miRNA content of human mast cell-derived exosomes and their role in cell-to-cell communication. As before, 116 miRNAs and ~1800 mRNAs were identified within exosomes derived from the human mast cell line, HMC-1. By using radioactive uridine to label exosomal RNA in parental source cells,

mast cell-derived exosomes were shown to transfer their RNA cargoes to both human mast cells and CD34+ cells[495].

In the second influential paper, Skog *et al.*[496] confirmed the presence of angiogenic proteins, mRNAs and miRNAs within exosomes derived from glioblastoma tumour cells. 11 tumour-specific mature miRNAs and 27,000 mRNA transcripts were detected within exosomes, 4,700 of which were not detected in parental source cells, again suggesting selective enrichment of specific mRNAs. Via Gaussia luciferase mRNA, fluorescently labelled glioblastoma-derived vesicles were shown to actively deliver reporter mRNA to recipient human brain endothelial cells where it was translated into protein. These vesicles triggered endothelial cell tubule formation and stimulated the proliferation of human glioma cells, demonstrating the pleotropic biological effects elicited by tumour-derived vesicles.

As miRNAs have become increasingly implicated in health and disease, the interest in them has grown and the principal findings from these two publications have been confirmed by others. The RNA-mediated functional effects exerted on recipient cells by EVs have been diverse. For example, Collino *et al.*[469] confirmed the presence of 113 and 133 mature miRNAs in vesicles derived from human MSCs and liver resident stem cells, respectively. Many of the miRNAs, which could be transferred to recipient murine tubular epithelial cells, were predicted to play important roles in a variety of processes including immune system regulation, multi-organ development, cell survival and differentiation[469]. Exosomes derived from T, B and dendritic immune cells are also highly enriched in small RNA[497]. These exosomes were found to participate in immune interactions by transferring encapsulated miRNAs from T-cells to antigen-presenting

cells. Notably, the exosome transfer was unidirectional and modulated gene expression in recipient cells[497].

Montecalvo *et al.*[498] also provided evidence for the transfer of functional miRNAs within exosomes secreted by mouse dendritic cells (DCs). Not only were 202 miRNAs identified within DC-derived exosomes, but the precise miRNA profile varied depending on maturity of the source cell. Incubation of recipient cells with DC-derived exosomes resulted in repression of target genes involved in a range of DC functions including cytokine synthesis, endocytosis, antigen cross-presentation, dendritic cell differentiation, TGF-β signalling and cell survival.

Interestingly, the precise exosomal RNA profile and resulting biological effects vary not only by cell type and parent cell maturity but also by growth conditions and pathological state. Eldh *et al.*[499] revealed that the RNA content of exosomes derived from mouse mast cells differed significantly when source cells were grown under conditions of oxidative stress. Furthermore, these exosomes conferred a protective signal to recipient cells subsequently exposed to oxidative stress. Similarly, Wang *et al.*[500] reported that serum deprivation caused a prompt increase in miRNA secretion from human cell lines. However, whether these vesicles confer similar protective effects was not assessed. Finally, the miRNA profile of secreted EVs may also be altered by the pathological state of the source cell in a variety of diseases including cancer and cardiovascular disease[501–505]. Thus, as EVs derived from a range of different cell types are found within a variety of biological fluids, they have attracted increasing attention as potential biomarkers.

Together, these findings confirm exosomes as natural nanocarriers of proteins, mRNA and endogenous RNAi molecules both *in vitro* and *in vivo.* These cargoes are functional and may fundamentally change the biological phenotype of recipient cells. As exosomes are stable in human biological fluids, encapsulate a range of genetic material and are able to deliver functionally active molecules to distant cells, this raises the prospect that these properties may be exploited for therapeutic purposes.

1.7 Therapeutic Applications of Exosomes

Although the field is still at an early stage, several studies have now highlighted the potential of exosomes for the delivery of exogenous RNAi-based effectors (**Table 1.2**). Exosomes also possess intrinsic therapeutic properties which may offer inherent potential for the treatment of disease.

1.7.1 Delivery of Exogenous Therapeutic Cargoes

Different strategies have been employed to load exogenous RNAi-based molecules into exosomes including endogenous and exogenous mechanisms. By endogenous methods, RNAi molecules are transfected into exosome source cells and rely upon endogenous loading pathways for encapsulation of exogenous RNAi molecules into EVs. In contrast, exogenous loading strategies first require the isolation of vesicles, after which they are loaded *ex vivo* by either electroporation or co-incubation techniques.

Exogenous miRNA and siRNA Delivery

Kosaka *et al.*[506] provided early evidence that overexpression of miRNAs within source cells resulted in their increased secretion within exosomes. The activity of a luciferase reporter containing a perfectly complementary binding site to miR-146a was reduced in recipient cells treated with conditioned medium derived from COS-7 and HEK293 cells pre-transfected with pri-miR-146a expression plasmids. These findings were supported by Zhang *et al.*[468] who showed that transfection of miR-150 mimics into human THP-1 monocytic cells resulted in their secretion within microvesicles. Microvesicles were

taken up by human HMEC-1 cells *in vitro*, where elevated levels of exogenous miR-150 reduced protein expression of the miR-150 target, c-Myb, and increased cell migration. Furthermore, miR-150 transfer also occurred *in vivo*. When C57BL/6 mice were injected intravenously with miR-150-loaded fluorescent THP-1 microvesicles, the blood vessel endothelium became fluorescently labelled and enriched in miR-150, confirming that EVs may deliver exogenous RNAi-molecules *in vivo.*

Similarly, Akao *et al.*[507] demonstrated that transfection of THP-1 cells with miR-143 resulted in miR-143 enriched microvesicles. When pre-transfected THP-1 cells were injected into nude mice, miR-143 levels were significantly increased in the serum, tumour and kidneys. Although no functional assessments of transported miR-143 were reported, these findings support those of Zhang *et al.*[468] by demonstrating that exogenous miRNAs may be delivered to recipient cells *in vivo*.

In 2011, Alvarez-Erviti *et al.*[508] provided the first proof-of-concept evidence that exosomes could be harnessed to deliver exogenously loaded siRNA. Bone marrow-derived immature DCs (BM-DCs) were used as a source of immunologically inert exosomes. It is imperative that therapeutics are developed which are specifically targeted and capable of penetrating the BBB. Therefore, a novel targeting strategy was employed in which the exosomal membrane protein, Lamp2B, was fused either to a muscle specific peptide (MSP)[509] or a rabies viral glycoprotein (RVG)-derived peptide[510], chosen for its ability to bind nicotinic acetylcholine receptors expressed on neurons and the vascular endothelium of the BBB. Once isolated, exosomes were loaded via electroporation with siRNA against Gapdh, cyclophilin B or Bace1. Importantly, exosomal expression of targeting peptides conferred specific targeting

capacities to the exosomes; the strongest knockdown in C2C12 (myoblast) cells was achieved with MSP-exosomes while RVG-exosomes elicited the strongest knockdown in Neuro2A (neuroblastoma) cells. The role of the RVG-peptide in specific targeting was confirmed as silencing was abolished when acetylcholine receptors were blocked using α-bungarotoxin.

Subsequently, siRNA-loaded RVG-exosomes were administered to C57BL/6 mice via intravenous injection. Strikingly, RVG-exosomes resulted in effective silencing throughout several brain regions including the striatum, midbrain and cortex with little silencing in the liver and spleen. This was in contrast to naked siRNA which was sequestered within the liver, kidneys and spleen. Significantly, *in vivo* delivery of Bace1 siRNA-loaded exosomes resulted in ~60% silencing of cortical Bace1 mRNA and protein, paired with a significant reduction (~55%) in amyloid-β (42). Exosome treatment was well-tolerated *in vivo* and did not appear to stimulate an immune response, even following repeated administration. This study therefore offered the first evidence that exosomes may be harnessed safely as natural delivery vehicles to effectively deliver exogenous RNAi-molecules across the previously insurmountable BBB.

Importantly, Wahlgren *et al*.[511] provided evidence that this nanotechnology could translate to human cells. The authors harvested plasma exosomes from the peripheral blood of human donors and successfully loaded them with fluorescently tagged MAPK-1 siRNA by electroporation. Exosomes were taken up by both monocytes and lymphocytes where exosome-delivered siRNA localized mainly to the cytoplasm and elicited effective silencing of MAPK1. Interestingly, silencing was more pronounced in

recipient monocytes than lymphocytes suggesting selectivity in exosome uptake, as mentioned previously.

Following these reports, further studies have shown that exosomes deliver both exogenous siRNA and miRNA and have extended applicability to other diseases[450,512–515]. For example, Shtam *et al*.[512] used a number of strategies, including electroporation, to introduce exogenous siRNAs against RAD51 and RAD52 into HeLa and human ascites-derived exosomes. Treatment of recipient HeLa and HT1080 fibrosarcoma cells with siRNA-loaded exosomes resulted in effective post-transcriptional gene silencing with RAD51 siRNA prompting reproductive cell death in recipient HeLa cells.

Three studies have provided further evidence for exosome-mediated delivery of synthetic miRNAs. In the first, Momen-Heravi and colleagues[450] used electroporation to load B-cell-derived exosomes with miR-155 synthetic mimics or inhibitors for delivery to hepatocytes or macrophages. Exosomes loaded with miR-155 mimics significantly increased miR-155 levels in primary mouse hepatocytes *in vitro* and in the liver of miR-155 knockout mice *in vivo*. Conversely, treatment of RAW macrophage cells with exosomes loaded with miR-155 inhibitors reduced both miR-155 expression and LPS-induced TNFα production, which partially prevented an LPS-induced decrease in *SOCS1* mRNA levels. Furthermore, exosome-mediated delivery of miR-155 inhibitors was more effective and less toxic compared to conventional transfection protocols. As one of the first reports of exosome-mediated delivery of miRNA inhibitors, this extends the exogenous RNAi-based cargoes which exosomes may potentially deliver.

In two companion studies, Lee *et al*.[514,515] showed that MSC-derived exosomes were able to deliver synthetic miR-124 and miR-125 mimics to a range of cells including glioma cells, glioma stem cells (GSCs), neural progenitor cells (NPCs) and astrocytes following co-culture *in vitro.* The role of exosomes in delivering exogenous miRNA mimics was confirmed following their isolation and direct application to recipient cells. In glioma cells and GSCs, exosome-mediated delivery of miR-124 and miR-125 mimics significantly reduced luciferase reporter activity for target genes, *SCP-1* and *Sox2*, and decreased the migration of glioma cells and self-renewal of GSCs[514]. In NPCs, exosome-mediated delivery of miR-124 significantly decreased expression of the target gene, *Sox9,* and enhanced neuronal differentiation[515]. Additionally, expression of the glutamate transporters, EEAT1 in NPCs and EAAT2 in NPCs and astrocytes, was increased following delivery of miR-124. Functional effects were also observed *in vivo* when intracranially administered MSCs delivered Cy3-labelled miR-124 mimics to glioma xenografts, resulting in increased expression of miR-124 within tumour cells[514]. Together, these two studies demonstrated that MSC-derived exosomes are able to deliver exogenous miRNA to a variety of cells both *in vitro* and *in vivo*.

Finally, Cooper and colleagues[513] reported that RVG-modified exosomes loaded with siRNA targeting α-synuclein could hold therapeutic utility in the treatment of PD. RVG-modified exosomes loaded with α-synuclein siRNA effectively silenced α-synuclein mRNA (80%) and protein (85%) in SH-SH5Y cells *in vitro*. These results extended *in vivo* with selective silencing of α-synuclein mRNA and protein in the brains (midbrain, striatum and cortex) of both wild-type mice and S129D α-synuclein PD transgenic mice. Furthermore, there was also a significant reduction in intraneuronal protein aggregates, including in the dopaminergic neurons of the substantia nigra, in the

brains of PD transgenic mice[513]. These findings not only extend the use of RVG-modified exosomes for the delivery of PD-relevant siRNA but confirm that exosomes are effective in reducing aggregates in a disease-model of PD. This is important as they suggest that aggregated proteins may be reduced by targeting mutant protein at the mRNA level.

In summary, although the number of experiments to-date is relatively small, combined, they provide strong support for the hypothesis that exosomes may be loaded with exogenous RNAi-based cargoes and exploited for their capacities as a natural *in vivo* delivery vehicle.

Delivery of Other Cargoes

While this thesis focuses upon RNA-based therapeutics, it is important to note that exosomes are also capable of delivering other exogenous cargoes (**Table 1.2**). For example, exosomes may be complexed with the anti-inflammatory agent, curcumin[516,517]. Curcumin was more stable *in vitro* and had a higher bioavailability *in vivo* when delivered in association with exosomes[516,517]. Exosome-curcumin complexes could be delivered noninvasively to microglia cells *in vivo* by intranasal delivery and protected mice against a range of inflammatory challenges[516,517]. Similarly, exosomes have been loaded with catalase, a potent anti-oxidant, and delivered to the brain intranasally, where they protected neurons against oxidative stress in a PD mouse model[518]. Two phase I clinical trials are currently recruiting to study the anti-inflammatory effects of plant exosomes either alone or in complex with curcumin for the treatment of cancer (NCT01294072, NCT01668849). This anti-inflammatory

potential of exosome-mediated therapies may therefore have relevance for the neuroinflammatory component within AD.

An alternative therapeutic use for exosomes has been proposed by Maguire and colleagues[519] who showed that during production of adeno-associated viruses (AAVs), a fraction were associated with EVs (vexosomes). Gene transduction efficiency in recipient cells was significantly enhanced by vexosome-mediated delivery and purified vexosomes were more resistant to an AAV-neutralising antibody. Ligands could also be incorporated into the vexosome membrane to improve targeting. This study suggests that exosomes may hold promise as co-delivery vectors and may improve existing AAV vectors which have suffered from off-target effects and low transduction efficiency in target tissues.

Exosomes may also be used to deliver cargoes for the treatment of cancer. For example, EV-mediated delivery of CD-UPRT mRNA/protein, a potent prodrug-activating combination, resulted in regression of Schwannoma tumours following systemic treatment with the prodrug 5-flurocytosine[520]. Other evidence has shown that exosomes encapsulating let-7a miRNA may be targeted to epidermal growth factor receptor (EGFR)-expressing breast cancer cells *in vivo* by engineering source cells to express the transmembrane domain of platelet-derived growth factor receptor fused to the GE11 peptide[521].

In summary, these studies highlight the therapeutic potential of exosome-mediated delivery for a wide range of cargoes and diseases and demonstrate cell-specific targeting following EV membrane modifications.

Table 1.2 Summary of Exogenous Exosome Cargoes and Their Functional Effects.

Ref.	Cell Type	Cargo	Vesicle-Mediated Effects
RNAi-Based Compounds			
468	THP-1	miR-150 mimic	Downregulation of target protein c-Myb in HMEC-1 cells and increased HMEC-1 cell migration. miR-150 transfer to mouse blood vessel endothelium *in vivo.*
506	HEK293, COS-7	pri-miR-146a	Downregulation of luciferase reporter protein and inhibition of tumour cell proliferation.
507	THP-1	Modified miR-143 mimic	miR-143 mimic accumulation in serum, tumour and kidneys of nude mice following intravenous injection of *ex vivo* transfected cells.
508	BM-DC	Gapdh and Bace1 siRNAs	Targeted *in vivo* silencing of mRNA and protein within the brain (striatum, midbrain and cortex).
522	Human hepatoma	HCV and CD81 shRNAs	*In vivo* siRNA transfer between native liver cells and engrafted cells in NOD/SCID mice. CD81 silencing in native liver cells.
523	MSC	GFP and mutant HTT shRNAs	HTT silencing in SH-SH5Y and U87 cells.
511	Human plasma	MAPK-1 siRNA	Silencing of MAPK1 in monocytes and lymphocytes.
521	HEK293	let-7a mimic	Exosome donor cells engineered to target EGFR-expressing breast cancer cells. Intravenously injected exosomes delivered let-7a miRNA to EGFR-expressing xenograft breast tissue in $RAG2^{-/-}$ mice and suppressed tumour growth.
512	HeLa and Ascites	RAD51 and RAD52 siRNAs	Post-transcriptional gene silencing in recipient HeLa and HT1080 cells. RAD51 delivery caused reproductive cell death of recipient HeLa cells.
514	MSC	miR-124 and miR-145 mimics	Transfer to glioma cells and GSCs. Silenced SCP-1 and Sox2 reporter activity and decreased migration of glioma cells and self-renewal of GSCs. Delivered Cy3-miR-124 mimic to glioma xenografts *in vivo* following intracranial administration.
515	BM-MSC	miR-124 and miR-145 mimics and pre-miR-124	Transfer to NPCs and astrocytes. Silencing of Sox9 and increased neuronal differentiation in NPCs. miR-124 increased glutamate transporter expression EAAT1 in NPCs and EAAT2 in NPCs and astrocytes.
450	Murine B-cells (M12.4)	miR-155 mimic or inhibitor	miR-155 mimic and inhibitor delivered to hepatocytes or macrophages. miR-155 inhibitor reduced LPS-induced TNFα production and prevented decrease in *SOCS1* mRNA levels in RAW macrophages.

Table 1.2 Continued.

Ref.	Cell Type	Cargo	Vesicle-Mediated Effects
524	HeLa	miR-16 mimic and AGO2	Co-expression of miR-16 and AGO2 increased miR-16 secretion in microvesicles. Enhanced silencing of BCL-2 protein in recipient HEK293T cells.
513	BM-DC	α-synuclein siRNA	Targeted *in vivo* silencing of α-synuclein mRNA and protein in the brain (striatum, midbrain and cortex). Significant reduction in intraneuronal protein aggregates including in dopaminergic neurons in substantia nigra.
525	Endothelial cells	Luciferase siRNA	Silencing of luciferase reporter in endothelial recipient cells.
526	U937	miR-21 mimic or inhibitor	miR-21 inhibitor reduced migration and increased apoptosis of gastric cancer cells.
Other Compounds			
519	HEK293T	AAVs	Enhanced AAV gene transduction, increased resistance to an AAV-neutralizing antibody.
520	HEK293T	CD-UPRT mRNA/protein	Regression and reduced growth of pre-established Schwannoma tumours in an orthotopic mouse model.
516	EL-4 and RAW 264.7	Curcumin	Enhanced *in vivo* bioavailability. Protection against LPS-induced septic shock in mice.
517	EL-4, 3T3L1, 4T1, CT26 and A20	Curcumin and Stat3 inhibitor, JSI124	Intranasal delivery to microglia. Protected mice against inflammation-mediated diseases.
527	Immature DC	Doxorubicin	DCs engineered to express Lamp2B fused to αv integrin-specific iRGD peptide for tumour targeting. Exosomes loaded with Doxorubicin inhibited tumour growth in BALB/c nude mice.
528	MDA, HUVEC, hMSC and hESC	Porphyrins of different hydrophobicities	Hydrophobic compounds loaded efficiently into vesicles. EV-mediated delivery significantly increased cellular uptake and the photodynamic effect of hydrophobic porphyrins.
518	RAW 264.7	Catalase	Catalase-loaded exosomes taken up by neuronal cells. Protected against neuronal stress and ROS *in vitro*. Protected against oxidative stress *in vivo* in a PD mouse model following intranasal administration.

THP-1, human acute monocytic leukaemia cell line; **HMEC-1**, human microvascular endothelial cell line; **HEK293**, human embryonic kidney 293 cell line; **COS-7**, African green monkey kidney cells; **BM-DC**, bone-marrow-derived dendritic cells; **HCV**, hepatitis C virus; **NOD/SCID**, Nonobese diabetic/severe combined immunodeficiency; **hMSCs**, human mesenchymal stem cells; **shRNA**, short hairpin RNA; **GFP**, green fluorescent protein; **HTT**, huntingtin; **SH-SH5Y**, human neuroblastoma cell line; **U87**, human primary glioblastoma cell line; **MAPK-1**, mitogen-activated protein kinase 1; **EGFR**, epidermal growth factor receptor; **HT1080**, human fibosarcoma cells; **GSCs**, glioma stem cells; **NPCs**, neural progenitor cells; **LPS**, lipopolysaccharide; **RAW**, murine leukaemic monocyte macrophage cell line; **AGO2**, argonaute 2; **U937**, human acute monocytic leukaemia cell line; **AAVs**, adeno-associated viruses; **CD-UPRT**, cytosine deaminase fused to uracil phosphoribosyltransferase; **EL-4**, murine T-lymphoma cell line; **3T3L1**, mouse embryonic fibroblast-adipose-like cell line; **4T1**, murine mammary tumour cell line; **CT26**, murine colon carcinoma cell line; **A20**, murine B lymphoma cell line; **Stat3**, Signal transducers and activators of transcription; **DC**, dendritic cell; **MDA**, MDA-MB231 breast cancer cell line; **HUVEC**, human umbilical vein endothelial cells; **hESC**, human embryonic stem cell line; **ROS**, reactive oxygen species.

1.7.2 Intrinsic Therapeutic Activity of Exosomes

In addition to their potential for the delivery of exogenous RNAi-based effectors it must be noted that exosomes also possess intrinsic therapeutic properties. Thus, it may be possible to combine intrinsic therapeutic potential with exogenous cargoes to enhance the therapeutic capabilities of exosomes.

Exosomes may confer both anti-inflammatory and immunosuppressive effects. They may therefore have therapeutic utility in the context of autoimmune diseases or those with an inflammatory component such as AD. Exosomes derived from immature DCs engineered to express immunosuppressive cytokines such as IL-4, IL-10, FasL and indoleamine 2,3-dioxygenase (IDO) reduced inflammatory responses in delayed-type hypersensitivity and suppressed the onset and severity of murine collagen-induced arthritis[529–532]. In these studies, exosomes were found to be as, if not more, immunosuppressive than the DCs from which they were derived.

Unmodified exosomes also display inherent therapeutic potential. A wealth of pre-clinical evidence has shown that MSC-derived exosomes improve organ function and promote recovery after injury and may inhibit tumour growth[533]. Indeed, MSC-derived exosomes are cardioprotective in the treatment of myocardial ischemia/reperfusion injury[534,535] and also promote neurite outgrowth and functional recovery after neurological injury[536]. Furthermore, MSC-derived exosomes have been used to treat a patient suffering from graft-versus-host disease (GvHD), where they appeared well-tolerated and ameliorated both the pro-inflammatory cytokine response and clinical GvHD symptoms[537].

Finally, exosomes derived from DCs, tumours and ascitic fluid may have intrinsic potential as a cell-free cancer vaccine by priming the immune system to evoke anti-tumour immunity. DC-derived exosomes (Dex) induce antigen-specific T-cell responses by direct and indirect display of antigens to T-cells[538–540] while tumour-derived exosomes (Tex) may function as antigen delivery systems[541,542]. Three clinical trials have assessed the safety and efficiency of Dex and ascites-derived exosomes (Aex) in patients with non-small cell lung cancer[543], metastatic melanoma[544] and colorectal cancer[545]. The treatments were well-tolerated and Aex, in combination with GM-CSF, produced beneficial anti-tumour cytotoxic T-lymphocyte responses[545]. Furthermore, exosomes derived from tumour cells genetically modified to express either IL-2 or glycolipid-anchored IL-12 had enhanced anti-tumour and anti-immunogenicity effects[546,547].

These findings support the proposal that combining the intrinsic therapeutic potential of exosomes with their ability to deliver exogenous cargoes may improve therapeutic outcomes. Together, these studies highlight the promise of exosome-mediated therapeutics and serve as evidence that exosomes may be delivered safely and efficiently in human clinical trials.

1.8 Conclusions

In summary, a novel disease-modifying therapy for AD is urgently required. Although seemingly promising compounds have been identified, many have subsequently failed at clinical trial. A novel, and most likely combinatorial, approach to therapy is therefore required. In this respect, the field of RNA-based therapeutics holds great promise. Nevertheless, development is currently limited by the lack of a suitable delivery vehicle able to target therapeutics across the BBB with minimal toxicity. In recent years, the potential for exosome-mediated delivery has been increasingly recognised. However, key challenges to realising this potential will be to characterise a safe and scalable source of exosomes, identify appropriate cargoes, establish efficient and sustainable loading protocols and develop methods to enable specific targeting of desired cells. This thesis will therefore focus on the development of RNA-based therapeutics and optimisation of exosome-mediated delivery for the treatment of AD.

1.9 Thesis Aims

The aims of this thesis were to:

1) Validate candidate RNAi-based therapeutics for the treatment of AD.
2) Optimise exosome-mediated delivery for AD-relevant RNAi-based therapeutics.
3) Develop combinatorial LNA-ASO-based approaches towards AD therapy.

2 Materials and Methods

2.1 siRNAs

siRNAs were purchased from Eurogentec or were a gift from Novartis. The Bace1 siRNA sequence chosen had previously been successfully validated in the literature[422,508]. APP siRNA sequences were designed utilising the Eurogentec siRNA design platform. A nonspecific siRNA sequence was used as a negative control for comparison to experimental siRNA activity. The siRNA sequences utilised in this study are provided in **Table 2.1**.

Table 2.1 siRNA Sequences.

siRNA	Sense Sequence	Antisense Sequence
BACE1	GCUUUGUGGAGAUGGUGGA	UCCACCAUCUCCACAAAGC
APP1	GUACCAACUUGCAUGACUA	UAGUCAUGCAAGUUGGUAC
APP2	GAUCACCAAUGUGGUAGAA	UUCUACCACAUUGGUGAUC
APP3	CUGGUACUUUGAUGUGACU	AGUCACAUCAAAGUACCAG
Negative Control	UGCGCUACGAUCGACGAUG	CAUCGUCGAUCGUAGCGCA

2.2 microRNA Mimics

Two sets of miRNA mimics were purchased; mirVana miRNA mimics (Life Technologies) and AccuTarget miRNA mimics (Bioneer). Cel-miR-39-3p was utilised as a normalisation control spike-in for RNA extractions and was purchased from IDT. The miRNAs utilised in this study are provided in **Table 2.2**.

Table 2.2 miRNA Mimics.

miRNA ID	Mature miRNA Sequence
hsa-miR-17-5p	CAAAGUGCUUACAGUGCAGGUAG
hsa-miR-20a-5p	UAAAGUGCUUAUAGUGCAGGUAG
hsa-miR-29a-5p	ACUGAUUUCUUUUGGUGUUCAG
hsa-miR-106b-5p	UAAAGUGCUGACAGUGCAGAU
cel-miR-39-3p	UCACCGGGUGUAAAUCAGCUUG
mirVana Negative Control #1	Sequence not provided (ID: 4464076)

2.3 Locked Nucleic Acid-Antisense Oligonucleotides (LNA-ASOs)

Multi-gene targeting LNA-ASOs were designed by Dr. Miguel Varela (Wood Lab) using a self-developed algorithm which identifies overlapping sequences between two or more genes of interest. The algorithm was utilised to design chimeric DNA/LNA "gapmer" ASOs which have a fully phosphorothioated backbone and comprise a core region of 7-9 DNA monomers flanked either end by 3 modified LNA bases. For multi-gene LNA-ASOs, these were based on sequences predicted to allow each LNA-ASO to target two genes simultaneously. Separate single-gene gapmer LNA-ASOs, predicted to target each desired gene individually, were also designed. A nonspecific LNA-ASO sequence was utilised as a negative control. All sequences were blasted against the human genome to ensure specificity to the genes of interest. LNA-ASOs were purchased from Exiqon. The LNA-ASOs utilised in this study are provided in **Table 2.3**.

Table 2.3 LNA-ASO Sequences.

LNA-ASO	Genes Targeted	Sequence
Multi-gene Targeting LNA-ASOs		
APGS	*APP, GSK3β*	+A+G+Agagactga+T+T+C
BACD	*BACE1, CDK5R1*	+C+C+Ttccaccgc+T+G+C
BAMT (human)	*BACE1, mTOR*	+G+A+Tagagaca+A+T+G
BAMT (mouse)	*Bace1, mTOR*	+T+T+Tggccagcag+G+G+A
BAPP1	*BACE1, APP*	+A+C+Ttcagactg+G+T+T
BAPP2	*BACE1, APP*	+A+C+Ttcagactg+G+T+T/idSp/+A
BAPP3	*BACE1, APP*	+A+C+Ttcagactg+G+T+T/idSp/+A/idSp/+G
BATA	*BACE1, Tau*	+T+G+Ctggtggctt+C+T+C
GRAGSB	*GRIA2, GSK3β*	+C+A+Aaaagatattc+A+G+A
GRANO	*GRIA2, NOX4*	+A+G+Gcatatttc+C+C+T
GRBCA	*GRIN2B, Caspase-9*	+G+A+Gtgagcccac+T+G+C
GSBGRB	*GSK3β, GRIN2B*	+C+C+Acccccctgga+T+C+T
Single-gene Targeting LNA-ASOs		
APP-1	*APP*	+C+A+Ccatgcgca+C+A+T
APP-2	*APP*	+T+A+Gcatattga+A+C+A
APP-3	*APP*	+T+G+Acgttctgc+C+T+C
BACE1-1	*BACE1*	+T+A+Acctcaccc+A+T+T
BACE1-2	*BACE1*	+C+C+Ataacagtg+C+C+C
GSK3β-1	*GSK3β*	+A+C+Accaaatga+T+C+C
GSK3β-2	*GSK3β*	+T+T+Ctcctgaat+C+A+C
mTOR-1	*mTOR*	+C+C+Acaccgtc+C+A+A
mTOR-2	*mTOR*	+T+T+Atctcgaa+C+C+C
mTOR-3	*mTOR*	+C+T+Cacggaga+A+C+C
mTOR-4	*mTOR*	+T+G+Gcaagacg+G+C+C
Control LNA-ASO		
Negative Control	N/A	+C+A+Gtgtgctag+T+C+A

All LNA-ASOs have a fully phosphorothioated backbone with 7-9 DNA monomers flanked either end by 3 LNA-modified bases, + indicates modified LNA monomer, idSp indicates inclusion of an abasic site.

2.4 Plasmids

2.4.1 Lamp2B-RVG Neuronal Cell Targeting Expression Plasmid

Where indicated, EVs were engineered to target neuronal cells through the use of the pEGFP-C1-Lamp2B-RVG plasmid[508] (a gift from Dr. Lydia Alvarez-Erviti, UCL). This plasmid had been constructed so that the exosomal protein, Lamp2B, was N-terminally fused with the Rabies Viral Glycoprotein (RVG)-derived peptide[510], a ligand for the acetylcholine receptor, with the removal of EGFP (**Fig. 2.1**). As a control, the pEGFP-C1-Lamp2B construct, lacking the RVG peptide, was used.

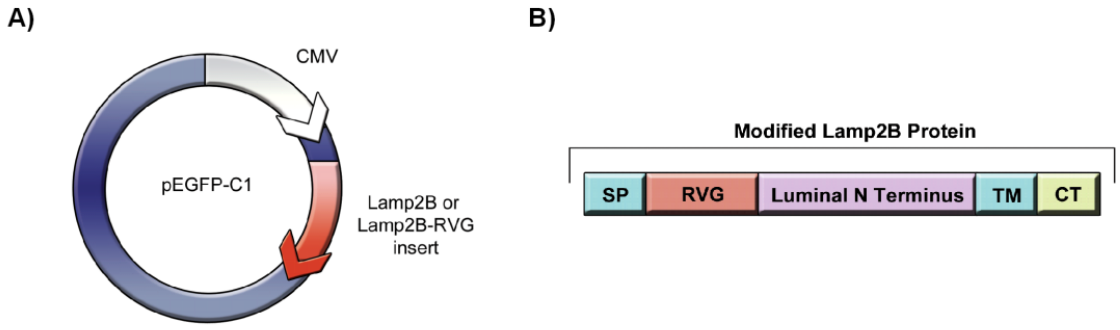

Figure 2.1 Structure of pEGFP-C1-Lamp2B-RVG Targeting Peptide. (**A)** The Lamp2B or Lamp2B-RVG fusion protein is inserted downstream of the CMV promoter between *Nhel* and *BamHI* restriction sites in the pEGFP-C1 plasmid with the EGFP sequence removed. **(B)** The Rabies Viral Glycoprotein (RVG)-derived peptide is cloned into the N-terminus of Lamp2B. SP, signal peptide, TM, transmembrane domain, CT, C terminus.

2.4.2 AGO2 and Membrane-associated AGO2 Expression Plasmids

To assess the effect of increased cellular expression of AGO2, the pEGFP-N1-hAGO2 plasmid (a gift from Giulia Corso, Karolinska Institute) was utilised. This plasmid had been constructed by amplification of the hAGO2 insert from the pEGFP-C1-hAGO2 plasmid[548] (Addgene, plasmid #21981) and subsequent insertion into the C-terminus of EGFP in the pEGFP-N1 plasmid (Clontech) between *NheI* and *BsrGI* restriction sites. To assess the impact of directing AGO2 towards the membrane, a membrane-associated (MT) form of the pEGFP-N1-hAGO2 plasmid (a gift from Giulia Corso) was utilised. This plasmid comprised an acylation domain inserted in the N-terminal region of the pEGFP-N1-hAGO2 fusion protein and is referred to as pEGFP-N1-hAGO2 (MT). The pEGFP-N1-His6 plasmid (a gift from Dr. Imre Mäger, Wood Lab) was utilised as a control GFP plasmid for AGO2 and TNRC6A co-transfection experiments.

2.4.3 TNRC6A Expression Plasmid

To assess the effect of increased cellular expression of TNRC6A, the pmyc-GFP-TNRC6A plasmid[388] was purchased from Addgene (Plasmid #41999). This plasmid contains the human TNRC6A protein fused to the C-terminus of pmyc-GFP.

2.5 Plasmid Cloning

2.5.1 shRNA Expression Plasmids

pU6-Neo shRNA expression plasmids expressing BACE1 or a nonspecific control shRNA were a gift from Dr. Thomas Roberts (Wood Lab). A further pU6-Neo shRNA expression plasmid expressing the APP1 siRNA sequence was designed using Serial Cloner v2.6.1 (SerialBasics). The following oligonucleotides were purchased from IDT in order to construct the APP shRNA expression plasmid: APP1 sense, 5'-CACCGTACCAACTTGCATGACTACCTGACCCATAGTCATGCAAGTTGGTAC and APP1 antisense, 5'-AAAAGTACCAACTTGCATGACTATGGGTCAGGTAGTC ATGCAAGTTGGTAC.

The oligonucleotides were phosphorylated and annealed in one step using 1 µl T4 Polynucleotide Kinase (PNK) Enzyme (New England Biolabs) and 2 µl each of sense and antisense 100 µM APP1 oligonucleotides per 20 µl reaction. The samples were phosphorylated by incubation at 37ºC for 30 minutes and then annealed by incubation at 95ºC for 5 minutes followed by cooling to 25ºC by 5ºC per minute using a G-Storm Quad Block Thermal Cycler (GMI). The pU6-Neo backbone was prepared by restriction digest with 1 µl *BbsI* and 1 µg pU6-Neo plasmid in 50 µl reactions. The digest was incubated at 37ºC for 1 hour followed by heat inactivation of the enzyme at 65ºC for 20 minutes. To prevent self-ligation, the digested plasmid was phosphatase treated. The following phosphatase mixture was prepared and added to the 50 µl restriction digest; 1 µl Antarctic Phosphatase Enzyme (New England Biolabs) and 5 µl Antarctic Phosphatase Buffer in 4 µl H_2O. The mixture was incubated at 37ºC for 1 hour followed

by heat inactivation at 65ºC for 20 minutes and the resulting product gel purified from a 1% agarose gel using the QIAquick Gel Extraction Kit (Qiagen) according to manufacturer's instructions. The purified digested pU6-Neo plasmid was then ligated with the previously annealed APP1 oligonucleotide using 100 ng plasmid backbone, a 4 x molar excess of the insert and 1.5 µl DNase Ligase (New England Biolabs) per 15 µl reaction. The ligation reaction was incubated for 1 hour at room temperature. 2 µl of the ligation mixture was then transformed in 50 µl Stellar Competent Cells (Clontech Laboratories) with heat shock for 1 minute at 42ºC followed by 2 minutes incubation on ice. 450 µl of S.O.C medium (Clontech) was added to the transformation mixture and incubated for 1 hour at 37ºC with shaking. 100 µl of transformation mixture was spread on lysogeny broth (LB)-Agar plates containing 100 µg/ml Ampicillin (Sigma-Aldrich) and incubated overnight at 37ºC. Resulting colonies were picked and grown in 5 ml LB containing 100 µg/ml Ampicillin overnight at 37ºC with shaking. The plasmid DNA was subsequently isolated using the QIAprep Spin Miniprep Kit (Qiagen) according to manufacturer's instructions and resuspended in 50 µl H_2O. Successful cloning was confirmed by sequencing (Source BioScience) using the primer; 5'-GGGTTATTGTCTCATGAGCG.

The APP, BACE1 and nonspecific control shRNA expression plasmids were constructed to express the same functional sequences as utilised for the corresponding siRNAs. The exact sequences cloned into the pU6-Neo shRNA expression plasmid are provided in **Table 2.4**.

Table 2.4 APP, BACE1 and Control pU6-Neo shRNA Sequences.

siRNA	Sense	Loop	Antisense
APP1 shRNA	caccGTACCAACTTGCATGACTA	CCTGACCCA	TAGTCATGCAAGTTGGTAC
BACE1 shRNA	caccGCTTTGTGGAGATGGTGGA	CCTGACCCA	TCCACCATCTCCACAAAGCT
Nonspecific shRNA	caccGATCGTCGATCGTAGCGCA	CCTGACCCA	TGCGCTACGATCGACGATGT

2.5.2 miRNA Expression Plasmids

Individual miRNA expression plasmids were constructed which expressed the primary transcripts for hsa-miR-17, hsa-miR-106b and hsa-miR-29a. The pri-miRNA sequence for each miRNA was subcloned between *BamH1* and *XhoI* restriction sites in the empty pCMV-miR Expression Plasmid (Origene Technologies). To obtain the primary transcript, the pre-miRNA sequence and ~200 base pairs of surrounding genomic sequence were identified for each miRNA using miRBase[549] and Ensembl Genome Browser (Release 71)[550]. A four base-pair string (TCGA) and *BamH1* restriction site (GGATCC) was added to the 5' end and a four base-pair string (CATG) and *XhoI* restriction site (CTCGAG) was added to the 3' end of each sequence. Insert sequences were purchased as "gBlocks Gene Fragments" from IDT and are provided in **Table 2.5**.

The inserts and plasmid were first prepared for cloning by double restriction digest at 37ºC for 1 hour with *BamH1* and *XhoI*. For the plasmid, 2.5 µg of pCMV-miR expression plasmid was digested in a total volume of 15 µl with 2 µl of each restriction enzyme. For the pri-miRNA inserts, 1 µg of gBlock Fragment was digested in a total volume of 15 µl with 1.5 µl of each restriction enzyme. The digested insert was then

purified using the QIAquick PCR Purification Kit (Qiagen) according to manufacturer's instructions. The digested pCMV-miR expression plasmid was phosphatase treated and gel purified using the QIAquick Gel Extraction Kit (Qiagen), as outlined above. The ligation reaction was performed with 50 ng digested pCMV-miR expression plasmid with a 5 x molar excess of insert in 20 µl reactions for 1 hour at room temperature. The ligation reaction was transformed in Stellar Competent Cells (Clontech Laboratories) as outlined above and 100 µl of the resulting mixture spread on LB-Agar plates containing 50 µg/ml Kanamycin (Sigma-Aldrich) and incubated overnight at 37ºC. Resulting colonies were picked and grown in 5 ml LB containing 50 µg/ml Kanamycin overnight at 37ºC with shaking. The plasmid DNA was subsequently isolated using the QIAprep Spin Miniprep Kit (Qiagen) according to manufacturer's instructions and resuspended in 50 µl H_2O. Successful cloning was confirmed by *BamH1* and *XhoI* double restriction digest and sequencing (Source BioScience) using the primer; 5'-CAACGGGACTTTCCAAAATG.

Table 2.5 Pri-miRNA Transcript Sequences for pCMV-miR Expression Plasmid Cloning.

miRNA	Sequence
hsa-miR-17-5p	tcgaGGATCC_CTTTGAGATAATTAAACTAATTTTTTCTTCCCCATTAGG GATTATGCTGAATTTGTATGGTTTATAGTTGTTAGAGTTTGAGGTGTT AATTCTAATTATCTATTTCAAATTTAGCAGGAAAAAAGAGAACATCAC CTTGTAAAACTGAAGATTGTGACCAGTCAGAATAATGTCAAAGTGCTT ACAGTGCAGGTAGTGATATGTGCATCTACTGCAGTGAAGGCACTTGT AGCATTATGGTGACAGCTGCCTCGGGAAGCCAAGTTGGGCTTTAAAG TGCAGGGCCTGCTGATGTTGAGTGCTTTTTGTTCTAAGGTGCATCTAG TGCAGATAGTGAAGTAGATTAGCATCTACTGCCCTAAGTGCTCCTTCT GGCATAAGAAGTTATGTATTCATCCAATAATTCAAGCCAAGCAAGTA TATAGGTGTTTTAATAGTTTTTGTTTGCAGTCCTCTGTTAGTTTTGCAT AGTTGCACTA_CTCGAGcatg
hsa-miR-29a-5p	tcgaGGATCC_AGGATACCAAGGGATGAATGTAATTGTACAGGATATCG CATTGTTGGAATTTTATACTTCTTTGTGGAATAAACCTATAGCACTTA ATAGATAGTACAGACTCATTCCATTGTGCCTGGGTTAAAGAGCCCAAT GTATGCTGGATTTAGTAAGATTTGGGCCCTCCCAACCCTCACGACCTT CTGTGACCCCTTAGAGGATGACTGATTTCTTTTGGTGTTCAGAGTCAA TATAATTTTCTAGCACCATCTGAAATCGGTTATAATGATTGGGGAAGA GCACCATGATGCTGACTGCTGAGAGGAAATGTATTGGTGACCGTTGG GGCCATGGACAAGAACTAAGAAAACAAATGCAAAGCAATAATGCAA AGGTGATTTTTCTTCTTCCAGTTTCTAAGTTGAATTTCACTGACCTGAA TTGCATGTGGTATAATACTAACAAATGGTTCACTATTAGCATATCATG AAT_CTCGAGcatg
hsa-miR-106b-5p	tcgaGGATCC_CAGCATACGTGGAGATGAGGCGAGAGGCTTGGGCTAGT AAGGATGCCACCTATACTTCTGCCCGGACCCTGCTGGCTATCCTGCGC CTTTCCACTGCTCTGGTAAGTGCCCAAATTGCTGGAGGGCCATCTGTT TTGACCCTTAAAGGGGTAGCTCCTTACCGTGCTCTCATTGCCGCCTCC CCACCTCCCGCTCCAGCCCTGCCGGGGCTAAAGTGCTGACAGTGCAG ATAGTGGTCCTCTCCGTGCTACCGCACTGTGGGTACTTGCTGCTCCAG CAGGGCACGCACAGCGTCCGTGGAGGGAAAGGCCTTTTCCCCACTTC TTAACCTTCACTGAGAGGGTGGTTGGGGTCTGTTTCACTCCATGTGTC CTAGATCCTGTGCTACAGACCTTCCTTTCTGTCCTCCCGTCTTGGACCT CAGTCCTGGGGGCTCCAAAGTGCTGTTCGTGCAGGTAGTGTGATTACC CAACCTACTGC_CTCGAGcatg

2.5.3 *APP* and *BACE1* 3' UTR Dual-Luciferase Reporter Plasmids

Dual-luciferase reporter plasmids were constructed which comprised the full length 3' UTR of either *APP* or *BACE1* subcloned downstream of *Renilla* luciferase between *XhoI* and *NotI* restriction sites in the psiCHECK-2 plasmid (Promega). This plasmid contains Firefly luciferase as an internal normalisation control. The full 3' UTRs of *APP* and *BACE1* were identified using Ensembl Genome Browser (Release 70)[550]. Forward and reverse PCR primers for *APP* and *BACE1* 3' UTRs were custom designed using Primer3[551] and purchased from IDT (**Table 2.6**). The forward primers contained a six base-pair string (AGAGAG) and an *XhoI* restriction site (CTCGAG) at the 5' end while reverse primers contained a six base-pair string (AGAGAG) and a *NotI* restriction site (GCGGCCGC) at the 5' end.

Table 2.6 Primers for Amplification of *APP* and *BACE1* 3' UTR.

Primer	Sequence
APP Forward	AGAGAGCTCGAGACCCCCGCCACAGCAGCC
APP Reverse	AGAGAGGCGGCCGCTGCTCCTCCAAGAATGTATTTATTTACATG
BACE1 Forward	AGAGAGCTCGAGTGATGACATCTCCCTGCTGA
BACE1 Reverse	AGAGAGGCGGCCGCAACCCTAGTAGTTTGACTTCTTATTGAATA

APP and *BACE1* 3' UTRs were PCR amplified from human genomic DNA using the KAPA HiFi PCR Kit (Kapa Biosystems) in 25 µl reactions according to manufacturer's instructions. Each 25 µl reaction comprised 0.5 µl KAPA HiFi DNA Polymerase, 0.3 µM forward and reverse primers, 5 µl GC KAPA HiFi buffer and 10 ng of human genomic DNA. PCR amplification was performed using a G-Storm Quad Block Thermal Cycler (GMI) under the parameters provided in **Table 2.7**.

Table 2.7 PCR Parameters for Amplification of *APP* and *BACE1* 3' UTR.

Step	Temperature	Duration	Number of Cycles
Initial Denaturation	95ºC	3 minutes	1
Denaturation	98ºC	20 seconds	35
Annealing	60ºC	15 seconds	
Extension	72ºC	1 minute (APP) 4 minutes (BACE1)	
Final extension	72ºC	1 minute (APP) 4 minutes (BACE1)	1
Cooling	4ºC	-	-

The amplified PCR product was gel purified using the QIAquick Gel Extraction Kit (Qiagen) as outlined above and resuspended in 40 µl H_2O. The purified PCR product and Psicheck-2 plasmid were prepared for ligation by double restriction digest at 37ºC for 1 hour with *XhoI* and *NotI*. 40 µl of purified PCR product was digested in 50 µl reactions with 2 µl of each restriction enzyme while 2.5 µg of Psicheck-2 plasmid was digested in 100 µl reactions with 2.5 µl of each enzyme. Ligation of the digested 3' UTR insert and Psicheck-2 plasmid was performed at room temperature for 1 hour in 20 µl reactions with 2 µl of digested plasmid to 6 µl of 3' UTR insert. The ligation reaction was then transformed in Stellar Competent Cells (Clontech Laboratories) as outlined above. 100 µl of the ligation reaction was spread on LB-Agar plates containing 100 µg/ml Ampicillin (Sigma-Aldrich) and incubated overnight at 37ºC. Resulting colonies were picked and grown in 5 ml of LB containing 100 µg/ml Ampicillin overnight at 37ºC with shaking. The plasmid DNA was isolated using the QIAprep Spin Miniprep Kit (Qiagen) according to manufacturer's instructions and resuspended in 50 µl H_2O.

Successful cloning was confirmed by *XhoI* and *NotI* double restriction digest and sequencing (Source BioScience) using the primers provided in **Table 2.8**.

Table 2.8 Sequencing Primers for *APP* and *BACE1* 3' UTR Luciferase Reporter Plasmids.

Primer	Sequence
***BACE1* 3' UTR Forward 1**	CGCTATTGTCGAGGGAGCTA
***BACE1* 3' UTR Forward 2**	GGCTGGAAAGAGGAGAAGGA
***BACE1* 3' UTR Forward 3**	ATGTCCTCCACCACAAGAGC
***BACE1* 3' UTR Forward 4**	AGTTACTTCCTTCCTGCCCC
***BACE1* 3' UTR Forward 5**	GCCACTCCAATCACCCTACA
***BACE1* 3' UTR Forward 6**	CAGACATCTCCTCACCCCAG
***APP* 3' UTR Forward 1**	CGCTATTGTCGAGGGAGCTA
***APP* 3' UTR Forward 2**	ACGTTTGTTTCTTCGTGCCT

2.5.4 miRNA Target Sequence Dual-Luciferase Reporter Plasmids

To improve the detection sensitivity of luciferase reporter regulation, 3 further miRNA dual-luciferase reporter plasmids were constructed. These plasmids comprised a "target" sequence containing four repeats exactly complementary to the mature miRNA sequence for hsa-miR-17, hsa-miR-106b and hsa-miR-29a. The desired target sequence was subcloned into the pmirGLO Dual-Luciferase miRNA Target Expression Plasmid (Promega) downstream of Firefly luciferase between *PmeI* and *XbaI* restriction sites with *Renilla* luciferase as a normalisation control. Sequences were designed to include the digested *PmeI* restriction site (AAAC) at the 5' end followed by a *NotI* internal restriction site for confirmation of clones (GCGGCCGC). This was followed by a four base-pair string (TAGT) and four repeats of the appropriate mature miRNA complement sequence with each repeat separated by a six base-pair string (GATATC).

The digested *Xbal* restriction site (T) was included at the 3' end. The full sequences were purchased as Ultramer DNA Oligos from IDT and are provided in **Table 2.9**. Sense and antisense oligonucleotides were phosphorylated individually at 37ºC for 1 hour with 2 µl T4 Polynucleotide Kinase (PNK) Enzyme (New England Biolabs) and 2 µl of 100 µM oligonucleotide per 20 µl reaction. 10 µl of phosphorylated sense and antisense oligonucleotides were then combined and annealed by incubation at 95ºC for 3 minutes followed by cooling to 25ºC by 5ºC per minute using a G-Storm Quad Block Thermal Cycler (GMI). The resulting annealed oligonucleotides were diluted 1:25 in nuclease-free H_2O. The pmirGLO dual-luciferase plasmid was prepared for ligation by double restriction digest at 37ºC for 1 hour with *PmeI* and *XbaI* followed by phosphatase treatment, as described previously. Ligation was performed at room temperature for 1 hour in a total volume of 20 µl with 100 ng of digested plasmid and a 3 x molar excess of target sequence insert. The ligation reaction was transformed in 50 µl Stellar Competent Cells (Clontech Laboratories) as outlined above and 100 µl spread on LB-Agar plates containing 100 µg/ml Ampicillin (Sigma-Aldrich) and grown overnight. Resulting colonies were grown in 5 ml of LB containing 100 µg/ml Ampicillin overnight at 37ºC with shaking. The plasmid DNA was isolated using the QIAprep Spin Miniprep Kit (Qiagen) according to manufacturer's instructions and resuspended in 50 µl H_2O. Successful cloning was confirmed by single restriction digest with *NotI* and by sequencing (Source BioScience) using the primer; 5'-TGAAGAGCCTGATCAAATA.

Table 2.9 miRNA Sequences for pmirGLO Dual-Luciferase Target Reporter Plasmids.

Corresponding miRNA	Sequence
hsa-miR-17-5p Sense	AAACTAGCGGCCGCTAGTCTACCTGCACTGTAAGCACTTTG GATATCCTACCTGCACTGTAAGCACTTTGGATATCCTACCTG CACTGTAAGCACTTTGGATATCCTACCTGCACTGTAAGCACT TTGT
hsa-miR-17-5p Antisense	ACAAAGTGCTTACAGTGCAGGTAGGATATCCAAAGTGCTTA CAGTGCAGGTAGGATATCCAAAGTGCTTACAGTGCAGGTAG GATATCCAAAGTGCTTACAGTGCAGGTAGACTAGCGGCCGC TAGTTT
hsa-miR-29a-5p Sense	AAACTAGCGGCCGCTAGTCTGAACACCAAAAGAAATCAGTG ATATCCTGAACACCAAAAGAAATCAGTGATATCCTGAACAC CAAAAGAAATCAGTGATATCCTGAACACCAAAAGAAATCAG TT
hsa-miR-29a-5p Antisense	AACTGATTTCTTTTGGTGTTCAGGATATCACTGATTTCTTTTG GTGTTCAGGATATCACTGATTTCTTTTGGTGTTCAGGATATC ACTGATTTCTTTTGGTGTTCAGACTAGCGGCCGCTAGTTT
hsa-miR-106b-5p Sense	AAACTAGCGGCCGCTAGTATCTGCACTGTCAGCACTTTAGAT ATCATCTGCACTGTCAGCACTTTAGATATCATCTGCACTGTC AGCACTTTAGATATCATCTGCACTGTCAGCACTTTAT
hsa-miR-106b-5p Antisense	ATAAAGTGCTGACAGTGCAGATGATATCTAAAGTGCTGACA GTGCAGATGATATCTAAAGTGCTGACAGTGCAGATGATATC TAAAGTGCTGACAGTGCAGATACTAGCGGCCGCTAGTTT

Underlined sequence indicates reverse complement miRNA target sequence.

2.5.5 Membrane-associated TNRC6A Expression Plasmid

Overlap extension PCR cloning[552] was utilised to construct a membrane-associated (MT) form of TNRC6A using the pmyc-GFP-TNRC6A plasmid[388] (Addgene, Plasmid #41999). To create a "membrane tag" to direct TNRC6A to the membrane, an acylation domain[553–556] (ATGGGCTGCATTAACAGCAAACGCAAAGAT) was inserted into the N-terminal region of the pmyc-GFP-TNRC6A fusion protein. To achieve this, two sets of primers were custom designed according to the principles of primer design for overlap extension PCR cloning (**Fig. 2.2**). The forward plasmid primer contained the reverse complement of the acylation domain sequence at the 5' end and the reverse

complement of the overlapping plasmid sequence at the 3' end while the reverse plasmid primer comprised the 3' end sequence of the TNRC6A protein. The forward insert primer comprised the acylation domain sequence at the 5' end and an overlapping plasmid sequence at the 3' end. The reverse insert primer was the reverse complement of the reverse plasmid primer. The full primers were purchased as DNA oligonucleotides from IDT and are provided in **Table 2.10**.

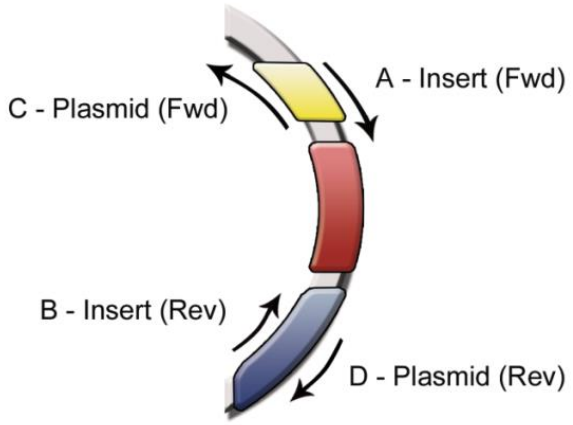

Figure 2.2 Primer Design for Overlap Extension PCR Cloning of the Membrane-associated TNRC6A Plasmid. The acylation domain was inserted into the N-terminal region of the fusion protein in the pmyc-GFP-TNRC6A plasmid[388] using custom designed primers. **(A)** The forward ("Fwd") insert primer comprised the acylation domain sequence at the 5' end and an overlapping plasmid sequence at the 3' end. **(B)** The reverse ("Rev") insert primer contained the reverse complement sequence from the 3' end of the TNRC6A protein. **(C)** The forward plasmid primer comprised the reverse complement of the acylation domain sequence at the 5' end and the reverse complement of the overlapping plasmid sequence at the 3' end. **(D)** The reverse plasmid primer comprised the sequence from the 3'end of the TNRC6A protein.

Table 2.10 Overlap Extension Primers for Membrane-associated TNRC6A Plasmid.

Primer	Sequence
Insert Forward	ATGGGCTGCATTAACAGCAAACGCAAAGATGAA CAAAAACTCATCTCAGAAGAGGATCTG
Insert Reverse	TCTAGATTACATGGACTCTCCACCCCCACCCAG
Plasmid Forward	ATCTTTGCGTTTGCTGTTAATGCAGCCCATCATT GGTGGGCTAGCCAGCTTGGG
Plasmid Reverse	CTGGGTGGGGGTGGAGAGTCCATGTAATCTAGA

Two separate PCR reactions were performed with each pair of primers using Phusion High-Fidelity DNA Polymerase (New England Biolabs) in 50 µl reactions. Each 50 µl reaction contained 2.5 µl each of 10 µM forward and reverse primer (either plasmid or insert pair) and 10 ng of the pmyc-GFP-TNRC6A template DNA. The PCR reaction was conducted using a G-Storm Quad Block Thermal Cycler (GMI) with the parameters provided in **Table 2.11**.

Table 2.11 Parameters for PCR Cloning of Membrane-associated TNRC6A Plasmid.

Step	Temperature	Duration	Number of Cycles
Initial Denaturation	98ºC	30 seconds	1
Denaturation	98ºC	10 seconds	30
Annealing	72ºC	30 seconds	
Extension	72ºC	160 seconds (plasmid PCR) 180 seconds (insert PCR)	
Final extension	72ºC	10 minutes	1
Cooling	4ºC	-	-

The resulting PCR products were gel purified using QIAquick Gel Extraction Kit (Qiagen) according to manufacturer's instructions. The two PCR products were then combined together using the Gibson Assembly method[557] and Gibson Assembly Master Mix (New England, Biolabs) in 20 µl reactions at 50ºC for 60 minutes. Each reaction contained 100 ng of plasmid PCR product to 300 ng of insert PCR product and 10 µl of Gibson Master Mix. 2 µl of assembled product was transformed in 50 µl of Stellar Competent Cells (Clontech Laboratories), as above, and 100 µl of transformation mixture was spread onto LB-Agar plates containing 100 µg/ml Ampicillin (Sigma-Aldrich) and incubated overnight at 37ºC. Resulting colonies were grown in 5 ml of LB containing 100 µg/ml Ampicillin overnight at 37ºC with shaking. The plasmid DNA was isolated using the QIAprep Spin Miniprep Kit (Qiagen) according to manufacturer's instructions and resuspended in 50 µl H_2O. Successful insertion of the membrane-targeting domain was confirmed by sequencing (Source Bioscience) using the primers in **Table 2.12**.

Table 2.12 Sequencing Primers for Membrane-associated TNRC6A Plasmid.

Primer	Sequence
TNRC6A Insert Forward 1	CCCTATGGTGCACTCTCAGT
TNRC6A Insert Forward 2	CAACGGGACTTTCCAAAATG
TNRC6A Insert Forward 3	ACCACTACCAGCAGAACACC
TNRC6A Insert Forward 4	ATCCTCAGATGCAGGCTCC
TNRC6A Insert Forward 5	ATCCCAAACCTGCTCTGAGG
TNRC6A Insert Forward 6	GGTAAGCCCATAGACAGTGGT
TNRC6A Insert Forward 7	ACCAGCTTTCTCAGATCTCCC
TNRC6A Insert Forward 8	AGGTCCCTTTGCCACCTAAA
TNRC6A Insert Reverse 1	TTGTCTTCCCAATCCTCCCC

2.6 Cell Culture

Immortalised Cell Lines

Neuro2A (mouse neuroblastoma cell line), HEK293T (human embryonic kidney cell line containing SV40 Large T-antigen) and HeLa (human epithelial cell line) cells were cultured in Dulbecco's Modified Eagle Medium (DMEM, Life Technologies) supplemented with 10% Fetal Bovine Serum (FBS) (Life Technologies) and 1% antibiotic/antimycotic (Life Technologies). SH-SH5Y cells (human neuroblastoma cell line) were cultured in DMEM supplemented with 10% Hyclone FBS (U.S.) Defined (GE Healthcare Life Sciences) and 1% antibiotic/antimycotic. BE(2)-M17 cells (human neuroblastoma cell line) were cultured in Opti-MEM Reduced Serum Medium (Life Technologies) supplemented with 10% FBS and 1% antibiotic/antimycotic. HEK293 APPswe cells (HEK293 cells stably transfected with the human Swedish mutation of APP_{695}[18]) were a gift from Professor Christian Haass (University of Munich). HEK293 APPswe cells were cultured in DMEM supplemented with 10% FBS, 1% L-Glutamine (Life Technologies), 1% antibiotic/antimycotic and 200 µg/ml G418 (Life Technologies). All cells were incubated at 37°C in 5% CO_2.

Primary Dendritic Cell Culture

All animal procedures were conducted at the Biomedical Sciences Unit, University of Oxford, according to the regulations of the Animals (Scientific Procedures) Act (1986) authorised by the UK Home Office. Bone-marrow-derived dendritic cells (BM-DCs) were harvested from the murine bone marrow from either C57BL/6 or CBA 9-week-old

male mice (The Jackson Laboratory) and cultured for 8 days in 6-well cell culture plates, seeded at a density of 3 x 10^6 cells/well. BM-DCs were maintained in DMEM supplemented with 10% FBS, 10% GM-CSF (Life Technologies) and 1% antibiotic/antimycotic and incubated at 37°C in 5% CO_2.

2.7 Transfections

2.7.1 Transfection of EV-secreting BM-DCs with Targeting Plasmids

BM-DCs were transfected 4 days after plating with 5 μg/well targeting plasmid, pEGFP-C1-Lamp2B-RVG, or the control plasmid, pEGFP-C1-Lamp2B, using 5 μl TransIT LT1 transfection reagent (Mirus Bio) according to manufacturer's instructions. Briefly, 5 μg plasmid DNA was added to 250 μl Opti-MEM Reduced-Serum Medium (Life Technologies) before 5 μl TransIT LT1 transfection reagent was added to the diluted DNA. The mixture was incubated at room temperature for 20 minutes before addition to cells. After 4 hours, the medium was removed and fresh medium added to each well. On day 7, medium was changed to fresh DMEM supplemented with 10% EV-depleted FBS (pre-spun at 120,000 x g for 70 minutes to remove bovine EVs) and 1% antibiotic/antimycotic. Cell culture supernatant containing BM-DC-secreted EVs was harvested 24 hours later by differential ultracentrifugation (**Fig. 2.3**).

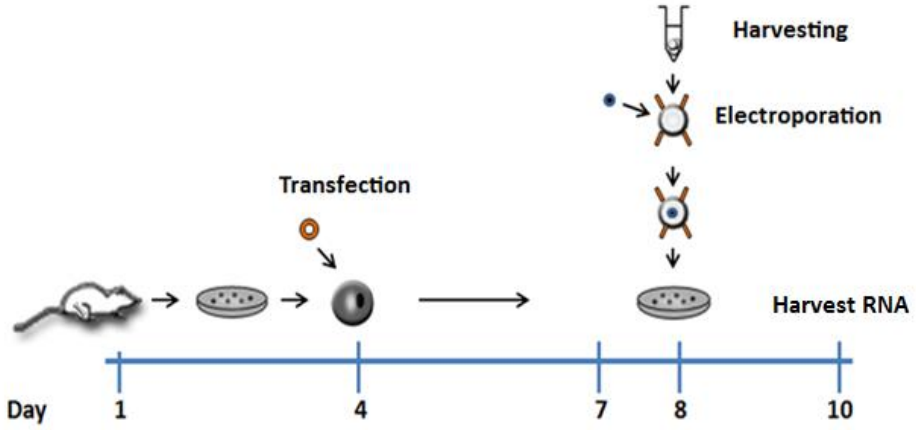

Figure 2.3 BM-DC-derived Extracellular Vesicle Isolation, Transfection and Harvesting Protocol. BM-DCs were harvested from 9-week-old male mice and cultured for 8 days in 6-well cell culture plates. On day 4, BM-DCs were transfected with 5 µg/well targeting plasmid using TransIT LT1 transfection reagent. On day 7, medium was replaced with fresh EV-depleted DMEM medium. BM-DC-secreted EVs were harvested 24 hours later from the cell culture supernatant via ultracentrifugation, loaded with siRNA by electroporation and applied to recipient cells. RNA was harvested from cells after 48 hours and gene expression assessed by qPCR.

2.7.2 Transfection of EV-secreting Neuro2As with Targeting Plasmids

EV-secreting Neuro2A source cells were plated at a density of 5 x 10^6 cells/15 cm cell culture dish (Corning) in DMEM supplemented with 10% FBS. After 24 hours, cells were transfected with 25 µg of the targeting plasmid, pEGFP-C1-Lamp2B-RVG, or the control plasmid, pEGFP-C1-Lamp2B, using 75 µl TransIT LT1 transfection reagent (Mirus Bio) diluted in 1 ml Opti-MEM. Four hours later, the medium was replaced with fresh DMEM supplemented with 10% EV-depleted FBS and 1% antibiotic/antimycotic. Neuro2A-secreted EVs were harvested by differential ultracentrifugation after 48 hours.

2.7.3 Transfection of small RNAs and Expression Plasmids

For validation of target gene silencing by siRNAs/shRNA expression plasmids or regulation of reporter plasmids by miRNA mimics/miRNA expression plasmids, cells were forward transfected using Lipofectamine 2000 (Life Technologies). HEK293T cells were plated at a density of 1 x 10^5 cells/well in 24-well cell culture plates in 400 µl DMEM supplemented with 10% FBS and incubated for 24 hours. After 24 hours, transfection complexes were prepared as follows; the required quantity of RNA/DNA was diluted in 50 µl Opti-MEM while 1.5 µl Lipofectamine 2000 was separately diluted in 50 µl Opti-MEM per replicate required. The mixtures were incubated for 5 minutes at room temperature before they were combined. The combined mixture was incubated for a further 20 minutes to allow complex formation before 100 µl was applied per well of the 24-well cell culture plate. After 4 hours, the medium was changed to fresh DMEM supplemented with 10% FBS without antibiotics. For siRNA/shRNA experiments, cells were incubated for 48 hours prior to cell harvesting while for miRNA experiments, cells were incubated for 24 hours before they were harvested for luciferase assay.

For endogenous exosomal loading experiments, typically performed in 15 cm cell culture dishes, cells were forward transfected using Polyethylenimine (PEI) (Sigma-Aldrich) as the transfection reagent at a ratio of 4 µg PEI: 1 µg RNA/DNA. Stock solutions of PEI at 4 mg/ml were prepared using nuclease-free H_2O, purified by filtration through 0.2 µm filters (Millipore) and stored at -20ºC in 1 ml aliquots. HEK293T cells were plated at a density of 6 x 10^6 cells/15 cm cell culture dish in DMEM supplemented with 10% FBS and incubated for 24 hours. After 24 hours, the transfection complexes were prepared. The required quantity (as stated for individual

experiments in the Results section) and combination of siRNA/miRNA mimics, miRNA/shRNA expression plasmids and/or AGO2/TNRC6A expression plasmids were diluted in 500 µl Opti-MEM. The required quantity of PEI was separately diluted in 500 µl Opti-MEM and incubated for 5 minutes. The diluted PEI was then added to the diluted RNA/DNA and incubated for a further 20 minutes to allow complex formation. 1 ml of the RNA/DNA and PEI complex was added per 15 cm cell culture dish. After 4 hours, the medium was removed and cells were washed once with Opti-MEM before the medium was replaced with Opti-MEM supplemented with 1% antibiotic/antimycotic. After 48 hours, the supernatant was collected and EVs isolated by differential ultracentrifugation, as outlined below. For co-culture experiments where transfections were performed in smaller volumes, the RNA/DNA and PEI dilutions were scaled from the quantities indicated above according to surface area.

2.7.4 Transfection of LNA-ASOs

For all LNA-ASO experiments, cells were reverse transfected using Lipofectamine 2000 according to manufacturer's instructions. Prior to transfection, cell culture plates were pre-coated with Poly-L-Lysine (Sigma-Aldrich) according to manufacturer's instructions, washed with Phosphate Buffered Saline (PBS) (Life Technologies) and allowed to air-dry for 1 hour. For transfections performed in 24-well cell culture plates, the required quantity of LNA-ASO was diluted up to 20 µl with Opti-MEM directly in each well. Separately, a mastermix comprising 0.75 µl Lipofectamine 2000 diluted in 44.25 µl Opti-MEM per well required was incubated for 5 minutes at room temperature. After 5 minutes, 45 µl of diluted Lipofectamine 2000 was added to each well with the diluted LNA-ASO molecules and mixed gently. The mixture was incubated for 15

minutes at room temperature to allow for complex formation. Following incubation, 2 x 10^5 cells (SH-SH5Y and HEK293 APPswe cells) or 1.5 x 10^5 cells (Neuro2A cells) were added per well in 435 µl of the appropriate growth medium supplemented only with 10% FBS (except for HEK293 APPswe cells where complete growth medium was applied). Typically, cells were incubated for 48 hours before they were harvested and RNA extracted. For transfections performed in different sized cell culture plates, transfection quantities were scaled from those indicated above according to surface area.

2.8 Extracellular Vesicle Isolation

EV-containing supernatant was collected and spun at 300 x g for 5 minutes, 2000 x g for 10 minutes and filtered through 0.2 µm filters (Millipore) to remove cell debris before a final spin at 120,000 x g for 70 minutes to pellet EVs. The pellet was resuspended in 100 µl 0.1 M ammonium acetate or PBS, as indicated. Where appropriate after pelleting, 75 µl of supernatant was also collected for further analysis.

2.9 Extracellular Vesicle Characterisation

Electron Microscopy

10 µl of EV sample was applied to Formvar/Carbon coated 200 Mesh Nickel grids (Agar Scientific) for 15 minutes before negative staining with 10 µl of 2% uranyl acetate diluted in distilled water. The grid was then washed with deionised H_2O to remove excess solution and salt from the preparation. The preparation was analysed

with a JEOL JEM-1010 transmission electron microscope at an accelerating voltage of 80 kV, with 1 second exposure and magnifications as indicated.

Nanoparticle Tracking Analysis

The particle size distribution and concentration of EV preparations was measured by nanoparticle tracking analysis (NTA) using the Nanosight NS500 system (NanoSight). This system relates the rate of particle Brownian motion to particle size given that particle movement is determined by the temperature and size of the particle and the viscosity of the liquid. As temperature and viscosity are controlled parameters, the system allows the visualisation, tracking and analysis of particles based upon the light scattered during motion. The rate of tracked particle movement permits the calculation of particle size through the Stokes-Einstein equation by integrated system software. For NTA analysis, 20 µl of EVs resuspended in PBS were first diluted to 500 µl with PBS. If required, EV samples were further diluted with PBS to achieve an optimal measurement concentration of between 5-10 x 10^8 particles/ml. Three 30 second videos tracking particle movement under Brownian motion were recorded and used to calculate particle size and concentration in each EV preparation using the integrated Nanosight NS500 software. The software settings for analysis were; camera level, 14, detection threshold, 5, particle size, 50 nm, minimum track length, 10, blur, auto, screen gain, 10.

Western Blotting

For cells, an equal quantity of protein was diluted up to 20 µl in protein extraction buffer (recipe below) and added to 20 µl 2x Laemmli Sample Buffer (Bio-Rad) supplemented with 5% β-mercaptoethanol (Sigma-Aldrich). For EVs, 20 µl of EV sample was added to 20 µl 2x Laemmli Sample Buffer supplemented with 5% β-mercaptoethanol. Cell and EV samples were heated for 10 minutes at 100°C to denature proteins. 30 µl of sample was then loaded onto a 10% polyacrylamide gel and run at 150 V for 75 minutes to separate proteins. The Immobilon-FL PVDF membrane (Merck Millipore) was soaked in methanol for 1 minute prior to gel to PVDF membrane transfer. Transfer was performed at 100 V for 70 minutes using the Bio-Rad transfer system. Membranes were blocked with 5% non-fat dry milk in TBST or 5% BSA in TBST (phosphorylated proteins) for 1 hour at room temperature with shaking before application of primary antibodies (Abcam) (**Table 2.13**). Primary antibodies were diluted in the respective blocking agent and incubated for 2 hours at room temperature or for 16 hours at 4ºC with shaking. The membrane was then washed for 3 x 10 minutes in TBST before incubation with the secondary antibody for 1 hour at room temperature with shaking. Secondary antibodies used were IRDye 680RD goat anti-rabbit IgG (LI-COR Biosciences) and IRDye 800CW goat anti-mouse IgG (LI-COR Biosciences) at a 1:10,000 concentration in TBST supplemented with 0.01% SDS. When multiple blotting of the same membrane was desired, blots were stripped with Restore PLUS Western Blot Stripping Buffer (Life Technologies) for 15 minutes at room temperature with shaking. Blots were washed in TBST and blocked again in the appropriate blocking agent for 1 hour at room temperature before the next primary antibody was

applied. Western blots were imaged using the Odyssey Fc Imaging System (LI-COR Biosciences).

Table 2.13 Primary Antibodies used for Western Blot Analysis.

Antibody	Host	Product Code	Expected Band Size	Dilution
Anti-AGO2	Rabbit polyclonal	ab32381	87 kDa	1:500
Anti-ALIX	Mouse monoclonal	ab117600	96 kDa	1:1000
Anti-APP	Rabbit polyclonal	ab15272	97 kDa	1:1000
Anti-BACE1	Rabbit polyclonal	ab2077	70 kDa	1:500
Anti-β-Actin	Mouse monoclonal	ab82618	42 kDa	1:200
Anti-Calnexin	Rabbit polyclonal	ab22595	75 kDa	1:1000
Anti-Flotillin 1	Rabbit polyclonal	ab41927	47 kDa	1:1000
Anti-GSK3β	Rabbit monoclonal	ab32391	46 kDa	1:10,000
Anti-GW182 (TNRC6A)	Rabbit polyclonal	ab84403	182 kDa	1:200
Anti-mTOR	Mouse monoclonal	ab87540	289 kDa	1:1000
Anti-Tau (pS396)	Rabbit monoclonal	ab109390	79 kDa	1:1000
Anti-Tau (total)	Rabbit monoclonal	ab32057	79 kDa	1:1000
Anti-TSG101	Rabbit polyclonal	ab30871	49 kDa	1:1000

2.10 Microscopy

To monitor transfection efficiency and to determine the localisation of membrane and non-membrane associated constructs, cells were imaged using an EVOS XL Core digital microscope (Electron Microscopy Sciences). GFP and phase images were captured and overlayed using the integrated computer software.

2.11 Loading of siRNA into Extracellular Vesicles by Electroporation

For In Vitro Use

EVs corresponding to 18-30 μg of protein, as measured by the Bradford Protein Assay Kit (Sigma-Aldrich) according to manufacturer's instructions, and 300 pmol BACE1 siRNA were diluted in 400 μl electroporation buffer (1.15 mM potassium phosphate pH 7.2, 25 mM potassium chloride, 21% Optiprep) and electroporated in a 4 mm cuvette (400 V, 125 μF) using a Bio-Rad Gene Pulser (Bio-Rad). Identical non-electroporated mixtures were used as a control. The electroporation mixture was diluted in 2 ml PBS and pelleted in 2 ml Quick Seal Ultracentrifugation Tubes (Beckman Coulter) by ultracentrifugation at 120,000 x g for 70 minutes. Pelleted EVs were either resuspended in 300 μl Opti-MEM and split equally between 3 wells of recipient Neuro2A cells, plated 24 hours previously at a density of 5 x 10^4 cells/well in 24-well cell culture plates, or resuspended in 80-100 μl PBS and stored for downstream analyses. Recipient cells were incubated for 48 hours before they were harvested for RNA analysis.

For In Vivo Use

The total yield of BM-DC-derived EVs from cells obtained from the equivalent of 1.5 mice was electroporated with 150 μg BACE1 siRNA per treated mouse. For electroporation, the EV and siRNA mixture was divided into aliquots containing 12 μg siRNA per 400 μl electroporation buffer and electroporated as above. Electroporated samples were then pooled, washed with PBS and pelleted by ultracentrifugation at 120,000 x g for 70 minutes. The EV pellet and naked siRNA was resuspended in a

volume of 5% glucose corresponding to 80 µl per mouse and administered intravenously via tail vein injections to 9 week-old male C57BL/6 mice. Untreated control mice received a 5% glucose control injection of the same volume. Mice were sacrificed after 48 hours and tissues immediately dissected, snap frozen in ice-cold isopentane and stored at -80ºC for later processing. The tissues harvested were cortex, striatum, midbrain, cerebellum, kidney, liver, spleen, heart and the tibialis anterior muscle.

2.12 Exploitation of Endogenous Extracellular Vesicle Loading Machinery

HEK293T cells to be used as EV-secreting source cells were plated at a density of 6 x 10^6 cells/15 cm cell culture dish. After 24 hours, cells were transfected with the required quantity and combination of siRNA, miRNA mimics or miRNA/shRNA expression plasmids and/or RNA-binding protein expression plasmids. After 4 hours, the medium was removed and cells were washed once with Opti-MEM before the medium was replaced with Opti-MEM supplemented with 1% antibiotic/antimycotic. The cells were incubated for 48 hours to allow expression and EV-packaging of transfected molecules before EVs were isolated as above. Cells were also collected for RNA analysis using 500 µl TRIzol (Life Technologies) (**Fig. 2.4**).

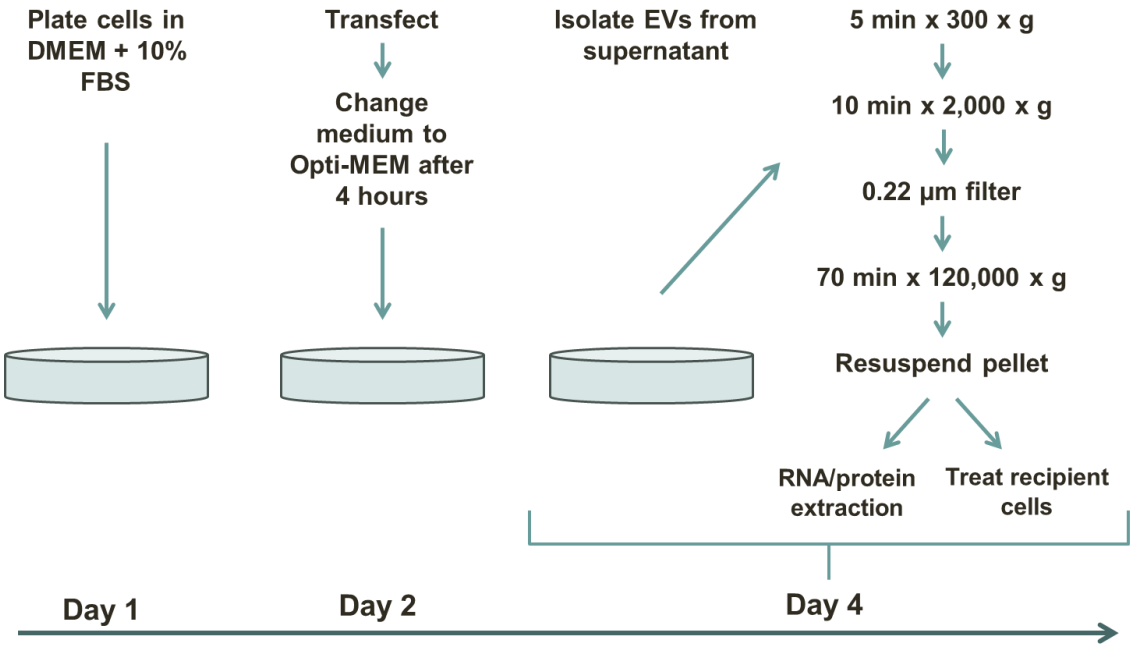

Figure 2.4 Method for Exploiting Endogenous Extracellular Vesicle Loading Capabilities. EV source cells were plated in 15 cm cell culture dishes on day 1. Cells were transfected with the relevant constructs 24 hours later. Following 4 hours incubation, the cells were washed and the medium changed to Opti-MEM. After 48 hours, EVs were isolated from the supernatant according to the differential ultracentrifugation protocol and the resulting pellet resuspended and either processed for downstream analysis or applied to recipient cells.

2.13 Co-culture Assay

For co-culture experiments, recipient HEK293T cells were first seeded in 6-well cell culture plates at a confluency of 1 x 10^6 cells/well while source HEK293T cells were seeded directly into 24-well cell culture plates at a confluency of 1 x 10^5 cells/well in 500 µl DMEM supplemented with 10% FBS. After 24 hours, recipient cells were transfected with 2 µg of the appropriate dual-luciferase target reporter plasmid for miRNA experiments or left untreated for shRNA experiments. Source cells were transfected with 500 ng of each required plasmid. After a further 24 hours, recipient cells were split into 24-well cell culture plate inserts at a ratio of 1:30 in 200 µL DMEM supplemented with 10% FBS. 24-Well Thinsert, 0.4 µm pore diameter inserts (Greiner

Bio-One) were chosen to allow movement of material less than 0.4 µm between source cells plated in the lower 24-well plate layer and recipient cells plated in the upper insert. After recipient cells had adhered, inserts were placed in the appropriate source cell well before source and recipient cells were incubated together for 24-72 hours as indicated. Recipient cells were harvested with 30 µl Passive Lysis Buffer (Promega) for luciferase experiments or 500 µl TRIzol (Life Technologies) for RNA analysis.

2.14 Recipient Cell Treatment with Endogenously Loaded Isolated EVs

Recipient HEK293T cells were first seeded in 12-well cell culture plates at a confluency of 5 x 10^5 cells/well in DMEM supplemented with 10% FBS. 24 hours later, cells were transfected with 1 µg of the appropriate dual-luciferase target reporter plasmid for miRNA experiments or left untreated for shRNA experiments. After 24 hours, recipient cells were split from 12-well cell culture plates to 96-well cell culture plates at a ratio of 1:30 in 100 µl DMEM supplemented with 10% FBS and allowed to adhere. During this time, EVs from source cells, plated in 15 cm cell culture dishes, which had been co-transfected with the relevant expression plasmids 48 hours previously, were isolated, pooled and washed by differential ultracentrifugation. EVs were resuspended in 350 µl Opti-MEM and applied to recipient cells at a volume of 50 µl per recipient well. The supernatant remaining after the first isolation was concentrated to a final volume of 350 µl using 10 kDa Amicon Ultra-15 Centrifugal Filter Units (Merck Millipore), according to manufacturer's instructions, and applied to recipient cells at a volume of 50 µl per well. 50 µl of Opti-MEM was also added to otherwise untreated cells as a further control. Recipient cells received the equivalent of the total yield of isolated EVs and concentrated supernatant from 1 x 15 cm dish per well of a 96-well plate. Following

treatment, recipient cells were incubated for 48 hours prior to luciferase or RNA analysis, performed as outlined above.

2.15 Protein Extraction

For cells, protein was extracted using Cell Extraction Buffer (Life Technologies) supplemented with Halt Protease and Phosphatase Inhibitor Cocktail (100x) (Life Technologies) and 1 mM PMSF. 200 µl of cell extraction buffer was used per well in a 6-well cell culture plate. Samples were incubated on ice for 30 minutes with shaking to lyse cells before centrifugation at 13,000 rpm for 10 minutes at 4ºC. The supernatant was transferred to clean microcentrifuge tubes and stored at -80ºC. For Western blotting, cell lysate protein concentration was assessed using the microBCA Protein Assay Kit (Life Technologies) according to manufacturer's instructions.

2.16 Enzyme-Linked Immunosorbent Assays (ELISAs)

Amyloid-β (42) Production

HEK293 APPswe cells were reverse transfected under the required LNA-ASO conditions and plated at a confluency of 4 x 10^5 cells/well in 12-well cell culture plates. After 48 hours, the supernatant was collected and Halt 100x Protease Inhibitor Cocktail (Life Technologies) was added. A human amyloid-β (42) ELISA kit was used (Life Technologies) to assess amyloid-β production according to manufacturer's instructions. For optimisation studies, supernatant was first concentrated by centrifugation at 4,000 x g for 30 minutes using Amicon Ultra-4 3 kDa Centrifugal Filter Units (Merck

Millipore). However, as HEK293 APPswe cells produced high levels of amyloid-β (42), unconcentrated supernatant samples were typically diluted 1:1 with diluent buffer to remain within the range of the kit. For comparability between samples and standards, amyloid-β (42) peptide standards were serially diluted in fresh HEK293 APPswe culture medium and diluent buffer at a ratio of 1:1 with the addition of Halt 100x Protease Inhibitor Cocktail (Life Technologies). 50 µl of standards and samples and 50 µl of Human Aβ42 Detection Antibody were added to each well except for the chromagen blank. The plate was incubated for 3 hours at room temperature with gentle shaking. Following incubation, the solution was aspirated and the wells washed 4 times. 100 µL Anti-Rabbit IgG HRP working solution was then added to each well, except for the chromagen blank, and incubated for a further 30 minutes at room temperature. The solution was aspirated and the wells washed 4 times before 100 µL of Stabilised Chromagen was added to each well. The plate was then incubated in the dark for 30 minutes at room temperature before 100 µL of Stop Solution was added. Absorbance was measured at 450 nm using a Victor3 1420 multilabel fluorescence microplate reader (Perkin Elmer). A standard curve was fitted to the data to determine the concentration of experimental supernatant samples and obtained values multiplied by two to correct for sample dilution.

Tau Phosphorylation

A Tau (Phospho-Ser396) Colorimetric Cell-Based ELISA Kit (Stratech) was used to assess tau phosphorylation at the Ser396 epitope following LNA-ASO treatment. HEK293 APPswe cells were reverse transfected with the required LNA-ASO and plated at a confluency of 3 x 10^4 cells/well in 96-well cell culture plates that had been pre-

coated with 10 µg/ml Poly-L-Lysine (Sigma-Aldrich) according to manufacturer's instructions. Tau phosphorylation was normalised to total tau and GAPDH levels. 9 replicates were therefore performed for each transfection condition, allowing 3 replicates for each protein of interest. After 48 hours incubation, cells were washed once in TBS and fixed with 100 µl 8% PFA (Sigma-Aldrich) for 20 minutes at room temperature. The fixing solution was then aspirated and the plate washed for 3 x 5 minutes with 200 µl Wash Buffer with gentle shaking. 100 µl of Quenching Buffer was then added per well and the plate incubated for a further 20 minutes at room temperature. The solution was aspirated and the plate washed for 3 x 5 minutes with 200 µl Wash Buffer with gentle shaking. 200 µl of Blocking Buffer was added to each well before the plate was incubated for 1 hour at room temperature. Following incubation, the plate was washed for 3 x 5 minutes before the addition of 50 µl of 1 x primary antibody (either rabbit Anti-Tau Phospho-Ser 396, rabbit Anti-Tau or mouse Anti-GAPDH antibody) to the corresponding wells. The plate was incubated for 2 hours at room temperature with gentle shaking before a further 3 x 5 minutes of washing. 50 µl of 1 x secondary antibody was then added to each corresponding well. HRP-Conjugated Anti-Rabbit IgG antibody was added to wells incubated with primary antibodies against total or phosphorylated tau and HRP-Conjugated Anti-Mouse IgG antibody was added to wells incubated with the GAPDH primary antibody. The plate was incubated for 1.5 hours at room temperature with gentle shaking. The plate was then washed for a further 3 x 5 minutes before 50 µl of Ready-to-Use Substrate was added per well and the plate incubated in the dark for 30 minutes at room temperature with shaking. Finally, 50 µl of Stop Solution was added per well and absorbance

measured at 450 nm using a Victor3 1420 multilabel fluorescence microplate reader (Perkin Elmer).

To allow normalisation to cell counts, Crystal Violet cell staining was performed. Cells were washed for 2 x 5 minutes with 200 µl of Wash Buffer and 2 x 5 minutes with 200 µl of 1 x TBS. The plate was allowed to air dry for 5 minutes at room temperature before the addition of 50 µl Crystal Violet solution. After 30 minutes of incubation at room temperature with shaking the solution was removed. Wells were gently rinsed with H_2O and washed for 3 x 5 minutes with 200 µl of TBS with shaking. 100 µl of SDS solution was added per well and incubated with shaking at room temperature for 1 hour. The absorbance was read at 595 nm with the Victor3 1420 multilabel fluorescence microplate reader (Perkin Elmer). Tau phosphorylation was normalised to both total tau and GAPDH expression (corrected for cell count) and then to negative control LNA-ASO treated wells.

2.17 Luciferase Assays

Validation of miRNA Mimic and miRNA Expression Plasmid Activity

To validate the regulation of reporter plasmids by miRNA mimics and miRNA expression plasmids, HEK293T cells were seeded in 24-well cell culture plates at a confluency of 1 x 10^5 cells/well in DMEM supplemented with 10% FBS. After 24 hours, each well was co-transfected with 200 ng of reporter plasmid and the required quantity of miRNA mimic or expression plasmid as indicated. Cells were harvested 24 hours later with 100 µl Passive Lysis Buffer (Promega) and active cell scraping. Firefly

and *Renilla* luciferase activity were quantified using the Dual-Luciferase Reporter Assay System (Promega) according to manufacturer's instructions.

Co-culture: miR-106b

Source and recipient HEK293T cells were plated and transfected as outlined above. Recipient cells were plated within inserts and allowed to adhere before inserts were added to the appropriate source cell well in 24-well cell culture plates and incubated together for 24-72 hours as indicated. Recipient cells were harvested with 30 µl Passive Lysis Buffer (Promega) and active cell scraping. Firefly and *Renilla* luciferase activity were quantified using the Dual-Luciferase Reporter Assay System (Promega) according to manufacturer's instructions. The effect of secreted miR-106b (released from miR-106b overexpressing source cells) on recipient cells (expressing the miR-106b pmirGLO dual-luciferase reporter) was normalised to the effect of endogenous miR-106b originating from untreated source cells.

Direct Treatment of Recipient Cells with miR-106b Isolated EVs

Source and recipient HEK293T cells were plated and transfected as outlined above. Following treatment of recipient cells with isolated EVs or concentrated supernatant, cells were incubated for 24 hours before the medium was changed. After a further 24 hours, recipient cells were harvested with 30 µl Passive Lysis Buffer (Promega) and Firefly and *Renilla* luciferase activity quantified as above. The effect of secreted miR-106b (from miR-106b overexpressing source cells) on recipient cells (expressing the

miR-106b pmirGLO dual-luciferase reporter) was normalised to the effect of endogenous miR-106b originating from untreated source cells.

2.18 MTS Cell Proliferation Assay

The CellTiter 96 Aqueous One Solution Cell Proliferation Assay (Promega) was used to assess cell viability following LNA-ASO treatment. SH-SH5Y, Neuro2A and HEK293 APPswe cells were reverse transfected with experimental or negative control LNA-ASOs in 96-well cell culture plates according to the transfection conditions outlined above. After 48 hours of incubation, 25 µl of CellTiter 96 Aqueous One Solution Reagent was added per well of the 96-well assay plate containing 125 µl of culture medium and cells. The cells were returned to the incubator for 3 hours at 37ºC before absorbance at 490 nm was measured using a 96-well microplate reader (Perkin Elmer). To determine sequence-specific effects upon cell viability, absorbance from cells treated with experimental LNA-ASOs was normalised to that from cells treated with the same dose of negative control LNA-ASO and the result compared to untreated cells.

2.19 RNA Extractions

Cells

RNA was extracted from cells using TRIzol (Life Technologies) according to manufacturer's instructions. Briefly, 500 µl of TRIzol was added per well in a 24-well cell culture plate and incubated for 5 minutes at room temperature to homogenize cells. 100 µl of chloroform was added to each sample, shaken vigorously and incubated for 10

minutes at room temperature. Samples were centrifuged at 12,000 x g for 15 minutes at 4°C to allow separation of the homogenate into a clear upper aqueous layer containing RNA and an interphase and lower organic layer containing DNA and proteins. The upper aqueous layer was carefully removed to a fresh tube and 250 µl of isopropanol added to precipitate RNA. Where the expected RNA yield was low, 1 µl of RNase-free glycogen (Roche) was added to the sample to increase the recovery of nucleic acids. The sample was vortexed and incubated for 10 minutes at room temperature before centrifugation at 12,000 x g for 10 minutes at 4°C. The supernatant was removed and the RNA pellet was washed with 400 µl of 75% ethanol before centrifugation at 7,500 x g for 5 minutes at 4°C. The supernatant was discarded and the pellet air-dried for 10 minutes. The RNA pellet was resuspended in 20-100 µl of nuclease-free H_2O and incubated at 55°C for 10 minutes to aid RNA resuspension. RNA quantity and quality, as measured by the $A_{260/280}$ and $A_{260/230}$ ratios, were then quantified using a Nanodrop 2000 spectrometer (Thermo Scientific).

Tissue

Tissue was snap frozen in ice-cold isopentane after harvesting and stored at -80ºC. Prior to RNA extraction, a section of tissue was removed and placed in a 2 ml soft tissue CK14 homogenisation tube containing 1.4 mm ceramic beads (Precellys) with 500 µl of TRIzol Reagent (Life Technologies). Tissue was homogenized by 2 x 30 seconds x 6500 rpm using a Precellys 24 homogenizer (Precellys). The homogenized tissue was removed to a fresh microcentrifuge tube (Axygen, Corning) and RNA extracted according to the protocol outlined above.

Extracellular Vesicles and Supernatant

To preserve small RNA species[558], TRIzol LS (Life Technologies) was used to extract RNA from EV and supernatant samples according to manufacturer's instructions. 225 µl of TRIzol LS was added to 75 µl of EV or supernatant sample in addition to 5 pg of cel-miR-39 spike-in for normalisation purposes. The sample was incubated for 5 minutes at room temperature before 60 µl of chloroform was added and the sample incubated for 10 minutes. Samples were centrifuged at 12,000 x g for 15 minutes at 4°C. As above, the upper aqueous layer was removed to a fresh tube before the addition of 1 µl of RNase-free glycogen (Roche) and 150 µl of isopropanol. The sample was vortexed and incubated for 10 minutes at room temperature before centrifugation at 12,000 x g for 10 minutes at 4°C. The supernatant was removed and the RNA pellet was washed with 300 µl of 75% ethanol before centrifugation at 7,500 x g for 5 minutes at 4°C. The supernatant was discarded and the pellet air-dried for 10 minutes. The RNA pellet was resuspended in 20 µl of nuclease-free H_2O and incubated at 55°C for 10 minutes to aid RNA resuspension. When required, RNA quantity of EV samples was assessed using Quant-iT RiboGreen RNA Assay Kit (Life Technologies).

2.20 RNA Quantification using Quant-iT RiboGreen RNA Assay

As the expected RNA quantity in EV samples was low, the low-range protocol of the Quant-iT RiboGreen RNA Assay Kit (Life Technologies) was applied to measure EV samples according to manufacturer's instructions. Briefly, 100 µg/ml of Ribosomal RNA standard (16S and 23S rRNA from *E. coli*) was serially diluted at a ratio of 1:5 with TE buffer to give a range of standards from 100 ng/µl to 0 ng/µl. 100 µl of each

standard was added per well in a 96-well black microplate (Corning). For test samples, 2 µl of EV sample was diluted with 98 µl of TE buffer and 100 µl added per 96-well. The Quant-iT RiboGreen reagent working solution was prepared by diluting the stock solution 2,000 fold with TE before 100 µl of working solution was added to standard and test samples in the microplate. Fluorescence emission intensity was measured at 530 nm using a Victor3 1420 multilabel fluorescence microplate reader (Perkin Elmer) and fluorescence emission intensity was plotted versus RNA concentration to calculate the RNA quantity present in test samples.

2.21 mRNA Quantification by Quantitative Real-time PCR (qPCR)

The High-Capacity cDNA Reverse Transcription Kit (Life Technologies) was used to obtain cDNA from extracted RNA by reverse transcription. Reverse transcription was performed in 20 µl reactions according to manufacturer's instructions. For cellular samples, RNA was diluted to 50-100 ng/µl and 10 µl was added per well of a 96-well low profile, skirted PCR plate (Life Technologies) for a total of 500-1000 ng per 20 µl reaction. For EV and supernatant samples, 5 µl of sample was added to 5 µl of nuclease-free H_2O per 20 µl reaction. 10 µl of cDNA Reverse Transcription mastermix with random primers was added to each well for a 20 µl reaction volume and reverse transcription performed using a G-Storm Quad Block Thermal Cycler (GMI) under the following parameters; 10 minutes at 25ºC, 120 minutes at 37ºC, 5 minutes at 85ºC before cooling to 4ºC.

A StepOnePlus Real-Time PCR system (Life Technologies) was used to perform qPCR in 20 µl singleplex reactions using Taqman Fast Universal Master Mix (2x) (Life

Technologies) and FAM-MGB labelled Taqman Gene Expression Assays (20x) (Life Technologies) (**Table 2.14**). cDNA from cellular and EV/supernatant samples was diluted with 80 µl or 20 µl of nuclease-free H_2O, respectively, and 5 µl of diluted cDNA was added per 20 µl reaction. The relative standard curve method was applied to determine the relative fold change in target gene expression. Standard curves were typically produced from serial dilutions (diluted either 1:5 or 1:10) of cDNA from untreated experimental samples. qPCR was performed using the following cycling parameters; initial activation at 95ºC for 20 seconds followed by forty cycles of 1 second at 95ºC and 20 seconds at 60ºC. The resulting data were analysed using the StepOne Software v2.2.2 (Life Technologies). Unless otherwise stated, mRNA target gene expression was normalised to *β-Actin*.

Table 2.14 Taqman Gene Expression Assays.

Gene Name	Assay ID
Human Assays	
β-Actin	Hs01060665_g1
AGO2	Hs01085579_m1
APP	Hs01552283_m1
BACE1	Hs00201573_m1
Caspase-9	Hs00154261_m1
CDK5R1	Hs00243655_s1
GAPDH	Hs02758991_g1
GRIA2	Hs00181331_m1
GRIN2B	Hs00168230_m1
GSK3β	Hs01047719_m1
HN1	Hs00993863_g1
MAPT	Hs00902194_m1
mTOR	Hs00234508_m1
NOX4	Hs00418356_m1
TNRC6A	Hs00325721_m1
Mouse Assays	
β-Actin	Mm01205647_g1
Bace1	Mm00478664_m1
Cyclophilin	Mm00478295_m1
Gapdh	Mm03302249_g1
mTOR	Mm00444968_m1
Human Primary miRNA Transcript Assays	
hsa-miR-17	Hs03295901_pri
hsa-miR-29a	Hs03302672_pri
hsa-miR-106b	Hs03295154_pri

2.22 miRNA Quantification by qPCR

Reverse transcription was performed using the High-Capacity cDNA Reverse Transcription Kit (Life Technologies) to obtain cDNA from extracted RNA. Cellular RNA was first diluted to 2 ng/µl before 5 µl was added per 15 µl reaction for a total RNA input of 10 ng. For exosomal and supernatant RNA, 5 µl of extracted RNA was added per 15 µl reaction. To denature double-stranded templates, 3 µl of 5x RT primer from the appropriate Taqman Small RNA Assay kit (**Table 2.15**) was added to 5 µl of RNA template and incubated for 5 minutes at 85ºC followed by 5 minutes at 60ºC. The mastermix was prepared according to manufacturer's instructions and 7 µl added to the RNA and 5x RT primer mix. Reverse transcription was performed using a G-Storm Quad Block Thermal Cycler (GMI) under the following parameters; 30 minutes at 16ºC, 30 minutes at 42ºC, 5 minutes at 85ºC before cooling to 4ºC.

qPCR was performed in 20 µl singleplex reactions using a StepOnePlus Real-Time PCR system (Life Technologies) under the parameters outlined above with Taqman Fast Universal Master Mix (2x) (Life Technologies) and Taqman Small RNA Assays (20x) (Life Technologies) (**Table 2.15**). A total of 1.33 µl undiluted cDNA was added per 20 µl reaction. The relative standard curve method was applied to determine the relative fold change in target gene expression. Standard curves were typically produced from serial dilutions (diluted 1:10) of the cDNA obtained from reverse transcription of 5 pg of input RNA from commercially purchased miRNA mimics/siRNA. The resulting data were analysed using the StepOne Software v2.2.2 (Life Technologies). For cellular samples, target miRNA/siRNA expression was normalised to total RNA volume. For

EV and supernatant samples, target miRNA/siRNA expression was normalised to expression of the cel-miR-39 spike-in, unless otherwise stated.

Table 2.15 Taqman Small RNA and Custom Small RNA Assays.

miRNAs	
Target	**Assay ID**
hsa-miR-17-5p	000393
hsa-miR-20a-5p	000580
hsa-miR-29a-5p	002447
hsa-miR-106b-5p	000442
cel-miR-39-3p	000200
siRNA	
Custom Small Assay	**Target Sequence**
APP siRNA	GUACCAACUUGCAUGACUA
BACE1 siRNA	GCUUUGUGGAGAUGGUGGA

2.23 Identification of Optimal *In Vivo* Reference Genes

The 12-gene geNorm Perfect Probe Plus Mouse Kit (PrimerDesign) was utilised to identity the most appropriate reference gene for *in vivo* data analysis. This kit compares expression, within experimental tissue samples, of 12 candidate reference genes which have been identified from more than 30,000 microarray experiments to express inherent levels of stability across different tissues, disease states and experimental designs. The expression of cyclophilin was also assessed using Taqman Gene Expression Assay (20x), ID: Mm00478295_m1 (Life Technologies). To determine reference gene stability, the expression of each of the 13 candidate reference genes was assessed in samples extracted from the cortex of 3 mice and from the liver of 2 mice from each of

the following treatment conditions; RVG-EV + siRNA, Lamp2B-EV + siRNA, siRNA alone and untreated. qPCR was performed with the StepOnePlus Real-Time PCR system (Life Technologies) in 20 µl singleplex reactions using Taqman Fast Universal Master Mix (2x) (Life Technologies) and the cycling parameters outlined above. cDNA was diluted 1:10 with nuclease-free H_2O for an input volume of 25 ng of cDNA and the resulting data analysed with the qbasePLUS software (Biogazelle). The software allows the identification of the most appropriate reference gene(s) for normalisation by ranking candidate genes by their expression stability across tissues and treatments.

2.24 Statistical Analyses

Statistical analyses were performed using GraphPad Prism (Version 6, GraphPad Software, La Jolla California USA). Student's 2-tailed t-test or one-way analysis of variance (ANOVA) followed by Tukey's multiple comparisons post-hoc test were used to assess the statistical significance of group differences. Experimental conditions were normalised to a nonspecific negative control or untreated condition as indicated. All experiments were performed in triplicate unless otherwise stated. Graphs represent mean ± standard error and differences were considered significant at $p \leq 0.05$. Asterisks indicate significant difference compared to untreated or negative control samples except where indicated by comparison bars. Asterisk (*) indicates $p \leq 0.05$, double asterisks (**) indicates $p \leq 0.01$ and triple asterisks (***) indicates $p \leq 0.001$.

3 Loading of siRNA into Extracellular Vesicles by Electroporation

3.1 Introduction

A predominant pathological hallmark of AD is the presence of amyloid-β plaques. As discussed previously, amyloid-β peptides are formed from the sequential cleavage of APP by BACE1 and γ-secretase. Therefore, one potential therapeutic strategy to decrease amyloid-β production is to reduce expression of APP, BACE1 or γ-secretase. Complete silencing is undesirable given the potential for deleterious consequences arising from disruption to the processing of alternative substrates and pathways. However, previous studies have shown, both *in vitro* and *in vivo*, that partial silencing of APP or BACE1, either through genetic deletion or RNAi-mediated silencing, significantly reduced amyloid-β production and tau hyperphosphorylation, rescuing memory impairments[290,296,297,422,423,425,426,559]. Typically, RNAi-mediated silencing has been assessed *in vitro* or following intracranial injections of viral vectors expressing shRNA against the target of interest *in vivo*[296,422,424–426]. However, as this strategy is not amenable for clinical translation, a novel delivery vehicle able to transport systemically-delivered RNAi effectors across the BBB to key areas within the brain is required.

Recent studies exploring exosome-mediated delivery of RNAi-based molecules have shown that exosomes appear capable of delivering exogenous siRNAs and miRNAs *in vivo*[468,507,508,513]. Importantly, two recent studies have demonstrated that exosomes modified to express a rabies virus glycoprotein (RVG)-derived targeting peptide were able to traverse the BBB to deliver cargoes to the brain[508,513]. Specifically, systemically-delivered RVG-exosomes, loaded by electroporation with siRNA against either Bace1

or α-synuclein, significantly silenced mRNA and protein expression within the cortex, striatum and midbrain in wild-type mice[508,513]. Strikingly, the delivery of α-synuclein siRNA-loaded exosomes also significantly reduced mRNA and protein expression, including protein aggregates, within the brains of a transgenic PD mouse model[513]. Together, these studies highlight the potential of exosome-mediated delivery of RNAi-based molecules for the treatment of neurodegenerative disease.

Thus, this study focused upon the optimisation of exosome-mediated delivery for siRNA cargoes as a therapeutic strategy for AD. siRNAs were first validated to target APP or Bace1 before their electroporation-based loading into exosomes was investigated. The efficacy of exosome-mediated siRNA delivery was assessed by treatment of Neuro2A cells *in vitro* and following intravenous injections of siRNA-loaded exosomes to wild-type mice *in vivo*. However, it proved challenging to replicate previous findings of exosome-mediated delivery of siRNA, both *in vitro* and *in vivo*. Further characterisation of the electroporation protocol revealed the formation of large siRNA aggregates following electroporation, which may contribute towards an overestimation of siRNA-loading efficiency. These findings therefore highlight the requirement for alternative exosome loading strategies.

3.2 Results

3.2.1 Identification and Validation of Candidate siRNA Cargoes

Potential siRNA cargoes targeting APP or BACE1 were first screened *in vitro* to identify siRNA sequences which efficiently silenced the target of interest. Three novel candidate siRNAs targeting APP (APP1, APP2 and APP3) were identified utilising the Eurogentec siRNA design platform. For BACE1 siRNA, a previously validated sequence[422] was chosen that had been utilised by Alvarez-Erviti and colleagues[508] for their demonstration of exosome-mediated siRNA delivery. APP siRNA sequences were human-specific while the BACE1 siRNA targeted a conserved coding sequence between human, mouse and rat[422]. To validate siRNA-mediated silencing of APP or BACE1, HEK293T cells were transfected with APP, BACE1 or a negative control (NC) siRNA using Lipofectamine 2000 and target gene knockdown, normalised to *β-Actin* expression, was analysed after 48 hours by qPCR (**Fig. 3.1**).

Initial screening of candidate APP sequences revealed that all three elicited significant silencing of *APP* mRNA expression although APP1 and APP3 were most potent (**Fig. 3.1A**). APP1 siRNA was selected for further study and a dose-response experiment confirmed strong silencing of *APP* mRNA expression at concentrations ≥ 100 nM (**Fig. 3.1B**). A dose-response experiment performed with BACE1 siRNA showed significant silencing of *BACE1* mRNA at concentrations ≥ 50 nM (**Fig. 3.1C**).

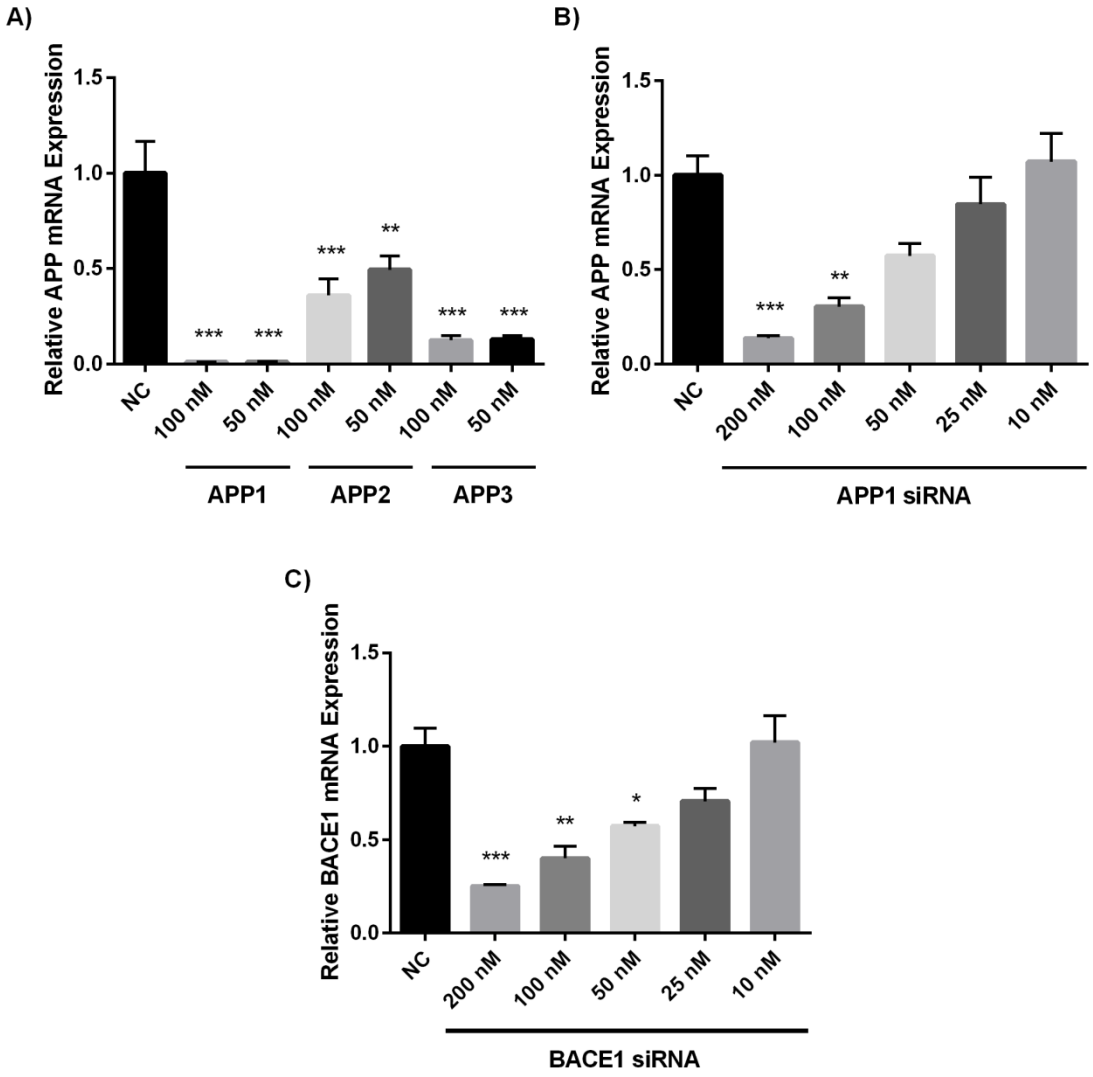

Figure 3.1 Identification and Validation of APP and BACE1 siRNAs. HEK293T cells were transfected with shown siRNAs at indicated concentrations using Lipofectamine 2000. Target gene knockdown, normalised to *β-Actin* expression, was measured after 48 hours by qPCR. **(A)** 3 candidate APP-targeting siRNAs (APP1, APP2 and APP3; identified utilising the Eurogentec siRNA design platform) were screened for silencing of *APP* mRNA. **(B)** Dose-response curve of selected APP1 siRNA. **(C)** Dose-response curve of BACE1 siRNA. Values are mean ± SEM, n = 3, "NC", negative control siRNA at 100 nM, ***p<0.001, **p<0.01, *p<0.05, one-way ANOVA followed by Tukey's post-hoc test.

3.2.2 Characterisation of BM-DC-derived Extracellular Vesicles

Immature bone-marrow-derived dendritic cells (BM-DCs) were chosen as the primary source of exosomes as their exosomes have previously been shown to lack lymphocyte stimulatory molecules including MHC-1, MHC-II, CD40 and CD86[560] and appeared well-tolerated following systemic delivery in two previous studies[508,513].

BM-DCs were harvested from 9-week-old male C57BL/6 mice and cultured for 8 days in 6-well cell culture plates. Four days after plating, BM-DCs were transfected with 5 μg/well of the Lamp2B-RVG targeting plasmid (RVG) or Lamp2B control plasmid (Lamp2B) using TransIT LT1 transfection reagent or were left untreated (UT). On day 7, the medium was changed to fresh DMEM supplemented with 10% extracellular vesicle (EV)-depleted FBS. Conditioned medium was collected 24 hours later and exosomes isolated by differential ultracentrifugation.

BM-DC-derived vesicles were characterised by a number of methods including Western blot, electron microscopy (EM) and nanoparticle tracking analysis (NTA) to assess the presence of exosomal markers, vesicle size and morphology and the number of particles obtained (**Fig. 3.2**). Western blot analysis confirmed the presence of the exosomal markers, Alix and Flotillin-1 and suggested that transfection of targeting or control plasmids did not significantly affect the yield of exosomes obtained (**Fig. 3.2A**). EM and NTA established that preparations contained vesicles comprising a lipid-bilayer membrane with typical exosomal morphology in the range of 50-200 nm (**Fig. 3.2B-F**). NTA confirmed a similar size and total particle count across each condition, again suggesting that transfection with targeting or control plasmids did not significantly

affect the size or yield of vesicles (**Fig. 3.2C-F**). EM and NTA also revealed that each preparation contained a mixed population of both smaller and larger vesicles in addition to potential aggregates of smaller vesicles (**Fig. 3.2B-F**). As such, vesicle preparations are referred to as EVs rather than exosomes specifically as they were purified based upon their size and density by differential ultracentrifugation.

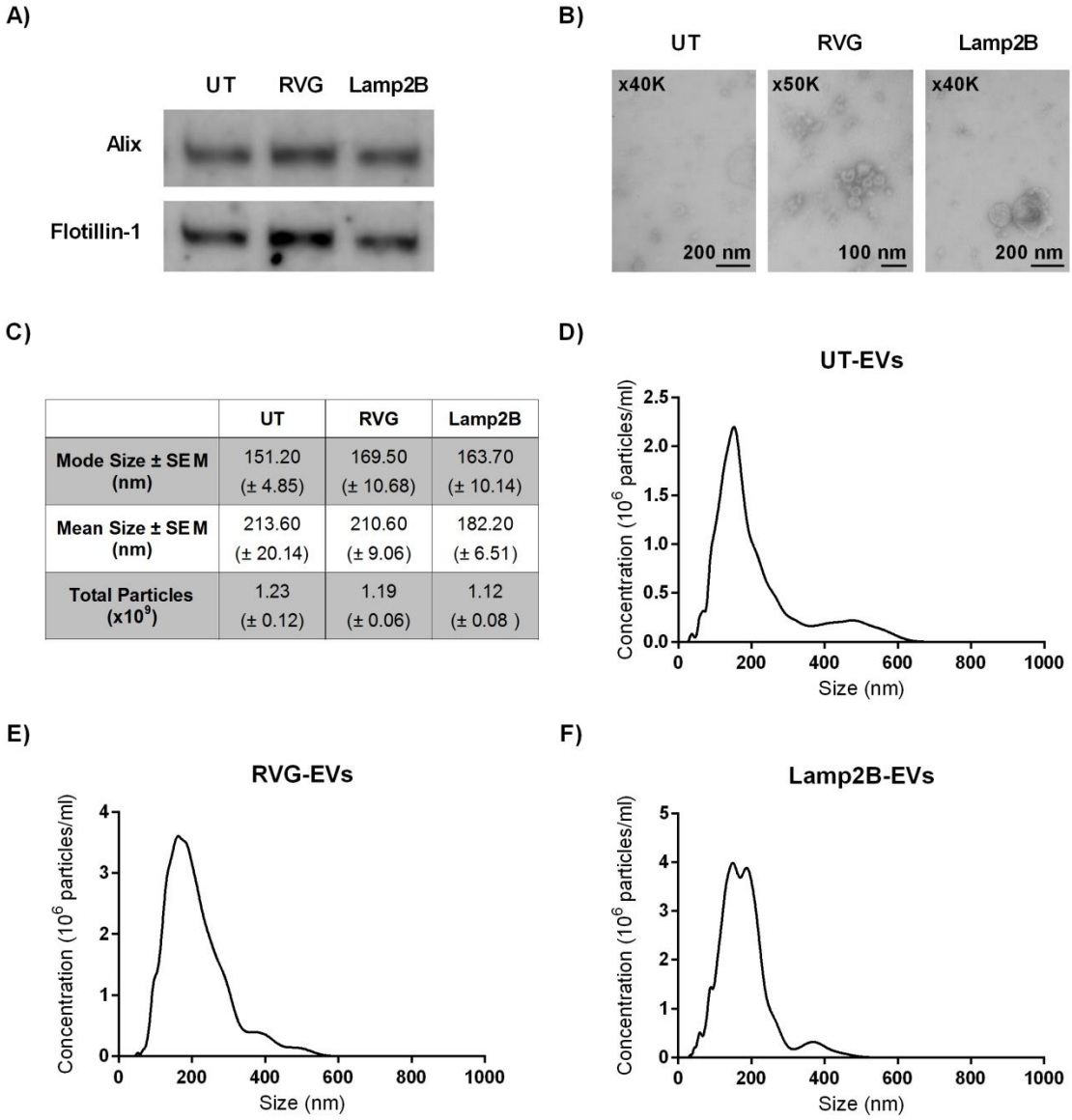

	UT	RVG	Lamp2B
Mode Size ± SEM (nm)	151.20 (± 4.85)	169.50 (± 10.68)	163.70 (± 10.14)
Mean Size ± SEM (nm)	213.60 (± 20.14)	210.60 (± 9.06)	182.20 (± 6.51)
Total Particles ($x10^9$)	1.23 (± 0.12)	1.19 (± 0.06)	1.12 (± 0.08)

Figure 3.2 Characterisation of BM-DC-derived Extracellular Vesicles. Extracellular vesicles (EVs) derived from BM-DCs that were pre-transfected with the Lamp2B-RVG targeting plasmid ("RVG"), Lamp2B control plasmid ("Lamp2B") or left untreated ("UT") were characterised by a number of methods. **(A)** EVs were purified from the conditioned medium of BM-DCs isolated from one mouse. 20% of the purified EVs were loaded onto a Western blot and probed for the exosomal markers, Alix and Flotillin-1, which suggested similar yields of exosomes were obtained from each condition. **(B)** Electron microscopy images revealed typical morphology of isolated exosomes. **(C)** Nanoparticle tracking analysis (NTA) showing the mean particle size and total number of particles secreted from BM-DCs isolated per one mouse (n = 3) is consistent with the earlier observation of similar exosome yield for each condition. **(D-F)** NTA analysis of size distribution histogram (n = 3) for **(D)** UT-EVs, peak = 151.2 nm, **(E)** RVG-EVs, peak = 169.5 nm and **(F)** Lamp2B-EVs, peak = 163.7 nm.

3.2.3 *Bace1* Expression was not Silenced by siRNA-loaded BM-DC-derived Extracellular Vesicles *In Vitro*

To assess the efficacy of EV-mediated siRNA delivery, the same experimental set-up reported by Alvarez-Erviti *et al*.[508] was utilised. Thus, the first aim of this study was to replicate *Bace1* mRNA silencing following EV-mediated delivery of Bace1 siRNA. BM-DC source cells were modified to express either the Lamp2B-RVG or Lamp2B control construct. EVs were loaded with Bace1 siRNA by electroporation or left unelectroporated as a control. Following electroporation, the mixture was washed and pelleted at 120,000 x g before addition to Neuro2A recipient cells in 24-well cell culture plates. Neuro2A cells were also directly transfected with 200 nM Bace1 siRNA or NC siRNA as further controls. *Bace1* mRNA expression was assessed, relative to *β-Actin*, 48 hours after EV treatment by qPCR.

A ratio of 6 μg EVs: 100 pmol (200 nM) Bace1 siRNA per well was first tested in line with Alvarez-Erviti *et al*.[508]. EVs were derived from BM-DCs harvested from two strains of mice, either C57BL/6 (**Fig. 3.3A**) or CBA (**Fig. 3.3B**), to determine whether BM-DC source affected outcome. Direct transfection of Bace1 siRNA elicited effective silencing (80-90% reduction) of *Bace1* mRNA expression, confirming efficacy of the siRNA sequence. However, EV-mediated delivery of siRNAs loaded by electroporation proved inconsistent. Across a number of replicates, *Bace1* expression was not consistently reduced following treatment with RVG-EVs obtained from either source (**Fig. 3.3A-B**). Although there appeared to be a non-significant trend towards silencing by C57/BL6 Lamp2B-EVs (**Fig. 3.3A**), this was not evident for CBA-derived Lamp2B-EVs (**Fig. 3.3B**).

It was hypothesised that an insufficient quantity of EVs may fail to deliver effective yields of siRNA particularly as EV protein quantification may be biased by medium contamination. Therefore, the experiment was repeated with a ratio of 8 μg (**Fig. 3.3C**) or 10 μg (**Fig. 3.3D**) EVs: 100 pmol (200 nM) Bace1 siRNA. Unmodified (UT) EVs were also included as an additional control. While direct transfection of Bace1 siRNA effectively silenced *Bace1* expression, there was no significant silencing following treatment with RVG-EVs, Lamp2B-EVs or UT-EVs (**Fig. 3.3C-D**). In fact, *Bace1* mRNA expression was significantly increased after treatment with electroporated/unelectroporated RVG-EVs and electroporated Lamp2B-EVs at the 8 μg EVs: 100 pmol siRNA ratio (**Fig. 3.3C**).

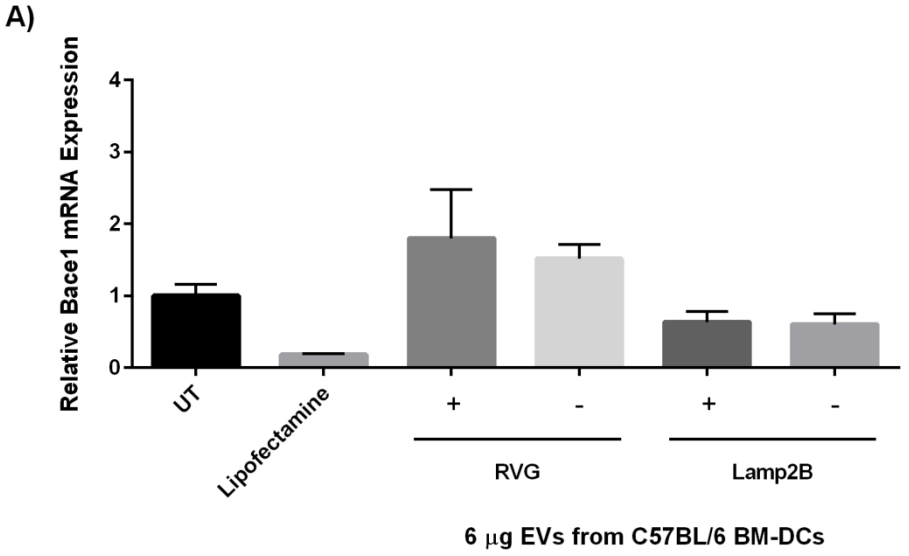
A)
Relative Bace1 mRNA Expression
4
3
2
1
0
UT
Lipofectamine
+
-
+
-
RVG
Lamp2B
6 μg EVs from C57BL/6 BM-DCs

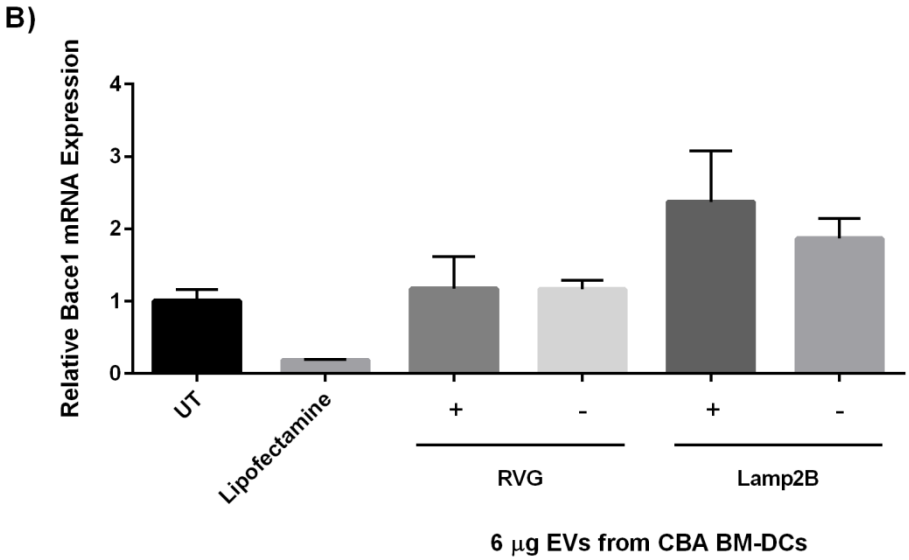
B)
Relative Bace1 mRNA Expression
4
3
2
1
0
UT
Lipofectamine
+
-
+
-
RVG
Lamp2B
6 μg EVs from CBA BM-DCs

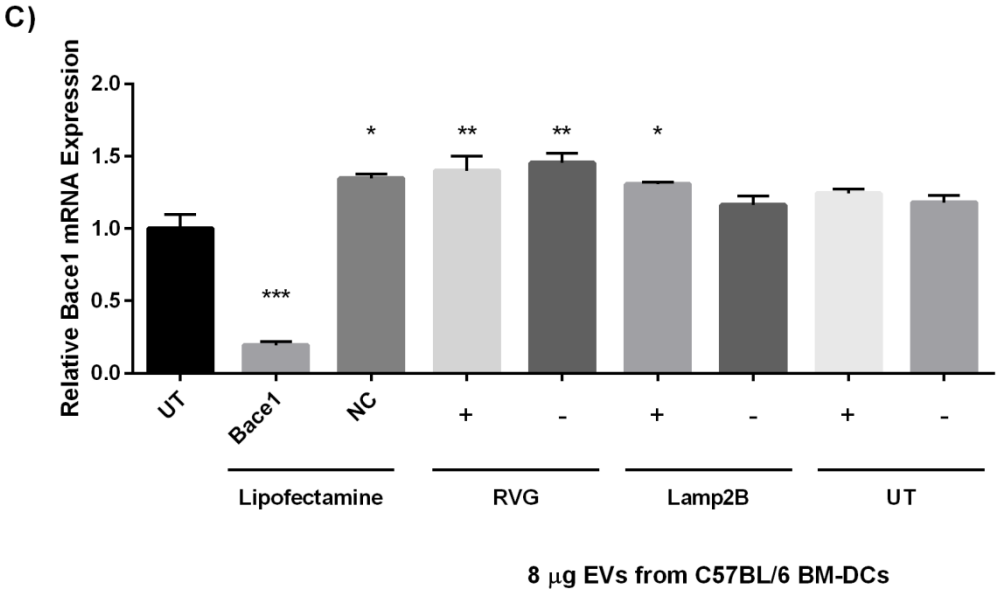
C)
Relative Bace1 mRNA Expression
2.0
1.5
1.0
0.5
0.0
***
*
**
**
*
UT
Bace1
NC
+
-
+
-
+
-
Lipofectamine
RVG
Lamp2B
UT
8 μg EVs from C57BL/6 BM-DCs

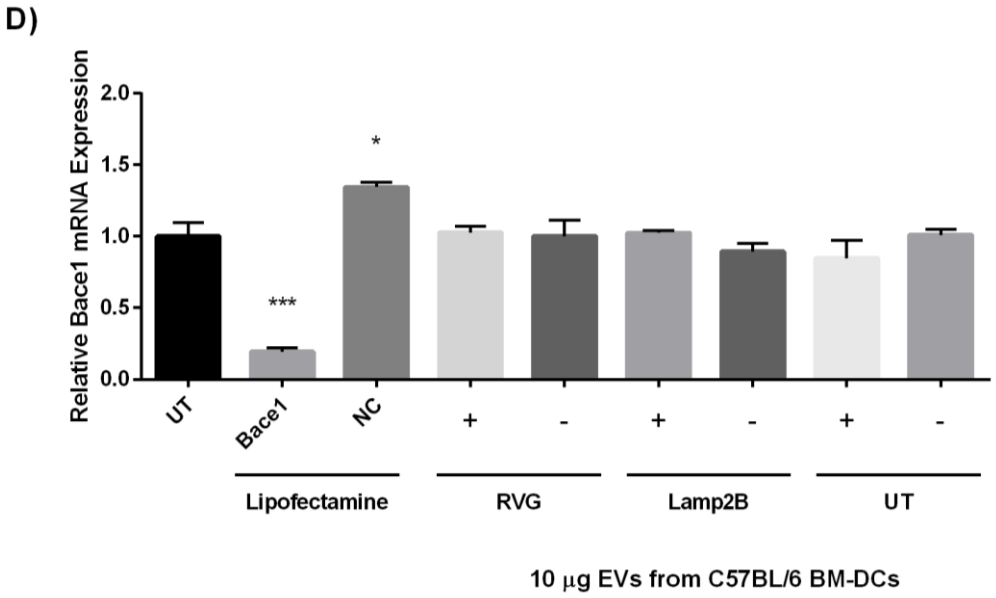

Figure 3.3 Treatment of Neuro2A Cells with BM-DC-derived Extracellular Vesicles. *Bace1* mRNA expression, relative to *β-Actin*, was analysed in Neuro2A cells by qPCR 48 hours after treating cells with Bace1 siRNA-loaded EVs or controls. EV source BM-DCs were transfected with the Lamp2B-RVG targeting construct ("RVG"), Lamp2B control construct ("Lamp2B") or left untreated ("UT"). **(A)** 6 µg EVs from C57BL/6 mice BM-DCs, **(B)** 6 µg EVs from CBA mice BM-DCs, **(C)** 8 µg EVs from C57BL/6 mice BM-DCs or **(D)** 10 µg EVs from C57BL/6 mice BM-DCs were mixed in electroporation buffer with Bace1 siRNA (100 pmol per replicate for 200 nM concentration in cells). To load EVs with siRNA, the mixture was electroporated using a 400 V / 125 µF pulse ("+") or left unelectroporated ("-"), washed and added to cells. As controls, Neuro2A cells were transfected with 200 nM Bace1 siRNA ("Bace1") or negative control siRNA ("NC") using Lipofectamine 2000. Values are mean ± SEM, n = 3, ***p<0.001, **p<0.01, *p<0.05, one-way ANOVA followed by Tukey's post-hoc test.

3.2.4 *Bace1* Expression was not Silenced by siRNA-loaded BM-DC-derived Extracellular Vesicles *In Vivo*

A disparity between the *in vitro* and *in vivo* efficacy of EV-mediated delivery of siRNA has previously been observed within the lab. Therefore, with the aim of replicating the results of Alvarez-Erviti *et al*.[508], EV-mediated delivery of Bace1 siRNA was assessed *in vivo* utilising the same experimental conditions.

Wild-type mice received intravenous injections of either 150 µg Bace1 siRNA alone or after electroporation with the total yield of RVG-EVs or Lamp2B-EVs obtained from cells derived from the equivalent of 1.5 mice. Control mice received an injection of 5% glucose only. After 48 hours, *Bace1* mRNA expression, relative to *β-Actin*, was assessed by qPCR in the cortex, midbrain, liver and kidney (**Fig. 3.4A-D**). Cortical *Bace1* expression was significantly reduced following all experimental treatments (**Fig. 3.4A**). RVG-EVs and Lamp2B-EVs significantly reduced cortical *Bace1* expression by ~54% and ~42%, respectively. Unexpectedly, naked Bace1 siRNA also significantly silenced cortical *Bace1* expression (~48% reduction) (**Fig. 3.4A**). There was no significant effect upon *Bace1* expression in any of the other tissues tested although there was a non-significant reduction in expression in the liver following treatment with naked Bace1 siRNA (**Fig. 3.4C**). In contrast, no silencing was observed in the kidney or liver following administration of modified EVs, suggesting a degree of selective targeting (**Fig. 3.4C-D**).

However, an important issue was discovered during analysis. Due to the unexpected silencing of cortical *Bace1* expression by naked Bace1 siRNA and variability within

conditions, the data were reanalysed with respect to an alternative normalisation gene, *cyclophilin* (**Fig. 3.4E**). This substantially affected the pattern of results with no significant silencing observed across any condition. In fact, *Bace1* mRNA expression appeared to be non-significantly increased following Lamp2B-EV treatment. However, there was variability in the expression of *cyclophilin* itself and the variability in *Bace1* mRNA expression appeared greater following normalisation to *cyclophilin* (**Fig. 3.4E**). These results therefore highlighted the importance of identifying the correct normalisation gene.

Consequently, the most stable and optimal number of reference genes for this experiment was determined using the geNorm Perfect Probe Mouse Kit and associated qbasePLUS software (**Fig. 3.5**). This kit compares expression within experimental tissue samples of 12 candidate reference genes which have been identified to express inherent levels of stability. *Cyclophilin* was also included for further clarification given the discrepancy in results following normalisation to *cyclophilin* or *β-Actin* (**Fig. 3.4A,E**). Identification of the most stable pair of reference genes is determined via calculation of the average expression stability value (geNorm M), which refers to the variation of a gene compared to all other candidate genes. The optimal number of reference genes required for normalisation is determined by pairwise variation (geNorm V) when V (n/n+1) < 0.15. In this study, the most stable pair of reference genes were found to be *Gapdh* and *β-Actin* (**Fig. 3.5A**) and the geometric mean of two reference genes was identified as optimal for *in vivo* normalisation (**Fig. 3.5B**).

The *in vivo* data were therefore reanalysed relative to the geometric mean of *Gapdh* and *β-Actin* (**Fig. 3.6**). Following re-analysis there was no significant silencing observed

following any treatment condition in the cortex, midbrain, liver or kidney (**Fig. 3.6A-D**). However, variability within conditions was relatively high and a non-significant trend towards reduced *Bace1* mRNA expression was observed in the cortex following all experimental treatments (**Fig. 3.6A**). Similarly, there appeared to be a non-significant trend towards reduced *Bace1* mRNA expression in the liver following treatment with Bace1 siRNA alone (**Fig. 3.6C**).

The quantity of Bace1 siRNA within the cortex, midbrain and liver following treatment with Bace1 siRNA alone or RVG-EVs was determined to assess the relationship between Bace1 siRNA quantity within tissues and the level of *Bace1* mRNA silencing (**Fig. 3.7A-C**). High variability precluded any observed increases in Bace1 siRNA expression from reaching significance. However, Bace1 siRNA appeared to be increased in the cortex following treatment with Bace1 siRNA alone or RVG-EVs (**Fig. 3.7A**) and in the midbrain (**Fig. 3.7B**) and liver (**Fig. 3.7C**) following RVG-EV treatment. There appeared to be an association between increased siRNA quantity and reduced *Bace1* mRNA expression in the cortex (**Fig. 3.6A**/**Fig. 3.7A**) but this was not true for the liver or midbrain. Despite high levels of Bace1 siRNA detected in liver samples from mice treated with RVG-EVs, no silencing of *Bace1* mRNA expression was observed (**Fig. 3.6C**/**Fig. 3.7C**). In contrast, *Bace1* mRNA expression appeared non-significantly reduced following Bace1 siRNA alone treatment but this was not associated with increased Bace1 siRNA quantity (**Fig. 3.6C**/**Fig. 3.7C**). This may reflect greater protection of the siRNA cargo within EVs, preventing the rapid degradation and excretion typically observed for naked siRNAs.

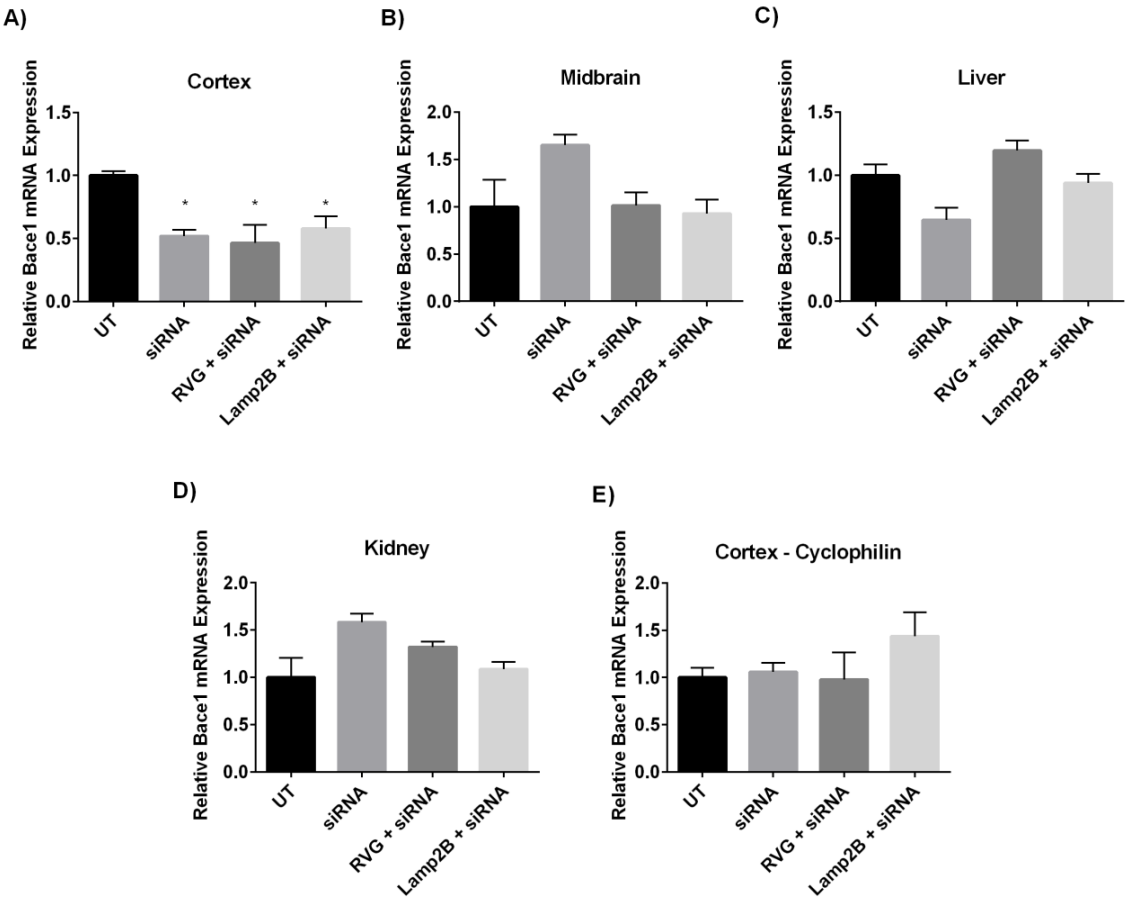

Figure 3.4 *In Vivo* Delivery of Bace1 siRNA By Targeted Extracellular Vesicles. *Bace1* expression, relative to *β-Actin*, was assessed by qPCR 48 hours after intravenous injection of 150 µg Bace1 siRNA alone or loaded within EVs. EV source BM-DCs were transfected with the Lamp2B-RVG targeting construct ("RVG") or Lamp2B control construct ("Lamp2B"). To load EVs with siRNA, the total yield of RVG-EVs or Lamp2B-EVs derived from the BM-DC cells obtained from 1.5 mice and 150 µg Bace1 siRNA was electroporated using a 400 V / 125 µF pulse. *Bace1* expression was analysed in the **(A)** cortex, **(B)** midbrain, **(C)** liver and **(D)** kidney, relative to *β-Actin* expression, and in the **(E)** cortex, relative to *cyclophilin* expression, in comparison to untreated ("UT", 5% glucose injection only) control mice. Values are mean ± SEM, n = 3, *$p<0.05$, one-way ANOVA followed by Tukey's post-hoc test.

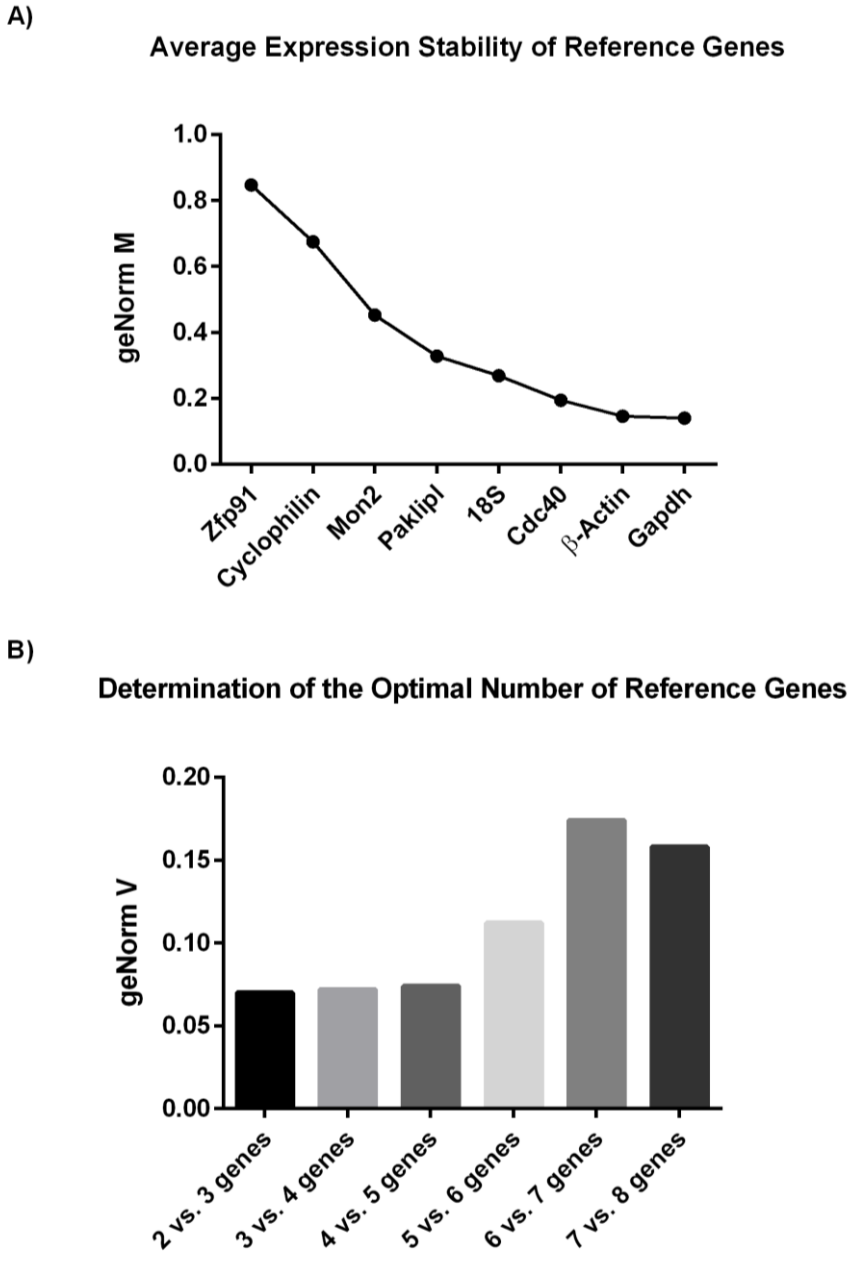

Figure 3.5 Identification of Optimal *In Vivo* Reference Gene. The expression of 13 candidate reference genes was assessed via qPCR using the geNorm Perfect Probe Plus Mouse Kit and qbasePLUS software. **(A)** Identification of the most stable reference genes by calculation of the average expression stability value (geNorm M, variation of a gene compared to all other candidate genes) of reference genes at each step during stepwise exclusion of the least stably expressed reference genes. The most stable and optimal pair of reference genes for this study are *Gapdh* and *β-Actin*, as indicated on the right. **(B)** The optimal number of reference genes required for normalisation was determined by pairwise variation (geNorm V) when V (n/n+1) < 0.15, where n = number of reference genes. In this study, the geometric mean of two reference genes (*Gapdh* and *β-Actin*) was identified as optimal for *in vivo* normalisation.

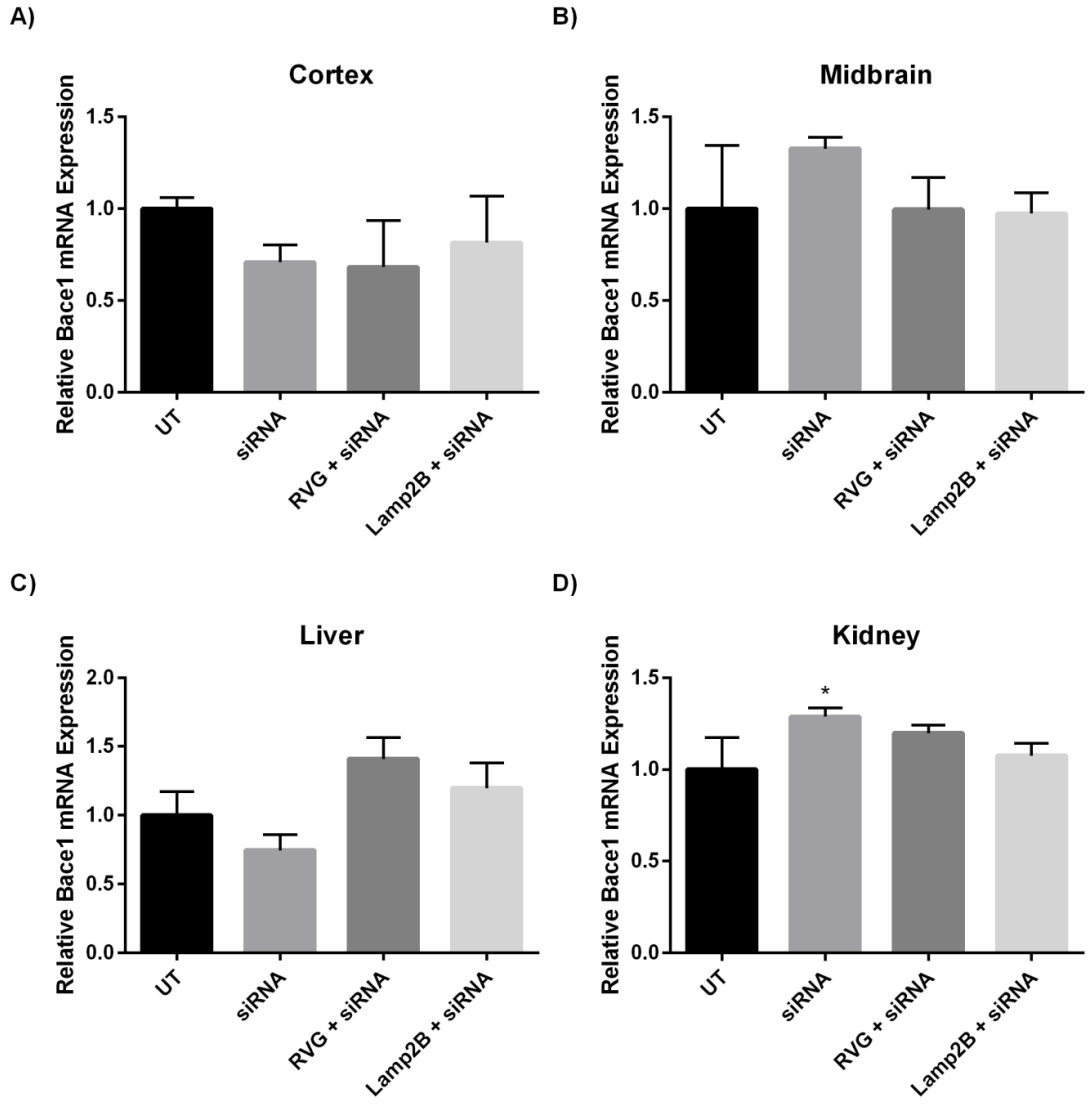

Figure 3.6 Re-analysis of EV-mediated Bace1 siRNA Delivery *In Vivo* Normalised to Optimal Reference Genes. *Bace1* mRNA expression, relative to the geometric mean of *Gapdh* and *β-Actin*, was assessed by qPCR 48 hours after intravenous injection of 150 µg Bace1 siRNA alone or loaded within EVs. EV source BM-DCs were transfected with the Lamp2B-RVG targeting construct ("RVG") or Lamp2B control construct ("Lamp2B"). To load EVs with siRNA, the total yield of RVG-EVs or Lamp2B-EVs derived from the BM-DC cells obtained from 1.5 mice and 150 µg Bace1 siRNA was electroporated using a 400 V / 125 µF pulse. Relative *Bace1* expression was analysed in the **(A)** cortex, **(B)** midbrain, **(C)** liver and **(D)** kidney in comparison to untreated ("UT", 5% glucose injection only) control mice. Values are mean ± SEM, n = 3, *p<0.05, one-way ANOVA followed by Tukey's post-hoc test.

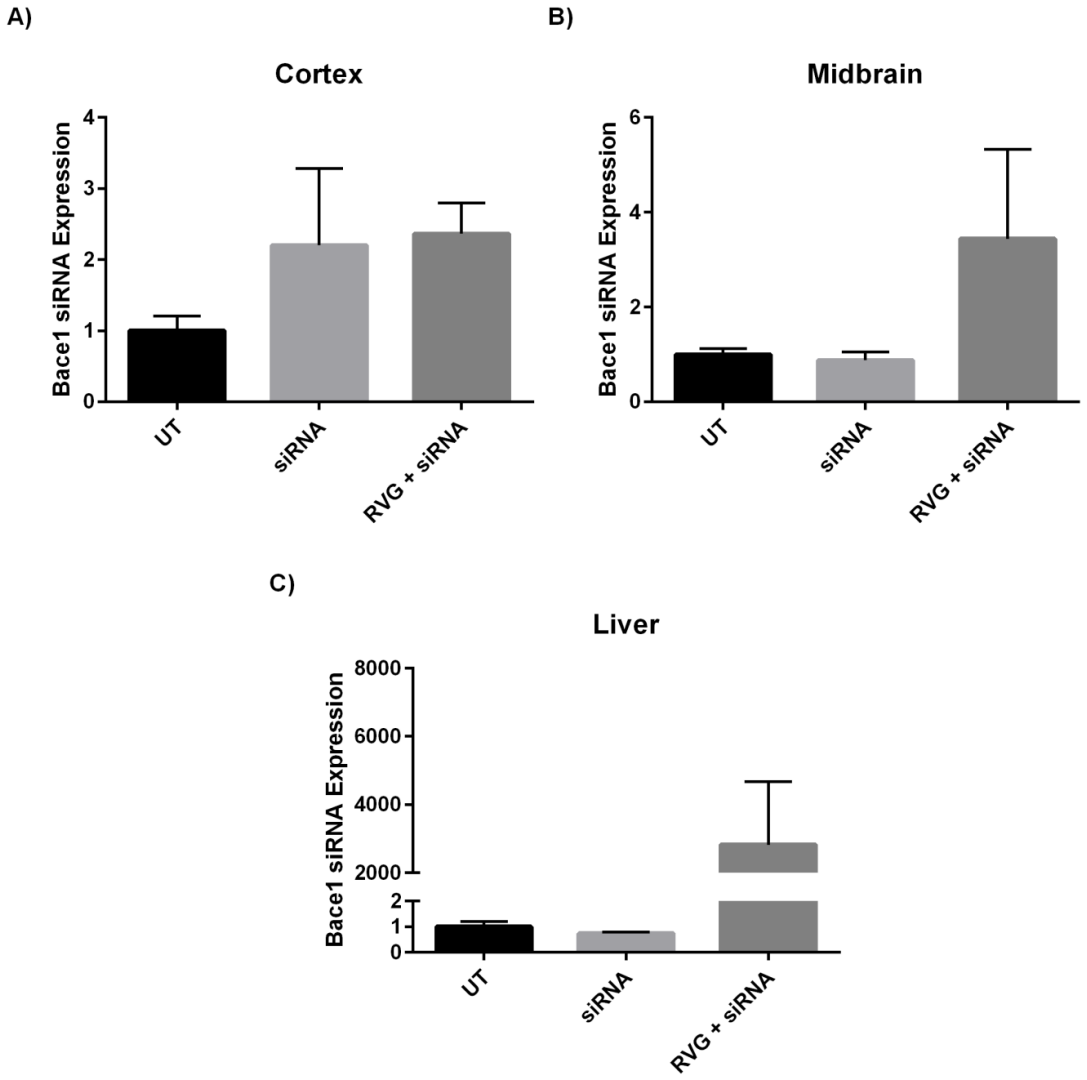

Figure 3.7 Quantification of *In Vivo* Bace1 siRNA Delivery. Bace1 siRNA, normalised to 10 ng total RNA input volume, was quantified by qPCR 48 hours after intravenous injection of 150 µg Bace1 siRNA alone ("siRNA") or loaded within EVs. EV source BM-DCs were transfected with the Lamp2B-RVG targeting construct ("RVG"). To load EVs with siRNA, the total yield of RVG-EVs derived from the BM-DC cells obtained from 1.5 mice and 150 µg Bace1 siRNA was electroporated using a 400 V / 125 µF pulse. Bace1 siRNA quantity was assessed in **(A)** cortex, **(B)** midbrain and **(C)** liver in comparison to untreated ("UT", 5% glucose injection only) control mice. Values are mean ± SEM, n = 3, one-way ANOVA.

3.2.5 Characterisation of Neuro2A-derived Extracellular Vesicles

The previous experiments failed to replicate the *in vitro* or *in vivo* results of Alvarez-Erviti *et al*.[508] using BM-DC-derived EVs to deliver Bace1 siRNA. To investigate this further, the *in vitro* experiments were repeated using Neuro2A-derived EVs. Neuro2A-derived EVs were chosen as a more feasible model for optimisation purposes and to determine whether replication failure could be related to the harvesting or yield of BM-DC-derived EVs.

EVs were derived from Neuro2A source cells after 48 hours of incubation by differential ultracentrifugation and characterised by Western blot, EM and NTA (**Fig. 3.8**). Neuro2A cells and derived EVs were probed for the exosomal markers, Alix and Tsg101, in addition to the ER membrane marker, Calnexin and loading control, β-Actin. This confirmed that typical exosome markers were enriched in EV preparations while the ER marker, usually associated with secreted apoptotic bodies, was absent (**Fig. 3.8A**). EM and NTA established that preparations contained vesicles comprising a lipid-bilayer membrane with typical exosomal morphology and size (**Fig. 3.8B-D**). In contrast to BM-DC-derived EVs, EM and NTA revealed that Neuro2A-derived EV preparations appeared more homogenous with fewer larger particles, evidenced by the relatively narrow mode peak at 94.6 nm (**Fig. 3.8B-D**).

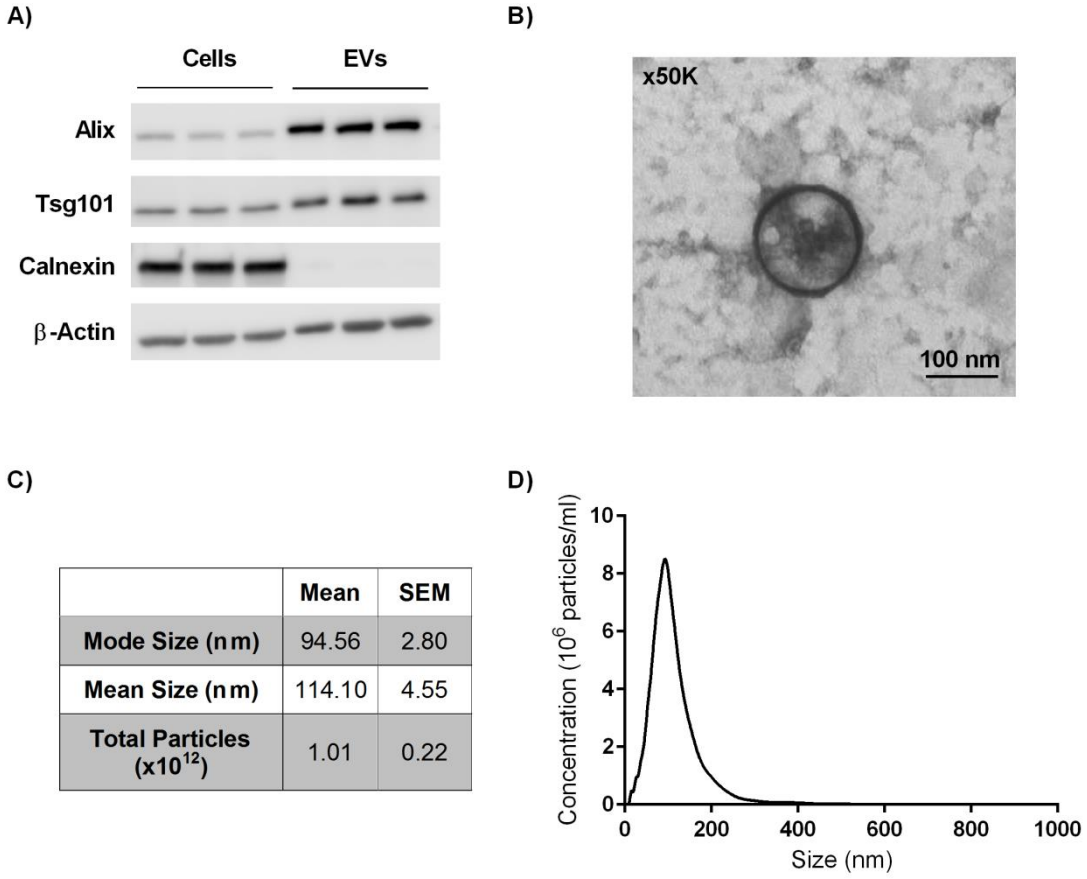

	Mean	SEM
Mode Size (nm)	94.56	2.80
Mean Size (nm)	114.10	4.55
Total Particles ($x10^{12}$)	1.01	0.22

Figure 3.8 Characterisation of Neuro2A-derived Extracellular Vesicles. EVs derived by differential ultracentrifugation from Neuro2A cells after 48 hours incubation were characterised by a number of methods. **(A)** EVs (25% of total EV preparation isolated from 1 x 15 cm cell culture dish) and Neuro2A cell lysates (50 µg) were probed by Western blot for the exosomal markers, Alix and Tsg101, the ER membrane marker, Calnexin and loading control, β-Actin. The typical exosome markers were enriched in EV preparations while the ER marker, usually observed in association with secreted apoptotic bodies, was absent. **(B)** Electron microscopy image of EV showing typical exosomal morphology and size. **(C)** NTA analysis of Neuro2A-derived EV samples (n = 3) showing the mean statistics for particle size and total particle count (total yield per 1 x 15 cm cell culture dish). **(D)** NTA analysis of size distribution histogram for Neuro2A-derived EV samples (n = 3), peak = 94.6 nm.

3.2.6 *Bace1* Expression was not Silenced by siRNA-loaded Neuro2A-derived Extracellular Vesicles *In Vitro*

To assess the efficacy of EV-mediated siRNA delivery by Neuro2A-derived EVs, the same experimental set-up as employed for BM-DC-derived EVs was utilised. Neuro2A source cells were modified to express either the Lamp2B-RVG or Lamp2B control construct or were left untreated. EVs were isolated by differential ultracentrifugation and loaded with Bace1 siRNA at various ratios by electroporation or left unelectroporated as a control. After electroporation the mixture was washed and pelleted at 120,000 x g before addition to Neuro2A recipient cells in 24-well cell culture plates. Neuro2A cells were also directly transfected with 200 nM Bace1 siRNA or NC siRNA as further controls. *Bace1* mRNA expression, relative to *β-Actin*, was assessed by qPCR 48 hours after EV treatment.

A ratio of 6 μg Neuro2A-EVs: 100 pmol (200 nM) Bace1 siRNA per well was first tested as above (**Fig. 3.9A-C**). Direct transfection of Bace1 siRNA elicited effective silencing of *Bace1* mRNA expression. However, there were no consistent effects following treatment with siRNA-loaded RVG-EVs or Lamp2B-EVs across a number of replicates (**Fig. 3.9A-C**). Furthermore, increased *Bace1* mRNA expression was sometimes observed following treatment with RVG-EVs or Lamp2B-EVs (**Fig. 3.9B-C**).

It was again hypothesised that a failure to achieve mRNA knockdown may be due to an insufficient yield of siRNA-loaded EVs. Therefore, the experiment was repeated with 10 μg EVs: 100 pmol (200 nM) Bace1 siRNA. This resulted in a significant reduction in

Bace1 mRNA expression following treatment with electroporated RVG-EVs (~34% reduction), and both electroporated and unelectroporated Lamp2B-EVs (~57% and 59% reduction, respectively) (**Fig. 3.9D**). To determine whether silencing could be enhanced by increasing the ratio of EVs: siRNA and reducing the number of recipient cells, 50% of the total EV yield obtained from 1 x 15 cm cell culture dish was electroporated with 300 pmol Bace1 siRNA (100 pmol per well) while the remaining 50% was mixed with 300 pmol Bace1 siRNA but left unelectroporated. After washing, the pellet was resuspended and divided equally amongst 3 wells of a 96-well cell culture plate (**Fig. 3.9E**). Under these conditions, there was no significant silencing; instead, *Bace1* mRNA expression was significantly upregulated following treatment with electroporated RVG-EVs (**Fig. 3.9E**).

Given the increased *Bace1* mRNA expression observed across several conditions and the failure to consistently replicate findings from the previous report[508] the role of endogenous EV cargoes was considered. Specifically, Neuro2A-derived EVs were assessed to determine whether they carry APP and Bace1 mRNA and protein by qPCR and Western blot, respectively (**Fig. 3.10**). This is important as several recent studies have suggested that exosomes may be secreted in association with full length APP, APP metabolites, including CTFs and amyloid-β peptides, and tau from a range of cells, including Neuro2As, both *in vitro* and *in vivo*[491,561–565]. The level of *APP* and *Bace1* mRNA expression in Neuro2A-EVs was determined relative to the quantity found within untreated Neuro2A cells. However, it should be noted that due to difficulties in matching RNA input (500 ng RNA input for cells compared to 10 µl (33%) EV sample) the quantities are not directly comparable but are intended to provide an indication as to the presence or absence of the given mRNA.

Both *APP* and *Bace1* mRNA were present at very low levels within Neuro2A-derived EVs (**Fig. 3.10A-B**). However, there was a relatively higher proportion of *Bace1* mRNA (mean CT values; cells, 29.89, EVs, 34.87) compared to *APP* mRNA (mean CT values; cells, 23.21, EVs, 32.18) when considered relative to the quantities within Neuro2A source cells (**Fig. 3.10A-B**). This is consistent with the relative expression of APP and Bace1 protein within Neuro2A cells and derived EVs as indicated by Western blot (**Fig. 3.10C**). Thus, while in Neuro2A cells, APP protein appears more abundant than Bace1, only Bace1 protein was detected within Neuro2A-derived EVs, suggesting a degree of selective enrichment (**Fig. 3.10C**). The transfer of Bace1 mRNA and protein within Neuro2A-derived EVs could therefore have contributed towards the increased *Bace1* mRNA expression observed previously. These findings highlight the importance of considering endogenous EV content when selecting EVs for therapeutic purposes.

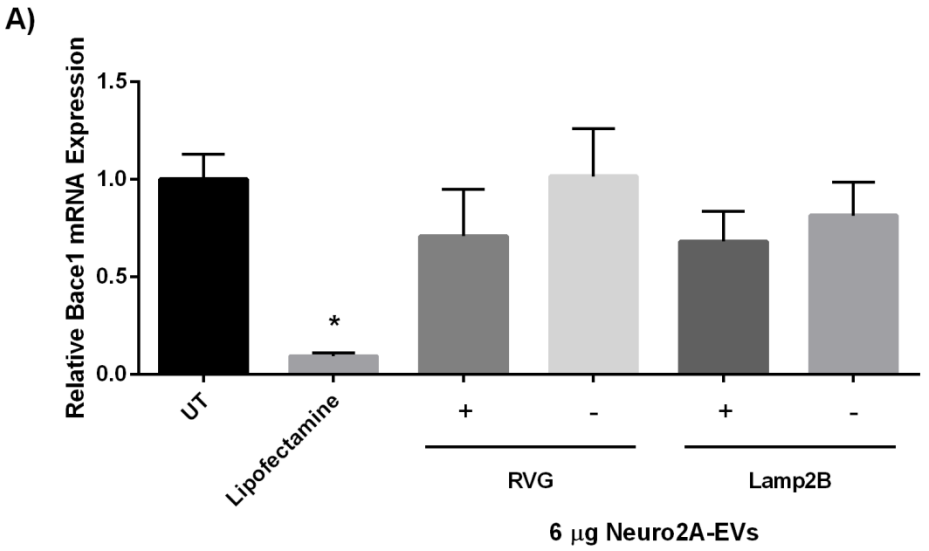
A)
Relative Bace1 mRNA Expression
1.5
1.0
0.5
0.0
*
UT
Lipofectamine
+
-
+
-
RVG
Lamp2B
6 μg Neuro2A-EVs

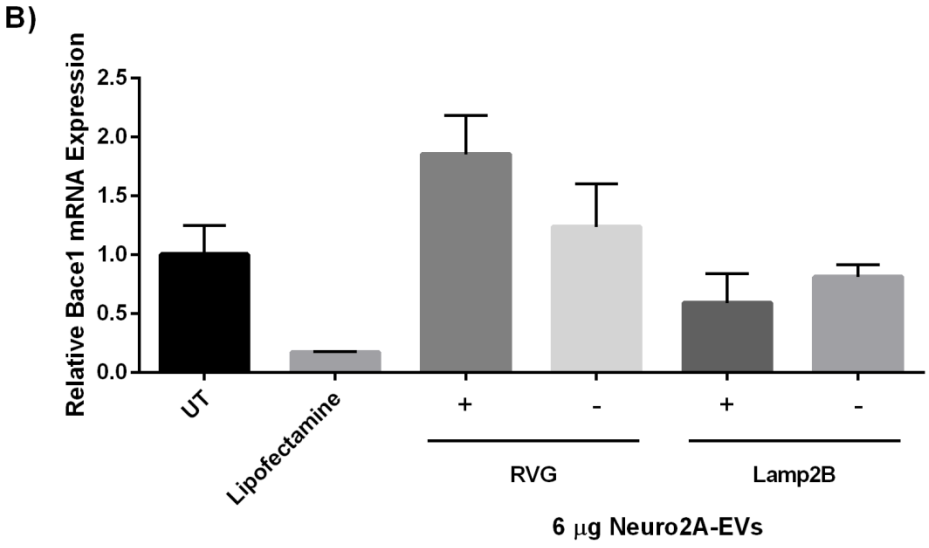
B)
Relative Bace1 mRNA Expression
2.5
2.0
1.5
1.0
0.5
0.0
UT
Lipofectamine
+
-
+
-
RVG
Lamp2B
6 μg Neuro2A-EVs

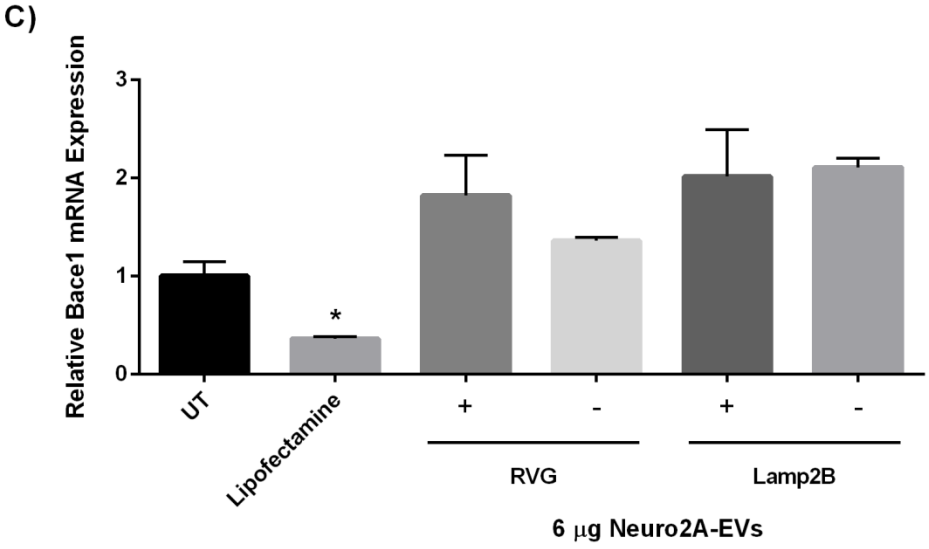
C)
Relative Bace1 mRNA Expression
3
2
1
0
*
UT
Lipofectamine
+
-
+
-
RVG
Lamp2B
6 μg Neuro2A-EVs

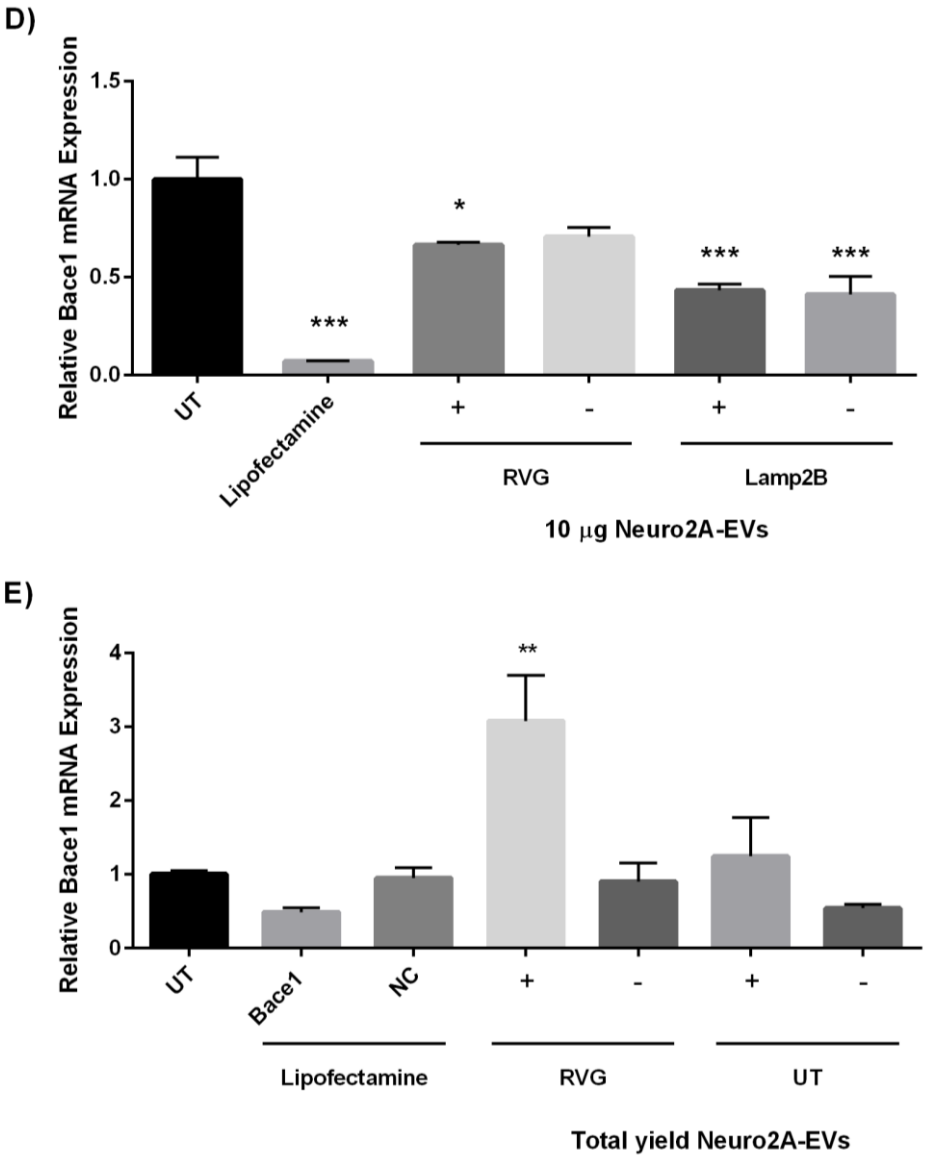

Figure 3.9 Treatment of Neuro2A Cells with Neuro2A-derived Extracellular Vesicles. *Bace1* mRNA expression, relative to *β-Actin*, was analysed in Neuro2A cells by qPCR 48 hours after treating cells with Bace1 siRNA-loaded EVs or controls. EV source Neuro2As were transfected with the Lamp2B-RVG targeting construct ("RVG"), Lamp2B control construct ("Lamp2B") or left untreated ("UT"). To load EVs with siRNA, EVs were mixed in electroporation buffer with 100 pmol Bace1 siRNA per replicate before the mixture was electroporated using a 400 V / 125 µF pulse ("+") or left unelectroporated ("-"), washed and added to cells. **(A-C)** 6 µg EVs or **(D)** 10 µg EVs were applied to Neuro2A cells in 24-well cell culture plates. **(E)** 50% of the total EV yield collected from 1 x 15 cm cell culture dish was applied to Neuro2A cells in 96-well cell culture plates. As controls, Neuro2A cells were transfected with 100 pmol Bace1 siRNA ("Bace1") or negative control siRNA ("NC") using Lipofectamine 2000. Values are mean ± SEM, n = 3, ***p<0.001, **p<0.01, *p<0.05, one-way ANOVA followed by Tukey's post-hoc test.

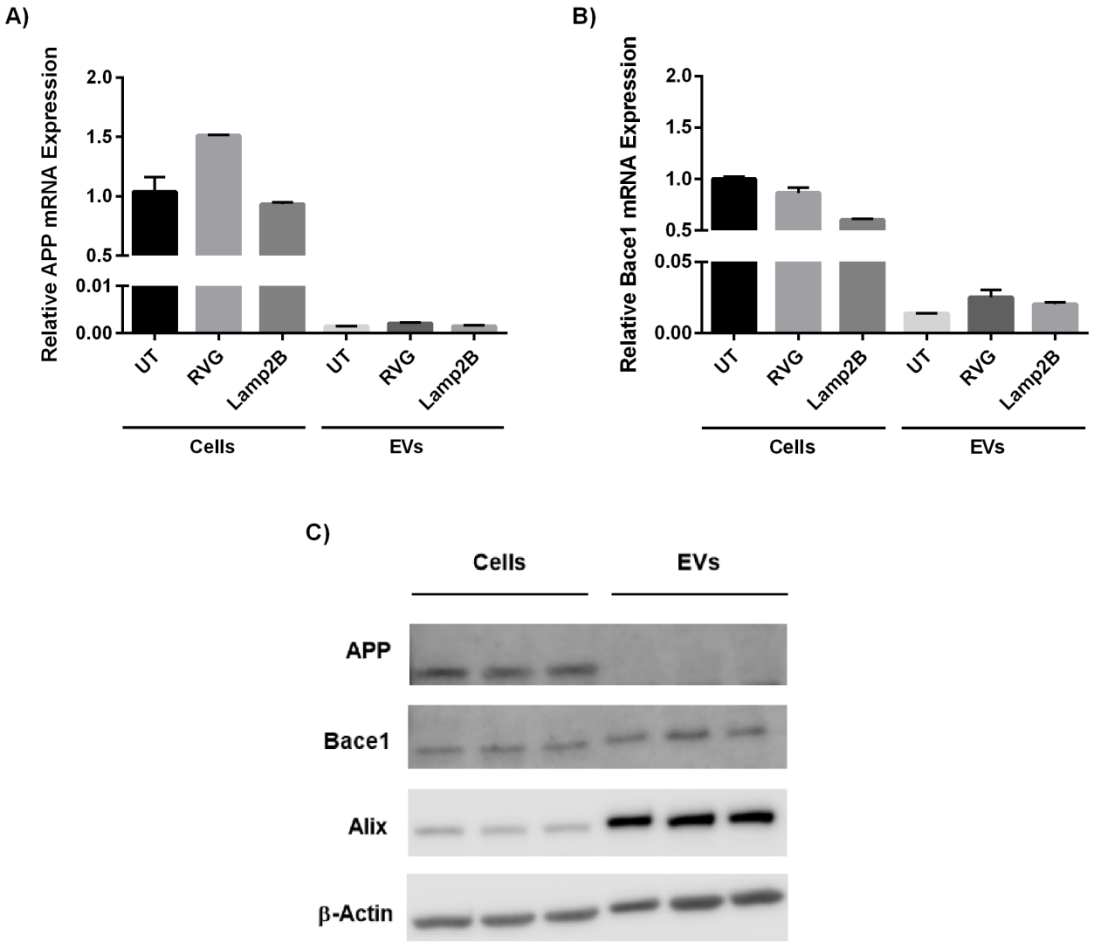

Figure 3.10 Quantification of APP and Bace1 mRNA and Protein within Neuro2A Cells and Extracellular Vesicles. Relative mRNA expression levels, normalised to *β-Actin* expression (cells) or input volume (EVs, 10 µl), compared to untreated cells, were determined by qPCR in Neuro2A cells and derived-EVs that were untreated ("UT") or had been transfected with the Lamp2B-RVG targeting construct ("RVG") or Lamp2B control construct ("Lamp2B") for **(A)** *APP* mRNA and **(B)** *Bace1* mRNA. Both *APP* and *Bace1* mRNA were detectable in cells and, at very low levels, in EVs (33% of total EV preparation). **(C)** APP and Bace1 protein expression in UT Neuro2A cells (50 µg protein loaded) and EVs (25% of total EV preparation) was probed by Western blot. Bace1 protein was detected in both cells and EVs, while APP protein was detected only in cells. β-Actin and the exosomal marker, Alix, are included as loading controls. Values are mean ± SEM, n = 3.

3.2.7 Quantification of Extracellular Vesicle Loading After Electroporation

An alternative explanation for the failure to replicate the results of Alvarez-Erviti *et al.*[508] may relate to inefficient and inconsistent loading of EVs by electroporation. Previous reports of electroporation loading efficiency have ranged from ~10 to ~55%[450,508,511]. However, despite extensive optimisation of electroporation parameters, electroporation loading efficacy has been acknowledged to vary significantly[511]. Thus, inefficient loading of EVs could potentially account for the failure to replicate previous findings.

To determine whether this might be the case, loading efficiency in terms of the percentage of Bace1 siRNA retained was assessed by qPCR normalised by total EV input volume (**Fig. 3.11**). EVs (18 µg) were derived from untreated Neuro2A cells and electroporated with Bace1 siRNA (300 pmol) or left unelectroporated as a control. Samples were washed and pelleted before Bace1 siRNA quantity was assessed. Electroporation of 300 pmol siRNA with 18 µg Neuro2A-derived EVs resulted in higher siRNA retention (75.0% retention) compared to unelectroporated samples (14.6%) (**Fig. 3.11A**). Bace1 siRNA expression was also assessed in EVs which had not been mixed with siRNA. In these samples, Bace1 siRNA detection was negligible (0.3% electroporated, 0.2% unelectroporated) (**Fig. 3.11A**).

The percentage of Bace1 siRNA retained following electroporation of Bace1 siRNA with increasing quantities of EVs (18, 24 and 30 µg) was also assessed (**Fig. 3.11B**). As before, increased siRNA retention was observed following electroporation of Bace1 siRNA with all three quantities of EVs in comparison to unelectroporated samples (**Fig.**

3.11B). Interestingly, the greatest siRNA retention was observed following electroporation with 18 µg EVs (75.0%) followed by 30 µg (67.3%) and 24 µg EVs (55.1%) (**Fig. 3.11B**). Together, these results suggest high loading efficiency of Bace1 siRNA following electroporation with a range of EV quantities.

However, as an additional control, Bace1 siRNA was also electroporated or left unelectroporated in the absence of EVs (**Fig. 3.11C**). Strikingly, this revealed that electroporation of siRNA in the absence of EVs resulted in similar, if not greater, levels of siRNA retention (86.7%) as when electroporated in the presence of 18 µg EVs (75.0%) (**Fig. 3.11C**). To determine what might be the cause of these unexpectedly high levels of siRNA retention in the absence of EVs, electroporated and unelectroporated samples of Bace1 siRNA alone or in the presence of 18 µg EVs were assessed by EM (**Fig. 3.12**). This revealed the formation of large aggregates in the vicinity of EVs following the electroporation of Bace1 siRNA with EVs (**Fig. 3.12A**). In contrast, no such aggregates were observed when Bace1 siRNA and EV samples were not electroporated (**Fig. 3.12B**). Intriguingly, large formations of siRNA aggregates were also observed in the absence of EVs following electroporation of Bace1 siRNA alone (**Fig. 3.12C**). Again, no aggregates were observed when Bace1 siRNA alone samples were left unelectroporated (**Fig. 3.12D**). Thus, these findings suggest that siRNA may be retained within large aggregates which might entrap EVs rather than being encapsulated within them and this may lead to overestimation of loading efficiency following electroporation.

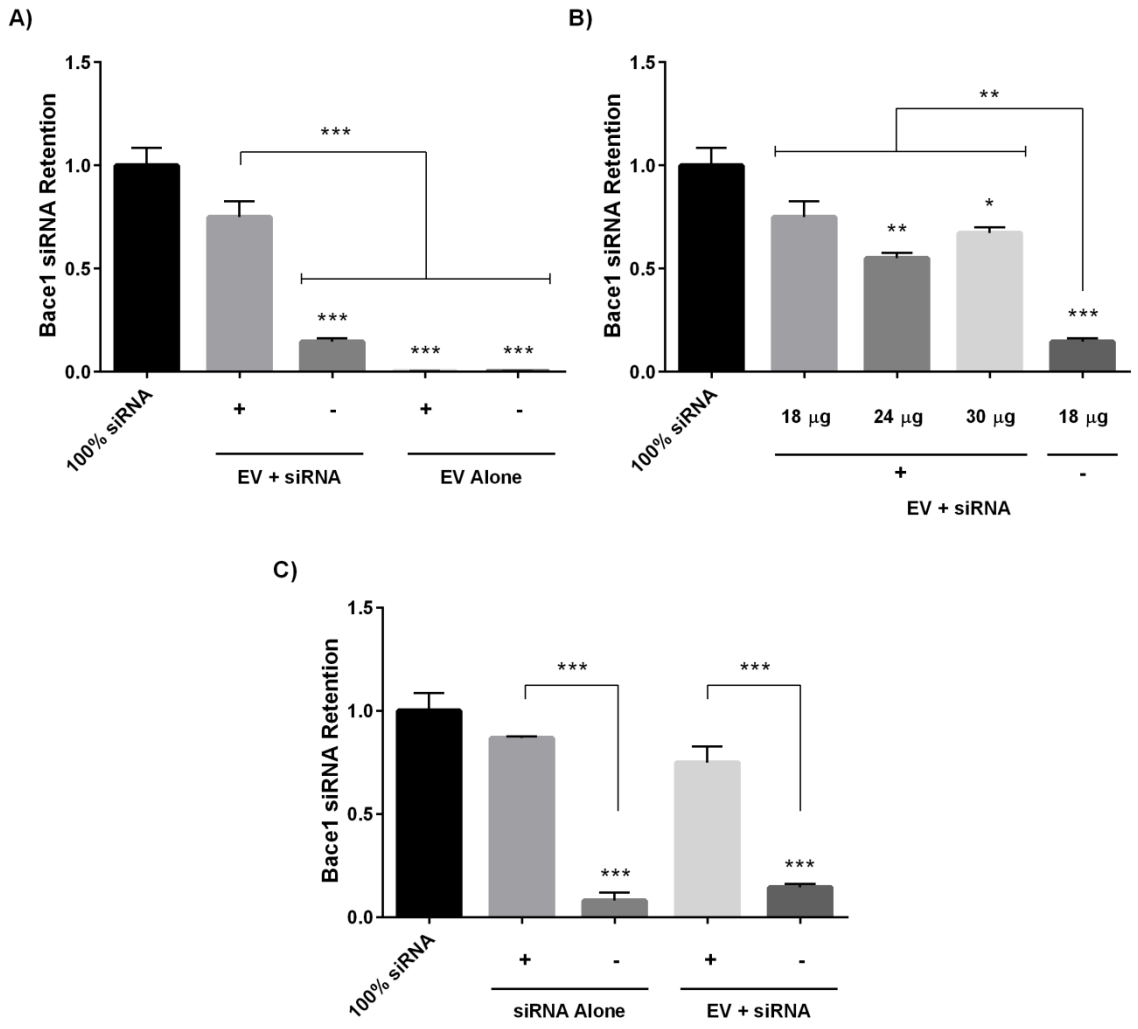

Figure 3.11 Quantification of Bace1 siRNA Retention Following Electroporation. Neuro2A-derived EVs were mixed with 300 pmol Bace1 siRNA and electroporated using a 400 V / 125 µF pulse ("+") or left unelectroporated ("–") in control experiments before pelleting at 120,000 x g. The quantity of retained Bace1 siRNA in the EV pellet was analysed by qPCR normalised to total input volume and compared to a total siRNA input control. **(A)** Electroporation of siRNA with 18 ug EVs led to higher siRNA retention compared to unelectroporated samples ("EV + siRNA"), whereas very little siRNA was detected in negative control samples ("EV Alone"). **(B)** Increased siRNA retention was also observed when using higher quantities of EVs (18, 24 and 30 µg) for electroporation. **(C)** Electroporation of siRNA in the absence of EVs ("siRNA Alone") produced similar levels of siRNA retention as when siRNA was electroporated in the presence of 18 µg EVs ("EV + siRNA"). Values are mean ± SEM, n = 3, ***p<0.001, **p<0.01, *p<0.05, one-way ANOVA followed by Tukey's post-hoc test.

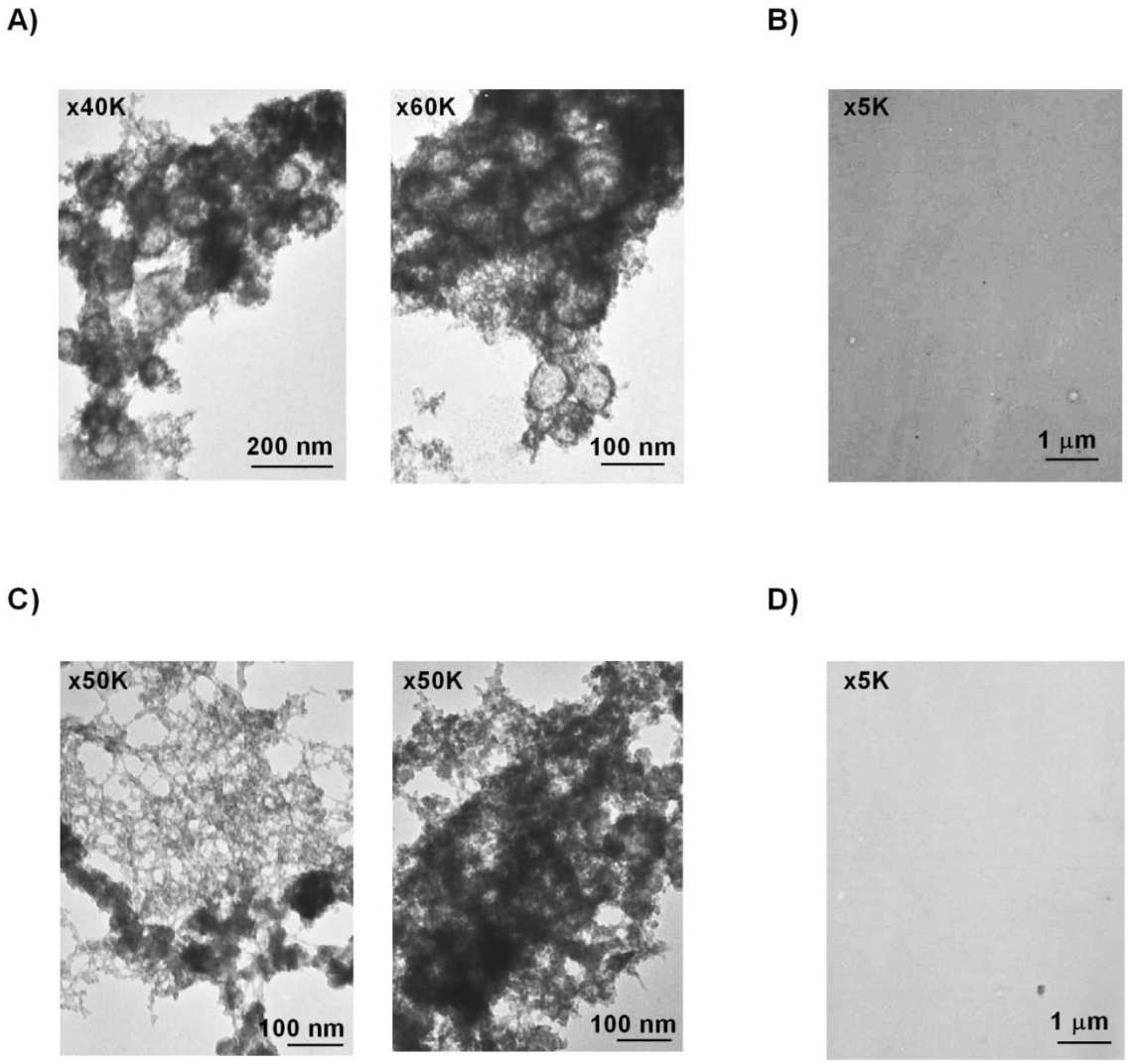

Figure 3.12 Aggregation of siRNA Following Electroporation. Bace1 siRNA (300 pmol) was added alone to electroporation buffer or in the presence of Neuro2A-derived EVs (18 µg) and electroporated using a 400 V / 125 µF pulse or left unelectroporated before pelleting at 120,000 x g. The resulting pellet was assessed by electron microscopy. **(A)** Formation of aggregates in the vicinity of EVs following the electroporation of EVs and Bace1 siRNA preparations. **(B)** There was no formation of aggregates in unelectroporated EV and Bace1 siRNA preparations. **(C)** Formation of siRNA aggregates in the absence of EVs following the electroporation of Bace1 siRNA alone. **(D)** There was no formation of aggregates in unelectroporated Bace1 siRNA alone preparations.

3.3 Discussion

This study assessed the efficacy of EV-mediated delivery of siRNA targeting AD-relevant genes. APP and Bace1 siRNA sequences were identified and confirmed to elicit potent silencing of their respective target mRNAs following direct transfection of HEK293T or Neuro2A cells *in vitro*. Subsequently, the remainder of the study focused upon the optimisation of EV-mediated delivery of Bace1 siRNA both *in vitro* and *in vivo*. However, contrary to previous findings upon which this chapter was originally based[508], EV-mediated delivery of siRNA did not produce consistent silencing of *Bace1* mRNA either *in vitro* or *in vivo*. A number of approaches were taken to determine the source of this discrepancy including alternative sources and quantities of EVs, assessment of endogenous cargoes and finally characterisation of electroporation efficiency. Strikingly, this revealed the presence of large aggregates following the electroporation of Bace1 siRNA either alone or in combination with EVs, with similar levels of retained siRNA. These results therefore suggest that loading efficiency may be greatly overestimated following electroporation and may be a confounding factor in EV-mediated delivery. Together, the results of this study suggest alternative loading mechanisms should be pursued.

Precipitation of siRNA following Electroporation

The large aggregates observed following electroporation of Bace1 siRNA alone or together with EVs are consistent with the findings from one other recent publication[566]. In this study, Kooijmans and colleagues[566] reported similar or greater levels of siRNA retention following the electroporation of siRNA alone compared to in the presence of

EVs, which was attributed to large insoluble siRNA aggregates induced by electroporation. siRNA aggregation was shown to result from complex formation between metal ions from the electrodes of the electroporation cuvettes and hydroxide ions within the electroporation buffer. Reduction of metal ions, through the use of different electrode materials, and/or hydroxide ions, by varying the composition of electroporation buffer, almost completely attenuated complex formation after electroporation. However, when this was the case the level of retained siRNA was less than 0.05% and of similar levels whether siRNA was electroporated alone or in the presence of EVs[566].

These findings are consistent with a previous report by Stapulionis *et al*.[567] who showed that electric discharges through solutions of biological macromolecules, including DNA, RNA and protein, induced their precipitation. Precipitation was attributed to an interaction between biological macromolecules and the metal ions solubilized from the anode electrode by the electric pulse. Stapulionis *et al*.[567] also reported that 30% of pulsed DNA and RNA could be pelleted at just 7,000 x g for two minutes. This is highly relevant given that in the current study, samples were washed and pelleted at 120,000 x g for 70 minutes after electroporation. This could therefore account for the apparently high loading efficiency observed (75.0%) following electroporation of Bace1 siRNA with 18 µg EVs. In combination with these two previous reports, the current findings strongly suggest that loading efficiency may be greatly overestimated following electroporation. It was previously believed that siRNA was encapsulated within exosomes following electroporation[508,511]. However, the extensive precipitates of siRNA observed here and in the previous report[566] in which exosomal fractions floated at a difference density to siRNA aggregates, suggest that this is not the case. Instead,

while a small proportion of siRNA may be encapsulated within EVs, the majority of siRNA retained following electroporation appears to be in the form of large siRNA aggregates.

However, it is important to note the findings of Momen-Heravi *et al*.[450] who used electroporation to load B-cell derived exosomes with miR-155 mimics or inhibitors. Momen-Heravi *et al*.[450] chose to include 1 mM EDTA in their electroporation buffer as Kooijmans and colleagues[566] had shown that EDTA prevented the interaction of cations with components within the electroporation buffer. Exosomes were also treated with RNase H to eliminate unloaded miR-155 mimic/inhibitor outside of exosomes. In contrast to Kooijmans and colleagues[566], who showed that EDTA reduced both aggregate formation and the percentage of siRNA retained to almost negligible levels, Momen-Heravi *et al*.[450] reported loading efficiency of 55%. Loaded exosomes produced functional effects both *in vitro* and *in vivo* and exosome-mediated miR-155 inhibitor delivery was functionally more efficient and less toxic compared to conventional transfection methods[450]. It is unclear why these results are discrepant to those of Kooijmans and colleagues[566], as based on their findings the presence of EDTA would be expected to significantly reduce loading efficiency and functional efficacy. However, while RNase H treatment was applied to degrade miR-155 not encapsulated within exosomes, given that RNase H targets RNA:DNA duplexes, any potential aggregates of miR-155 mimics outside of EVs may not have been degraded as intended.

One key difference between the two studies is the method of exosome isolation following electroporation. While Kooijmans and colleagues[566] utilised differential ultracentrifugation and sucrose density gradient centrifugation to isolate exosomes,

Momen-Heravi *et al.*[450] used Exoquick-TC (System Biosciences), a commercial polymer-based exosome precipitation reagent. A recent comparison study between more conventional methods such as ultracentrifugation or sucrose density gradient centrifugation and precipitation-based methods such as Exoquick revealed that Exoquick also precipitated non-exosomal contaminants[568]. Momen-Heravi *et al.*[450] tested three different methods for re-isolation of exosomes including ultracentrifugation, immunomagnetic isolation and Exoquick-TC. Based on relative miR-155 expression, Exoquick-TC was identified as the recovery method of choice. However, no electron microscopy data were provided. Therefore, it is unclear whether the use of Exoquick-TC improved the retained miR-155 yield by precipitation of any miR-155 aggregates that may have remained following EDTA and RNase H treatment. It should also be noted that both Kooijmans and colleagues[566] and the current study revealed large precipitates following electroporation of siRNA while Momen-Heravi *et al.*[450] utilised miR-155 mimics and inhibitors. Although miRNA mimics may be expected to form similar aggregates, this remains to be shown.

Discrepancy with Previous Literature – Quantification of EV Protein Concentration and Importance of Normalisation Gene?

While the presence of large siRNA aggregates may account for why the current study failed to elicit silencing of *Bace1* mRNA, they do not explain the discrepancy with the results of Alvarez-Erviti *et al.*[508] who utilised similar experimental conditions. One potential area for discrepancy is the quantity of exosomes included in each electroporation. Alvarez-Erviti *et al.*[508] and the current study used Bradford protein assay reagent to quantify EV protein concentration. However, this method is

challenging given the potential for contamination by medium proteins. The precise quantity of EVs is an important factor as Wahlgren *et al.*[511] reported that loading efficiency was reduced with increasing exosome quantities within electroporation samples. This may link to reduced precipitation of siRNA aggregates as Kooijmans *et al.*[566] also showed that retained siRNA levels were reduced with increasing exosome quantities. They suggested that this may be due to the capture of multivalent ions by the negatively charged EV membrane or by changes to buffer conductivity following the addition of EVs. Wahlgren *et al.*[511] also noted that electroporation efficiency varied significantly despite extensive optimisation. This suggests that the degree of siRNA precipitation may sensitively depend on a range of different parameters. Therefore, it is possible that the discrepancy between the current results and those of Alvarez-Erviti *et al.*[508] may perhaps be explained by inherent variability in both exosome protein quantification and electroporation-induced precipitation. Together, these factors may contribute to different proportions of aggregated siRNA as opposed to siRNA which is more directly associated or encapsulated within EVs.

An alternative explanation that must be considered relates to the identity of the normalisation gene. As shown in the current study, the choice of normalisation gene substantially altered the pattern of results. When *β-Actin* was used for normalisation, significant silencing of cortical *Bace1* mRNA was observed following all experimental treatments. However, this apparent silencing was eliminated following normalisation to *cyclophilin*. Subsequently, *β-Actin* and *Gapdh* were identified as the optimal pair of normalisation genes by geNorm-based analysis. When the data were reanalysed with respect to the geometric norm of these two genes, the pattern of silencing was similar to that originally obtained with respect to *β-Actin*, but no longer reached significance.

These findings clearly highlight the importance of identifying the correct normalisation gene as apparently reduced expression may be an artefact of the normalisation gene chosen. It is therefore of note that in the study of Alvarez-Erviti *et al*.[508], *in vitro* and *in vivo* data were normalised relative to *18S*. Although it is important to note that optimal reference genes vary across experiments, *18S* was identified as the 4th most stable gene by geNorm analysis in the current study. It is therefore feasible that a different choice of normalisation gene may have contributed towards the inconsistent results.

In the previous two studies[508,513], RVG-EVs selectively targeted neuronal cells both *in vitro* and *in vivo*. While there was a trend towards cortical targeting of EVs *in vivo* in the current study, this was not observed *in vitro*. Furthermore, both Lamp2B-EVs and RVG-EVs appeared to achieve similar effects *in vivo*, while *in vitro* treatment with Lamp2B-EVs often produced an inconsistent trend towards greater mRNA silencing than RVG-EV treatment. Whether this relates to differences in the level of siRNA aggregation is unclear. However, it is important to note that Lamp2B has previously been implicated in a role in cell adhesion[569]. Expression of the Lamp2B control construct may therefore have contributed to EV and recipient cell binding and uptake. As discussed previously, the mechanisms determining the selectivity of EV uptake are not fully understood. However, cell adhesion molecules are thought to play a key role in mediating EV and recipient cell interactions[457–459]. Whether Lamp2B may contribute towards EV uptake and whether this effect might be blocked by fusion to the RVG-peptide is unclear.

A preliminary analysis of Bace1 siRNA quantity *in vivo* revealed a trend towards a small increase in Bace1 siRNA in cortical tissues following siRNA alone or RVG-EV

treatment and a large increase in liver following RVG-EV treatment. Whether these increases relate to the presence of siRNA aggregates or a small proportion of siRNA associated with EVs remains to be seen. Indeed, whether siRNA aggregates may be taken up by recipient cells, either neuronal or otherwise, is unknown. Naked siRNA is typically degraded and excreted rapidly by the liver and kidneys. Whether aggregates are not so quickly degraded or whether association with EVs offers some form of protection against degradation may account for the large increase in Bace1 siRNA expression in the liver. An inability of siRNA to escape either EVs or aggregated precipitates could explain why such high levels of Bace1 siRNA were not associated with enhanced silencing of *Bace1* expression in the liver following RVG-EV treatment.

Potential Role of Endogenous Protein and RNA Cargoes

This study also highlighted the importance of considering endogenous cargoes when choosing the source of EVs as Neuro2A-derived EVs were found to contain Bace1 mRNA and protein and *APP* mRNA. Furthermore, given the relative proportions observed in source cells there appeared to be selective EV enrichment of Bace1 mRNA and protein. These findings complement previous reports in which APP, amyloid-β peptides and tau have been identified within EVs, both *in vitro* and *in vivo*[491,561–565]. Indeed, a number of studies have now suggested that exosomes may be involved in the spread of pathology in a prion-like manner as EVs carrying disease-associated forms of proteins may induce pathological protein folding in near and distant recipient cells[489,570].

In contrast, other reports suggest that EVs may also play a beneficial role in AD. For example, neuronal-derived EVs, enriched with abundant glycosphingolipids, were able

to capture amyloid-β and promote clearance by microglia. Interestingly, this did not appear to be the case for glial-derived EVs, highlighting cell-source specific EV properties[571–573]. Similarly, adipose-derived MSCs (AD-MSCs) secreted exosomes carrying neprilysin, an enzyme important for amyloid-β degradation within the brain[574]. AD-MSC-derived exosomes decreased both secreted and intracellular amyloid-β levels in Neuro2A cells. This effect was more pronounced for AD-MSC-derived EVs compared to EVs secreted from bone-marrow-derived MSCs[574]. Together, these findings demonstrate the importance of carefully selecting EV source cells for each specific therapeutic purpose to avoid any potential pathological consequences of endogenous cargoes.

In summary, the current study revealed that EV-loading efficiency may be greatly overestimated due to the formation of large siRNA aggregates during electroporation. These findings therefore highlight the need for alternative EV-loading methods.

4 Endogenous Loading of RNAi-based Therapeutic Cargoes

4.1 Introduction

EV-loading efficiency appears to be inflated by the presence of large siRNA aggregates following electroporation. Therefore, an alternative EV-loading strategy is required. Several recent reports have described the loading of miRNA mimics and inhibitors into EVs following transfection of either mature mimics/inhibitors or expression plasmids into EV source cells[468,507,514,515]. This strategy relies upon exploitation of the endogenous loading machinery for secretion of exogenous RNAi-based molecules within EVs. Given that electroporation induces the formation of siRNA aggregates and may disrupt the integrity and functional properties of EVs and their cargoes, endogenous loading techniques may produce loaded EVs that are more biologically-relevant.

The mechanisms which direct the selective loading of specific miRNAs into EVs are not fully understood. Furthermore, it is unclear whether endogenous miRNAs carried by EVs require association with other components to elicit functional effects in recipient cells. Such a functional association would not necessarily be achieved by exogenous loading methods in which the cargo of interest is simply electroporated or co-incubated with isolated EVs. Endogenous loading techniques may therefore represent a more promising approach in terms of ensuring exogenous RNAi effectors are loaded into EVs in association with any proteins required for functional activity in recipient cells.

One potentially important association may be with RNA-binding proteins such as AGO2, GW182, Stau1 and Stau2, all of which have been reported within EVs[385,387,468,470]. Indeed, AGO2 has been found to associate with miRNAs, both within and independently of cell-secreted vesicles[470,575–577] and miRNA secretion within EVs is decreased following silencing of AGO2 or GW182[385,471]. The interaction with AGO2 appears to be important for promoting the stability of miRNAs and protecting them from degradation[470,575,578]. However, it appears to be selective with certain miRNAs associated with AGO2 to a greater extent than others[470]. Importantly, a recent study suggested that AGO2 association may also contribute towards the function of miRNAs within recipient cells[524]. Co-expression of RNAi-based molecules with AGO2 and/or TNRC6A (the human orthologue of GW182) might therefore serve to enhance EV-mediated secretion and function of exogenous RNAi effectors.

Thus, the focus of this study was to explore the viability of endogenous EV-loading techniques for RNAi-based therapeutics relevant to AD. Candidate miRNAs and siRNAs were first identified and confirmed to silence appropriate targets. Consistent with previous studies, exogenous RNAi effectors were secreted within EVs following source cell transfection. The remainder of the study focused upon methods to optimise this loading technique. Two main strategies were employed for this purpose. Firstly, given their proposed role in miRNA stability and function, AGO2 or TNRC6A were co-expressed with exogenous RNAi effectors to determine if this enhanced their EV-mediated loading and functional activity. Secondly, this study investigated whether inclusion of a membrane-targeting acylation domain within AGO2 and TNRC6A constructs would further enhance exogenous RNAi effector secretion within EVs[553]. The acylation domain employed here results in a post-translational modification in

which myristic (myristoylation) and palmitic (palmitoylation) fatty acids are covalently linked to the N-terminal region of the protein, serving to target the protein to the membrane[554,556]. Inclusion of the acylation domain has previously been shown to target cystolic proteins to vesicles[555,556]. Thus, it was hypothesised that increasing the membrane localisation of AGO2/TNRC6A may enhance their incorporation into EVs along with any associated nucleic acids.

The findings from this study revealed that co-expression of exogenous RNAi molecules with the RNA-binding proteins, AGO2 and TNRC6A, enhanced loading and secretion of exogenous RNAi effectors within EVs. This effect appeared to be further enhanced by inclusion of the acylation domain within RNA-binding proteins. These results demonstrate the feasibility of endogenous loading methods for AD-relevant RNAi-based therapeutics and highlight the importance of RISC components in promoting the stability and EV-based secretion of RNAi molecules.

4.2 Results

4.2.1 Characterisation of HEK293T-derived Extracellular Vesicles

HEK293T cells were chosen as the source of EVs given their amenability to transfection[579]. This was important as the endogenous loading technique relies upon transfection of the desired RNAi molecules into EV source cells. HEK293T source cells were first plated in DMEM supplemented with 10% FBS. After 24 hours, cells were washed and the medium replaced with Opti-MEM, supplemented with antibiotics. After a further 48 hours, HEK293T-derived EVs were isolated by differential ultracentrifugation. Cells were grown in Opti-MEM prior to EV collection as previous data indicated that this enhances vesicle production while reducing contamination by serum vesicles[580].

HEK293T-derived EVs were first characterised by Western blot, EM, and NTA (**Fig. 4.1A-D**). Western blotting confirmed the enrichment of typical exosome markers within EV preparations while the ER marker, usually associated with secreted apoptotic bodies, was absent (**Fig. 4.1A**). EM and NTA established that preparations contained vesicles with typical exosomal morphology in the size range of 50-200 nm (**Fig. 4.1B-D**). EM also suggested the potential aggregation or fusion of smaller vesicles (**Fig. 4.1B**).

As outlined previously, it is important to consider endogenous EV cargoes. Therefore, HEK293T-derived EVs were assessed to determine whether they carry APP and BACE1 mRNA and protein by qPCR and Western blot, respectively (**Fig. 4.2**). This is

important given recent reports suggesting exosomes may be secreted in association with a number of AD-relevant proteins both *in vitro* and *in vivo*[491,561–564]. The level of *APP* and *BACE1* mRNA expression in HEK293T-derived EVs was determined relative to the quantity within untreated HEK293T cells. However, due to difficulties in matching RNA input (500 ng RNA input for cells compared to 10 µl (33%) EV sample) the quantities between EVs and cells are not directly comparable but intended as an indication as to the presence or absence of a given mRNA.

Both *APP* and *BACE1* mRNA were present at very low levels within HEK293T-derived EVs (**Fig. 4.2A**). However, there was a relative enrichment of *BACE1* mRNA (mean CT values; cells, 28.54, EVs, 33.03) compared to *APP* mRNA (mean CT values; cells, 22.00, EVs, 31.98) when compared to quantities within HEK293T source cells (**Fig. 4.2A**). BACE1 protein was also detected in cells, and at lower levels in EVs, while APP protein was only detected at low levels in cells (**Fig. 4.2B**). As *APP* and *BACE1* mRNA and BACE1 protein only appeared to be present in relatively low levels in HEK293T-derived EVs, this suggests HEK293T cells may represent a good choice of EV source cell for the current study. However, the potential impact of endogenous cargoes should be noted.

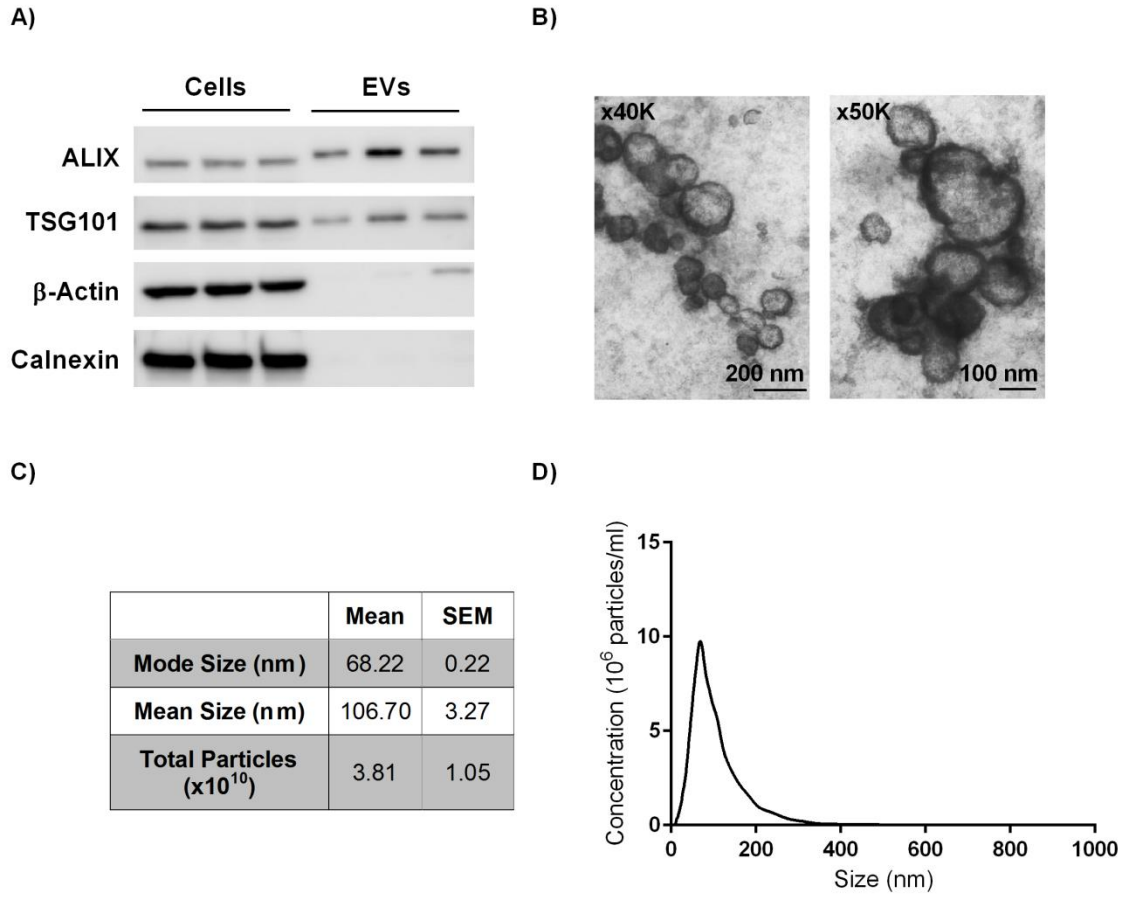

	Mean	SEM
Mode Size (nm)	68.22	0.22
Mean Size (nm)	106.70	3.27
Total Particles ($x10^{10}$)	3.81	1.05

Figure 4.1 Characterisation of HEK293T-derived Extracellular Vesicles. EVs derived from HEK293T cells by differential ultracentrifugation after 48 hours incubation were characterised by a number of methods. **(A)** EVs (25% of total EV preparation) and HEK293T lysates (50 µg) were probed by Western blot for the exosomal markers, ALIX and TSG101, the ER membrane marker, Calnexin and loading control, β-Actin. The typical exosome markers were enriched in the EV preparation while the ER marker, usually observed in association with secreted apoptotic bodies, was absent. **(B)** Electron microscopy images revealed typical morphology of isolated exosomes in addition to larger particle aggregates. **(C)** Nanoparticle tracking analysis (NTA) showing the mean particle size and total number of particles across 3 preparations (total yield per 1 x 15 cm cell culture dish). **(D)** NTA analysis of size distribution histogram for HEK293T-derived EV samples (n = 3), peak = 68.22 nm.

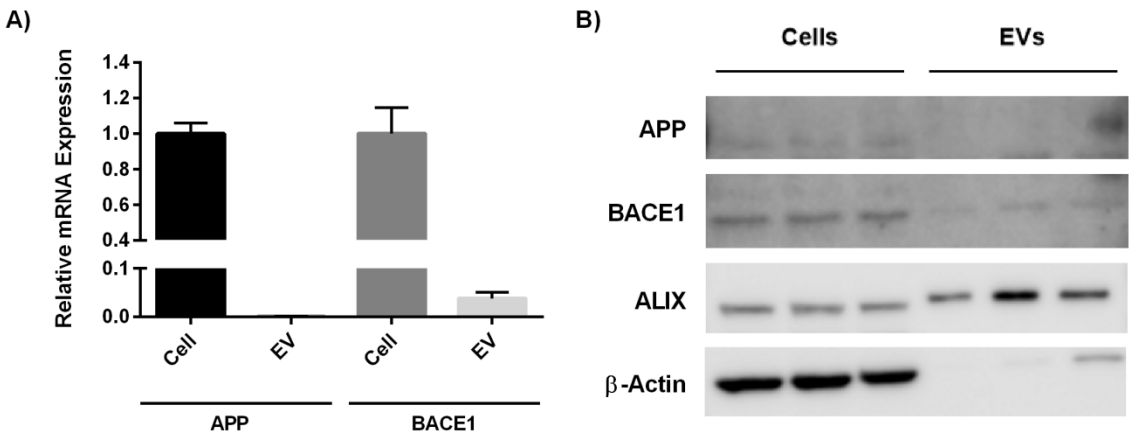

Figure 4.2 Quantification of APP and BACE1 mRNA and Protein within HEK293T Cells and Extracellular Vesicles. (A) Relative mRNA expression levels, normalised to *β-Actin* expression (cells) or input volume (EVs, 10 µl), compared to untreated cells, were determined by qPCR in HEK293T cells and EVs. Both *APP* and *BACE1* mRNA were detectable in cells and, at very low levels, in EVs (33% of total EV preparation). **(B)** APP and BACE1 protein expression in HEK293T lysates (50 µg) and EVs (25% of total EV preparation) was probed by Western blot. BACE1 protein was detected in cells and at low levels in EVs, while APP protein was detected only at low levels in cells. β-Actin and the exosomal marker, ALIX are included as loading controls. Values are mean ± SEM, n = 3.

4.2.2 Exogenous siRNAs are Secreted within Extracellular Vesicles

The endogenous loading method relies upon cellular loading machinery to package exogenous cargoes for their secretion within EVs. As mentioned previously, direct transfection of dsRNA is relatively transient as RNAi molecules are degraded or become successively diluted with each cell division. In contrast, expression plasmids, driven by a strong constitutive promoter, may induce longer-term expression. For the future development of EV-mediated RNAi-based therapeutics the use of expression plasmids, particularly within stably transfected cells, may reflect a more sustainable strategy. APP and BACE1 shRNA expression plasmids were therefore designed which expressed identical sequences as the siRNAs validated in Chapter 3 (**Fig. 4.3**).

The shRNA expression plasmids were assessed to confirm that they silenced target mRNA expression. HEK293T cells were transfected with either APP or BACE1 shRNA expression plasmids before target mRNA expression, relative to *β-Actin*, was determined by qPCR after 48 hours. This confirmed strong silencing of both *APP* (**Fig. 4.4A**) and *BACE1* mRNA expression (**Fig. 4.4B**) following treatment with the respective shRNA expression plasmids.

To determine whether siRNAs and shRNAs processed from shRNA expression plasmids can be endogenously packaged for secretion within EVs, HEK293T source cells were transfected with APP or BACE1 siRNAs or shRNA expression plasmids. After 48 hours, EVs were isolated by differential ultracentrifugation and siRNA/shRNA expression in cells and EVs, relative to total RNA input (cells) or cel-miR-39 spike-in expression (EVs), quantified by qPCR.

This revealed a significant dose-dependent increase in the quantity of siRNA/shRNA in cells and secreted EVs following transfection with the APP shRNA expression plasmid (**Fig. 4.5A-B**), APP siRNA (**Fig. 4.5C-D**), BACE1 shRNA expression plasmid (**Fig. 4.5E-F**), and BACE1 siRNA (**Fig. 4.5G-H**). These results suggest that, following transfection, exogenous siRNA/shRNA molecules are packaged and secreted within EVs by endogenous loading mechanisms.

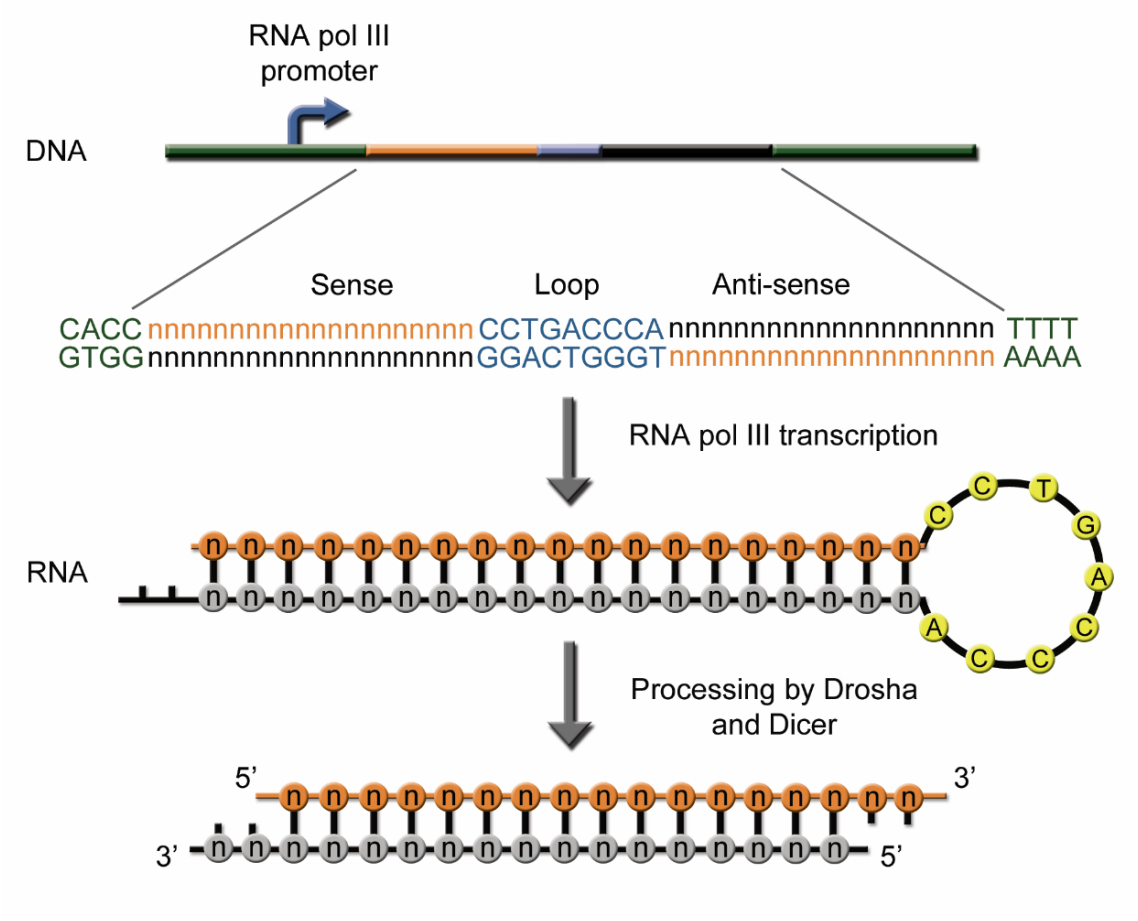

Figure 4.3 Design of pU6-Neo APP and BACE1 shRNA Expression Plasmids. APP and BACE1 shRNA expression plasmids were designed to include identical sequences to selected APP and BACE1 siRNAs which were cloned into the pU6-Neo shRNA expression plasmid. Following transfection into cells, the shRNA transcript is transcribed in the nucleus by the polymerase III U6 promoter before it is processed by Drosha and exported by Exportin-5 to the cytoplasm. In the cytoplasm, the hairpin is removed by Dicer to produce the mature double-stranded siRNA.

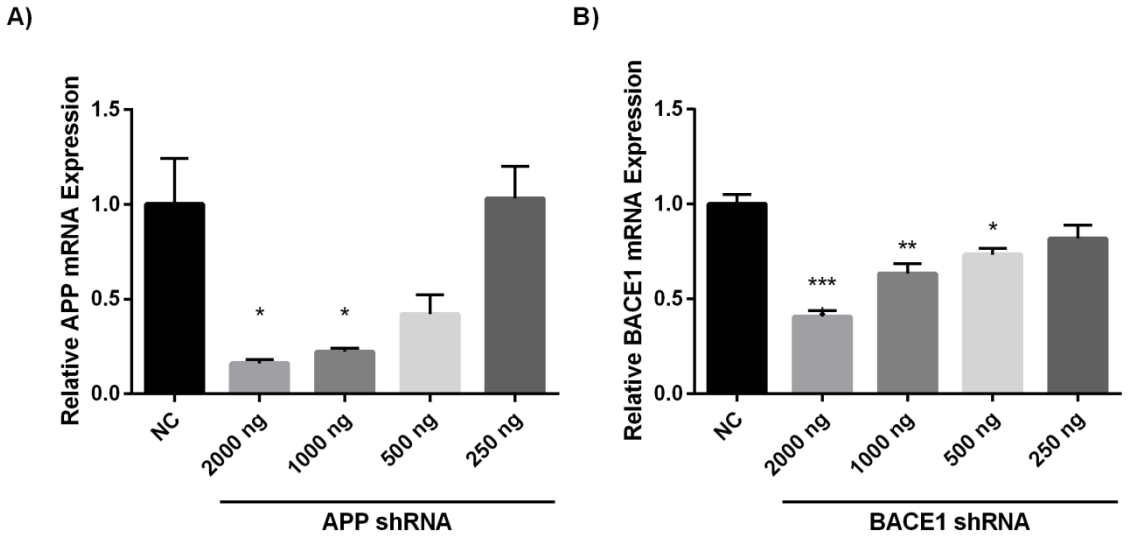

Figure 4.4 Validation of APP and BACE1 Silencing by shRNA Expression Plasmids. HEK293T cells were transfected with APP, BACE1 or negative control ("NC", 1000 ng) shRNA expression plasmids at shown concentrations in 24-well cell culture plates and target mRNA expression, normalised to *β-actin*, analysed by qPCR after 48 hours. **(A)** APP and **(B)** BACE1 shRNA expression plasmids resulted in significant silencing of the targeted mRNA. Values are mean ± SEM, n = 3, ***p<0.001, **p<0.01, *p<0.05, one-way ANOVA followed by Tukey's post-hoc test.

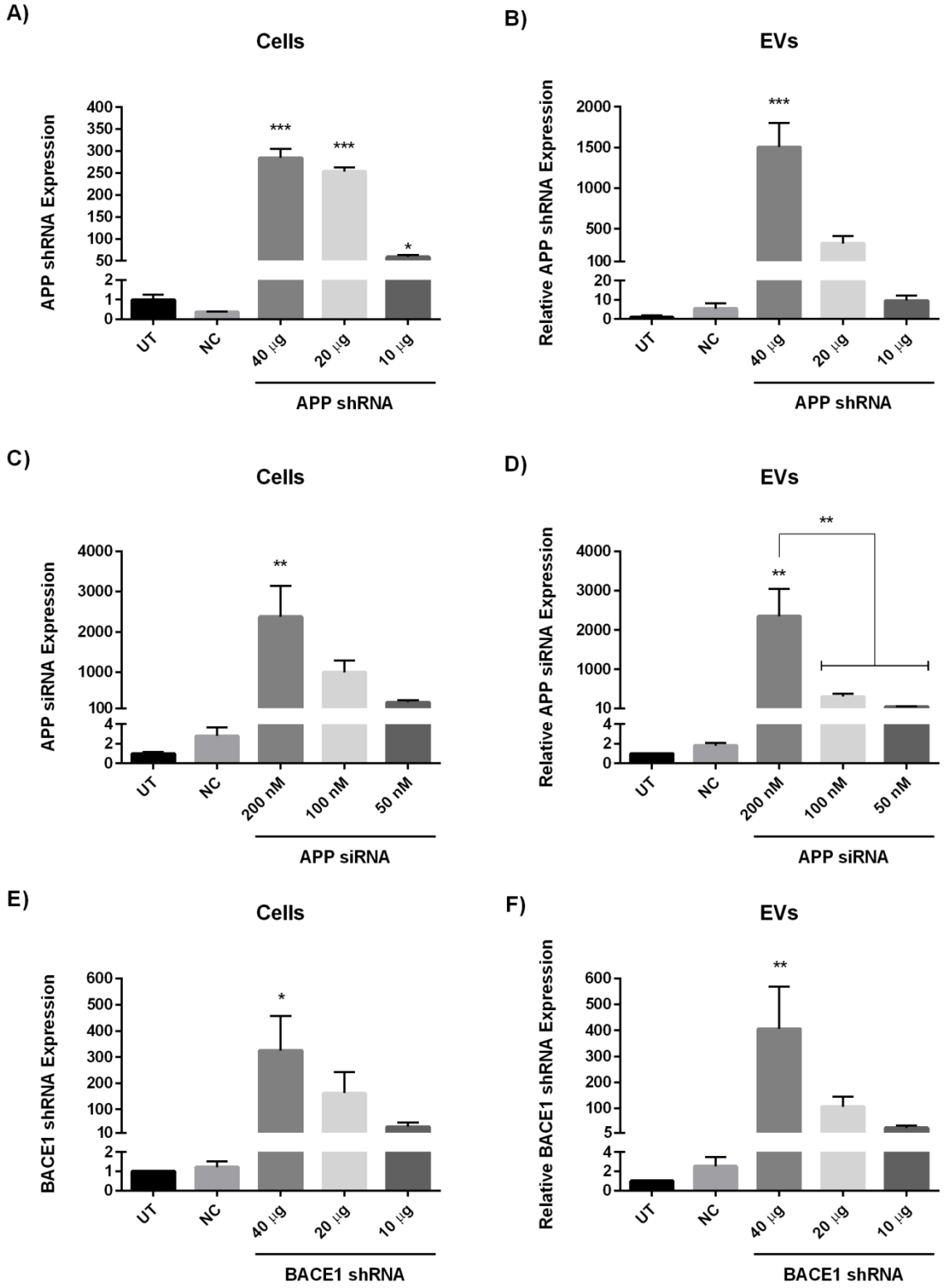
A)
Cells
APP shRNA Expression
400
350
300
250
200
150
100
50
2
1
0
***
***
*
UT
NC
40 µg
20 µg
10 µg
APP shRNA
B)
EVs
Relative APP shRNA Expression
2000
1500
1000
500
100
20
10
0
***
UT
NC
40 µg
20 µg
10 µg
APP shRNA
C)
Cells
APP siRNA Expression
4000
3000
2000
1000
100
4
2
0
**
UT
NC
200 nM
100 nM
50 nM
APP siRNA
D)
EVs
Relative APP siRNA Expression
4000
3000
2000
1000
10
4
2
0
**
**
UT
NC
200 nM
100 nM
50 nM
APP siRNA
E)
Cells
BACE1 shRNA Expression
600
500
400
300
200
100
10
2
1
0
*
UT
NC
40 µg
20 µg
10 µg
BACE1 shRNA
F)
EVs
Relative BACE1 shRNA Expression
600
500
400
300
200
100
5
4
2
0
**
UT
NC
40 µg
20 µg
10 µg
BACE1 shRNA

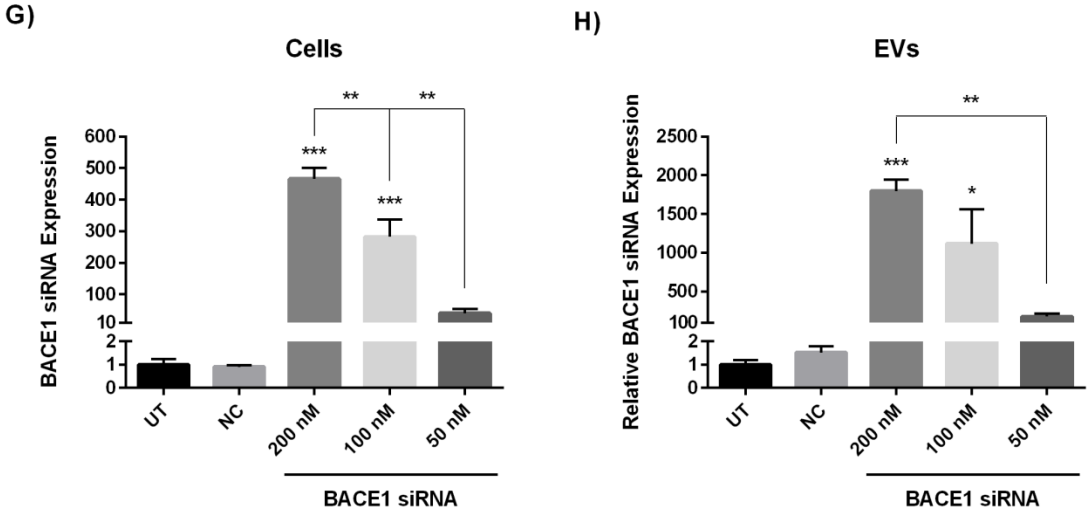

Figure 4.5 Transfection of siRNA and shRNA Expression Plasmids Results in their Secretion within Extracellular Vesicles. HEK293T cells, plated in 15 cm cell culture dishes, were left untreated ("UT") or transfected with APP, BACE1 or negative control ("NC", siRNA, 100 nM; shRNA, 20 µg) siRNAs or shRNA expression plasmids at shown concentrations. EVs were isolated after 48 hours and siRNA/shRNA expression in source cells and EVs, normalised to total RNA input (cells) or cel-miR-39 spike-in expression (EVs), quantified by qPCR. **(A-D)** APP shRNA/siRNA expression was significantly increased in **(A)** cells and **(B)** EVs following APP shRNA transfection and in **(C)** cells and **(D)** EVs following APP siRNA transfection. **(E-H)** BACE1 shRNA/siRNA expression was significantly increased in **(E)** cells and **(F)** EVs following BACE1 shRNA transfection and in **(G)** cells and **(H)** EVs following BACE1 siRNA transfection. Values are mean ± SEM, n = 3, ***p<0.001, **p<0.01, *p<0.05, one-way ANOVA followed by Tukey's post-hoc test.

4.2.3 Identification and Validation of Candidate miRNA Cargoes

As discussed previously, the miRNA network is perturbed in AD. A number of miRNAs shown to regulate AD-relevant genes, such as APP and BACE1, are downregulated or upregulated in AD patients and mouse models[245,247,249,250,253,256,257,260,266,267,581]. Downregulation of key miRNAs in disease may result in increased protein expression of disease-associated genes. Therefore, an alternative strategy to reduce APP and BACE1 expression is to restore expression of the miRNA network through delivery of exogenous miRNAs. As discussed previously, miRNAs may modulate multiple targets. Therefore, this method has the additional benefit that the expression of other targets of the deregulated miRNA may also be normalised and thus this may represent an intrinsically combinatorial approach towards therapy.

The miRNAs of interest in the current study were identified from a literature search and are provided in **Table 4.1**. hsa-miR-17, hsa-miR-20a and hsa-miR-106b are all part of the hsa-miR-20a cluster and regulate expression of APP[247]. hsa-miR-106b has been shown to be downregulated in sporadic AD patients while polymorphisms in the 3' UTR of APP disrupt hsa-miR-20a binding[247,265]. In contrast, hsa-miR-29a/b-1 regulates expression of BACE1 and is downregulated in a subset of AD patients showing elevated BACE1 expression[250].

Table 4.1 miRNAs of Interest for Current Study.

miRNA	Target	Evidence	Ref.
hsa-miR-17	APP	• Regulates APP at endogenous level *in vitro*. • Tight correlation between expression of miRNA and APP during brain development and in primary neuronal culture.	247,265
hsa-miR-20a	APP	• Polymorphisms in *APP* 3'UTR disrupt binding activity of hsa-miR-20a. • Regulates APP at endogenous level *in vitro*. • Correlation between expression of miRNA and APP during brain development and in primary neuronal culture.	247,265
hsa-miR-106b	APP	• Decreased in sporadic AD patients. • Regulates APP at endogenous level *in vitro*. • Correlation between expression of miRNA and APP during brain development and in primary neuronal culture. • Regulator of ATP-binding cassette transporter A1 (ABCA1) involved in cholesterol efflux in neuronal cells. • Influences amyloid-β metabolism through suppression of ABCA1 expression.	247,582
hsa-miR-29a	BACE1	• Decreased in subset of patients with elevated BACE1 expression. • Regulates BACE1 at endogenous level *in vitro*; APP β-CTFs and amyloid-β peptides reduced following hsa-miR-29a expression. • Correlation between expression of miRNA and BACE1 during brain development and in primary neuronal culture.	250

To confirm that the identified miRNAs regulate either APP or BACE1 expression, two reporter constructs were generated. These contained the full-length human *APP* 3' UTR (~1100 base pairs) or *BACE1* 3' UTR (~3900 base pairs) downstream of *Renilla* luciferase in the psiCHECK-2 expression plasmid (**Fig. 4.6**). HEK293T cells were co-transfected with either the *APP* 3' UTR luciferase reporter plasmid and synthetic miRNA mimics for hsa-miR-17, hsa-miR-20a or hsa-miR-106b or the *BACE1* 3' UTR luciferase reporter plasmid and hsa-miR-29a miRNA mimics. Relative luciferase activity (*Renilla* normalised to Firefly luciferase activity) was quantified 24 hours later (**Fig. 4.7**). This confirmed that miRNA mimics for hsa-miR-17 (**Fig. 4.7A**), hsa-miR-20a (**Fig. 4.7B**) and hsa-miR-106b (**Fig. 4.7C**) significantly reduced luciferase activity of the *APP* 3' UTR reporter. Similarly, luciferase activity of the *BACE1* 3' UTR reporter was significantly reduced following co-transfection with hsa-miR-29a miRNA mimics (**Fig. 4.7D**). While the level of silencing is relatively low this is typical of miRNA regulation and consistent with the degree of silencing of full length 3' UTR luciferase plasmids reported by previous studies[247,250].

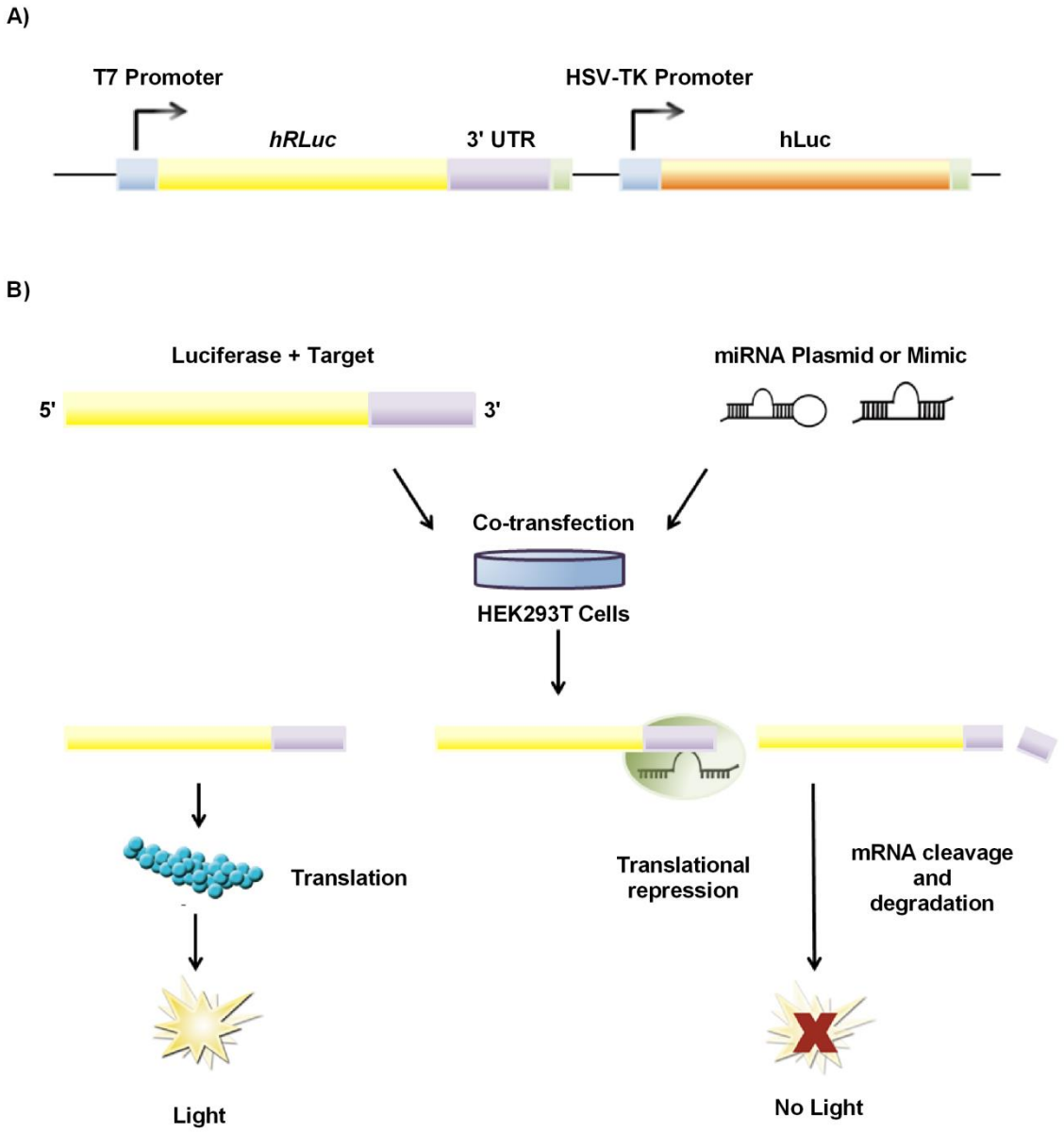

Figure 4.6 Structure of 3' UTR Dual-Luciferase Reporter Plasmids and Experimental Design. (A) The *APP* or *BACE1* 3' UTR was cloned downstream of *Renilla* luciferase ("*hRLuc*") in the psiCHECK-2 plasmid with Firefly luciferase ("hLuc") as an internal control. **(B)** Luciferase constructs were co-transfected with miRNA expression plasmids or miRNA mimics in HEK293T cells and relative luciferase activity quantified 24 hours later. Luminescence is reduced if the miRNA regulates expression of the target sequence either through translational repression or cleavage and degradation of the mRNA. If the miRNA does not regulate the sequence of interest, translation proceeds resulting in luminescence.

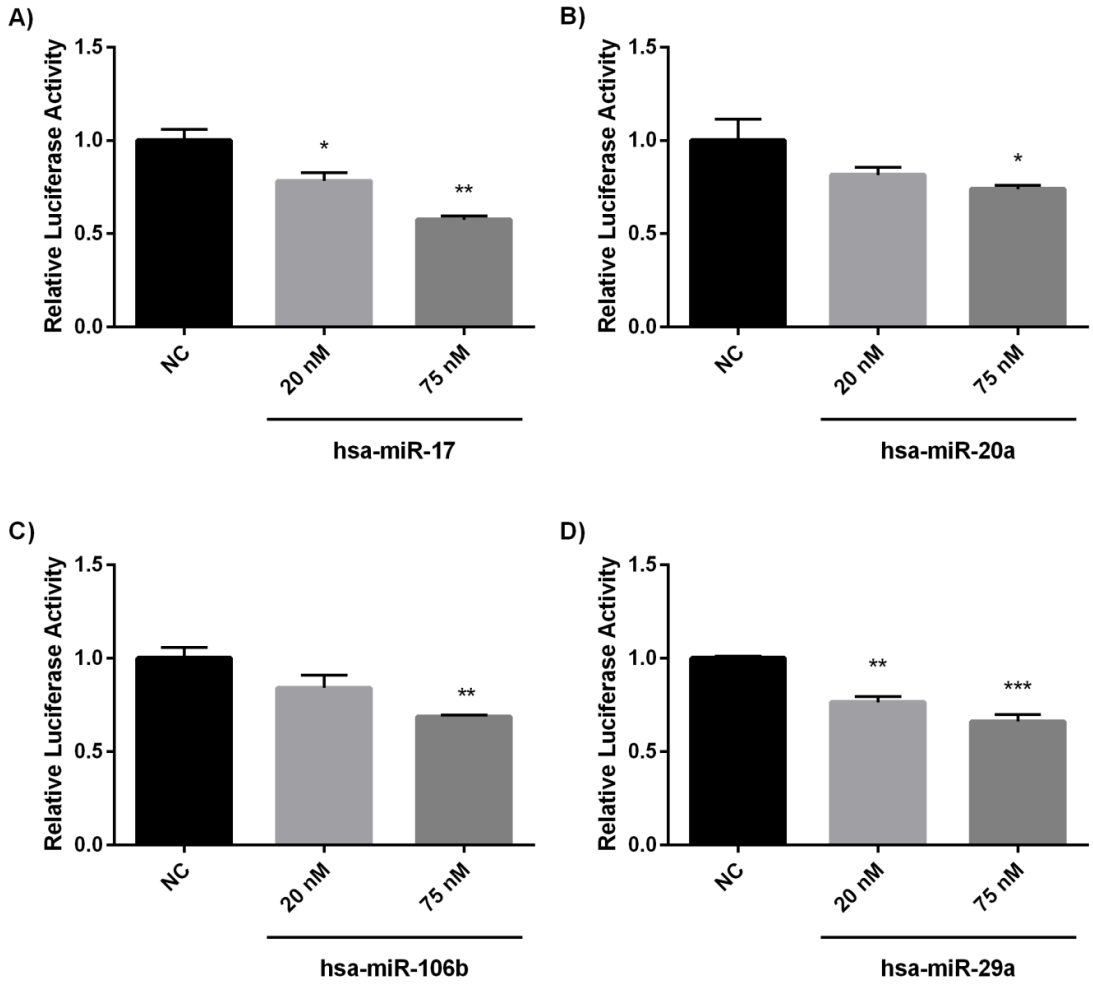

Figure 4.7 Validation of miRNA Mimic Regulation of *APP* and *BACE1* 3' UTR Dual-Luciferase Reporter Plasmids. HEK293T cells were co-transfected with 200 ng *APP/BACE1* 3' UTR dual-luciferase reporter plasmids and shown concentrations of experimental miRNA mimics or negative control mimic ("NC", 20 nM) in 24-well cell culture plates. Cells were incubated for 24 hours before *Renilla* normalised to Firefly luciferase activity was assessed. The *APP* 3' UTR dual-luciferase reporter plasmid was significantly silenced by **(A)** hsa-miR-17, **(B)** hsa-miR-20a and **(C)** hsa-miR-106b miRNA mimics. **(D)** The *BACE1* 3' UTR dual-luciferase reporter plasmid was significantly silenced by hsa-miR-29a miRNA mimics. Values are mean ± SEM, n = 3, ***p<0.001, **p<0.01, *p<0.05, one-way ANOVA followed by Tukey's post-hoc test.

Endogenous RNA cargoes may be selectively enriched within EVs compared to their relative proportions within source cells. Furthermore, the association between AGO2 and miRNAs varies depending on the identity of the specific miRNA[470]. However, the factors which drive selective EV enrichment or association with AGO2 are currently unknown. It was hypothesised that the relative abundance of endogenous miRNAs may influence the extent to which exogenously applied miRNAs could be packaged and secreted within EVs.

The relative endogenous abundance of the four chosen miRNAs was therefore assessed by qPCR in cells (**Fig. 4.8A**) and EVs (**Fig. 4.8B**) across five different cell lines. This revealed a similar pattern of miRNA abundance across the five cell lines and their corresponding EVs. Specifically, hsa-miR-17 and hsa-miR-20a were expressed at relatively high levels, hsa-miR-106b at medium levels and hsa-miR-29a at relatively low levels in both cells and EVs (**Fig. 4.8A-B**). Given these expression levels, three miRNAs were selected for further study; hsa-miR-17 (high abundance), hsa-miR-106b (medium abundance) and hsa-miR-29a (low abundance).

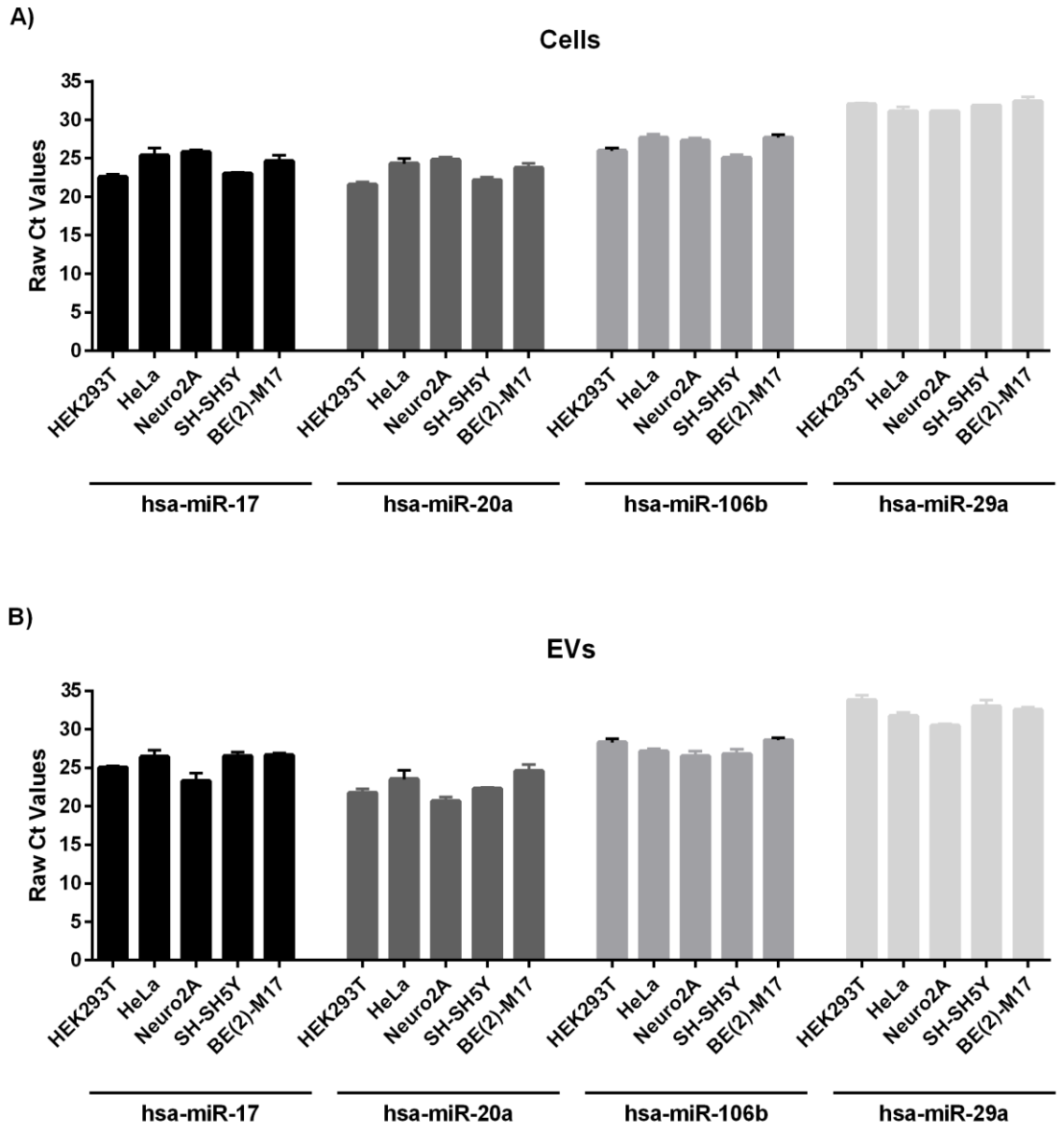

Figure 4.8 Endogenous Expression of miRNAs in Cells and Extracellular Vesicles. The endogenous expression of hsa-miR-17, hsa-miR-20a, hsa-miR-106b and hsa-miR-29a was assessed by qPCR in **(A)** cells and **(B)** EVs derived from HEK293T, HeLa, Neuro2A, SH-SH5Y and BE(2)-M17 cell lines. hsa-miR-17 and hsa-miR-20a were expressed at relatively high levels, hsa-miR-106b at medium levels and hsa-miR-29a at relatively low levels across 5 different cell lines and their corresponding EVs. Values are mean ± SEM of raw Ct values (lower values indicate higher endogenous expression), n = 3.

Similar to siRNAs, miRNAs may be delivered as synthetic miRNA mimics or expressed from pre/pri-miRNA expression plasmids. Both endogenous and exogenous forms of mature miRNAs and pre-miRNAs are found within EVs[515,583]. Within the endogenous miRNA pathway, Dicer plays an important role in loading pre-miRNAs into RISC prior to their cleavage to produce the mature guide strand[584–586]. The Dicer-directed relationship between pre-miRNAs and RISC might therefore suggest potential differences in the loading efficiency of synthetic mature miRNAs versus those expressed from pre/pri-miRNA expression plasmids which undergo processing by the endogenous RNA pathway. Furthermore, these effects may be more evident following co-transfection of miRNAs with AGO2 or TNRC6A. Individual pri-miRNA expression plasmids were therefore constructed which expressed the primary transcript of hsa-miR-17, hsa-miR-106b or hsa-miR-29a. This allowed comparison of EV-mediated miRNA secretion following transfection of exogenous miRNAs either as mature mimics or as pri-miRNA expression plasmids.

As discussed above, the regulation of *APP* and *BACE1* 3' UTR luciferase reporters by mature miRNA mimics was relatively low (**Fig. 4.7**). More sensitive luciferase reporters were therefore required as it is unlikely that exogenous miRNAs secreted within EVs would reach recipient cells in the required concentrations shown here to elicit detectable silencing of full 3' UTR reporters. Thus, to improve detection sensitivity of reporter regulation, three further miRNA dual-luciferase reporter plasmids were constructed. These plasmids comprised a "target" sequence, containing four repeats exactly complementary to the miRNA sequence for hsa-miR-17, hsa-miR-106b or hsa-miR-29a, downstream of Firefly luciferase within the pmirGLO dual-luciferase reporter plasmid (**Fig. 4.9**).

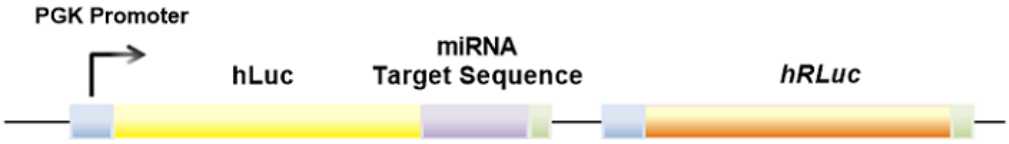

Figure 4.9 Structure of Complementary miRNA Target Sequence Dual-Luciferase Reporter Plasmids. miRNA target sequences comprising four repeats of a sequence fully complementary to each mature miRNA sequence were cloned downstream of Firefly luciferase ("hLuc") in the pmirGLO dual-luciferase target reporter plasmid with *Renilla* luciferase as an internal control ("*hRLuc*").

To confirm whether these luciferase reporters were regulated by miRNAs, HEK293T cells were co-transfected with mature miRNA mimics (**Fig. 4.10**/**Fig. 4.11**) or pri-miRNA expression plasmids (**Fig. 4.12**) and the corresponding target sequence luciferase reporter. This confirmed dose-dependent silencing of the respective luciferase target reporter by mature miRNAs mimics for hsa-miR-17 (**Fig. 4.10A**), hsa-miR-106b (**Fig. 4.10B**) and hsa-miR-29a (**Fig. 4.10C**). To further confirm this effect, miRNA mimics from two different sources, mirVana (Life Technologies) and AccuTarget (Bioneer), were directly compared for their regulatory effect upon the corresponding luciferase target reporter (**Fig. 4.11**). This revealed that the each luciferase target reporter was significantly silenced by miRNA mimics from both sources for hsa-miR-17 (**Fig. 4.11A**), hsa-miR-106b (**Fig. 4.11B**) and hsa-miR-29a (**Fig. 4.11C**), although mirVana miRNA mimics were more effective at reducing luciferase activity. Similarly, the corresponding target luciferase reporter was also significantly silenced, but in a more subtle dose-dependent manner, following co-transfection with pri-miRNA expression plasmids for hsa-miR-17 (**Fig. 4.12A**), hsa-miR-106b (**Fig. 4.12B**) and hsa-miR-29a (**Fig. 4.12C**).

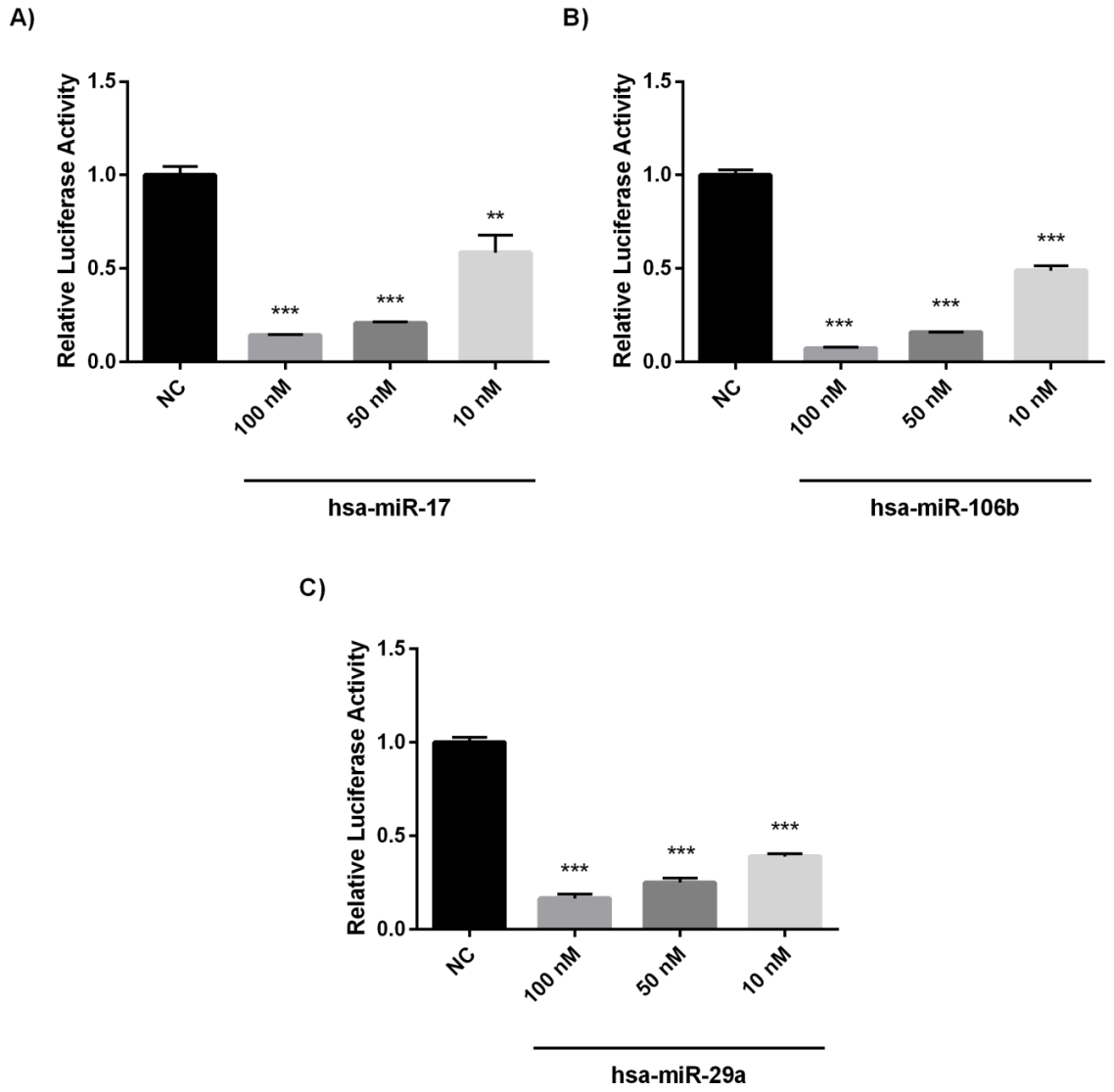

Figure 4.10 Validation of miRNA Mimic Regulation of pmirGLO Dual-Luciferase Target Reporters. HEK293T cells were co-transfected with 200 ng pmirGLO dual-luciferase target reporter and shown concentrations of the corresponding miRNA mimic or negative control mimic ("NC", 100 nM) in 24-well cell culture plates. Cells were incubated for 24 hours before Firefly luciferase normalised to *Renilla* luciferase activity was assessed. The corresponding pmirGLO dual-luciferase target reporter was significantly silenced by **(A)** hsa-miR-17, **(B)** hsa-miR-106b and **(C)** hsa-miR-29a miRNA mimics. Values are mean ± SEM, n = 3, ***p<0.001, **p<0.01, *p<0.05, one-way ANOVA followed by Tukey's post-hoc test.

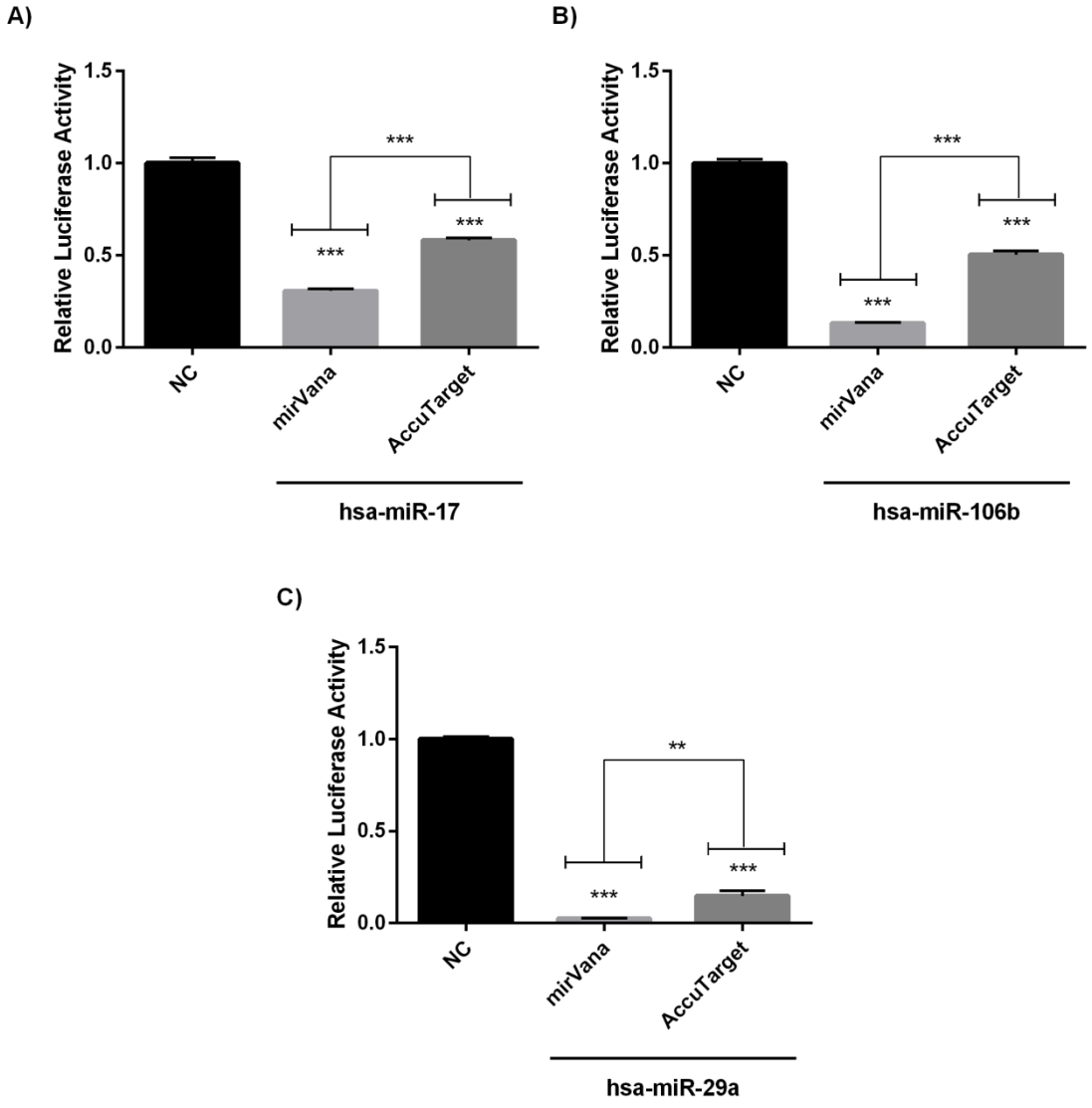

Figure 4.11 Regulation of pmirGLO Dual-Luciferase Target Reporters By miRNA Mimics. HEK293T cells were co-transfected with 200 ng pmirGLO dual-luciferase target reporter and either 50 nM mirVana (Life Technologies) or AccuTarget (Bioneer) miRNA mimics or a negative control mimic ("NC", 50 nM) in 24-well cell culture plates. Firefly luciferase activity, normalised to *Renilla* luciferase activity, was assessed 24 hours later. The corresponding pmirGLO dual-luciferase target reporter for **(A)** hsa-miR-17, **(B)** hsa-miR-106b and **(C)** hsa-miR-29a was significantly silenced by miRNA mimics from both sources although mirVana miRNA mimics were most effective. Values are mean ± SEM, n = 3, ***p<0.001, **p<0.01, *p<0.05, one-way ANOVA followed by Tukey's post-hoc test.

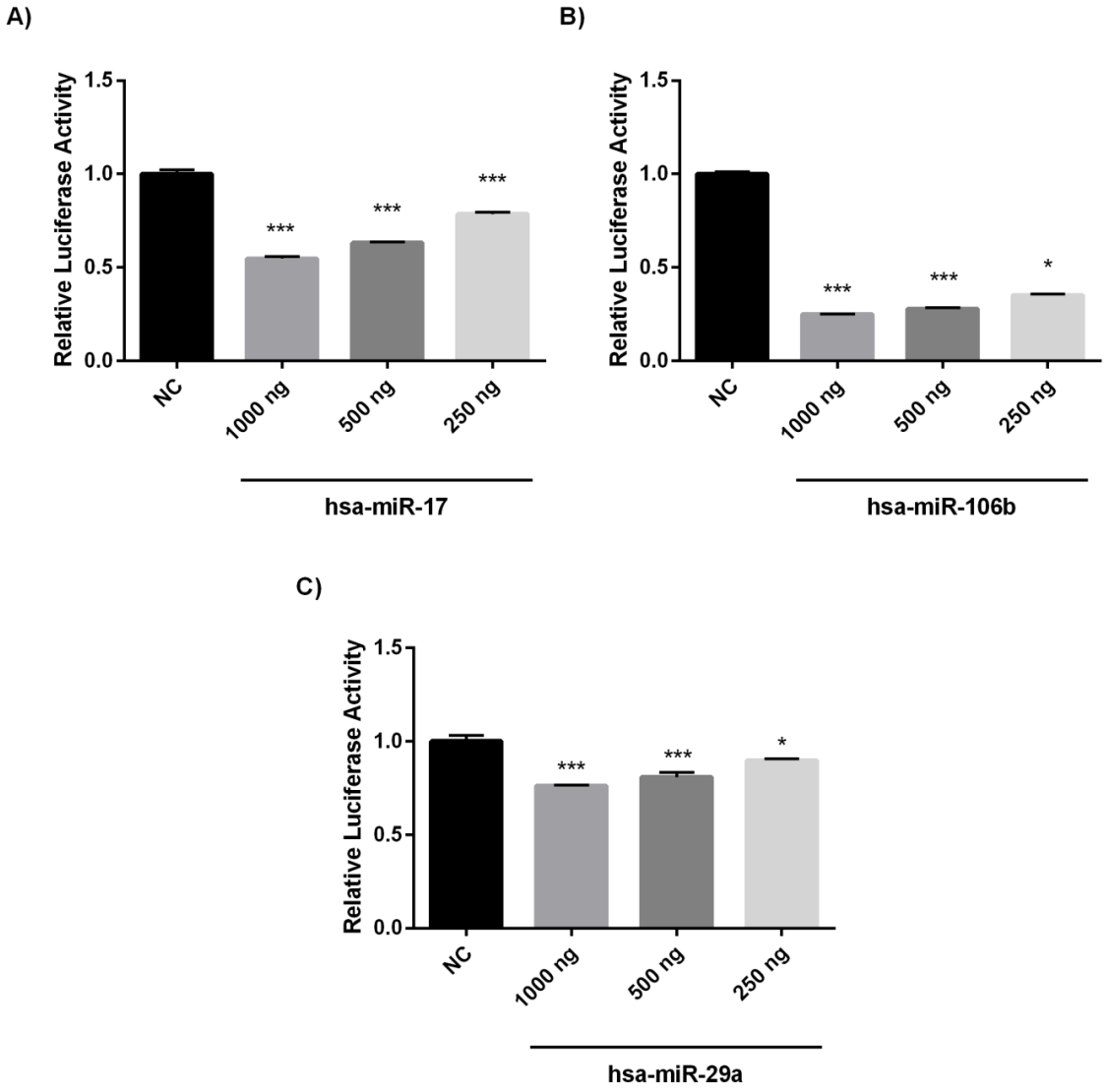

Figure 4.12 Validation of pri-miRNA Expression Plasmid Regulation of pmirGLO Dual-Luciferase Target Reporters. HEK293T cells were co-transfected with 200 ng pmirGLO dual-luciferase target reporter and shown concentrations of the corresponding miRNA expression plasmid or negative control plasmid ("NC", 500 ng) in 24-well cell culture plates. Cells were incubated for 24 hours before Firefly luciferase activity, normalised to *Renilla* luciferase activity, was assessed. The corresponding pmirGLO dual-luciferase target reporter was significantly silenced by pri-miRNA expression plasmids encoding **(A)** hsa-miR-17, **(B)** hsa-miR-106b and **(C)** hsa-miR-29a. Values are mean ± SEM, n = 3, ***p<0.001, **p<0.01, *p<0.05, one-way ANOVA followed by Tukey's post-hoc test.

4.2.4 Exogenous miRNAs are Secreted within Extracellular Vesicles

Given their more sustainable nature, this study first focused upon the packaging and secretion of exogenous miRNAs processed from pri-miRNA expression plasmids. HEK293T source cells were transfected with hsa-miR-17, hsa-miR-106b or hsa-miR-29a pri-miRNA expression plasmids and EVs isolated by differential ultracentrifugation after 48 hours. Mature miRNA expression in source cells and EVs was quantified by qPCR, relative to total RNA input (cells) or cel-miR-39 spike-in expression (EVs) (**Fig. 4.13**).

Variability in miRNA expression following transfection was high in both cells and EVs and precluded some of the observed increases from reaching significance. However, generally there appeared to be an increase in cellular and EV expression of miRNAs following transfection with hsa-miR-17 (**Fig. 4.13A-B**), hsa-miR-106b (**Fig. 4.13C-D**) and hsa-miR-29a (**Fig. 4.13E-F**) pri-miRNA expression plasmids. The observed increase reached significance following transfection of the hsa-miR-106b pri-miRNA expression plasmid in cells and EVs (**Fig. 4.13C-D**) and in EVs following transfection of the hsa-miR-29a pri-miRNA expression plasmid (**Fig. 4.13F**). Intriguingly, the degree of increased miRNA expression following pri-miRNA expression plasmid transfection varied inversely with the abundance of endogenous miRNAs. Thus, hsa-miR-17, which has the highest abundance, showed the smallest increase relative to endogenous expression while hsa-miR-29a, which has the lowest abundance, showed the greatest increase relative to endogenous expression following transfection.

To ascertain whether miRNA expression was also increased following transfection of miRNA mimics, the decision was taken to focus upon hsa-miR-29a mimics given that hsa-miR-29a showed the greatest fold change in expression following transfection of pri-miRNA expression plasmids. HEK293T cells were transfected with hsa-miR-29a mature mimics and EVs isolated by differential ultracentrifugation after 48 hours. Mature miRNA expression was assessed in cells and EVs, as outlined above. This revealed a non-significant increase in cellular hsa-miR-29a levels (**Fig. 4.13G**) and a significant increase in EV hsa-miR-29a levels (**Fig. 4.13H**) at the highest transfection concentration. Together, these results suggest that following transfection of either pri-miRNA expression plasmids or mature mimics, endogenous loading mechanisms may package exogenous miRNAs for secretion within EVs.

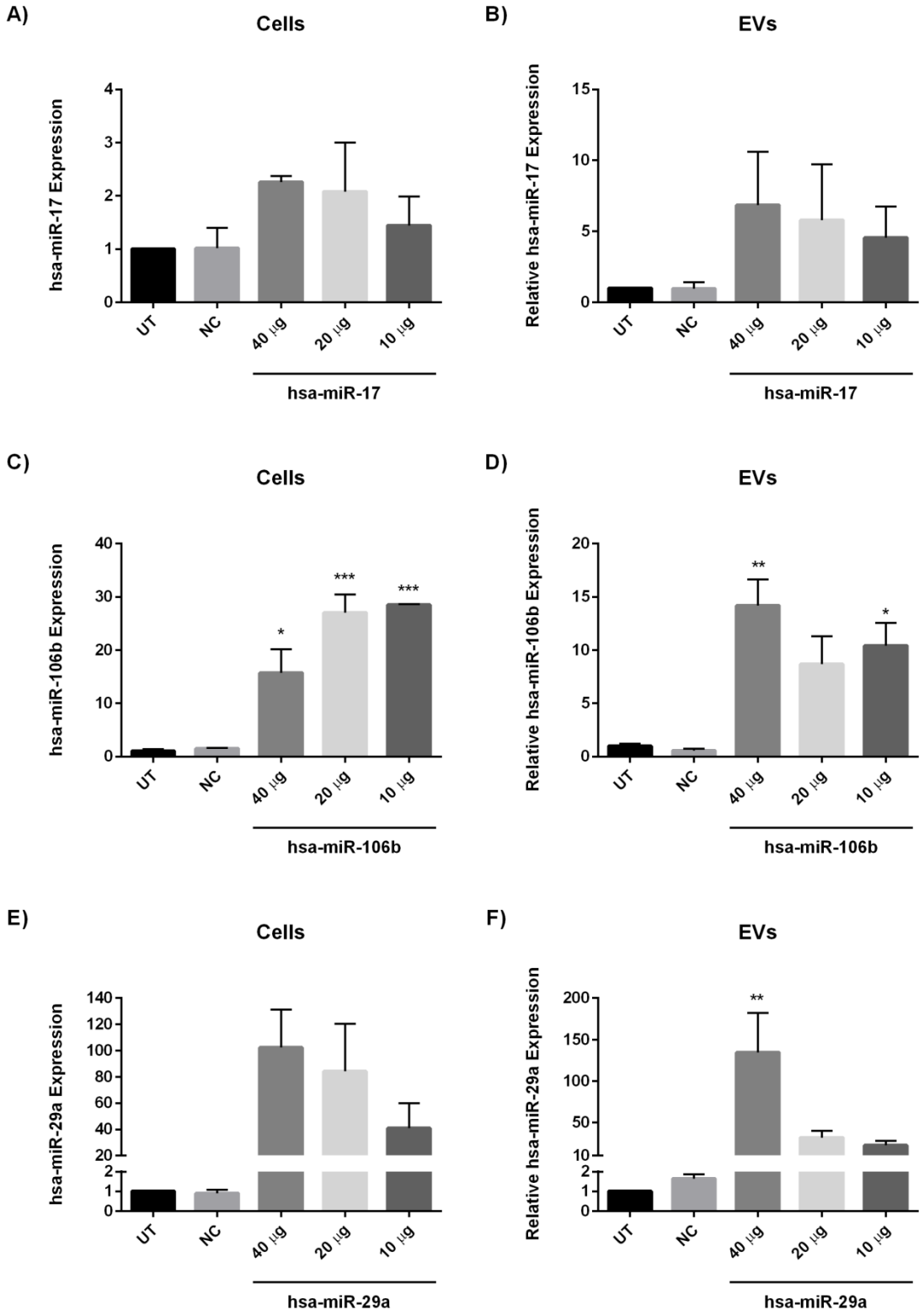
A)
Cells
hsa-miR-17 Expression
UT
NC
40 µg
20 µg
10 µg
hsa-miR-17
B)
EVs
Relative hsa-miR-17 Expression
hsa-miR-17
C)
Cells
hsa-miR-106b Expression
hsa-miR-106b
D)
EVs
Relative hsa-miR-106b Expression
hsa-miR-106b
E)
Cells
hsa-miR-29a Expression
hsa-miR-29a
F)
EVs
Relative hsa-miR-29a Expression
hsa-miR-29a

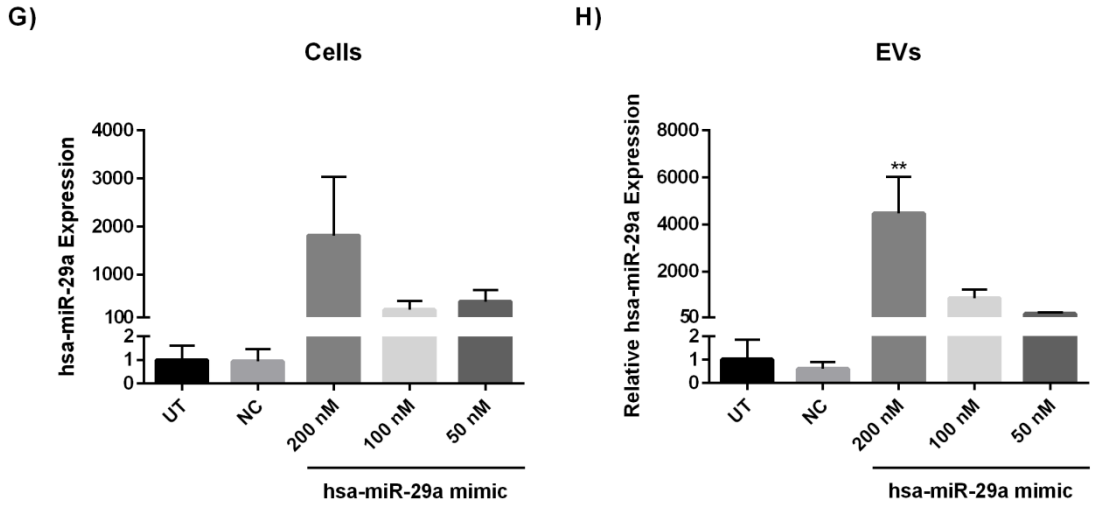

Figure 4.13 Mature miRNA Expression in Cells and Extracellular Vesicles Following Transfection of miRNA Expression Plasmids and hsa-miR-29a Mimic. HEK293T cells, plated in 15 cm cell culture dishes, were transfected with miRNA expression plasmids, hsa-miR-29a mimics or the negative control plasmid/mimic ("NC", plasmid, 20 µg; mimic, 100 nM). Mature miRNA expression, normalised to total RNA input (cells) or cel-miR-39 spike-in expression (EVs), was quantified by qPCR after 48 hours. **(A)** Mature hsa-miR-17 expression was non-significantly increased in cells and **(B)** EVs following hsa-miR-17 plasmid transfection. **(C)** Mature hsa-miR-106b expression was significantly increased in cells and **(D)** EVs following hsa-miR-106b plasmid transfection. **(E)** Mature hsa-miR-29a expression was increased in cells (non-significantly) and **(F)** EVs (significantly) following hsa-miR-29a plasmid transfection. **(G)** Mature hsa-miR-29a expression was increased in cells (non-significantly) and **(H)** EVs (significantly) following hsa-miR-29a miRNA mimic transfection. Values are mean ± SEM, n = 3, ***p<0.001, **p<0.01, *p<0.05, one-way ANOVA followed by Tukey's post-hoc test.

4.2.5 Acylation Domain Targets AGO2 and TNRC6A to the Membrane and Increases Extracellular Vesicle Expression of AGO2

RNA-binding proteins, such as AGO2 and GW182, are found in association with miRNAs within EVs and their silencing reduces EV-mediated miRNA secretion[385,387,468,470,471,575–577]. It was therefore hypothesised that co-expression of exogenous miRNAs with AGO2 or TNRC6A (the human orthologue of GW182) may increase packaging and secretion of exogenous miRNAs within EVs. It was also proposed that inclusion of an acylation domain within AGO2 or TNRC6A, to target proteins towards the membrane, would further enhance EV-mediated miRNA secretion by increasing the incorporation of AGO2/TNRC6A along with any associated nucleic acids.

To investigate this, an acylation domain was inserted into the N-terminal region of the myc-EGFP-TNRC6A plasmid to produce a "membrane-tagged" (MT) expression product of myc-EGFP-TNRC6A (**Fig. 4.14**). A similar plasmid in which the acylation domain was inserted in the N-terminal region of the pEGFP-N1-hAGO2 plasmid to produce a "membrane-tagged" (MT) expression product of EGFP-hAGO2 was a gift from Giulia Corso (Karolinska Institute). To investigate the effects of the acylation domain, HEK293T cells were transfected with plasmids encoding either the wild-type (WT) or membrane-tagged (MT) forms of AGO2 or TNRC6A before cells and EVs were characterised by a number of methods after 48 hours.

EVs were first assessed by NTA to determine whether plasmid transfections influenced EV secretion either in terms of size or particle count (**Fig. 4.15**). While there was no

change in particle size, there was a significant reduction in the number of secreted EVs following transfection with either AGO2 (WT and MT) (**Fig. 4.15A-B**) or TNRC6A (WT and MT) (**Fig. 4.15A,C**) expression plasmids.

Next, mRNA and protein expression in HEK293T cells and EVs was assessed by qPCR (**Fig. 4.16**) and Western blotting (**Fig. 4.17**) following transfection of AGO2 (WT and MT) or TNRC6A (WT and MT) expression plasmids. *AGO2* mRNA expression was significantly increased in cells following transfection of both WT and MT AGO2 expression plasmids and in EVs following transfection of the AGO2 MT expression plasmid (**Fig. 4.16A-B**). Similarly, *TNRC6A* mRNA expression was significantly increased in cells following transfection of both WT and MT TNRC6A expression plasmids and in EVs following transfection of the TNRC6A MT expression plasmid (**Fig. 4.16C-D**). Interestingly, *AGO2* mRNA expression was also significantly increased following transfection of the TNRC6A WT plasmid in cells (**Fig. 4.16C**).

Western blotting revealed that transfection of AGO2 WT and MT expression plasmids increased both cellular and EV protein expression of AGO2 (**Fig. 4.17A-B**). AGO2 expression was increased to a similar extent following transfection of either WT or MT forms of AGO2 in cells (**Fig. 4.17A**). However, in line with the hypothesis above, transfection of the AGO2 MT plasmid resulted in higher expression of AGO2 in EVs when compared to AGO2 WT plasmid transfections (**Fig. 4.17B**). This suggests that incorporation of AGO2 protein within EVs is increased following inclusion of the acylation domain. In contrast, while transfection of TNRC6A WT and MT plasmids increased TNRC6A protein expression in cells (**Fig. 4.17C**) there appeared to be no effect upon the very low levels of TNRC6A detected in EVs **(Fig. 4.17D**).

Finally, the localisation of AGO2 and TNRC6A was assessed by fluorescence microscopy following transfection of either WT or MT plasmids (**Fig. 4.18**). This revealed that inclusion of the acylation domain directed the GFP-AGO2 and GFP-TNRC6A fusion proteins towards the membrane (**Fig. 4.18B,D**) while expression from WT plasmids produced a more punctate distribution (**Fig. 4.18A,C**).

Together, these results suggest that mRNA and protein expression of AGO2 and TNRC6A are increased following transfection of their respective plasmids. Furthermore, inclusion of the acylation domain appears to direct AGO2 and TNRC6A towards the membrane resulting in increased levels of AGO2 protein within EVs.

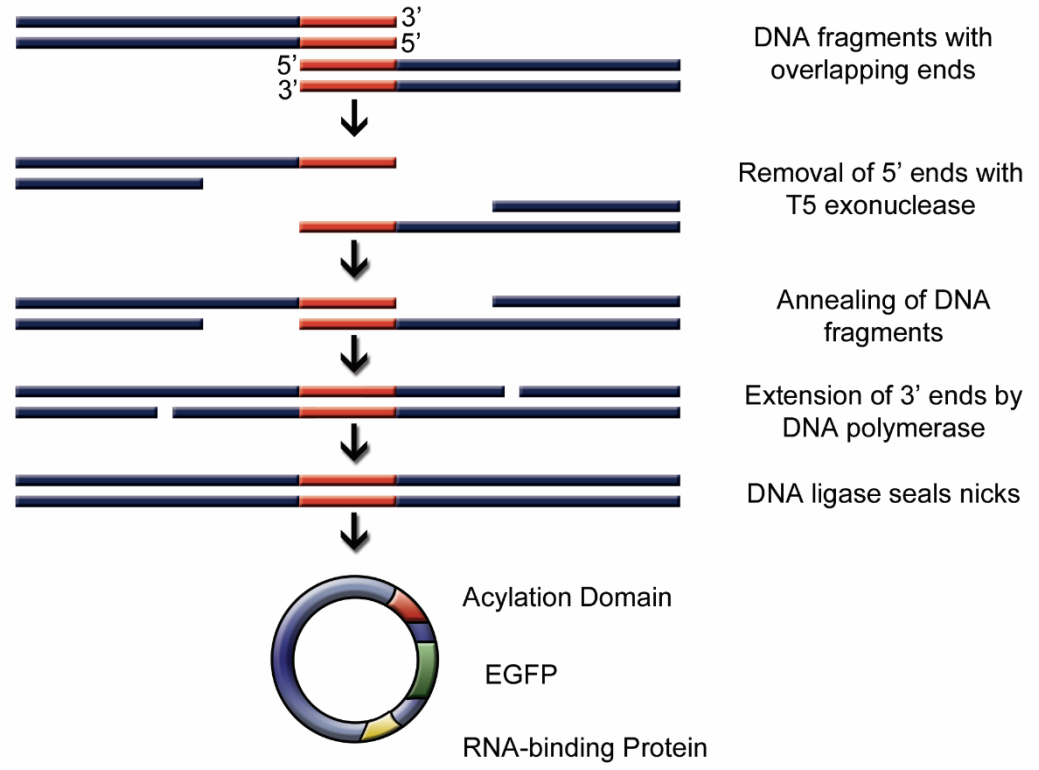

Figure 4.14 Cloning of Membrane-associated pmyc-EGFP-TNRC6A Plasmid by Overlap Extension PCR. The acylation domain was inserted in the N-terminal domain of the myc-EGFP-TNRC6A fusion protein according to the concepts of overlap extension PCR in which two DNA fragments with overlapping ends may be combined[557].

A)

	UT	AGO2 (WT)	AGO2 (MT)	TNRC6A (WT)	TNRC6A (MT)
Mode Size (± SEM) (nm)	79.00 (± 6.11)	78.00 (± 4.04)	79.67 (± 1.20)	79.67 (± 7.69)	74.33 (± 2.03)
Mean Size (± SEM) (nm)	120.50 (± 2.67)	114.10 (± 3.63)	109.30 (± 4.71)	121.00 (± 6.32)	105.50 (± 2.42)
Total Particles ($x10^{10}$) (± SEM)	6.12 (± 0.59)	3.07 * (± 0.65)	2.73 ** (± 0.19)	2.58 ** (± 0.54)	3.21 * (± 0.49)

B)

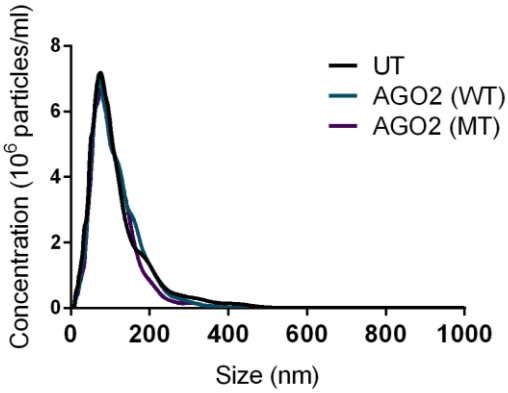

C)

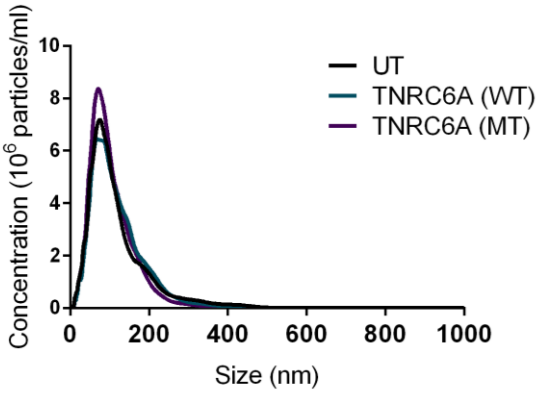

Figure 4.15 Particle Size and Concentration Following Transfection of AGO2 and TNRC6A Expression Plasmids. HEK293T cells, plated in 15 cm cell culture dishes, were transfected with 17.5 µg of either AGO2 or TNRC6A wild-type ("WT") or membrane-tagged ("MT") expression plasmids or left untreated ("UT"). EVs were isolated after 48 hours and analysed by nanoparticle tracking analysis ("NTA"). **(A)** NTA showing mean particle size and total particle count (total yield from 1 x 15 cm dish). **(B-C)** NTA analysis of size distribution histogram for **(B)** EVs derived from UT and AGO2 (WT and MT) transfected cells or **(C)** EVs derived from UT and TNRC6A (WT and MT) transfected cells. There was no significant difference in the mode and mean size of EVs but total particle count was significantly reduced for EVs derived from transfected cells compared to UT cells. Values are mean ± SEM, n = 3, **p<0.01, *p<0.05, one-way ANOVA followed by Tukey's post-hoc test.

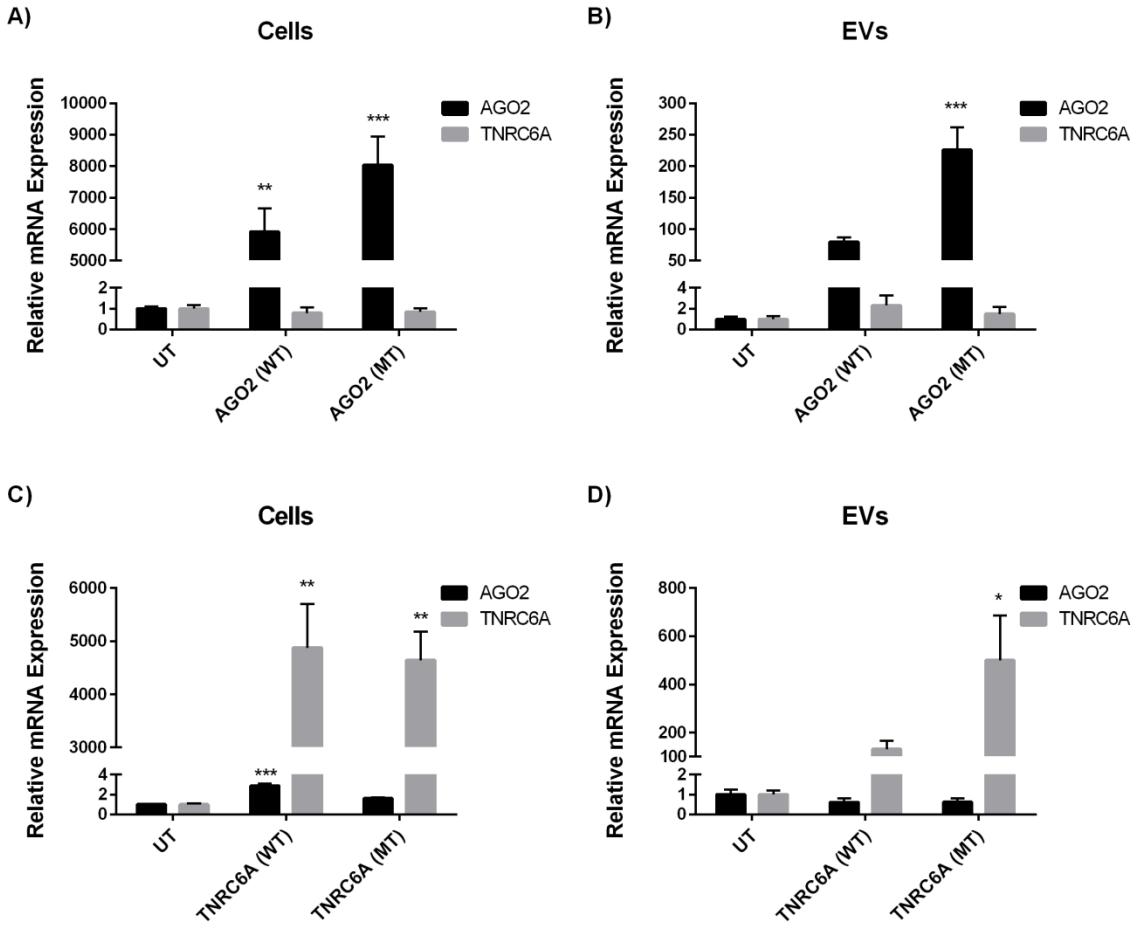

Figure 4.16 AGO2 and TNRC6A mRNA Expression in Cells and Extracellular Vesicles Following Transfection of AGO2 and TNRC6A Expression Plasmids. HEK293T cells, plated in 15 cm cell culture dishes, were transfected with 17.5 µg of either AGO2 or TNRC6A wild-type ("WT") or membrane-tagged ("MT") expression plasmids or left untreated ("UT"). *AGO2* and *TNRC6A* mRNA expression in cells and EVs was quantified, relative to *β-Actin* expression, by qPCR after 48 hours. **(A-B)** *AGO2* mRNA expression was significantly increased in **(A)** cells and **(B)** EVs following transfection of AGO2 WT and MT expression plasmids while *TNRC6A* expression was unaffected. **(C-D)** *TNRC6A* mRNA expression was significantly increased in **(C)** cells and **(D)** EVs following transfection of TNRC6A WT and MT expression plasmids. *AGO2* mRNA expression was also increased in cells following transfection of the TNRC6A WT plasmid. Values are mean ± SEM, n = 3, ***p<0.001, **p<0.01, *p<0.05, one-way ANOVA followed by Tukey's post-hoc test.

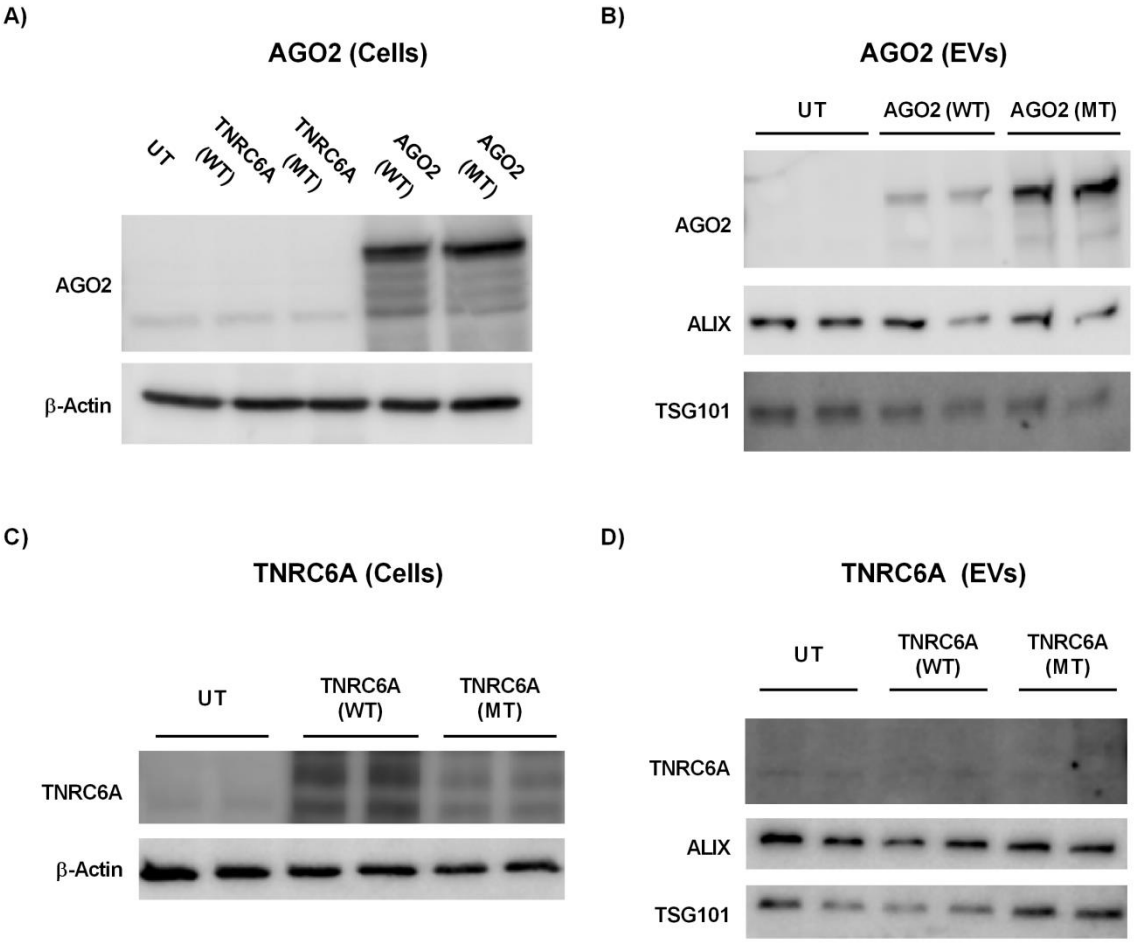

Figure 4.17 AGO2 and TNRC6A Protein Expression in Cells and Extracellular Vesicles Following Transfection of AGO2 and TNRC6A Expression Plasmids. HEK293T cells, plated in 15 cm cell culture dishes, were transfected with 17.5 µg of either AGO2 or TNRC6A wild-type ("WT") or membrane-tagged ("MT") expression plasmids or left untreated ("UT"). Protein was harvested 48 hours later and AGO2 and TNRC6A expression assessed by Western blotting in cells (50 µg) and EVs (25% of total EV yield). Transfection of AGO2 expression plasmids resulted in increased **(A)** cellular and **(B)** EV AGO2 protein expression. **(C)** Transfection of TNRC6A expression plasmids only increased cellular TNRC6A protein expression. **(D)** There was no increase in TNRC6A protein expression in EVs. β-Actin and the exosomal markers, ALIX and TSG101, are included as loading controls.

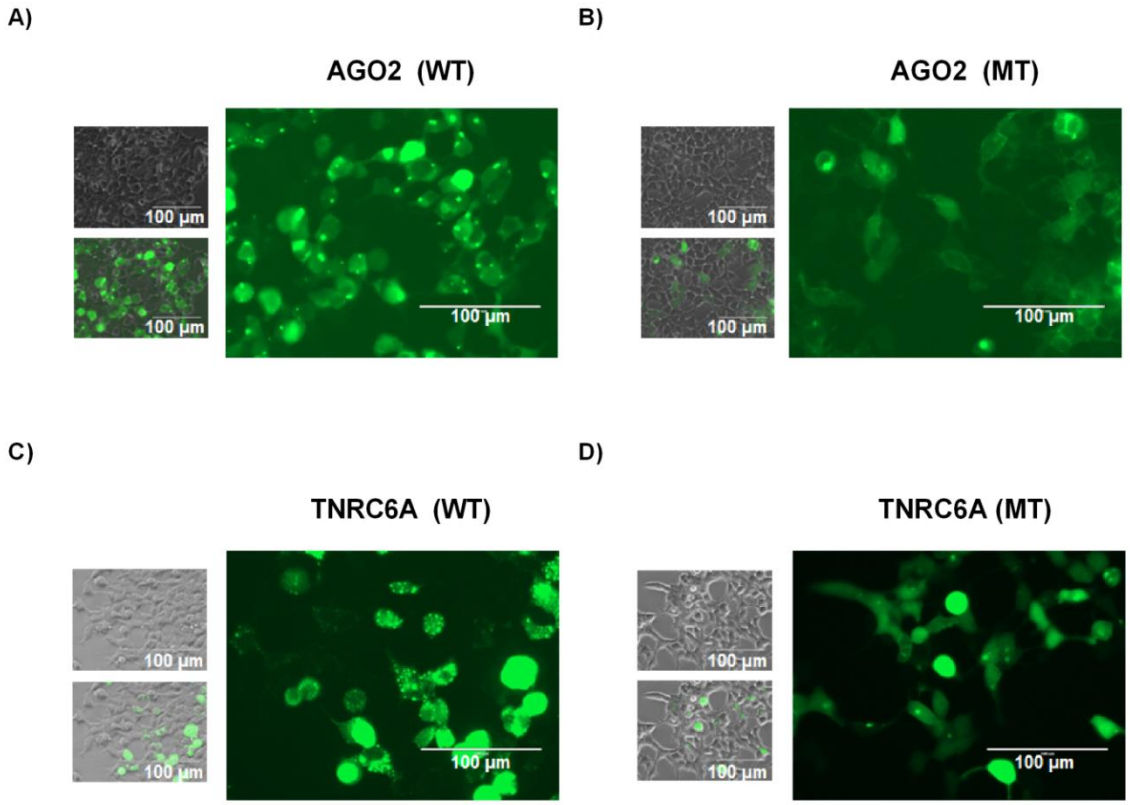

Figure 4.18 Localisation of AGO2 and TNRC6A Expression Products in HEK293T Cells. HEK293T cells, plated in 15 cm cell culture dishes, were transfected with 17.5 µg of **(A)** AGO2 wild-type ("WT"), **(B)** AGO2 membrane-tagged ("MT"), **(C)** TNRC6A WT or **(D)** TNRC6A MT expression plasmids and localisation of GFP assessed by fluorescence microscopy after 48 hours. Inclusion of the membrane-targeting acylation domain (MT plasmids) resulted in localisation of GFP-AGO2 and GFP-TNRC6A fusion proteins towards the membrane while expression of WT plasmids produced a more punctate distribution. Fluorescence is optimised for each image set and is not constant across different image sets.

4.2.6 Co-expression with AGO2 Increases Secretion of Exogenous miRNAs within Extracellular Vesicles

Given the proposed role of AGO2 in the biogenesis and EV-mediated secretion of miRNAs, it was hypothesised that co-expression of AGO2 with exogenous miRNAs would further increase their packaging into EVs. However, preliminary experiments revealed no increased effect upon miRNA secretion within EVs following co-transfection of synthetic mature miRNA mimics with AGO2 expression plasmids (data not shown). Therefore, the decision was taken to focus upon co-expression of pri-miRNA expression plasmids with AGO2, particularly given their more scalable nature.

AGO2 WT and MT expression plasmids were co-transfected with hsa-miR-17 (**Fig. 4.19**), hsa-miR-29a (**Fig. 4.20**) or hsa-miR-106b (**Fig. 4.21**) pri-miRNA expression plasmids in HEK293T cells and EVs isolated after 48 hours. Expression of the mature miRNA transcript was assessed in cells, EVs and supernatant. Cellular expression of the corresponding primary miRNA transcript was assessed in addition to the expression of *AGO2* mRNA in cells and EVs. Primary miRNA transcripts could not be reliably assessed in EVs due to low expression levels.

Generally, expression of the mature miRNA transcript was increased in cells, EVs and supernatant following co-transfection of AGO2 with pri-miRNA expression plasmids for hsa-miR-17 (**Fig. 4.19A-C**), hsa-miR-29a (**Fig. 4.20A-C**) and hsa-miR-106b (**Fig. 4.21A-C**). As noted before, the increase in miRNA secretion displayed an inverse relationship to endogenous miRNA abundance. Interestingly, AGO2 MT appeared to further increase mature miRNA expression within EVs in comparison to the AGO2 WT

form, although this was not significant. Conversely, mature miRNA expression was most increased within supernatant following co-transfection of the AGO2 WT form. This may correspond to the increased secretion of vesicle-independent miRNA-AGO2 complexes[575,576]. There was no significant effect upon cellular expression of the primary transcript for hsa-miR-17 (**Fig. 4.19D**), hsa-miR-29a (**Fig. 4.20D**) or hsa-miR-106b (**Fig. 4.21D**) following any co-transfection. As expected, *AGO2* mRNA expression was increased in cells and EVs following co-transfection of AGO2 WT and MT plasmids with hsa-miR-17 (**Fig. 4.19E-F**), hsa-miR-29a (**Fig. 4.20E-F**) and hsa-miR-106b (**Fig. 4.21E-F**) expression plasmids.

To explore the specificity of increased miRNA expression following co-transfection of pri-hsa-miR-106b and AGO2 expression plasmids, the expression of two unrelated miRNAs was assessed in cells and EVs (**Fig. 4.22**). This included hsa-let-7a-1, which has relatively high endogenous abundance, and hsa-miR-29a which was shown above to have relatively low endogenous abundance. There was no significant effect upon cellular hsa-let-7a-1 expression (**Fig. 4.22A**) or cellular and EV expression of hsa-miR-29a (**Fig. 4.22C-D**). However, expression of hsa-let-7a-1 did appear to be reduced in EVs following all co-transfection conditions (**Fig. 4.22B**).

In summary, co-expression of pri-miRNAs with AGO2 increased exogenous miRNA secretion within EVs. Furthermore, AGO2 MT plasmids appeared to non-significantly enhance this effect in comparison to AGO2 WT plasmids. However, a number of observed increases did not reach significance due to a high degree of variability within treatment conditions. This will be discussed further in **Section 4.2.10**.

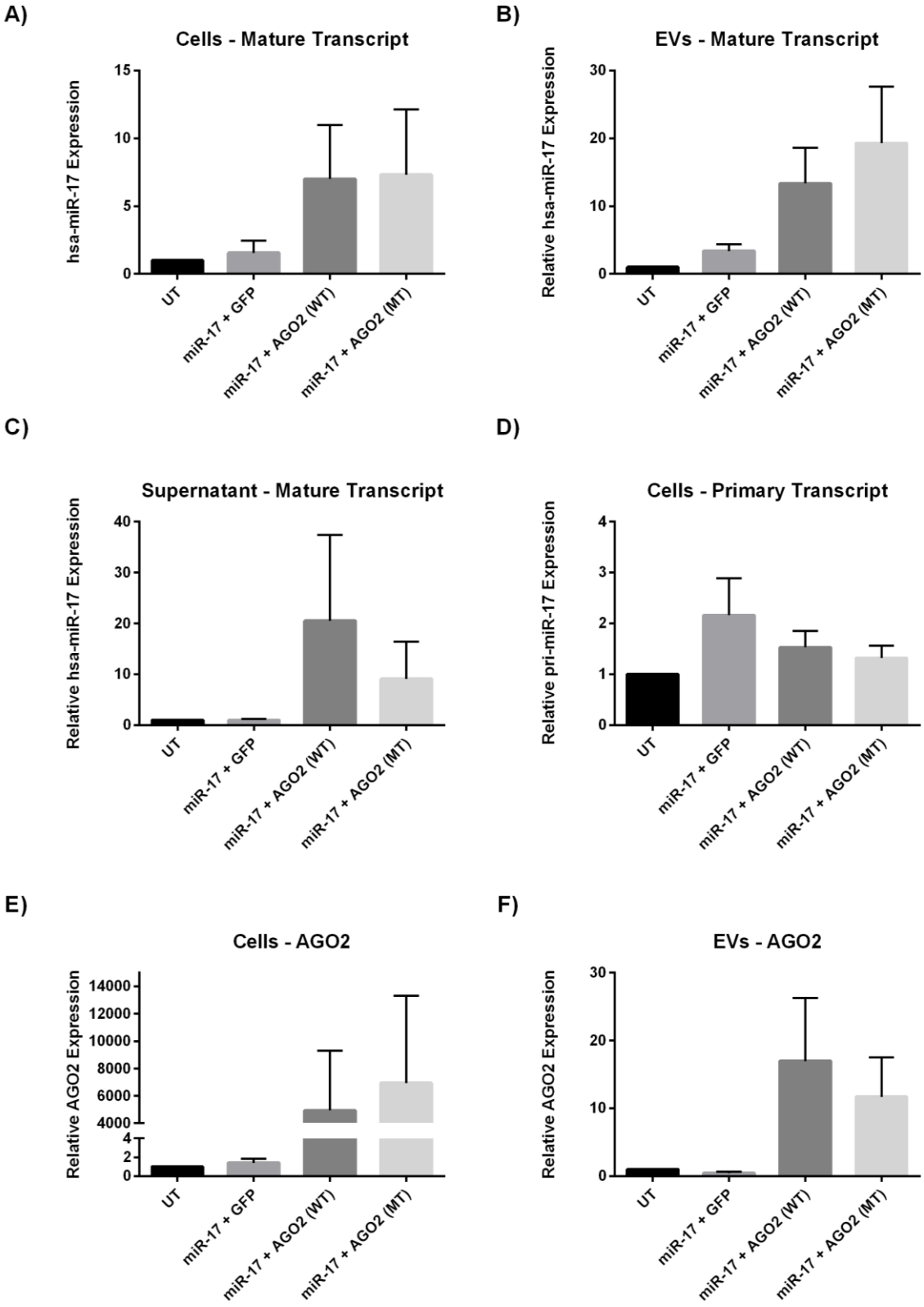
A)
Cells - Mature Transcript
hsa-miR-17 Expression
15
10
5
0
UT
miR-17 + GFP
miR-17 + AGO2 (WT)
miR-17 + AGO2 (MT)
B)
EVs - Mature Transcript
Relative hsa-miR-17 Expression
30
20
10
0
UT
miR-17 + GFP
miR-17 + AGO2 (WT)
miR-17 + AGO2 (MT)
C)
Supernatant - Mature Transcript
Relative hsa-miR-17 Expression
40
30
20
10
0
UT
miR-17 + GFP
miR-17 + AGO2 (WT)
miR-17 + AGO2 (MT)
D)
Cells - Primary Transcript
Relative pri-miR-17 Expression
4
3
2
1
0
UT
miR-17 + GFP
miR-17 + AGO2 (WT)
miR-17 + AGO2 (MT)
E)
Cells - AGO2
Relative AGO2 Expression
14000
12000
10000
8000
6000
4000
4
2
0
UT
miR-17 + GFP
miR-17 + AGO2 (WT)
miR-17 + AGO2 (MT)
F)
EVs - AGO2
Relative AGO2 Expression
30
20
10
0
UT
miR-17 + GFP
miR-17 + AGO2 (WT)
miR-17 + AGO2 (MT)

Figure 4.19 hsa-miR-17 Expression following Co-transfection of hsa-miR-17 and AGO2 Expression Plasmids. HEK293T cells, plated in 15 cm cell culture dishes, were left untreated ("UT") or co-transfected with 17.5 µg each of hsa-miR-17 and either a control GFP plasmid ("GFP") or AGO2 wild-type ("WT") or membrane-tagged ("MT") expression plasmids. EVs were isolated after 48 hours and mature hsa-miR-17 expression, normalised to total RNA input (cells) or cel-miR-39 spike-in (EVs and supernatant), assessed by qPCR. Expression of *AGO2* and primary hsa-miR-17, normalised to *β-Actin*, was also quantified. **(A-C)** hsa-miR-17 expression was non-significantly increased in **(A)** cells, **(B)** EVs and **(C)** supernatant following co-transfection of hsa-miR-17 and AGO2 (WT and MT) plasmids. **(D)** There was no significant effect upon hsa-miR-17 primary transcript expression in cells following co-transfection of hsa-miR-17 and AGO2 plasmids. **(E-F)** *AGO2* mRNA expression was non-significantly increased in **(E)** cells and **(F)** EVs following co-transfection of hsa-miR-17 and AGO2 (WT and MT) plasmids. Values are mean ± SEM, n = 3, one-way ANOVA.

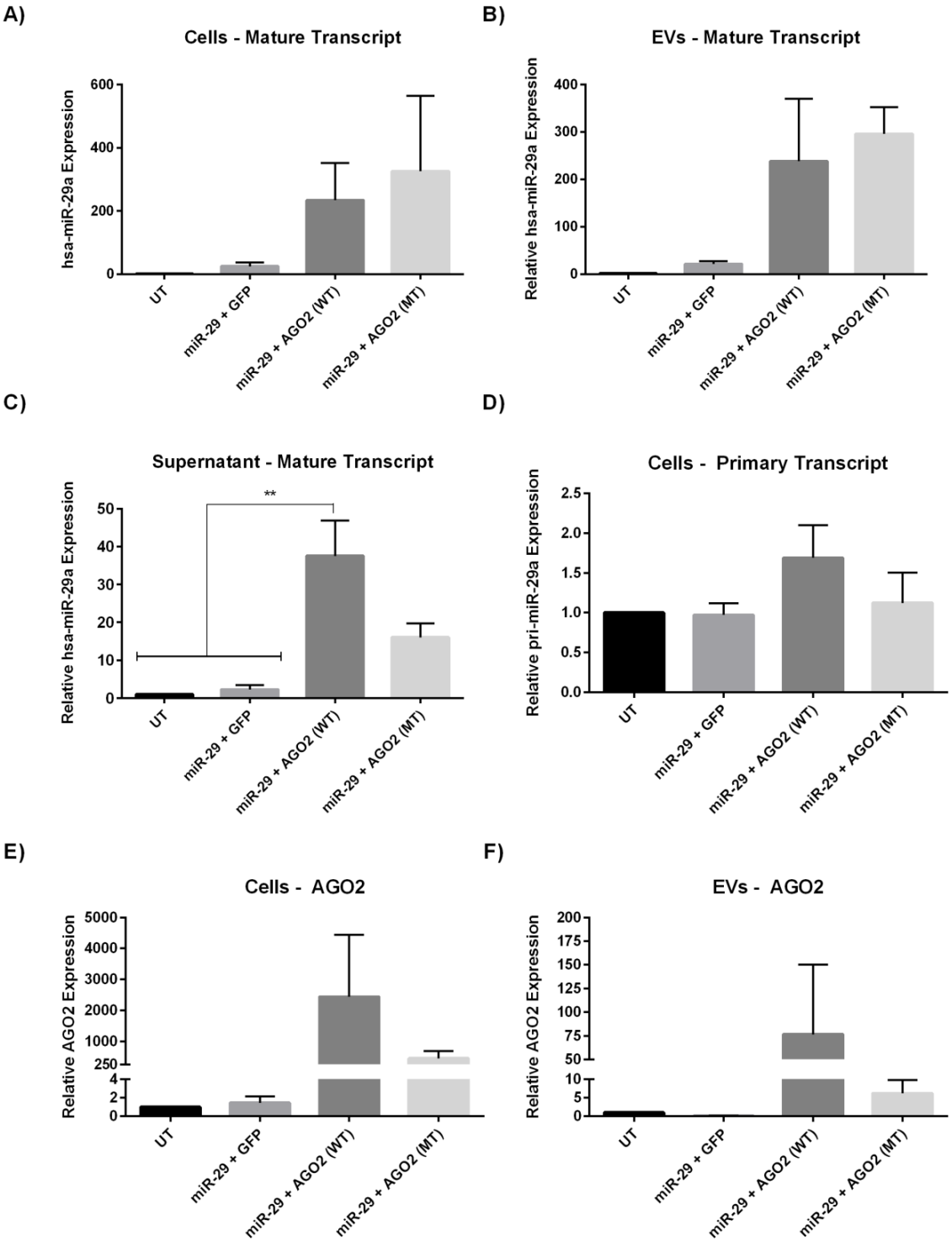
A)
Cells - Mature Transcript
hsa-miR-29a Expression
600
400
200
0
UT
miR-29 + GFP
miR-29 + AGO2 (WT)
miR-29 + AGO2 (MT)
B)
EVs - Mature Transcript
Relative hsa-miR-29a Expression
400
300
200
100
0
UT
miR-29 + GFP
miR-29 + AGO2 (WT)
miR-29 + AGO2 (MT)
C)
Supernatant - Mature Transcript
Relative hsa-miR-29a Expression
**
50
40
30
20
10
0
UT
miR-29 + GFP
miR-29 + AGO2 (WT)
miR-29 + AGO2 (MT)
D)
Cells - Primary Transcript
Relative pri-miR-29a Expression
2.5
2.0
1.5
1.0
0.5
0.0
UT
miR-29 + GFP
miR-29 + AGO2 (WT)
miR-29 + AGO2 (MT)
E)
Cells - AGO2
Relative AGO2 Expression
5000
4000
3000
2000
1000
250
4
2
0
UT
miR-29 + GFP
miR-29 + AGO2 (WT)
miR-29 + AGO2 (MT)
F)
EVs - AGO2
Relative AGO2 Expression
200
175
150
125
100
75
50
10
5
0
UT
miR-29 + GFP
miR-29 + AGO2 (WT)
miR-29 + AGO2 (MT)

Figure 4.20 hsa-miR-29a Expression following Co-transfection of hsa-miR-29a and AGO2 Expression Plasmids. HEK293T cells, plated in 15 cm cell culture dishes, were left untreated ("UT") or co-transfected with 17.5 µg each of hsa-miR-29a and either a control GFP plasmid ("GFP") or AGO2 wild-type ("WT") or membrane-tagged ("MT") expression plasmids. EVs were isolated after 48 hours and mature hsa-miR-29a expression, normalised to total RNA input (cells) or cel-miR-39 spike-in (EVs and supernatant), assessed by qPCR. Expression of *AGO2* and primary hsa-miR-29a, normalised to *β-Actin*, was also quantified. **(A-C)** hsa-miR-29a expression was increased in **(A)** cells, **(B)** EVs and **(C)** supernatant following co-transfection of hsa-miR-29a and AGO2 (WT and MT) plasmids. **(D)** There was no significant effect upon hsa-miR-29a primary transcript expression in cells following co-transfection of hsa-miR-29a and AGO2 plasmids. **(E-F)** *AGO2* mRNA expression was non-significantly increased in **(E)** cells and **(F)** EVs following co-transfections of hsa-miR-29a and AGO2 (WT and MT) plasmids. Values are mean ± SEM, n = 3, **p<0.01, one-way ANOVA followed by Tukey's post-hoc test.

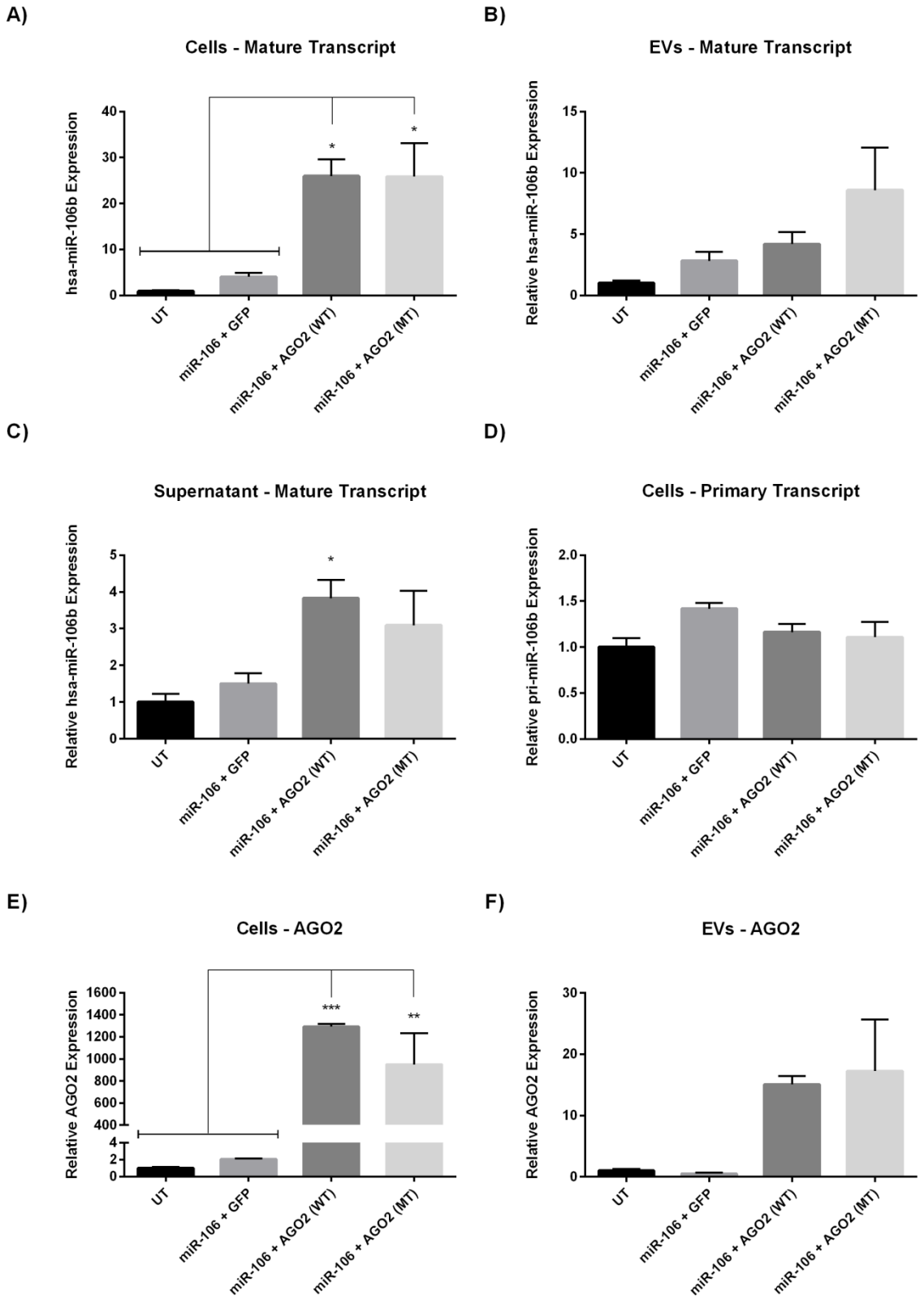
A)
Cells - Mature Transcript
hsa-miR-106b Expression
40
30
20
10
0
*
*
UT
miR-106 + GFP
miR-106 + AGO2 (WT)
miR-106 + AGO2 (MT)
B)
EVs - Mature Transcript
Relative hsa-miR-106b Expression
15
10
5
0
UT
miR-106 + GFP
miR-106 + AGO2 (WT)
miR-106 + AGO2 (MT)
C)
Supernatant - Mature Transcript
Relative hsa-miR-106b Expression
5
4
3
2
1
0
*
UT
miR-106 + GFP
miR-106 + AGO2 (WT)
miR-106 + AGO2 (MT)
D)
Cells - Primary Transcript
Relative pri-miR-106b Expression
2.0
1.5
1.0
0.5
0.0
UT
miR-106 + GFP
miR-106 + AGO2 (WT)
miR-106 + AGO2 (MT)
E)
Cells - AGO2
Relative AGO2 Expression
1600
1400
1200
1000
800
600
400
4
2
0
***
**
UT
miR-106 + GFP
miR-106 + AGO2 (WT)
miR-106 + AGO2 (MT)
F)
EVs - AGO2
Relative AGO2 Expression
30
20
10
0
UT
miR-106 + GFP
miR-106 + AGO2 (WT)
miR-106 + AGO2 (MT)

Figure 4.21 hsa-miR-106b Expression following Co-transfection of hsa-miR-106b and AGO2 Expression Plasmids. HEK293T cells, plated in 15 cm cell culture dishes, were left untreated ("UT") or co-transfected with 17.5 µg each of hsa-miR-106b and either a control GFP plasmid ("GFP") or AGO2 wild-type ("WT") or membrane-tagged ("MT") expression plasmids. EVs were isolated after 48 hours and mature hsa-miR-106b expression, normalised to total RNA input (cells) or cel-miR-39 spike-in (EVs and supernatant), assessed by qPCR. Expression of *AGO2* and primary hsa-miR-106b, normalised to *β-Actin*, was also quantified. **(A)** hsa-miR-106b expression was significantly increased in cells following co-transfection of hsa-miR-106b and AGO2 plasmids (WT and MT). **(B)** hsa-miR-106b was non-significantly increased in EVs following co-transfection of hsa-miR-106b and AGO2 MT. **(C)** Supernatant expression of hsa-miR-106b was significantly increased following co-transfection of hsa-miR-106b and AGO2 WT. **(D)** There was no significant effect upon hsa-miR-106b primary transcript expression in cells following co-transfection of hsa-miR-106b and AGO2 plasmids. **(E-F)** *AGO2* mRNA expression was increased in **(E)** cells and **(F)** EVs following co-transfection of hsa-miR-106b and AGO2 (WT and MT) plasmids. Values are mean ± SEM, n = 3, ***$p<0.001$, **$p<0.01$, *$p<0.05$, one-way ANOVA followed by Tukey's post-hoc test.

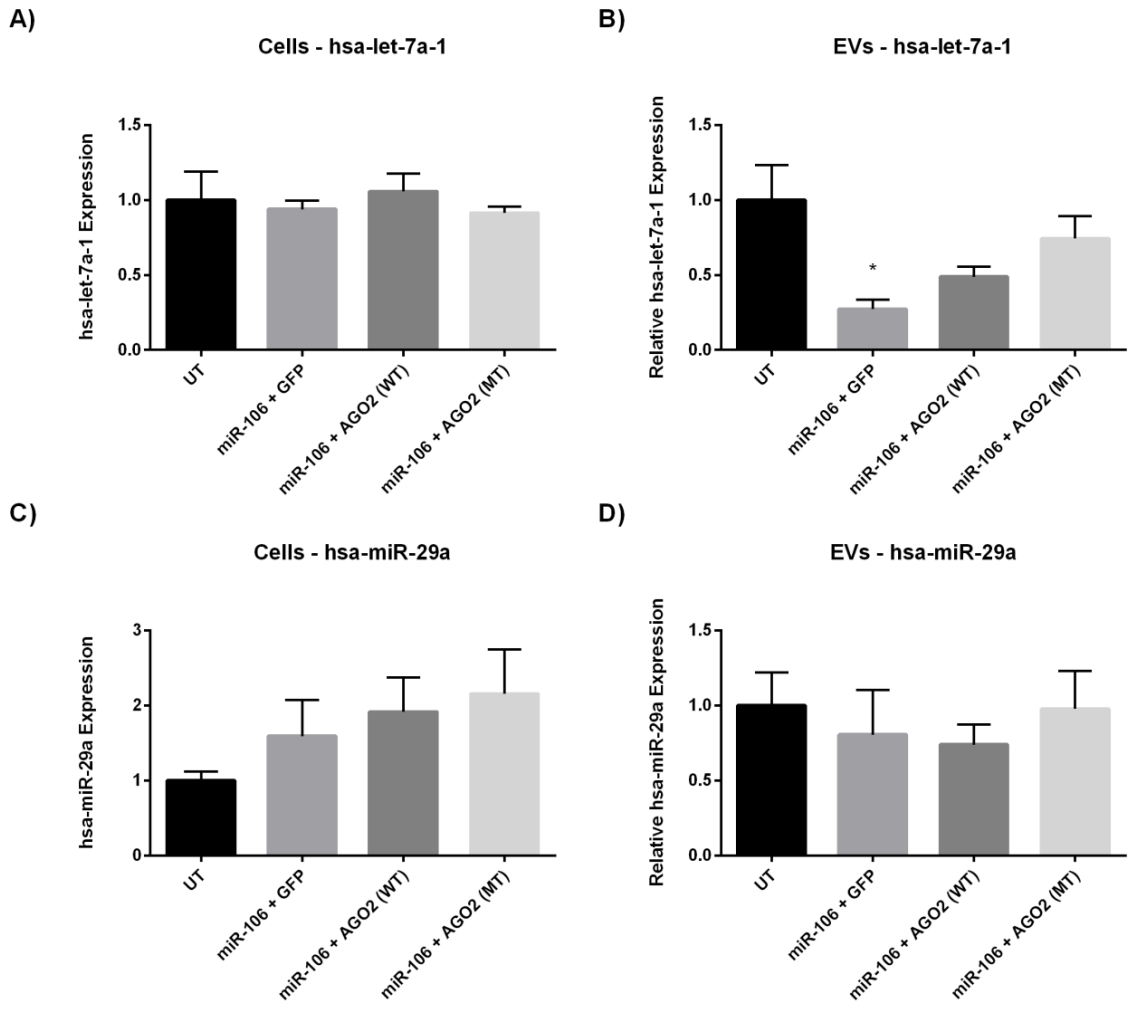

Figure 4.22 Specificity of Increased miRNA Expression following Co-transfection of hsa-miR-106b and AGO2 Expression Plasmids. HEK293T cells, plated in 15 cm cell culture dishes, were left untreated ("UT") or co-transfected with 17.5 µg each of hsa-miR-106b and either a control GFP plasmid ("GFP") or AGO2 wild-type ("WT") or membrane-tagged ("MT") expression plasmids. hsa-let-7a-1 and hsa-miR-29a expression, normalised to total RNA input (cells) or cel-miR-39 spike-in (EVs), was determined by qPCR after 48 hours. **(A)** There was no significant effect upon cellular hsa-let-7a-1 expression. **(B)** hsa-let-7a-1 expression was significantly reduced in EVs following co-expression of hsa-miR-106b and GFP control plasmids. **(C)** Cellular and **(D)** EV expression levels of hsa-miR-29a were not significantly affected following co-expression of hsa-miR-106b and AGO2 expression plasmids. Values are mean ± SEM, n = 3, *$p<0.05$, one-way ANOVA followed by Tukey's post-hoc test.

4.2.7 Co-expression with AGO2 Increases Secretion of shRNA within Extracellular Vesicles

Source cell transfection of siRNAs and shRNA plasmids resulted in their secretion within EVs. It was therefore of interest to determine whether co-transfection with AGO2 would further increase their secretion as observed for pri-miRNA expression plasmids. To investigate this, HEK293T cells were co-transfected with AGO2 (WT or MT) plasmids and APP shRNA (**Fig. 4.23**), APP siRNA (**Fig. 4.24**), BACE1 shRNA (**Fig. 4.25**) or BACE1 siRNA (**Fig. 4.26**). EVs were isolated after 48 hours and expression of APP/BACE1 siRNA/shRNA and *APP*, *BACE1* and *AGO2* mRNA in cells, EV and supernatant assessed by qPCR.

Expression of APP shRNA was significantly increased in cells, EVs and supernatant following co-expression with AGO2 WT (**Fig. 4.23A-C**). This effect was further enhanced in EVs following co-expression with AGO2 MT (**Fig. 4.23B**). *APP* mRNA expression was not significantly reduced in cells (**Fig. 4.23D**) or EVs (**Fig. 4.23E**) following co-transfection with control or AGO2 plasmids. However, this may have arisen from an insufficient quantity of transfected shRNA, as suggested by the earlier shRNA dose-response (**Fig. 4.4A**). In contrast, *AGO2* mRNA expression was increased in cells (**Fig. 4.23F**) and EVs (**Fig. 4.23G**) following co-transfection with AGO2 plasmids.

A similar pattern was observed for APP siRNA. APP siRNA was significantly increased in cells (**Fig. 4.24A**) and EVs (**Fig. 4.24B**) following co-expression with both AGO2 plasmids and in supernatant following co-expression with AGO2 WT (**Fig. 4.24C**). In

contrast to the results above, *APP* mRNA expression was significantly decreased in cells (**Fig. 4.24D**) and EVs (**Fig. 4.24E**) following all co-transfections with APP siRNA. As expected, *AGO2* mRNA expression was increased in cells (**Fig. 4.24F**) and EVs (**Fig. 4.24G**) following co-transfection with AGO2 plasmids.

Co-expression of BACE1 shRNA and AGO2 plasmids produced similar results. BACE1 shRNA expression was increased in cells, EVs and supernatant following co-transfection with AGO2 plasmids (**Fig. 4.25A-C**). *BACE1* mRNA expression was reduced in cells (**Fig. 4.25D**) and EVs (**Fig. 4.25E**) while *AGO2* mRNA expression was significantly increased in cells (**Fig. 4.25F**) and EVs (**Fig. 4.25G**) following co-transfection with AGO2 plasmids.

Increased BACE1 siRNA expression was also observed in cells, EVs and supernatant following co-transfection with AGO2 plasmids (**Fig. 4.26A-C**). As expected, *BACE1* mRNA expression was reduced in cells (**Fig. 4.26D**) and EVs (**Fig. 4.26E**) while *AGO2* mRNA expression was increased in both cells (**Fig. 4.26F**) and EVs (**Fig. 4.26G**) following AGO2 WT and MT plasmid co-transfections.

In summary, these results suggest that co-expression with AGO2 increased the secretion of exogenous siRNAs/shRNAs within EVs. Interestingly, AGO2 MT appeared to increase EV-mediated secretion above that achieved by AGO2 WT for shRNAs but not for siRNAs. Expression of *APP* and *BACE1* mRNA within cells and EVs was generally reduced following co-transfection, which is of interest given the potential for endogenous cargoes to influence recipient cell expression. However, as noted in the case of pri-miRNAs, high variability within treatment conditions was observed.

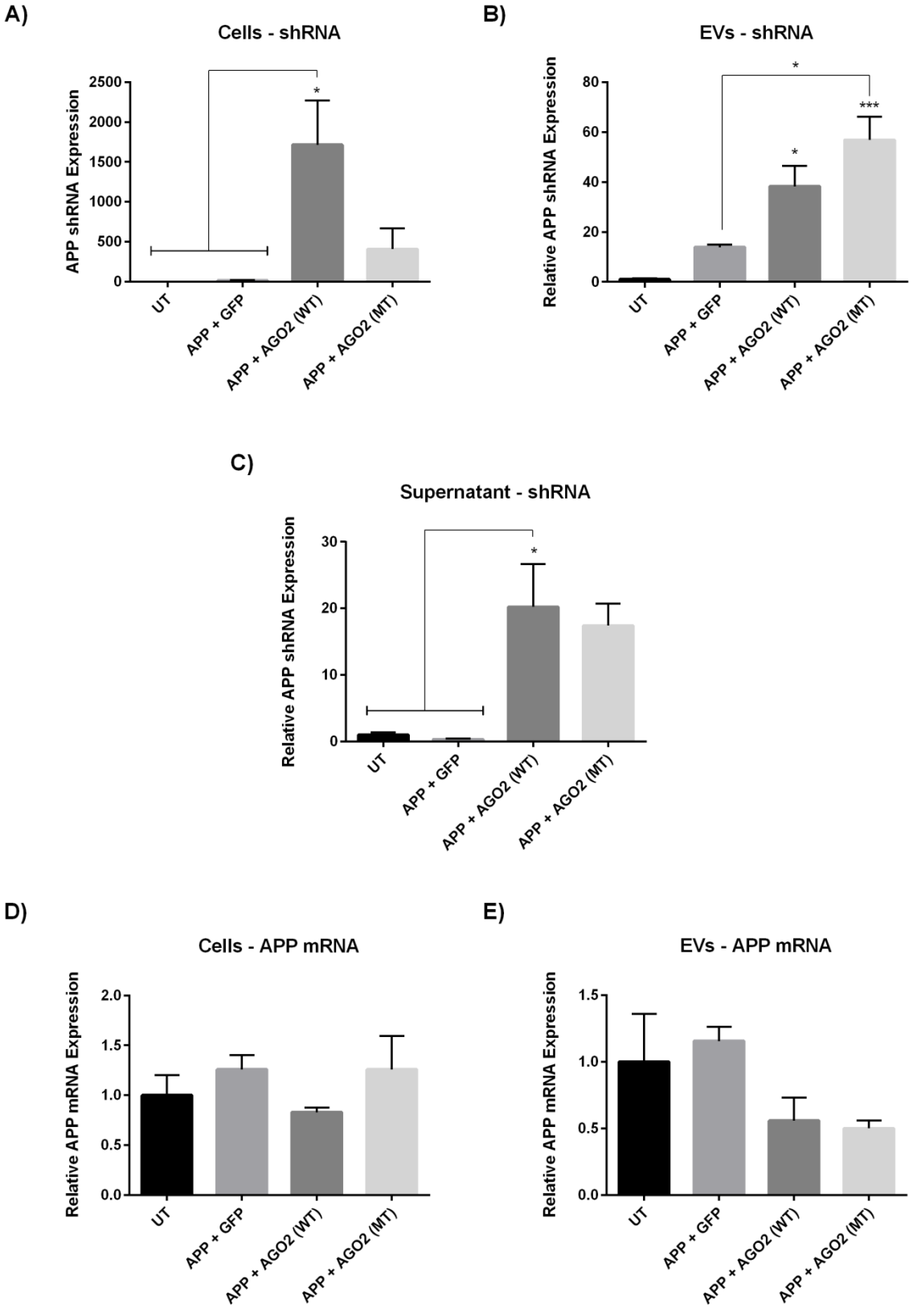
A)
Cells - shRNA
APP shRNA Expression
2500
2000
1500
1000
500
0
*
UT
APP + GFP
APP + AGO2 (WT)
APP + AGO2 (MT)
B)
EVs - shRNA
Relative APP shRNA Expression
80
60
40
20
0
*
*
***
UT
APP + GFP
APP + AGO2 (WT)
APP + AGO2 (MT)
C)
Supernatant - shRNA
Relative APP shRNA Expression
30
20
10
0
*
UT
APP + GFP
APP + AGO2 (WT)
APP + AGO2 (MT)
D)
Cells - APP mRNA
Relative APP mRNA Expression
2.0
1.5
1.0
0.5
0.0
UT
APP + GFP
APP + AGO2 (WT)
APP + AGO2 (MT)
E)
EVs - APP mRNA
Relative APP mRNA Expression
1.5
1.0
0.5
0.0
UT
APP + GFP
APP + AGO2 (WT)
APP + AGO2 (MT)

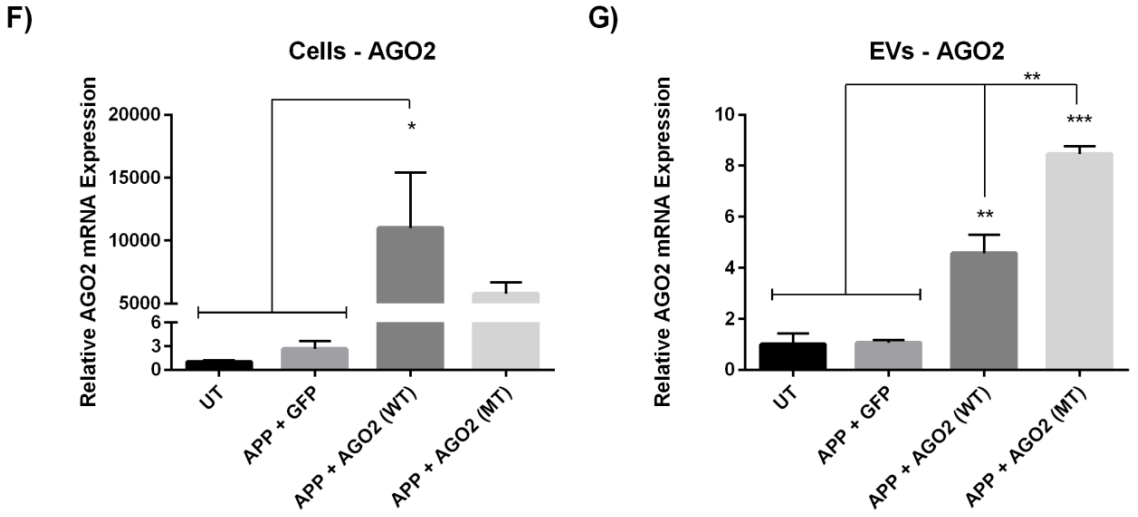

Figure 4.23 APP shRNA Expression following Co-transfection of APP shRNA and AGO2 Expression Plasmids. HEK293T cells, plated in 15 cm cell culture dishes, were left untreated ("UT") or co-transfected with 17.5 µg each of APP shRNA and either a control GFP plasmid ("GFP") or AGO2 wild-type ("WT") or membrane-tagged ("MT") expression plasmids. APP shRNA expression, normalised to total RNA input (cells) or cel-miR-39 spike-in (EVs and supernatant), was quantified by qPCR after 48 hours. *AGO2* and *APP* mRNA expression, normalised to *β-Actin*, was also assessed. **(A)** APP shRNA expression was significantly increased in cells following co-expression of APP shRNA and AGO2 WT plasmids. **(B)** APP shRNA expression was significantly increased in EVs following co-expression of APP shRNA and AGO2 (WT and MT) plasmids. **(C)** APP shRNA expression was significantly increased in supernatant following co-transfection of APP shRNA and AGO2 WT plasmids. **(D)** Cellular and **(E)** EV *APP* mRNA expression was not significantly affected following co-expression of APP shRNA with AGO2 (WT and MT) plasmids. **(F)** Cellular and **(G)** EV expression of *AGO2* mRNA was significantly increased following co-expression of APP shRNA and AGO2 plasmids. Values are mean ± SEM, n = 3, ***p<0.001, **p<0.01, *p<0.05, one-way ANOVA followed by Tukey's post-hoc test.

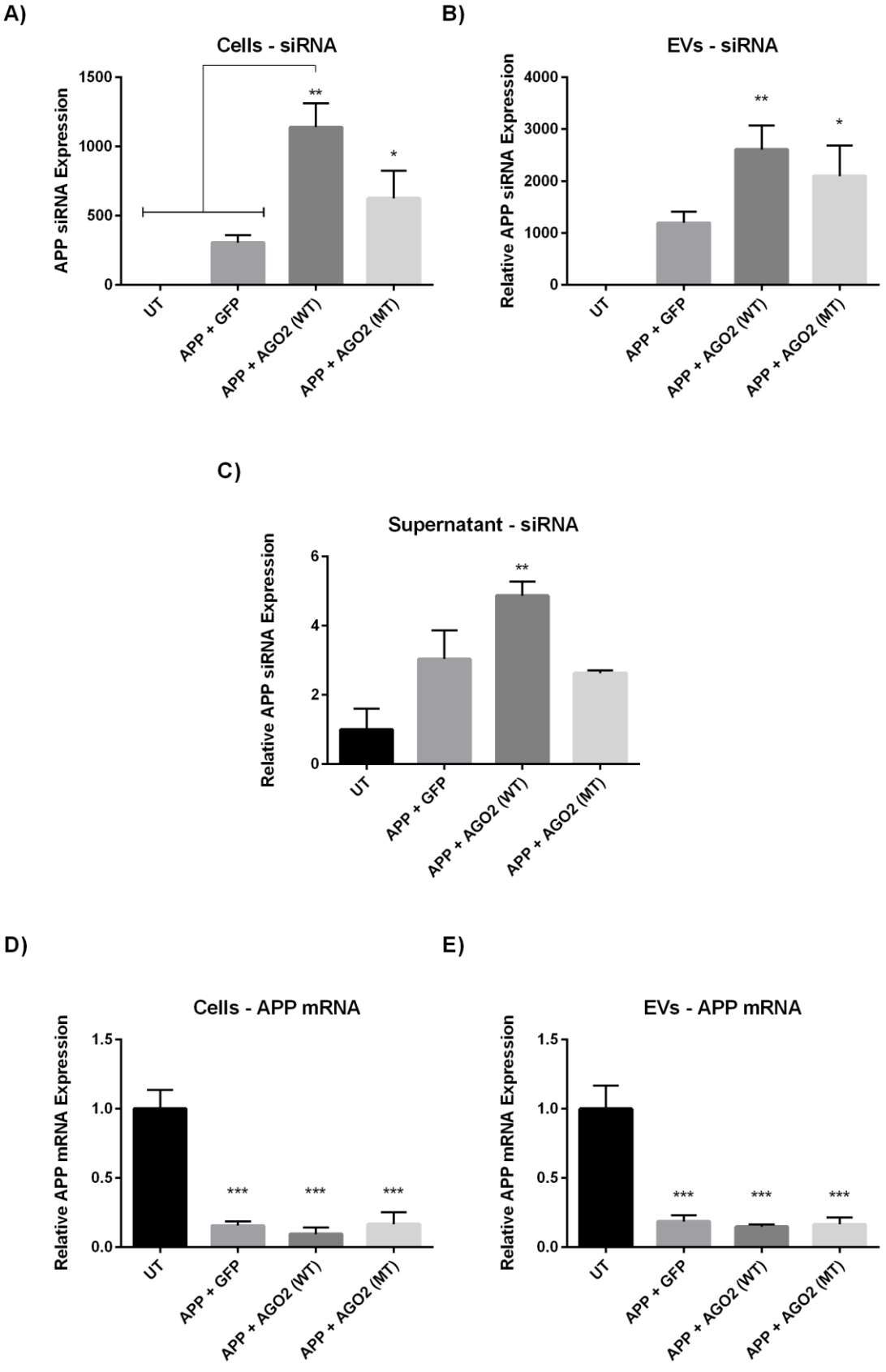
A)
Cells - siRNA
APP siRNA Expression
1500
1000
500
0
**
*
UT
APP + GFP
APP + AGO2 (WT)
APP + AGO2 (MT)
B)
EVs - siRNA
Relative APP siRNA Expression
4000
3000
2000
1000
0
**
*
UT
APP + GFP
APP + AGO2 (WT)
APP + AGO2 (MT)
C)
Supernatant - siRNA
Relative APP siRNA Expression
6
4
2
0
**
UT
APP + GFP
APP + AGO2 (WT)
APP + AGO2 (MT)
D)
Cells - APP mRNA
Relative APP mRNA Expression
1.5
1.0
0.5
0.0
***
***
***
UT
APP + GFP
APP + AGO2 (WT)
APP + AGO2 (MT)
E)
EVs - APP mRNA
Relative APP mRNA Expression
1.5
1.0
0.5
0.0
***
***
***
UT
APP + GFP
APP + AGO2 (WT)
APP + AGO2 (MT)

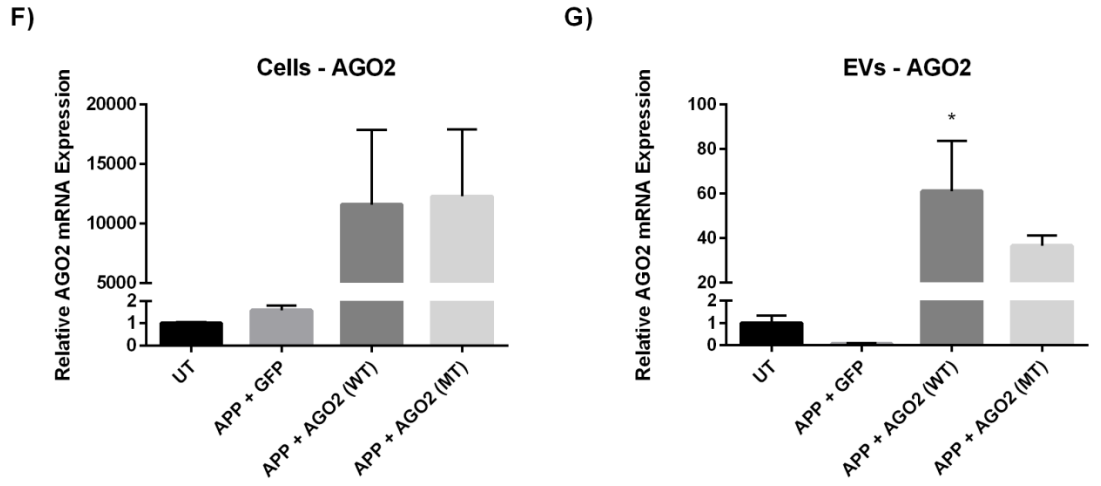

Figure 4.24 APP siRNA Expression following Co-transfection of APP siRNA and AGO2 Expression Plasmids. HEK293T cells, plated in 15 cm cell culture dishes, were left untreated ("UT") or co-transfected with 100 nM of APP siRNA and 17.5 µg of either a control GFP plasmid ("GFP") or AGO2 wild-type ("WT") or membrane-tagged ("MT") expression plasmids. APP siRNA expression, normalised to total RNA input (cells) or cel-miR-39 spike-in (EVs and supernatant), was quantified by qPCR after 48 hours. *AGO2* and *APP* mRNA expression, normalised to *β-Actin*, was also assessed. **(A-C)** APP siRNA expression was significantly increased in **(A)** cells and **(B)** EVs following co-expression of APP siRNA and both AGO2 plasmids and in **(C)** supernatant following co-expression of APP siRNA and AGO2 WT. **(D)** Cellular and **(E)** EV *APP* mRNA expression was significantly reduced following co-expression of APP siRNA and all plasmids. **(F)** Cellular and **(G)** EV expression of *AGO2* mRNA was increased following co-expression of APP siRNA and AGO2 plasmids reaching significance in EVs following co-expression with AGO2 WT. Values are mean ± SEM, n = 3, ***p<0.001, **p<0.01, *p<0.05, one-way ANOVA followed by Tukey's post-hoc test.

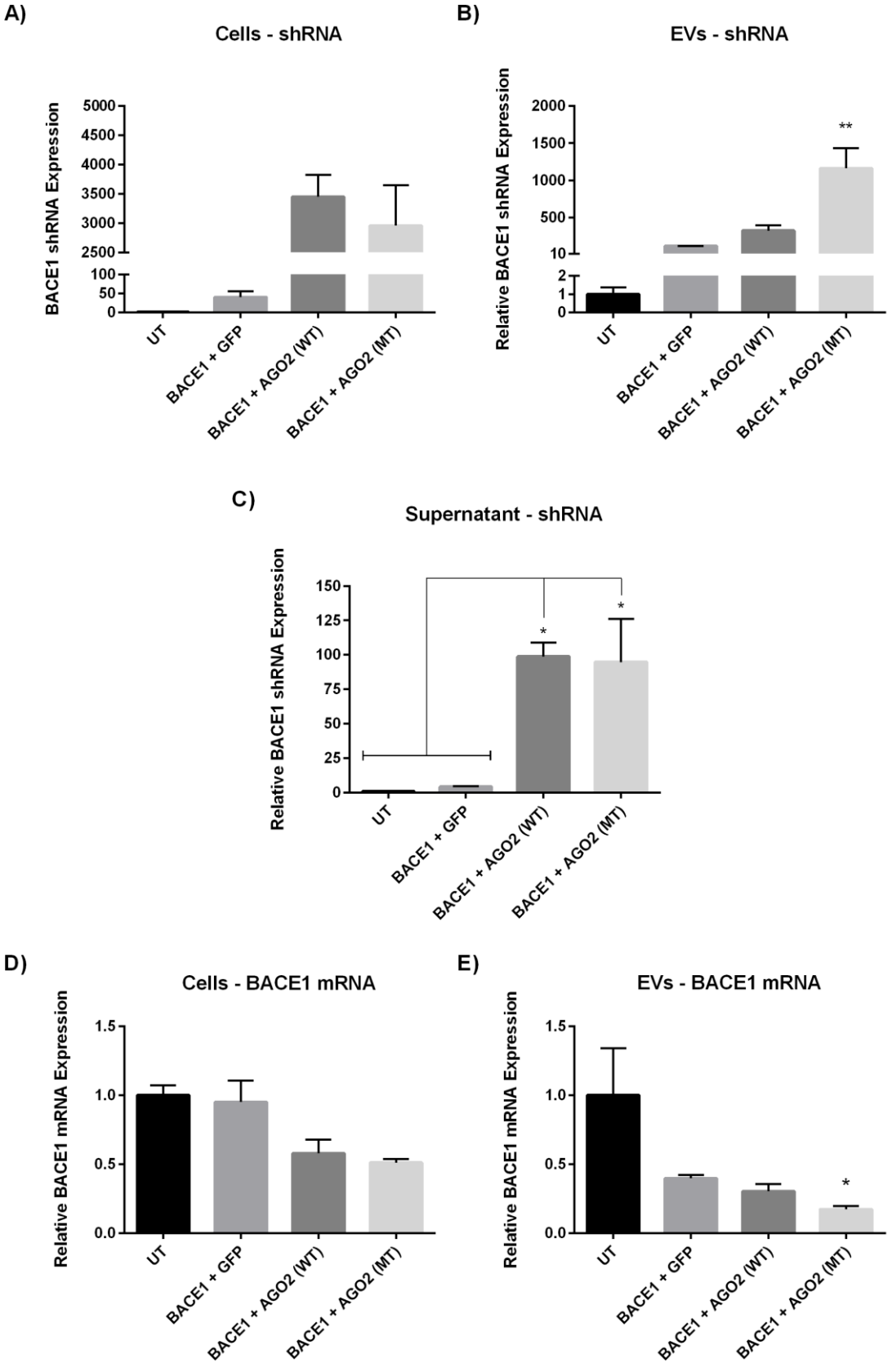
A)
Cells - shRNA
BACE1 shRNA Expression
5000
4500
4000
3500
3000
2500
100
50
0
UT
BACE1 + GFP
BACE1 + AGO2 (WT)
BACE1 + AGO2 (MT)
B)
EVs - shRNA
Relative BACE1 shRNA Expression
2000
1500
1000
500
10
2
1
0
**
UT
BACE1 + GFP
BACE1 + AGO2 (WT)
BACE1 + AGO2 (MT)
C)
Supernatant - shRNA
Relative BACE1 shRNA Expression
150
125
100
75
50
25
0
*
*
UT
BACE1 + GFP
BACE1 + AGO2 (WT)
BACE1 + AGO2 (MT)
D)
Cells - BACE1 mRNA
Relative BACE1 mRNA Expression
1.5
1.0
0.5
0.0
UT
BACE1 + GFP
BACE1 + AGO2 (WT)
BACE1 + AGO2 (MT)
E)
EVs - BACE1 mRNA
Relative BACE1 mRNA Expression
1.5
1.0
0.5
0.0
*
UT
BACE1 + GFP
BACE1 + AGO2 (WT)
BACE1 + AGO2 (MT)

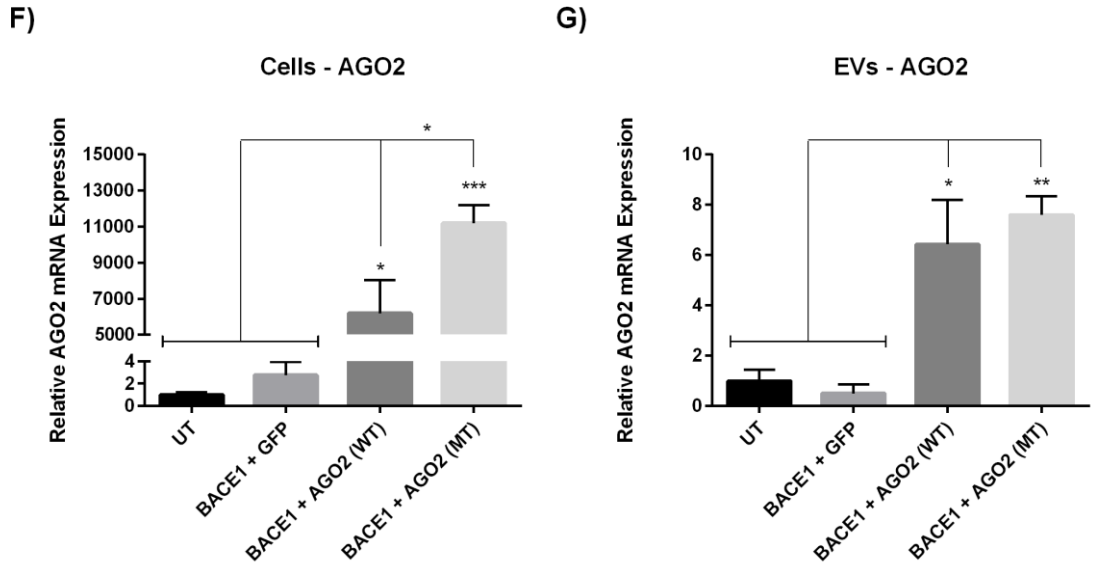

Figure 4.25 BACE1 shRNA Expression following Co-transfection of BACE1 shRNA and AGO2 Expression Plasmids. HEK293T cells, plated in 15 cm cell culture dishes, were left untreated ("UT") or co-transfected with 17.5 µg each of BACE1 shRNA and either a control GFP plasmid ("GFP") or AGO2 wild-type ("WT") or membrane-tagged ("MT") expression plasmids. BACE1 shRNA expression, normalised to total RNA input (cells) or cel-miR-39 spike-in (EVs and supernatant), was quantified by qPCR after 48 hours. *AGO2* and *BACE1* mRNA expression, normalised to *β-Actin*, was also assessed. **(A)** BACE1 shRNA expression was non-significantly increased in cells following co-expression of BACE1 shRNA and AGO2 (WT and MT) plasmids. **(B)** BACE1 shRNA expression was significantly increased in EVs following co-expression of BACE1 shRNA and AGO2 MT. **(C)** BACE1 shRNA expression was significantly increased in supernatant following co-transfection of BACE1 shRNA and AGO2 plasmids. **(D)** Cellular *BACE1* mRNA expression was non-significantly reduced following co-expression of BACE1 shRNA with AGO2 plasmids. **(E)** EV *BACE1* mRNA expression was significantly reduced following co-expression of BACE1 shRNA and AGO2 MT plasmids. **(F)** Cellular and **(G)** EV expression of *AGO2* mRNA was significantly increased following co-expression of BACE1 shRNA and AGO2 plasmids. Values are mean ± SEM, n = 3, ***$p<0.001$, **$p<0.01$, *$p<0.05$, one-way ANOVA followed by Tukey's post-hoc test.

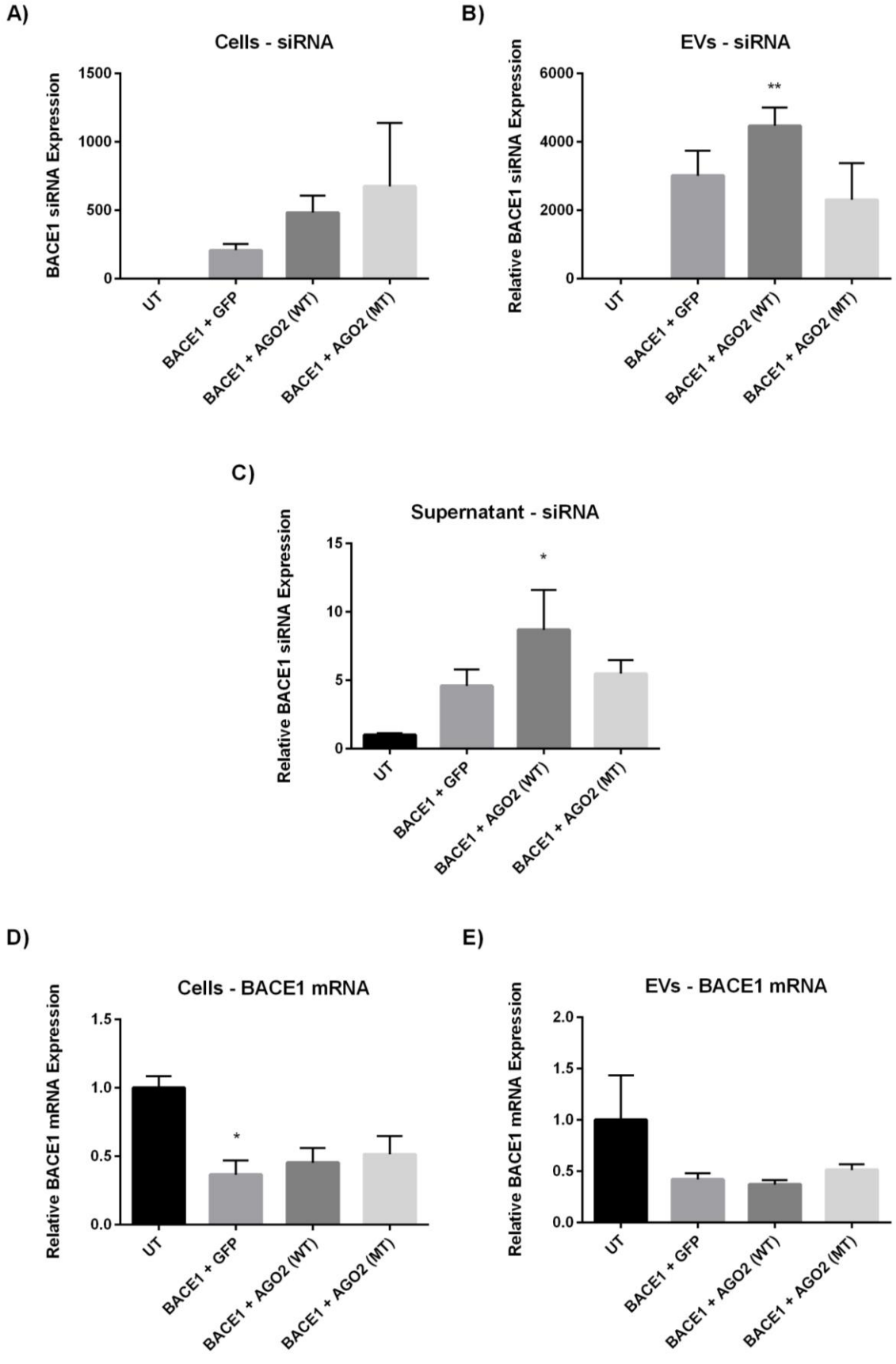
A)
Cells - siRNA
BACE1 siRNA Expression
1500
1000
500
0
UT
BACE1 + GFP
BACE1 + AGO2 (WT)
BACE1 + AGO2 (MT)
B)
EVs - siRNA
Relative BACE1 siRNA Expression
6000
4000
2000
0
**
UT
BACE1 + GFP
BACE1 + AGO2 (WT)
BACE1 + AGO2 (MT)
C)
Supernatant - siRNA
Relative BACE1 siRNA Expression
15
10
5
0
*
UT
BACE1 + GFP
BACE1 + AGO2 (WT)
BACE1 + AGO2 (MT)
D)
Cells - BACE1 mRNA
Relative BACE1 mRNA Expression
1.5
1.0
0.5
0.0
*
UT
BACE1 + GFP
BACE1 + AGO2 (WT)
BACE1 + AGO2 (MT)
E)
EVs - BACE1 mRNA
Relative BACE1 mRNA Expression
2.0
1.5
1.0
0.5
0.0
UT
BACE1 + GFP
BACE1 + AGO2 (WT)
BACE1 + AGO2 (MT)

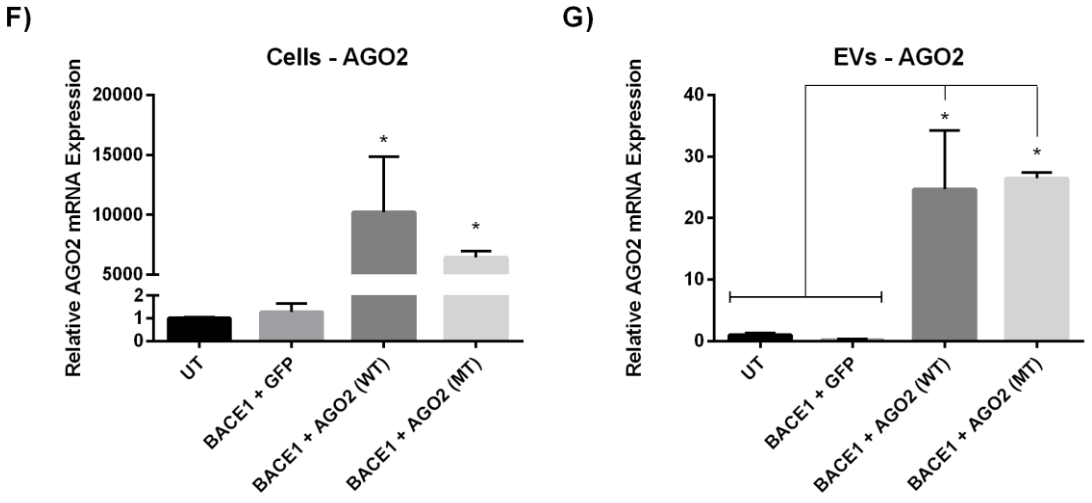

Figure 4.26 BACE1 siRNA Expression following Co-transfection of BACE1 siRNA and AGO2 Expression Plasmids. HEK293T cells, plated in 15 cm cell culture dishes, were left untreated ("UT") or co-transfected with 100 nM of BACE1 siRNA and 17.5 µg of either a control GFP plasmid ("GFP") or AGO2 wild-type ("WT") or membrane-tagged ("MT") expression plasmids. BACE1 siRNA expression, normalised to total RNA input (cells) or cel-miR-39 spike-in (EVs and supernatant), was quantified by qPCR after 48 hours. *AGO2* and *BACE1* mRNA expression, normalised to *β-Actin*, was also assessed. **(A)** Cellular BACE1 siRNA expression was non-significantly increased following co-expression of BACE1 siRNA and AGO2 (WT and MT) plasmids. **(B)** BACE1 siRNA expression was significantly increased in EVs and **(C)** supernatant following co-transfection of BACE1 siRNA and AGO2 WT. **(D)** Cellular and **(E)** EV levels of *BACE1* mRNA were reduced following co-expression of BACE1 siRNA with all plasmids. **(F)** Cellular and **(G)** EV expression of *AGO2* mRNA was significantly increased following co-expression of BACE1 siRNA and AGO2 plasmids. Values are mean ± SEM, n = 3, **p<0.01, *p<0.05, one-way ANOVA followed by Tukey's post-hoc test.

4.2.8 Co-expression with TNRC6A (MT) Increases Secretion of Exogenous miRNAs within Extracellular Vesicles

Co-expression with AGO2, and particularly AGO2 MT, appeared to increase endogenous EV-loading of exogenous pri-miRNAs. Therefore, it was hypothesised that co-expression with TNRC6A, another member of RISC, may also increase miRNA packaging within EVs. To investigate this, HEK293T cells were co-transfected with pri-miRNA expression plasmids for hsa-miR-17 (**Fig. 4.27**), hsa-miR-29a (**Fig. 4.28**) or hsa-miR-106b (**Fig. 4.29**) and either a control GFP plasmid or TNRC6A WT or MT plasmids.

Similar to the results with AGO2 above, mature miRNA expression was increased in cells, EVs and supernatant following co-transfection of TNRC6A plasmids with hsa-miR-17 (**Fig. 4.27A-C**), hsa-miR-29a (**Fig. 4.28A-C**) or hsa-miR-106b (**Fig. 4.29A-C**). Furthermore, miRNA expression within EVs was typically enhanced following co-transfection with the TNRC6A MT plasmid in comparison to the WT form. There was no significant effect upon the primary miRNA transcript following co-transfection of hsa-miR-17 (**Fig. 4.27D**), hsa-miR-29a (**Fig. 4.28D**) or hsa-miR-106b (**Fig. 4.29D**) with either control or TNRC6A plasmids. However, as expected, *TNRC6A* mRNA expression was increased in cells and EVs following co-transfection of hsa-miR-17 (**Fig. 4.27E-F**), hsa-miR-29a (**Fig. 4.28E-F**) or hsa-miR-106b (**Fig. 4.29E-F**) with TNRC6A expression plasmids.

As before, the specificity of increased miRNA expression following co-transfection of TNRC6A (WT and MT) and hsa-miR-106b pri-miRNA expression plasmids was

assessed by analysis of hsa-let-7a-1 and hsa-miR-29a expression. This again indicated a degree of specificity as there was no significant effect upon cellular or EV expression of either hsa-let-7a-1 (**Fig. 4.30A-B**) or hsa-miR-29a (**Fig. 4.30C-D**) following co-transfections.

In summary, these results suggested that co-expression with TNRC6A produced a general increase in cellular and EV expression of exogenous miRNAs. In contrast to AGO2, the fold increase in miRNA expression did not appear to vary inversely with endogenous miRNA abundance. Instead, co-transfection with hsa-miR-106b appeared to produce the greatest increase in expression within EVs. However, it should be noted that variability within treatment conditions was again relatively high.

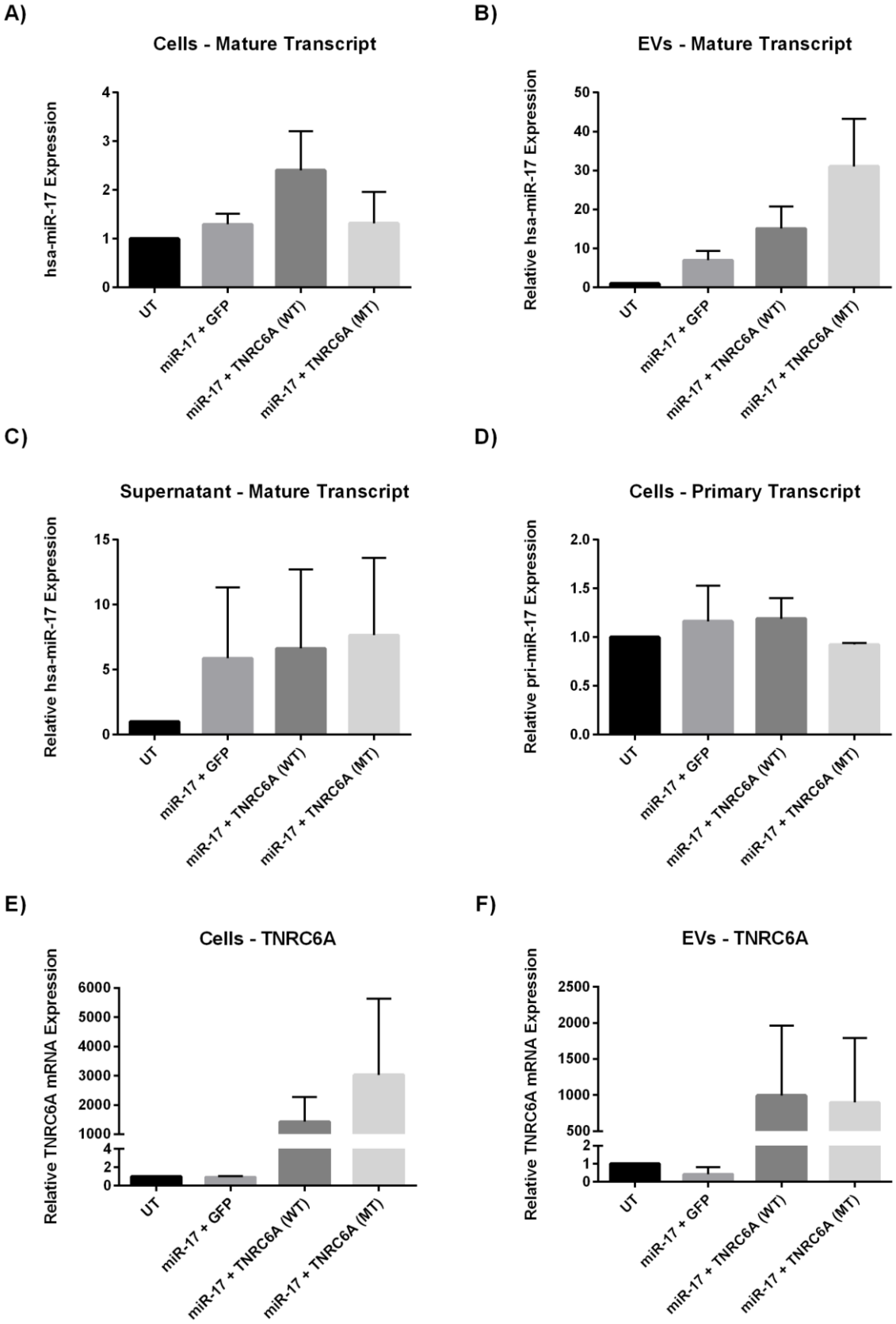
A)
Cells - Mature Transcript
hsa-miR-17 Expression
0
1
2
3
4
UT
miR-17 + GFP
miR-17 + TNRC6A (WT)
miR-17 + TNRC6A (MT)
B)
EVs - Mature Transcript
Relative hsa-miR-17 Expression
0
10
20
30
40
50
UT
miR-17 + GFP
miR-17 + TNRC6A (WT)
miR-17 + TNRC6A (MT)
C)
Supernatant - Mature Transcript
Relative hsa-miR-17 Expression
0
5
10
15
UT
miR-17 + GFP
miR-17 + TNRC6A (WT)
miR-17 + TNRC6A (MT)
D)
Cells - Primary Transcript
Relative pri-miR-17 Expression
0.0
0.5
1.0
1.5
2.0
UT
miR-17 + GFP
miR-17 + TNRC6A (WT)
miR-17 + TNRC6A (MT)
E)
Cells - TNRC6A
Relative TNRC6A mRNA Expression
0
2
4
1000
2000
3000
4000
5000
6000
UT
miR-17 + GFP
miR-17 + TNRC6A (WT)
miR-17 + TNRC6A (MT)
F)
EVs - TNRC6A
Relative TNRC6A mRNA Expression
0
1
2
500
1000
1500
2000
2500
UT
miR-17 + GFP
miR-17 + TNRC6A (WT)
miR-17 + TNRC6A (MT)

Figure 4.27 Expression of hsa-miR-17 following Co-transfection of hsa-miR-17 and TNRC6A Expression Plasmids. HEK293T cells, plated in 15 cm cell culture dishes, were left untreated ("UT") or co-transfected with 17.5 µg each of hsa-miR-17 and either a control GFP plasmid ("GFP") or TNRC6A wild-type ("WT") or membrane-tagged ("MT") expression plasmids. EVs were isolated after 48 hours and mature hsa-miR-17 expression, normalised to total RNA input (cells) or cel-miR-39 spike-in (EVs and supernatant), assessed by qPCR. Expression of *TNRC6A* and hsa-miR-17 primary transcript mRNA, normalised to *β-Actin*, was also quantified. **(A-C)** hsa-miR-17 expression was assessed in **(A)** cells, **(B)** EVs and **(C)** supernatant. The observed increases in expression in EVs and supernatant were not significant. **(D)** There was no effect of co-expression upon hsa-miR-17 primary transcript expression. **(E-F)** *TNRC6A* mRNA expression was increased, but not significantly, in **(E)** cells and **(F)** EVs following co-expression of hsa-miR-17 with TNRC6A (WT and MT) plasmids. Values are mean ± SEM, n = 3, one-way ANOVA.

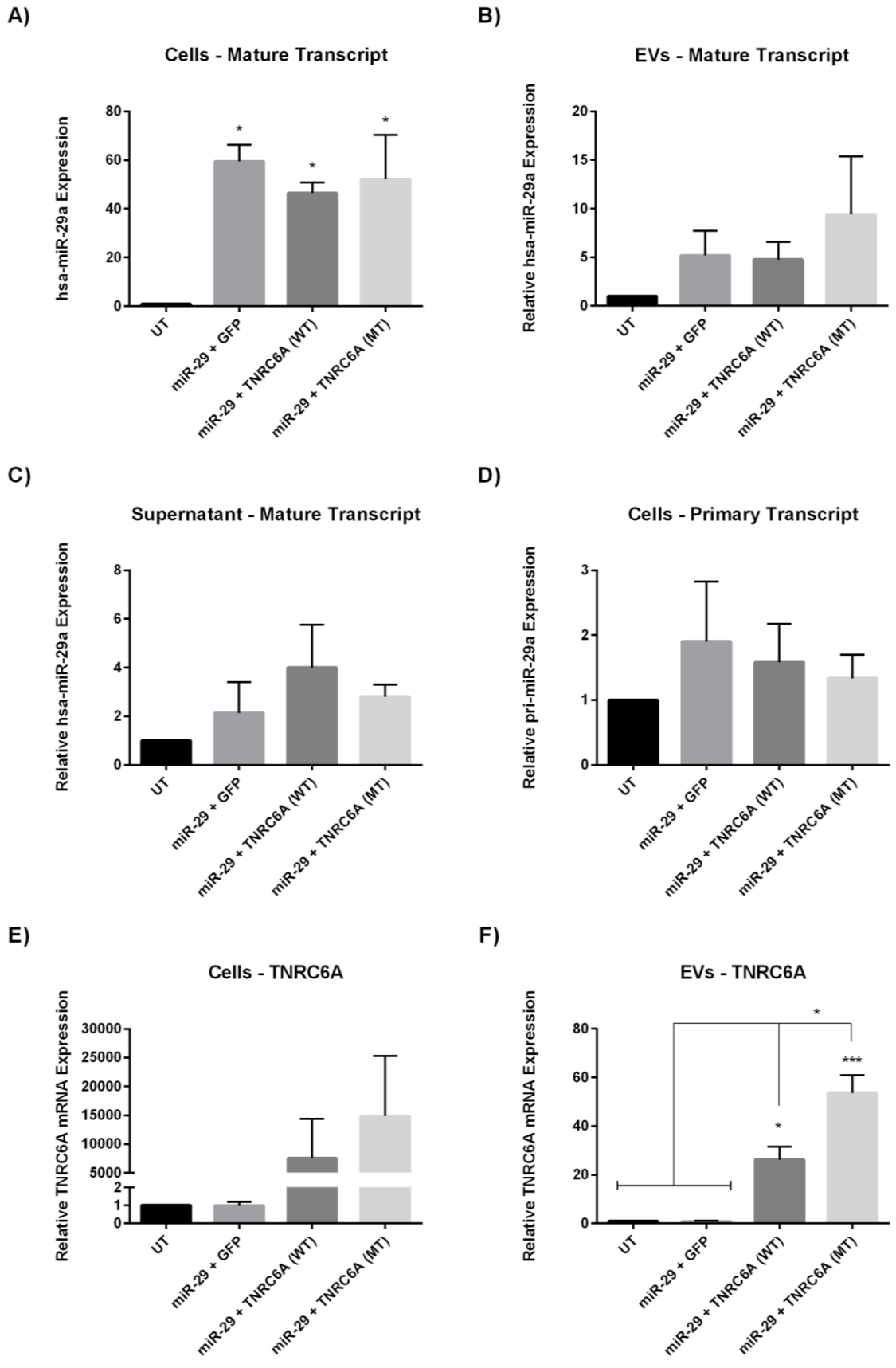
A)
Cells - Mature Transcript
hsa-miR-29a Expression
80
60
40
20
0
*
*
*
UT
miR-29 + GFP
miR-29 + TNRC6A (WT)
miR-29 + TNRC6A (MT)
B)
EVs - Mature Transcript
Relative hsa-miR-29a Expression
20
15
10
5
0
UT
miR-29 + GFP
miR-29 + TNRC6A (WT)
miR-29 + TNRC6A (MT)
C)
Supernatant - Mature Transcript
Relative hsa-miR-29a Expression
8
6
4
2
0
UT
miR-29 + GFP
miR-29 + TNRC6A (WT)
miR-29 + TNRC6A (MT)
D)
Cells - Primary Transcript
Relative pri-miR-29a Expression
3
2
1
0
UT
miR-29 + GFP
miR-29 + TNRC6A (WT)
miR-29 + TNRC6A (MT)
E)
Cells - TNRC6A
Relative TNRC6A mRNA Expression
30000
25000
20000
15000
10000
5000
2
1
0
UT
miR-29 + GFP
miR-29 + TNRC6A (WT)
miR-29 + TNRC6A (MT)
F)
EVs - TNRC6A
Relative TNRC6A mRNA Expression
80
60
40
20
0
*
*
***
UT
miR-29 + GFP
miR-29 + TNRC6A (WT)
miR-29 + TNRC6A (MT)

Figure 4.28 Expression of hsa-miR-29a following Co-transfection of hsa-miR-29a and TNRC6A Expression Plasmids. HEK293T cells, plated in 15 cm cell culture dishes, were left untreated ("UT") or co-transfected with 17.5 µg each of hsa-miR-29a and either a control GFP plasmid ("GFP") or TNRC6A wild-type ("WT") or membrane-tagged ("MT") expression plasmids. EVs were isolated after 48 hours and mature hsa-miR-29a expression, normalised to total RNA input (cells) or cel-miR-39 spike-in (EVs and supernatant), assessed by qPCR. Expression of *TNRC6A* and hsa-miR-29a primary transcript mRNA, normalised to *β-Actin*, was also quantified. **(A)** hsa-miR-29a expression was significantly increased in cells following co-expression with all plasmids but was not increased further by co-transfection with TNRC6A (WT or MT) plasmids. **(B)** hsa-miR-29a expression was slightly increased, but not significantly, following co-transfection with TNRC6A MT in EVs and **(C)** with TNRC6A WT in supernatant. **(D)** There was no effect of co-expression upon hsa-miR-29a primary transcript expression. **(E-F)** *TNRC6A* mRNA expression was increased in **(E)** cells (non-significantly) and in **(F)** EVs (significantly) following co-expression of hsa-miR-29a with TNRC6A (WT and MT) plasmids. Values are mean ± SEM, n = 3, ***$p<0.001$, *<0.05, one-way ANOVA followed by Tukey's post-hoc test.

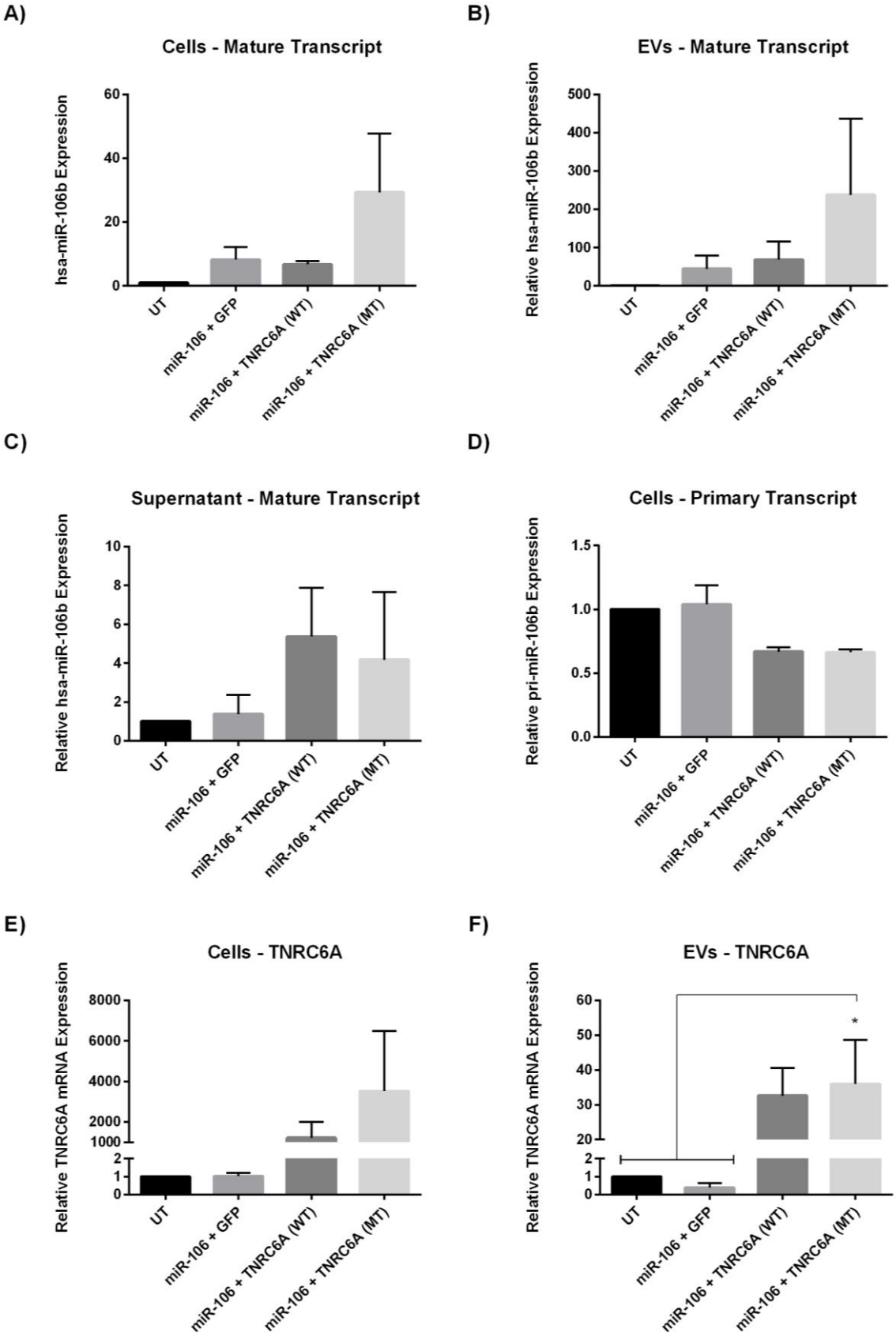
A)
Cells - Mature Transcript
hsa-miR-106b Expression
60
40
20
0
UT
miR-106 + GFP
miR-106 + TNRC6A (WT)
miR-106 + TNRC6A (MT)
B)
EVs - Mature Transcript
Relative hsa-miR-106b Expression
500
400
300
200
100
0
UT
miR-106 + GFP
miR-106 + TNRC6A (WT)
miR-106 + TNRC6A (MT)
C)
Supernatant - Mature Transcript
Relative hsa-miR-106b Expression
10
8
6
4
2
0
UT
miR-106 + GFP
miR-106 + TNRC6A (WT)
miR-106 + TNRC6A (MT)
D)
Cells - Primary Transcript
Relative pri-miR-106b Expression
1.5
1.0
0.5
0.0
UT
miR-106 + GFP
miR-106 + TNRC6A (WT)
miR-106 + TNRC6A (MT)
E)
Cells - TNRC6A
Relative TNRC6A mRNA Expression
8000
6000
4000
2000
1000
2
1
0
UT
miR-106 + GFP
miR-106 + TNRC6A (WT)
miR-106 + TNRC6A (MT)
F)
EVs - TNRC6A
Relative TNRC6A mRNA Expression
60
50
40
30
20
2
1
0
*
UT
miR-106 + GFP
miR-106 + TNRC6A (WT)
miR-106 + TNRC6A (MT)

Figure 4.29 Expression of hsa-miR-106b following Co-transfection of hsa-miR-106b and TNRC6A Expression Plasmids. HEK293T cells, plated in 15 cm cell culture dishes, were left untreated ("UT") or co-transfected with 17.5 µg each of hsa-miR-106b and either a control GFP plasmid ("GFP") or TNRC6A wild-type ("WT") or membrane-tagged ("MT") expression plasmids. EVs were isolated after 48 hours and mature hsa-miR-106b expression, normalised to total RNA input (cells) or cel-miR-39 spike-in (EVs and supernatant), assessed by qPCR. Expression of *AGO2* and hsa-miR-106b primary transcript mRNA, normalised to *β-Actin*, was also quantified. **(A-C)** hsa-miR-106b expression was assessed in **(A)** cells, **(B)** EVs and **(C)** supernatant. The increase in hsa-miR-106b expression in cells and EVs following co-expression with TNRC6A MT did not reach significance. **(D)** There was no effect upon hsa-miR-106b primary transcript expression following co-expression with TNRC6A (WT and MT) plasmids. **(E-F)** *TNRC6A* mRNA expression was increased in **(E)** cells (non-significantly) and **(F)** EVs (significantly) following co-expression of hsa-miR-106b with TNRC6A plasmids. Values are mean ± SEM, n = 3, *<0.05, one-way ANOVA followed by Tukey's post-hoc test.

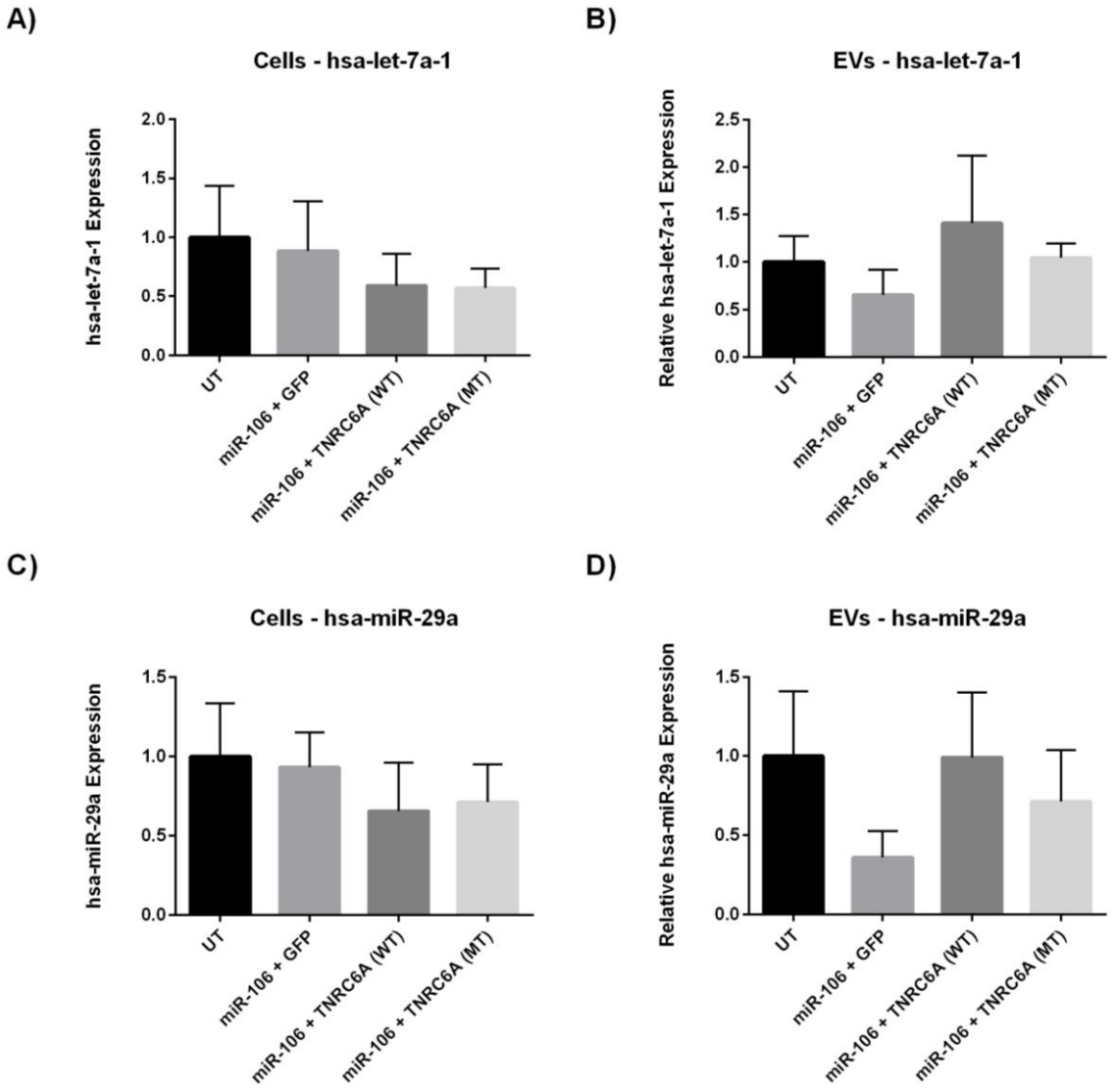

Figure 4.30 Specificity of miRNA Expression following Co-transfection of hsa-miR-106b and TNRC6A Expression Plasmids. HEK293T cells, plated in 15 cm cell culture dishes, were left untreated ("UT") or co-transfected with 17.5 µg each of hsa-miR-106b and either a control GFP plasmid ("GFP") or TNRC6A wild-type ("WT") or membrane-tagged ("MT") expression plasmids. hsa-let-7a-1 and hsa-miR-29a expression, normalised to total RNA input (cells) or cel-miR-39 spike-in (EVs), was determined by qPCR after 48 hours. **(A)** There was no significant effect upon cellular or **(B)** EV hsa-let-7a-1 expression levels or upon **(C)** cellular or **(D)** EV hsa-miR-29a expression levels. Values are mean ± SEM, n = 3, one-way ANOVA.

4.2.9 Co-expression with TNRC6A Increases Secretion of shRNA within Extracellular Vesicles

To determine whether increased TNRC6A expression would also enhance packaging and EV-mediated secretion of siRNA/shRNAs, HEK293T cells were co-transfected with TNRC6A WT or MT plasmids and APP shRNA (**Fig. 4.31**), APP siRNA (**Fig. 4.32**), BACE1 shRNA (**Fig. 4.33**) or BACE1 siRNA (**Fig. 4.34**). After 48 hours, expression of APP/BACE1 siRNA/shRNA and *TNRC6A* mRNA was assessed in cells, EVs and supernatant by qPCR.

APP shRNA expression was increased following co-transfection with both TNRC6A plasmids in cells, EVs and supernatant (**Fig. 4.31A-C**). *TNRC6A* mRNA expression was also increased in cells and EVs (**Fig. 4.31D-E**). This is in contrast to the results observed with APP siRNA. Co-transfection with TNRC6A plasmids did not increase APP siRNA expression above that observed following co-transfection with the control GFP plasmid in cells, EVs or supernatant (**Fig. 4.32A-C**). This was despite a significant increase in *TNRC6A* mRNA expression in both cells and EVs following TNRC6A (WT and MT) plasmid co-transfections (**Fig. 4.32D-E**).

BACE1 shRNA expression was increased in cells, EVs and supernatant following all co-transfections (**Fig. 4.33A-C**). However, co-transfection with TNRC6A only produced a greater fold increase in BACE1 shRNA expression compared to control GFP co-transfections with TNRC6A MT in EVs and with TNRC6A WT in supernatant. This was similar to the results following co-transfection of BACE1 siRNA with TNRC6A plasmids as BACE1 siRNA expression was not increased above that achieved

with the control GFP plasmid in cells, EVs or supernatant (**Fig. 4.34A-C**). *TNRC6A* mRNA expression was increased in cells and EVs following co-transfection with both BACE1 shRNA plasmids (**Fig. 4.33D-E**) and BACE1 siRNA (**Fig. 4.34D-E**). Interestingly however, the increase was relatively low compared to that achieved previously with APP siRNA/shRNA and did not reach significance, suggesting that co-transfection of BACE1 siRNA/shRNA with TNRC6A plasmids may result in relatively inefficient expression of TNRC6A.

Similar to the results obtained with AGO2, these findings suggested that co-expression with TNRC6A MT may increase packaging of shRNAs into EVs when expressed from shRNA expression plasmids but not when directly transfected as siRNAs. This indicates that processing through the endogenous miRNA pathway may be important for EV-loading. Co-expression with AGO2 rather than TNRC6A generally appeared to be more effective at enhancing shRNA/siRNA secretion within EVs. However, relatively high variability was observed within conditions following co-transfections with either AGO2 or TNRC6A and pri-miRNA or siRNA/shRNA expression plasmids.

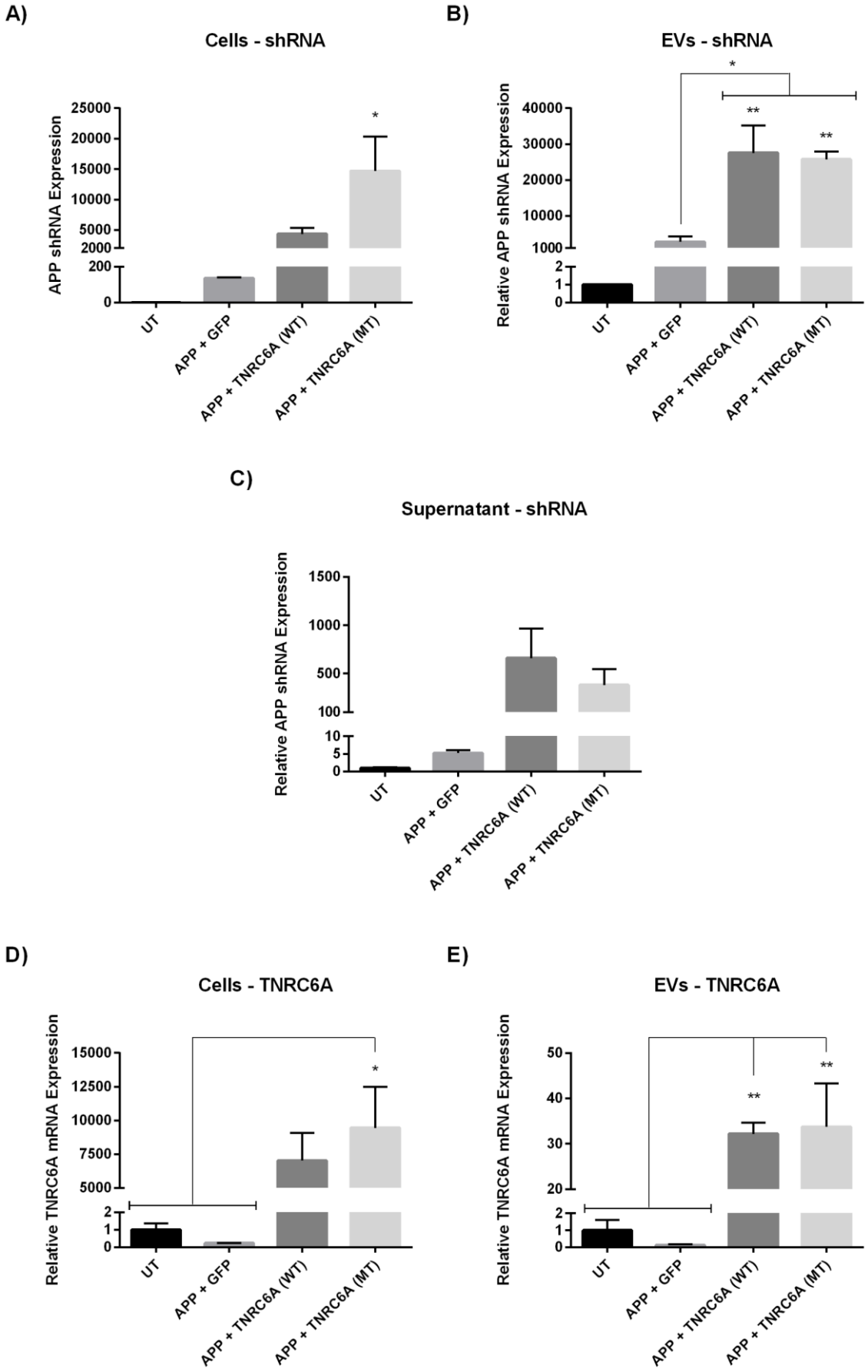
A)
Cells - shRNA
APP shRNA Expression
25000
20000
15000
10000
5000
2000
200
0
*
UT
APP + GFP
APP + TNRC6A (WT)
APP + TNRC6A (MT)
B)
EVs - shRNA
Relative APP shRNA Expression
40000
30000
20000
10000
1000
2
1
0
*
**
**
UT
APP + GFP
APP + TNRC6A (WT)
APP + TNRC6A (MT)
C)
Supernatant - shRNA
Relative APP shRNA Expression
1500
1000
500
100
10
5
0
UT
APP + GFP
APP + TNRC6A (WT)
APP + TNRC6A (MT)
D)
Cells - TNRC6A
Relative TNRC6A mRNA Expression
15000
12500
10000
7500
5000
2
1
0
*
UT
APP + GFP
APP + TNRC6A (WT)
APP + TNRC6A (MT)
E)
EVs - TNRC6A
Relative TNRC6A mRNA Expression
50
40
30
20
2
1
0
**
**
UT
APP + GFP
APP + TNRC6A (WT)
APP + TNRC6A (MT)

Figure 4.31 APP shRNA Expression following Co-transfection of APP shRNA and TNRC6A Expression Plasmids. HEK293T cells, plated in 15 cm cell culture dishes, were left untreated ("UT") or co-transfected with 17.5 µg each of APP shRNA and either a control GFP plasmid ("GFP") or TNRC6A wild-type ("WT") or membrane-tagged ("MT") expression plasmids. APP shRNA expression, normalised to total RNA input (cells) or cel-miR-39 spike-in (EVs and supernatant), was quantified by qPCR after 48 hours. *TNRC6A* expression, normalised to *β-Actin*, was also assessed. **(A-C)** APP shRNA expression was significantly increased following co-transfection with TNRC6A MT in **(A)** cells and **(B)** with TNRC6A (WT and MT) in EVs. **(C)** The increased expression observed in supernatant following TNRC6A (WT and MT) co-transfections was not significant. **(D-E)** *TNRC6A* mRNA expression was significantly increased in **(D)** cells following co-transfection with TNRC6A MT and **(E)** EVs following co-transfection with TNRC6A (WT and MT) plasmids. Values are mean ± SEM, n = 3, $^{**}p<0.01$, $^{*}p<0.05$, one-way ANOVA followed by Tukey's post-hoc test.

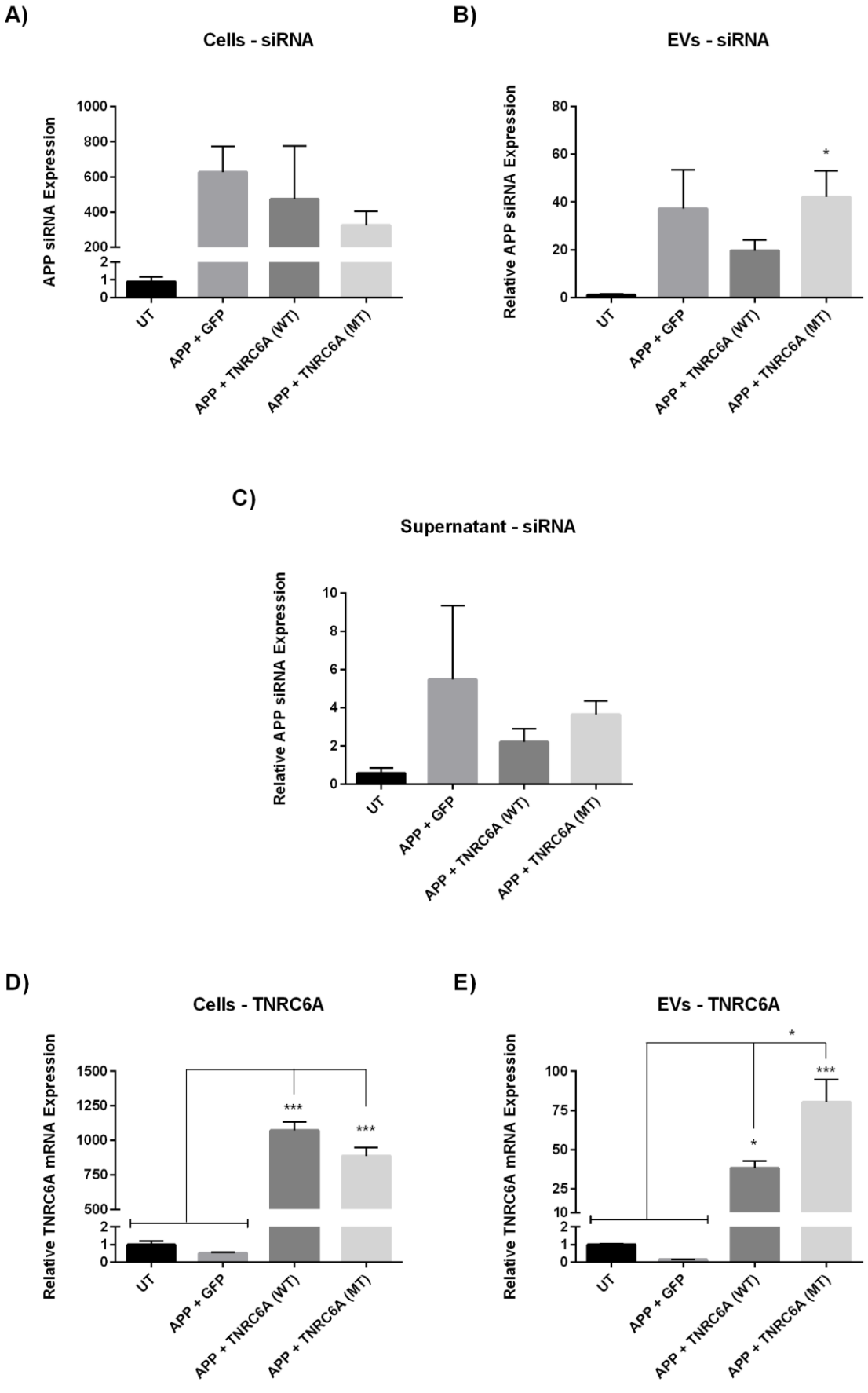
A)
Cells - siRNA
APP siRNA Expression
1000
800
600
400
200
2
1
0
UT
APP + GFP
APP + TNRC6A (WT)
APP + TNRC6A (MT)
B)
EVs - siRNA
Relative APP siRNA Expression
80
60
40
20
0
*
UT
APP + GFP
APP + TNRC6A (WT)
APP + TNRC6A (MT)
C)
Supernatant - siRNA
Relative APP siRNA Expression
10
8
6
4
2
0
UT
APP + GFP
APP + TNRC6A (WT)
APP + TNRC6A (MT)
D)
Cells - TNRC6A
Relative TNRC6A mRNA Expression
1500
1250
1000
750
500
2
1
0
***
***
UT
APP + GFP
APP + TNRC6A (WT)
APP + TNRC6A (MT)
E)
EVs - TNRC6A
Relative TNRC6A mRNA Expression
100
75
50
25
10
2
1
0
*
*
***
UT
APP + GFP
APP + TNRC6A (WT)
APP + TNRC6A (MT)

Figure 4.32 APP siRNA Expression following Co-transfection of APP siRNA and TNRC6A Expression Plasmids. HEK293T cells, plated in 15 cm cell culture dishes, were left untreated ("UT") or co-transfected with 100 nM APP siRNA and 17.5 µg each of a control GFP plasmid ("GFP") or TNRC6A wild-type ("WT") or membrane-tagged ("MT") expression plasmids. APP siRNA expression, normalised to total RNA input (cells) or cel-miR-39 spike-in (EVs and supernatant), was quantified by qPCR after 48 hours. *TNRC6A* mRNA expression, normalised to *β-Actin*, was also assessed. **(A)** APP siRNA expression was non-significantly increased in cells following all co-transfection conditions. **(B)** APP siRNA expression was significantly increased following co-transfection with TNRC6A MT in EVs. **(C)** No significant increase in APP siRNA expression was observed in supernatant. **(D-E)** *TNRC6A* expression was significantly increased in **(D)** cells and **(E)** EVs following co-transfection with both TNRC6A (WT and MT) plasmids. Values are mean ± SEM, n = 3, ***$p<0.001$, *$p<0.05$, one-way ANOVA followed by Tukey's post-hoc test.

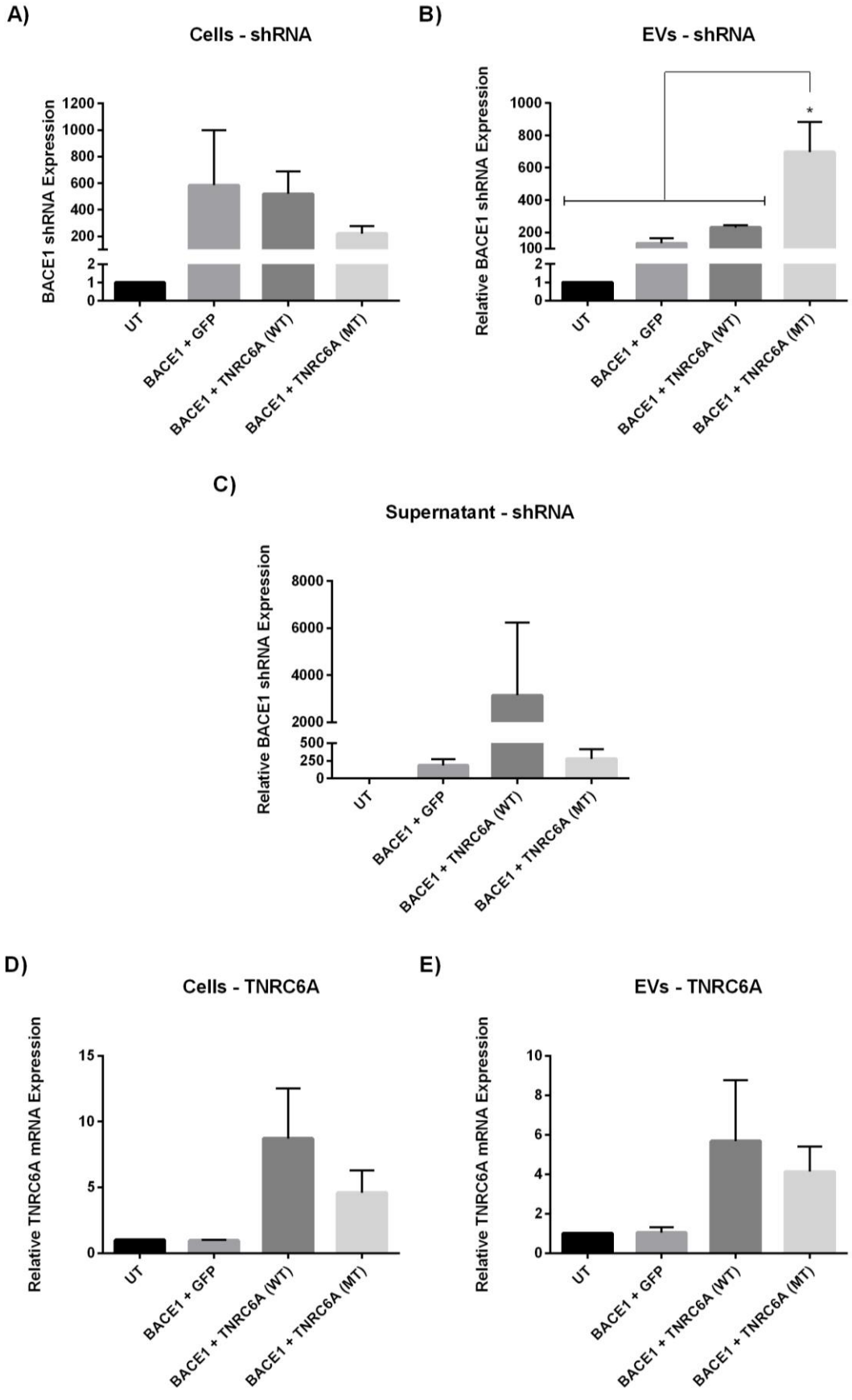
A)
Cells - shRNA
BACE1 shRNA Expression
1200
1000
800
600
400
200
2
1
0
UT
BACE1 + GFP
BACE1 + TNRC6A (WT)
BACE1 + TNRC6A (MT)
B)
EVs - shRNA
Relative BACE1 shRNA Expression
1000
800
600
400
200
100
2
1
0
*
UT
BACE1 + GFP
BACE1 + TNRC6A (WT)
BACE1 + TNRC6A (MT)
C)
Supernatant - shRNA
Relative BACE1 shRNA Expression
8000
6000
4000
2000
500
250
0
UT
BACE1 + GFP
BACE1 + TNRC6A (WT)
BACE1 + TNRC6A (MT)
D)
Cells - TNRC6A
Relative TNRC6A mRNA Expression
15
10
5
0
UT
BACE1 + GFP
BACE1 + TNRC6A (WT)
BACE1 + TNRC6A (MT)
E)
EVs - TNRC6A
Relative TNRC6A mRNA Expression
10
8
6
4
2
0
UT
BACE1 + GFP
BACE1 + TNRC6A (WT)
BACE1 + TNRC6A (MT)

Figure 4.33 BACE1 shRNA Expression following Co-transfection of BACE1 shRNA and TNRC6A Expression Plasmids. HEK293T cells, plated in 15 cm cell culture dishes, were left untreated ("UT") or co-transfected with 17.5 µg each of BACE1 shRNA and either a control GFP plasmid ("GFP") or TNRC6A wild-type ("WT") or membrane-tagged ("MT") expression plasmids. BACE1 shRNA expression, normalised to total RNA input (cells) or cel-miR-39 spike-in (EVs and supernatant), was quantified by qPCR after 48 hours. *TNRC6A* expression, normalised to *β-Actin*, was also assessed. **(A)** BACE1 shRNA expression in cells was not increased above that achieved following co-transfection with the control GFP plasmid. **(B)** BACE1 shRNA expression was significantly increased in EVs following co-transfection with the TNRC6A MT plasmid. **(C)** The increase in BACE1 shRNA expression in supernatant following co-transfection with the TNRC6A WT plasmid did not reach significance. **(D-E)** Levels of *TNRC6A* mRNA expression were increased, but not significantly, in **(D)** cells and **(E)** EVs following co-transfection with TNRC6A (WT and MT) plasmids. Values are mean ± SEM, n = 3, *$p<0.05$, one-way ANOVA followed by Tukey's post-hoc test.

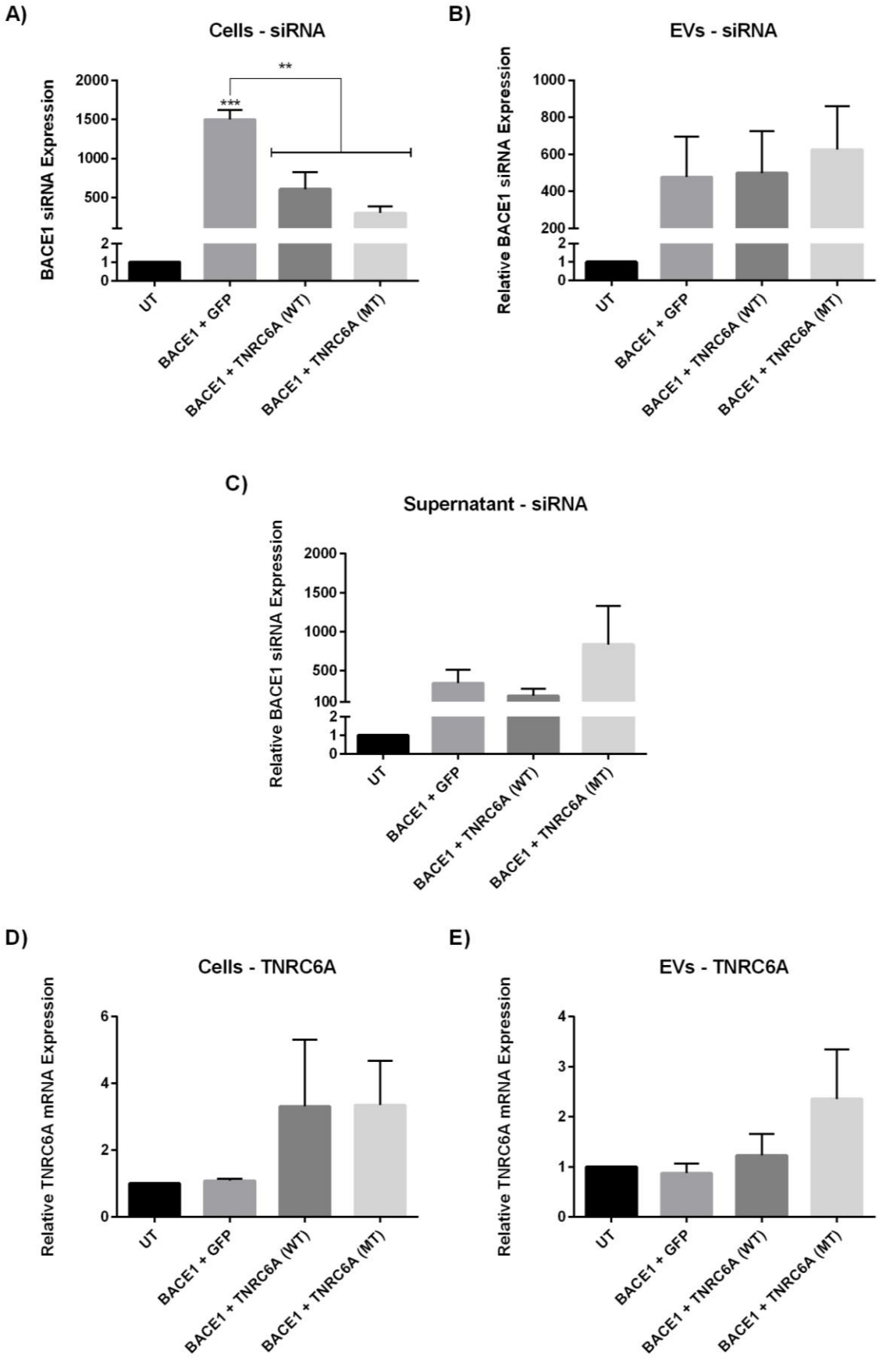
A)
Cells - siRNA
BACE1 siRNA Expression
**
***
2000
1500
1000
500
2
1
0
UT
BACE1 + GFP
BACE1 + TNRC6A (WT)
BACE1 + TNRC6A (MT)
B)
EVs - siRNA
Relative BACE1 siRNA Expression
1000
800
600
400
200
2
1
0
UT
BACE1 + GFP
BACE1 + TNRC6A (WT)
BACE1 + TNRC6A (MT)
C)
Supernatant - siRNA
Relative BACE1 siRNA Expression
2000
1500
1000
500
100
2
1
0
UT
BACE1 + GFP
BACE1 + TNRC6A (WT)
BACE1 + TNRC6A (MT)
D)
Cells - TNRC6A
Relative TNRC6A mRNA Expression
6
4
2
0
UT
BACE1 + GFP
BACE1 + TNRC6A (WT)
BACE1 + TNRC6A (MT)
E)
EVs - TNRC6A
Relative TNRC6A mRNA Expression
4
3
2
1
0
UT
BACE1 + GFP
BACE1 + TNRC6A (WT)
BACE1 + TNRC6A (MT)

Figure 4.34 BACE1 siRNA Expression following Co-transfection of BACE1 siRNA and TNRC6A Expression Plasmids. HEK293T cells, plated in 15 cm cell culture dishes, were left untreated ("UT") or co-transfected with 100 nM BACE1 siRNA and 17.5 µg each of a control GFP plasmid ("GFP") or TNRC6A wild-type ("WT") or membrane-tagged ("MT") expression plasmids. BACE1 siRNA expression, normalised to total RNA input (cells) or cel-miR-39 spike-in (EVs and supernatant), was quantified by qPCR after 48 hours. *TNRC6A* mRNA expression, normalised to *β-Actin*, was also assessed. **(A-C)** BACE1 siRNA expression was not increased above that achieved following co-transfection with the control GFP plasmid in **(A)** cells, **(B)** EVs or **(C)** supernatant. **(D-E)** *TNRC6A* expression was increased, but not significantly, in **(D)** cells and **(E)** EVs following co-transfection of BACE1 siRNA and TNRC6A (WT or MT) plasmids. Values are mean ± SEM, n = 3, ***p<0.001, **p<0.01, one-way ANOVA followed by Tukey's post-hoc test.

4.2.10 Efficiency of Transfection and Extracellular Vesicle Isolation Contributes to Variability Following Co-transfections

Co-transfection of RNA-binding proteins with exogenous shRNA and pri-miRNA expression plasmids tended to increase EV secretion of RNAi effectors. However, high variability was often apparent which precluded some observed increases in expression from reaching significance. The source of this variability was therefore investigated.

As high variability was observed in both cellular and EV samples, it was hypothesised that variability may result from inconsistent transfection efficiency and/or the efficiency of EV isolations between different replicates. Transfections were performed in 15 cm cell culture dishes using Polyethylenimine (PEI) as the transfection reagent at a previously optimised ratio of 4 µg PEI: 1 µg RNA/DNA. Therefore, it was hypothesised that variability may result either from the use of PEI or the large-scale nature of transfections. Indeed, it had been noted that cells were not always evenly distributed across the 15 cm cell culture dish. To explore this further, co-transfection of AGO2 and hsa-miR-29a pri-miRNA expression plasmids was repeated on a smaller scale in 12-well cell culture plates using either PEI or Lipofectamine 2000 as the transfection reagent. Expression of the mature hsa-miR-29a transcript and *AGO2* mRNA was assessed in cells after 48 hours by qPCR (**Fig. 4.35**).

Mature hsa-miR-29a and *AGO2* mRNA expression were both significantly increased following PEI-mediated co-transfections (**Fig. 4.35A,C**). In contrast, only *AGO2* mRNA expression was significantly increased following Lipofectamine 2000-mediated transfections (**Fig. 4.35B,D**). Interestingly, PEI-mediated transfections appeared more

effective in terms of increased hsa-miR-29a and *AGO2* expression while the extent of variability appeared lower than that observed in the previous experiments. This therefore suggested that the use of PEI was not a primary cause of variability but instead suggested that inconsistent co-transfection efficiency arising from larger-scale transfections might be one factor contributing towards variability.

Inconsistent EV isolation efficiency might also increase variability. This may relate either to the differential loss of material between replicates during isolation or to contamination by non-vesicular RNA within the supernatant. If so, an additional wash might help to remove contaminating RNA from EV preparations. To assess this further, HEK293T cells were left untreated or co-transfected with hsa-miR-29a pri-miRNA expression plasmids and either a control GFP plasmid or AGO2 plasmids. EV samples were isolated after 48 hours before EV particle count and RNA quantity were assessed by NTA and the Quant-iT RiboGreen RNA Assay Kit, respectively (**Fig. 4.36**). To assess the extent of material lost at each step, a "filtrate" sample was removed after purification through 0.2 µm filters prior to the first ultracentrifugation isolation. After ultracentrifugation, the pellet was resuspended and divided equally between unwashed and washed samples. For washed samples, the pellet was diluted in PBS and re-isolated by a further ultracentrifugation step.

EVs were first derived from six separate replicates of untreated cells and total particle count assessed by NTA for each filtrate, unwashed and washed sample (**Fig. 4.36A-C**). This revealed variability in the total particle count between the six replicates both in the initial filtrate sample and in that retained following each ultracentrifugation step (**Fig. 4.36A-C**). Consistent with previous data within the lab, a significant reduction in

retained material was observed following each isolation step. Thus, 36.5% of the initial starting number of particles was retained after the first ultracentrifugation step and only 4.2% of the initial starting material was retained following a further wash (**Fig. 4.36C**).

It was previously observed that transfection of AGO2 and TNRC6A plasmids resulted in a significant reduction in secreted particles when compared to untreated cells (**Fig. 4.15A**). It was therefore important to assess whether a difference in the original starting quantity of EVs would affect the variability and percentage of retained particles. Consistent with the previous results, the obtained particle count was reduced following co-transfections of hsa-miR-29a with either control GFP or AGO2 (WT and MT) plasmids when compared to untreated cells (**Fig. 4.36D-E**). Variability was again observed between three separate replicates both in the initial filtrate samples and following each ultracentrifugation step (**Fig. 4.36D-E**). A higher starting yield in untreated samples did appear to improve the percentage of recovery following the first ultracentrifugation step but did not improve yields following an additional wash and ultracentrifugation step (**Fig. 4.36D-E**).

The RNA concentration within each unwashed or washed EV sample was assessed to determine whether variability in particle count was also reflected in the EV RNA yield (**Fig. 4.36F-H**). As for particle count, variability in RNA concentration was observed between each of the three replicates within each condition while untreated samples provided the highest yield of RNA (**Fig. 4.36F**). RNA concentration was also compared against total particle count for unwashed and washed samples and revealed a positive correlation between RNA quantity and particle count for both unwashed ($r = 0.94$, $p < 0.001$) and washed ($r = 0.71$, $p < 0.01$) samples (**Fig. 4.36G-H**).

Together, these results suggest that co-transfection efficiency combined with inherent variability in the initial starting material and variable recovery following EV isolation may contribute towards the variability observed in the previous experiments. Including an additional wash step may be desirable to reduce miRNA quantification bias by removing contaminating non-vesicular miRNAs. However, these results suggest that this might also increase variability and may require a larger quantity of starting material than utilised in the current study.

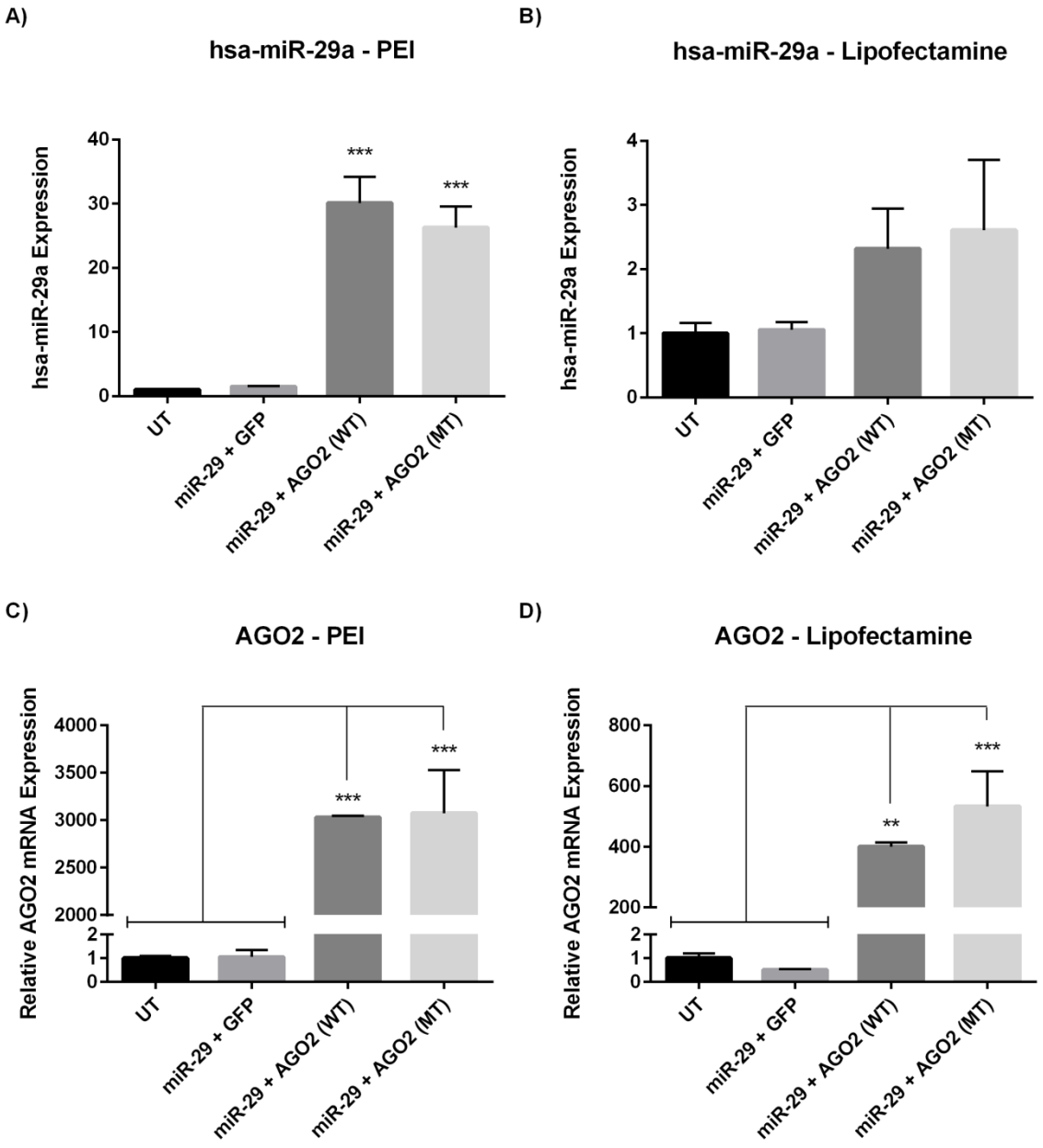

Figure 4.35 Comparison of Transfection Efficiency after PEI and Lipofectamine-mediated Transfections. HEK293T cells were left untreated ("UT") or co-transfected with 800 ng each of hsa-miR-29a and either a control GFP plasmid ("GFP") or AGO2 wild-type ("WT") or membrane-tagged ("MT") expression plasmids in 12-well cell culture plates using either PEI or Lipofectamine 2000 for the transfection reagent. Cellular RNA was harvested after 48 hours and hsa-miR-29a expression, normalised to total RNA input, and *AGO2* expression, normalised to *β-Actin*, determined by qPCR. **(A)** hsa-miR-29a expression was significantly increased in cells following PEI-mediated co-transfections. **(B)** The increase in hsa-miR-29a expression following Lipofectamine-mediated co-transfections was not significant. **(C-D)** *AGO2* mRNA expression was increased in cells following both **(C)** PEI-mediated and **(D)** Lipofectamine-mediated co-transfections of hsa-miR-29a and AGO2 plasmids. Values are mean ± SEM, n = 3, ***p<0.001, **p<0.01, one-way ANOVA followed by Tukey's post-hoc test.

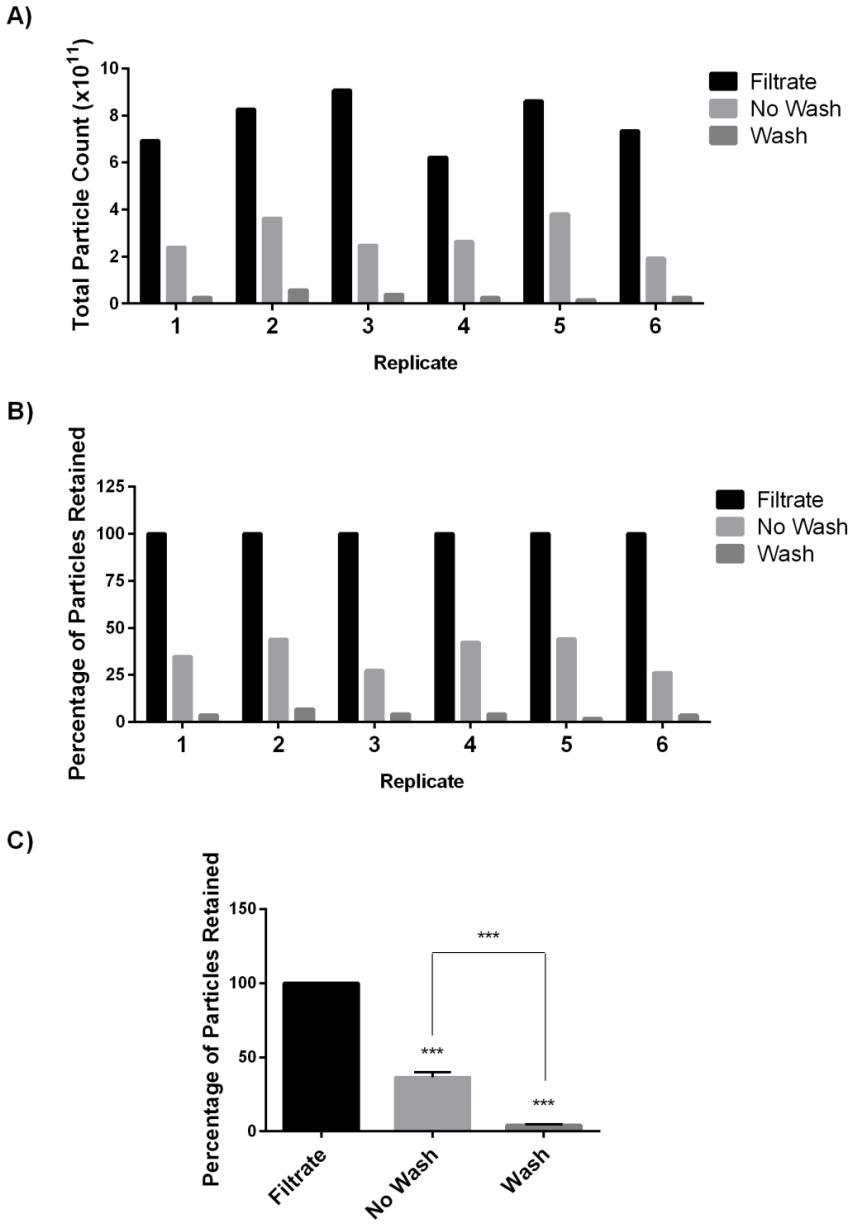

Figure 4.36 Quantification of Particle Count and RNA Yield following Extracellular Vesicle Isolation. HEK293T cells, plated in 15 cm cell culture dishes, were left untreated ("UT") or transfected with 17.5 µg each of hsa-miR-29a and either a control GFP plasmid ("GFP") or AGO2 wild-type ("WT") or membrane-tagged ("MT") plasmids. EV samples were isolated after 48 hours before particle count and RNA concentration were assessed. A "filtrate" sample was removed prior to ultracentrifugation and isolated EV samples were designated as either no wash or washed (PBS wash followed by repeat isolation). **(A-C)** EVs derived from UT cells (6 replicates) were assessed by nanoparticle tracking analysis (NTA) to determine **(A)** total particle count, **(B)** percentage of particles retained after isolation per replicate and **(C)** mean percentage of particles retained per isolation (n = 6). This showed variability in the starting material and particles retained following each isolation step. Each wash significantly reduced the quantity of retained material. Values are mean ± SEM, ***p<0.001, one-way ANOVA followed by Tukey's post-hoc test. (Figure continued overleaf).

D)

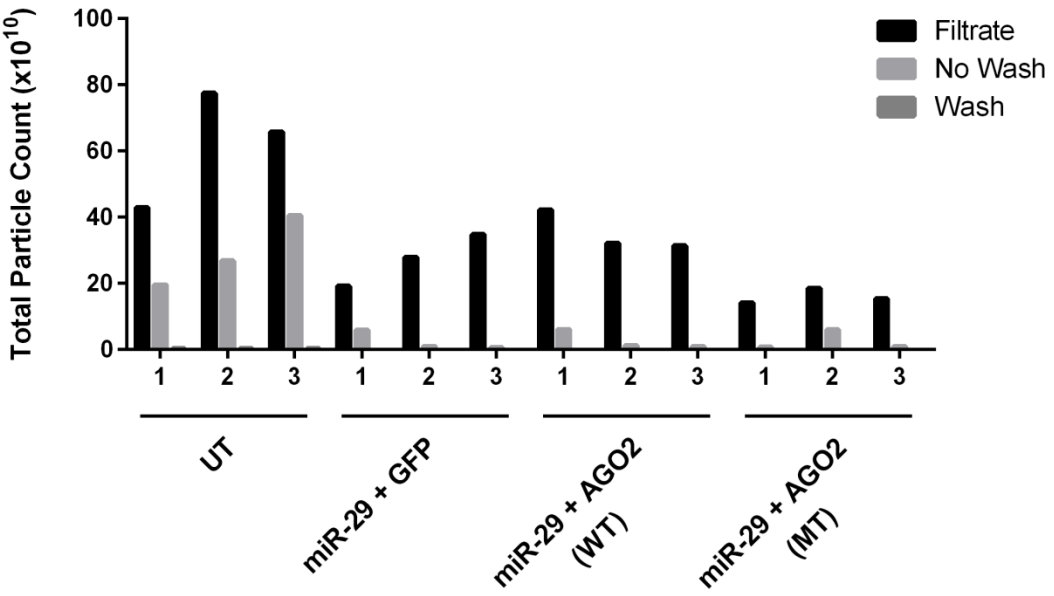
Total Particle Count (x10^10)
100
80
60
40
20
0
Filtrate
No Wash
Wash
1 2 3 1 2 3 1 2 3 1 2 3
UT
miR-29 + GFP
miR-29 + AGO2 (WT)
miR-29 + AGO2 (MT)

E)

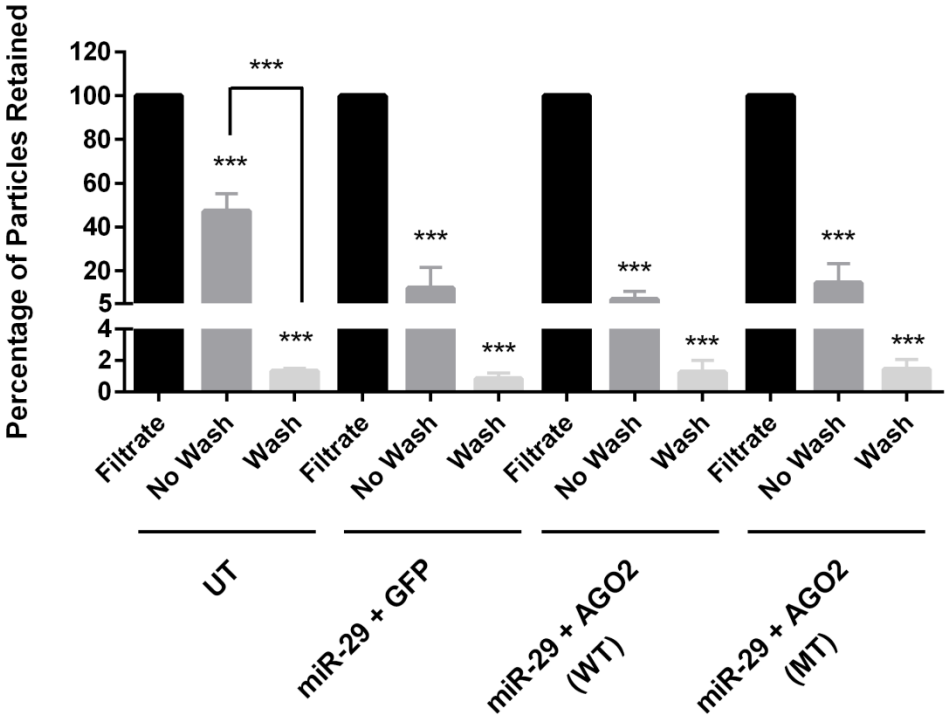
Percentage of Particles Retained
120
100
80
60
40
20
5
4
2
0
***
Filtrate
No Wash
Wash
UT
miR-29 + GFP
miR-29 + AGO2 (WT)
miR-29 + AGO2 (MT)

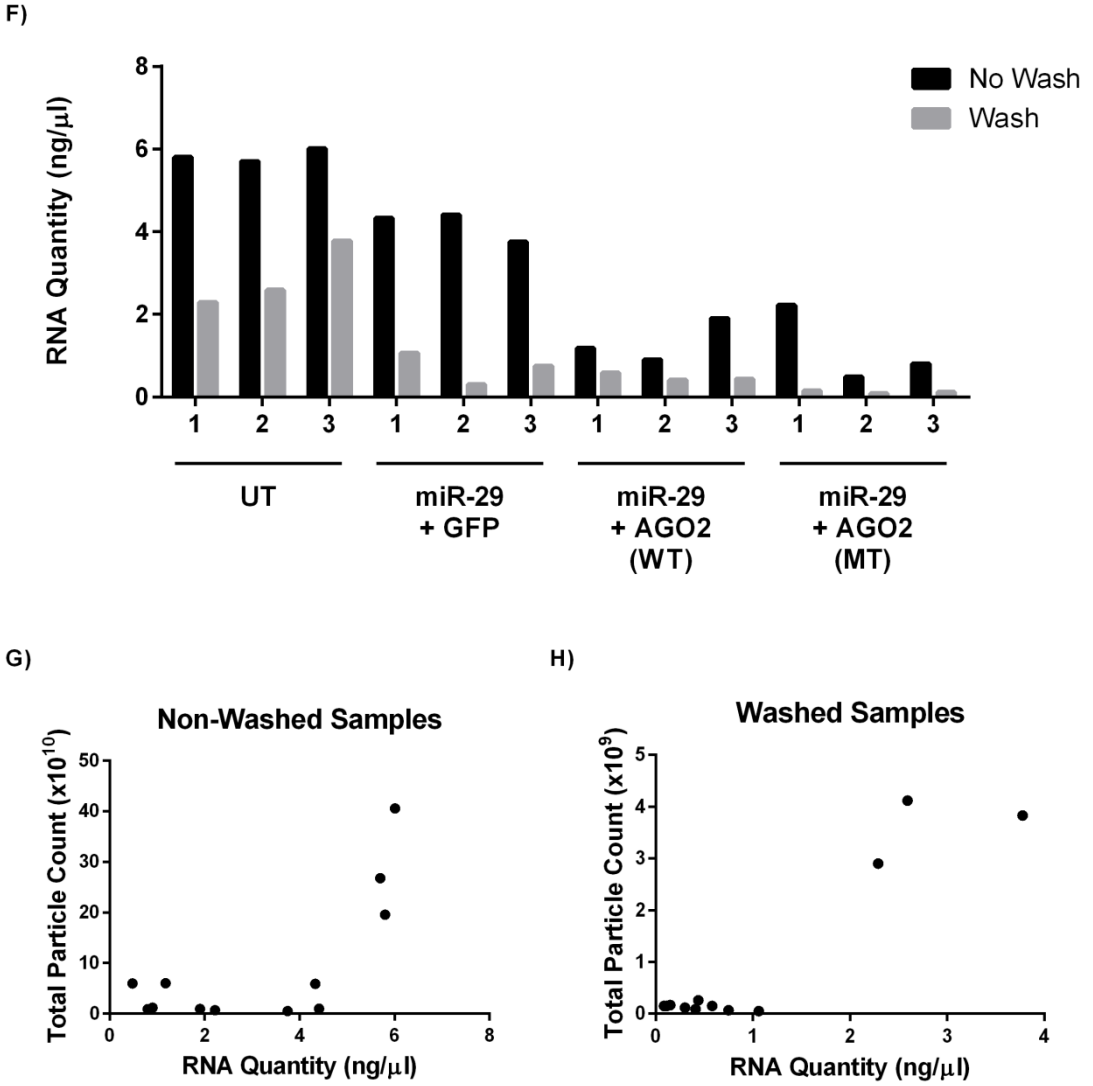

Figure 4.36 Quantification of Particle Count and RNA Yield following Extracellular Vesicle Isolation – Continued. (D-H) EVs derived from UT or transfected cells (n = 3) were assessed by NTA and for RNA yield. NTA revealed variability in **(D)** the total particle count and **(E)** the mean percentage of particles retained after each isolation/wash. **(F)** Variability in RNA concentration within EV samples was observed between replicates for both UT and transfected cells. **(G-H)** A positive relationship between particle count and RNA quantity was observed for both **(G)** non-washed (positive correlation; $r = 0.94$, $p < 0.001$) and **(H)** washed samples (positive correlation; $r = 0.71$, $p < 0.01$) (Pearson product-moment correlation test). Values are mean ± SEM, ***$p<0.001$, one-way ANOVA followed by Tukey's post-hoc test.

4.2.11 Co-expression with RNA-binding Proteins did not Enhance Silencing of Luciferase Activity Following Co-culture with hsa-miR-106b Source Cells

Despite the issue of variability discussed above, transfection of exogenous pri-miRNA expression plasmids alone or in combination with RNA-binding proteins appeared to result in their packaging and secretion within EVs. It was therefore important to determine whether exogenous miRNAs secreted within EVs produced functional effects within recipient cells.

Expression of hsa-miR-106b was selected for this purpose. Although the relative increase in exogenous hsa-miR-29a expression within EVs was greater than that of hsa-miR-106b following transfection of the respective pri-miRNA expression plasmids, hsa-miR-106b more strongly regulated its dual-luciferase target reporter (**Fig. 4.12**). hsa-miR-106b was therefore chosen to maximise detection sensitivity for functional activity within recipient cells.

The functional effects of exogenous hsa-miR-106b expression were first assessed by a transwell co-culture approach utilising 24-well cell culture plate inserts comprising 0.4 µm diameter pores. This system permits the movement of material less than 0.4 µm between source cells plated in the lower 24-well plate layer and recipient cells plated in the upper insert and hence was used to assess transfer of hsa-miR-106b between source and recipient cells. HEK293T source cells were transfected with the hsa-miR-106b pri-miRNA expression plasmid while recipient HEK293T cells were transfected with either the hsa-miR-106b dual-luciferase target reporter alone or, as a positive control, directly

with 50 nM hsa-miR-106b miRNA mimic. Recipient and source cells were combined in co-culture 24 hours after transfection and incubated together for a further 48 hours before relative luciferase activity was assessed (**Fig. 4.37**). As the hsa-miR-106b plasmid expresses GFP, source cells were first confirmed to express the hsa-miR-106b plasmid by fluorescence microscopy (**Fig. 4.37A**). Promisingly, luciferase activity of the hsa-miR-106b target reporter was significantly reduced (**Fig. 4.37B**) while expression of the mature transcript of hsa-miR-106b was significantly increased (**Fig. 4.37C**) following co-culture with source cells transfected with the hsa-miR-106b pri-miRNA expression plasmid. There was no significant effect upon recipient cell expression of the primary transcript of hsa-miR-106b or *APP* mRNA (**Fig. 4.37D**).

Whether this functional effect could be enhanced by co-expression with RNA-binding proteins was then addressed. HEK293T source cells were left untreated or co-transfected with either a negative control miRNA expression plasmid and control GFP plasmid or the hsa-miR-106b pri-miRNA expression plasmid and either control GFP, AGO2 (WT or MT) or TNRC6A (WT or MT) expression plasmids. Recipient cells were transfected with either a negative control luciferase reporter, the hsa-miR-106b dual-luciferase reporter alone, or, as a positive control, with 50 nM hsa-miR-106b miRNA mimic. Recipient and source cells were combined in co-culture 24 hours after transfection and incubated together for a further 48 hours before relative luciferase activity was assessed (**Fig. 4.38**).

As before, hsa-miR-106b plasmid expression was confirmed in source cells by fluorescence microscopy (**Fig. 4.38A**). Luciferase activity appeared reduced to a similar level following co-culture with source cells expressing either hsa-miR-106b and control

GFP or hsa-miR-106b and AGO2 WT although this did not reach significance (**Fig. 4.38B**). There was no effect following co-expression of hsa-miR-106b and TNRC6A in source cells (**Fig. 4.38C**). Recipient cell reporter expression was only significantly reduced following direct treatment with the hsa-miR-106b mimic (**Fig. 4.38D**). Similarly, expression of the mature transcript of hsa-miR-106b was only significantly increased in recipient cells treated directly with the hsa-miR-106b mimic (**Fig. 4.38E-G**). There was no significant effect upon expression of the primary transcript of hsa-miR-106b or *APP* mRNA following any condition (**Fig. 4.38H**).

While 48 hours of co-incubation resulted in regulation of the luciferase reporter within recipient cells following expression of hsa-miR-106b alone in source cells, it was hypothesised that association with RNA-binding proteins may influence silencing dynamics. Therefore, the experiment was repeated but source and recipient cells were co-cultured for either 24 or 72 hours. However, only direct treatment with the positive control hsa-miR-106b mimic significantly silenced recipient cell reporter activity following 24 or 72 hours co-incubation, suggesting 48 hours co-culture may be optimal (**Fig. 4.38I-K**).

A)

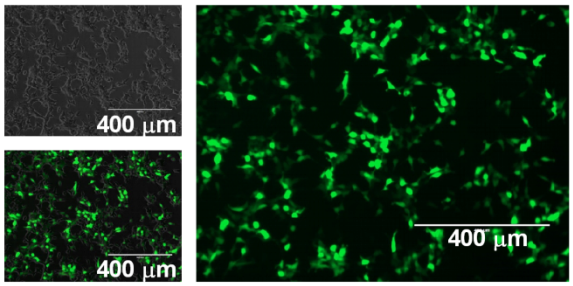
400 µm
400 µm
400 µm

B)

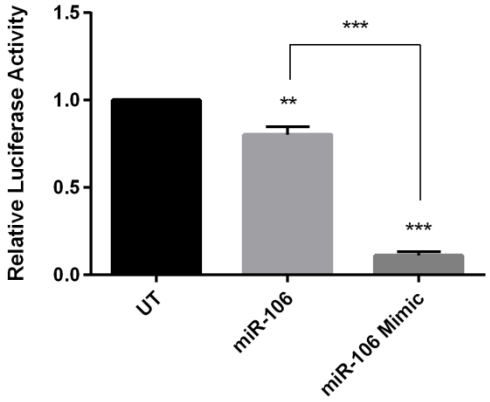
Relative Luciferase Activity
1.5
1.0
0.5
0.0
***
**
***
UT
miR-106
miR-106 Mimic

C)

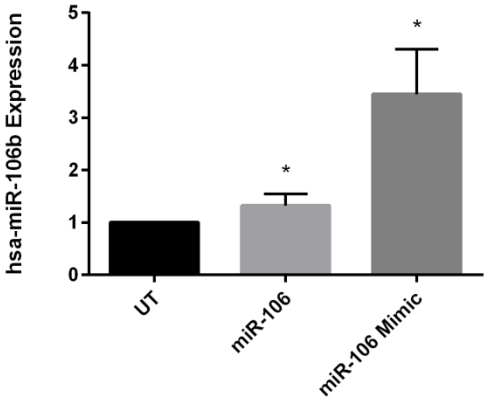
hsa-miR-106b Expression
5
4
3
2
1
0
*
*
UT
miR-106
miR-106 Mimic

D)

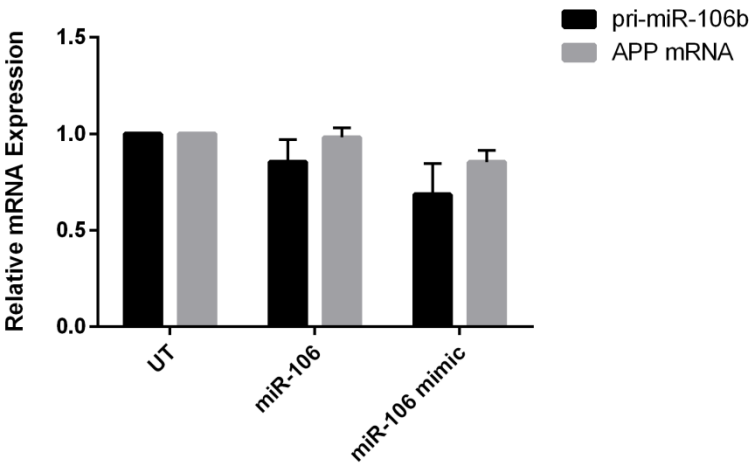
pri-miR-106b
APP mRNA
Relative mRNA Expression
1.5
1.0
0.5
0.0
UT
miR-106
miR-106 mimic

Figure 4.37 Functional Effects of hsa-miR-106b in Co-culture. HEK293T source cells, plated in 24-well cell culture plates, were left untreated ("UT") or transfected with 500 ng hsa-miR-106b pri-miRNA expression plasmid ("miR-106"). Recipient HEK293T cells, plated in 6-well cell culture plates, were transfected with 2 µg of hsa-miR-106b dual-luciferase target reporter alone or, as a positive control, with 50 nM hsa-miR-106b miRNA mimic ("miR-106 mimic"). Recipient and source cells were combined in co-culture 24 hours after transfection and incubated together for a further 48 hours before relative luciferase activity (Firefly luciferase normalised to Renilla luciferase) was assessed. Source cell expression of mature hsa-miR-106b (normalised to RNA input volume) and the primary transcript of hsa-miR-106b and *APP* mRNA, normalised to *β-Actin*, was assessed by qPCR. **(A)** Source cells showed high transfection efficiency of the hsa-miR-106b expression plasmid. **(B)** Recipient cell luciferase activity was significantly reduced following co-culture with hsa-miR-106b source cells and direct treatment with the hsa-miR-106b miRNA mimic. **(C)** Recipient cell expression of mature hsa-miR-106b was significantly increased following co-culture with hsa-miR-106b source cells and direct treatment with the hsa-miR-106b miRNA mimic. **(D)** There was no significant effect upon expression of the primary transcript of hsa-miR-106b or *APP* mRNA. Values are mean ± SEM, n = 3, ***$p<0.001$, **$p<0.01$, *$p<0.05$, one-way ANOVA followed by Tukey's post-hoc test.

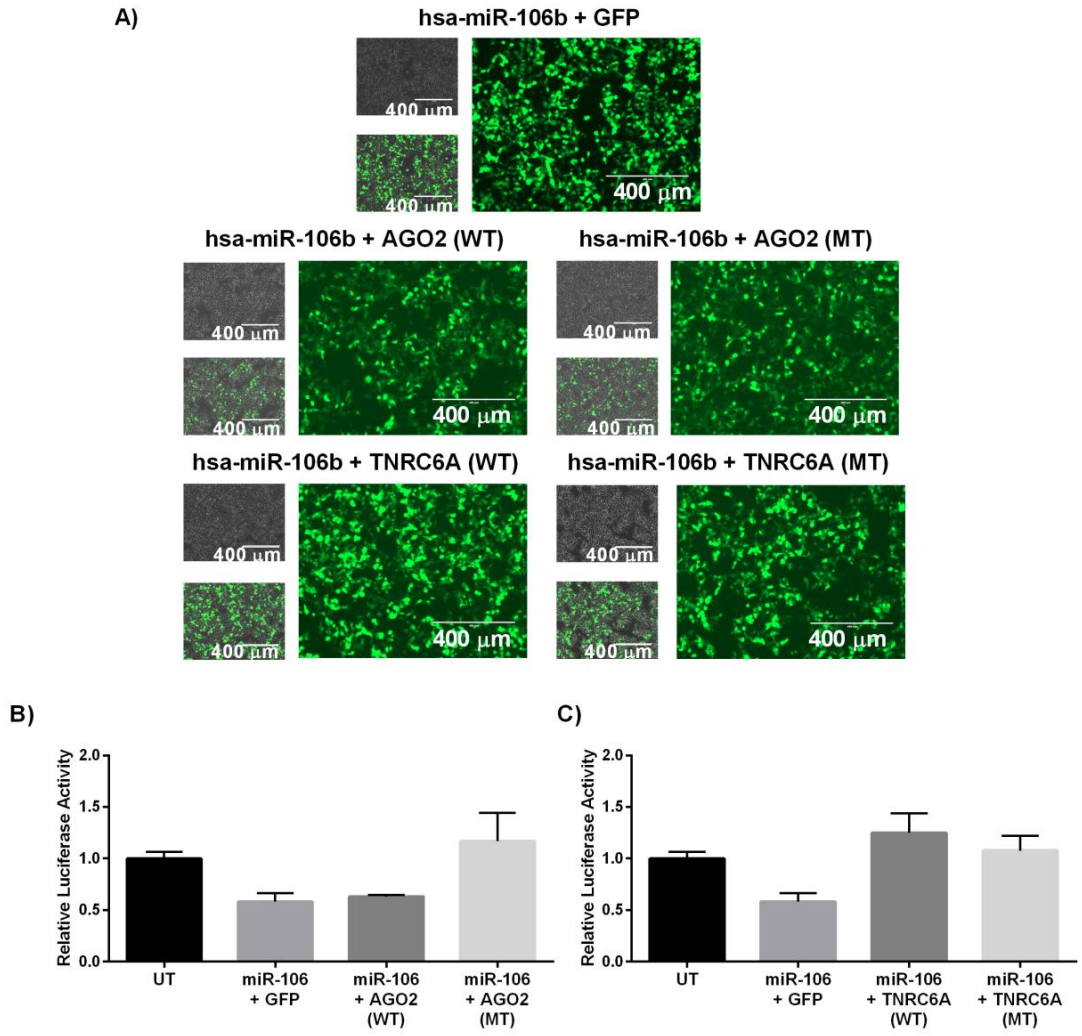

Figure 4.38 Functional Effects of hsa-miR-106b and RNA-binding Proteins in Co-culture. HEK293T source cells, plated in 24-well cell culture plates, were left untreated ("UT") or co-transfected with 500 ng each of the hsa-miR-106b miRNA plasmid or a negative control miRNA expression plasmid ("NC") and either a control GFP plasmid ("GFP") or wild-type ("WT") or membrane-tagged ("MT") forms of AGO2 and TNRC6A plasmids. Recipient HEK293T cells, plated in 6-well cell culture plates, were transfected with 2 µg of a negative control dual-luciferase reporter ("NC reporter") or the hsa-miR-106b dual-luciferase target reporter alone or, as a positive control, with 50 nM hsa-miR-106b miRNA mimic ("miR-106 mimic"). Recipient and source cells were combined in co-culture 24 hours after transfection and incubated together for a further 24, 48 or 72 hours before relative luciferase activity in source cells was assessed. Recipient cell expression of mature hsa-miR-106b (normalised to RNA input volume) and the primary transcript of hsa-miR-106b and *APP*, normalised to *β-Actin*, was assessed by qPCR. **(A)** Source cells showed high transfection efficiency of the respective plasmids. **(B-C)** Source and recipient cells were co-cultured for 48 hours. **(B)** Luciferase activity was reduced, but not significantly, following co-culture with hsa-miR-106b + GFP and hsa-miR-106b + AGO2 WT source cells. **(C)** There was no effect following co-culture with hsa-miR-106b + TNRC6A (WT or MT) source cells. Values are mean ± SEM, n = 3, one-way ANOVA. (Figure continued on opposite page).

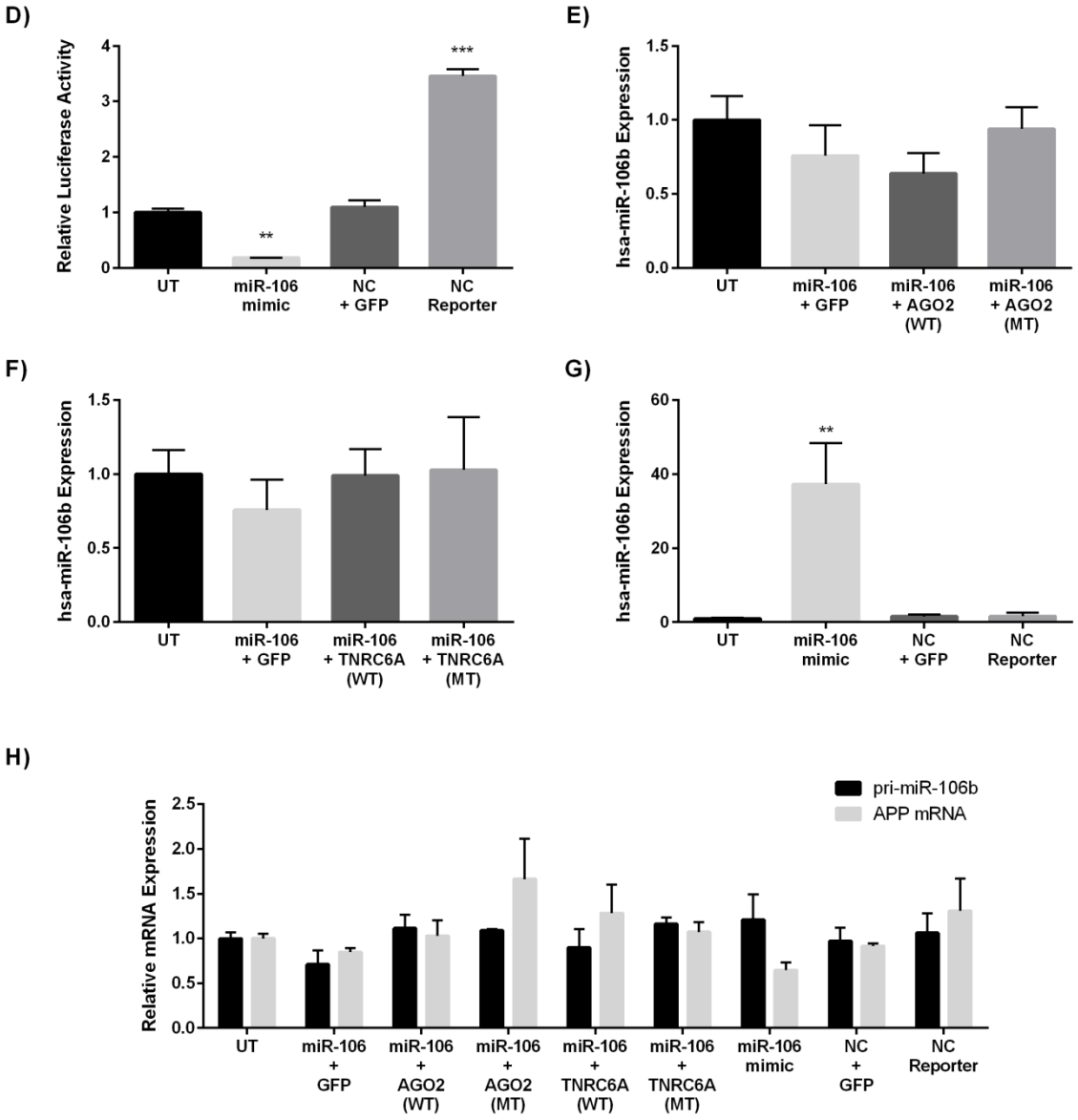

Figure 4.38 Functional Effects of hsa-miR-106b and RNA-Binding Proteins in Co-culture – Continued. (D-H) Source and recipient cells were co-cultured for 48 hours. **(D)** Luciferase activity was significantly silenced by direct treatment of recipient cells with the positive control hsa-miR-106b miRNA mimic. **(E-F)** There was no significant effect upon recipient cell expression of the mature transcript of hsa-miR-106b following co-culture with source cells co-transfected with hsa-miR-106b and **(E)** AGO2 plasmids or **(F)** TNRC6A plasmids. **(G)** Expression of the mature transcript of hsa-miR-106b was significantly increased in recipient cells treated directly with the hsa-miR-106b miRNA mimic. **(H)** There was no significant effect upon expression of either the primary transcript of hsa-miR-106b or *APP* mRNA. Values are mean ± SEM, n = 3, ***p<0.001, **p<0.01, one-way ANOVA followed by Tukey's post-hoc test. (Figure continued overleaf).

I)

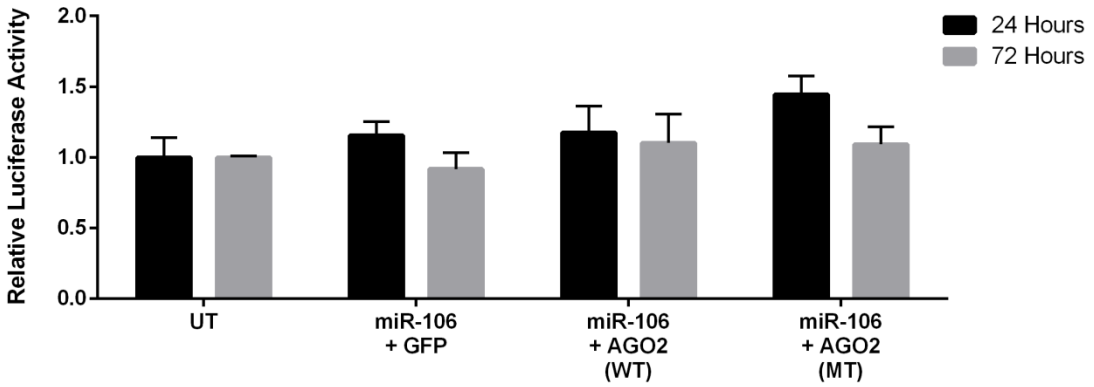
Relative Luciferase Activity
2.0
1.5
1.0
0.5
0.0
24 Hours
72 Hours
UT
miR-106 + GFP
miR-106 + AGO2 (WT)
miR-106 + AGO2 (MT)

J)

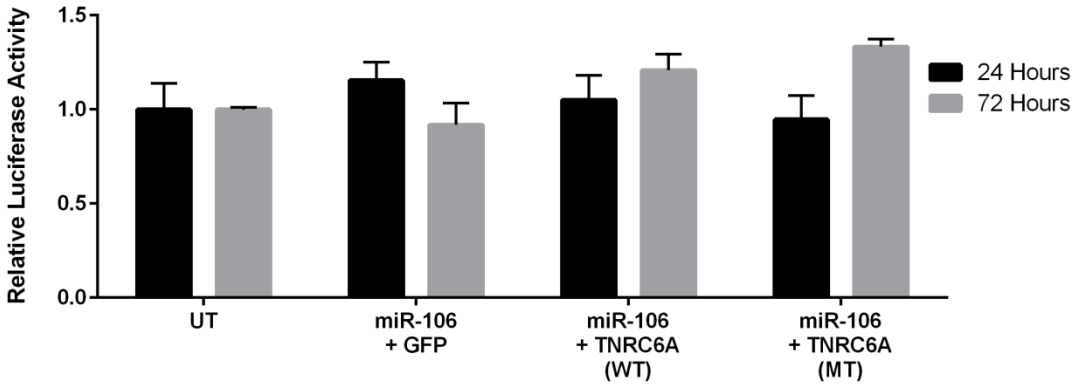
Relative Luciferase Activity
1.5
1.0
0.5
0.0
24 Hours
72 Hours
UT
miR-106 + GFP
miR-106 + TNRC6A (WT)
miR-106 + TNRC6A (MT)

K)

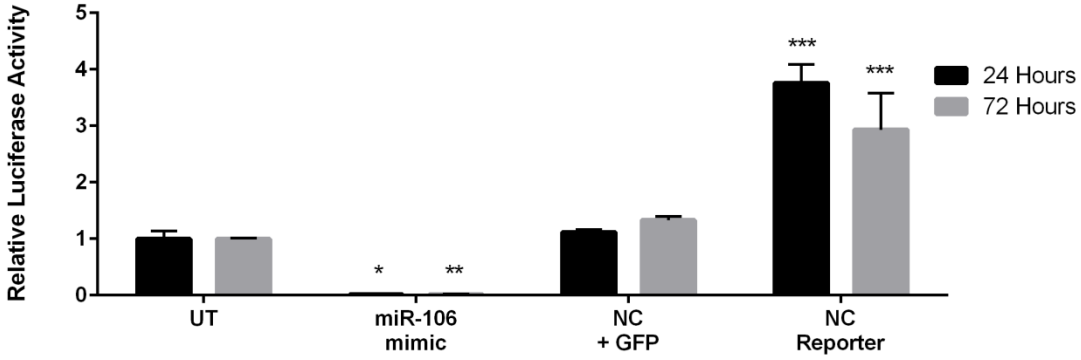
Relative Luciferase Activity
5
4
3
2
1
0
***
***
*
**
24 Hours
72 Hours
UT
miR-106 mimic
NC + GFP
NC Reporter

Figure 4.38 Functional Effects of hsa-miR-106b and RNA-binding Proteins in Co-culture – Continued. (I-K) Source and recipient cells were co-cultured for 24 or 72 hours. There was no effect upon luciferase reporter activity in recipient cells following co-culture with **(I)** hsa-miR-106b + AGO2 (WT or MT) or **(J)** hsa-miR-106b + TNRC6A (WT or MT) source cells. **(K)** Luciferase activity was significantly silenced by direct treatment of recipient cells with the positive control hsa-miR-106b miRNA mimic. Values are mean ± SEM, n = 3, ***p<0.001, **p<0.01, *p<0.05, one-way ANOVA followed by Tukey's post-hoc test.

4.2.12 Luciferase Activity Was Reduced Following Treatment with Isolated hsa-miR-106b Extracellular Vesicles and Concentrated Supernatant

The results above indicate that co-expression of RNA-binding proteins with hsa-miR-106b in source cells did not enhance regulation of the luciferase reporter in recipient cells above that following co-transfection with the control GFP plasmid. As observed previously, transfection of AGO2 and TNRC6A plasmids alone or in combination with a pri-miRNA expression plasmid reduced the yield of EVs compared to untreated cells. It was therefore hypothesised that the quantity of exogenous hsa-miR-106b carried by the number of vesicles secreted from cells within a 24-well cell culture plate may have been too low to influence luciferase reporter activity within recipient cells. To investigate this, EVs were isolated from 15 cm cell culture dishes, 48 hours after transfection, and applied directly to recipient cells within 96-well cell culture plates (**Fig. 4.39**). The equivalent of the total yield of EVs obtained from 1 x 15 cm dish was applied per well of a 96-well plate. As a control, supernatant remaining after EV isolation was concentrated and applied directly to recipient cells within 96-well plates.

Plasmid expression was confirmed by fluorescence microscopy (**Fig. 4.39A**). Promisingly, luciferase reporter activity was significantly reduced in recipient cells following treatment with both isolated EVs and concentrated supernatant obtained from source cells co-transfected with hsa-miR-106b and either the control GFP plasmid or AGO2 (WT or MT) plasmids (**Fig. 4.39B-C**). Unexpectedly however, mature hsa-miR-106b expression was reduced, although not significantly, in recipient cells treated with EVs isolated from source cells co-transfected with hsa-miR-106b and either the control GFP plasmid or AGO2 (WT or MT) plasmids (**Fig. 4.39D**). In contrast, mature hsa-

miR-106b expression was unchanged in recipient cells treated with concentrated supernatant across all conditions (**Fig. 4.39E**). There was no significant effect upon primary hsa-miR-106b or *AGO2* mRNA expression following treatment with either EVs or concentrated supernatant (**Fig. 4.39F-G**).

As the results concerning mature hsa-miR-106b expression were surprising given the level of reporter regulation, expression of hsa-miR-106b was reanalysed relative to *U6* expression. This had no effect upon the pattern of reduced hsa-miR-106b expression observed (data not shown). It should be noted that variability was relatively high in recipient cells treated with EVs and concentrated supernatant derived from untreated cells. As mentioned previously, hsa-miR-106b endogenous levels are comparatively high. It is therefore possible that variability in expression of endogenous hsa-miR-106b within untreated cells may have contributed towards the apparent reduction in hsa-miR-106b expression in recipient cells following experimental treatments. Furthermore, the miRNA network is under a high degree of regulatory control and it has been suggested that cells may have a compensatory mechanism to maintain overall miRNA production to prevent saturation of the endogenous miRNA pathway[587,588]. Therefore, an alternative explanation is that an increased concentration of exogenous hsa-miR-106b following treatment with isolated EVs may have downregulated production of endogenous hsa-miR-106b. Although there was no significant effect upon primary transcript expression of hsa-miR-106b, a slight reduction was observed following treatment with EVs derived from source cells co-transfected with hsa-miR-106b and AGO2 plasmids (**Fig. 4.39F**).

A results summary for all experiments concerning miRNA loading into EVs is provided in **Table 4.2**.

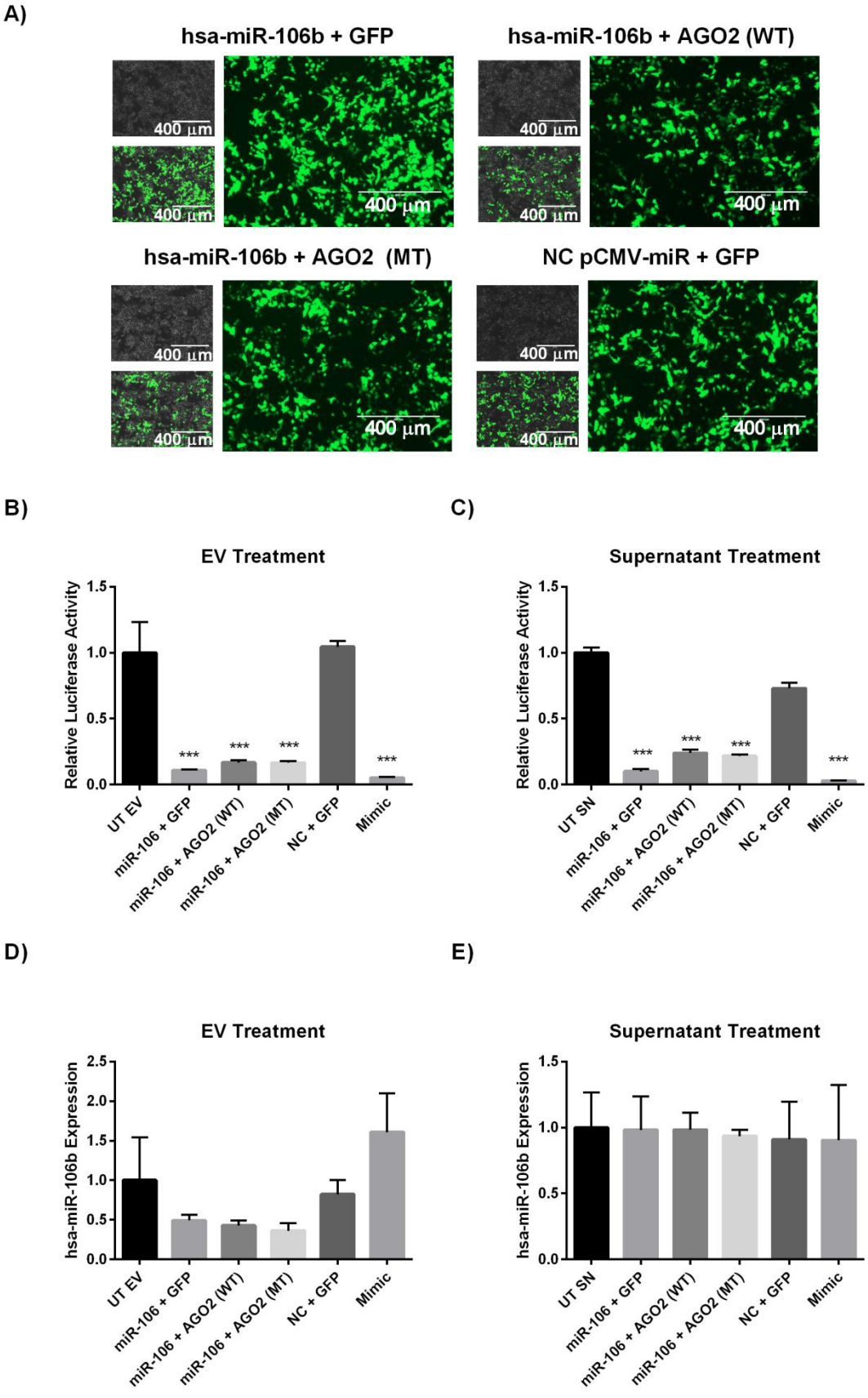
A)
hsa-miR-106b + GFP
hsa-miR-106b + AGO2 (WT)
hsa-miR-106b + AGO2 (MT)
NC pCMV-miR + GFP
400 µm
B)
EV Treatment
Relative Luciferase Activity
UT EV
miR-106 + GFP
miR-106 + AGO2 (WT)
miR-106 + AGO2 (MT)
NC + GFP
Mimic
C)
Supernatant Treatment
UT SN
D)
hsa-miR-106b Expression
E)

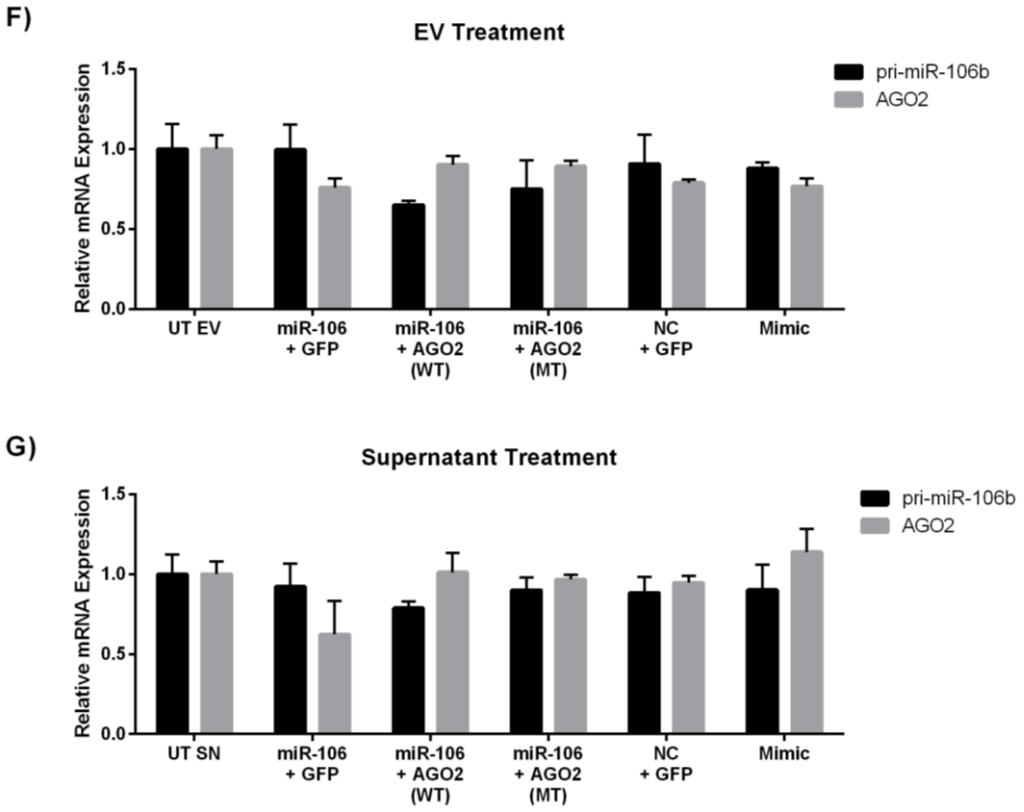

Figure 4.39 Direct Treatment of Recipient Cells with Isolated hsa-miR-106b Extracellular Vesicles. HEK293T source cells, plated in 15 cm cell culture dishes, were left untreated ("UT") or co-transfected with 17.5 µg each of a negative control ("NC") or hsa-miR-106b miRNA expression plasmid and either a control GFP ("GFP") or AGO2 wild-type ("WT") or membrane-tagged ("MT") plasmid, 48 hours prior to isolation. Recipient HEK293T cells, plated in 12-well cell culture dishes, were transfected 48 hours prior to EV treatment with 1 µg of hsa-miR-106b dual-luciferase target reporter alone, or as a positive control, with 50 nM hsa-miR-106b miRNA mimic. 24 hours prior to isolation, recipient cells were divided at a ratio of 1:30 into 96-well cell culture plates. EVs were isolated, pooled, washed, re-isolated and split equally between recipient cells in a 96-well cell culture plate. The remaining supernatant was concentrated and divided equally between recipient cells in a 96-well cell culture plate. Firefly luciferase activity normalised to *Renilla* luciferase was determined after 48 hours. Recipient cell expression of the mature transcript of hsa-miR-106b (normalised to RNA input volume) and the primary transcript of hsa-miR-106b and *AGO2* mRNA, normalised to *β-Actin*, was assessed by qPCR. **(A)** High transfection efficiency of plasmids within source cells. **(B-C)** Luciferase activity was significantly decreased in cells treated with **(B)** EVs and **(C)** concentrated supernatant derived from source cells transfected with hsa-miR-106b + GFP or AGO2 (WT and MT) plasmids. **(D)** Mature hsa-miR-106b expression was non-significantly reduced following treatment with EVs derived from hsa-miR-106b + GFP or hsa-miR-106b + AGO2 (WT and MT) source cells. **(E)** There was no significant effect upon mature hsa-miR-106b expression following supernatant treatment. **(F-G)** There was no significant effect upon primary hsa-miR-106b or *AGO2* mRNA expression following treatment with **(F)** EVs or **(G)** supernatant. Values are mean ± SEM, n = 3, ***p<0.001, one-way ANOVA followed by Tukey's post-hoc test.

Table 4.2 Results Summary for miRNA EV-Loading Experiments.

RNA	Experimental Condition	Results	Ref.
hsa-miR-17	miRNA overexpression alone	• Small increase (non sig.) in miRNA expression in cells and EVs.	**Fig. 4.13**
	Co-expression of miRNA with AGO2	• miRNA expression increased (non sig.) in cells, EVs and SN following AGO2 co-transfection. • Trend towards higher miRNA expression with AGO2 (MT) in EVs and with AGO2 (WT) in SN. • No effect upon primary miRNA transcript. • High variability within replicates.	**Fig. 4.19**
	Co-expression of miRNA with TNRC6A	• miRNA expression increased (non sig.) in cells, EVs and SN following TNRC6A co-transfection. • Trend towards higher miRNA expression with TNRC6A (MT) in EVs. • No effect upon primary miRNA transcript. • High variability within replicates.	**Fig. 4.27**
hsa-miR-29a	miRNA overexpression alone	• Increase in miRNA expression in cells (non sig.) and EVs (sig.).	**Fig. 4.13**
	Co-expression of miRNA with AGO2	• miRNA expression increased in cells and EVs (non sig.) and SN (sig.) following AGO2 co-transfection. • Trend towards higher miRNA expression with AGO2 (MT) in cells and EVs and with AGO2 (WT) in SN. • No effect upon primary miRNA transcript. • High variability within replicates.	**Fig. 4.20**
	Co-expression of miRNA with TNRC6A	• miRNA expression increased in cells (sig.), EVs and SN (non sig.) following TNRC6A co-transfection. • Trend towards higher miRNA expression with TNRC6A (MT) in EVs and with TNRC6A (WT) in SN. • No effect upon primary miRNA transcript. • High variability within replicates.	**Fig. 4.28**
hsa-miR-106b	miRNA overexpression alone	• Significant increase in miRNA expression in cells and EVs.	**Fig. 4.13**
	Co-expression of miRNA with AGO2	• miRNA expression increased in cells and SN (sig.) and EVs (non sig.) following co-transfection with AGO2. • Trend towards higher miRNA expression with AGO2 (MT) in EVs and AGO2 (WT) in SN. • No effect upon primary miRNA transcript. • Specificity: hsa-let-7a-1 expression significantly reduced in EVs after hsa-miR-106b + AGO2 co-transfection.	**Fig. 4.21** **Fig. 4.22**

Table 4.2 Continued.

RNA	Experimental Condition	Results	Ref.
hsa-miR-106b	Co-expression of miRNA with TNRC6A	• miRNA expression increased (non sig.) in cells, EVs and SN following co-transfection with TNRC6A. • Trend towards higher miRNA expression with TNRC6A (MT) in EVs and with TNRC6A (WT) in SN. • No effect upon primary miRNA transcript. • High variability within replicates. • Specificity: no significant effect upon hsa-let-7a-1 and hsa-miR-29a expression in cells and EVs after hsa-miR-106b + TNRC6A co-transfection.	**Fig. 4.29** **Fig. 4.30**
	Functional effects in recipient cells (co-culture): hsa-miR-106b alone	• Recipient cell target reporter activity significantly reduced while mature hsa-miR-106b expression significantly increased after 48 hours co-culture with hsa-miR-106b transfected source cells. • No significant effect upon pri-miR-106b or *APP* mRNA expression.	**Fig. 4.37**
	Functional effects in recipient cells (co-culture): hsa-miR-106b + AGO2/ TNRC6A	• Recipient cell target reporter activity significantly reduced to a similar degree after 48 hours co-culture with hsa-miR-106b + GFP and hsa-miR-106b + AGO2 co-transfected source cells. • Recipient cell expression of mature hsa-miR-106b was only increased followed direct treatment with the hsa-miR-106b mimic. • Target reporter activity was not significantly reduced after 24 or 72 hours co-culture with hsa-miR-106b + GFP, AGO2 or TNRC6A co-transfected source cells.	**Fig. 4.38**
	Functional effects in recipient cells (isolated EVs): hsa-miR-106b + AGO2	• Recipient cell target reporter activity significantly reduced following treatment with EVs and concentrated SN isolated from hsa-miR-106b + GFP and hsa-miR-106b + AGO2 (WT and MT) co-transfected source cells. • Non-significant reduction in hsa-miR-106b expression in recipient cells after treatment with EVs isolated from hsa-miR-106b + GFP or AGO2 co-transfected source cells. • No significant effect upon pri-miR-106b expression or *AGO2* mRNA expression following EV or SN treatment.	**Fig. 4.39**

Sig., significant; **EVs**, extracellular vesicles; **AGO2**, argonaute 2; **SN**, supernatant; **MT**, membrane tagged/associated; **WT**, wild-type; **TNRC6A**, Trinucleotide Repeat-Containing 6A (GW182 orthologue).

4.2.13 Co-expression of shRNA and RNA-binding Proteins in Source Cells did not Enhance mRNA Silencing Following Co-culture

Co-transfection of shRNA expression plasmids with RNA-binding proteins increased exogenous shRNA expression within secreted EVs. Therefore, co-culture was used to ascertain whether shRNA-loaded EVs would have functional effects in recipient cells.

HEK293T source cells were left untreated or co-transfected with APP (**Fig. 4.40**) or BACE1 shRNA (**Fig. 4.41**) and either control GFP, AGO2 (WT or MT) or TNRC6A (WT or MT) plasmids. Recipient HEK293T cells were left untreated or, as a positive control, directly transfected with the APP or BACE1 shRNA plasmid. Recipient and source cells were combined 24 hours after transfection and incubated together for a further 48 hours.

Similar results were obtained for both APP and BACE1 shRNA. Thus, recipient cell expression of target mRNA (*APP* or *BACE1*) was only significantly reduced following direct transfection of recipient cells with either APP shRNA (**Fig. 4.40A**) or BACE1 shRNA (**Fig. 4.41A**). Correspondingly, a significant increase in shRNA expression within recipient cells was only observed following direct transfection of recipient cells with either APP shRNA (**Fig. 4.40B**) or BACE1 shRNA (**Fig. 4.41B**).

However, there did appear to be either transfer or upregulation of *AGO2* and *TNRC6A* mRNA following co-culture with co-transfected source cells. *AGO2* expression was non-significantly increased following co-culture with APP shRNA + AGO2 (WT and MT) co-transfected source cells while *TNRC6A* expression was non-significantly

increased following co-culture with APP shRNA + TNRC6A MT co-transfected source cells (**Fig. 4.40C-D**). Similarly, *AGO2* expression was significantly increased following co-culture with BACE1 shRNA + AGO2 MT co-transfected source cells while *TNRC6A* expression was significantly increased following co-culture with BACE1 shRNA + TNRC6A MT co-transfected source cells (**Fig. 4.41C-D**).

These results suggest that there may be some transfer of exogenous cargoes. As discussed previously, a failure to elicit a reduction in mRNA expression may be the result of too low a quantity of loaded EVs.

A)

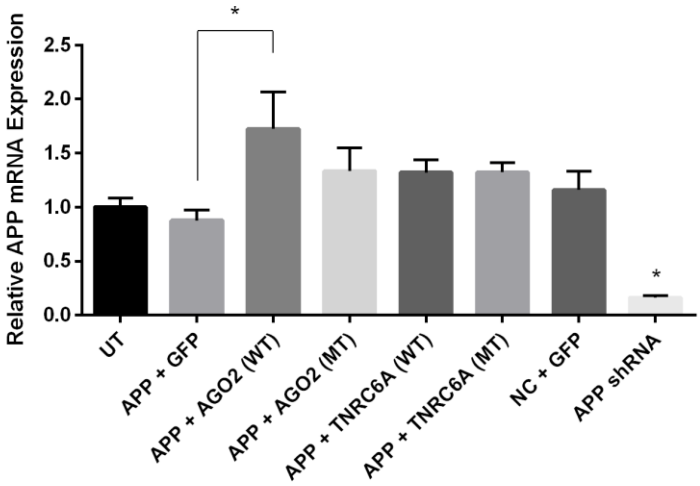
Relative APP mRNA Expression
2.5
2.0
1.5
1.0
0.5
0.0
*
*
UT
APP + GFP
APP + AGO2 (WT)
APP + AGO2 (MT)
APP + TNRC6A (WT)
APP + TNRC6A (MT)
NC + GFP
APP shRNA

B)

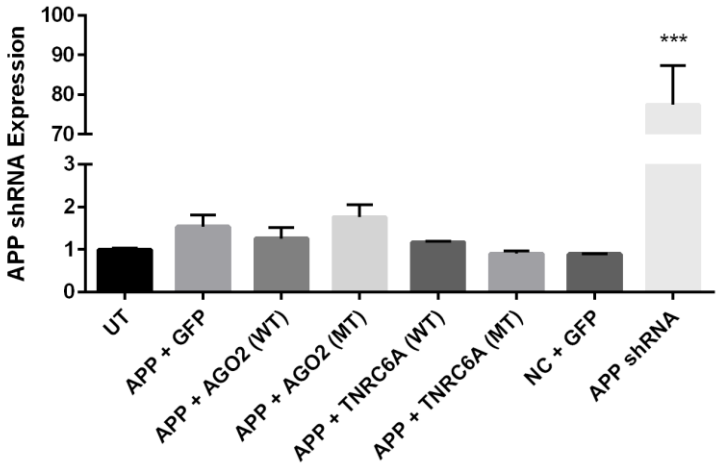
APP shRNA Expression
100
90
80
70
3
2
1
0
***
UT
APP + GFP
APP + AGO2 (WT)
APP + AGO2 (MT)
APP + TNRC6A (WT)
APP + TNRC6A (MT)
NC + GFP
APP shRNA

C)

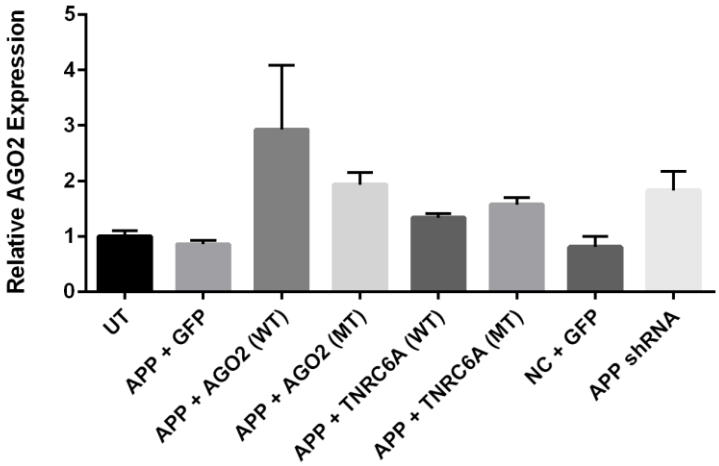
Relative AGO2 Expression
5
4
3
2
1
0
UT
APP + GFP
APP + AGO2 (WT)
APP + AGO2 (MT)
APP + TNRC6A (WT)
APP + TNRC6A (MT)
NC + GFP
APP shRNA

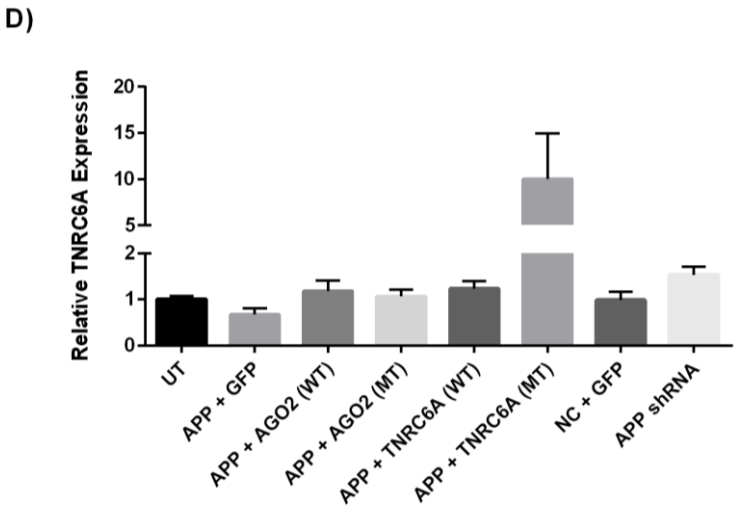

Figure 4.40 Functional Effects of APP shRNA and RNA-binding Proteins in Co-culture. HEK293T source cells, plated in 24-well cell culture plates, were left untreated ("UT") or co-transfected with 500 ng each of the APP shRNA or a negative control shRNA plasmid ("NC") and either a control GFP plasmid ("GFP") or wild-type ("WT") or membrane-tagged ("MT") forms of AGO2 or TNRC6A plasmids. Recipient HEK293T cells, plated in 6-well cell culture plates were left UT or, as a positive control, directly transfected with 2 µg of the APP shRNA plasmid ("APP shRNA"). Recipient and source cells were combined in co-culture 24 hours after transfection and incubated together for a further 48 hours. Recipient cell expression of APP shRNA (normalised to RNA input volume) and *APP*, *AGO2* and *TNRC6A* mRNA, normalised to *β-Actin*, was assessed by qPCR. **(A)** *APP* mRNA expression was only significantly decreased following direct transfection with APP shRNA. **(B)** APP shRNA expression was only significantly increased following direct transfection with APP shRNA. **(C)** There was a non-significant increase in *AGO2* mRNA expression following co-culture with APP + AGO2 (WT and MT) source cells and **(D)** *TNRC6A* mRNA expression following co-culture with APP + TNRC6A MT source cells. Values are mean ± SEM, n = 3, ***$p<0.001$, *$p<0.05$, one-way ANOVA followed by Tukey's post-hoc test.

A)

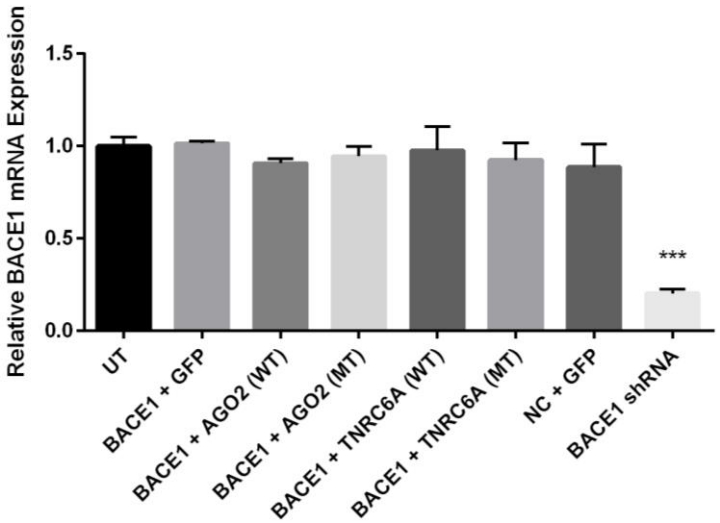
Relative BACE1 mRNA Expression
1.5
1.0
0.5
0.0
***
UT
BACE1 + GFP
BACE1 + AGO2 (WT)
BACE1 + AGO2 (MT)
BACE1 + TNRC6A (WT)
BACE1 + TNRC6A (MT)
NC + GFP
BACE1 shRNA

B)

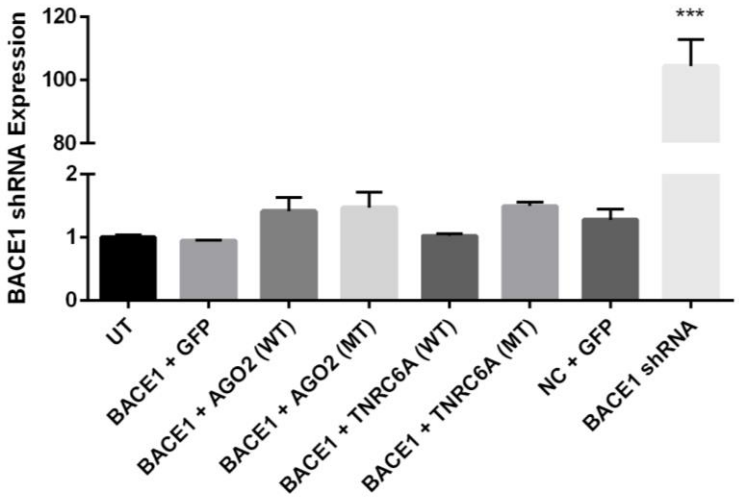
BACE1 shRNA Expression
120
100
80
2
1
0
***
UT
BACE1 + GFP
BACE1 + AGO2 (WT)
BACE1 + AGO2 (MT)
BACE1 + TNRC6A (WT)
BACE1 + TNRC6A (MT)
NC + GFP
BACE1 shRNA

C)

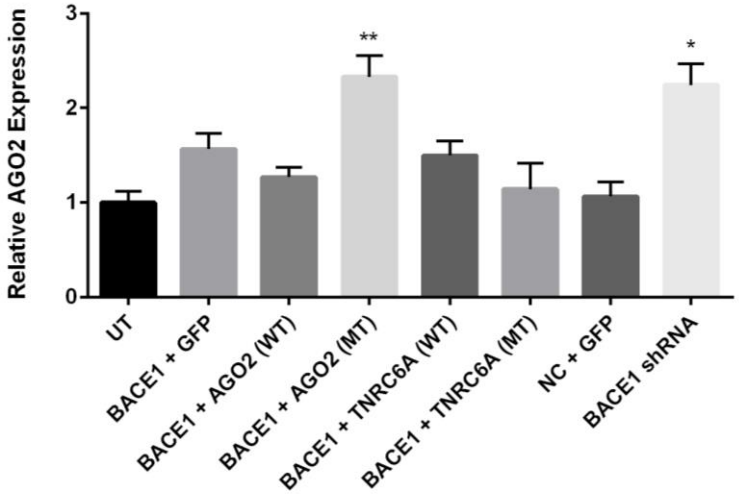
Relative AGO2 Expression
3
2
1
0
**
*
UT
BACE1 + GFP
BACE1 + AGO2 (WT)
BACE1 + AGO2 (MT)
BACE1 + TNRC6A (WT)
BACE1 + TNRC6A (MT)
NC + GFP
BACE1 shRNA

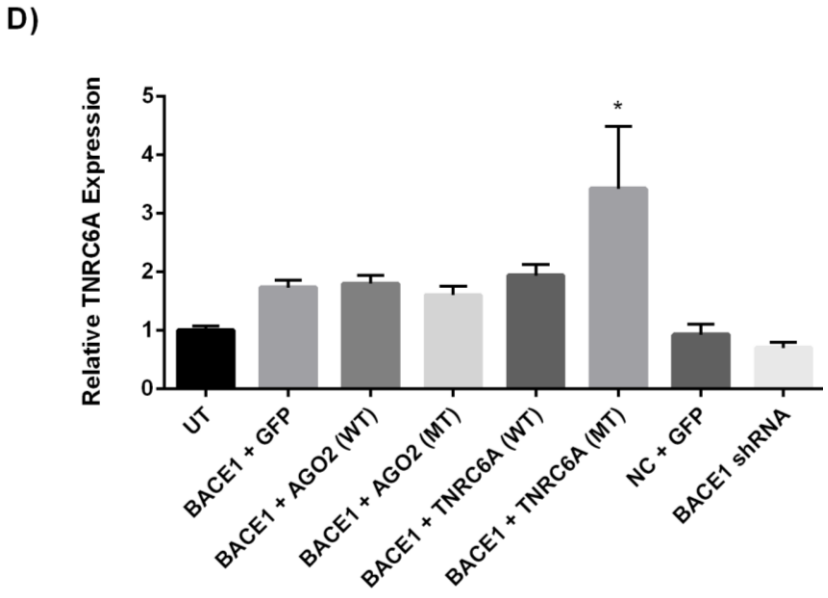

Figure 4.41 Functional Effects of BACE1 shRNA and RNA-binding Proteins in Co-culture. HEK293T source cells, plated in 24-well cell culture plates, were left untreated ("UT") or co-transfected with 500 ng each of the BACE1 shRNA or a negative control shRNA plasmid ("NC") and either a control GFP plasmid ("GFP") or wild-type ("WT") or membrane-tagged ("MT") forms of AGO2 or TNRC6A plasmids. Recipient HEK293T cells, plated in 6-well cell culture plates, were left UT or, as a positive control, directly transfected with 2 µg of the BACE1 shRNA plasmid ("BACE1 shRNA"). Recipient and source cells were combined in co-culture 24 hours after transfection and incubated together for a further 48 hours. Recipient cell expression of BACE1 shRNA (normalised to RNA input volume) and *BACE1*, *AGO2* and *TNRC6A* mRNA, normalised to *β-Actin*, was assessed by qPCR. **(A)** *BACE1* mRNA expression was only significantly decreased by direct transfection with BACE1 shRNA. **(B)** BACE1 shRNA expression was only significantly increased following direct transfection with BACE1 shRNA. **(C)** *AGO2* mRNA expression was significantly increased following co-culture with BACE1 shRNA + AGO2 MT source cells and by direct BACE1 shRNA transfection. **(D)** *TNRC6A* mRNA expression was significantly increased following co-culture with BACE1 shRNA + TNRC6A MT. Values are mean ± SEM, n = 3, ***p<0.001, **p<0.01, *p<0.05, one-way ANOVA followed by Tukey's post-hoc test.

4.2.14 Co-expression of AGO2 with shRNAs did not Enhance mRNA Silencing Following Treatment with Isolated Extracellular Vesicles

To investigate whether a larger quantity of shRNA-loaded EVs was required to silence target mRNA expression within recipient cells, EVs were isolated from HEK293T cells 48 hours after transfection and applied directly to recipient cells as above. The equivalent of the total yield of EVs obtained from 1 x 15 cm cell culture dish was applied per well of a 96-well cell culture plate. As a further control, the supernatant remaining after EV isolation was concentrated and applied directly to recipient cells within 96-well cell culture plates.

As before, plasmid expression was confirmed by fluorescence microscopy following co-transfection of APP shRNA with control GFP and AGO2 plasmids (**Fig. 4.42A**). Promisingly, there was a significant increase in APP shRNA expression in recipient cells following treatment with EVs isolated from source cells co-transfected with APP shRNA and either AGO2 WT or MT plasmids (**Fig. 4.42B**). A significant increase in APP shRNA expression was also observed following treatment with concentrated supernatant derived from source cells co-transfected with APP shRNA and AGO2 WT (**Fig. 4.42C**). However, this did not translate to increased silencing of *APP* mRNA. Instead, *APP* mRNA expression was only significantly decreased following treatment with EVs isolated from source cells co-transfected with APP shRNA + control GFP (**Fig. 4.42D**). No significant silencing of *APP* mRNA expression was observed following treatment with concentrated supernatant (**Fig. 4.42E**).

Similar results were obtained following co-transfections with BACE1 shRNA (**Fig. 4.43**). BACE1 shRNA expression was significantly increased in recipient cells treated with EVs derived from BACE1 shRNA + AGO2 (WT and MT) source cells (**Fig. 4.43B**). BACE1 shRNA was also significantly increased in cells treated with concentrated supernatant derived from BACE1 shRNA + AGO2 WT source cells (**Fig. 4.43C**). However, *BACE1* mRNA expression was only significantly decreased in recipient cells following treatment with EVs derived from BACE1 shRNA + control GFP and BACE1 + AGO2 WT transfected source cells (**Fig. 4.43D**). There was no effect upon *BACE1* mRNA expression following treatment with concentrated supernatant (**Fig. 4.43E**).

A results summary for all experiments concerning siRNA/shRNA loading into EVs is provided in **Table 4.3**.

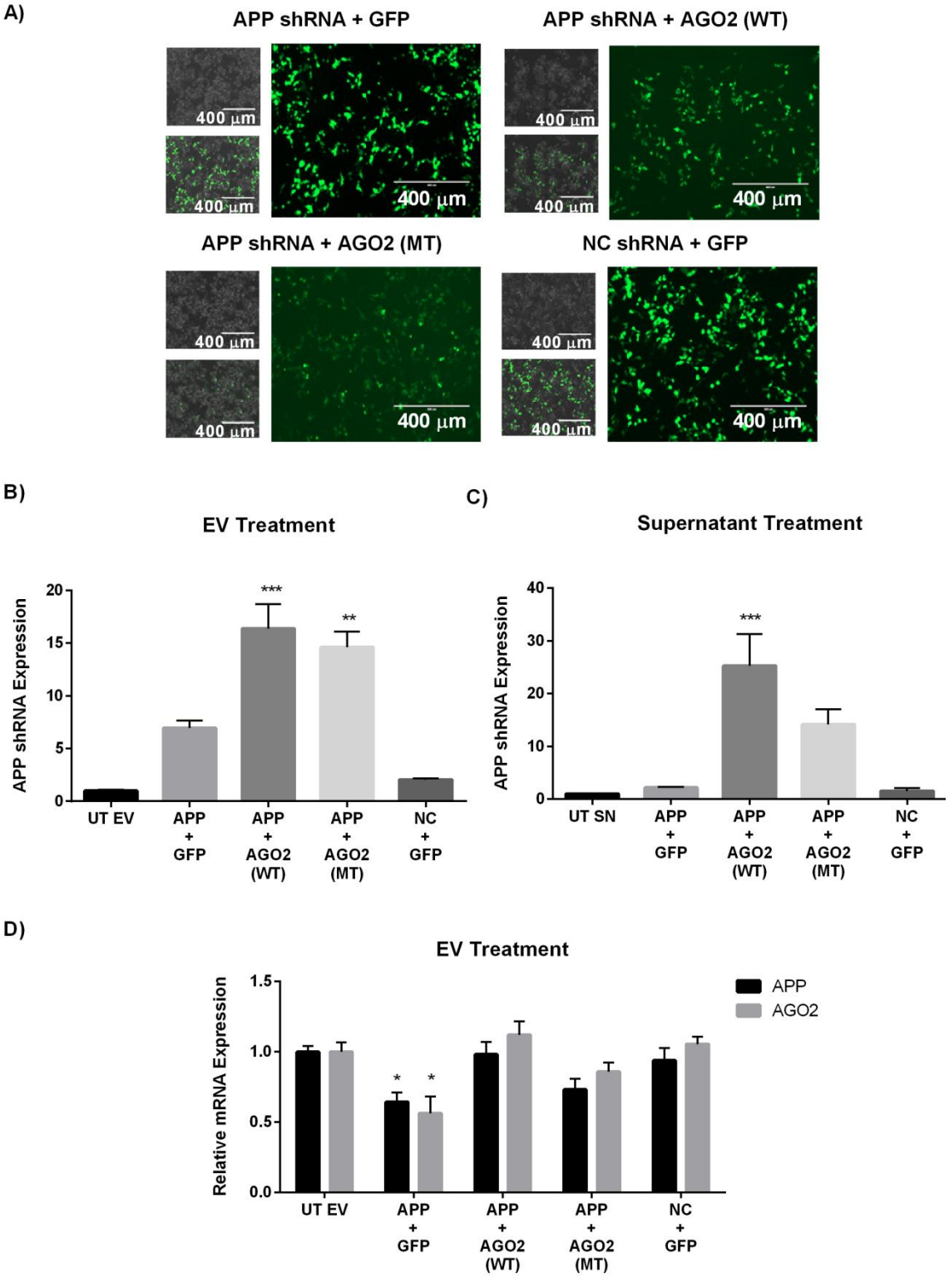
A)
APP shRNA + GFP
APP shRNA + AGO2 (WT)
APP shRNA + AGO2 (MT)
NC shRNA + GFP
400 μm
B)
EV Treatment
APP shRNA Expression
UT EV
APP + GFP
APP + AGO2 (WT)
APP + AGO2 (MT)
NC + GFP
C)
Supernatant Treatment
UT SN
D)
Relative mRNA Expression
APP
AGO2

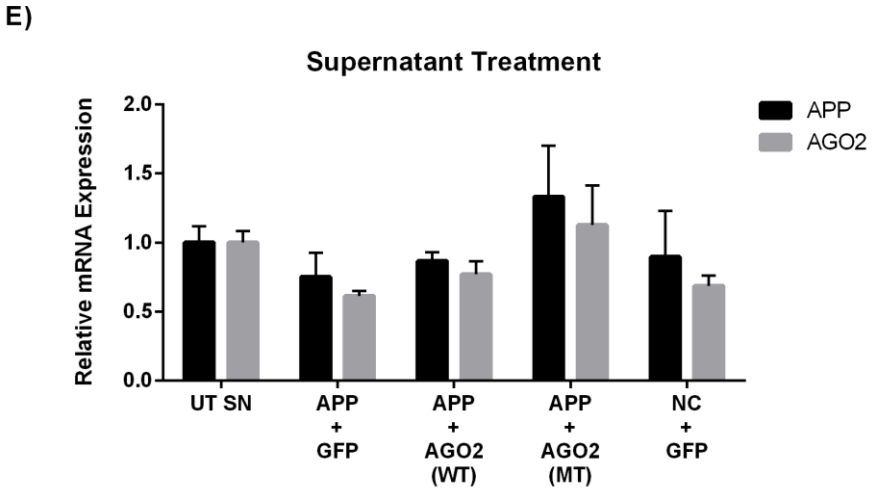

Figure 4.42 Direct Treatment of Recipient Cells with Isolated APP shRNA Loaded Extracellular Vesicles. HEK293T source cells, plated in 15 cm cell culture dishes, were left untreated ("UT") or co-transfected with 17.5 µg each of the APP shRNA or a negative control shRNA ("NC") plasmid and either a control GFP plasmid ("GFP") or wild-type ("WT") or membrane-tagged ("MT") forms of AGO2, 48 hours prior to isolation. Recipient HEK293T cells were plated 24 hours prior to treatment in 96-well cell culture plates and left UT. EVs were isolated, pooled, washed with PBS, re-isolated and split equally between recipient cells in a 96-well cell culture plate. The remaining supernatant was concentrated and divided equally between recipient cells in a 96-well cell culture plate ("SN"). Recipient cell expression of APP shRNA (normalised to RNA input volume) and *APP* and *AGO2* mRNA, normalised to *β-Actin*, was assessed by qPCR. **(A)** Source cells showed high transfection efficiency of the respective plasmids. **(B)** APP shRNA expression was significantly increased in cells treated with EVs derived from APP shRNA + AGO2 (WT and MT) source cells. **(C)** APP shRNA expression was significantly increased in cells treated with concentrated supernatant derived from APP shRNA + AGO2 WT source cells. **(D)** Both *APP* and *AGO2* mRNA expression was significantly decreased following treatment with EVs derived from APP shRNA + control GFP source cells. **(E)** There was no effect upon either *APP* or *AGO2* mRNA expression following treatment with concentrated supernatant. Values are mean ± SEM, n = 3, ***$p<0.001$, **$p<0.01$, *$p<0.05$, one-way ANOVA followed by Tukey's post-hoc test.

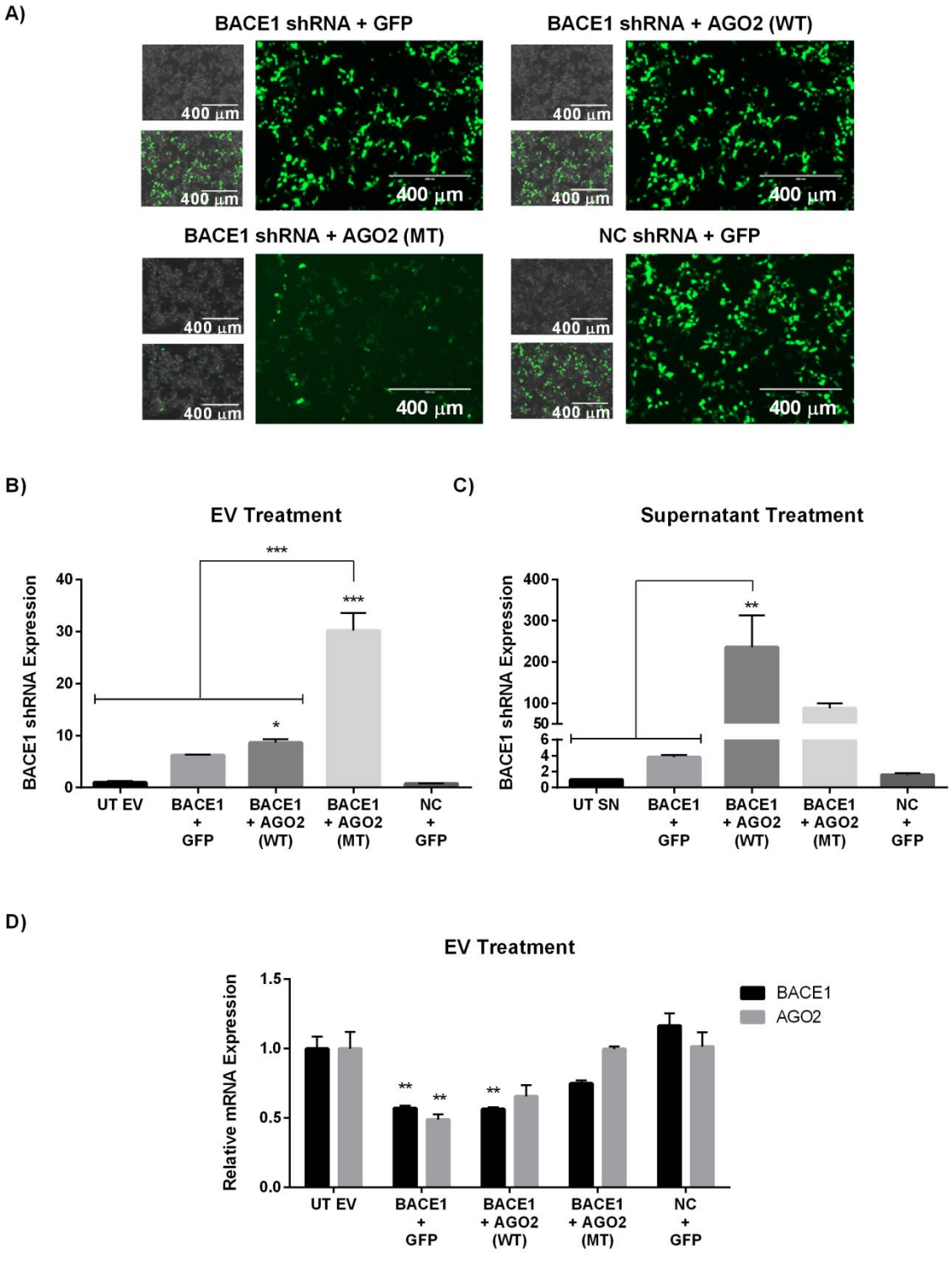
A)
BACE1 shRNA + GFP
BACE1 shRNA + AGO2 (WT)
BACE1 shRNA + AGO2 (MT)
NC shRNA + GFP
400 μm
B)
EV Treatment
BACE1 shRNA Expression
UT EV
BACE1 + GFP
BACE1 + AGO2 (WT)
BACE1 + AGO2 (MT)
NC + GFP
C)
Supernatant Treatment
BACE1 shRNA Expression
UT SN
D)
EV Treatment
Relative mRNA Expression
BACE1
AGO2

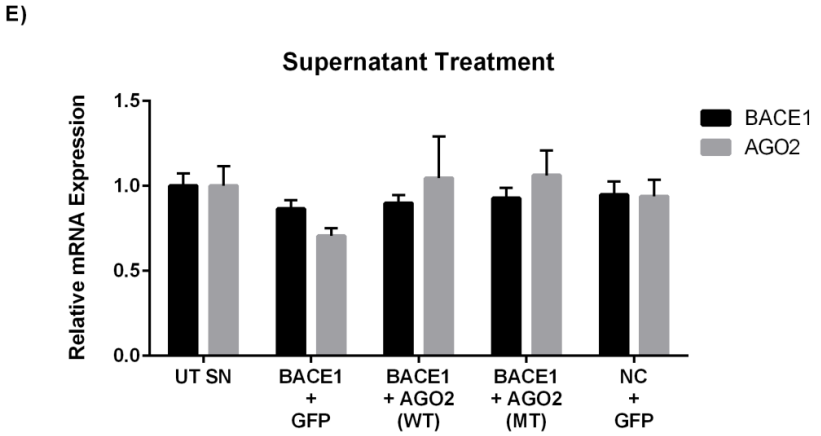

Figure 4.43 Direct Treatment of Recipient Cells with Isolated BACE1 shRNA Loaded Extracellular Vesicles. HEK293T source cells, plated in 15 cm cell culture dishes, were left untreated ("UT") or co-transfected with 17.5 µg each of the BACE1 shRNA or a negative control shRNA ("NC") plasmid and either a control GFP plasmid ("GFP") or wild-type ("WT") or membrane-tagged ("MT") forms of AGO2, 48 hours prior to isolation. Recipient HEK293T cells were plated in 96-well cell culture plates 24 hours prior to treatment and left UT. EVs were isolated, pooled, washed with PBS, re-isolated and split equally between recipient cells in a 96-well cell culture plate. The remaining supernatant was concentrated and divided equally between recipient cells in a 96-well cell culture plate ("SN"). Recipient cell expression of BACE1 shRNA (normalised to RNA input volume) and *BACE1* and *AGO2* mRNA, normalised to *β-Actin*, was assessed by qPCR. **(A)** Source cells showed high transfection efficiency of the respective plasmids. **(B)** BACE1 shRNA expression was significantly increased in cells treated with EVs derived from BACE1 shRNA + AGO2 (WT and MT) source cells. **(C)** BACE1 shRNA expression was significantly increased in cells treated with concentrated supernatant derived from BACE1 shRNA + AGO2 WT source cells. **(D)** *BACE1* mRNA expression was significantly decreased following treatment with EVs derived from BACE1 shRNA + control GFP and BACE1 + AGO2 WT source cells. *AGO2* expression was significantly decreased by EVs derived from BACE1 shRNA + control GFP source cells. **(E)** There was no effect upon either *BACE1* or *AGO2* mRNA expression following treatment with concentrated supernatant. Values are mean ± SEM, n = 3, ***p<0.001, **p<0.01, *p<0.05, one-way ANOVA followed by Tukey's post-hoc test.

Table 4.3 Results Summary for siRNA/shRNA EV-Loading Experiments.

RNA	Experimental Condition	Results	Ref.
APP shRNA	shRNA transfection alone	• shRNA expression increased significantly in cells and EVs.	**Fig. 4.5**
	Co-transfection of shRNA with AGO2	• shRNA expression increased (sig.) in cells, EVs and SN following co-transfection with AGO2. • Trend towards higher shRNA expression with AGO2 (MT) in EVs and with AGO2 (WT) in SN.	**Fig. 4.23**
	Co-transfection of shRNA with TNRC6A	• shRNA expression increased in cells and EVs (sig.) and SN (non sig.) following co-transfection with TNRC6A. • Trend towards higher shRNA expression with TNRC6A (WT) in SN.	**Fig. 4.31**
	Functional effects in recipient cells (co-culture): APP shRNA + AGO2/TNRC6A	• *APP* mRNA expression was not silenced following co-culture with APP shRNA + GFP, AGO2 or TNRC6A co-transfected source cells. • Trend towards increased *AGO2* mRNA expression in recipient cells following co-culture with APP shRNA + AGO2 (WT and MT) source cells. • Trend towards increased *TNRC6A* mRNA expression in recipient cells following co-culture with APP shRNA + TNRC6A (MT) source cells.	**Fig. 4.40**
	Functional effects in recipient cells (isolated EVs): APP shRNA + AGO2	• Significant increase in APP shRNA expression in recipient cells following treatment with EVs and SN isolated from APP shRNA + AGO2 source cells. • *APP* mRNA expression in recipient cells significantly reduced only following treatment with EVs isolated from APP shRNA + GFP source cells.	**Fig. 4.42**
APP siRNA	siRNA transfection alone	• siRNA expression increased significantly in cells and EVs.	**Fig. 4.5**
	Co-transfection of siRNA with AGO2	• siRNA expression significantly increased in cells, EVs and SN following co-transfection with AGO2. • Trend towards highest siRNA expression with AGO2 (WT) in cells, EVs and SN.	**Fig. 4.24**
	Co-transfection of siRNA with TNRC6A	• siRNA expression increased in cells and SN (non sig.) and EVs (sig.) following co-transfection with TNRC6A, but not above the level obtained following control co-transfections. • High variability within replicates.	**Fig. 4.32**
BACE1 shRNA	shRNA transfection alone	• shRNA expression increased significantly in cells and EVs.	**Fig. 4.5**
	Co-transfection of shRNA with AGO2	• shRNA expression increased in cells (non sig.), EVs and SN (sig.) following co-transfection with AGO2. • Trend towards higher shRNA expression with AGO2 (MT) in EVs.	**Fig.4.25**

Table 4.3 Continued.

RNA	Experimental Condition	Results	Ref.
BACE1 shRNA	Co-transfection of shRNA with TNRC6A	• shRNA expression increased in cells and SN (non sig.) and EVs (sig.) following co-transfection with TNRC6A but high variability within replicates. • Higher shRNA expression with TNRC6A (MT) in EVs (sig.) and with TNRC6A (WT) in SN (non sig.).	**Fig. 4.33**
	Functional effects in recipient cells (co-culture): BACE1 shRNA + AGO2/TNRC6A	• *BACE1* mRNA expression was not silenced following co-culture with BACE1 shRNA + GFP, AGO2 or TNRC6A co-transfected source cells. • Significantly increased *AGO2* mRNA expression in recipient cells following co-culture with BACE1 shRNA + AGO2 (MT) source cells. • Significantly increased *TNRC6A* mRNA expression in recipient cells following co-culture with BACE1 shRNA + TNRC6A (MT) source cells.	**Fig. 4.41**
	Functional effects in recipient cells (isolated EVs): BACE1 shRNA + AGO2	• Significant increase in BACE1 shRNA expression in recipient cells following treatment with EVs and SN isolated from BACE1 + AGO2 source cells. • *APP* mRNA expression in recipient cells significantly reduced following treatment with EVs isolated from BACE1 + GFP and BACE1 + AGO2 (WT) source cells.	**Fig. 4.43**
BACE1 siRNA	siRNA transfection alone	• siRNA expression increased significantly in cells and EVs.	**Fig. 4.5**
	Co-transfection of siRNA with AGO2	• siRNA expression increased in cells (non sig.) and EVs and SN (sig.) following AGO2 co-transfection. • Trend towards highest siRNA expression with AGO2 (WT) in EVs and SN.	**Fig. 4.26**
	Co-transfection of siRNA with TNRC6A	• siRNA expression increased in cells (sig.), EVs and SN (non sig.) following co-transfection with TNRC6A, but not above the level obtained following control co-transfections. • High variability within replicates.	**Fig. 4.34**

Sig., significant; **EVs**, extracellular vesicles; **AGO2**, argonaute 2; **SN**, supernatant; **MT**, membrane tagged/associated; **WT**, wild-type; **TNRC6A**, Trinucleotide Repeat-Containing 6A (GW182 orthologue).

4.3 Discussion

This study assessed the efficacy of an endogenous EV-loading strategy for RNAi effectors relevant to AD. Appropriate siRNA and miRNA-based candidates were identified and validated to regulate either *APP* or *BACE1* expression. Consistent with previous studies which have employed endogenous EV-loading techniques[468,507,514,515], transfection of RNAi effectors within source cells resulted in their secretion within EVs. The remainder of the study therefore focused upon methods to optimise the endogenous EV-loading technique. This included co-expression of RNA-binding proteins with exogenous RNAi molecules within EV source cells and the inclusion of an acylation domain to target RNA-binding proteins towards the membrane. As EVs are formed following inward budding of the plasma membrane, it was hypothesised that increasing the membrane localisation of RNA-binding proteins may enhance their incorporation into EVs along with any associated RNA. Indeed, findings from this study suggest that co-expression of exogenous RNAi-based molecules with AGO2 and TNRC6A enhanced their cellular expression and secretion within EVs. Furthermore, inclusion of the acylation domain within RNA-binding proteins appeared to enhance this effect when co-transfected with pri-miRNA and shRNA expression plasmids. Together, these findings suggest that members of RISC are important not only for promoting the stability of RNAi-based molecules but also for their inclusion and secretion within EVs.

Co-expression with RNA-binding Proteins Increased EV-loading of Small RNAs

The findings of the current study are generally consistent with those of a recently published study by Lv *et al.*[524] who showed that co-transfection of an AGO2-expressing plasmid with miR-16 mimics resulted in increased miR-16 expression in both cells and EVs. Specifically, AGO2 was shown to increase the level of miR-16 in cells by protecting miRNAs from degradation within lysosomes. However, while these results are consistent in terms of implicating AGO2 in increased cellular expression and EV secretion of RNAi effectors, it should be noted that in the current study this was only observed following expression of exogenous miRNAs from pri-miRNA expression plasmids. Preliminary experiments revealed no significant increase in miRNA expression within EVs following co-transfection of AGO2 with miRNA mimics and thus the decision was taken to focus upon pri-miRNA expression plasmids.

One potential explanation for this discrepancy is the different identity of miRNAs used between the two studies. This is an important factor as it has previously been shown that different miRNA species are differentially associated with AGO2[470,587]. Indeed, miR-16 has been found to associate more strongly with AGO2 in comparison to a range of other miRNAs including miR-30a, miR-223 and let-7b[470]. While there has been no focused assessment of AGO2 association with the miRNAs of interest in the current study, a recent paper assessed miRNA expression profiles in HEK293T cells stably expressing miR-155[589]. Interestingly, it was reported that miR-17 and miR-106b were in the top 30 miRNAs associated with AGO2 although miR-29a was not mentioned. In this study, a selective enrichment was also noted in AGO2-miRNA associations suggesting that expression of a miRNA might not always be a true reflection of its activity[589]. However,

it should be noted that ectopic expression of miR-155 was reported to cause changes in both mRNA and miRNA expression profiles, which resulted in increased cellular proliferation. As both miR-17[590] and miR-106b[591] have been linked to roles in proliferation these results should be viewed with caution.

In this respect, it is also of interest that the degree of miRNA association with AGO2 has been found to vary depending upon both the condition of source cells and the availability of the mRNA target[470,592]. For example, serum depletion significantly increased the percentage of miR-16 associated with AGO2 while the total quantity of miR-16 remained unchanged[470]. Together, these results again suggest that the level of miRNA expression is not necessarily the best indication of activity. In the current study, EV source cells were grown in Opti-MEM under conditions of serum deprivation. It is therefore possible that this may have influenced the level of association between AGO2 and the miRNAs of interest. Furthermore, while miRNAs may associate with AGO2, it is also apparent that they are afforded extra protection by associations with other, as yet unidentified, proteins[470].

It would therefore be of interest to investigate the level of association between AGO2 and TNRC6A with the miRNAs in the current study. Following co-expression of miRNAs with AGO2, there appeared to be an inverse relationship between the increase in cellular and EV expression of exogenous miRNAs and the level of endogenous miRNA abundance. While this might point towards a compensatory mechanism of miRNA expression[587], it might also relate to differences in the extent of miRNA association with AGO2. Thus, if a miRNA has a relatively high association with AGO2, or indeed TNRC6A, co-expression with either of these proteins might be expected to

increase the stability of the miRNA above that observed for miRNAs with which they are not so strongly associated. There did not appear to be such a strong inverse relationship between the increase in exogenous miRNA expression and their endogenous abundance following co-transfection with TNRC6A. This may potentially be explained either by a difference in association of certain miRNAs with AGO2 or TNRC6A or the relative importance of AGO2 versus TNRC6A in stabilising miRNAs.

There are several approaches that may be undertaken to explore the level of association between miRNAs and AGO2 or TNRC6A. A miRNA pull-down assay may be utilised to isolate miRNAs of interest followed by probing for AGO2/TNRC6A proteins. Conversely, AGO2 or TNRC6A may be immunoprecipitated and the association between each protein and specific miRNAs assessed by qPCR. More detailed proteomic and transcriptomic analyses within both cells and EVs would also be informative to determine how co-expression with AGO2 or TNRC6A may affect the composition of cells and EVs. In the current study, AGO2 protein appeared significantly upregulated in EVs following transfection of both AGO2 plasmids. In contrast, only low levels of TNRC6A were detectable in EVs and were not increased following TNRC6A transfections. This is in contrast to the results of Gibbings *et al*.[387] who reported an enrichment of GW182 (TNRC6A orthologue) within EVs. Whether this relates to a Western blotting detection issue or to specific differences in expression between different cell types is unclear. Similarly, while the expression of two further miRNAs suggested a degree of specificity in increased exogenous miRNA expression following co-transfections, more detailed transcriptomic analyses would further clarify the consequences of RNA-binding protein overexpression upon EV cargoes.

As mentioned previously, specific sequence motifs (EXOmotifs) may selectively target specific miRNAs for EV-loading[474]. However, sequence motifs have also been identified which are over-represented in miRNAs specifically retained in cells (CLmotifs)[474]. Mutagenesis to convert EXOmotifs into CLmotifs and vice versa has been shown to reverse the pattern of exosome enrichment or cellular retention of miRNAs, respectively[474]. Of note, three miRNAs within the current study (hsa-miR-17, hsa-miR-20a and hsa-miR106b) contained the CLmotif "UGCA". It is possible that this may have influenced the EV-loading for these miRNAs. It would therefore be of interest to explore whether insertion of the EXOmotif into these miRNAs would enhance their loading into EVs without disrupting regulation of their target mRNAs.

AGO2 and TNRC6A Did Not Enhance Functional Activity of Small RNA in Recipient Cells

Importantly, the study of Lv *et al*.[524] reported that increased EV expression of miR-16 was associated with functional effects in recipient cells. Treatment of HEK293T cells with HeLa EVs enriched in miR-16 and AGO2 enhanced silencing of the miR-16 target, BCL-2, when compared to EVs derived from control source cells or those transfected only with miR-16. In contrast, enhanced functional activity following co-transfection with AGO2 (or TNRC6A) was not consistently observed in the current study. Thus, silencing of reporter activity or target mRNA was generally observed following treatment with EVs derived from source cells co-transfected with the control GFP plasmid and either hsa-miR-106, APP shRNA or BACE1 shRNA. When silencing was observed following treatment with EVs derived from source cells co-transfected with RNAi effectors and AGO2 plasmids it was at a similar level to that achieved with the

control GFP plasmid. Therefore, in contrast to Lv *et al.*[524], the results of the current study do not suggest that functional activity in recipient cells was enhanced following co-transfection with AGO2 or TNRC6A.

The exact reasons for this inconsistency are unclear; however, there are a number of potential explanations. Firstly, it should be noted that while EV yield was reduced following co-transfection of RNAi effectors with all plasmids, co-transfection with AGO2 plasmids reduced EV yield to a greater extent than co-transfections with control GFP plasmids. This could partly account for why co-transfection with AGO2 did not enhance target silencing above that achieved following co-transfections with the control GFP plasmid if fewer EVs loaded with exogenous RNAi-based effectors were secreted.

Furthermore, the threshold level of exogenous RNAi cargoes within EVs required to elicit functional activity in recipient cells is unknown. Therefore, it is possible that the quantity of loaded EVs produced an insufficient concentration of RNAi molecules to elicit functional effects in recipient cells. In this respect, the relatively high endogenous levels of hsa-miR-106b may have made it more challenging to significantly increase hsa-miR-106b expression in recipient cells following EV-mediated delivery in co-culture. This is particularly important as the luciferase reporter is already under regulation by endogenous hsa-miR-106b in recipient cells. While the use of hsa-miR-29a may have been more optimal, the choice of hsa-miR-106b was determined by reporter sensitivity. In contrast, in the case of isolated EVs loaded with hsa-miR-106b, a near ceiling effect was achieved in the level of silencing of the luciferase reporter within recipient cells. Treatment with isolated EVs elicited a similar level of silencing as that achieved following direct transfection of the hsa-miR-106b mimic. High silencing

efficiency may therefore have precluded any difference in efficacy from becoming apparent.

As noted above, miRNA expression might not be a true reflection of activity[470,589,592]. Therefore, even though miRNA/shRNA expression appeared increased following co-expression with AGO2 and TNRC6A, this may not necessarily translate into increased activity. It should also be noted that in the current study both AGO2 and TNRC6A were fused to GFP and this may have affected their functional activity. It will be important to assess this using constructs from which AGO2/TNRC6A are expressed in the absence of GFP. Finally, the current study focused upon silencing of luciferase activity and mRNA expression. Future studies should therefore explore the effects upon endogenous protein levels.

Two different strategies were employed to assess the functional activity of loaded EVs upon recipient cells including co-culture and the direct application of isolated EVs. While the direct application of EVs appeared more promising, suggesting that increasing the quantity of EVs may increase functional activity, this requires further optimisation. In the current study, the equivalent yield from 1 x 15 cm cell culture dish was applied to 1 well of a 96-well cell culture plate. In contrast, Lv *et al*.[524] reported the use of 10 µg EVs to treat 1 x 10^5 cells. When samples are washed prior to quantification, the EVs obtained from 1 x 15 cm dish may yield ~1-5 µg of protein. EVs were applied based upon yield obtained per plate rather than protein quantity given the potential for medium protein contamination. However, this strategy is associated with its own issues given the potential for variability in isolation efficiency and the reduced

secretion of EVs observed following co-transfection. In future, normalisation by particle number may prove a more optimal approach.

Another factor which may potentially contribute towards the discrepancy in functional activity observed between the current study and previous reports[468,507,514,515,524] is the choice of source and recipient cells. As discussed previously, the interactions driving recipient cell uptake of EVs are not fully elucidated, although a role for cell adhesion molecules, and in particular the tetraspanins, has been postulated[457,458,493]. In the current study, HEK293T cells were used as both source and recipient cells largely due to their amenability to transfection. However, previous studies have utilised a range of cell types often differing in their choice for source and recipient cells. It is therefore possible that the ideal cell combination was not used in the present study and this will be an important area for future research.

Finally, it should be noted that, where appropriate, the results of the current study are focused on the expression of mature miRNA. As mentioned previously, endogenous and exogenous pre-miRNAs and mature miRNAs may be found within EVs and it has been suggested that pre-miRNAs may be preferentially loaded over mature forms in some cell types[469,494,515,583]. The level of pri-miRNA expression was therefore also considered following transfections of pri-miRNA expression plasmids in the current study. However, this revealed that pri-miRNA levels within EVs were either undetectable, at very low levels or were actually reduced following co-expression of pri-miRNA expression plasmids. These results therefore suggest that preferential loading of pre-miRNAs may be limited to specific cell types or miRNA species.

Co-transfection and EV Isolation Efficiency Contributed to High Variability between Replicates

Throughout this study, relatively high variability was noted in cellular and EV expression of miRNAs/siRNAs and mRNAs. This issue was investigated and appeared to arise from variability in the efficiency of large-scale transfections and EV isolation. Combined, these two sources of variability may contribute towards the lack of enhanced silencing following co-transfections with AGO2/TNRC6A proteins. In this respect, further optimisation of transfection parameters is likely required. In the current study, equal quantities of miRNA/shRNA expression plasmids and AGO2/TNRC6A plasmids were applied during co-transfections. However, whether this represents the optimal strategy remains to be determined. It may be that a higher ratio of AGO2/TNRC6A to RNAi effectors or vice versa may be more effective at increasing the expression and functional activity of exogenous RNAi molecules within EVs.

The issue of variable isolation efficiency is an important one. While differential ultracentrifugation currently remains the standard technique within the field, it may not be the most efficient. As demonstrated in the current study, there is substantial loss of material with each isolation step and this may vary between replicates. Furthermore, it is not yet fully understood how ultracentrifugation may influence the structure or function of EVs. Indeed, evidence from electron microscopy provided in the current study suggests particles may become aggregated or fused. Alternative isolation methods are therefore required which are more scalable and not as subject to variability in retained yield of EVs. Current work within the lab and with collaborators is aimed at developing new isolation strategies which includes the use of ultrafiltration paired with

size-exclusion liquid chromatography (UF-LC)[593]. When compared to ultracentrifugation, UF-LC appears to produce a significantly higher EV yield without affecting vesicle protein composition. Furthermore, EVs derived by UF-LC and ultracentrifugation show different *in vivo* biodistributions[593], suggesting that the biophysical properties of EVs may be significantly altered by the isolation method chosen. This technique was unavailable for the current study and therefore future studies should explore whether UF-LC isolations may produce different functional outcomes.

A Role for Non-Vesicular Small RNA-Protein Complexes?

It is of interest that concentrated supernatant samples also produced significant silencing of reporter activity following co-transfection of miR-106b with either control GFP or AGO2 plasmids. There are a number of factors which may have contributed towards this silencing. Firstly, as discussed above, a large proportion of particles are not retained following each centrifugation step. While some of the observed particles measured within filtrate may relate to protein contamination, it is also possible that those vesicles which were not retained were subsequently concentrated within the supernatant by ultrafiltration and contributed to silencing of reporter activity within recipient cells.

Alternatively, it has also been clearly established that there are a population of AGO2-miRNA complexes which associate independently of vesicles[575,576]. Indeed, it has been suggested that the majority of circulating miRNAs may be associated with protein complexes such as AGO2 rather than with vesicles, although this is debated[470,575,576]. Therefore, it is possible that some of these complexes may have been concentrated by

ultrafiltration and taken up by recipient cells where they were able to silence the target reporter. Indeed, increased supernatant expression of exogenous RNAi molecules was frequently observed following co-transfection with AGO2 or TNRC6A WT plasmids, suggesting that secretion of non-vesicular RNAi effectors and AGO2/TNRC6A complexes may have been increased. In contrast to the results with hsa-miR-106b, neither *APP* nor *BACE1* mRNA expression was significantly silenced despite increased APP and BACE1 shRNA expression following treatment with concentrated supernatant. It is possible that this might relate to differences in readout sensitivity and the quantity of RNAi effectors required to silence a luciferase reporter with four complementary binding sites versus *APP* or *BACE1* mRNA.

In summary, the current study adds support to previous evidence suggesting that an endogenous EV-loading method is a viable alternative to exogenous-based loading methods. Indeed, this is one of the first studies to demonstrate enhanced EV-loading of exogenous RNAi-based effectors, including miRNAs and siRNAs, following co-expression with RNA-binding proteins such as AGO2 and TNRC6A. Moreover, this effect appeared to be further increased by the inclusion of an acylation domain within the N-terminus of these RNA-binding proteins. While the assessment of functional effects in recipient cells requires further optimisation, this remains a promising strategy for future research.

5 Multi-gene LNA-ASO Silencing of Alzheimer's Disease Targets[†]

5.1 Introduction

While a minority of AD cases are caused by mutations in key genes such as APP and presenilin, for most, AD is multi-faceted involving a large number of different risk factors. Thus, although approaches focused upon silencing specific gene expression may prove promising, it is increasingly recognised that a combinatorial approach may have the strongest chance of therapeutic success[40,594–596]. Combinatorial therapies are now utilised for the treatment of a range of other complex diseases including cancer, AIDS and cardiovascular disease[597–599]. Therefore, it is perhaps unrealistic to expect a compound targeting one single aspect of the complex disease process to demonstrate significant disease-modifying properties in AD. While a number of amyloid-β-based drugs have failed at clinical trial, it may be that targeting amyloid-β in combination with other pathogenic processes may hold more promise. Indeed, the Accelerate Cure/Treatments for Alzheimer's Disease Coalition recently highlighted the need for combinatorial approaches and began planning clinical trials to test compounds targeting different pathogenic pathways or multiple targets within the same pathway[595,596].

While the concept of combinatorial therapy for AD is relatively new, a number of studies have begun to investigate its potential. Chow *et al.*[594] showed that partially silencing both Bace1 and γ-secretase additively reduced amyloid-β burden and cognitive deficits in an aged transgenic mouse model of AD. Similarly, treatment of

[†] This study was completed in collaboration with Dr. Miguel Varela, Wood Lab, University of Oxford. Dr. Varela conducted bioinformatics analyses to identify potential multi-gene targeting LNA-ASO sequences while C. Woffindale performed *in vitro* screening of candidate LNA-ASOs.

APP transgenic mice with the anti-amyloid-β antibody, Gantenerumab, in combination with a Bace1 inhibitor significantly enhanced the anti-amyloid effect produced by either compound alone[600]. Combined targeting of other pathogenic processes has also been successful. Treatment with both anti-oxidants and essential fatty acids reduced the inflammatory response, loss of cholinergic neurons and cognitive deficits in a mouse model of AD[601]. Similarly, the repurposing of two existing drugs aimed at restoring the balance between excitatory and inhibitory signalling within AD resulted in neuroprotective effects against amyloid-β-mediated toxicity *in vitro* and alleviated cognitive deficits in two different AD mouse models *in vivo*[602].

Combinatorial strategies have also been trialled in AD patients. A recent meta-review of several studies investigating combined treatment with acetylcholinesterase inhibitors and Memantine revealed beneficial effects in moderate-to-severe AD across a range of measures[603]. Similarly, combining Vitamin E supplements with acetylcholinesterase inhibitors may reduce the rate of functional decline[604]. Together, these results offer support for the notion that combinatorial approaches represent the most promising therapeutic hope for the future.

Based upon developments in the field of therapeutic antisense oligonucleotides (ASOs) and recent findings highlighting their promise for AD[401,403,404,406–413], the current study investigated the utility of locked nucleic acid-modified-ASOs (LNA-ASOs) as a combinatorial approach towards AD therapy. As outlined previously, the methylene bridge between the 2' oxygen and 4' carbon of LNA bases imposes a conformational constraint which increases binding affinity and specificity for target mRNA. The addition of flanking LNA bases also protects against exonucleolytic degradation and

increases *in vivo* stability[417,418]. Thus, LNA-ASO gapmers are able to induce potent and highly specific RNase H-mediated gene silencing and as such are emerging as a popular choice for ASO-based therapeutics.

Therefore, this study focused upon a novel oligonucleotide-based combinatorial approach in which LNA-ASO gapmers were designed to specifically and simultaneously target two separate AD-relevant genes. Two promising candidate multi-gene LNA-ASOs targeting human transcripts were identified; one targeting *APP* and *GSK3β* (APGS) and the second targeting *BACE1* and *mTOR* (BAMT). APGS and BAMT multi-gene LNA-ASOs elicited potent silencing of both their respective target genes and significantly reduced amyloid-β production in the HEK293 APPswe cell line[18]. Promisingly, a further multi-gene LNA-ASO (mBAMT) targeting murine *Bace1* and *mTOR* was also identified, paving the way for future *in vivo* studies. This study therefore identified three novel multi-gene targeting LNA-ASOs with the potential to moderate two different disease pathways within AD.

5.2 Results

5.2.1 Identification of Potential Gene Targets

Candidate gene targets were identified by a literature search and are provided in **Table 5.1**. Potential targets were selected if they had previously been linked to pathological pathways in AD or if their silencing had been shown to have therapeutic relevance for AD. Candidate multi-gene targeting LNA-ASOs were designed by Dr. Miguel Varela (Wood Lab) using an algorithm which identifies overlapping sequences, 13-15 nucleotides in length, between two or more genes of interest. Sequences were blasted against the human genome to ensure specificity to the genes of interest and subsequently used to design candidate multi-gene targeting LNA-ASO gapmers which were predicted to target two separate genes simultaneously (**Fig. 5.1**). LNA-ASO gapmers contained a fully phosphorothioated backbone and comprised a core region of 7-9 DNA monomers flanked either end by 3 LNA-modified bases, as this structure has previously been shown to elicit potent and specific RNase H-mediated gene silencing[417]. Candidate multi-gene targeting LNA-ASOs identified by this method are provided in **Tables 5.2** and **5.3**.

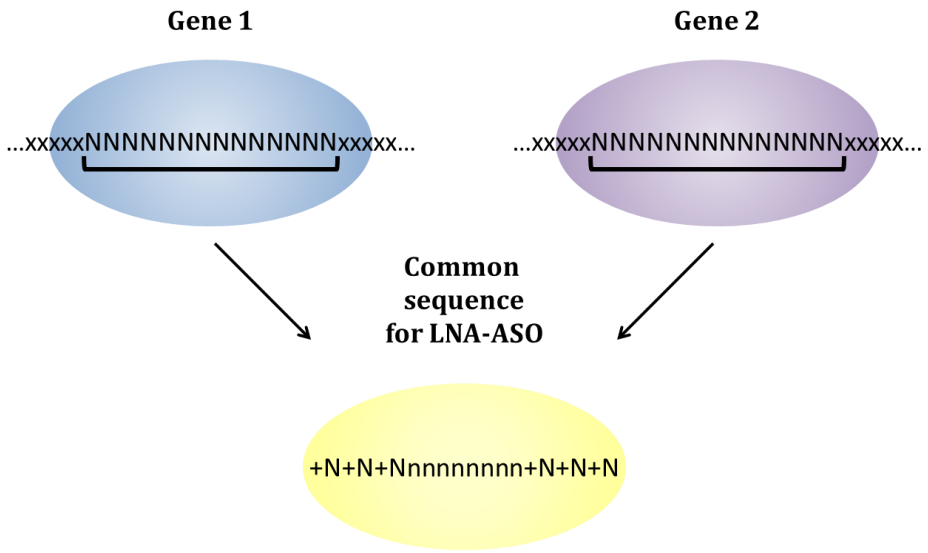

Figure 5.1 Design of LNA-ASOs for Multi-gene Targeting. Common sequences, 13-15 nucleotides in length, present within two candidate genes of interest, were identified by the use of an algorithm which detects overlapping sequences between two or more genes. Candidate sequences were blasted against the human genome to ensure specificity to the desired target genes and utilised to design multi-gene targeting LNA-ASO gapmers. LNA-ASO gapmers were designed to have a fully phosphorothioated backbone and comprised a core region of 7-9 DNA bases flanked either end by 3 LNA-modified bases, indicated by + signs.

Table 5.1 Candidate Genes of Interest as Multi-gene LNA-ASO Targets.

Gene of Interest	Evidence	Ref.
AChE	• Loss of cholinergic neurons in AD leads to reduction in levels of key neurotransmitter, acetylcholine (ACh). • Acetylcholinesterase (AChE) inhibitors prolong the activity of ACh, enhancing neurotransmission. • AChE inhibitors are approved to treat mild-to-moderate AD.	1,281,605
APOE	• *APOE ε4* is strongest genetic risk factor for sporadic AD. • APOE is the most prevalent neuronal lipoprotein, colocalizes with amyloid-β plaques and linked to disrupted clearance and aggregation of amyloid-β. • Monoclonal antibody against APOE significantly reduced amyloid-β load when administered prior to or after plaque deposition in transgenic mouse model of AD.	25,324, 325, 606–608
APP	• Sequential cleavage of APP by BACE1 and γ-secretase results in amyloid-β production. • Mutations in *APP* linked to early and late-onset AD through enhanced production of toxic amyloid-β (42) monomers.	609,610
AS-BDNF	• BDNF is a secreted neurotrophic growth factor important for supporting neuronal survival, plasticity, learning and memory. • *AS-BDNF* forms duplexes with *sense-BDNF* mRNA. • Silencing of *AS-BDNF* increased both mRNA and protein BDNF levels resulting in increased neurite outgrowth and maturation.	611–613
AS-GDNF	• GDNF is a secreted neurotrophic growth factor important for regulating neuronal survival, branching and plasticity. • *GDNF* and *AS-GDNF* display inverse pattern of expression in human middle temporal gyrus in AD patients. • Inhibition of *AS-GDNF* resulted in upregulation of *GDNF* mRNA.	613,614
BACE1	• Successive proteolytic processing of APP by BACE1 results in production of amyloid-β. • BACE1 expression is elevated in AD patients, resulting in increased production of amyloid-β. • Inhibition of Bace1 in primary cortical neurons, WT and AD transgenic mice lowered amyloid-β production with a reduction in amyloid-β plaques, reversal of synaptic pathology and rescue of memory deficits. • BACE1 inhibitors have reached human clinical trials.	290,296, 297,299, 305,422, 615–618

Table 5.1 Continued.

Gene of Interest	Evidence	Ref.
Caspase-3	• "Effector" protease activated in apoptosis cell death pathway. • Chronic, non-apoptotic activation of caspase-3 in hippocampal dendritic spines in transgenic AD mice. • Increased amyloid-β production through caspase-3 mediated cleavage of APP and formation of tau filaments following caspase-3 cleavage of tau. • Inhibition of caspase-3 rescued AD phenotype.	619,620
Caspase-9	• "Initiator" protease activated as part of apoptotic pathway. • Activation of caspase-9 in human hippocampal AD sections and hippocampal synaptic fractions in transgenic AD mice. • Caspase-cleaved tau fragments found in neurofibrillary tangles and dystrophic neurons. • Inhibition of caspase-9 activity rescued synaptic plasticity and memory deficits in transgenic mice.	621,622
CDK1	• Interacts with cyclin B1 to form a heterodimer that determines the timing of mitosis in the cell-division cycle. • Activation of CDK1 important in determining initiation of apoptosis and aberrant expression of CDK1/cyclin B1 observed in degenerating neurons in AD brain. • CDK1 phosphorylates amyloid-β. CDK1 inhibitor reduced amyloid-β phosphorylation, preventing amyloid-β toxicity.	623–625
CDK5R1	• Encodes p35, a neuron-specific activator of CDK5, which is required for correct CNS development. • Cleavage of p35 produces a truncated form, p25, which is found to accumulate in the neurons of patients with AD. • p25 constitutively activates CDK5, altering its cellular location and resulting in hyperphosphorylation of tau.	626–629
C-Jun	• Transcription factor that is an effector of the JNK signal transduction pathway with can lead to neuroprotective adaptations or apoptosis depending upon the stressor. • Phosphorylated c-Jun is strongly associated with neurofibrillary tangles and nuclei in hippocampal neurons in AD brains. • Inhibition of JNK ameliorated cognitive deficits and reduced amyloid-β production, amyloid plaque load, tau hyper-phosphorylation and synaptic loss in transgenic AD mice.	630–632

Table 5.1 Continued.

Gene of Interest	Evidence	Ref.
GRIA2	• Encodes GRIA2 subunit of AMPA receptor. • Expressed in cortical neurons and plays a role in excitatory glutamatergic neurotransmission. • Differential expression reported at post-mortem in AD patients and in young *APOE* Ɛ4 carriers prior to AD occurrence. • Hippocampus-specific defective GRIA2 RNA-editing reported within AD patient samples.	633–636
GRIN2A/B	• Encodes NR2A/B subunit of NMDA receptor. • Deregulated expression of GRIN2A/B in AD. • Amyloid-β oligomers interfere with NMDA receptor function and trafficking. • Association between GRIN2B polymorphisms and AD. • Silencing of NMDA receptors in hippocampal neurons blocked neuronal oxidative stress induced by amyloid-β oligomers. • Inhibition of NR2B-containing NMDA receptors abolished amyloid-β-induced tau phosphorylation and toxicity.	637–641
GSK3α	• Protein kinase involved in phosphorylation of tau and cleavage of APP. • Two GSK3 inhibitors blocked production and accumulation of amyloid-β in transgenic APP mice by interfering with γ-secretase processing of APP. • Selective RNAi-silencing of GSK3α resulted in significant reduction in amyloid-β (40/42) in APP mutant cell line while overexpression of GSK3α resulted in a dose-dependent increase in amyloid-β.	150,161, 642
GSK3β	• Protein kinase involved in the phosphorylation of tau. • Increased activation of GSK3β in frontal cortex and colocalization with neurofibrillary tangles in brains of AD patients. • Inhibition of GSK3β reduced Bace1-mediated cleavage of APP and amyloid-β production by decreasing *Bace1* gene transcription and expression. • Inhibition of GSK3β rescued cognitive deficits and synaptic plasticity in mice. • GSK3β inhibitors have reached clinical trial.	151,346, 643–647

Table 5.1 Continued.

Gene of Interest	Evidence	Ref.
mTOR	• Ser/Thr kinase involved in regulation of protein synthesis, autophagy and cell growth, proliferation and survival. • Increased expression of mTOR in hippocampus and in neurons bearing neurofibrillary tangles in AD patients. • Amyloid-β increases mTOR signalling while inhibition of mTOR results in reduction in amyloid-β levels. • mTOR inhibition reduced amyloid-β and tau phosphorylation, rescuing cognitive deficits in transgenic AD mice models.	648–654
NOX2/ NOX4	• NADPH oxidases (NOX2/4 - isoforms of the catalytic subunit) are enzyme complexes responsible for production of reactive oxygen species in microglia, neurons and astrocytes. • NOX activity and expression upregulated in MCI and AD patients and NOX4 subunit increased in APP transgenic mice in age-dependent manner. • Amyloid-β induces activation of NOX2 resulting in superoxide production while ibuprofen treatment inhibits NOX2 activation, reduces oxidative damage and increases plaque clearance. • AD transgenic mice lacking the catalytic subunit, NOX2, protected against oxidative stress, cerebrovascular dysfunction and behavioural deficits. • Positive linear relationship between NOX4 activity and deposition of amyloid-β which was inversely related to cognitive performance.	655–663
Tau	• Hyperphosphorylated tau is primary component of neurofibrillary tangles. • Oligomeric tau found to be a toxic species which reduces cell viability and may play a role in initiation and spread of tau pathology. • Tau appears to play important role in propagating excitotoxic-mediated amyloid-β pathology through post-synaptic targeting of Src kinase Fyn. Silencing of tau or inhibition of post-synaptic targeting of Fyn prevents memory and synaptic deficits and improves survival in AD transgenic mouse model. • RNAi-silencing of tau in SH-SH5Y cells improved mitochondrial function and synaptic activity. • Reduction of endogenous tau levels protected AD mice against excitotoxicity and prevented behavioural deficits.	126,141, 145,186, 664–666

AD, Alzheimer's Disease; **ACh**, acetylcholine; **AChE**, acetylcholinesterase; **APP**, amyloid precursor protein; **AS-BDNF**, antisense brain-derived neurotrophic factor; **AS-GDNF**, antisense glial cell-derived neurotrophic factor; **BACE1**, β-secretase; **NR2A/B**, N-methyl D-aspartate receptor subtype 2A/B; **NMDA**, N-methyl D-aspartate; **mTOR**, mammalian target of rapamycin; **Ser/Thr**, serine/threonine; **NADPH**, nicotinamide adenine dinucleotide phosphate (reduced); **NOX**, NADPH oxidase.

Table 5.2 Human Multi-gene LNA-ASO Candidates.

LNA-ASO	Genes Targeted		Sequence
	Gene 1	Gene 2	
APGS	*APP*	*GSK3β*	+A+G+Agagactga+T+T+C
BACD	*BACE1*	*CDK5R1*	+C+C+Ttccaccgc+T+G+C
BAMT	*BACE1*	*mTOR*	+G+A+Tagagaca+A+T+G
BAPP1	*BACE1*	*APP*	+A+C+Ttcagactg+G+T+T
BAPP2*	*BACE1*	*APP*	+A+C+Ttcagactg+G+T+T/idSp/+A
BAPP3**	*BACE1*	*APP*	+A+C+Ttcagactg+G+T+T/idSp/+A/idSp/+G
BATA	*BACE1*	*Tau*	+T+G+Ctggtggctt+C+T+C
GRAGSB	*GRIA2*	*GSK3β*	+C+A+Aaaagatattc+A+G+A
GRANO	*GRIA2*	*NOX4*	+A+G+Gcatatttc+C+C+T
GRBCA	*GRIN2B*	*Caspase-9*	+G+A+Gtgagcccac+T+G+C
GSBGRB	*GSK3β*	*GRIN2B*	+C+C+Acccccctgga+T+C+T

BAPP sequences were identical but included the addition of 1* or 2** abasic sites (idSp). This allowed the design of longer LNA-ASOs by covering mismatches between APP and BACE1 sequences. All LNA-ASOs have a fully phosphorothioated backbone with 7-9 DNA monomers flanked on either end by 3 LNA-modified bases, + indicates LNA-modified base.

Table 5.3 Chromosome Location of LNA-ASO Target Sequences.

LNA-ASO	Chromosome Location of Target Sequence (GRCh38)
APGS	*APP*: Chr. 21: 26097025-26097038 *GSK3β*: Chr. 3: 120090373-120090386
BACD	*BACE1*: Chr. 11: 117311680-117311693 *CDK5R1*: Chr. 17: 32490184-32490197
BAMT	*BACE1*: Chr. 11: 117312772-117312784 *mTOR*: Chr. 1: 11155629-11155641
BAPP1	*BACE1*: Chr. 11: 117307558-117307571 *APP*: Chr. 21: 26170967-26170980
BAPP2	*BACE1*: Chr. 11: 117307556-117307571 *APP*: Chr. 21: 26170965-26170980
BAPP3	*BACE1*: Chr. 11: 117307554-117307571 *APP*: Chr. 21: 26170963-26170980
BATA	*BACE1*: Chr. 11: 117285578-117285592 *Tau*: Chr. 17: 45983557-45983571
GRAGSB	*GRIA2*: Chr. 4: 157364444-157364459 *GSK3β*: Chr. 3: 120091488-120091503
GRANO	*GRIA2*: Chr. 4: 157360007-157360020 *NOX4*: Chr. 11: 89496453-89496466
GRBCA	*GRIN2B*: Chr. 12: 13904052-13904066 *Caspase-9*: Chr. 1: 15523433-15523447
GSBGRB	*GSK3β*: Chr. 3: 120089164-120089178 *GRIN2B*: Chr. 12: 13653364-13653378

5.2.2 Multi-gene LNA-ASOs Effectively Silenced Target Genes in SH-SH5Y Cells

Candidate LNA-ASO gapmers were first screened *in vitro* in the human neuroblastoma SH-SH5Y cell line. SH-SH5Y cells were reverse transfected with 20 nM of either the candidate multi-gene LNA-ASO or a negative control LNA-ASO using Lipofectamine 2000. Expression of each relevant target mRNA, normalised to *β-Actin*, was assessed by qPCR after 48 hours. *Caspase 9*, *GRIA2*, *GRIN2B* and *NOX4* mRNA were not detectable in SH-SH5Y cells so the following multi-gene LNA-ASOs could not be screened; GRAGSB, GRANO, GRBCA and GSBGRB.

Promisingly, a number of candidate LNA-ASOs silenced both of their predicted targets including APGS (*APP* and *GSK3β*), BAMT (*BACE1* and *mTOR*) and BATA (*BACE1* and *tau*) (**Fig. 5.2A,C,E**). In contrast, BACD (*BACE1* and *CDK5R1*) and BAPP1 (*APP* and *BACE1*) produced significant silencing of only one target gene (**Fig. 5.2B,D**). Given that targeting both APP and BACE1 may prove potentially additive in reducing amyloid-β production, two further multi-gene LNA-ASOs were designed to target both *BACE1* and *APP*; BAPP2 and BAPP3. BAPP2 and BAPP3 LNA-ASOs were based upon the same sequence as BAPP1 but included the addition of either one (BAPP2) or two (BAPP3) abasic sites within the 3' end of the LNA-ASO sequence. The abasic site allowed the design of longer LNA-ASOs despite a mismatch between the *APP* and *BACE1* sequences. As above, BAPP2 and BAPP3 were screened at 20 nM in SH-SH5Y cells. Encouragingly, BAPP2 and BAPP3 produced significant silencing of both *APP* and *BACE1* mRNA expression (**Fig. 5.3**).

A)

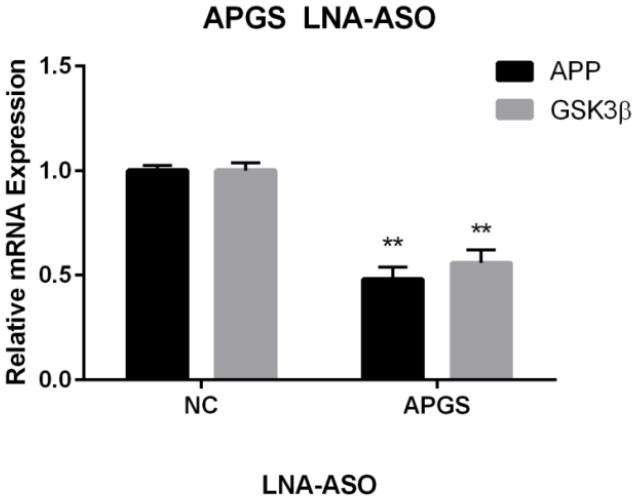
APGS LNA-ASO
APP
GSK3β
Relative mRNA Expression
1.5
1.0
0.5
0.0
**
**
NC
APGS
LNA-ASO

B)

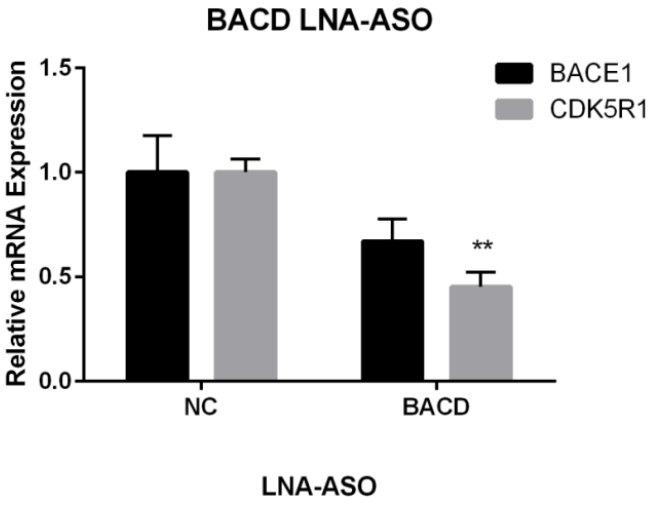
BACD LNA-ASO
BACE1
CDK5R1
Relative mRNA Expression
1.5
1.0
0.5
0.0
**
NC
BACD
LNA-ASO

C)

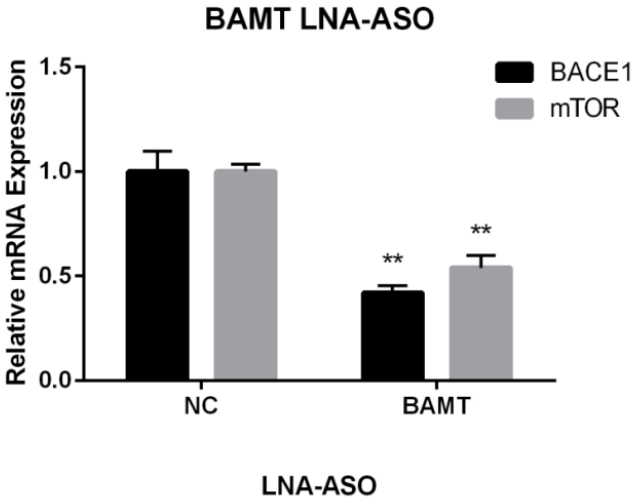
BAMT LNA-ASO
BACE1
mTOR
Relative mRNA Expression
1.5
1.0
0.5
0.0
**
**
NC
BAMT
LNA-ASO

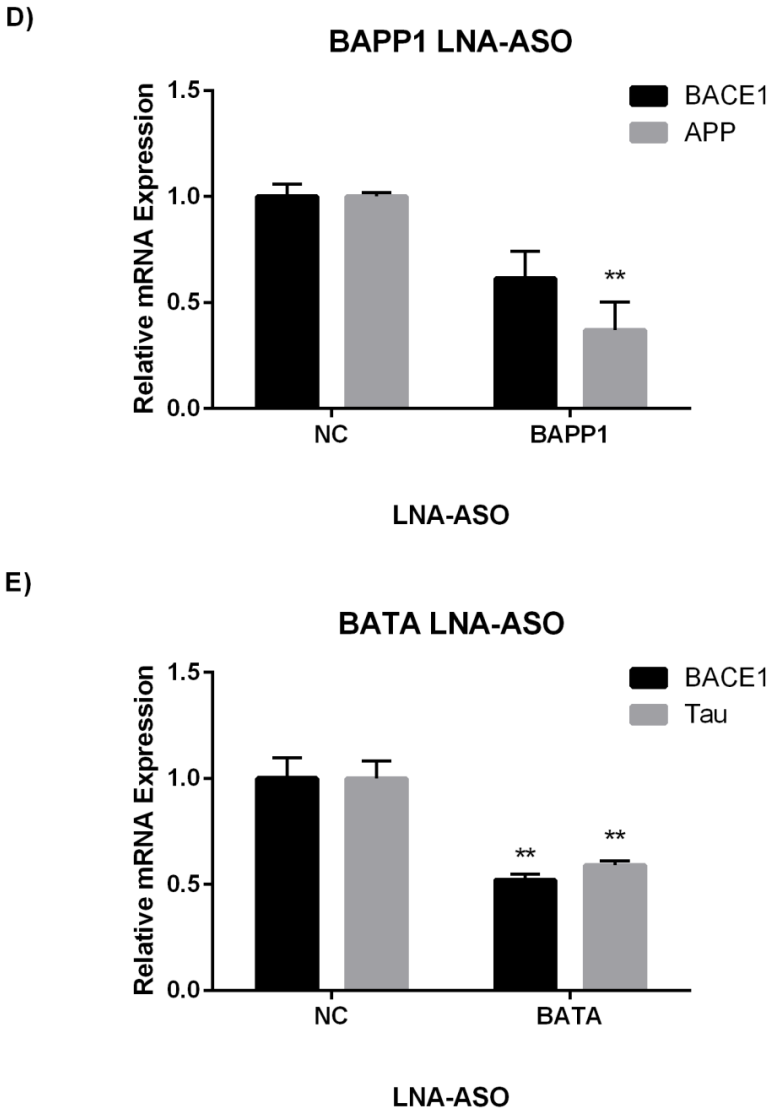

Figure 5.2 Candidate Multi-gene LNA-ASO Screening in SH-SH5Y Cells. SH-SH5Y cells were reverse transfected with 20 nM of each candidate multi-gene LNA-ASO or a negative control LNA-ASO ("NC"). Expression of the appropriate genes, normalised to *β-Actin*, was assessed by qPCR after 48 hours. Gene silencing observed following treatment with **(A)** APGS, **(B)** BACD, **(C)** BAMT, **(D)** BAPP1 and **(E)** BATA multi-gene LNA-ASOs. Values are mean ± SEM, n = 3, **p<0.01, Student's t-test.

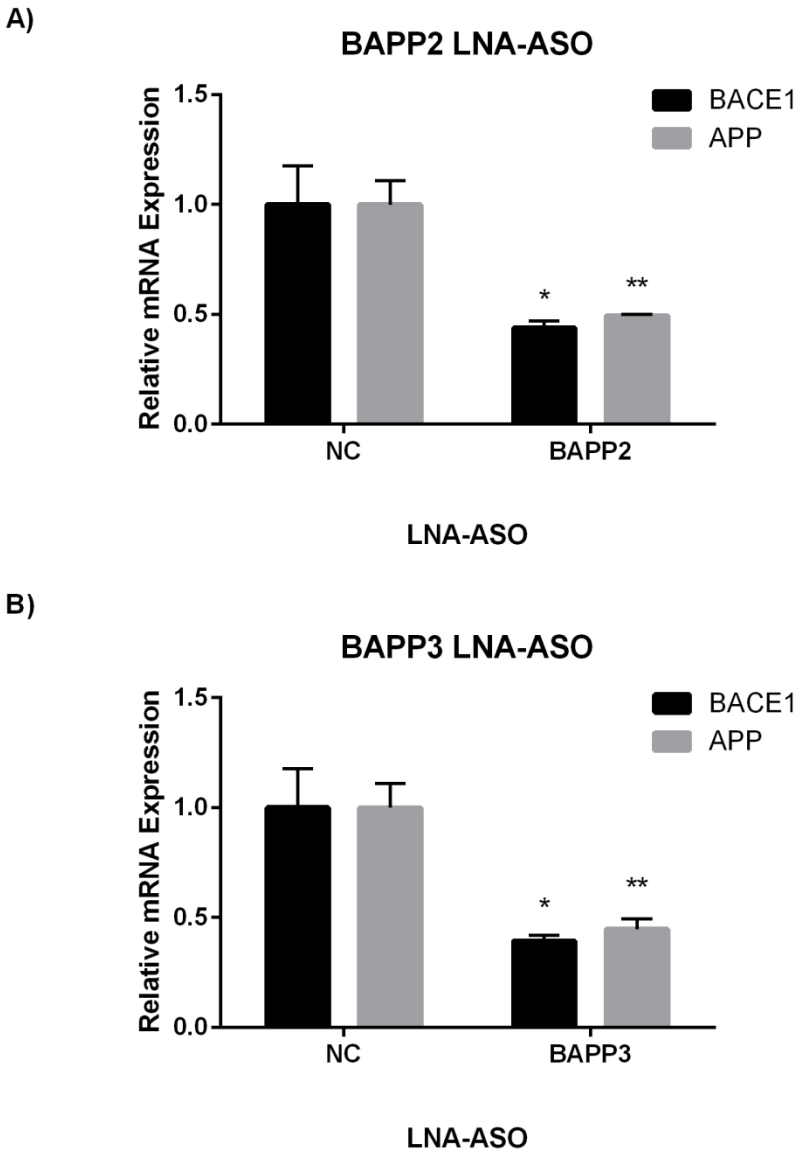

Figure 5.3 Screening of Candidate BAPP Multi-gene LNA-ASOs in SH-SH5Y Cells. SH-SH5Y cells were reverse transfected with 20 nM of each candidate BAPP multi-gene LNA-ASO or a negative control LNA-ASO ("NC"). RNA was harvested after 48 hours and *BACE1* and *APP* mRNA expression, normalised to *β-Actin*, assessed by qPCR. Both *BACE1* and *APP* mRNA expression was significantly decreased following treatment with **(A)** BAPP2 and **(B)** BAPP3 multi-gene LNA-ASOs. Values are mean ± SEM, n = 3, **p<0.01, *p<0.05, Student's t-test.

5.2.3 Multi-gene LNA-ASOs Effectively Silenced Target Genes in HEK293 APPswe Cells

Candidate LNA-ASO gapmers were also screened in HEK293 APPswe cells as a more relevant model of AD. HEK293 APPswe cells refer to a line of HEK293 cells stably transfected with the human Swedish mutation of APP_{695}[18,667]. Stable expression of the mutated form of APP_{695} increases amyloid-β production by 6-8 fold in comparison to cells expressing normal APP_{695}[18].

GRIA2 and *NOX4* mRNA were not detectable so GRAGSB and GRANO multi-gene LNA-ASOs could not be screened in HEK293 APPswe cells. As before, HEK293 APPswe cells were reverse transfected with 20 nM of either the candidate multi-gene LNA-ASO or a negative control LNA-ASO using Lipofectamine 2000. Expression of each relevant target mRNA, normalised to *β-Actin*, was assessed by qPCR after 48 hours. This revealed that a number of candidate multi-gene LNA-ASOs silenced both of their predicted targets including APGS (*APP* and *GSK3β*), BAMT (*BACE1* and *mTOR*), BATA (*BACE1* and *tau*) and GRBCA (*GRIN2B* and *caspase-9*) (**Fig. 5.4A,C,E,F**). As in SH-SH5Y cells, BAPP1 (*APP* and *BACE1*) and BACD (*BACE1* and *CDK5R1*) significantly silenced only one of their target genes (**Fig. 5.4B,D**) while GSBGRB (*GSK3β* and *GRIN2B*) did not silence either target (**Fig. 5.4G**).

As it was desirable to identify a multi-gene LNA-ASO targeting both *APP* and *BACE1*, the additional BAPP2 and BAPP3 LNA-ASOs were also screened at 20 nM in HEK293 APPswe cells. However, in contrast to the dual-silencing observed in SH-SH5Y cells, only *BACE1* was significantly silenced (**Fig. 5.5A-B**). To determine whether an

increased concentration was required to elicit silencing, HEK293 APPswe cells were transfected with 50 nM of BAPP1, BAPP2 or BAPP3 multi-gene LNA-ASOs. Despite the increased concentration, all three failed to silence *APP* mRNA expression (**Fig. 5.5C-E**). This may relate to an inaccessible binding site if a different conformational structure is imposed upon *APP* mRNA by the presence of the Swedish mutation. As the design of new LNA-ASOs was limited by the requirement for overlapping sequences between *APP* and *BACE1* no further LNA-ASOs could be developed.

Based upon the results in both SH-SH5Y and HEK293 APPswe cells, two LNA-ASOs were selected for further study; APGS (*APP* and *GSK3β*) and BAMT (*BACE1* and *mTOR*). BATA also elicited silencing of both *BACE1* and *tau*, however the decision was taken to focus upon APGS and BAMT given the essential neuronal functions of tau as outlined previously. Both GSK3β and mTOR are implicated in the hyperphosphorylation of tau and thus may provide an alternative strategy to target the tau pathological pathway.

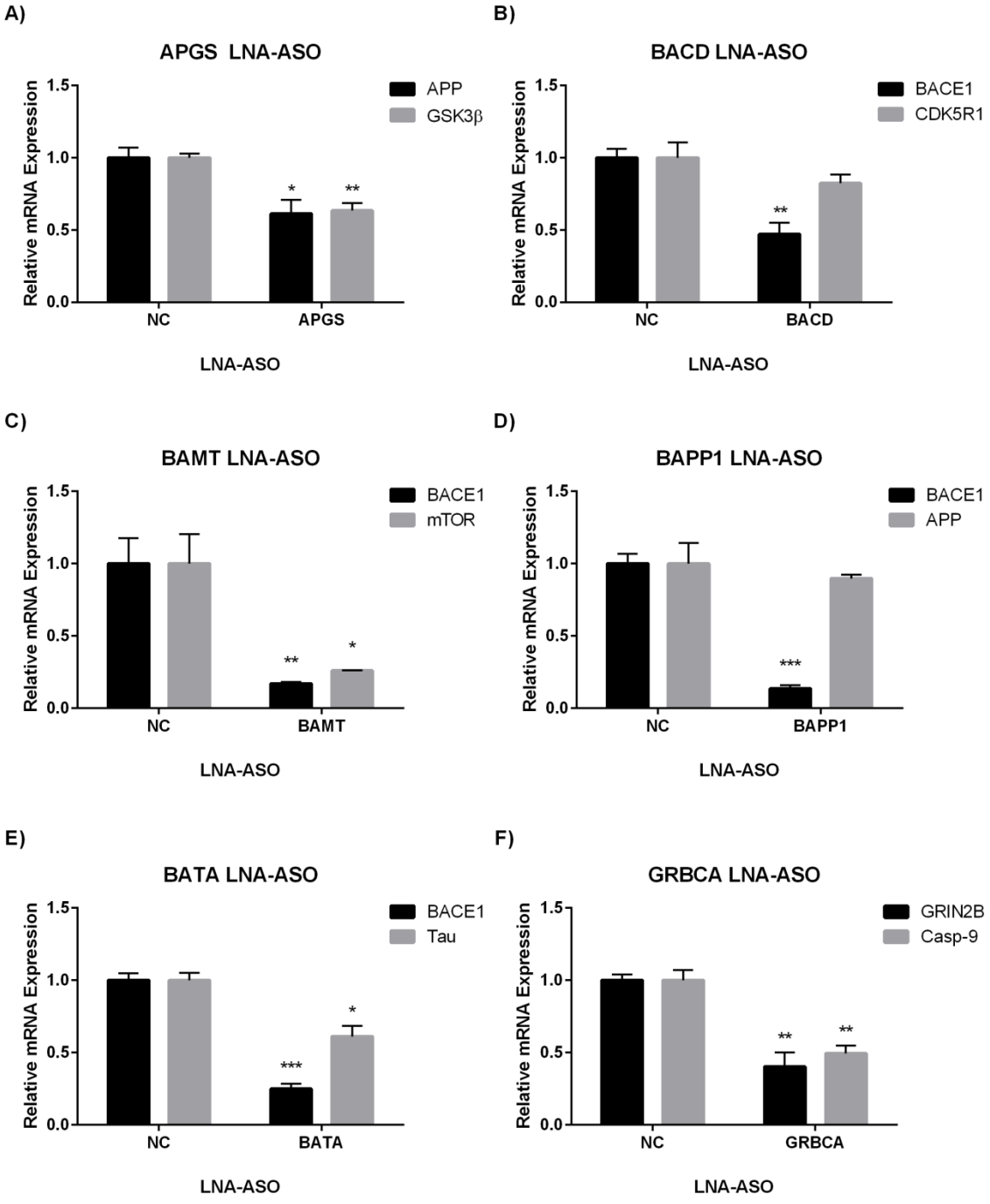
A)
APGS LNA-ASO
Relative mRNA Expression
1.5
1.0
0.5
0.0
APP
GSK3β
*
**
NC
APGS
LNA-ASO
B)
BACD LNA-ASO
Relative mRNA Expression
BACE1
CDK5R1
**
NC
BACD
LNA-ASO
C)
BAMT LNA-ASO
Relative mRNA Expression
BACE1
mTOR
**
*
NC
BAMT
LNA-ASO
D)
BAPP1 LNA-ASO
Relative mRNA Expression
BACE1
APP
***
NC
BAPP1
LNA-ASO
E)
BATA LNA-ASO
Relative mRNA Expression
BACE1
Tau
***
*
NC
BATA
LNA-ASO
F)
GRBCA LNA-ASO
Relative mRNA Expression
GRIN2B
Casp-9
**
**
NC
GRBCA
LNA-ASO

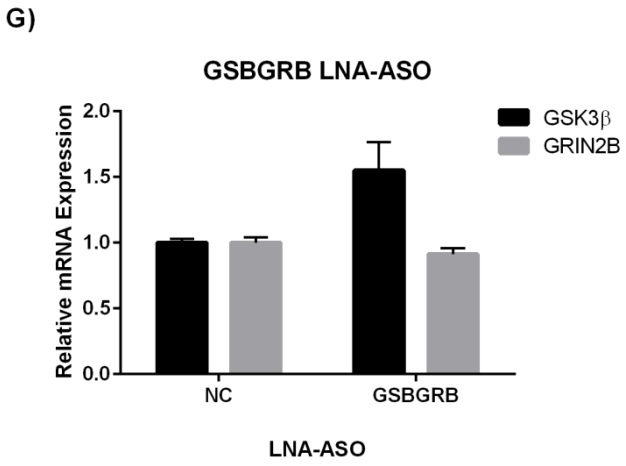

Figure 5.4 Candidate Multi-gene LNA-ASO Screening in HEK293 APPswe Cells. HEK293 APPswe cells were reverse transfected with 20 nM of each candidate multi-gene LNA-ASO or a negative control LNA-ASO ("NC"). RNA was harvested after 48 hours and mRNA expression of the appropriate genes, normalised to *β-Actin*, assessed by qPCR. Gene silencing observed following treatment with **(A)** APGS, **(B)** BACD, **(C)** BAMT, **(D)** BAPP1, **(E)** BATA, **(F)** GRBCA and **(G)** GSBGRB multi-gene LNA-ASOs. Values are mean ± SEM, n = 3, ***p<0.001, **p<0.01, *p<0.05, Student's t-test.

A)

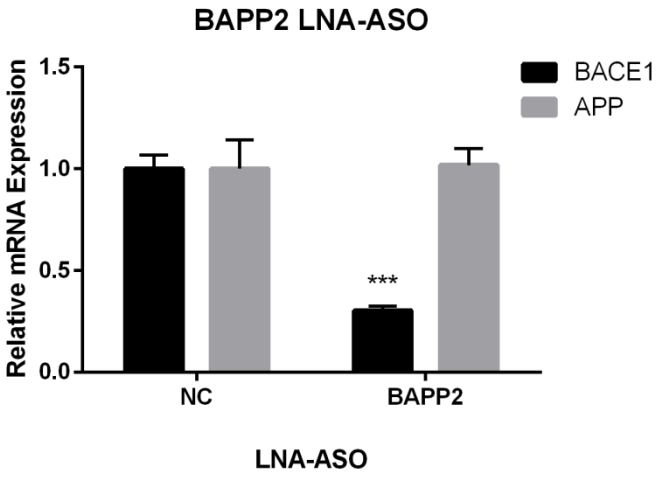
BAPP2 LNA-ASO
Relative mRNA Expression
1.5
1.0
0.5
0.0
BACE1
APP
***
NC
BAPP2
LNA-ASO

B)

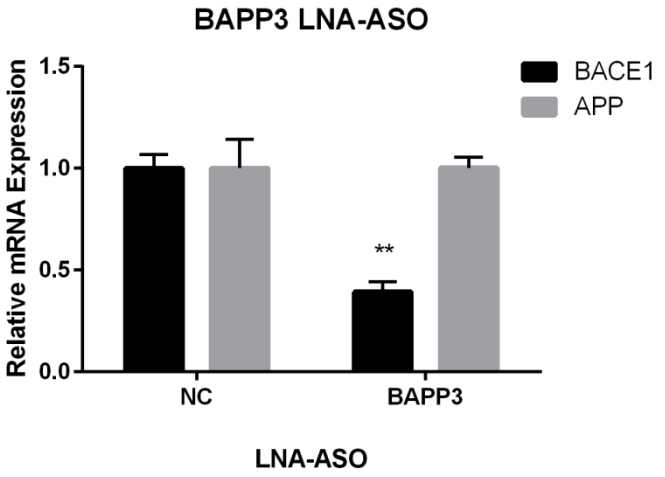
BAPP3 LNA-ASO
Relative mRNA Expression
1.5
1.0
0.5
0.0
BACE1
APP
**
NC
BAPP3
LNA-ASO

C)

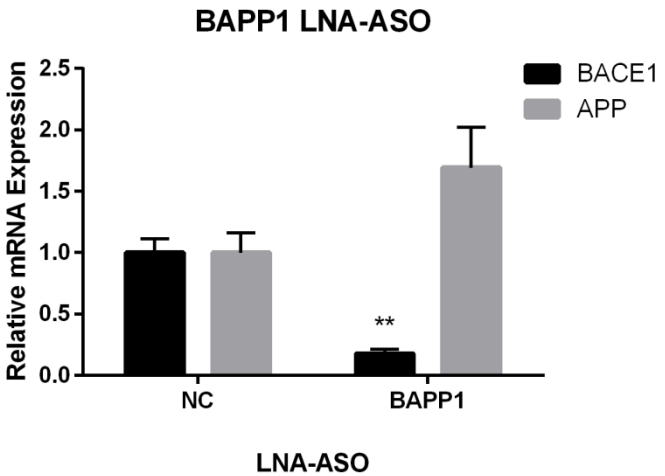
BAPP1 LNA-ASO
Relative mRNA Expression
2.5
2.0
1.5
1.0
0.5
0.0
BACE1
APP
**
NC
BAPP1
LNA-ASO

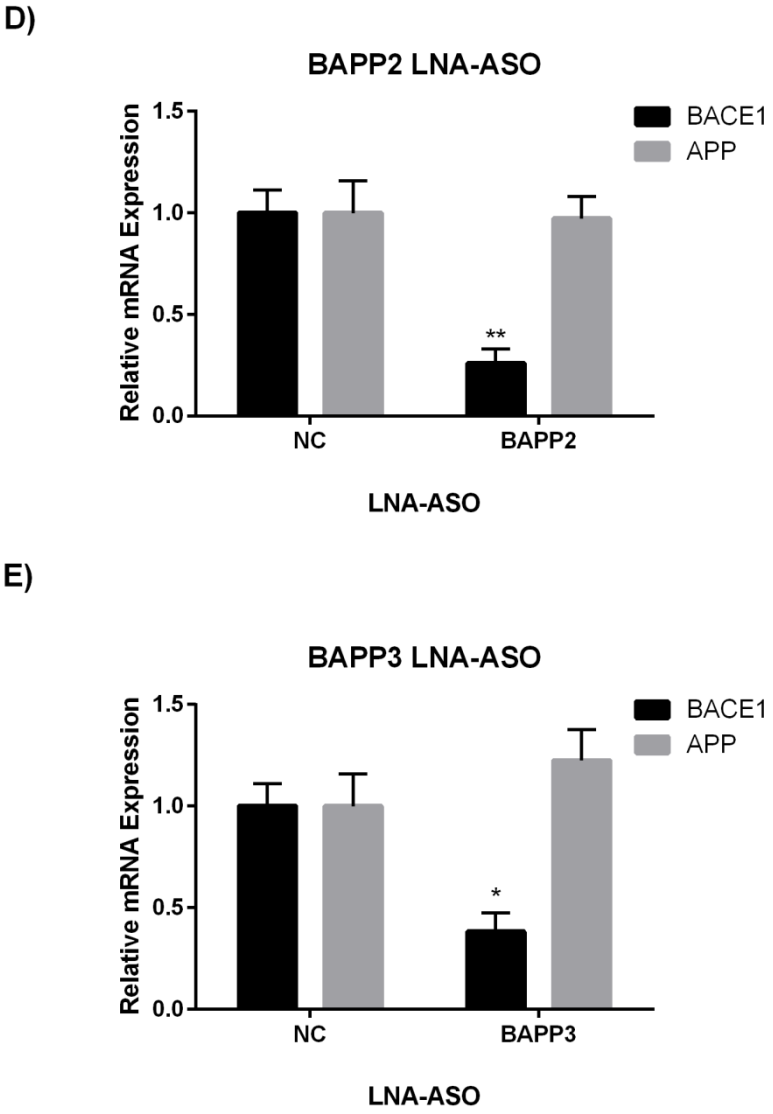

Figure 5.5 Screening of Candidate BAPP Multi-gene LNA-ASOs in HEK293 APPswe Cells. HEK293 APPswe cells were reverse transfected with either 20 nM or 50 nM of candidate BAPP multi-gene LNA-ASOs or a negative control LNA-ASO ("NC"). RNA was harvested after 48 hours and *BACE1* and *APP* mRNA expression, normalised to *β-Actin*, assessed by qPCR. **(A)** BAPP2 and **(B)** BAPP3 multi-gene LNA-ASOs applied at 20 nM dose. **(C)** BAPP1, **(D)** BAPP2 and **(E)** BAPP3 multi-gene LNA-ASOs applied at 50 nM dose. Values are mean ± SEM, n = 3, ***p<0.001, **p<0.01, *p<0.05, Student's t-test.

5.2.4 Characterisation of APGS and BAMT Multi-gene LNA-ASOs in SH-SH5Y Cells

Further characterisation of APGS (**Fig. 5.6**) and BAMT (**Fig. 5.7**) multi-gene LNA-ASOs was performed in SH-SH5Y cells to assess the kinetics of mRNA silencing, LNA-ASO toxicity and effect upon target gene protein expression.

The APGS multi-gene LNA-ASO elicited significant silencing of both *APP* and *GSK3β* mRNA at concentrations ≥ 2.5 nM (IC_{50}: *APP*, 1.60 nM; *GSK3β*, 1.28 nM) (**Fig. 5.6A-C**) which persisted for up to 72 hours (**Fig. 5.6D**). The relatively flat dose-response curve above these concentrations was attributed to saturation of transfection efficiency of SH-SH5Y cells. Although LNA-ASOs are often stated to be of low toxicity *in vivo*, several studies have demonstrated that they may be associated with hepatotoxicity, the extent of which may vary by sequence length and specific sequence motifs[668–670]. Cellular toxicity of the APGS multi-gene LNA-ASO was therefore assessed by the MTS viability assay (**Fig. 5.6E**). This assay measures the conversion of the MTS tetrazolium compound into formazan by NAD(P)H dehydrogenase enzymes in metabolically active cells to provide a measure of cell viability. The MTS assay revealed a dose-dependent reduction in cell viability 48 hours after treatment with the APGS multi-gene LNA-ASO (**Fig. 5.6E**). Protein expression of APP and GSK3β, relative to β-Actin, was assessed by Western blotting 48 hours after LNA-ASO treatment (**Fig. 5.6F**). Both APP and GSK3β protein were expressed at relatively low levels in SH-SH5Y cells. However, there appeared to be a slight reduction in both APP and GSK3β protein expression following treatment with the APGS multi-gene LNA-ASO (**Fig. 5.6F**).

The BAMT multi-gene LNA-ASO also elicited strong silencing of both *BACE1* and *mTOR* mRNA at concentrations ≥ 1 nM (IC_{50}: *BACE1*, 15.81 nM; *mTOR*, 2.74 nM) (**Fig. 5.7A-C**) and this effect persisted 72 hours after LNA-ASO transfection (**Fig. 5.7D**). Promisingly, the BAMT multi-gene LNA-ASO did not appear to significantly decrease cellular viability, even up to concentrations of 100 nM (**Fig. 5.7E**). Both BACE1 and mTOR protein were expressed at relatively low levels in SH-SH5Y cells but there appeared to be a slight reduction in both BACE1 and mTOR protein expression, 48 hours after treatment with the BAMT multi-gene LNA-ASO (**Fig. 5.7F**).

A)

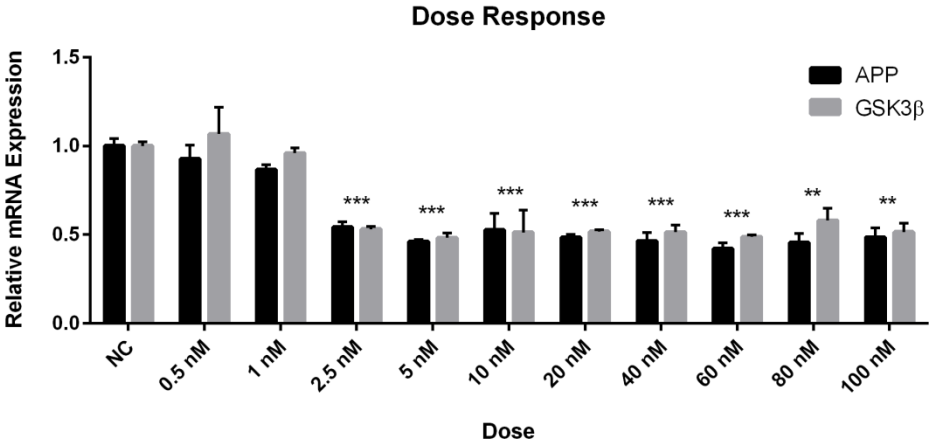
Dose Response
Relative mRNA Expression
1.5
1.0
0.5
0.0
APP
GSK3β
***
***
***
***
***
***
**
**
NC
0.5 nM
1 nM
2.5 nM
5 nM
10 nM
20 nM
40 nM
60 nM
80 nM
100 nM
Dose

B)

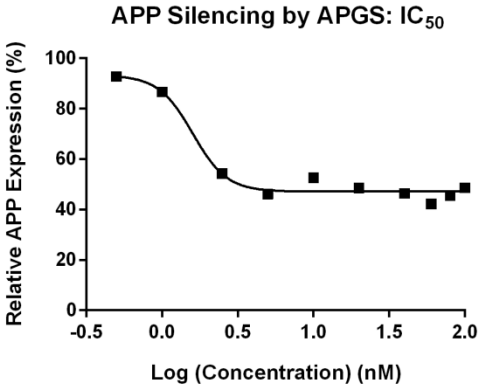
APP Silencing by APGS: IC50
Relative APP Expression (%)
100
80
60
40
20
0
-0.5
0.0
0.5
1.0
1.5
2.0
Log (Concentration) (nM)

C)

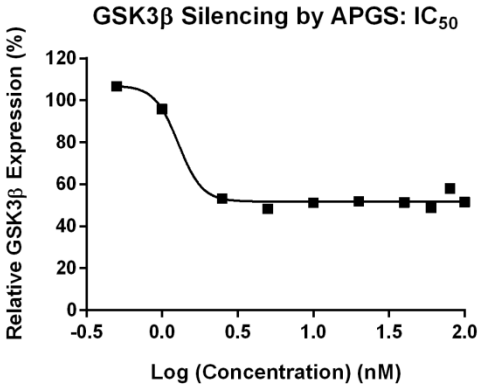
GSK3β Silencing by APGS: IC50
Relative GSK3β Expression (%)
120
100
80
60
40
20
0
-0.5
0.0
0.5
1.0
1.5
2.0
Log (Concentration) (nM)

D)

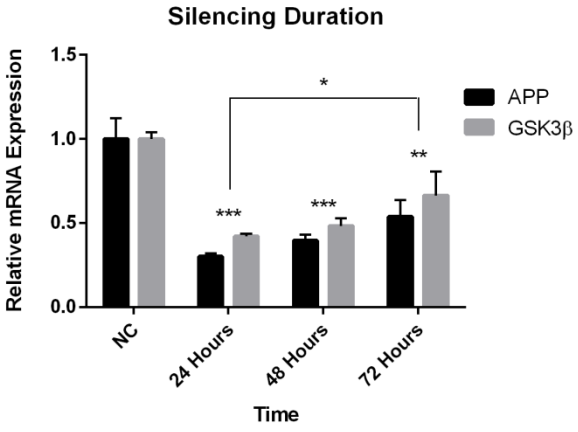
Silencing Duration
Relative mRNA Expression
1.5
1.0
0.5
0.0
*
**
***
***
APP
GSK3β
NC
24 Hours
48 Hours
72 Hours
Time

E)

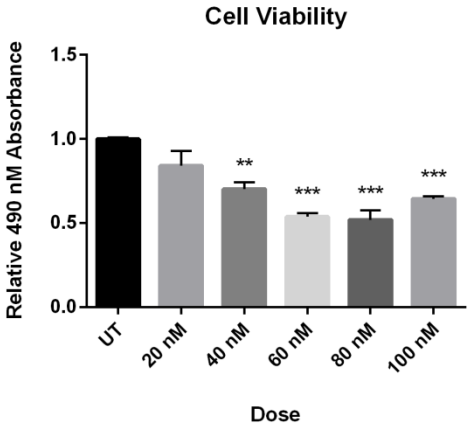
Cell Viability
Relative 490 nM Absorbance
1.5
1.0
0.5
0.0
**
***
***
***
UT
20 nM
40 nM
60 nM
80 nM
100 nM
Dose

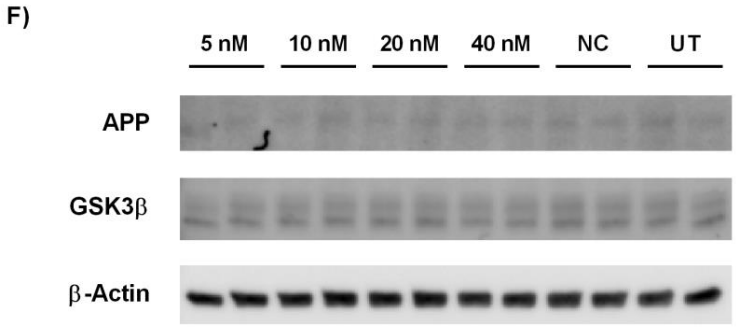

Figure 5.6 Characterisation of APGS LNA-ASO Silencing in SH-SH5Y Cells. SH-SH5Y cells were left untreated ("UT") or transfected with the APGS multi-gene LNA-ASO or a negative control LNA-ASO ("NC", 20 nM) at shown concentrations. mRNA and protein expression, normalised to β-Actin, was assessed by qPCR and Western blotting after 48 hours. **(A)** Dose-response curve of *APP* and *GSK3β* mRNA expression following APGS multi-gene LNA-ASO treatment relative to NC. **(B-C)** IC_{50} plots for **(B)** *APP* and **(C)** *GSK3β* mRNA expression following APGS multi-gene LNA-ASO treatment relative to NC. **(D)** Duration of gene silencing following transfection of 20 nM APGS or NC LNA-ASOs after 24, 48 and 72 hours. **(E)** Cell viability assessed by MTS assay 48 hours after LNA-ASO treatment. **(F)** SH-SH5Y cell lysates (50 µg) probed by Western blot for APP, GSK3β, and the loading control, β-Actin. Values are mean ± SEM, n = 3, ***p<0.001, **p<0.01, *p<0.05, one-way ANOVA followed by Tukey's post-hoc test.

A)

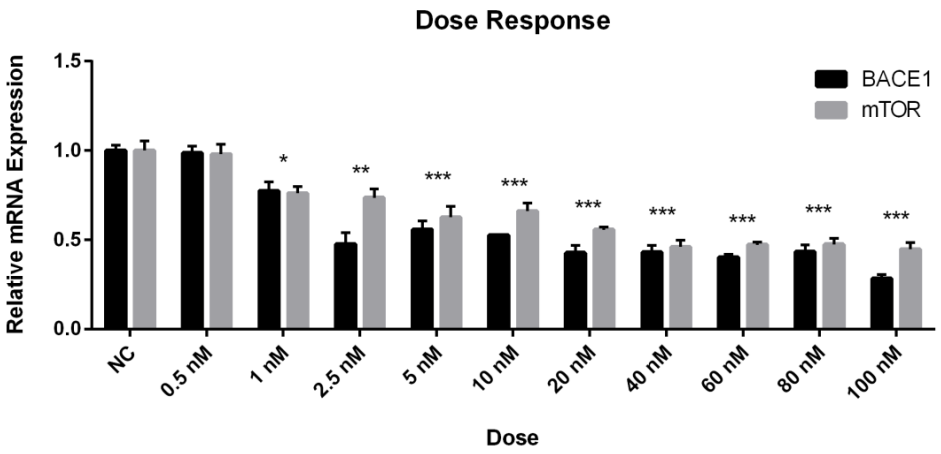
Dose Response
Relative mRNA Expression
1.5
1.0
0.5
0.0
BACE1
mTOR
*
**
***
***
***
***
***
***
NC
0.5 nM
1 nM
2.5 nM
5 nM
10 nM
20 nM
40 nM
60 nM
80 nM
100 nM
Dose

B)

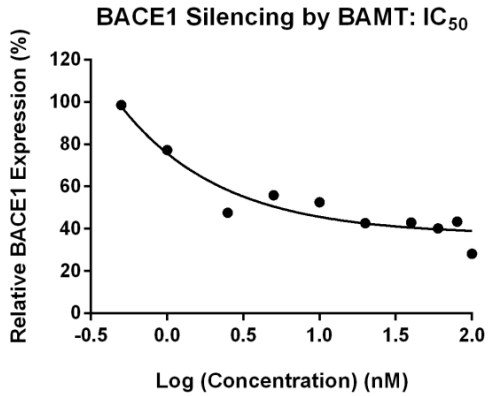
BACE1 Silencing by BAMT: IC50
Relative BACE1 Expression (%)
120
100
80
60
40
20
0
-0.5
0.0
0.5
1.0
1.5
2.0
Log (Concentration) (nM)

C)

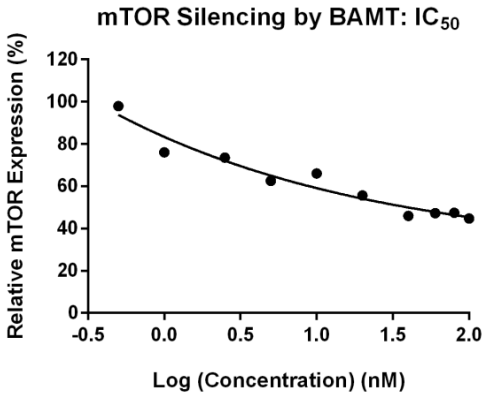
mTOR Silencing by BAMT: IC50
Relative mTOR Expression (%)
120
100
80
60
40
20
0
-0.5
0.0
0.5
1.0
1.5
2.0
Log (Concentration) (nM)

D)

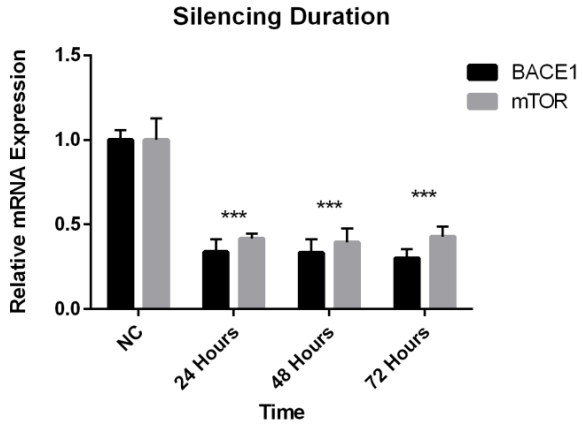
Silencing Duration
Relative mRNA Expression
1.5
1.0
0.5
0.0
BACE1
mTOR
***
***
***
NC
24 Hours
48 Hours
72 Hours
Time

E)

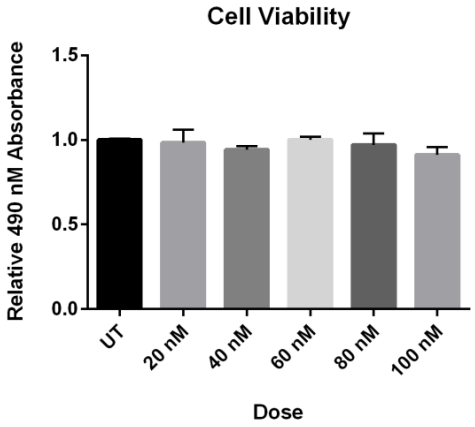
Cell Viability
Relative 490 nM Absorbance
1.5
1.0
0.5
0.0
UT
20 nM
40 nM
60 nM
80 nM
100 nM
Dose

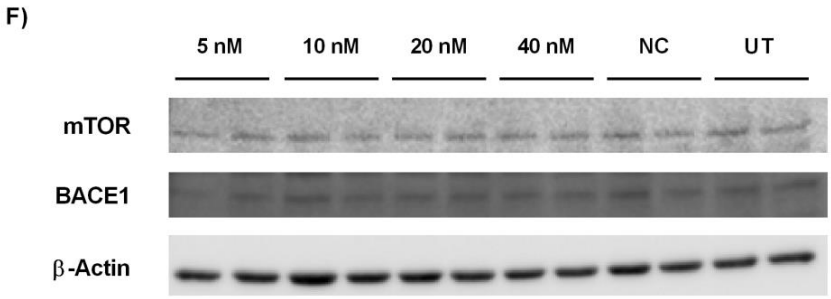

Figure 5.7 Characterisation of BAMT LNA-ASO Silencing in SH-SH5Y Cells. SH-SH5Y cells were left untreated ("UT") or transfected with the BAMT multi-gene LNA-ASO or a negative control LNA-ASO ("NC", 20 nM) at shown concentrations. mRNA and protein expression, normalised to β-Actin, was assessed by qPCR and Western blotting after 48 hours. **(A)** Dose-response curve of *BACE1* and *mTOR* mRNA expression following BAMT multi-gene treatment relative to NC LNA-ASO. **(B-C)** IC_{50} plots for **(B)** *BACE1* and **(C)** *mTOR* mRNA expression following BAMT multi-gene LNA-ASO treatment relative to NC. **(D)** Duration of gene silencing following transfection of 20 nM BAMT or NC LNA-ASOs after 24, 48 and 72 hours. **(E)** Cell viability assessed by MTS assay 48 hours after BAMT LNA-ASO treatment. **(F)** SH-SH5Y cell lysates (50 µg) probed by Western blot for BACE1, mTOR and the loading control, β-Actin. Values are mean ± SEM, n = 3, ***p<0.001, **p<0.01, *p<0.05, one-way ANOVA followed by Tukey's post-hoc test.

5.2.5 Characterisation of APGS and BAMT Multi-gene LNA-ASOs in HEK293 APPswe Cells

Further characterisation of APGS (**Fig. 5.8**) and BAMT (**Fig. 5.9**) multi-gene LNA-ASOs was also performed in HEK293 APPswe cells. The APGS multi-gene LNA-ASO significantly silenced *APP* and *GSK3β* mRNA expression in a dose-dependent manner at concentrations ≥ 1 nM (IC_{50}: *APP*, 2.86 nM; *GSK3β*, 1.82 nM) (**Fig. 5.8A-C**). There was a time-dependent reduction in mRNA silencing from 24 to 72 hours with silencing alleviated 72 hours after treatment (**Fig. 5.8D**). As in SH-SH5Y cells, the APGS multi-gene LNA-ASO was associated with a dose-dependent increase in cellular toxicity (**Fig. 5.8E**). However, in contrast to SH-SH5Y cells, APP and GSK3β protein were expressed at higher levels and revealed a dose-dependent reduction in protein expression of both APP and the longer isoform 1 of GSK3β[671,672] (**Fig. 5.8F**).

Similarly, the BAMT multi-gene LNA-ASO elicited strong dose-dependent silencing of both *BACE1* and *mTOR* mRNA at concentrations ≥ 10 nM (IC_{50}: *BACE1,* 6.90 nM; *mTOR,* 10.18 nM) (**Fig. 5.9A-C**). In contrast to SH-SH5Y cells, there was a time-dependent alleviation of silencing from 24 to 72 hours which resulted in a significant upregulation of mTOR expression at 72 hours (**Fig. 5.9D**). There appeared to be a dose-dependent reduction in cellular viability following BAMT multi-gene LNA-ASO treatment but this was only significant at the highest concentrations (**Fig. 5.9E**). BACE1 protein expression was relatively low in HEK293 APPswe cells making it challenging to identify changes in protein expression (**Fig. 5.9F**). However, there did appear to a dose-dependent reduction in mTOR protein expression following BAMT LNA-ASO treatment (**Fig. 5.9F**).

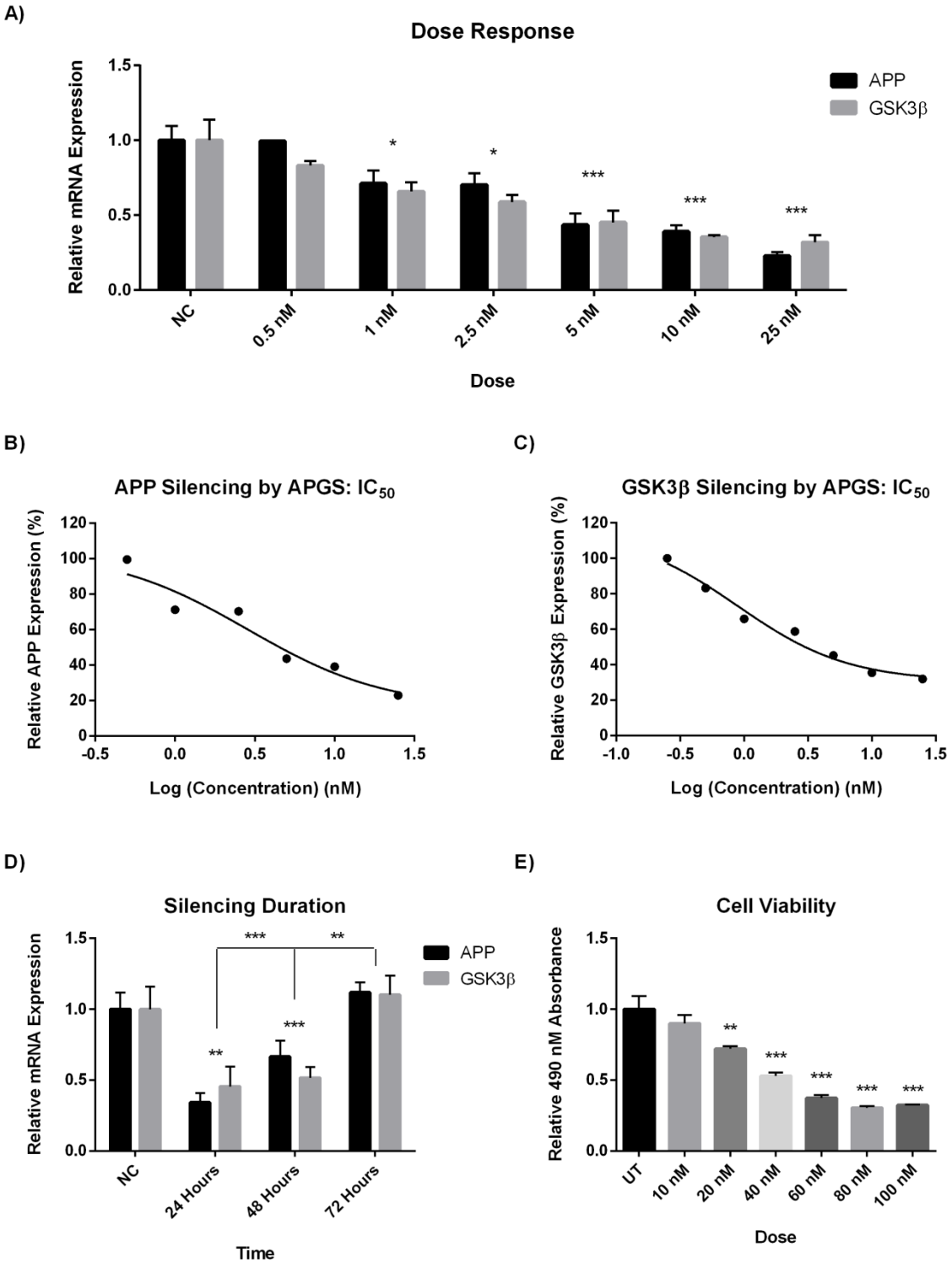
A)
Dose Response
Relative mRNA Expression
1.5
1.0
0.5
0.0
APP
GSK3β
*
*
***
***
***
NC
0.5 nM
1 nM
2.5 nM
5 nM
10 nM
25 nM
Dose
B)
APP Silencing by APGS: IC50
Relative APP Expression (%)
120
100
80
60
40
20
0
-0.5
0.0
0.5
1.0
1.5
Log (Concentration) (nM)
C)
GSK3β Silencing by APGS: IC50
Relative GSK3β Expression (%)
120
100
80
60
40
20
0
-1.0
-0.5
0.0
0.5
1.0
1.5
Log (Concentration) (nM)
D)
Silencing Duration
Relative mRNA Expression
1.5
1.0
0.5
0.0
***
**
**
***
APP
GSK3β
NC
24 Hours
48 Hours
72 Hours
Time
E)
Cell Viability
Relative 490 nM Absorbance
1.5
1.0
0.5
0.0
**
***
***
***
***
UT
10 nM
20 nM
40 nM
60 nM
80 nM
100 nM
Dose

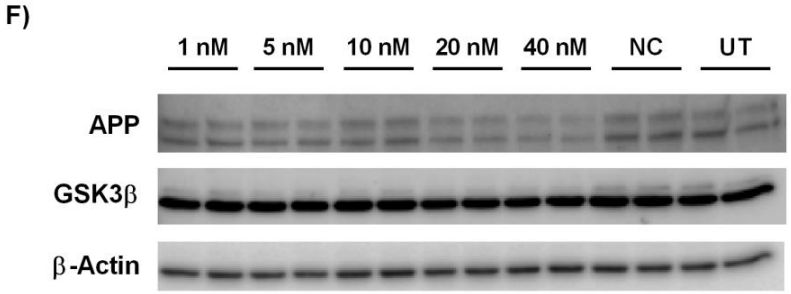

Figure 5.8 Characterisation of APGS LNA-ASO Silencing in HEK293 APPswe Cells. HEK293 APPswe cells were left untreated ("UT") or transfected with the APGS multi-gene LNA-ASO or a negative control LNA-ASO ("NC") at shown concentrations. mRNA and protein expression, normalised to β-Actin, was assessed by qPCR and Western blotting after 48 hours. **(A)** Dose-response curve of *APP* and *GSK3β* mRNA expression following APGS multi-gene LNA-ASO treatment relative to a NC LNA-ASO (10 nM). **(B-C)** IC_{50} plots for **(B)** *APP* and **(C)** *GSK3β* mRNA expression following APGS multi-gene LNA-ASO treatment relative to NC. **(D)** Duration of gene silencing following transfection of 20 nM APGS or NC LNA-ASOs. **(E)** Cell viability assessed by MTS assay 48 hours after APGS LNA-ASO treatment. **(F)** HEK293 APPswe cell lysates (50 μg) probed by Western blot for APP, GSK3β and the loading control, β-Actin. Values are mean ± SEM, n = 3, ***p<0.001, **p<0.01, *p<0.05, one-way ANOVA followed by Tukey's post-hoc test.

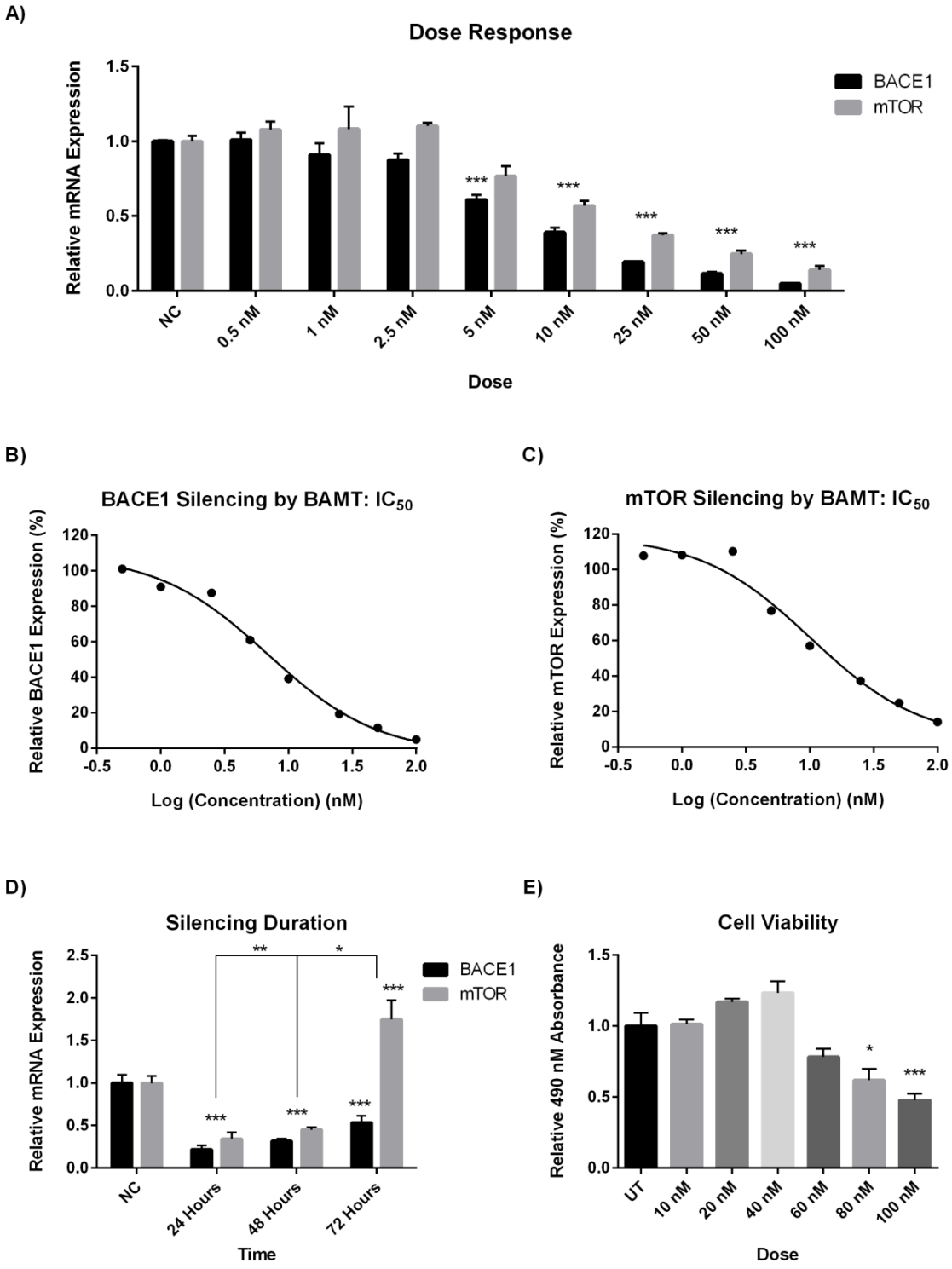
A)
Dose Response
Relative mRNA Expression
1.5
1.0
0.5
0.0
BACE1
mTOR
***
***
***
***
***
NC
0.5 nM
1 nM
2.5 nM
5 nM
10 nM
25 nM
50 nM
100 nM
Dose
B)
BACE1 Silencing by BAMT: IC50
Relative BACE1 Expression (%)
120
100
80
60
40
20
0
-0.5
0.0
0.5
1.0
1.5
2.0
Log (Concentration) (nM)
C)
mTOR Silencing by BAMT: IC50
Relative mTOR Expression (%)
120
100
80
60
40
20
0
-0.5
0.0
0.5
1.0
1.5
2.0
Log (Concentration) (nM)
D)
Silencing Duration
Relative mRNA Expression
2.5
2.0
1.5
1.0
0.5
0.0
**
*
***
***
***
***
BACE1
mTOR
NC
24 Hours
48 Hours
72 Hours
Time
E)
Cell Viability
Relative 490 nM Absorbance
1.5
1.0
0.5
0.0
*
***
UT
10 nM
20 nM
40 nM
60 nM
80 nM
100 nM
Dose

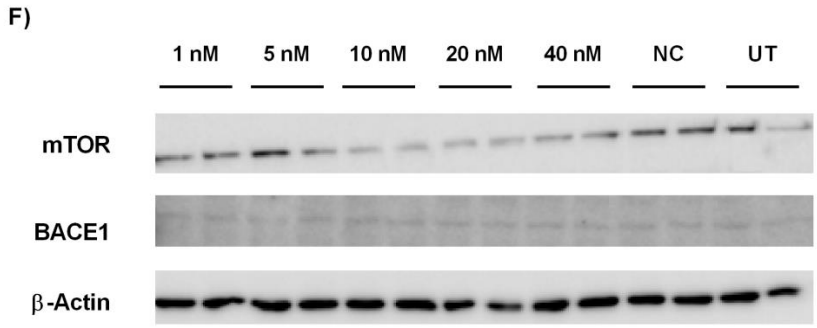

Figure 5.9 Characterisation of BAMT LNA-ASO Silencing in HEK293 APPswe Cells. HEK293 APPswe cells were left untreated ("UT") or transfected with the BAMT multi-gene LNA-ASO or a negative control LNA-ASO ("NC"). mRNA and protein expression, normalised to β-Actin, was assessed by qPCR and Western blotting after 48 hours. **(A)** Dose-response curve of *BACE1* and *mTOR* mRNA expression following BAMT multi-gene LNA-ASO treatment relative to NC LNA-ASO (10 nM). **(B-C)** IC_{50} plots for **(B)** *BACE1* and **(C)** *mTOR* mRNA expression following BAMT multi-gene LNA-ASO treatment relative to NC. **(D)** Duration of gene silencing following transfection of 20 nM BAMT or NC LNA-ASOs. **(E)** Cell viability assessed by MTS assay 48 hours after BAMT LNA-ASO treatment. **(F)** HEK293 APPswe cell lysates (50 μg) probed by Western blot for BACE1, mTOR and the loading control, β-Actin. Values are mean ± SEM, n = 3, ***p<0.001, **p<0.01, *p<0.05, one-way ANOVA followed by Tukey's post-hoc test.

5.2.6 Gene Silencing by BAMT Multi-gene LNA-ASO is Specific to Targeted Genes

The LNA-ASOs in this study were of a short length (13-14 nucleotides). Given the high potential binding affinity of LNA-ASOs, this raised concern for potential off-target effects due to the increasing likelihood of similar sequences with shorter sequence lengths. While candidate sequences were blasted to minimise the risk of off-target binding within non-targeted genes, the specificity of gene silencing was assessed.

To address this, a gene target, *HN1*, was identified which contained a sequence highly similar to that targeted by the BAMT multi-gene LNA-ASO, differing only by a single nucleotide (adenine instead of thymine at penultimate position within targeted sequence; CATTGTCTCTA**A**C). Both SH-SH5Y and HEK293 APPswe cells were reverse transfected with the BAMT multi-gene LNA-ASO at varying doses and *HN1* mRNA expression assessed, relative to *β-Actin*, after 48 hours. Promisingly, there was no effect upon *HN1* expression at any dose in either HEK293 APPswe cells or SH-SH5Y cells, suggesting specificity of the BAMT multi-gene LNA-ASO (**Fig. 5.10**).

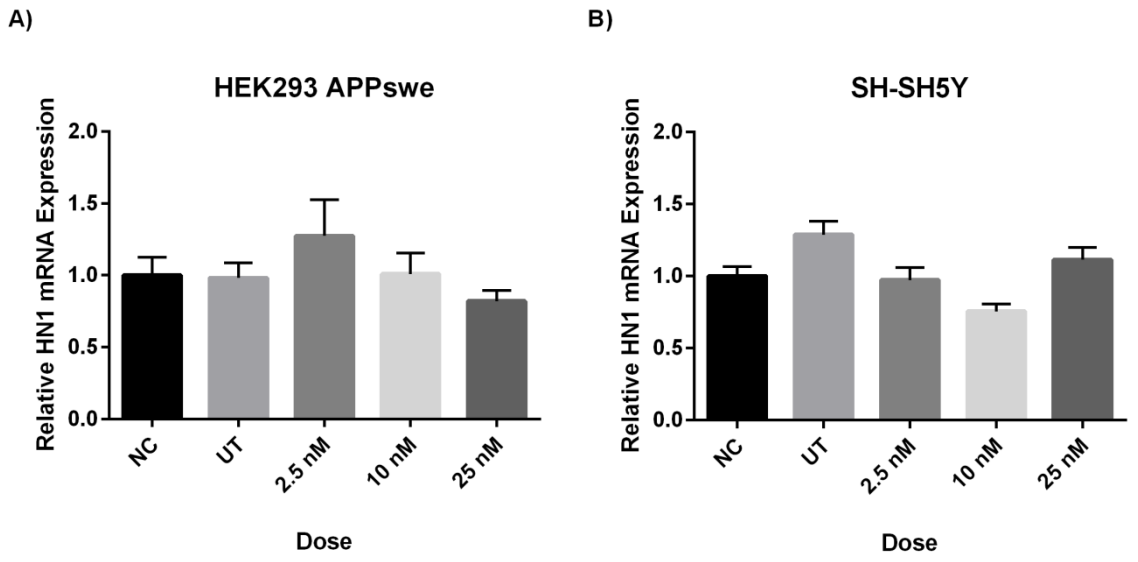

Figure 5.10 Specificity of Gene Targeting by BAMT Multi-gene LNA-ASO. HEK293 APPswe cells and SH-SH5Y cells were left untreated ("UT") or transfected with 2.5 nM, 10 nM or 25 nM of the BAMT multi-gene LNA-ASO or with a negative control LNA-ASO ("NC", 10 nM). Expression of *HN1* mRNA was assessed, relative to *β-Actin*, after 48 hours by qPCR. There was no effect upon *HN1* expression in either **(A)** HEK293 APPswe cells or **(B)** SH-SH5Y cells following BAMT multi-gene LNA-ASO treatment. Values are mean ± SEM, n = 3, one-way ANOVA.

5.2.7 APGS and BAMT Multi-gene LNA-ASOs Reduce Amyloid-β (42) Production by HEK293 APPswe Cells

APGS and BAMT multi-gene LNA-ASOs were next assessed for their effect upon an AD-relevant phenotype; amyloid-β production. To ensure that samples fell within the optimal concentration parameters of the amyloid-β ELISA kit, a preliminary study was performed to assess the quantity of amyloid-β (42) produced by SH-SH5Y and HEK293 APPswe cells. SH-SH5Y and HEK293 APPswe cells were plated in 12-well cell culture plates. After 48 hours, cell lysates and supernatant were collected before the supernatant was concentrated using centrifugal filters with a 3 kDa molecular weight cut-off. The quantity of amyloid-β (42) present in cell lysates, concentrated supernatant and in concentrated supernatant diluted 1:5 was then determined. As expected, HEK293 APPswe cells produced a much higher quantity of secreted amyloid-β (42) than SH-SH5Y cells and the non-linear constraints of the kit were evident at high concentrations of amyloid-β (42) (**Fig. 5.11**). For further amyloid-β experiments, non-concentrated supernatant was derived from HEK293 APPswe cells and diluted at a ratio of 1:1 with ELISA kit diluent.

To assess the impact upon amyloid-β (42) production, HEK293 APPswe cells were reverse transfected with either APGS (**Fig. 5.12**) or BAMT (**Fig. 5.13**) multi-gene LNA-ASOs and amyloid-β (42) levels assessed after 48 hours. Promisingly, this resulted in a dose-dependent reduction in amyloid-β (42) production which paralleled the dose-dependent silencing of target mRNA following treatment with both APGS (89.3% amyloid-β (42) reduction at 10 nM dose) (**Fig. 5.12**) and BAMT LNA-ASOs (75.6% amyloid-β (42) reduction at 20 nM dose) (**Fig. 5.13**). These results suggest that

treatment with APGS and BAMT multi-gene LNA-ASOs results in both mRNA and protein silencing of target genes which serves to attenuate amyloid-β production. This is presumably driven by a reduction in total APP expression (APGS) or in APP processing following the silencing of BACE1 (BAMT).

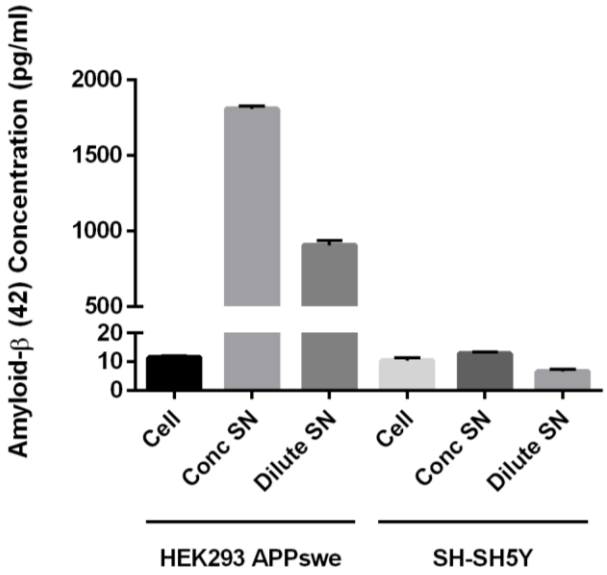

Figure 5.11 Quantification of Amyloid-β (42) Production by HEK293 APPswe and SH-SH5Y Cells. HEK293 APPswe cells and SH-SH5Y cells were plated in 12-well cell culture plates at a confluency of 4 x 10^5 cells/well. After 48 hours, the cell lysates and supernatant were collected and the supernatant concentrated using centrifugal filters with a 3 kDa molecular weight cut-off. The quantity of amyloid-β (42) present in cell lysates ("cell"), concentrated supernatant ("conc SN") and concentrated supernatant diluted 1:5 with kit standard diluent ("dilute SN") was determined by an amyloid-β (42) ELISA. Values are mean ± SEM, n = 3.

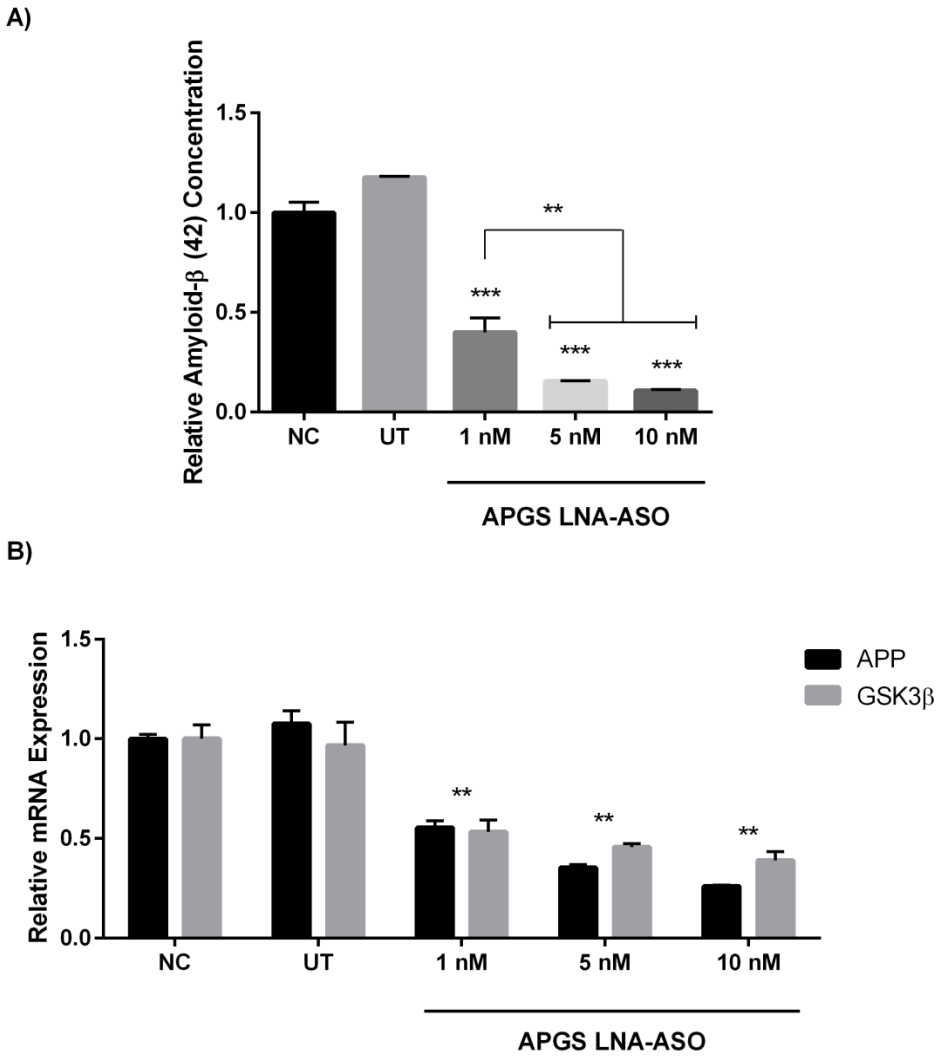

Figure 5.12 Reduced Amyloid-β (42) Production Following Treatment with APGS Multi-gene LNA-ASO. HEK293 APPswe cells were left untreated ("UT") or reverse transfected with the APGS multi-gene LNA-ASO or a negative control LNA-ASO ("NC", 10 nM). Supernatant was collected 48 hours after transfection, diluted 1:1, and amyloid-β (42) concentration assessed by ELISA. *APP* and *GSK3β* mRNA expression, normalised to *β-Actin*, was also assessed after 48 hours by qPCR. Both **(A)** amyloid-β (42) concentration and **(B)** *APP* and *GSK3β* mRNA expression were significantly silenced following APGS multi-gene LNA-ASO treatment. Values are mean ± SEM, n = 3, ***p<0.001, **p<0.01, one-way ANOVA followed by Tukey's post-hoc test.

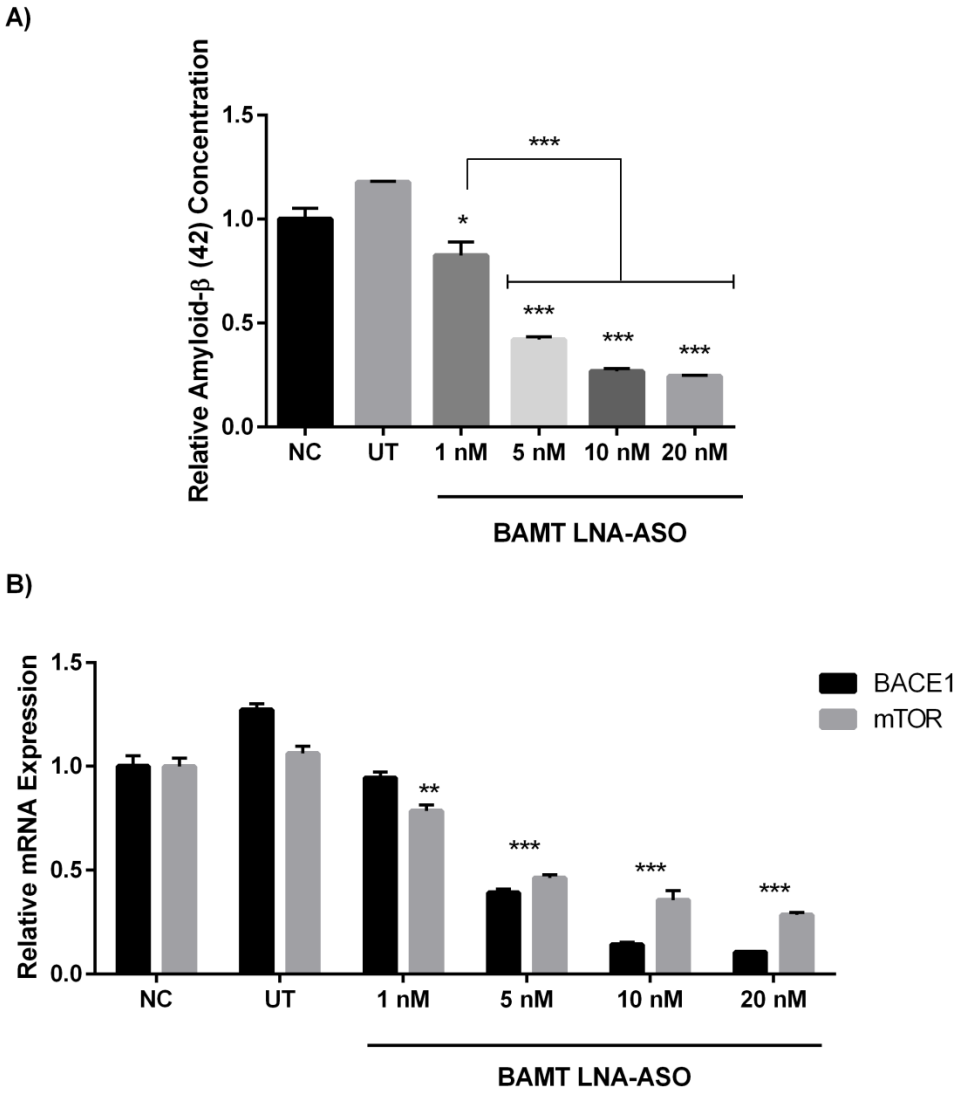

Figure 5.13 Reduced Amyloid-β (42) Production Following Treatment with BAMT Multi-gene LNA-ASO. HEK293 APPswe cells were left untreated ("UT") or reverse transfected with the BAMT multi-gene LNA-ASO or a negative control LNA-ASO ("NC", 10 nM). Supernatant was collected 48 hours after transfection, diluted 1:1, and amyloid-β (42) concentration assessed by ELISA. *BACE1* and *mTOR* mRNA expression, normalised to *β-Actin*, was assessed after 48 hours by qPCR. Both **(A)** amyloid-β (42) concentration and **(B)** *BACE1* and *mTOR* mRNA expression were significantly silenced following BAMT multi-gene LNA-ASO treatment. Values are mean ± SEM, n = 3, ***p<0.001, **p<0.01, *p<0.05, one-way ANOVA followed by Tukey's post-hoc test.

5.2.8 Amyloid-β (42) Production is Reduced to Comparable Levels by Single-gene and Multi-gene Targeting LNA-ASOs

The novel advantage of multi-gene targeting LNA-ASOs is that they are potentially able to simultaneously silence the expression of two different genes either within one or two different pathways. Depending upon the identity of the genes targeted, this could produce either relatively independent or synergistic effects upon phenotypic outcomes. Therefore, it was important to assess the impact of targeting two separate genes simultaneously in comparison to silencing each alone.

For this purpose, single-gene LNA-ASOs were designed which comprised a similar structure to the multi-gene LNA-ASOs but which were predicted to individually target *APP*, *GSK3β*, *BACE1* or *mTOR* (**Table 5.4**). HEK293 APPswe cells were reverse transfected with 10 nM of each single-gene LNA-ASO, the corresponding multi-gene LNA-ASO or a negative control LNA-ASO and the relevant mRNA expression, relative to *β-Actin*, assessed by qPCR after 48 hours (**Fig. 5.14**). This showed successful single-gene targeting of mRNA expression, at a similar level to that achieved by multi-gene targeting LNA-ASOs, by APP-3 and GSK3β-2 (**Fig. 5.14A**) and by BACE1-2, mTOR-1 and mTOR-3 (**Fig. 5.14B**). APP-3, GSK3β-2, BACE1-2 and mTOR-3 were selected for further study.

Subsequently, multi-gene and single-gene LNA-ASOs, targeting either *APP* and *GSK3β* (**Fig. 5.15**) or *BACE1* and *mTOR* (**Fig. 5.16**), were compared for their ability to attenuate amyloid-β (42) production. HEK293 APPswe cells were reverse transfected with either 10 nM of APGS (**Fig. 5.15**) or BAMT (**Fig. 5.16**) multi-gene LNA-ASO, 10

nM of the corresponding single-gene LNA-ASOs or a combination of either 5 nM or 10 nM of each corresponding single-gene LNA-ASO (i.e. 5/10 nM APP-3 and 5/10 nM GSK3β-2) to control for the multi-gene aspect. This revealed that the APGS multi-gene LNA-ASO resulted in a similar level of silencing of both mRNA and amyloid-β (42) production as either APP-3 alone or the combination of 5/10 nM of APP-3 and GSK3β-2 single-gene LNA-ASOs (**Fig. 5.15**). Correspondingly, the BAMT multi-gene LNA-ASO also significantly silenced amyloid-β (42) production to a similar extent as either BACE1-2 alone or the combination of 5/10 nM of BACE1-2 and mTOR-3 single-gene LNA-ASOs (**Fig. 5.16B**). This was despite a slightly higher degree of silencing of *BACE1* mRNA by BACE1-2 alone in comparison to the BAMT multi-gene LNA-ASO (**Fig. 5.16A**).

Together, these results suggest that APGS and BAMT multi-gene LNA-ASOs produce effective silencing of amyloid-β (42) expression, with comparable efficacy to that elicited by single-gene LNA-ASOs.

Table 5.4 Human Single-gene LNA-ASO Candidates.

LNA-ASO	Gene Targeted	Sequence	Chromosome Location of Target Sequence (GRCh38)
APP-1	*APP*	+C+A+Ccatgcgca+C+A+T	*APP:* Chr. 21: 26096006-26096019
APP-2	*APP*	+T+A+Gcatattga+A+C+A	*APP:* Chr. 21: 26095934-26095947
APP-3	*APP*	+T+G+Acgttctgc+C+T+C	*APP:* Chr. 21: 26075669-26075682
BACE1-1	*BACE1*	+T+A+Acctcaccc+A+T+T	*BACE1:* Chr. 11: 117310519-117310532
BACE1-2	*BACE1*	+C+C+Ataacagtg+C+C+C	*BACE1:* Chr. 11: 117310885-117310898
GSK3β-1	*GSK3β*	+A+C+Accaaatga+T+C+C	*GSK3β:* Chr. 3: 119913606-119913619
GSK3β-2	*GSK3β*	+T+T+Ctcctgaat+C+A+C	*GSK3β:* Chr. 3: 119913640-119913653
mTOR-1	*mTOR*	+C+C+Acaccgtc+C+A+A	*mTOR:* Chr. 1: 11259319-11259331
mTOR-2	*mTOR*	+T+T+Atctcgaa+C+C+C	*mTOR:* Chr. 1: 11259733-11259745
mTOR-3	*mTOR*	+C+T+Cacggaga+A+C+C	*mTOR:* Chr. 1: 11112856-11112868
mTOR-4	*mTOR*	+T+G+Gcaagacg+G+C+C	*mTOR:* Chr. 1: 11111997-11112009

LNA-ASOs have a fully phosphorothioated backbone with 7-8 DNA monomers flanked on either end by 3 LNA-modified bases, + indicates LNA-modified base.

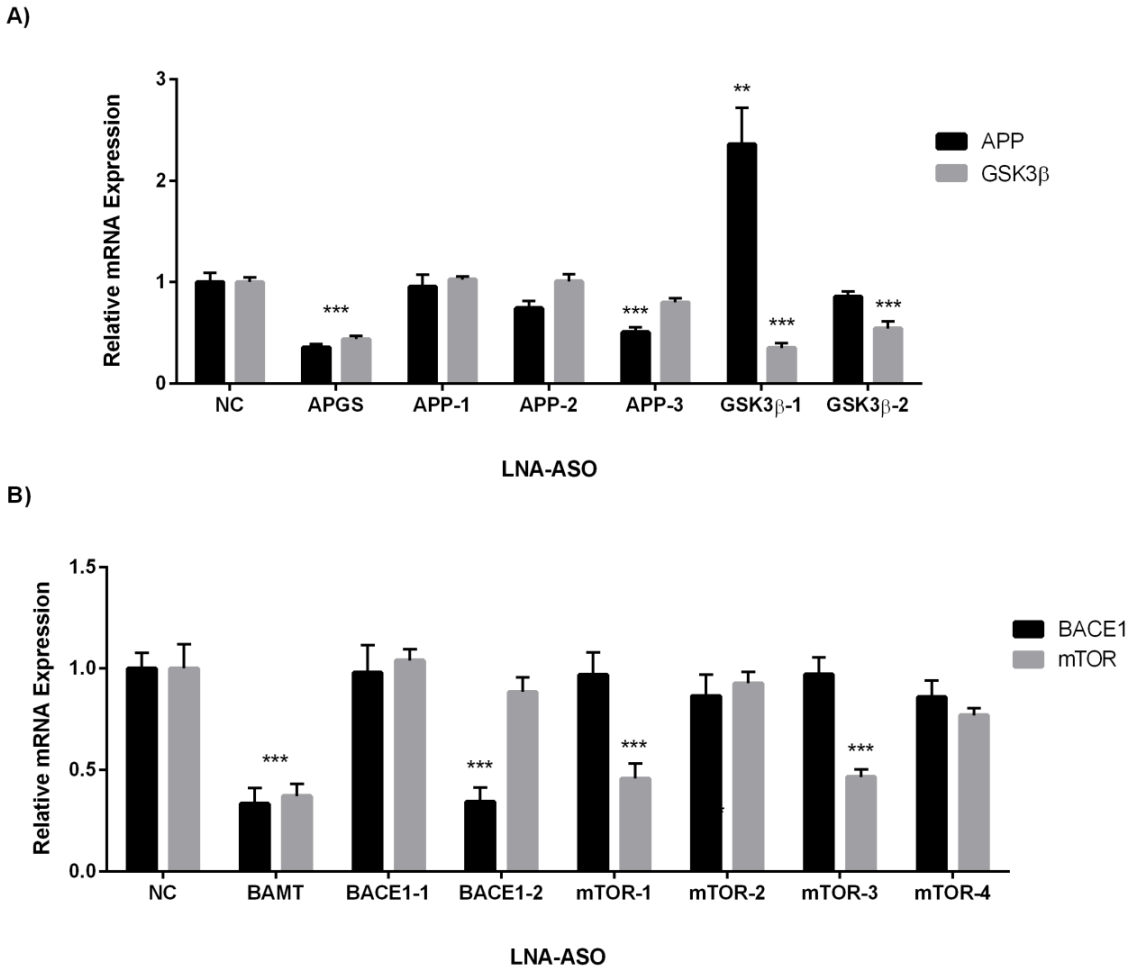

Figure 5.14 Candidate Single-gene LNA-ASO Screening in HEK293 APPswe Cells. HEK293 APPswe cells were reverse transfected with 10 nM of the candidate single-gene LNA-ASOs, multi-gene LNA-ASOs ("APGS" or "BAMT") or a negative control LNA-ASO ("NC"). RNA was harvested after 48 hours and mRNA expression of the appropriate genes, normalised to *β-Actin*, assessed by qPCR. **(A)** *APP* and *GSK3β* mRNA expression following treatment with single-gene and multi-gene targeting LNA-ASOs. **(B)** *BACE1* and *mTOR* mRNA expression following treatment with single-gene and multi-gene targeting LNA-ASOs. Values are mean ± SEM, n = 6, ***p<0.001, one-way ANOVA followed by Tukey's post-hoc test.

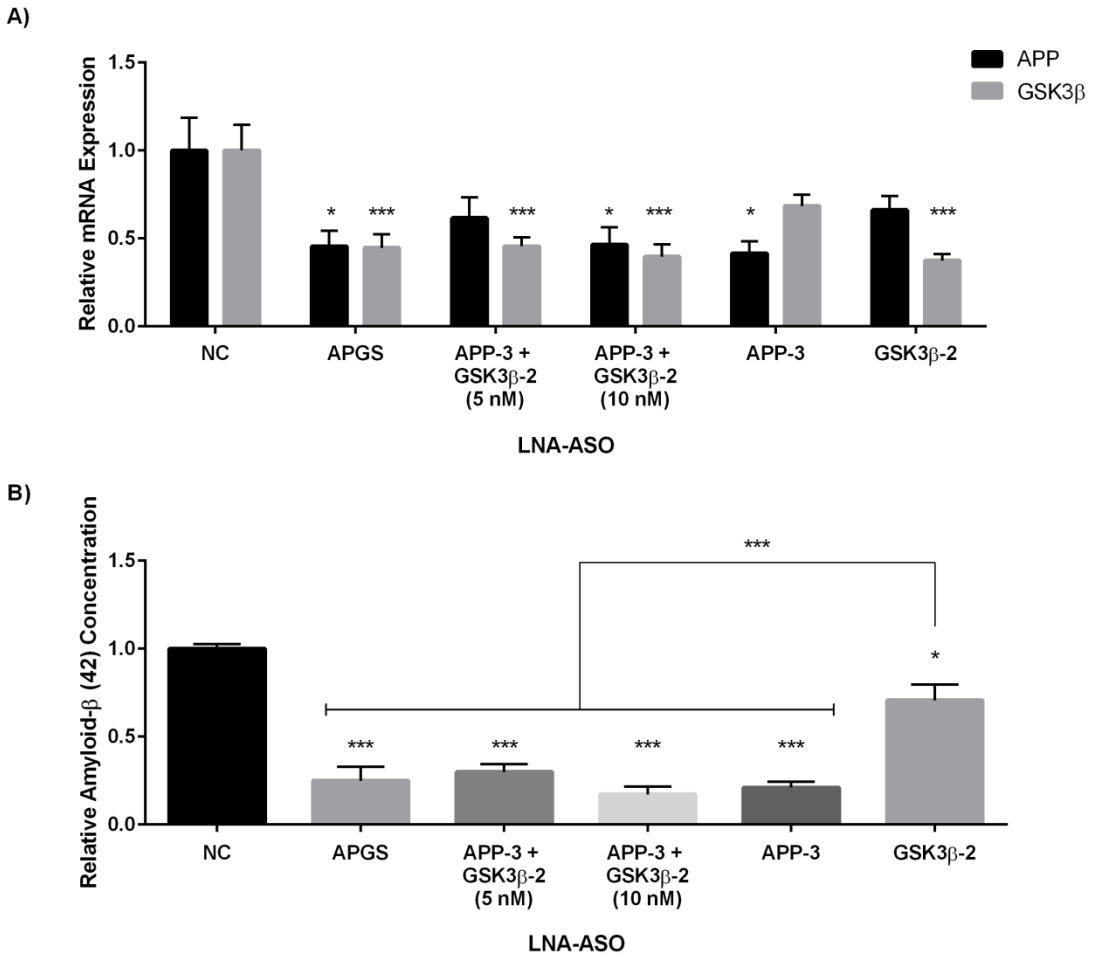

Figure 5.15 Amyloid-β (42) Production is Similarly Reduced by APP and GSK3β Targeting Multi-gene and Single-gene LNA-ASOs. HEK293 APPswe cells were reverse transfected with 10 nM of a negative control LNA-ASO ("NC"), the APGS multi-gene LNA-ASO or APP-3 and GSK3β-2 single-gene LNA-ASOs. As a further control for the multi-gene element, APP-3 and GSK3β-2 single-gene LNA-ASOs were also reverse transfected in combination at either 5 nM or 10 nM each. Amyloid-β (42) concentration and mRNA expression, normalised to *β-Actin*, was assessed by ELISA and qPCR, respectively, after 48 hours. **(A)** *APP* and *GSK3β* mRNA expression was significantly silenced following multi-gene and single-gene targeting LNA-ASO treatment. **(B)** Amyloid-β (42) concentration was reduced to a similar extent by multi-gene and single-gene targeting LNA-ASO treatments. Values are mean ± SEM, n = 6, ***p<0.001, *p<0.05, one-way ANOVA followed by Tukey's post-hoc test.

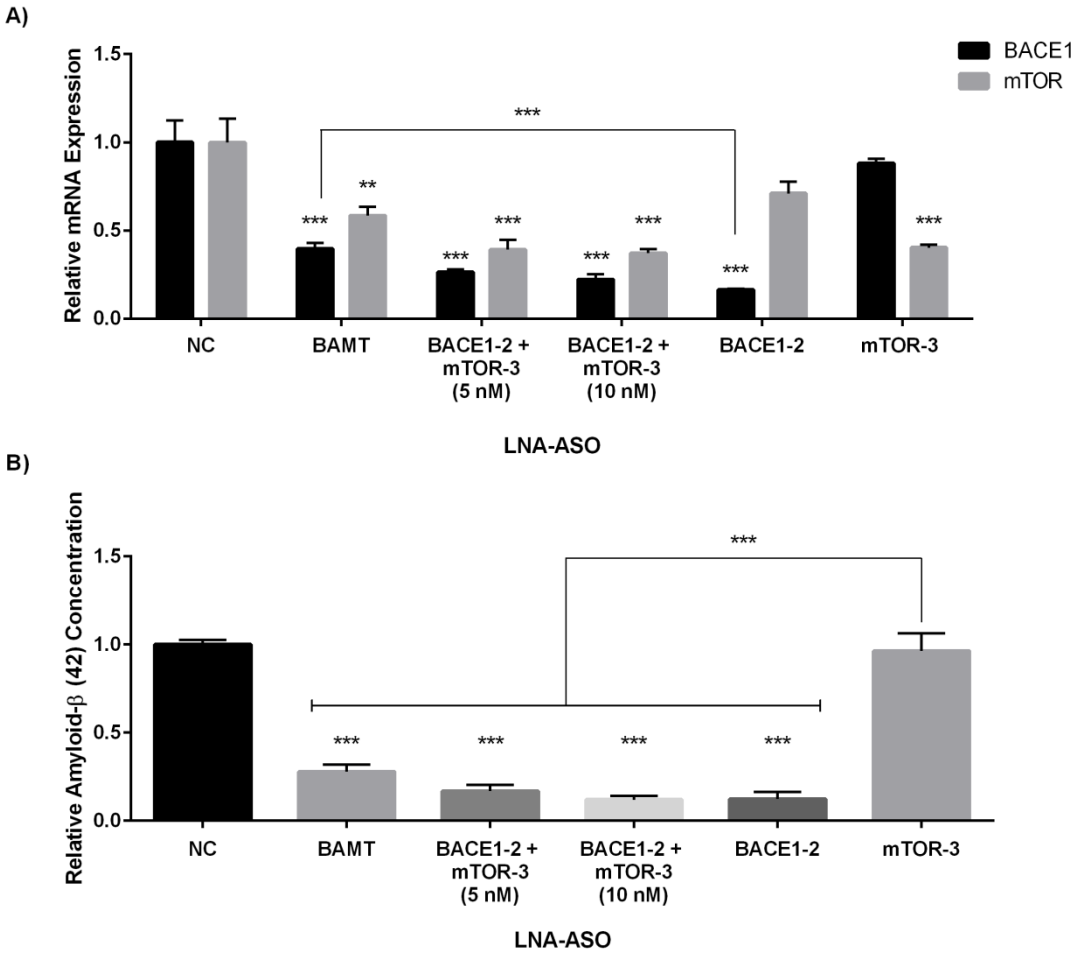

Figure 5.16 Amyloid-β (42) Production is Similarly Reduced by BACE1 and mTOR Targeting Multi-gene and Single-gene LNA-ASOs. HEK293 APPswe cells were reverse transfected with 10 nM of a negative control LNA-ASO ("NC"), the BAMT multi-gene LNA-ASO or BACE1-2 and mTOR-3 single-gene LNA-ASOs. As a further control for the multi-gene element, BACE1-2 and mTOR-3 single-gene LNA-ASOs were also reverse transfected in combination at either 5 nM or 10 nM each. Amyloid-β (42) concentration and mRNA expression, normalised to *β-Actin*, was assessed by ELISA and qPCR, respectively, after 48 hours. **(A)** *BACE1* and *mTOR* mRNA expression was significantly silenced following multi-gene and single-gene targeting LNA-ASO treatment. **(B)** Amyloid-β (42) concentration was reduced to a similar extent by multi-gene and single-gene targeting LNA-ASO treatments. Values are mean ± SEM, n = 6, ***p<0.001, **p<0.01, one-way ANOVA followed by Tukey's post-hoc test.

5.2.9 Tau Phosphorylation Following Multi-gene LNA-ASO Treatment in HEK293 APPswe and SH-SH5Y Cells

The findings above suggest that APGS and BAMT multi-gene LNA-ASOs regulate the production of amyloid-β (42) with similar efficacy to single-gene targeting LNA-ASOs, presumably by silencing APP or BACE1 expression. However, the potentially advantageous property of multi-gene targeting LNA-ASOs is that they are theoretically able to target two different genes and hence may be used to modulate two different disease-relevant pathways. Therefore, APGS and BAMT multi-gene LNA-ASOs were assessed for their ability to modulate a second pathway, tau phosphorylation, through their targeting of GSK3β and mTOR.

Given the promising results concerning amyloid-β (42) production, APGS and BAMT multi-gene LNA-ASOs were tested for their effects upon tau phosphorylation in HEK293 APPswe cells (**Fig. 5.17**). Both GSK3β and mTOR have been shown to modulate the phosphorylation of tau at multiple epitopes, including the Ser396 epitope (pS396)[643,649,673,674]. Therefore, HEK293 APPswe cells were transfected with a negative control LNA-ASO or the APGS or BAMT multi-gene LNA-ASOs before tau phosphorylation (pS396) was assessed by ELISA after 48 hours. There appeared to be a small decrease in tau phosphorylation following treatment with APGS (**Fig. 5.17A**) and BAMT multi-gene LNA-ASOs (**Fig. 5.17B**). To assess this further, tau phosphorylation (pSer396) was also assessed by Western blot 48 hours after treatment with APGS (**Fig. 5.17C**) or BAMT (**Fig. 5.17D**) multi-gene LNA-ASOs. This showed that tau phosphorylation at the Ser396 epitope was barely detectable across all treatment conditions, including in untreated and negative control treated cells. Total tau

expression was also probed by Western blot but could not be detected suggesting that HEK293 APPswe cells are not the optimal model in which to assess tau phosphorylation (**Fig. 5.17C-D**).

Therefore, tau phosphorylation (pS396) was also assessed in SH-SH5Y cells by Western blotting, following treatment with either APGS or BAMT multi-gene LNA-ASOs (**Fig. 5.18**). Higher levels of tau phosphorylation at the Ser396 epitope were evident in SH-SH5Y cells and there appeared to be a small reduction in tau phosphorylation following treatment with APGS (**Fig. 5.18A**) or BAMT (**Fig. 5.18B**) multi-gene LNA-ASOs. However, it should be noted that there also appeared to be a slight reduction in total tau expression, as assessed by Western blotting, following treatment with either APGS or BAMT multi-gene LNA-ASOs (**Fig. 5.18**).

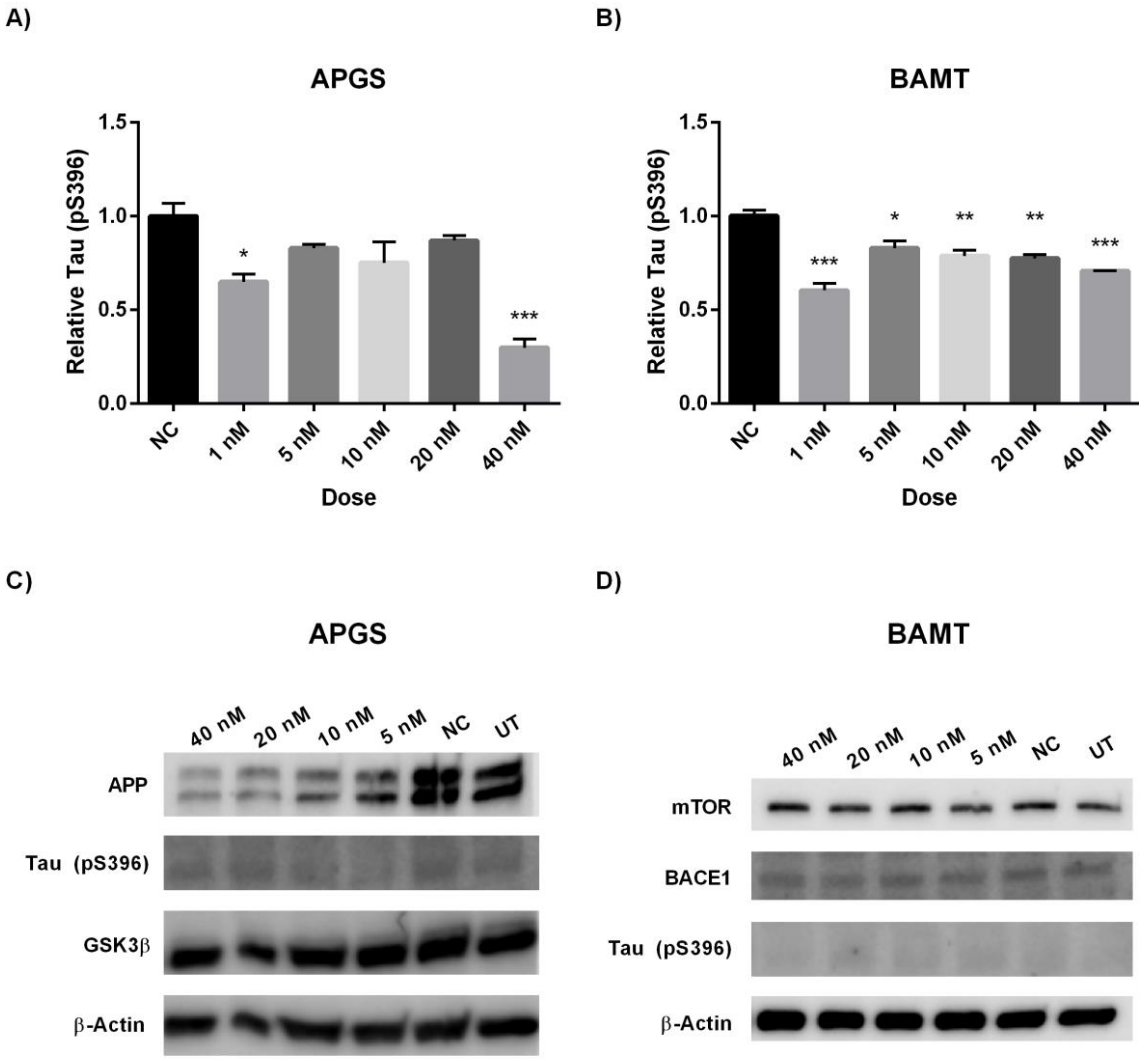

Figure 5.17 Tau Phosphorylation Following Multi-gene LNA-ASO Treatment in HEK293 APPswe Cells. HEK293 APPswe cells were left untreated ("UT") or reverse transfected with either the APGS or BAMT multi-gene LNA-ASO or a negative control LNA-ASO ("NC", 20 nM). Tau phosphorylation at the Ser396 epitope ("Tau pS396") was assessed by ELISA and Western blotting after 48 hours. **(A-B)** ELISA showed reduced tau phosphorylation following treatment with either **(A)** APGS or **(B)** BAMT multi-gene LNA-ASOs. **(C-D)** Western blotting revealed very low levels of tau phosphorylation at the Ser396 epitope across all treatment conditions including both UT and NC cell lysates following **(C)** APGS or **(D)** BAMT multi-gene LNA-ASO treatment (50 µg cell lysate). ELISA values are mean ± SEM, n = 3, ***p<0.001, **p<0.01, *p<0.05, one-way ANOVA followed by Tukey's post-hoc test.

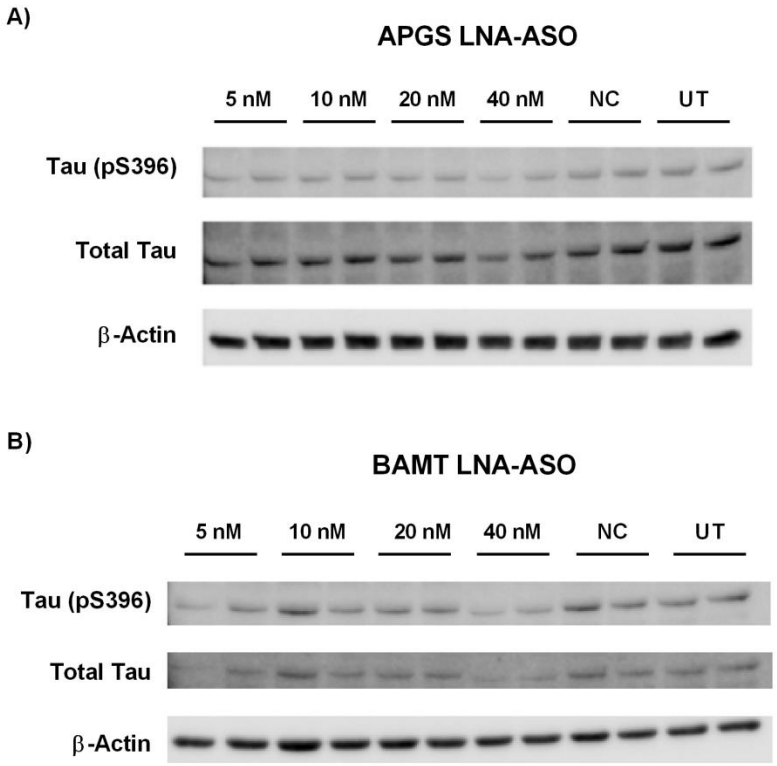

Figure 5.18 Tau Phosphorylation Following Multi-gene LNA-ASO Treatment in SH-SH5Y Cells. SH-SH5Y cells were left untreated ("UT") or reverse transfected with either the APGS or BAMT multi-gene LNA-ASO or a negative control LNA-ASO ("NC", 20 nM). Tau phosphorylation at the Ser396 epitope ("pS396") was assessed by Western blotting after 48 hours. SH-SH5Y cell lysates (50 µg) probed for tau (pS396), total tau and the loading control, β-Actin, following treatment with **(A)** APGS or **(B)** BAMT multi-gene LNA-ASOs.

5.2.10 Tau Phosphorylation in SH-SH5Y Cells Following Treatment with Single-gene and Multi-gene Targeting LNA-ASOs

Subsequently, multi-gene and single-gene LNA-ASOs were compared for their ability to attenuate tau phosphorylation at the Ser396 epitope in SH-SH5Y cells. SH-SH5Y cells were reverse transfected with either 20 nM of APGS (**Fig. 5.19**) or BAMT (**Fig. 5.20**) multi-gene LNA-ASOs, 20 nM of the corresponding single-gene LNA-ASOs or a combination of either 10 nM or 20 nM of each appropriate single-gene LNA-ASO (i.e. 10/20 nM APP-3 and 10/20 nM GSK3β-2) to control for the multi-gene aspect. Cell viability and protein and mRNA expression of relevant genes, relative to β-Actin, was assessed by MTS assay, Western blotting and qPCR after 48 hours.

As in HEK293 APPswe cells, *APP* and *GSK3β* mRNA expression was significantly reduced following treatment with multi-gene and single-gene LNA-ASOs (**Fig. 5.19A**). However, it should be noted that the APP-3 LNA-ASO also produced significant silencing of *GSK3β* mRNA expression. As discussed previously, APP and GSK3β protein expression was relatively low in SH-SH5Y cells, making it challenging to assess protein silencing following treatment with multi-gene and single-gene LNA-ASOs (**Fig. 5.19B**). Nevertheless, there appeared to be a reduction in both APP and GSK3β protein expression and tau phosphorylation at the Ser396 epitope following all experimental treatment conditions (**Fig. 5.19B**). As this was again associated with an apparent reduction in total tau protein expression (**Fig. 5.19B**), *tau* mRNA expression was also assessed by qPCR. This revealed a small non-significant reduction following treatment with all LNA-ASOs (**Fig. 5.19C**). There was no effect upon cell viability following any treatment (**Fig. 5.19D**).

The results were more inconclusive following treatment with BACE1 and mTOR targeting multi-gene and single-gene LNA-ASOs (**Fig. 5.20**). *BACE1* and *mTOR* mRNA expression was significantly reduced following treatment with the BAMT multi-gene LNA-ASO and the BACE1-2 and mTOR-3 single-gene LNA-ASOs either alone or in combination (**Fig. 5.20A**). The effects on BACE1, mTOR, phosphorylated tau or total tau at the protein level were milder (**Fig. 5.20B**). A discrepancy in the potency of gene silencing evaluated at RNA and protein levels may occur for several reasons; most commonly due to the different half-life of proteins or the sensitivity of the antibodies utilised for Western blotting. Furthermore, protein expression for the genes of interest was relatively low, particularly for mTOR and total tau, and this may also have been a contributing factor (**Fig. 5.20B**). Again, there appeared to be a slight reduction in *tau* mRNA expression following treatment with single-gene LNA-ASOs either alone or in combination but this effect was not significant (**Fig. 5.20C**). There was no significant effect upon cell viability following any treatment condition (**Fig. 5.20D**).

In summary, despite extensive optimisation efforts in two different cell lines, the results concerning the effect of multi-gene LNA-ASOs upon tau phosphorylation proved inconclusive due to low and variable baseline levels of tau phosphorylation at the Ser396 epitope. Alternative *in vitro* or *in vivo* models are therefore required to clarify the effect of multi-gene LNA-ASO treatment upon tau phosphorylation. A results summary for all experiments concerning APGS and BAMT multi-gene LNA-ASOs is provided in **Table 5.5**.

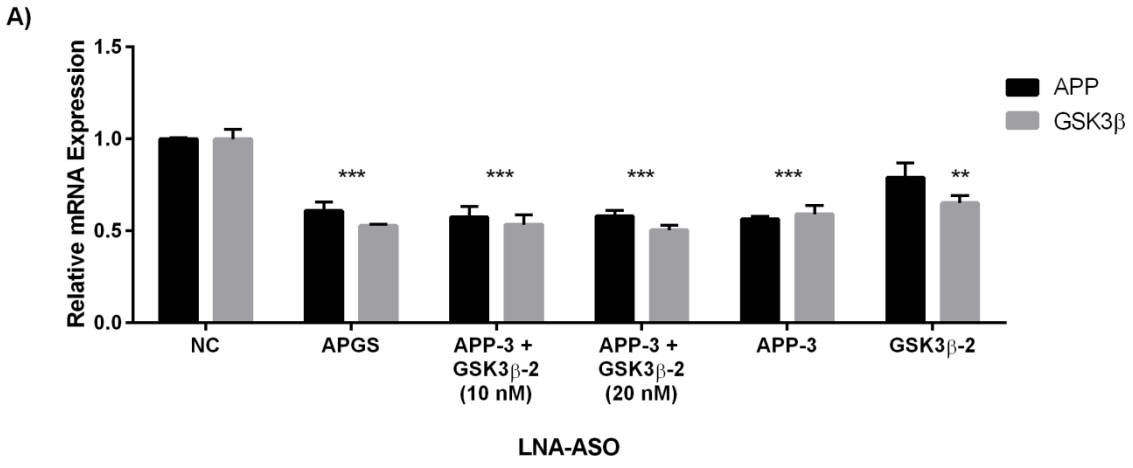
A)
Relative mRNA Expression
1.5
1.0
0.5
0.0
APP
GSK3β
***
***
***
***
**
NC
APGS
APP-3 + GSK3β-2 (10 nM)
APP-3 + GSK3β-2 (20 nM)
APP-3
GSK3β-2
LNA-ASO

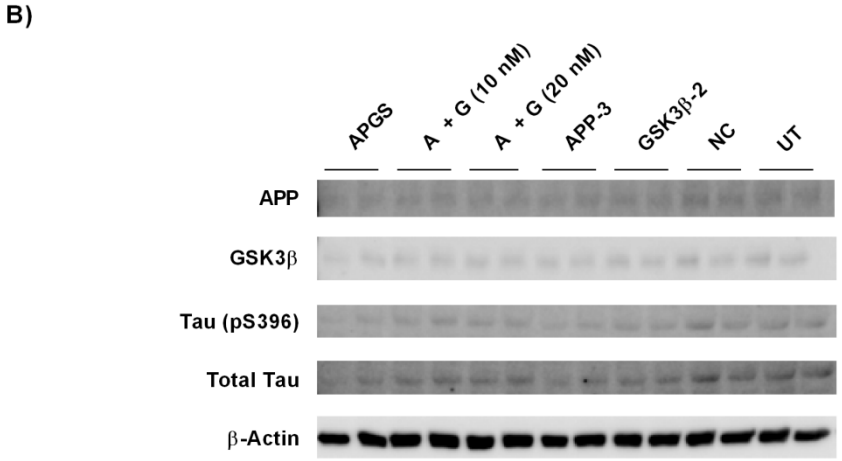
B)
APGS
A + G (10 nM)
A + G (20 nM)
APP-3
GSK3β-2
NC
UT
APP
GSK3β
Tau (pS396)
Total Tau
β-Actin

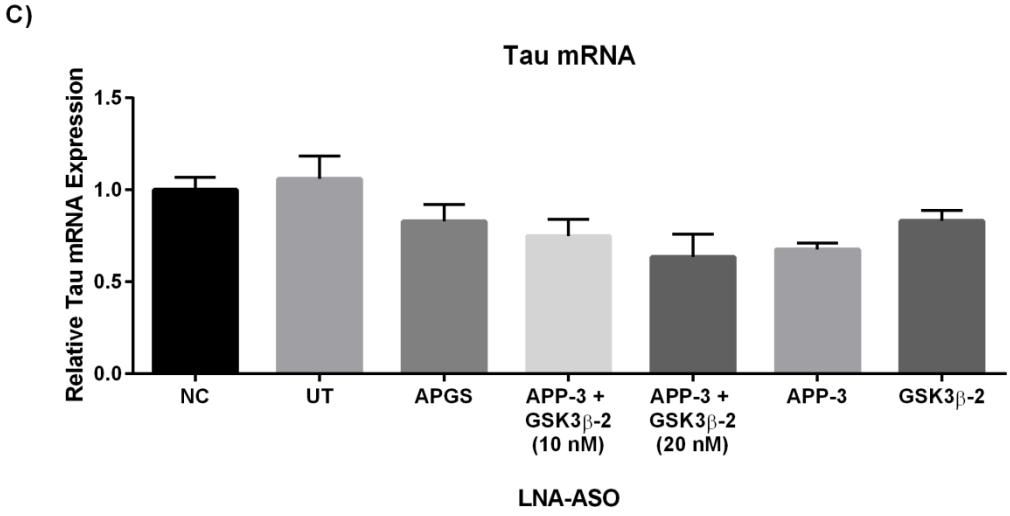
C)
Tau mRNA
Relative Tau mRNA Expression
1.5
1.0
0.5
0.0
NC
UT
APGS
APP-3 + GSK3β-2 (10 nM)
APP-3 + GSK3β-2 (20 nM)
APP-3
GSK3β-2
LNA-ASO

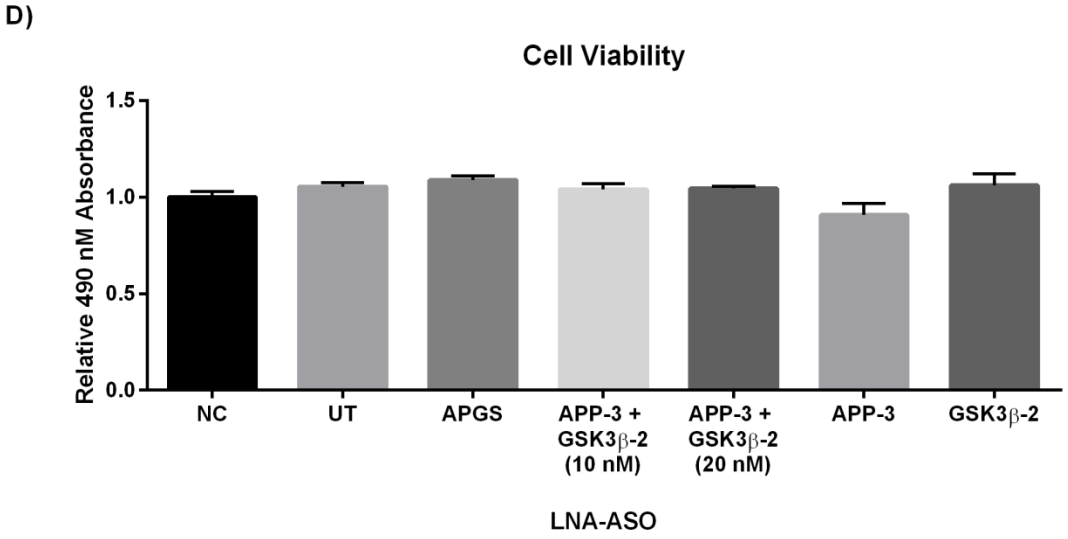

Figure 5.19 Tau Phosphorylation Following APP and GSK3β Targeting Multi-gene and Single-gene LNA-ASO Treatment. SH-SH5Y cells were left untreated ("UT") or were reverse transfected with 20 nM of a negative control LNA-ASO ("NC"), the APGS multi-gene LNA-ASO or APP-3 or GSK3β-2 single-gene LNA-ASOs. As a further control for the multi-gene element, APP-3 and GSK3β-2 single-gene LNA-ASOs were also applied in combination at 10 nM or 20 nM each ("APP-3 + GSK3β-2", "A + G"). Tau, APP and GSK3β mRNA and protein expression and tau phosphorylation at the Ser396 epitope ("pS396"), normalised to β-Actin, was assessed by qPCR and Western blotting after 48 hours. **(A)** *APP* and *GSK3β* mRNA expression was significantly reduced by both multi-gene and single-gene LNA-ASOs. **(B)** SH-SH5Y lysates (50 µg) probed for APGS, GSK3β, tau (pS396), total tau and β-Actin. **(C)** There was a slight but non-significant reduction in *tau* mRNA expression following all LNA-ASO treatments. **(D)** There was no effect upon cell viability following either multi-gene or single-gene LNA-ASO treatments. Values are mean ± SEM, n = 3, ***p<0.001, **p<0.01, one-way ANOVA followed by Tukey's post-hoc test.

A)

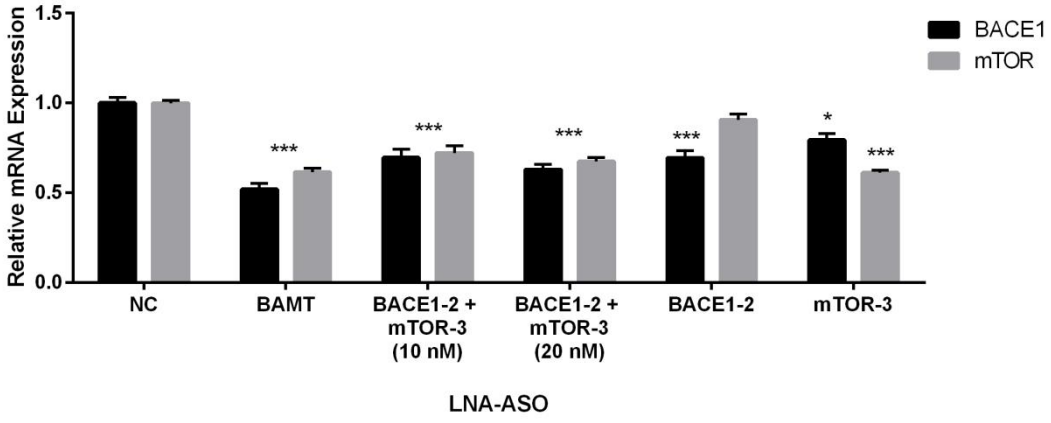
BACE1
mTOR
Relative mRNA Expression
1.5
1.0
0.5
0.0
***
***
***
***
*
***
NC
BAMT
BACE1-2 + mTOR-3 (10 nM)
BACE1-2 + mTOR-3 (20 nM)
BACE1-2
mTOR-3
LNA-ASO

B)

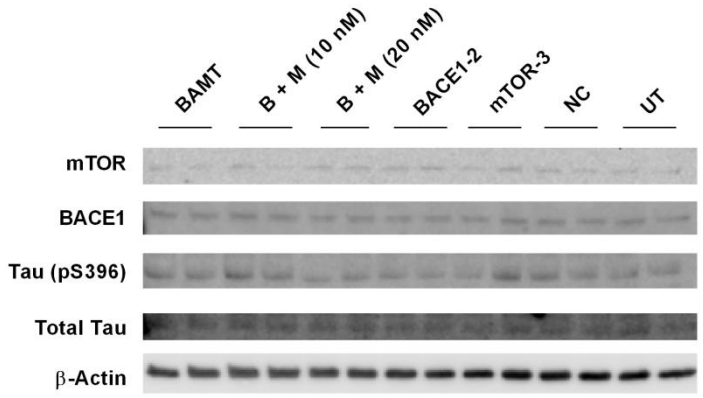
BAMT
B + M (10 nM)
B + M (20 nM)
BACE1-2
mTOR-3
NC
UT
mTOR
BACE1
Tau (pS396)
Total Tau
β-Actin

C)

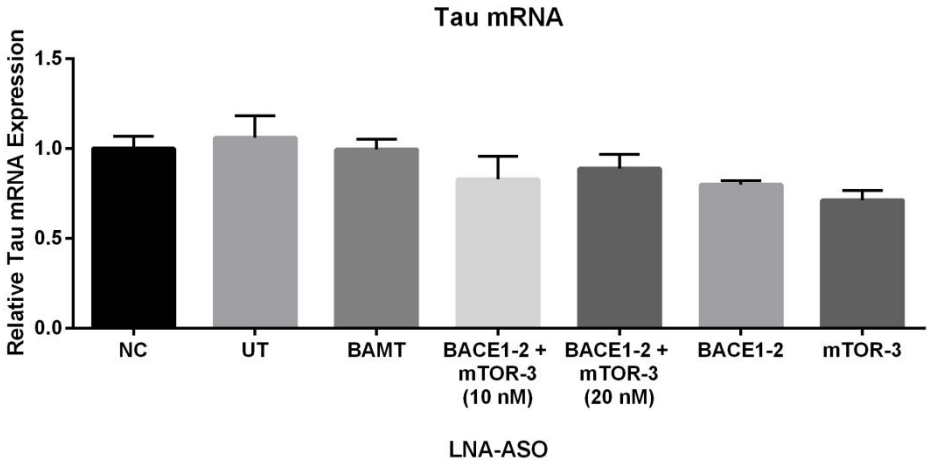
Tau mRNA
Relative Tau mRNA Expression
1.5
1.0
0.5
0.0
NC
UT
BAMT
BACE1-2 + mTOR-3 (10 nM)
BACE1-2 + mTOR-3 (20 nM)
BACE1-2
mTOR-3
LNA-ASO

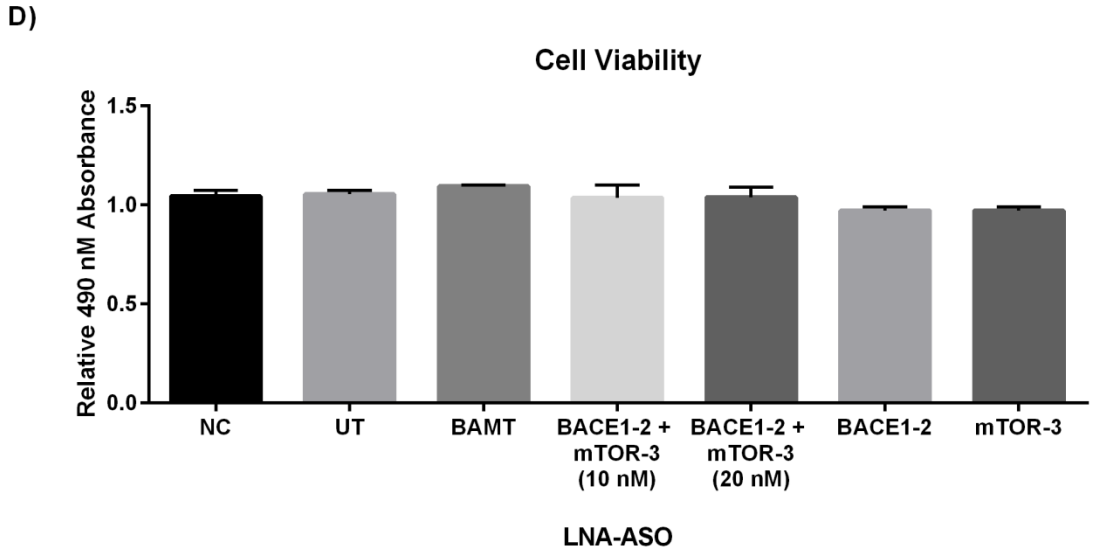

Figure 5.20 Tau Phosphorylation Following BACE1 and mTOR Targeting Multi-gene and Single-gene LNA-ASO Treatment. SH-SH5Y cells were left untreated ("UT") or were reverse transfected with 20 nM of a negative control LNA-ASO ("NC"), the BAMT multi-gene LNA-ASO or BACE1-2 or mTOR-3 single-gene LNA-ASOs. As a further control for the multi-gene element, BACE1-2 and mTOR-3 single-gene LNA-ASOs were also applied in combination at 10 nM or 20 nM each ("BACE1-2 + mTOR-3", "B + M"). BACE1, mTOR and Tau mRNA and protein expression and tau phosphorylation at the Ser396 epitope ("pS396"), normalised to β-Actin, was assessed by qPCR and Western blotting after 48 hours. **(A)** *BACE1* and *mTOR* mRNA expression was significantly reduced by multi-gene and single-gene LNA-ASOs. **(B)** SH-SH5Y lysates (50 µg) probed for BACE1, mTOR, tau (pS396), total tau and β-Actin. **(C)** There appeared to be a small but non-significant reduction in *tau* mRNA expression following treatment with single-gene LNA-ASOs both alone or combined. **(D)** There was no significant effect upon cell viability following either multi-gene or single-gene LNA-ASO treatment. Values are mean ± SEM, n = 3, ***$p<0.001$, *$p<0.05$, one-way ANOVA followed by Tukey's post-hoc test.

Table 5.5 Results Summary for APGS and BAMT LNA-ASO Experiments.

LNA-ASO	Cell Line	Results	Ref.
APGS	SH-SH5Y	• Significant silencing of *APP* and *GSK3β* mRNA at doses ≥ 2.5 nM (IC_{50}: *APP*, 1.60 nM; *GSK3β*, 1.28 nM). • Silencing persisted for 72 hours after treatment. • Dose-dependent reduction in cell viability at doses ≥ 40 nM. • Low endogenous protein expression levels but slight silencing of APP and GSK3β protein expression, 48 hours after APGS treatment. • Dose-dependent reduction in phosphorylated tau at pS396 epitope by Western blotting, 48 hours after treatment. • Comparison between single-gene and multi-gene LNA-ASOs for effect upon tau phosphorylation at pS396 epitope inconclusive by Western blotting due to low and variable baseline levels of tau phosphorylation.	**Fig. 5.6** **Fig. 5.18** **Fig. 5.19**
APGS	HEK293 APPswe	• Significant silencing of *APP* and *GSK3β* mRNA at doses ≥ 1 nM (IC_{50}: *APP*, 2.86 nM; *GSK3β*, 1.82 nM). • Silencing persisted for 48 hours after treatment. • Dose-dependent reduction in cell viability at doses ≥ 20 nM. • Dose-dependent reduction in APP and GSK3β protein expression, 48 hours after APGS treatment. • Significant dose-dependent reduction in amyloid-β (42) levels (89.3% reduced by 10 nM dose), 48 hours after APGS treatment. • Amyloid-β (42) production similarly reduced by APP and GSK3β-targeting multi-gene and single-gene LNA-ASOs. • Slight reduction in phosphorylated tau at pS396 epitope observed by ELISA, 48 hours after APGS treatment. • Levels of phosphorylated tau at pS396 epitope too low to detect by Western blotting.	**Fig. 5.8** **Fig. 5.12** **Fig. 5.15** **Fig. 5.17**
BAMT	SH-SH5Y	• Significant silencing of *BACE1* and *mTOR* mRNA at doses ≥ 1 nM (IC_{50}: *BACE1*, 15.81 nM; *mTOR*, 2.74 nM). • Silencing persisted for 72 hours after treatment. • No reduction in cell viability for doses ≤ 100 nM. • Low endogenous levels of BACE1 and mTOR protein precluded clear effect of BAMT upon expression. • Specificity of silencing – *HN1* gene containing a single mismatch nucleotide to LNA-ASO target sequence was not silenced by BAMT treatment. • Dose-dependent reduction in phosphorylated tau at pS396 epitope by Western blotting, 48 hours after BAMT treatment. • Comparison between single-gene and multi-gene LNA-ASOs for effect upon tau phosphorylation at pS396 epitope inconclusive by Western blotting due to low and variable baseline levels of tau phosphorylation.	**Fig. 5.7** **Fig. 5.10** **Fig. 5.18** **Fig. 5.20**

Table 5.5 Continued.

LNA-ASO	Cell Line	Results	Ref.
BAMT	HEK293 APPswe	• Significant silencing of *BACE1* and *mTOR* mRNA at doses ≥ 10 nM (IC_{50}: *BACE1*, 6.90 nM; *mTOR*, 10.18 nM). • Silencing persisted for 48 hours after treatment. • Dose-dependent reduction in cell viability for doses ≥ 60 nM. • Low endogenous levels of BACE1 protein precluded clear effect upon expression. • Dose-dependent reduction in mTOR protein expression, 48 hours after BAMT treatment. • Specificity of silencing – *HN1* gene containing a single mismatch nucleotide to LNA-ASO target sequence was not silenced by BAMT treatment. • Significant dose-dependent reduction in amyloid-β (42) levels (75.6% reduced by 20 nM dose), 48 hours after BAMT treatment. • Amyloid-β (42) production similarly reduced by BACE1 and mTOR-targeting multi-gene and single-gene LNA-ASOs. • Slight reduction in phosphorylated tau at pS396 epitope observed by ELISA, 48 hours after BAM T treatment. • Levels of phosphorylated tau at pS396 epitope too low to detect by Western blotting.	**Fig. 5.9** **Fig. 5.10** **Fig. 5.13** **Fig. 5.16** **Fig. 5.17**

5.2.11 Identification of mBAMT Multi-gene LNA-ASO Targeting Mouse Transcripts

The results above are promising as they suggest that both APGS and BAMT multi-gene LNA-ASOs reduce the production of amyloid-β (42), presumably via silencing of APP and BACE1. However, the above experiments were all conducted *in vitro* and therefore preliminary *in vivo* assessments are required. Not only will this allow investigation of the *in vivo* efficacy of multi-gene LNA-ASOs in terms of gene silencing, BBB penetrance and toxicity, but it may also help to clarify the effects upon tau phosphorylation.

The sequences targeted by the APGS and BAMT multi-gene LNA-ASOs described above are not conserved between mouse and human. Therefore, to allow for *in vivo* testing, the mouse sequences for the genes of interest outlined in **Table 5.1** were again compared using the algorithm described previously. Promisingly, this resulted in the identification of a multi-gene LNA-ASO (mBAMT) which was predicted to target the mouse sequences for both *Bace1* and *mTOR* (**Table 5.6**).

Table 5.6 Candidate Multi-gene LNA-ASO Targeting Mouse Transcripts.

LNA-ASO	Genes Targeted		Sequence	Chromosome Location of Target Sequence (GRCh38)
	Gene 1	Gene 2		
mBAMT	*Bace1*	*mTOR*	+T+T+Tggccagcag+G+G+A	*Bace1*: Chr. 9: 45860719-45860733 *mTOR*: Chr. 4: 148469440-148469454

LNA-ASO has a fully phosphorothioated backbone with 9 DNA monomers flanked on either end by 3 LNA-modified bases, + indicates LNA-modified base.

The mBAMT multi-gene LNA-ASO was first screened in the mouse neuroblastoma Neuro2A cell line. Neuro2A cells were reverse transfected with 20 nM of the mBAMT multi-gene LNA-ASO or the negative control LNA-ASO before *Bace1* and *mTOR* mRNA expression, relative to *β-Actin*, was assessed by qPCR after 48 hours. Promisingly, this resulted in significant silencing of both *Bace1* and *mTOR* expression following mBAMT multi-gene LNA-ASO treatment (**Fig. 5.21A**).

Consequently, the mBAMT multi-gene LNA-ASO underwent further screening to assess the kinetics of mRNA silencing, LNA-ASO toxicity and effect upon target gene protein expression, as above (**Fig. 5.21B-H**). This revealed that the mBAMT multi-gene LNA-ASO elicited strong silencing of both *Bace1* and *mTOR* mRNA expression at doses as low as 0.5 nM (IC_{50}: *Bace1*, 0.18 nM; *mTOR*, 0.38 nM) (**Fig. 5.21B-D**). The relatively flat dose-response was again attributed to saturation of transfection efficiency of Neuro2A cells. Silencing of mRNA expression was apparent 24 and 48 hours after treatment with the mBAMT LNA-ASO although a significant rebound in expression was observed for both *Bace1* and *mTOR* after 72 hours (**Fig. 5.21E**). A slight dose-dependent reduction in cell viability was observed following treatment with the

mBAMT multi-gene LNA-ASO but this was only significant at the highest dose (100 nM) (**Fig. 5.21F**). Promisingly, treatment with the mBAMT multi-gene LNA-ASO resulted in strong silencing of Bace1 protein expression (**Fig. 5.21G**). There also appeared to be a small reduction in mTOR expression although the relatively low levels of this protein made it challenging to quantify. While phosphorylated and total tau protein could not reliably be detected, *tau* mRNA did appear slightly, but non-significantly, reduced (**Fig. 5.21H**). Together, these results (summarised in **Table 5.7**) highlight the mBAMT multi-gene LNA-ASO as a promising candidate for further *in vitro* and *in vivo* assessments.

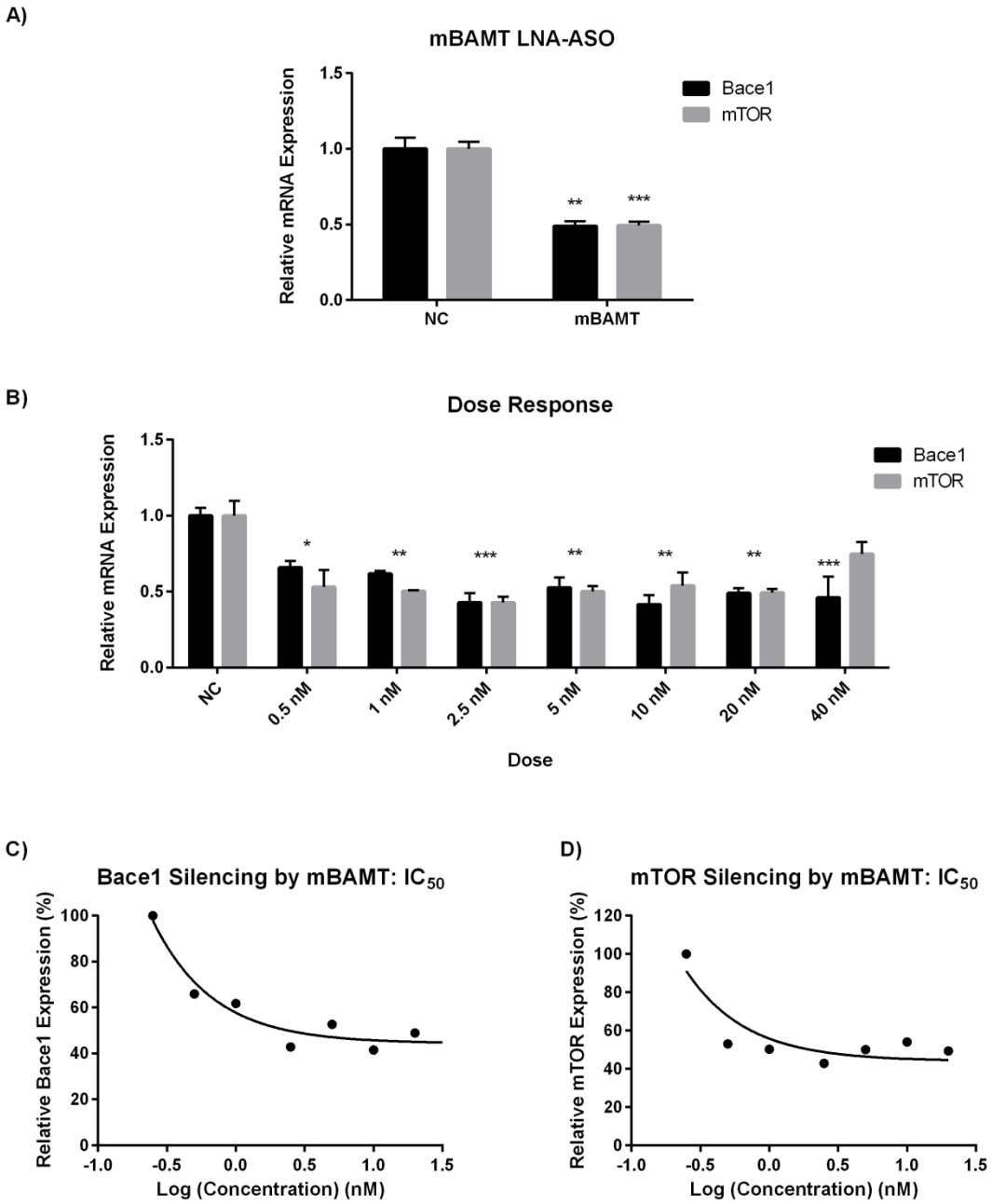

Figure 5.21 Characterisation of mBAMT Multi-gene LNA-ASO in Neuro2A Cells. Neuro2A cells were left untreated ("UT") or were reverse transfected with either the mBAMT multi-gene LNA-ASO or a negative control LNA-ASO ("NC") at shown concentrations. mRNA and protein expression, normalised to β-Actin, was assessed by qPCR and Western blotting, respectively, after 48 hours. **(A)** Both *Bace1* and *mTOR* mRNA expression were significantly silenced by a 20 nM dose of mBAMT LNA-ASO in comparison to the NC LNA-ASO (20 nM) (Student's t-test). **(B)** Dose-response curve of *Bace1* and *mTOR* mRNA expression following mBAMT multi-gene LNA-ASO treatment in comparison to the NC LNA-ASO (20 nM). **(C-D)** IC_{50} plots for **(C)** *Bace1* and **(D)** *mTOR* mRNA expression following mBAMT multi-gene LNA-ASO treatment relative to NC. Values are mean ± SEM, n = 3, ***p<0.001, **p<0.01, *p<0.05, one-way ANOVA followed by Tukey's post-hoc test. (Figure continued overleaf).

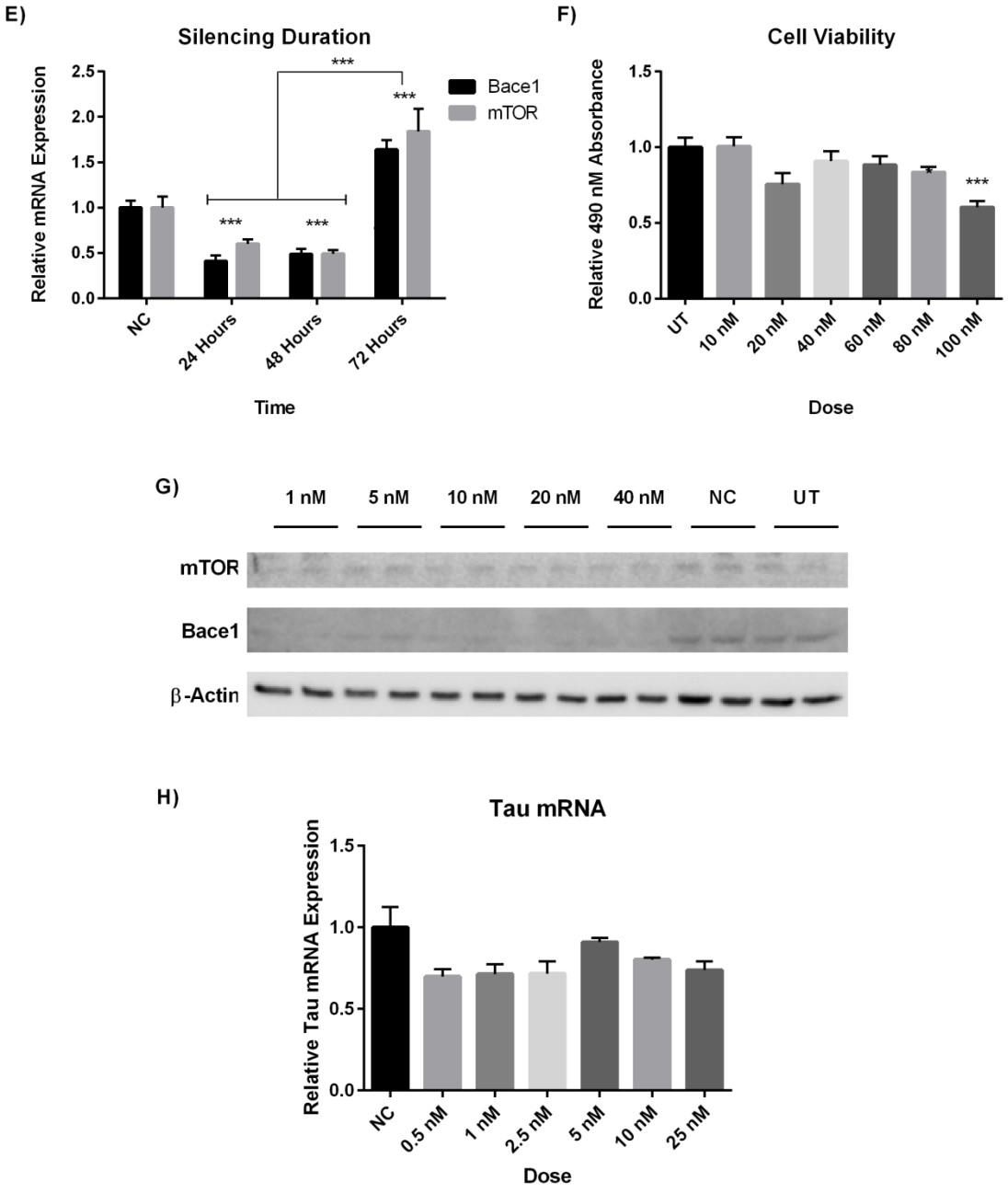

Figure 5.21 Characterisation of mBAMT Multi-gene LNA-ASO in Neuro2A Cells – Continued. (E) Duration of gene silencing following transfection of 20 nM mBAMT multi-gene LNA-ASO compared to NC LNA-ASO (20 nM). **(F)** Cell viability assessed by MTS assay. **(G)** Neuro2A cell lysates (50 µg) probed by Western blot for Bace1, mTOR and the loading control, β-Actin. **(H)** There was a non-significant reduction in *tau* mRNA expression following treatment with the mBAMT LNA-ASO. Values are mean ± SEM, n = 3, ***p<0.001, one-way ANOVA followed by Tukey's post-hoc test.

Table 5.7 Results Summary for mBAMT Multi-Gene LNA-ASO Experiments.

LNA-ASO	Cell Line	Results	Ref.
mBAMT	Neuro2A	• Significant silencing of *Bace1* and *mTOR* mRNA at doses ≥ 0.5 nM (IC_{50}: *Bace1*, 0.18 nM; *mTOR*, 10.38 nM). • Silencing persisted for 48 hours after mBAMT treatment. • Dose-dependent reduction in cell viability, significant only at 100 nM dose. • Strong dose-dependent silencing of Bace1 and mTOR protein expression, 48 hours after BAMT treatment. • Non-significant reduction in *tau* mRNA, 48 hours after mBAMT treatment.	**Fig. 5.21**

5.3 Discussion

This study investigated the potential of a novel multi-gene targeting approach in which single LNA-ASO gapmers were designed to target two separate AD-relevant genes simultaneously. Initial screening revealed a number of promising multi-gene LNA-ASOs targeting a range of AD-relevant genes. Two of these, APGS and BAMT, underwent further characterisation and were shown to produce potent silencing of target genes associated with a significant reduction in amyloid-β (42) production by HEK293 APPswe cells. Unfortunately, it proved challenging to assess the second potential pathway of action for these LNA-ASOs *in vitro* as baseline levels of tau phosphorylation were low and variable in two cell lines studied. Promisingly, an additional murine-specific multi-gene LNA-ASO was also identified (mBAMT), paving the way for preliminary *in vivo* studies. These findings highlight the potential of novel multi-gene targeting LNA-ASOs. However, they require further *in vitro* and *in vivo* assessment to determine whether they are able to modulate both potential pathways without significant toxicity.

Multi-gene LNA-ASO Treatment Significantly Reduced Amyloid-β (42) Levels

The findings from this study build upon recent data within the literature which have highlighted the promise of ASO-based therapeutics for AD[406–415,675,676]. In an array of complementary studies, Farr and colleagues[406–413] showed that ASOs targeting APP, GSK3β or presenilin-1 reduced target gene expression, amyloid-β production, markers of both neuroinflammation and oxidative stress and reversed learning and memory deficits in two mouse models of AD. These effects could be achieved not only by direct

intracerebroventricular injections but also following intravenous administration, where small but therapeutically effective quantities of ASO were able to penetrate the BBB[407,409,410]. Similarly, ASOs directed against the Swedish mutant sequence of APP significantly increased levels of sAPPα while reducing levels of amyloid-β (40/42) in the brains of transgenic mice following repeated intracerebroventricular injections[675]. Alternatively modified ASOs, in which the sugar phosphate backbone was replaced by amide linkages to produce PNAs, have also been shown to silence APP expression both *in vitro* and *in vivo* when administered systemically[414,415]. ASOs have also been used to elicit exon skipping of tau which resulted in potent gene silencing at both the mRNA and protein level *in vitro* and *in vivo*[676]. Together, these findings demonstrate the potential for ASO-mediated gene silencing and highlight the range of genes which may be targeted for therapeutic purposes.

Promisingly, APGS and BAMT multi-gene LNA-ASOs were shown here to strongly attenuate the production of amyloid-β (42) at very low doses, presumably through silencing of APP and BACE1. Furthermore, the use of a sequence which was identical between two targets did not appear to reduce the efficacy of multi-gene LNA-ASOs when compared to LNA-ASOs targeting a single gene. This may be due to the action of RNase H as upon binding to the target mRNA the DNA strand is released intact, allowing a single LNA-ASO molecule to direct the degradation of many individual transcripts[677]. Thus, these findings add to the existing literature to highlight the promise of LNA-ASO-based therapeutics for the reduction of amyloid-β in AD.

As discussed previously, the likely requirement for a combinatorial approach towards AD therapy is increasingly recognised[40,594–596]. RNA-based therapeutics may be

particularly amenable to this approach given that a combination of highly specific individual RNA-targeting molecules could feasibly be delivered together. However, for a combinatorial effect to be achieved this may require each separate effector to be taken up by the same cell. In contrast, multi-gene targeting LNA-ASOs possess the advantage that once taken up by a cell, a single multi-gene LNA-ASO is theoretically able to silence two different gene targets, which may have independent or synergistic effects upon disease pathways. For example, APGS may be able to target both APP and GSK3β to separately ameliorate amyloid-β and tau hyperphosphorylation-based pathologies. Furthermore, amyloid-β and tau-based downstream pathologies have been shown to interact to mediate pathogenic processes[126,170,172,173,175,185,186]. Indeed, amyloid-β may upregulate GSK3β activity[170] while GSK3β activation may increase production of amyloid-β through regulation of APP processing[161]. Thus, the simultaneous silencing of both APP and GSK3β may have additive feedback effects upon the mitigation of downstream pathology which are greater than that achieved by silencing each target alone. Additionally, targeting multiple genes or pathways by a single molecule may reduce the requirement for many individual toxicity studies which would otherwise be required for combinatorial approaches in which a number of separate therapeutic molecules, each targeting a single gene/pathway, are utilised. This may help to reduce both the cost and timescale for therapeutic drug development.

In Vitro Assessment of Tau Phosphorylation Proved Inconclusive

GSK3β and mTOR protein expression appeared reduced following treatment with either APGS or BAMT multi-gene LNA-ASOs in HEK293 APPswe cells. However, it proved challenging to assess the extent of tau phosphorylation in two cell lines *in vitro*. It was

hypothesised that tau phosphorylation may be relatively high in HEK293 APPswe cells due to the increased production of amyloid-β (42)[170,174,175]. Conversely, baseline levels of both total tau and phosphorylation at the Ser396 epitope (pS396) were low when assessed by ELISA and Western blotting. SH-SH5Y cells showed slightly higher, but also variable, expression of tau (both total and pS396) while both GSK3β and mTOR protein expression was lower than in HEK293 APPswe cells. Despite extensive optimisation attempts, the results concerning modulation of tau phosphorylation by APGS and BAMT multi-gene LNA-ASOs were inconclusive, especially as total tau protein expression also often appeared reduced. It is unclear from the present study if this relates to an antibody issue or an actual reduction in tau protein expression. However, a slight but non-significant reduction in *tau* mRNA was also observed following multi-gene and single-gene LNA-ASO treatment. Further assessments are therefore required to determine the potential of these multi-gene LNA-ASOs to target both amyloid-β and tau-based pathways.

In this respect, there are several alternative strategies which may be employed. Firstly, the current study focused upon the Ser396 epitope as this has been shown to be modulated by both GSK3β and mTOR in AD patients and disease models[643,673,674]. However, a number of other epitopes are also influenced by GSK3β and mTOR activity and therefore may offer alternative options to assess tau phosphorylation[643,649,650,673,674]. Secondly, given that endogenous baseline levels of pS396 were relatively low, pharmacological induction of tau phosphorylation followed by multi-gene LNA-ASO treatment may prove more informative. Okadaic acid, a serine/threonine phosphatase inhibitor, has been utilised in previous studies to induce tau phosphorylation[678–681]. In the present study, Western blotting and ELISA analyses were performed 48 hours after

transfection. However, given the different half-life of proteins, it may be that protein silencing would be more evident following shorter or longer durations. This will be assessed in future studies. Alternatively, it may be that the effects upon tau phosphorylation would be better assessed *in vivo* in either wild-type mice or disease models of AD.

Selectivity and Toxicity of Multi-gene LNA-ASOs

An important step in the characterisation of LNA-ASOs is *in vivo* screening. This is important not only to determine the *in vivo* potency of the LNA-ASOs in question but also their potential toxicity. LNA-ASOs are often stated to be of low toxicity *in vivo*. However, as discussed previously, several studies have demonstrated that they may be associated with increased hepatotoxicity which may depend upon both sequence length and specific sequence motifs[668–670,682]. While cell viability following multi-gene LNA-ASO treatment was assessed as a measure of toxicity, previous studies have shown that *in vitro* toxicity may not necessarily reflect that observed *in vivo*[670], highlighting the importance of *in vivo* screening.

Another potential concern relating to the use of LNA-ASOs is the potential for off-target effects given their short sequence length and high affinity binding. This issue was partially addressed in the current study by an assessment of *HN1* expression; an unrelated gene possessing an identical sequence, except for one mismatch, to the sequence targeted by the BAMT multi-gene LNA-ASO. Promisingly, there was no significant effect upon *HN1* mRNA expression, suggesting the specificity of this approach. However, whether other off-target effects are observed following *in vivo*

treatment remains to be seen. Thus, preliminary *in vivo* screening will be required, first in wild-type mice to assess silencing potency and potential toxicity, and given promising data, followed by more detailed assessments in an AD mouse model. This will be important to determine whether multi-gene LNA-ASOs are able to silence both targets and modulate two separate disease pathways *in vivo* and if so, whether this translates to preventative or disease-modifying outcomes in AD models.

Delivery of Multi-gene LNA-ASOs

As discussed previously, the BBB is a key limitation to the delivery of many therapeutics. While APP-targeting ASOs were shown to cross the BBB when administered intravenously, it is important to note that this equated to 1% of the same dose administered intracerebroventricularly[407,410]. Thus, the majority of recent studies, including the first two clinical trials assessing the use of ASOs for neurodegenerative diseases, have utilised either intrathecal or intracerebroventricular injections to directly administer ASOs to the CSF *in vivo*[402,675,683–686]. While these methods are relatively well-tolerated, resulting in a high concentration and wide distribution of ASOs within the CNS, they are invasive and may be associated with their own adverse effects. Therefore, alternative delivery strategies for systemic delivery are under development.

One approach aims to exploit receptor-mediated transcytosis through conjugation of ASOs to a monoclonal antibody to the mouse transferrin receptor[687,688]. Alternative strategies have focused upon cell-penetrating peptide-based delivery systems in which ASOs are tagged with arginine-rich cell-penetrating peptides, which are able to cross the BBB, resulting in a wide distribution of the ASO throughout the brain[689]. EV-

mediated delivery may represent another promising approach. As discussed previously, EVs encapsulate both endogenous and exogenous small RNA and are able to deliver their RNA cargoes to recipient cells, where they may exert pleotropic functional effects[494,496,497,499,508,513,515]. Therefore, given the potential for EV-mediated delivery, a preliminary experiment was performed in the current study to determine whether EVs derived from LNA-ASO transfected source cells could transfer LNA-ASO cargoes to recipient cells. No functional effects were observed in recipient cells. However, as LNA-ASOs could not be quantified by qPCR it is unclear whether this is due to insufficient loading of EVs or the challenge of identifying detectable readouts in recipient cells, as discussed above. Previous data within the lab has shown that LNA-ASOs are able to cross the BBB to elicit potent target silencing when administered to mice at very early postnatal stages when the BBB is not yet fully formed. Thus, this strategy will be employed for initial *in vivo* screening of multi-gene LNA-ASOs in wild-type mice. However, for future testing in AD mice models where it would be desirable to assess the effect of multi-gene LNA-ASOs applied both prior to and after disease onset, it is likely that direct injections or infusions would be required until an alternative delivery method is developed.

In the current study, the duration of *in vitro* mRNA silencing was relatively short. Typically, mRNA expression was maximally silenced between 24-48 hours with an attenuation of silencing at 72 hours. However, LNA-ASOs have been shown to have much longer half-lives *in vivo.* Indeed, previous studies have shown that target mRNAs may still be suppressed up to 6 months after ASO infusions[685,690]. While dosing regimens for any promising LNA-ASOs would obviously require optimisation in AD

models, these findings suggest that LNA-ASOs may provide a feasible approach to long-term silencing.

Alternative Multi-gene LNA-ASOs and Importance of a Combinatorial Approach

Finally, it is important to note that while APGS and BAMT multi-gene LNA-ASOs were chosen for further characterisation in the current study, a number of other candidate LNA-ASOs were also identified. These included BATA (*BACE1* and *tau*), BAPP2 and BAPP3 (*BACE1* and *APP*, in SH-SH5Y cells) and GRBCA (*GRIN2B* and *caspase-9*). Further investigation of these is warranted, particularly as they may target alternative pathways. Given the importance of a combinatorial approach it would also be of interest to assess whether combining multiple multi-gene LNA-ASOs in one treatment would be of value for targeting an even greater range of pathways. Alternatively, multi-gene LNA-ASOs could also be combined with other existing therapeutic strategies such as immunotherapy. Data from two previous studies suggest that this may be a promising approach. For example, memory deficits were reversed in an AD mouse model following combined treatment with a single dose of APP-directed ASOs and a monoclonal amyloid-β antibody while application of either treatment alone had no effect[406]. Similarly, Rapozzi and colleagues[419] showed that anti-proliferative effects were enhanced when an ASO targeting the BCR/ABL fusion gene was applied in combination with STI571, a tyrosine kinase inhibitor of $p210^{BCR/ABL}$. Together, these studies highlight the potential of combining novel multi-gene LNA-ASOs with additional therapeutic agents.

In summary, the recent transition to clinical trial for two ASOs directed at the treatment of SMA and ALS demonstrate the promise of ASO-mediated therapies for neurodegenerative disease[398,402,684]. This study has identified novel multi-gene LNA-ASOs, which are able to silence the expression of two target genes relevant to AD simultaneously. Although these require further validation *in vivo*, they may offer an alternative option towards combinatorial-based therapies for the treatment of AD.

6 Discussion

6.1 Summary of Results

The work presented in this thesis has explored the utility of RNA-based therapeutics for the treatment of AD. This work was divided into two themes; 1) the identification and EV-mediated delivery of potential RNAi-based therapeutics and 2) the development of novel multi-gene targeting LNA-ASOs as a combinatorial approach to AD therapy.

Amyloid-β peptides, a key pathogenic hallmark of AD, are produced through the sequential cleavage of APP by BACE1 and γ-secretase. As such, silencing either APP or the secretases is at the forefront of drug development. Furthermore, mounting evidence has demonstrated deregulation of the miRNA network within AD, with the potential to contribute towards disease. Thus, RNAi-based therapeutics may be well-suited to a role in AD therapy. However, their development thus far has been hindered by challenges associated with their delivery to the brain. This study therefore explored the potential of EV-mediated delivery for RNAi-based therapeutics. Promising APP and BACE1-targeting siRNAs were identified and the regulation of APP and BACE1 by several miRNAs, shown to be downregulated in AD, was confirmed. Subsequently, EV-mediated delivery of validated siRNAs and miRNAs was investigated *in vitro* and *in vivo*. Electroporation was first assessed as a method to load exogenous siRNA cargoes into BM-DC and Neuro2A-derived EVs. Following a lack of functional activity in recipient cells both *in vitro* and *in vivo*, EVs and siRNAs were carefully characterised after electroporation. This revealed the formation of large siRNA aggregates both in the presence and absence of EVs, which confound estimates of loading efficiency and may

contribute towards the lack of observed functional activity. Consequently, an alternative endogenous EV-loading method was explored. Both siRNA and miRNA cargoes were endogenously loaded into EVs following transfection of either dsRNA effectors or RNAi-expression plasmids into source cells. Strategies to optimise this technique were then investigated. Promisingly, co-expression with RNA-binding proteins increased EV-loading of exogenous RNAi effectors. Furthermore, this effect appeared enhanced by inclusion of an acylation domain which served to anchor RNA-binding proteins to the membrane. While assessment of functional activity in recipient cells requires further optimisation, this study highlighted the importance of detailed EV characterisation after loading and demonstrated potential strategies by which endogenous EV-loading methods may be enhanced.

It is increasingly recognised that a combinatorial approach likely holds the most promise for the development of disease-modifying therapeutics for AD. Therefore, the remainder of this thesis focused upon the development of novel multi-gene targeting LNA-ASOs as a combinatorial approach towards AD therapy. Promisingly, two multi-gene targeting LNA-ASOs were identified and each shown to silence their two target genes simultaneously. Importantly, this translated to a significant reduction in amyloid-β (42) production by HEK293 APPswe cells. Unfortunately, the effect upon tau phosphorylation proved more challenging to assess *in vitro*. However, the identification of a multi-gene LNA-ASO targeting two separate mouse transcripts paves the way for future *in vivo* studies. Thus, this work demonstrated the promise of a multi-gene targeting LNA-ASO approach towards a combinatorial therapy for AD.

6.2 Challenges to Realising the Therapeutic Potential of Extracellular Vesicles

The results of the present study add to a wealth of emerging evidence which highlights the therapeutic potential of EVs both as delivery vehicles of exogenous cargoes and as therapeutic effectors in their own right. Indeed, EV-based therapeutics have recently progressed to clinical trial both as vaccines and anti-inflammatory agents in the treatment of cancer[543–545] (Clinical Trials: NCT01668849, NCT01294072). Promisingly, these clinical trials have shown that EV-based therapies appear well-tolerated and offer preliminary evidence for their efficacy in halting disease progression in some patients[543–545]. However, while these findings highlight the promise of EV-based therapeutics, important challenges still remain which must be resolved for their potential to be fully realised. These include the identification of scalable and sustainable sources of well-characterised EVs and the development of robust isolation, purification, loading, delivery and targeting protocols. A lack of understanding concerning the fundamental biology of EV-mediated delivery also limits clinical translation.

Currently, EVs are derived from a range of source cells including MSCs, DCs and tumour cells. However, a wide variety of cells produce exosomes, all of which possess different intrinsic properties in terms of targeting and function. In the current study, BM-DCs, Neuro2A and HEK293T cells were utilised as EV source cells. However, for future therapeutic purposes it is unlikely that cell-line-derived EVs represent the ideal choice given their oncogenic potential. It is therefore important to identify an optimum scalable source of EVs which possess the appropriate properties for each therapeutic application. In this respect, ESCs or induced pluripotent stem cells (iPSCs),

differentiated along desired lineage pathways, may represent more promising options[691,692]. Not only do primary cell-derived EVs possess inherent therapeutic characteristics which may enhance the therapeutic potential of exogenous cargoes[529–532,534–536,693], but EVs derived from autologous patient sources are more likely to be immunologically compatible. Efforts are currently underway to identify techniques by which EV production may be up-scaled from such sources[692,694]. One group have produced an immortalised line of hESC-MSCs by transfection of the oncogene, MYC. EVs derived from immortalised hESC-MSC cells retained the ability to ameliorate myocardial infarct size, suggesting that the therapeutic potential of EVs was maintained[694]. Alternatively, plant-derived EVs may represent another promising option. Grape EVs are internalised by mammalian cells in culture, display limited toxicity *in vivo* and have recently progressed to clinical trial based upon their anti-inflammatory properties[695] (NCT01668849, NCT01294072). Thus, while a number of potential EV sources have now been identified, which represents the best option for each therapeutic purpose remains to be determined.

Indeed, EVs may also carry pathogenic cargoes linked to a number of diseases including neurodegenerative disorders, cancer, rheumatoid arthritis and HIV[489,491,496,561–563,696–698]. EVs have been shown to be secreted in association with APP, amyloid-β and tau both *in vitro* and *in vivo*[491,561–563]. Similarly, in the current study, *APP* and *BACE1* mRNA and BACE1 protein were found within both HEK293T and Neuro2A-derived EVs. However, as discussed previously, EVs may also play a beneficial role in AD either by promoting microglial clearance of amyloid-β or through EV-mediated secretion of neprilysin, an enzyme important for amyloid-β degradation[571–574]. Together, these findings highlight the importance of selecting the correct EV source for a specific

therapeutic purpose. Detailed transcriptomic and proteomic analyses of all EV preparations intended for clinical use are therefore required to screen natural cargoes to minimise the risk of undesired off-target effects. Not only are such analyses critical with regards to exploiting EVs for the delivery of therapeutic nucleic acids, but they may also help to inform strategies to target the proposed pathogenic role for EVs in disease.

EVs are currently harvested using a variety of isolation and purification protocols. To date, ultracentrifugation reflects the most accepted method for EV isolation and hence was the method chosen in the current study. However, due to concerns relating to operator-dependent variability, low yields, protein contamination and disruption to exosomal integrity, alternative methods are being explored. These have included ultrafiltration, sucrose density gradients, immunoaffinity capture with beads and microfluidic-based approaches[593,699–701]. Given the variety of potential techniques available, further optimisation is required to identify the optimal protocol for achieving clinical grade EV preparations. Indeed, while EVs are often described as a homogenous population, work within the lab and by others[702] has revealed two distinct populations within tumour cell-derived EVs. Whether distinct populations mediate separate biological processes and whether this is specific to tumour-derived EVs remains to be seen. However, these findings highlight the importance of identifying a highly characterised source of EVs for therapeutic applications.

While this work focused upon EV-mediated delivery of RNAi-based molecules, EVs may be suitable for the delivery of a wide range of therapeutics. However, as highlighted throughout this thesis, EV-loading protocols require refinement. While previous studies have used electroporation to load EVs, this represents a relatively

inefficient method and has often proved inconsistent despite identical parameters[450,508,511,513]. The results of the current study and those of Kooijmans *et al*.[566] suggest that this may be related to the formation of siRNA aggregates during electroporation. Although endogenous loading mechanisms, such as those explored here, may represent a promising alternative it is important to note that simple overexpression of exogenous cargoes in source cells may not necessarily reflect the most efficient mechanism either. While the current study aimed to optimise this approach through the co-expression of RNA-binding proteins, more cost-effective and knowledge-driven loading methods are required. In this respect, a growing understanding of the fundamental processes underlying EV biogenesis should help to inform the development of future loading methods. Thus, the identification of sequence motifs which may direct the sequestration of proteins, mRNAs and miRNAs within EVs suggests the existence of endogenous enrichment mechanisms which in future may be exploited for specific loading of exogenous cargoes[467,472–475].

A better understanding of EV biology may also inform strategies to improve EV targeting and uptake by recipient cells. While EVs may possess intrinsic targeting abilities dependent upon their cellular origin, they may also be engineered to display targeting moieties, such as the RVG-ligand employed in this study, which confer targeting to a desired tissue or cellular subtype[467,508,513,519]. While tetraspanin complexes are thought to play a role in determining target cell specificity[458,459], a fuller understanding of the factors which permit endogenous EV targeting to recipient cells is required. Similarly, while adhesion molecules may be important for exosome and recipient cell binding[457,458,493,703], the mechanisms controlling recipient cell uptake are not fully elucidated. A clearer understanding of the inherent properties driving these

interactions may guide the development of modifications to further enhance specificity and selectivity of therapeutic EVs. Furthermore, the development of additional targeting strategies may allow for a wider array of delivery methods for the EVs themselves. Current routes of delivery have involved intranasal application or intravenous, intradermal and subcutaneous injections[508,513,517,543–545]. However, current clinical trials designed to evaluate the efficacy of grape exosomes will administer EVs in either powder or tablet form. This may represent a promising strategy for other diseases if EVs may be engineered to efficiently direct them towards tissues of interest and away from excretory organs.

Delineating answers to the outstanding issues above will be important in furthering our understanding of the biological processes underpinning EVs as successful nanocarriers and in guiding their development for therapeutic purposes. Furthermore, an understanding of the necessary components which endow EVs with the capacity for drug delivery may facilitate the design of artificial "exosome-like" vesicles which possess only those characteristics required for delivery and are devoid of endogenous content which may interfere with therapeutic applications. This approach may be particularly valuable given the recent association of EVs with pathogenic cargoes as outlined above. Indeed, recent studies have begun to explore the concept of artificial "exosome-like" vesicles through the use of liposomes whose lipid composition is designed to resemble that of exosomes. These studies demonstrated increased bioactivity and treatment efficacy of proteins tethered or coated onto the surface of exosome-like vesicles with no evidence for systemic toxicity[704–707]. Together, these studies highlight how an understanding of inherent exosome properties may be

exploited to allow the delivery of exogenous therapeutic molecules, without the risk of potentially harmful endogenous cargoes.

Finally, while this thesis has focused upon EVs as delivery vehicles for RNAi-based therapeutics, EVs may have further utility in the context of AD in terms of their biomarker potential[708]. Several recent studies have suggested that the content of blood derived-EVs could be used to distinguish AD patients from controls[709–713]. Fiandaca and colleagues[709] reported that plasma-derived EVs from AD patients contained significantly higher levels of amyloid-β (42), phosphorylated tau-181 and phosphorylated tau-396. Individually, each protein predicted AD with an accuracy of more than 95%, while combined, their predictive ability approached 100%, suggesting that they could be used to distinguish AD patients accurately from controls[709]. Furthermore, all three proteins were elevated in the early blood samples of those who later developed AD, suggesting that they may have utility in predicting disease at preclinical stages[709]. In a series of further papers, Kapogiannis and colleagues[711–713] demonstrated differential expression in neural exosomes derived from AD patients relative to controls, for a range of proteins including lysosomal proteins, cellular survival factors and type 1 insulin receptor substrate. Altered protein expression was apparent up to 10 years prior to clinical diagnosis and could be used to accurately classify 100% of AD patients[711–713].

Alternatively, Cheng *et al.*[710] suggested that the miRNA content of EVs may represent a biomarker for AD. In their study, the profile of 16 miRNAs within serum-derived EVs combined with established risk factors including age, sex and *APOE ε4* status allowed the prediction of AD with a sensitivity and specificity of 87% and 77%, respectively[710].

While these results await validation in larger populations, together they suggest the promise of EV-based biomarkers in the context of AD. As discussed previously, identifying sensitive and less invasive biomarkers is crucial. Not only would accurate biomarkers aid the diagnosis of AD, which currently can only be confirmed post-mortem, but they may also help to identify homogenous populations of AD patients for clinical trials and provide alternative markers of disease progression and drug efficacy.

In summary, the findings from the current study add to existing literature suggesting that EVs hold promise for the delivery of a range of therapeutic cargoes. However, future work must address the challenges outlined above if the promise of EV-mediated therapeutics is to be achieved.

6.3 Multi-gene Targeting by LNA-ASOs

ASOs represent a promising option for the therapeutic silencing of both normal and mutant gene expression. To date, two phosphorothioate-modified ASOs have been approved for the treatment of AIDS and familial hypercholesterolemia[400,401]. However, a growing number of ASOs are now progressing towards clinical trial for a range of diseases including cancer, HCV, DMD and neurodegenerative disease[398,399,402,403,684,714–716]. Indeed, the first two clinical trials for ASO-based therapeutics targeting the neurodegenerative diseases, SMA and ALS, are now underway[398,402,684]. Promisingly, intrathecal-based delivery of both ASOs appears well-tolerated with SMA-based trials reaching phase III (NCT02292537)[402]. Furthermore, ASOs targeting SMA appear functional, with increased CSF SMN protein levels and improved muscle function observed in children treated with multiple doses of ISIS-SMNRx[717]. Together, these studies highlight the safety and efficacy of ASOs directly administered to the CNS, paving the way for the development of ASOs for the treatment of other neurological disorders.

The results of the current study suggest that multi-gene targeting LNA-ASOs have potential for the silencing of AD-relevant genes. These findings are consistent with those of previous studies which have shown that modified-ASOs, utilising a range of different chemistries, elicit potent silencing of APP, GSK3β, presenilin-1 and tau-based targets *in vitro* and *in vivo*[406–413]. Importantly, these studies revealed that silencing of these genes resulted not only in a reduction of amyloid-β and markers of neuroinflammation and oxidative stress but was also associated with the reversal of memory deficits in two mouse models of AD[406–413]. Thus, it will be important for future

work to determine whether the multi-gene LNA-ASOs in the current study may have similar disease-modifying properties. In this respect, the identification of a multi-gene LNA-ASO which targets mouse transcripts for *Bace1* and *mTOR* (mBAMT) is important as it will allow preliminary *in vivo* screens of this novel multi-gene targeting technology. While the multi-gene mBAMT LNA-ASO reduced both Bace1 and mTOR expression, further studies are required to determine whether this translates to a reduction in amyloid-β production and tau phosphorylation.

The design of multi-gene LNA-ASOs was based upon previous reports suggesting that a gapmer design of 7-9 DNA bases flanked by three LNA bases within a phosphorothioate-modified backbone is sufficient to induce potent RNase H-mediated gene silencing[417]. This chemistry has been shown not only to increase the binding affinity of LNA-ASOs but also to increase their stability in serum[417]. However, it should be noted that LNA-ASOs may be associated with hepatotoxicity *in vivo* although this may depend crucially on specific sequence motifs and length[668–670,682]. While shorter LNA-ASOs may be less toxic, it will be important to determine whether the LNA-ASOs investigated in the current study induce toxicity *in vivo*. It has been suggested that combining structural elements of different modifications, such as those of 2'-O-methoxyethyl residues and LNAs, may improve potency while reducing hepatotoxicity[718]. Thus, given the promise of ASOs capable of targeting multiple genes, it will be interesting to compare the efficacy of such modifications for the sequences upon which the current multi-gene LNA-ASOs are based.

Once delivered to the CSF, ASOs may be taken up by neuronal cells widely distributed throughout the brain[684–686]. Furthermore, ASO-based therapeutics have been shown to

elicit long-term silencing of their targets in neuronal cells following direct ASO infusions[685,690]. This may relate not only to the presence of the BBB which helps to maintain high ASO concentrations within the CNS following direct CSF delivery but also to reduced intrinsic nuclease activity in neuronal cells compared to the periphery[719]. This suggests that ASOs are well-suited to the treatment of chronic neurodegenerative disease, where long-term silencing of disease-relevant proteins is required. As outlined above, promising data from the ongoing ASO-based clinical trial in SMN indicates that repeated administrations are well-tolerated and associated with functional muscle improvements[717]. This is important as it is likely that regular dosing will be required to maintain optimal levels of silencing for a range of neurodegenerative diseases. The current data from clinical trials investigating ASOs in the context of neurodegenerative disease therefore appear encouraging. However, long-term studies are required to determine optimal dosing regimens and any long-term consequences upon efficacy and safety.

The two human clinical trials investigating the feasibility of ASOs for ALS and SMN employ intrathecal delivery. While this strategy appears well-tolerated, it is an invasive procedure and may be associated with adverse effects including post-lumbar puncture syndrome, back pain and nausea[402]. Future studies should therefore investigate alternative methods for less-invasive effective delivery. A preliminary experiment was performed in the current study to investigate the utility of EV-mediated delivery of multi-gene LNA-ASOs. While no functional effects were observed in recipient cells, EV-mediated delivery requires much optimisation as discussed previously. Thus, EV-based delivery remains one potential avenue which should be explored alongside other potential strategies such as conjugation or complexation of ASOs with either receptor

ligands to induce receptor-mediated transcytosis or cell-penetrating peptides for transport across the BBB[687,688].

The novel multi-gene LNA-ASOs described in this study are of particular interest given the drive towards a combinatorial approach for AD therapy. While further clarification is required to fully elucidate the effects upon tau phosphorylation, the current data suggest that both gene targets were significantly silenced by multi-gene LNA-ASOs. Furthermore, a substantial reduction in amyloid-β (42) production was achieved by partial gene silencing following LNA-ASO treatment. This is crucial given that targets may be involved in a range of key processes and thus require a degree of preserved function. Future studies will be required to determine if a similar reduction in amyloid-β is achieved following partial silencing *in vivo* and, if so, to calculate the degree of silencing required to reach a therapeutic threshold for disease modification while avoiding adverse effects.

The multi-gene LNA-ASOs identified here allow a combinatorial approach towards therapy in their own right. However, it is feasible that their efficacy might be further enhanced when applied in combination with other therapeutic compounds. Thus, if they are successfully validated in future studies, another promising option will be to explore their combined administration with a range of other compounds. Indeed, one limitation of the multi-gene LNA-ASO approach outlined here is that they are crucially dependent upon overlapping sequences between different genes of interest. While the inclusion of abasic sites may help to cover mismatches between sequences of interest, combined administration of multi-gene targeting LNA-ASOs, either with each other or with other

compounds, may allow targeting of an even greater number of pathways without the strict requirement for appropriately overlapping sequences.

In summary, ASOs are emerging as a promising class of therapeutics for the treatment of neurodegenerative disease. The findings from the current study add to the existing literature suggesting that ASOs represent a feasible strategy towards AD therapy and highlight the potential of a combinatorial multi-gene targeting LNA-ASO-based approach.

6.4 Concluding Remarks

The work in this thesis has contributed towards the development and delivery of novel RNA-based therapeutics for the treatment of AD. Promising miRNA and siRNA candidates regulating key AD-associated genes have been identified and their EV-mediated delivery to recipient cells explored. Electroporation as a method of EV-loading was shown to be confounded by the formation of large siRNA aggregates. In contrast, RNAi-based candidates could be loaded more effectively by exploitation of endogenous loading mechanisms. Loading was further enhanced by co-expression with RNA-binding proteins, particularly when they were tagged with a membrane-anchoring acylation domain. Finally, a novel multi-gene targeting LNA-ASO-based approach was identified and the simultaneous silencing of crucial AD genes demonstrated. This strategy may represent a novel approach towards the combinatorial treatment of AD.

7 References

1. Davies, P. & Maloney, A. J. Selective loss of central cholinergic neurons in Alzheimer's disease. *Lancet* **2,** 1403 (1976).

2. Alzheimer's Association. Alzheimer's disease facts and figures. *Alzheimer's Dement.* **11,** 332 (2015).

3. Alzheimer's Disease International. World Alzheimer Report 2013. (2013).

4. Dementia UK. *Prevalence and Economic Cost of Dementia in the UK*. (Kings College London and the London School of Economics, 2007).

5. De Jonghe, C. *et al.* Pathogenic APP mutations near the gamma-secretase cleavage site differentially affect Abeta secretion and APP C-terminal fragment stability. *Hum. Mol. Genet.* **10,** 1665–1671 (2001).

6. Murrell, J., Farlow, M., Ghetti, B. & Benson, M. D. A mutation in the amyloid precursor protein associated with hereditary Alzheimer's disease. *Science* **254,** 97–99 (1991).

7. Sherrington, R. *et al.* Cloning of a gene bearing missense mutations in early-onset familial Alzheimer's disease. *Nature* **375,** 754–760 (1995).

8. Levy-Lahad, E. *et al.* Candidate gene for the chromosome 1 familial Alzheimer's disease locus. *Science* **269,** 973–977 (1995).

9. Rogaev, E. I. *et al.* Familial Alzheimer's disease in kindreds with missense mutations in a gene on chromosome 1 related to the Alzheimer's disease type 3 gene. *Nature* **376,** 775–778 (1995).

10. De Strooper, B. Loss-of-function presenilin mutations in Alzheimer disease. Talking point on the role of presenilin mutations in Alzheimer disease. *EMBO Rep.* **8,** 141–146 (2007).

11. Reitz, C. & Mayeux, R. Alzheimer disease: epidemiology, diagnostic criteria, risk factors and biomarkers. *Biochem. Pharmacol.* **88,** 640–651 (2014).

12. Goate, A. *et al.* Segregation of a missense mutation in the amyloid precursor protein gene with familial Alzheimer's disease. *Nature* **349,** 704–706 (1991).

13. Di Fede, G. *et al.* Good gene, bad gene: new APP variant may be both. *Prog. Neurobiol.* **99,** 281–292 (2012).

14. Rovelet-Lecrux, A. *et al.* APP locus duplication causes autosomal dominant early-onset Alzheimer disease with cerebral amyloid angiopathy. *Nat. Genet.* **38,** 24–26 (2006).

15. Tomiyama, T. *et al.* A new amyloid beta variant favoring oligomerization in Alzheimer's-type dementia. *Ann. Neurol.* **63,** 377–387 (2008).

16. Bird, T. D. Early-onset familial Alzheimer disease. *GeneReviews* (2012).

17. Di Fede, G. *et al.* A recessive mutation in the APP gene with dominant-negative effect on amyloidogenesis. *Science* **323,** 1473–1477 (2009).

18. Citron, M. *et al.* Mutation of the beta-amyloid precursor protein in familial Alzheimer's disease increases beta-protein production. *Nature* **360,** 672–674 (1992).

19. De Strooper, B. *et al.* Deficiency of presenilin-1 inhibits the normal cleavage of amyloid precursor protein. *Nature* **391,** 387–390 (1998).

20. Hartley, D. *et al.* Down syndrome and Alzheimer's disease: common pathways, common goals. *Alzheimer's Dement.* **14,** 1–10 (2014).

21. Jonsson, T. *et al.* A mutation in APP protects against Alzheimer's disease and age-related cognitive decline. *Nature* **488,** 96–99 (2012).

22. Pericak-Vance, M. A. *et al.* Linkage studies in familial Alzheimer disease: evidence for chromosome 19 linkage. *Am. J. Hum. Genet.* **48,** 1034–1050 (1991).

23. Corder, E. H. *et al.* Gene dose of apolipoprotein E type 4 allele and the risk of Alzheimer's disease in late onset families. *Science* **261,** 921–923 (1993).

24. Mahley, R. W. & Rall, S. C. Apolipoprotein E: far more than a lipid transport protein. *Annu. Rev. Genomics Hum. Genet.* **1,** 507–537 (2000).

25. Castellano, J. M. *et al.* Human apoE isoforms differentially regulate brain amyloid-β peptide clearance. *Sci. Transl. Med.* **3,** 89ra57 (2011).

26. Chen, Y., Durakoglugil, M. S., Xian, X. & Herz, J. ApoE4 reduces glutamate receptor function and synaptic plasticity by selectively impairing ApoE receptor recycling. *Proc. Natl. Acad. Sci.* **107,** 12011–12016 (2010).

27. Mahley, R. W., Weisgraber, K. H. & Huang, Y. Apolipoprotein E4: a causative factor and therapeutic target in neuropathology, including Alzheimer's disease. *Proc. Natl. Acad. Sci. U. S. A.* **103,** 5644–5651 (2006).

28. Huang, Y. Molecular and cellular mechanisms of apolipoprotein E4 neurotoxicity and potential therapeutic strategies. *Curr. Opin. Drug Discov. Devel.* **9,** 627–641 (2006).

29. de-Almada, B. V. P. *et al.* Protective effect of the APOE-e3 allele in Alzheimer's disease. *Braz. J. Med. Biol. Res.* **45,** 8–12 (2012).

30. Rebeck, G. W., Kindy, M. & LaDu, M. J. Apolipoprotein E and Alzheimer's disease: the protective effects of ApoE2 and E3. *J. Alzheimers. Dis.* **4,** 145–154 (2002).

31. Farrer, L. A. *et al.* Effects of age, sex, and ethnicity on the association between apolipoprotein E genotype and Alzheimer disease. A meta-analysis. APOE and Alzheimer Disease Meta Analysis Consortium. *JAMA* **278,** 1349–1356 (1997).

32. Kurz, A. *et al.* Apolipoprotein E type 4 allele and Alzheimer's disease: effect on age at onset and relative risk in different age groups. *J. Neurol.* **243,** 452–456 (1996).

33. Breitner, J. C. *et al.* APOE-epsilon4 count predicts age when prevalence of AD increases, then declines: the Cache County Study. *Neurology* **53,** 321–331 (1999).

34. Holtzman, D. M. *et al.* Apolipoprotein E isoform-dependent amyloid deposition and neuritic degeneration in a mouse model of Alzheimer's disease. *Proc. Natl. Acad. Sci.* **97,** 2892–2897 (2000).

35. Hashimoto, T. *et al.* Apolipoprotein E, especially apolipoprotein E4, increases the oligomerization of amyloid β peptide. *J. Neurosci.* **32,** 15181–15192 (2012).

36. Drzezga, A. *et al.* Effect of APOE genotype on amyloid plaque load and gray matter volume in Alzheimer disease. *Neurology* **72,** 1487–1494 (2009).

37. Valla, J. *et al.* Reduced posterior cingulate mitochondrial activity in expired young adult carriers of the APOE ε4 allele, the major late-onset Alzheimer's susceptibility gene. *J. Alzheimers. Dis.* **22,** 307–313 (2010).

38. Shaw, P. *et al.* Cortical morphology in children and adolescents with different apolipoprotein E gene polymorphisms: an observational study. *Lancet Neurol.* **6,** 494–500 (2007).

39. Grouselle, D. *et al.* Loss of somatostatin-like immunoreactivity in the frontal cortex of Alzheimer patients carrying the apolipoprotein epsilon 4 allele. *Neurosci. Lett.* **255,** 21–24 (1998).

40. Huang, Y. & Mucke, L. Alzheimer mechanisms and therapeutic strategies. *Cell* **148,** 1204–1222 (2012).

41. Filippini, N. *et al.* Distinct patterns of brain activity in young carriers of the APOE-epsilon4 allele. *Proc. Natl. Acad. Sci. U. S. A.* **106,** 7209–7214 (2009).

42. Harold, D. *et al.* Genome-wide association study identifies variants at CLU and PICALM associated with Alzheimer's disease. *Nat. Genet.* **41,** 1088–1093 (2009).

43. Hollingworth, P., Harold, D., Jones, L., Owen, M. J. & Williams, J. Alzheimer's disease genetics: current knowledge and future challenges. *Int. J. Geriatr. Psychiatry* **26,** 793–802 (2011).

44. Lambert, J. *et al.* Genome-wide association study identifies variants at CLU and CR1 associated with Alzheimer's disease. *Nat. Genet.* **41,** 1094–1099 (2009).

45. Naj, A. C. *et al.* Common variants at MS4A4/MS4A6E, CD2AP, CD33 and EPHA1 are associated with late-onset Alzheimer's disease. *Nat. Genet.* **43,** 436–441 (2011).

46. Seshadri, S. *et al.* Genome-wide analysis of genetic loci associated with Alzheimer disease. *JAMA* **303,** 1832–1840 (2010).

47. Escott-Price, V. *et al.* Gene-wide analysis detects two new susceptibility genes for Alzheimer's disease. *PLoS One* **9,** e94661 (2014).

48. Lambert, J. C. *et al.* Meta-analysis of 74,046 individuals identifies 11 new susceptibility loci for Alzheimer's disease. *Nat. Genet.* **45,** 1452–1458 (2013).

49. Jun, G. *et al.* A novel Alzheimer disease locus located near the gene encoding tau protein. *Mol. Psychiatry* 1–10 (2015).

50. Reitz, C. Genetic loci associated with Alzheimer's disease. *Future Neurol.* **9,** 119–122 (2014).

51. Liang, Y., Buckley, T. R., Tu, L., Langdon, S. D. & Tedder, T. F. Structural organization of the human MS4A gene cluster on Chromosome 11q12. *Immunogenetics* **53,** 357–368 (2001).

52. Kim, W. S., Weickert, C. S. & Garner, B. Role of ATP-binding cassette transporters in brain lipid transport and neurological disease. *J. Neurochem.* **104,** 1145–1166 (2008).

53. Jones, L., Harold, D. & Williams, J. Genetic evidence for the involvement of lipid metabolism in Alzheimer's disease. *Biochim. Biophys. Acta - Mol. Cell Biol. Lipids* **1801,** 754–761 (2010).

54. De Silva, H. *et al.* A 70-kDa apolipoprotein designated ApoJ is a marker for subclasses of human plasma high density lipoproteins. *J. Biol. Chem.* **265,** 13240–13247 (1990).

55. Jehle, A. W. *et al.* ATP-binding cassette transporter A7 enhances phagocytosis of apoptotic cells and associated ERK signaling in macrophages. *J. Cell Biol.* **174,** 547–556 (2006).

56. Tebar, F., Bohlander, S. K. & Sorkin, A. Clathrin assembly lymphoid myeloid leukemia (CALM) protein: localization in endocytic-coated pits, interactions with clathrin, and the impact of overexpression on clathrin-mediated traffic. *Mol. Biol. Cell* **10,** 2687–2702 (1999).

57. Wigge, P. *et al.* Amphiphysin heterodimers: potential role in clathrin-mediated endocytosis. *Mol. Biol. Cell* **8,** 2003–2015 (1997).

58. Tateno, H. *et al.* Distinct endocytic mechanisms of CD22 (Siglec-2) and Siglec-F reflect roles in cell signaling and innate immunity. *Mol. Cell. Biol.* **27,** 5699–5710 (2007).

59. Lynch, D. K. *et al.* A Cortactin-CD2-associated protein (CD2AP) complex provides a novel link between epidermal growth factor receptor endocytosis and the actin cytoskeleton. *J. Biol. Chem.* **278,** 21805–21813 (2003).

60. Nuutinen, T., Suuronen, T., Kauppinen, A. & Salminen, A. Clusterin: a forgotten player in Alzheimer's disease. *Brain Res. Rev.* **61,** 89–104 (2009).

61. Hazrati, L. *et al.* Genetic association of CR1 with Alzheimer's disease: a tentative disease mechanism. *Neurobiol. Aging* **33,** 2949.e5–2949.e12 (2012).

62. Keenan, B. T. *et al.* A coding variant in CR1 interacts with APOE-ε4 to influence cognitive decline. *Hum. Mol. Genet.* **21,** 2377–2388 (2012).

63. Harel, A., Wu, F., Mattson, M. P., Morris, C. M. & Yao, P. J. Evidence for CALM in directing VAMP2 trafficking. *Traffic* **9,** 417–429 (2008).

64. Reitz, C. *et al.* Meta-analysis of the association between variants in SORL1 and Alzheimer disease. *Arch. Neurol.* **68,** 99–106 (2011).

65. Bertram, L., Lill, C. M. & Tanzi, R. E. The genetics of Alzheimer disease: back to the future. *Neuron* **68,** 270–281 (2010).

66. Hardy, J. & Higgins, G. Alzheimer's disease: the amyloid cascade hypothesis. *Science* **256,** 184–185 (1992).

67. Zhang, Y., Thompson, R., Zhang, H. & Xu, H. APP processing in Alzheimer's disease. *Mol. Brain* **4,** 3 (2011).

68. Kitazume, S. *et al.* Brain endothelial cells produce amyloid-beta from amyloid precursor protein 770 and preferentially secrete the O-glycosylated form. *J. Biol. Chem.* **285,** 40097–40103 (2010).

69. Greenfield, J. P. *et al.* Endoplasmic reticulum and trans-Golgi network generate distinct populations of Alzheimer beta-amyloid peptides. *Proc. Natl. Acad. Sci. U. S. A.* **96,** 742–747 (1999).

70. Hartmann, T. *et al.* Distinct sites of intracellular production for Alzheimer's disease A beta40/42 amyloid peptides. *Nat. Med.* **3,** 1016–1020 (1997).

71. Kaether, C., Haass, C. & Steiner, H. Assembly, trafficking and function of gamma-secretase. *Neurodegener. Dis.* **3,** 275–283 (2006).

72. Kamenetz, F. *et al.* APP processing and synaptic function. *Neuron* **37,** 925–937 (2003).

73. Weyer, S. W. *et al.* APP and APLP2 are essential at PNS and CNS synapses for transmission, spatial learning and LTP. *EMBO J.* **30,** 2266–2280 (2011).

74. Aydin, D., Weyer, S. W. & Müller, U. C. Functions of the APP gene family in the nervous system: insights from mouse models. *Exp. Brain Res.* **217,** 423–434 (2012).

75. Chasseigneaux, S. & Allinquant, B. Functions of Aβ, sAPPα and sAPPβ: Similarities and differences. *J. Neurochem.* **120,** 99–108 (2012).

76. Tyan, S. *et al.* Amyloid precursor protein (APP) regulates synaptic structure and function. *Mol. Cell. Neurosci.* **51,** 43–52 (2012).

77. Nikolaev, A., McLaughlin, T., O'Leary, D. D. M. & Tessier-Lavigne, M. APP binds DR6 to trigger axon pruning and neuron death via distinct caspases. *Nature* **457,** 981–989 (2009).

78. Sonnen, J. A. *et al.* Pathological correlates of dementia in a longitudinal, population-based sample of aging. *Ann. Neurol.* **62,** 406–413 (2007).

79. Terry, R. D. *et al.* Physical basis of cognitive alterations in Alzheimer's disease: synapse loss is the major correlate of cognitive impairment. *Ann. Neurol.* **30,** 572–580 (1991).

80. Dickson, D. W. *et al.* Correlations of synaptic and pathological markers with cognition of the elderly. *Neurobiol. Aging* **16,** 285–304 (1995).

81. Holmes, C. *et al.* Long-term effects of Abeta42 immunisation in Alzheimer's disease: follow-up of a randomised, placebo-controlled phase I trial. *Lancet* **372,** 216–223 (2008).

82. Nicoll, J. A. R. *et al.* Neuropathology of human Alzheimer disease after immunization with amyloid-beta peptide: a case report. *Nat. Med.* **9,** 448–452 (2003).

83. Elobeid, A., Rantakömi, S., Soininen, H. & Alafuzoff, I. Alzheimer's disease-related plaques in nondemented subjects. *Alzheimers. Dement.* **10,** 522–529 (2014).

84. Ferreira, S. T. & Klein, W. L. The Aβ oligomer hypothesis for synapse failure and memory loss in Alzheimer's disease. *Neurobiol. Learn. Mem.* **96,** 529–543 (2011).

85. Zempel, H., Thies, E., Mandelkow, E. & Mandelkow, E.-M. Abeta oligomers cause localized Ca(2+) elevation, missorting of endogenous Tau into dendrites, Tau phosphorylation, and destruction of microtubules and spines. *J. Neurosci.* **30,** 11938–11950 (2010).

86. Lacor, P. N. *et al.* Synaptic targeting by Alzheimer's-related amyloid beta oligomers. *J. Neurosci.* **24,** 10191–10200 (2004).

87. Klein, W. L. Abeta toxicity in Alzheimer's disease: globular oligomers (ADDLs) as new vaccine and drug targets. *Neurochem. Int.* **41,** 345–352 (2002).

88. Larson, M. E. & Lesné, S. E. Soluble Aβ oligomer production and toxicity. *J. Neurochem.* **120,** 125–139 (2012).

89. Haass, C. & Selkoe, D. J. Soluble protein oligomers in neurodegeneration: lessons from the Alzheimer's amyloid beta-peptide. *Nat. Rev. Mol. Cell Biol.* **8,** 101–112 (2007).

90. McLean, C. A. *et al.* Soluble pool of Abeta amyloid as a determinant of severity of neurodegeneration in Alzheimer's disease. *Ann. Neurol.* **46,** 860–866 (1999).

91. Lue, L. F. *et al.* Soluble amyloid beta peptide concentration as a predictor of synaptic change in Alzheimer's disease. *Am. J. Pathol.* **155,** 853–862 (1999).

92. Cohen, R. M. *et al.* A transgenic Alzheimer rat with plaques, tau pathology, behavioral impairment, oligomeric aβ, and frank neuronal loss. *J. Neurosci.* **33,** 6245–6256 (2013).

93. Selkoe, D. J. Alzheimer's disease is a synaptic failure. *Science* **298,** 789–791 (2002).

94. Treusch, S., Cyr, D. M. & Lindquist, S. Amyloid deposits: protection against toxic protein species? *Cell Cycle* **8,** 1668–1674 (2009).

95. Hardy, J. The amyloid hypothesis for Alzheimer's disease: a critical reappraisal. *J. Neurochem.* **110,** 1129–1134 (2009).

96. Shankar, G. M. *et al.* Amyloid-beta protein dimers isolated directly from Alzheimer's brains impair synaptic plasticity and memory. *Nat. Med.* **14,** 837–842 (2008).

97. Walsh, D. M. *et al.* Naturally secreted oligomers of amyloid beta protein potently inhibit hippocampal long-term potentiation in vivo. *Nature* **416,** 535–539 (2002).

98. Walsh, D. M., Tseng, B. P., Rydel, R. E., Podlisny, M. B. & Selkoe, D. J. The oligomerization of amyloid beta-protein begins intracellularly in cells derived from human brain. *Biochemistry* **39,** 10831–10839 (2000).

99. Ono, K., Condron, M. M. & Teplow, D. B. Structure-neurotoxicity relationships of amyloid beta-protein oligomers. *Proc. Natl. Acad. Sci. U. S. A.* **106,** 14745–14750 (2009).

100. Lesné, S. *et al.* A specific amyloid-beta protein assembly in the brain impairs memory. *Nature* **440,** 352–357 (2006).

101. Reed, M. N. *et al.* Cognitive effects of cell-derived and synthetically derived Aβ oligomers. *Neurobiol. Aging* **32,** 1784–1794 (2011).

102. Sherman, M. A. & Lesné, S. E. Detecting aβ*56 oligomers in brain tissues. *Methods Mol. Biol.* **670,** 45–56 (2011).

103. Lesné, S. E. *et al.* Brain amyloid-β oligomers in ageing and Alzheimer's disease. *Brain* **136,** 1383–1398 (2013).

104. Togo, T. & Dickson, D. W. Tau accumulation in astrocytes in progressive supranuclear palsy is a degenerative rather than a reactive process. *Acta Neuropathol.* **104,** 398–402 (2002).

105. Goedert, M. & Jakes, R. Mutations causing neurodegenerative tauopathies. *Biochim. Biophys. Acta - Mol. Basis Dis.* **1739,** 240–250 (2005).

106. Spillantini, M. G. *et al.* Mutation in the tau gene in familial multiple system tauopathy with presenile dementia. *Proc. Natl. Acad. Sci. U. S. A.* **95,** 7737–7741 (1998).

107. Arai, T. *et al.* Distinct isoforms of tau aggregated in neurons and glial cells in brains of patients with Pick's disease, corticobasal degeneration and progressive supranuclear palsy. *Acta Neuropathol.* **101,** 167–173 (2001).

108. Binder, L. I., Frankfurter, A. & Rebhun, L. I. The distribution of tau in the mammalian central nervous system. *J. Cell Biol.* **101,** 1371–1378 (1985).

109. Goedert, M., Spillantini, M. G., Jakes, R., Rutherford, D. & Crowther, R. A. Multiple isoforms of human microtubule-associated protein tau: sequences and localization in neurofibrillary tangles of Alzheimer's disease. *Neuron* **3,** 519–526 (1989).

110. Andreadis, A., Brown, W. M. & Kosik, K. S. Structure and novel exons of the human tau gene. *Biochemistry* **31,** 10626–10633 (1992).

111. Liu, F. & Gong, C. Tau exon 10 alternative splicing and tauopathies. *Mol. Neurodegener.* **3,** 8 (2008).

112. Kosik, K. S., Orecchio, L. D., Bakalis, S. & Neve, R. L. Developmentally regulated expression of specific tau sequences. *Neuron* **2,** 1389–1397 (1989).

113. D'Souza, I. & Schellenberg, G. D. Regulation of tau isoform expression and dementia. *Biochim. Biophys. Acta* **1739,** 104–115 (2005).

114. Baker, M. *et al.* Association of an extended haplotype in the tau gene with progressive supranuclear palsy. *Hum. Mol. Genet.* **8,** 711–715 (1999).

115. Stefansson, H. *et al.* A common inversion under selection in Europeans. *Nat. Genet.* **37,** 129–137 (2005).

116. Caffrey, T. M. & Wade-Martins, R. Functional MAPT haplotypes: bridging the gap between genotype and neuropathology. *Neurobiol. Dis.* **27,** 1–10 (2007).

117. Kwok, J. B. J. *et al.* Tau haplotypes regulate transcription and are associated with Parkinson's disease. *Ann. Neurol.* **55,** 329–334 (2004).

118. Skipper, L. *et al.* Linkage disequilibrium and association of MAPT H1 in Parkinson disease. *Am. J. Hum. Genet.* **75,** 669–677 (2004).

119. Myers, A. J. *et al.* The H1c haplotype at the MAPT locus is associated with Alzheimer's disease. *Hum. Mol. Genet.* **14,** 2399–2404 (2005).

120. Hayesmoore, J. B. G. *et al.* The effect of age and the H1c MAPT haplotype on MAPT expression in human brain. *Neurobiol. Aging* **30,** 1652–1656 (2009).

121. Rademakers, R. *et al.* High-density SNP haplotyping suggests altered regulation of tau gene expression in progressive supranuclear palsy. *Hum. Mol. Genet.* **14,** 3281–3292 (2005).

122. Caffrey, T. M., Joachim, C., Paracchini, S., Esiri, M. M. & Wade-Martins, R. Haplotype-specific expression of exon 10 at the human MAPT locus. *Hum. Mol. Genet.* **15,** 3529–3537 (2006).

123. Caffrey, T. M., Joachim, C. & Wade-Martins, R. Haplotype-specific expression of the N-terminal exons 2 and 3 at the human MAPT locus. *Neurobiol. Aging* **29,** 1923–1929 (2008).

124. Makrides, V., Massie, M. R., Feinstein, S. C. & Lew, J. Evidence for two distinct binding sites for tau on microtubules. *Proc. Natl. Acad. Sci. U. S. A.* **101,** 6746–6751 (2004).

125. Magnani, E. *et al.* Interaction of tau protein with the dynactin complex. *EMBO J.* **26,** 4546–4554 (2007).

126. Ittner, L. M. *et al.* Dendritic function of tau mediates amyloid-β toxicity in Alzheimer's disease mouse models. *Cell* **142,** 387–397 (2010).

127. Morris, M., Maeda, S., Vossel, K. & Mucke, L. The many faces of tau. *Neuron* **70,** 410–426 (2011).

128. Iqbal, K. & Grundke-Iqbal, I. Pharmacological approaches of neurofibrillary degeneration. *Curr. Alzheimer Res.* **2,** 335–341 (2005).

129. Bhaskar, K., Yen, S. & Lee, G. Disease-related modifications in Tau affect the interaction between Fyn and Tau. *J. Biol. Chem.* **280,** 35119–35125 (2005).

130. Cohen, T. J. *et al.* The acetylation of tau inhibits its function and promotes pathological tau aggregation. *Nat. Commun.* **2,** 252 (2011).

131. Bierer, L. M. *et al.* Neocortical neurofibrillary tangles correlate with dementia severity in Alzheimer's disease. *Arch. Neurol.* **52,** 81–88 (1995).

132. Mitchell, T. W. *et al.* Parahippocampal tau pathology in healthy aging, mild cognitive impairment, and early Alzheimer's disease. *Ann. Neurol.* **51,** 182–189 (2002).

133. Gómez-Isla, T. *et al.* Neuronal loss correlates with but exceeds neurofibrillary tangles in Alzheimer's disease. *Ann. Neurol.* **41,** 17–24 (1997).

134. Giannakopoulos, P. *et al.* Tangle and neuron numbers, but not amyloid load, predict cognitive status in Alzheimer's disease. *Neurology* **60,** 1495–1500 (2003).

135. Ingelsson, M. *et al.* Early Abeta accumulation and progressive synaptic loss, gliosis, and tangle formation in AD brain. *Neurology* **62,** 925–931 (2004).

136. Spires-Jones, T. L., Kopeikina, K. J., Koffie, R. M., de Calignon, A. & Hyman, B. T. Are tangles as toxic as they look? *J. Mol. Neurosci.* **45,** 438–444 (2011).

137. Ittner, L. M., Ke, Y. D. & Götz, J. Phosphorylated Tau interacts with c-Jun N-terminal kinase-interacting protein 1 (JIP1) in Alzheimer disease. *J. Biol. Chem.* **284,** 20909–20916 (2009).

138. Li, X. *et al.* Novel diffusion barrier for axonal retention of Tau in neurons and its failure in neurodegeneration. *EMBO J.* **30,** 4825–4837 (2011).

139. Dubey, M., Chaudhury, P., Kabiru, H. & Shea, T. B. Tau inhibits anterograde axonal transport and perturbs stability in growing axonal neurites in part by displacing kinesin cargo: neurofilaments attenuate tau-mediated neurite instability. *Cell Motil. Cytoskeleton* **65,** 89–99 (2008).

140. Stamer, K., Vogel, R., Thies, E., Mandelkow, E. & Mandelkow, E.-M. Tau blocks traffic of organelles, neurofilaments, and APP vesicles in neurons and enhances oxidative stress. *J. Cell Biol.* **156,** 1051–1063 (2002).

141. Kopeikina, K. J., Hyman, B. T. & Spires-Jones, T. L. Soluble forms of tau are toxic in Alzheimer's disease. *Transl. Neurosci.* **3,** 223–233 (2012).

142. Hoover, B. R. *et al.* Tau mislocalization to dendritic spines mediates synaptic dysfunction independently of neurodegeneration. *Neuron* **68,** 1067–1081 (2010).

143. Berger, Z. *et al.* Accumulation of pathological tau species and memory loss in a conditional model of tauopathy. *J. Neurosci.* **27,** 3650–3662 (2007).

144. Yoshiyama, Y. *et al.* Synapse loss and microglial activation precede tangles in a P301S tauopathy mouse model. *Neuron* **53,** 337–351 (2007).

145. Lasagna-Reeves, C. A. *et al.* Alzheimer brain-derived tau oligomers propagate pathology from endogenous tau. *Sci. Rep.* **2,** (2012).

146. Van der Jeugd, A. *et al.* Cognitive defects are reversible in inducible mice expressing pro-aggregant full-length human Tau. *Acta Neuropathol.* **123,** 787–805 (2012).

147. Sydow, A. *et al.* Tau-induced defects in synaptic plasticity, learning, and memory are reversible in transgenic mice after switching off the toxic Tau mutant. *J. Neurosci.* **31,** 2511–2525 (2011).

148. Hooper, C., Killick, R. & Lovestone, S. The GSK3 hypothesis of Alzheimer's disease. *J. Neurochem.* **104,** 1433–1439 (2008).

149. Hanger, D. P. & Noble, W. Functional implications of glycogen synthase kinase-3-mediated tau phosphorylation. *Int. J. Alzheimers. Dis.* **2011,** 352805 (2011).

150. Asuni, A. A. *et al.* GSK3alpha exhibits beta-catenin and tau directed kinase activities that are modulated by Wnt. *Eur. J. Neurosci.* **24,** 3387–3392 (2006).

151. Lovestone, S. *et al.* Alzheimer's disease-like phosphorylation of the microtubule-associated protein tau by glycogen synthase kinase-3 in transfected mammalian cells. *Curr. Biol.* **4,** 1077–1086 (1994).

152. Ferrer, I., Barrachina, M. & Puig, B. Glycogen synthase kinase-3 is associated with neuronal and glial hyperphosphorylated tau deposits in Alzheimer's disease, Pick's disease, progressive supranuclear palsy and corticobasal degeneration. *Acta Neuropathol.* **104,** 583–591 (2002).

153. Lucas, J. J. *et al.* Decreased nuclear beta-catenin, tau hyperphosphorylation and neurodegeneration in GSK-3beta conditional transgenic mice. *EMBO J.* **20,** 27–39 (2001).

154. Blalock, E. M. *et al.* Incipient Alzheimer's disease: microarray correlation analyses reveal major transcriptional and tumor suppressor responses. *Proc. Natl. Acad. Sci. U. S. A.* **101,** 2173–2178 (2004).

155. Leroy, K., Yilmaz, Z. & Brion, J. Increased level of active GSK-3beta in Alzheimer's disease and accumulation in argyrophilic grains and in neurones at different stages of neurofibrillary degeneration. *Neuropathol. Appl. Neurobiol.* **33,** 43–55 (2007).

156. Pei, J. J. *et al.* Distribution of active glycogen synthase kinase 3beta (GSK-3beta) in brains staged for Alzheimer disease neurofibrillary changes. *J. Neuropathol. Exp. Neurol.* **58,** 1010–1019 (1999).

157. Yamaguchi, H. *et al.* Preferential labeling of Alzheimer neurofibrillary tangles with antisera for tau protein kinase (TPK) I/glycogen synthase kinase-3 beta and cyclin-dependent kinase 5, a component of TPK II. *Acta Neuropathol.* **92,** 232–241 (1996).

158. Li, X. *et al.* Activation of glycogen synthase kinase-3 induces Alzheimer-like tau hyperphosphorylation in rat hippocampus slices in culture. *J. Neural Transm.* **113,** 93–102 (2006).

159. Wang, Y. *et al.* Temporal correlation of the memory deficit with Alzheimer-like lesions induced by activation of glycogen synthase kinase-3. *J. Neurochem.* **106,** 2364–2374 (2008).

160. Xu, G., Deng, Y., Liu, S., Li, H. & Wang, J. Prolonged Alzheimer-like tau hyperphosphorylation induced by simultaneous inhibition of phosphoinositol-3 kinase and protein kinase C in N2a cells. *Acta Biochim. Biophys. Sin. (Shanghai).* **37,** 349–354 (2005).

161. Phiel, C. J., Wilson, C. A., Lee, V. M. & Klein, P. S. GSK-3alpha regulates production of Alzheimer's disease amyloid-beta peptides. *Nature* **423,** 435–439 (2003).

162. Forde, J. E. & Dale, T. C. Glycogen synthase kinase 3: a key regulator of cellular fate. *Cell. Mol. Life Sci.* **64,** 1930–1944 (2007).

163. Song, L., De Sarno, P. & Jope, R. S. Central role of glycogen synthase kinase-3beta in endoplasmic reticulum stress-induced caspase-3 activation. *J. Biol. Chem.* **277,** 44701–44708 (2002).

164. Contestabile, A. *et al.* Lithium rescues synaptic plasticity and memory in Down syndrome mice. *J. Clin. Invest.* **123,** 348–361 (2013).

165. Hong, M., Chen, D. C. R., Klein, P. S. & Lee, V. M. Y. Lithium reduces tau phosphorylation by inhibition of glycogen synthase kinase-3. *J. Biol. Chem.* **272,** 25326–25332 (1997).

166. Muñoz-Montaño, J. R., Moreno, F. J., Avila, J. & Diaz-Nido, J. Lithium inhibits Alzheimer's disease-like tau protein phosphorylation in neurons. *FEBS Lett.* **411,** 183–188 (1997).

167. Noble, W. *et al.* Inhibition of glycogen synthase kinase-3 by lithium correlates with reduced tauopathy and degeneration in vivo. *Proc. Natl. Acad. Sci. U. S. A.* **102,** 6990–6995 (2005).

168. Pérez, M., Hernández, F., Lim, F., Díaz-Nido, J. & Avila, J. Chronic lithium treatment decreases mutant tau protein aggregation in a transgenic mouse model. *J. Alzheimers. Dis.* **5,** 301–308 (2003).

169. Trujillo-Estrada, L. *et al.* In vivo modification of Abeta plaque toxicity as a novel neuroprotective lithium-mediated therapy for Alzheimer's disease pathology. *Acta Neuropathol. Commun.* **1,** 73 (2013).

170. Takashima, A. *et al.* Activation of tau protein kinase I/glycogen synthase kinase-3beta by amyloid beta peptide (25-35) enhances phosphorylation of tau in hippocampal neurons. *Neurosci. Res.* **31,** 317–323 (1998).

171. Mateo, I. *et al.* Association between glycogen synthase kinase-3beta genetic polymorphism and late-onset Alzheimer's disease. *Dement. Geriatr. Cogn. Disord.* **21,** 228–232 (2006).

172. Hernández, F. *et al.* Glycogen synthase kinase-3 plays a crucial role in tau exon 10 splicing and intranuclear distribution of SC35. Implications for Alzheimer's disease. *J. Biol. Chem.* **279,** 3801–3806 (2004).

173. Chen, K., Yuan, R., Hu, C. & Hsu, C. Y. Amyloid-β peptide alteration of tau exon-10 splicing via the GSK3β-SC35 pathway. *Neurobiol. Dis.* **40,** 378–385 (2010).

174. Johansson, S. *et al.* Increased tau phosphorylation at the Ser396 epitope after amyloid beta-exposure in organotypic cultures. *Neuroreport* **17,** 907–911 (2006).

175. Zheng, W., Bastianetto, S., Mennicken, F., Ma, W. & Kar, S. Amyloid beta peptide induces tau phosphorylation and loss of cholinergic neurons in rat primary septal cultures. *Neuroscience* **115,** 201–211 (2002).

176. Götz, J., Schild, A., Hoerndli, F. & Pennanen, L. Amyloid-induced neurofibrillary tangle formation in Alzheimer's disease: insight from transgenic mouse and tissue-culture models. *Int. J. Dev. Neurosci.* **22,** 453–465 (2004).

177. Echeverria, V. *et al.* Altered mitogen-activated protein kinase signaling, tau hyperphosphorylation and mild spatial learning dysfunction in transgenic rats expressing the β-amyloid peptide intracellularly in hippocampal and cortical neurons. *Neuroscience* **129,** 583–592 (2004).

178. Chabrier, M. A. *et al.* Soluble amyloid-beta promotes wild-type tau pathology in vivo. *J. Neurosci.* **32,** 17345–17350 (2012).

179. Götz, J., Chen, F., van Dorpe, J. & Nitsch, R. M. Formation of neurofibrillary tangles in P301l tau transgenic mice induced by Abeta 42 fibrils. *Science* **293,** 1491–1495 (2001).

180. Killick, R. *et al.* Clusterin regulates β-amyloid toxicity via Dickkopf-1-driven induction of the wnt-PCP-JNK pathway. *Mol. Psychiatry* **19,** 88–98 (2014).

181. Caricasole, A. *et al.* Induction of Dickkopf-1, a negative modulator of the Wnt pathway, is associated with neuronal degeneration in Alzheimer's brain. *J. Neurosci.* **24,** 6021–6027 (2004).

182. Rosi, M. C. *et al.* Increased Dickkopf-1 expression in transgenic mouse models of neurodegenerative disease. *J. Neurochem.* **112,** 1539–1551 (2010).

183. Purro, S. A., Dickins, E. M. & Salinas, P. C. The secreted Wnt antagonist Dickkopf-1 is required for amyloid β-mediated synaptic loss. *J. Neurosci.* **32,** 3492–3498 (2012).

184. Thambisetty, M. *et al.* Association of plasma clusterin concentration with severity, pathology, and progression in Alzheimer disease. *Arch. Gen. Psychiatry* **67,** 739–748 (2010).

185. Rapoport, M., Dawson, H. N., Binder, L. I., Vitek, M. P. & Ferreira, A. Tau is essential to beta-amyloid-induced neurotoxicity. *Proc. Natl. Acad. Sci.* **99,** 6364–6369 (2002).

186. Roberson, E. D. *et al.* Reducing endogenous tau ameliorates amyloid beta-induced deficits in an Alzheimer's disease mouse model. *Science* **316,** 750–754 (2007).

187. Vossel, K. A. *et al.* Tau reduction prevents Abeta-induced defects in axonal transport. *Science* **330,** 198 (2010).

188. Palop, J. J. & Mucke, L. Amyloid-beta-induced neuronal dysfunction in Alzheimer's disease: from synapses toward neural networks. *Nat. Neurosci.* **13,** 812–818 (2010).

189. Perry, V. H., Nicoll, J. A. R. & Holmes, C. Microglia in neurodegenerative disease. *Nat. Rev. Neurol.* **6,** 193–201 (2010).

190. Nayak, D., Roth, T. L. & McGavern, D. B. Microglia development and function. *Annu. Rev. Immunol.* **32,** 367–402 (2014).

191. Shastri, A., Bonifati, D. M. & Kishore, U. Innate immunity and neuroinflammation. *Mediators Inflamm.* **2013,** 342931 (2013).

192. Lieberman, A. P., Pitha, P. M., Shin, H. S. & Shin, M. L. Production of tumor necrosis factor and other cytokines by astrocytes stimulated with lipopolysaccharide or a neurotropic virus. *Proc. Natl. Acad. Sci. U. S. A.* **86,** 6348–6352 (1989).

193. Van Neerven, S. *et al.* Inflammatory cytokine release of astrocytes in vitro is reduced by all-trans retinoic acid. *J. Neuroimmunol.* **229,** 169–179 (2010).

194. Stewart, C. R. *et al.* CD36 ligands promote sterile inflammation through assembly of a Toll-like receptor 4 and 6 heterodimer. *Nat. Immunol.* **11,** 155–161 (2010).

195. El Khoury, J. B. *et al.* CD36 mediates the innate host response to beta-amyloid. *J. Exp. Med.* **197,** 1657–1666 (2003).

196. Bamberger, M. E., Harris, M. E., McDonald, D. R., Husemann, J. & Landreth, G. E. A cell surface receptor complex for fibrillar beta-amyloid mediates microglial activation. *J. Neurosci.* **23,** 2665–2674 (2003).

197. Liu, Y. LPS receptor (CD14): a receptor for phagocytosis of Alzheimer's amyloid peptide. *Brain* **128,** 1778–1789 (2005).

198. Fiala, M., Cribbs, D. H., Rosenthal, M. & Bernard, G. Phagocytosis of amyloid-beta and inflammation: two faces of innate immunity in Alzheimer's disease. *J. Alzheimers. Dis.* **11,** 457–463 (2007).

199. Guerreiro, R. *et al.* TREM2 variants in Alzheimer's disease. *N. Engl. J. Med.* **368,** 117–127 (2013).

200. Bradshaw, E. M. *et al.* CD33 Alzheimer's disease locus: altered monocyte function and amyloid biology. *Nat. Neurosci.* **16,** 848–850 (2013).

201. Fiala, M. *et al.* Ineffective phagocytosis of amyloid-beta by macrophages of Alzheimer's disease patients. *J. Alzheimers. Dis.* **7,** 221–262 (2005).

202. Mawuenyega, K. G. *et al.* Decreased clearance of CNS beta-amyloid in Alzheimer's disease. *Science* **330,** 1774 (2010).

203. Lue, L. F. *et al.* Inflammatory repertoire of Alzheimer's disease and nondemented elderly microglia in vitro. *Glia* **35,** 72–79 (2001).

204. Patel, N. S. *et al.* Inflammatory cytokine levels correlate with amyloid load in transgenic mouse models of Alzheimer's disease. *J. Neuroinflammation* **2,** 9 (2005).

205. Hu, W. *et al.* Development of a novel therapeutic suppressor of brain proinflammatory cytokine up-regulation that attenuates synaptic dysfunction and behavioral deficits. *Bioorg. Med. Chem. Lett.* **17,** 414–418 (2007).

206. Munoz, L. *et al.* A novel p38 alpha MAPK inhibitor suppresses brain proinflammatory cytokine up-regulation and attenuates synaptic dysfunction and behavioral deficits in an Alzheimer's disease mouse model. *J. Neuroinflammation* **4,** 21 (2007).

207. Tarkowski, E., Andreasen, N., Tarkowski, A. & Blennow, K. Intrathecal inflammation precedes development of Alzheimer's disease. *J. Neurol. Neurosurg. Psychiatry* **74,** 1200–1205 (2003).

208. Goldgaber, D. *et al.* Interleukin 1 regulates synthesis of amyloid beta-protein precursor mRNA in human endothelial cells. *Proc. Natl. Acad. Sci. U. S. A.* **86,** 7606–7610 (1989).

209. Buxbaum, J. D. *et al.* Cholinergic agonists and interleukin 1 regulate processing and secretion of the Alzheimer beta/A4 amyloid protein precursor. *Proc. Natl. Acad. Sci. U. S. A.* **89,** 10075–10078 (1992).

210. Ramlackhansingh, A. F. *et al.* Inflammation after trauma: microglial activation and traumatic brain injury. *Ann. Neurol.* **70,** 374–383 (2011).

211. Fain, J. N. Release of interleukins and other inflammatory cytokines by human adipose tissue is enhanced in obesity and primarily due to the nonfat cells. *Vitam. Horm.* **74,** 443–477 (2006).

212. Holmes, C. *et al.* Systemic inflammation and disease progression in Alzheimer disease. *Neurology* **73,** 768–774 (2009).

213. Persson, T., Popescu, B. O. & Cedazo-Minguez, A. Oxidative stress in Alzheimer's disease: why did antioxidant therapy fail? *Oxid. Med. Cell. Longev.* **2014,** 427318 (2014).

214. Poulsen, H. E. *et al.* RNA modifications by oxidation: a novel disease mechanism? *Free Radic. Biol. Med.* **52,** 1353–1361 (2012).

215. Ding, Q., Markesbery, W. R., Chen, Q., Li, F. & Keller, J. N. Ribosome dysfunction is an early event in Alzheimer's disease. *J. Neurosci.* **25,** 9171–9175 (2005).

216. Headlam, H. A. & Davies, M. J. Markers of protein oxidation: different oxidants give rise to variable yields of bound and released carbonyl products. *Free Radic. Biol. Med.* **36,** 1175–1184 (2004).

217. Resende, R. *et al.* Brain oxidative stress in a triple-transgenic mouse model of Alzheimer disease. *Free Radic. Biol. Med.* **44,** 2051–2057 (2008).

218. Takuma, K. *et al.* ABAD enhances Abeta-induced cell stress via mitochondrial dysfunction. *FASEB J.* **19,** 597–598 (2005).

219. Lustbader, J. W. *et al.* ABAD directly links Abeta to mitochondrial toxicity in Alzheimer's disease. *Science* **304,** 448–452 (2004).

220. Paola, D. *et al.* Oxidative stress induces increase in intracellular amyloid beta-protein production and selective activation of betaI and betaII PKCs in NT2 cells. *Biochem. Biophys. Res. Commun.* **268,** 642–646 (2000).

221. Bradley, M. A., Xiong-Fister, S., Markesbery, W. R. & Lovell, M. A. Elevated 4-hydroxyhexenal in Alzheimer's disease (AD) progression. *Neurobiol. Aging* **33,** 1034–1044 (2012).

222. Markesbery, W. R., Kryscio, R. J., Lovell, M. A. & Morrow, J. D. Lipid peroxidation is an early event in the brain in amnestic mild cognitive impairment. *Ann. Neurol.* **58,** 730–735 (2005).

223. Lovell, M. A., Gabbita, S. P. & Markesbery, W. R. Increased DNA oxidation and decreased levels of repair products in Alzheimer's disease ventricular CSF. *J. Neurochem.* **72,** 771–776 (1999).

224. Nunomura, A. *et al.* Oxidative damage is the earliest event in Alzheimer disease. *J. Neuropathol. Exp. Neurol.* **60,** 759–767 (2001).

225. Praticò, D., MY Lee, V., Trojanowski, J. Q., Rokach, J. & Fitzgerald, G. A. Increased F2-isoprostanes in Alzheimer's disease: evidence for enhanced lipid peroxidation in vivo. *FASEB J.* **12,** 1777–1783 (1998).

226. Ramassamy, C. *et al.* Oxidative insults are associated with apolipoprotein E genotype in Alzheimer's disease brain. *Neurobiol. Dis.* **7,** 23–37 (2000).

227. Glodzik-Sobanska, L. *et al.* The effects of normal aging and ApoE genotype on the levels of CSF biomarkers for Alzheimer's disease. *Neurobiol. Aging* **30,** 672–681 (2009).

228. Miyata, M. & Smith, J. D. Apolipoprotein E allele–specific antioxidant activity and effects on cytotoxicity by oxidative insults and β–amyloid peptides. *Nat. Genet.* **14,** 55–61 (1996).

229. Vodovotz, Y. *et al.* Inducible nitric oxide synthase in tangle-bearing neurons of patients with Alzheimer's disease. *J. Exp. Med.* **184,** 1425–1433 (1996).

230. Fang, Z. & Rajewsky, N. The impact of miRNA target sites in coding sequences and in 3'UTRs. *PLoS One* **6,** e18067 (2011).

231. Baek, D. *et al.* The impact of microRNAs on protein output. *Nature* **455,** 64–71 (2008).

232. Goodall, E. F., Heath, P. R., Bandmann, O., Kirby, J. & Shaw, P. J. Neuronal dark matter: the emerging role of microRNAs in neurodegeneration. *Front. Cell. Neurosci.* **7,** 178 (2013).

233. Guo, H., Ingolia, N. T., Weissman, J. S. & Bartel, D. P. Mammalian microRNAs predominantly act to decrease target mRNA levels. *Nature* **466,** 835–840 (2010).

234. Eulalio, A., Huntzinger, E. & Izaurralde, E. Getting to the root of miRNA-mediated gene silencing. *Cell* **132,** 9–14 (2008).

235. Meister, G. miRNAs get an early start on translational silencing. *Cell* **131,** 25–28 (2007).

236. Behm-Ansmant, I., Rehwinkel, J. & Izaurralde, E. MicroRNAs silence gene expression by repressing protein expression and/or by promoting mRNA decay. *Cold Spring Harb. Symp. Quant. Biol.* **71,** 523–530 (2006).

237. Selbach, M. *et al.* Widespread changes in protein synthesis induced by microRNAs. *Nature* **455,** 58–63 (2008).

238. Lewis, B. P., Burge, C. B. & Bartel, D. P. Conserved seed pairing, often flanked by adenosines, indicates that thousands of human genes are microRNA targets. *Cell* **120,** 15–20 (2005).

239. Fiore, R., Siegel, G. & Schratt, G. MicroRNA function in neuronal development, plasticity and disease. *Biochim. Biophys. Acta* **1779,** 471–478 (2008).

240. Lau, P. & De Strooper, B. Dysregulated microRNAs in neurodegenerative disorders. *Semin. Cell Dev. Biol.* **21,** 768–773 (2010).

241. Nana-Sinkam, S. P. & Croce, C. M. MicroRNAs as therapeutic targets in cancer. *Transl. Res.* **157,** 216–225 (2011).

242. Beveridge, N. J. & Cairns, M. J. MicroRNA dysregulation in schizophrenia. *Neurobiol. Dis.* **46,** 263–271 (2012).

243. Provost, P. MicroRNAs as a molecular basis for mental retardation, Alzheimer's and prion diseases. *Brain Res.* **1338,** 58–66 (2010).

244. De Smaele, E., Ferretti, E. & Gulino, A. MicroRNAs as biomarkers for CNS cancer and other disorders. *Brain Res.* **1338,** 100–111 (2010).

245. Hébert, S. S. & De Strooper, B. Alterations of the microRNA network cause neurodegenerative disease. *Trends Neurosci.* **32,** 199–206 (2009).

246. Wang, G. *et al.* Variation in the miRNA-433 binding site of FGF20 confers risk for Parkinson disease by overexpression of alpha-synuclein. *Am. J. Hum. Genet.* **82,** 283–289 (2008).

247. Hébert, S. S. *et al.* MicroRNA regulation of Alzheimer's amyloid precursor protein expression. *Neurobiol. Dis.* **33,** 422–428 (2009).

248. Patel, N. *et al.* MicroRNAs can regulate human APP levels. *Mol. Neurodegener.* **3,** 10 (2008).

249. Vilardo, E., Barbato, C., Ciotti, M., Cogoni, C. & Ruberti, F. MicroRNA-101 regulates amyloid precursor protein expression in hippocampal neurons. *J. Biol. Chem.* **285,** 18344–18351 (2010).

250. Hébert, S. S. *et al.* Loss of microRNA cluster miR-29a/b-1 in sporadic Alzheimer's disease correlates with increased BACE1/beta-secretase expression. *Proc. Natl. Acad. Sci. U. S. A.* **105,** 6415–6420 (2008).

251. Shioya, M. *et al.* Aberrant microRNA expression in the brains of neurodegenerative diseases: miR-29a decreased in Alzheimer disease brains targets neurone navigator 3. *Neuropathol. Appl. Neurobiol.* **36,** 320–330 (2010).

252. Wang, W.-X. *et al.* The expression of microRNA miR-107 decreases early in Alzheimer's disease and may accelerate disease progression through regulation of beta-site amyloid precursor protein-cleaving enzyme 1. *J. Neurosci.* **28,** 1213–1223 (2008).

253. Nelson, P. T. & Wang, W. MiR-107 is reduced in Alzheimer's disease brain neocortex: validation study. *J. Alzheimers. Dis.* **21,** 75–79 (2010).

254. Yao, J. *et al.* MicroRNA-related cofilin abnormality in Alzheimer's disease. *PLoS One* **5,** e15546 (2010).

255. Smith, P. Y. *et al.* MicroRNA-132 loss is associated with tau exon 10 inclusion in progressive supranuclear palsy. *Hum. Mol. Genet.* **20,** 4016–4024 (2011).

256. Cogswell, J. P. *et al.* Identification of miRNA changes in Alzheimer's disease brain and CSF yields putative biomarkers and insights into disease pathways. *J. Alzheimers. Dis.* **14,** 27–41 (2008).

257. Schonrock, N. *et al.* Neuronal microRNA deregulation in response to Alzheimer's disease amyloid-beta. *PLoS One* **5,** e11070 (2010).

258. Lau, P. *et al.* Alteration of the microRNA network during the progression of Alzheimer's disease. *EMBO Mol. Med.* **5,** 1613–1634 (2013).

259. Smith, P., Al Hashimi, A., Girard, J., Delay, C. & Hébert, S. S. In vivo regulation of amyloid precursor protein neuronal splicing by microRNAs. *J. Neurochem.* **116,** 240–247 (2011).

260. Wang, X. *et al.* miR-34a, a microRNA up-regulated in a double transgenic mouse model of Alzheimer's disease, inhibits bcl2 translation. *Brain Res. Bull.* **80,** 268–273 (2009).

261. Bhatnagar, S. *et al.* Increased microRNA-34c abundance in Alzheimer's disease circulating blood plasma. *Front. Mol. Neurosci.* **7,** 2 (2014).

262. Schipper, H. M., Maes, O. C., Chertkow, H. M. & Wang, E. MicroRNA expression in Alzheimer blood mononuclear cells. *Gene Regul. Syst. Bio.* **1,** 263–274 (2007).

263. Absalon, S., Kochanek, D. M., Raghavan, V. & Krichevsky, A. M. MiR-26b, upregulated in Alzheimer's disease, activates cell cycle entry, tau-phosphorylation, and apoptosis in postmitotic neurons. *J. Neurosci.* **33,** 14645–14659 (2013).

264. Banzhaf-Strathmann, J. *et al.* MicroRNA-125b induces tau hyperphosphorylation and cognitive deficits in Alzheimer's disease. *EMBO J.* **33,** 1667–1680 (2014).

265. Delay, C., Calon, F., Mathews, P. & Hébert, S. S. Alzheimer-specific variants in the 3'UTR of Amyloid precursor protein affect microRNA function. *Mol. Neurodegener.* **6,** 70 (2011).

266. Lukiw, W. J. Micro-RNA speciation in fetal, adult and Alzheimer's disease hippocampus. *Neuroreport* **18,** 297–300 (2007).

267. Boissonneault, V., Plante, I., Rivest, S. & Provost, P. MicroRNA-298 and microRNA-328 regulate expression of mouse beta-amyloid precursor protein-converting enzyme 1. *J. Biol. Chem.* **284,** 1971–1981 (2009).

268. Wang, H. *et al.* MiR-106b aberrantly expressed in a double transgenic mouse model for Alzheimer's disease targets TGF-beta type II receptor. *Brain Res.* **1357,** 166–174 (2010).

269. Faghihi, M. A. *et al.* Evidence for natural antisense transcript-mediated inhibition of microRNA function. *Genome Biol.* **11,** R56 (2010).

270. Wang, W., Huang, Q., Hu, Y., Stromberg, A. J. & Nelson, P. T. Patterns of microRNA expression in normal and early Alzheimer's disease human temporal cortex: white matter versus gray matter. *Acta Neuropathol.* **121,** 193–205 (2010).

271. Schonrock, N., Humphreys, D. T., Preiss, T. & Götz, J. Target gene repression mediated by miRNAs miR-181c and miR-9 both of which are down-regulated by amyloid-β. *J. Mol. Neurosci.* **46,** 324–335 (2011).

272. Müller, M., Kuiperij, H. B., Claassen, J. A., Küsters, B. & Verbeek, M. M. MicroRNAs in Alzheimer's disease: Differential expression in hippocampus and cell-free cerebrospinal fluid. *Neurobiol. Aging* **35,** 152–158 (2014).

273. Long, J. M., Ray, B. & Lahiri, D. K. MicroRNA-339-5p down-regulates protein expression of β-site amyloid precursor protein-cleaving enzyme 1 (BACE1) in human primary brain cultures and is reduced in brain tissue specimens of Alzheimer disease subjects. *J. Biol. Chem.* **289,** 5184–5198 (2014).

274. Prado, M. A. . *et al.* Regulation of acetylcholine synthesis and storage. *Neurochem. Int.* **41,** 291–299 (2002).

275. Anand, P. & Singh, B. A review on cholinesterase inhibitors for Alzheimer's disease. *Arch. Pharm. Res.* **36,** 375–399 (2013).

276. Watkins, P. B., Zimmerman, H. J., Knapp, M. J., Gracon, S. I. & Lewis, K. W. Hepatotoxic effects of tacrine administration in patients with Alzheimer's disease. *JAMA* **271,** 992–998 (1994).

277. Raskind, M. A., Peskind, E. R., Wessel, T. & Yuan, W. Galantamine in AD: a 6-month randomized, placebo-controlled trial with a 6-month extension. The Galantamine USA-1 Study Group. *Neurology* **54,** 2261–2268 (2000).

278. Burns, A. *et al.* The effects of donepezil in Alzheimer's disease - results from a multinational trial. *Dement. Geriatr. Cogn. Disord.* **10,** 237–244 (1999).

279. Farlow, M., Anand, R., Messina, J., Hartman, R. & Veach, J. A 52-week study of the efficacy of rivastigmine in patients with mild to moderately severe Alzheimer's disease. *Eur. Neurol.* **44,** 236–241 (2000).

280. Winblad, B. *et al.* Donepezil treatment in severe Alzheimer's disease: a pooled analysis of three clinical trials. *Curr. Med. Res. Opin.* **25,** 2577–2587 (2009).

281. Birks, J. Cholinesterase inhibitors for Alzheimer's disease. *Cochrane Libr.* (2012).

282. Giacobini, E. Is anti-cholinesterase therapy of Alzheimer's disease delaying progression? *Aging (Milano).* **13,** 247–254 (2001).

283. Lipton, S. A. The molecular basis of memantine action in Alzheimer's disease and other neurologic disorders: low-affinity, uncompetitive antagonism. *Curr. Alzheimer Res.* **2,** 155–165 (2005).

284. Bullock, R. Efficacy and safety of memantine in moderate-to-severe Alzheimer disease: the evidence to date. *Alzheimer Dis. Assoc. Disord.* **20,** 23–29 (2006).

285. Schneider, L. S., Dagerman, K. S., Higgins, J. P. T. & McShane, R. Lack of evidence for the efficacy of memantine in mild Alzheimer disease. *Arch. Neurol.* **68,** 991–998 (2011).

286. McShane, R., Areosa Sastre, A. & Minakaran, N. Memantine for dementia. *Cochrane database Syst. Rev.* CD003154 (2006).

287. Van Dyck, C. H., Tariot, P. N., Meyers, B. & Malca Resnick, E. A 24-week randomized, controlled trial of memantine in patients with moderate-to-severe Alzheimer disease. *Alzheimer Dis. Assoc. Disord.* **21,** 136–143 (2007).

288. Farrimond, L. E., Roberts, E. & McShane, R. Memantine and cholinesterase inhibitor combination therapy for Alzheimer's disease: a systematic review. *BMJ Open* **2,** (2012).

289. Muayqil, T. & Camicioli, R. Systematic review and meta-analysis of combination therapy with cholinesterase inhibitors and memantine in Alzheimer's disease and other dementias. *Dement. Geriatr. Cogn. Dis. Extra* **2,** 546–572 (2012).

290. McConlogue, L. *et al.* Partial reduction of BACE1 has dramatic effects on Alzheimer plaque and synaptic pathology in APP transgenic mice. *J. Biol. Chem.* **282,** 26326–26334 (2007).

291. Roberds, S. L. *et al.* BACE knockout mice are healthy despite lacking the primary beta-secretase activity in brain: implications for Alzheimer's disease therapeutics. *Hum. Mol. Genet.* **10,** 1317–1324 (2001).

292. Dominguez, D. *et al.* Phenotypic and biochemical analyses of BACE1- and BACE2-deficient mice. *J. Biol. Chem.* **280,** 30797–30806 (2005).

293. Vassar, R., Kovacs, D. M., Yan, R. & Wong, P. C. The beta-secretase enzyme BACE in health and Alzheimer's disease: regulation, cell biology, function, and therapeutic potential. *J. Neurosci.* **29,** 12787–12794 (2009).

294. Hu, X. *et al.* BACE1 deficiency causes altered neuronal activity and neurodegeneration. *J. Neurosci.* **30,** 8819–8829 (2010).

295. Kim, D. Y. *et al.* BACE1 regulates voltage-gated sodium channels and neuronal activity. *Nat. Cell Biol.* **9,** 755–764 (2007).

296. Singer, O. *et al.* Targeting BACE1 with siRNAs ameliorates Alzheimer disease neuropathology in a transgenic model. *Nat. Neurosci.* **8,** 1343–1349 (2005).

297. Nishitomi, K. *et al.* BACE1 inhibition reduces endogenous Abeta and alters APP processing in wild-type mice. *J. Neurochem.* **99,** 1555–1563 (2006).

298. Laird, F. M. *et al.* BACE1, a major determinant of selective vulnerability of the brain to amyloid-beta amyloidogenesis, is essential for cognitive, emotional, and synaptic functions. *J. Neurosci.* **25,** 11693–11709 (2005).

299. Ohno, M. *et al.* BACE1 deficiency rescues memory deficits and cholinergic dysfunction in a mouse model of Alzheimer's disease. *Neuron* **41,** 27–33 (2004).

300. Luo, Y. *et al.* Mice deficient in BACE1, the Alzheimer's beta-secretase, have normal phenotype and abolished beta-amyloid generation. *Nat. Neurosci.* **4,** 231–232 (2001).

301. Fukumoto, H., Cheung, B. S., Hyman, B. T. & Irizarry, M. C. Beta-secretase protein and activity are increased in the neocortex in Alzheimer disease. *Arch. Neurol.* **59,** 1381–1389 (2002).

302. Yang, L. *et al.* Elevated β-secretase expression and enzymatic activity detected in sporadic Alzheimer disease. *Nat. Med.* **9,** 3–4 (2003).

303. Li, R. *et al.* Amyloid beta peptide load is correlated with increased beta-secretase activity in sporadic Alzheimer's disease patients. *Proc. Natl. Acad. Sci. U. S. A.* **101,** 3632–3637 (2004).

304. Lahiri, D. K., Maloney, B., Long, J. M. & Greig, N. H. Lessons from a BACE1 inhibitor trial: Off-site but not off base. *Alzheimer's Dement.* 1–9 (2014).

305. Vassar, R. BACE1 inhibitor drugs in clinical trials for Alzheimer's disease. *Alzheimers. Res. Ther.* **6,** 1 (2014).

306. Menting, K. W. & Claassen, J. A. H. R. β-secretase inhibitor; a promising novel therapeutic drug in Alzheimer's disease. *Front. Aging Neurosci.* **6,** 165 (2014).

307. Tomita, T. Secretase inhibitors and modulators for Alzheimer's disease treatment. *Expert Rev. Neurother.* **9,** 661–679 (2009).

308. Krishnaswamy, S., Verdile, G., Groth, D., Kanyenda, L. & Martins, R. N. The structure and function of Alzheimer's gamma secretase enzyme complex. *Crit. Rev. Clin. Lab. Sci.* **46,** 282–301 (2009).

309. Bateman, R. J. *et al.* Human amyloid-β synthesis and clearance rates as measured in cerebrospinal fluid in vivo. *Nat. Med.* **12,** 856–861 (2006).

310. Siemers, E. R. *et al.* Effects of a γ-secretase inhibitor in a randomized study of patients with Alzheimer disease. *Neurology* **66,** 602–604 (2006).

311. Doody, R. S. *et al.* A phase 3 trial of semagacestat for treatment of Alzheimer's disease. *N. Engl. J. Med.* **369,** 341–350 (2013).

312. Mangialasche, F., Solomon, A., Winblad, B., Mecocci, P. & Kivipelto, M. Alzheimer's disease: clinical trials and drug development. *Lancet Neurol.* **9,** 702–716 (2010).

313. Martone, R. L. *et al.* Begacestat (GSI-953): a novel, selective thiophene sulfonamide inhibitor of amyloid precursor protein gamma-secretase for the treatment of Alzheimer's disease. *J. Pharmacol. Exp. Ther.* **331,** 598–608 (2009).

314. Jacobsen, S. *et al.* GSI-953 is a potent APP-selective gamma-secretase inhibitor for the treatment of Alzheimer's disease. *Alzheimer's Dement.* **5,** P139 (2009).

315. Soares, H. *et al.* Aβ variability and effect of gamma secretase inhibition on cerebrospinal fluid levels of Aβ in healthy volunteers. *Alzheimer's Dement.* **5,** P252–P253 (2009).

316. Grossman, H. *et al.* NIC5-15 as a treatment for Alzheimer's: safety, pharmacokinetics and clinical variables. *Alzheimer's Dement.* **5,** P259 (2009).

317. Weggen, S. *et al.* A subset of NSAIDs lower amyloidogenic Abeta42 independently of cyclooxygenase activity. *Nature* **414,** 212–216 (2001).

318. Green, R. C. *et al.* Effect of tarenflurbil on cognitive decline and activities of daily living in patients with mild Alzheimer disease: a randomized controlled trial. *JAMA* **302,** 2557–2564 (2009).

319. Crump, C. J. *et al.* Piperidine acetic acid based γ-secretase modulators directly bind to presenilin-1. *ACS Chem. Neurosci.* **2,** 705–710 (2011).

320. Ohki, Y. *et al.* Phenylpiperidine-type γ-secretase modulators target the transmembrane domain 1 of presenilin 1. *EMBO J.* **30,** 4815–4824 (2011).

321. Aisen, P. S. *et al.* A Phase II study targeting amyloid-beta with 3APS in mild-to-moderate Alzheimer disease. *Neurology* **67,** 1757–1763 (2006).

322. Aisen, P. S. *et al.* Tramiprosate in mild-to-moderate Alzheimer's disease - a randomized, double-blind, placebo-controlled, multi-centre study (the Alphase Study). *Arch. Med. Sci.* **7,** 102–111 (2011).

323. Karran, E. & Hardy, J. A critique of the drug discovery and phase 3 clinical programs targeting the amyloid hypothesis for Alzheimer disease. *Ann. Neurol.* **76,** 185–205 (2014).

324. Kim, J. *et al.* Anti-apoE immunotherapy inhibits amyloid accumulation in a transgenic mouse model of Aβ amyloidosis. *J. Exp. Med.* **209,** 2149–2156 (2012).

325. Liao, F. *et al.* Anti-ApoE antibody given after plaque onset decreases Aβ accumulation and improves brain function in a mouse model of Aβ amyloidosis. *J. Neurosci.* **34,** 7281–7292 (2014).

326. Schenk, D. *et al.* Immunization with amyloid-beta attenuates Alzheimer-disease-like pathology in the PDAPP mouse. *Nature* **400,** 173–177 (1999).

327. Bard, F. *et al.* Peripherally administered antibodies against amyloid beta-peptide enter the central nervous system and reduce pathology in a mouse model of Alzheimer disease. *Nat. Med.* **6,** 916–919 (2000).

328. Gilman, S. *et al.* Clinical effects of Abeta immunization (AN1792) in patients with AD in an interrupted trial. *Neurology* **64,** 1553–1562 (2005).

329. Boche, D., Denham, N., Holmes, C. & Nicoll, J. A. R. Neuropathology after active Aβ42 immunotherapy: implications for Alzheimer's disease pathogenesis. *Acta Neuropathol.* **120,** 369–384 (2010).

330. Panza, F., Logroscino, G., Imbimbo, B. P. & Solfrizzi, V. Is there still any hope for amyloid-based immunotherapy for Alzheimer's disease? *Curr. Opin. Psychiatry* **27,** 128–137 (2014).

331. Spencer, B. & Masliah, E. Immunotherapy for Alzheimer's disease: past, present and future. *Front. Aging Neurosci.* **6,** 114 (2014).

332. Rinne, J. O. *et al.* 11C-PiB PET assessment of change in fibrillar amyloid-beta load in patients with Alzheimer's disease treated with bapineuzumab: a phase 2, double-blind, placebo-controlled, ascending-dose study. *Lancet. Neurol.* **9,** 363–372 (2010).

333. Salloway, S. *et al.* Two phase 3 trials of bapineuzumab in mild-to-moderate Alzheimer's disease. *N. Engl. J. Med.* **370,** 322–333 (2014).

334. Blennow, K. *et al.* Effect of immunotherapy with bapineuzumab on cerebrospinal fluid biomarker levels in patients with mild to moderate Alzheimer disease. *Arch. Neurol.* **69,** 1002–1010 (2012).

335. Samadi, H. & Sultzer, D. Solanezumab for Alzheimer's disease. *Expert Opin. Biol. Ther.* **11,** 787–798 (2011).

336. Doody, R. S. *et al.* Phase 3 trials of solanezumab for mild-to-moderate Alzheimer's disease. *N. Engl. J. Med.* **370,** 311–321 (2014).

337. Garber, K. Genentech's Alzheimer's antibody trial to study disease prevention. *Nat. Biotechnol.* **30,** 731–732 (2012).

338. Reiman, E. M. *et al.* Alzheimer's Prevention Initiative: a plan to accelerate the evaluation of presymptomatic treatments. *J. Alzheimers. Dis.* **26 Suppl 3,** 321–329 (2011).

339. Carrillo, M. C. *et al.* Can we prevent Alzheimer's disease? Secondary 'prevention' trials in Alzheimer's disease. *Alzheimer's Dement.* **9,** 123–131 (2013).

340. Churcher, I. Tau therapeutic strategies for the treatment of Alzheimer's disease. *Curr. Top. Med. Chem.* **6,** 579–595 (2006).

341. Roder, H. M. & Hutton, M. L. Microtubule-associated protein tau as a therapeutic target in neurodegenerative disease. *Expert Opin. Ther. Targets* **11,** 435–442 (2007).

342. Tariot, P. N. & Aisen, P. S. Can lithium or valproate untie tangles in Alzheimer's disease? *J. Clin. Psychiatry* **70,** 919–921 (2009).

343. Hampel, H. *et al.* Lithium trial in Alzheimer's disease: a randomized, single-blind, placebo-controlled, multicenter 10-week study. *J. Clin. Psychiatry* **70,** 922–931 (2009).

344. Tariot, P. N. *et al.* Chronic divalproex sodium to attenuate agitation and clinical progression of Alzheimer disease. *Arch. Gen. Psychiatry* **68,** 853–861 (2011).

345. Tolosa, E. *et al.* A phase 2 trial of the GSK-3 inhibitor tideglusib in progressive supranuclear palsy. *Mov. Disord.* **29,** 470–478 (2014).

346. Lovestone, S. *et al.* A Phase II trial of Tideglusib in Alzheimer's disease. *J. Alzheimers. Dis.* **45,** 75–88 (2014).

347. Del Ser, T. *et al.* Treatment of Alzheimer's disease with the GSK-3 inhibitor tideglusib: a pilot study. *J. Alzheimers. Dis.* **33,** 205–215 (2013).

348. Rosenmann, H. *et al.* Tauopathy-like abnormalities and neurologic deficits in mice immunized with neuronal tau protein. *Arch. Neurol.* **63,** 1459–1467 (2006).

349. Asuni, A. A., Boutajangout, A., Quartermain, D. & Sigurdsson, E. M. Immunotherapy targeting pathological tau conformers in a tangle mouse model reduces brain pathology with associated functional improvements. *J. Neurosci.* **27,** 9115–9129 (2007).

350. Chai, X. *et al.* Passive immunization with anti-tau antibodies in two transgenic models: Reduction of tau pathology and delay of disease progression. *J. Biol. Chem.* **286,** 34457–34467 (2011).

351. Kontsekova, E., Zilka, N., Kovacech, B., Novak, P. & Novak, M. First-in-man tau vaccine targeting structural determinants essential for pathological tau–tau interaction reduces tau oligomerisation and neurofibrillary degeneration in an Alzheimer's disease model. *Alzheimers. Res. Ther.* **6,** 44 (2014).

352. Deiana, S., Harrington, C. R., Wischik, C. M. & Riedel, G. Methylthioninium chloride reverses cognitive deficits induced by scopolamine: comparison with rivastigmine. *Psychopharmacology (Berl).* **202,** 53–65 (2009).

353. Wischik, C. M. *et al.* Tau aggregation inhibitor therapy: an exploratory phase 2 study in mild or moderate Alzheimer's disease. *J. Alzheimers. Dis.* **44,** 705–720 (2015).

354. Rogers, J. *et al.* Clinical trial of indomethacin in Alzheimer's disease. *Neurology* **43,** 1609–1611 (1993).

355. De Jong, D. *et al.* No effect of one-year treatment with indomethacin on Alzheimer's disease progression: a randomized controlled trial. *PLoS One* **3,** e1475 (2008).

356. Bentham, P. *et al.* Aspirin in Alzheimer's disease (AD2000): a randomised open-label trial. *Lancet. Neurol.* **7,** 41–49 (2008).

357. Simons, M. *et al.* Treatment with simvastatin in normocholesterolemic patients with Alzheimer's disease: A 26-week randomized, placebo-controlled, double-blind trial. *Ann. Neurol.* **52,** 346–350 (2002).

358. Harrington, C. *et al.* Rosiglitazone does not improve cognition or global function when used as adjunctive therapy to AChE inhibitors in mild-to-moderate Alzheimer's disease: two phase 3 studies. *Curr. Alzheimer Res.* **8,** 592–606 (2011).

359. Breitner, J. C. *et al.* Extended results of the Alzheimer's disease anti-inflammatory prevention trial. *Alzheimer's Dement.* **7,** 402–411 (2011).

360. Sano, M. *et al.* A controlled trial of selegiline, alpha-tocopherol, or both as treatment for Alzheimer's disease. The Alzheimer's Disease Cooperative Study. *N. Engl. J. Med.* **336,** 1216–1222 (1997).

361. Dysken, M. W. *et al.* Effect of vitamin E and memantine on functional decline in Alzheimer disease: the TEAM-AD VA cooperative randomized trial. *JAMA* **311,** 33–44 (2014).

362. Tuszynski, M. H. *et al.* A phase 1 clinical trial of nerve growth factor gene therapy for Alzheimer disease. *Nat. Med.* **11,** 551–555 (2005).

363. Bjelakovic, G., Nikolova, D., Gluud, L. L., Simonetti, R. G. & Gluud, C. Mortality in randomized trials of antioxidant supplements for primary and secondary prevention: systematic review and meta-analysis. *JAMA* **297,** 842–857 (2007).

364. Chiu, C. *et al.* The effects of omega-3 fatty acids monotherapy in Alzheimer's disease and mild cognitive impairment: a preliminary randomized double-blind placebo-controlled study. *Prog. Neuropsychopharmacol. Biol. Psychiatry* **32,** 1538–1544 (2008).

365. Chan, A. *et al.* A vitamin/nutriceutical formulation improves memory and cognitive performance in community-dwelling adults without dementia. *J. Nutr. Health Aging* **14,** 224–230 (2010).

366. Arlt, S., Müller-Thomsen, T., Beisiegel, U. & Kontush, A. Effect of one-year vitamin C- and E-supplementation on cerebrospinal fluid oxidation parameters and clinical course in Alzheimer's disease. *Neurochem. Res.* **37,** 2706–2714 (2012).

367. Galasko, D. R. *et al.* Antioxidants for Alzheimer disease. *Arch. Neurol.* **69,** 836–841 (2012).

368. Wahlberg, L. U. *et al.* Targeted delivery of nerve growth factor via encapsulated cell biodelivery in Alzheimer disease: a technology platform for restorative neurosurgery. *J. Neurosurg.* **117,** 340–347 (2012).

369. Shinto, L. *et al.* A randomized placebo-controlled pilot trial of omega-3 fatty acids and alpha lipoic acid in Alzheimer's disease. *J. Alzheimers. Dis.* **38,** 111–120 (2014).

370. Remington, R. *et al.* A phase II randomized clinical trial of a nutritional formulation for cognition and mood in Alzheimer's disease. *J. Alzheimers. Dis.* **45,** 395–405 (2015).

371. Kryscio, R. J. *et al.* A randomized controlled Alzheimer's disease prevention trial's evolution into an exposure trial: the PREADViSE Trial. *J. Nutr. Health Aging* **17,** 72–75 (2013).

372. McKhann, G. M. *et al.* The diagnosis of dementia due to Alzheimer's disease: recommendations from the National Institute on Aging-Alzheimer's Association workgroups on diagnostic guidelines for Alzheimer's disease. *Alzheimers. Dement.* **7,** 263–269 (2011).

373. Waldemar, G. *et al.* Recommendations for the diagnosis and management of Alzheimer's disease and other disorders associated with dementia: EFNS guideline. *Eur. J. Neurol.* **14,** e1–26 (2007).

374. Sabri, O. *et al.* Florbetaben PET imaging to detect amyloid plaques in Alzheimer disease: phase 3 study. *Alzheimers. Dement.* **11,** 964–974 (2015).

375. Diniz, B. S. O., Pinto Júnior, J. A. & Forlenza, O. V. Do CSF total tau, phosphorylated tau, and beta-amyloid 42 help to predict progression of mild cognitive impairment to Alzheimer's disease? A systematic review and meta-analysis of the literature. *World J. Biol. Psychiatry* **9,** 172–182 (2008).

376. Hampel, H. *et al.* Value of CSF beta-amyloid(1-42) and tau as predictors of Alzheimer's disease in patients with mild cognitive impairment. *Mol. Psychiatry* **9,** 705–710 (2004).

377. Lovestone, S. *et al.* AddNeuroMed - The European collaboration for the discovery of novel biomarkers for Alzheimer's disease. *Ann. N. Y. Acad. Sci.* **1180,** 36–46 (2009).

378. Lunnon, K. *et al.* A blood gene expression marker of early Alzheimer's disease. *J. Alzheimer's Dis.* **33,** 737–753 (2013).

379. Dorval, V., Nelson, P. T. & Hébert, S. S. Circulating microRNAs in Alzheimer's disease: the search for novel biomarkers. *Front. Mol. Neurosci.* **6,** 24 (2013).

380. Rosenblum, W. I. Why Alzheimer trials fail: removing soluble oligomeric beta amyloid is essential, inconsistent, and difficult. *Neurobiol. Aging* **35,** 969–974 (2014).

381. Bartel, D. P. MicroRNAs: genomics, biogenesis, mechanism, and function. *Cell* **116,** 281–297 (2004).

382. Yi, R., Qin, Y., Macara, I. G. & Cullen, B. R. Exportin-5 mediates the nuclear export of pre-microRNAs and short hairpin RNAs. *Genes Dev.* **17,** 3011–3016 (2003).

383. Meister, G. *et al.* Human Argonaute2 mediates RNA cleavage targeted by miRNAs and siRNAs. *Mol. Cell* **15,** 185–197 (2004).

384. Liu, J. *et al.* Argonaute2 is the catalytic engine of mammalian RNAi. *Science* **305,** 1437–1441 (2004).

385. Yao, B., La, L. B., Chen, Y., Chang, L. & Chan, E. K. L. Defining a new role of GW182 in maintaining miRNA stability. *EMBO Rep.* **13,** 1102–1108 (2012).

386. Eulalio, A., Huntzinger, E. & Izaurralde, E. GW182 interaction with Argonaute is essential for miRNA-mediated translational repression and mRNA decay. *Nat. Struct. Mol. Biol.* **15,** 346–353 (2008).

387. Gibbings, D. J., Ciaudo, C., Erhardt, M. & Voinnet, O. Multivesicular bodies associate with components of miRNA effector complexes and modulate miRNA activity. *Nat. Cell Biol.* **11,** 1143–1149 (2009).

388. Nishi, K., Nishi, A., Nagasawa, T. & Ui-Tei, K. Human TNRC6A is an Argonaute-navigator protein for microRNA-mediated gene silencing in the nucleus. *RNA* **19,** 17–35 (2013).

389. Lian, S. L. *et al.* The C-terminal half of human Ago2 binds to multiple GW-rich regions of GW182 and requires GW182 to mediate silencing. *RNA* **15,** 804–813 (2009).

390. Duursma, A. M., Kedde, M., Schrier, M., le Sage, C. & Agami, R. miR-148 targets human DNMT3b protein coding region. *RNA* **14,** 872–877 (2008).

391. Ørom, U. A., Nielsen, F. C. & Lund, A. H. MicroRNA-10a binds the 5'UTR of ribosomal protein mRNAs and enhances their translation. *Mol. Cell* **30,** 460–471 (2008).

392. Lytle, J. R., Yario, T. A. & Steitz, J. A. Target mRNAs are repressed as efficiently by microRNA-binding sites in the 5' UTR as in the 3' UTR. *Proc. Natl. Acad. Sci. U. S. A.* **104,** 9667–9672 (2007).

393. Lee, I. *et al.* New class of microRNA targets containing simultaneous 5'-UTR and 3'-UTR interaction sites. *Genome Res.* **19,** 1175–1183 (2009).

394. Place, R. F., Li, L., Pookot, D., Noonan, E. J. & Dahiya, R. MicroRNA-373 induces expression of genes with complementary promoter sequences. *Proc. Natl. Acad. Sci. U. S. A.* **105,** 1608–1613 (2008).

395. Friedman, R. C., Farh, K. K., Burge, C. B. & Bartel, D. P. Most mammalian mRNAs are conserved targets of microRNAs. *Genome Res.* **19,** 92–105 (2009).

396. Zeng, Y., Yi, R. & Cullen, B. R. MicroRNAs and small interfering RNAs can inhibit mRNA expression by similar mechanisms. *Proc. Natl. Acad. Sci. U. S. A.* **100,** 9779–9784 (2003).

397. Kim, D. H. & Rossi, J. J. Strategies for silencing human disease using RNA interference. *Nat. Rev. Genet.* **8,** 173–184 (2007).

398. Evers, M. M., Toonen, L. J. A. & van Roon-Mom, W. M. C. Antisense oligonucleotides in therapy for neurodegenerative disorders. *Adv. Drug Deliv. Rev.* **87,** 90–103 (2015).

399. Aoki, Y., Yokota, T. & Wood, M. J. A. Development of multiexon skipping antisense oligonucleotide therapy for duchenne muscular dystrophy. *Biomed Res. Int.* **2013,** 1–8 (2013).

400. De Smet, M. D., Meenken, C. J. & van den Horn, G. J. Fomivirsen - a phosphorothioate oligonucleotide for the treatment of CMV retinitis. *Ocul. Immunol. Inflamm.* **7,** 189–198 (1999).

401. Santos, R. D. *et al.* Mipomersen, an antisense oligonucleotide to apolipoprotein B-100, reduces lipoprotein(a) in various populations with Hypercholesterolemia: results of 4 phase III trials. *Arterioscler. Thromb. Vasc. Biol.* **35,** 689–699 (2015).

402. Miller, T. M. *et al.* An antisense oligonucleotide against SOD1 delivered intrathecally for patients with SOD1 familial amyotrophic lateral sclerosis: a phase 1, randomised, first-in-man study. *Lancet. Neurol.* **12,** 435–442 (2013).

403. Bianchini, D. *et al.* First-in-human phase I study of EZN-4176, a locked nucleic acid antisense oligonucleotide to exon 4 of the androgen receptor mRNA in patients with castration-resistant prostate cancer. *Br. J. Cancer* **109,** 2579–2586 (2013).

404. Gupta, N. *et al.* A locked nucleic acid antisense oligonucleotide (LNA) silences PCSK9 and enhances LDLR expression in vitro and in vivo. *PLoS One* **5,** e10682 (2010).

405. Laxton, C. *et al.* Selection, optimization, and pharmacokinetic properties of a novel, potent antiviral locked nucleic acid-based antisense oligomer targeting hepatitis C virus internal ribosome entry site. *Antimicrob. Agents Chemother.* **55,** 3105–3114 (2011).

406. Kumar, V. B. *et al.* Site-directed antisense oligonucleotide decreases the expression of amyloid precursor protein and reverses deficits in learning and memory in aged SAMP8 mice. *Peptides* **21,** 1769–1775 (2000).

407. Banks, W. A. *et al.* Delivery across the blood-brain barrier of antisense directed against amyloid beta: reversal of learning and memory deficits in mice overexpressing amyloid precursor protein. *J. Pharmacol. Exp. Ther.* **297,** 1113–1121 (2001).

408. Poon, H. F. *et al.* Antisense directed at the Abeta region of APP decreases brain oxidative markers in aged senescence accelerated mice. *Brain Res.* **1018,** 86–96 (2004).

409. Erickson, M. A. *et al.* Peripheral administration of antisense oligonucleotides targeting the amyloid-β protein precursor reverses AβPP and LRP-1 overexpression in the aged SAMP8 mouse brain. *J. Alzheimers. Dis.* **28,** 951–960 (2012).

410. Farr, S. A., Erickson, M. A., Niehoff, M. L., Banks, W. A. & Morley, J. E. Central and peripheral administration of antisense oligonucleotide targeting amyloid-β protein precursor improves learning and memory and reduces neuroinflammatory cytokines in Tg2576 (AβPPswe) mice. *J. Alzheimers. Dis.* **40,** 1005–1016 (2014).

411. Armbrecht, H. J. *et al.* Antisense against amyloid-β protein precursor reverses memory deficits and alters gene expression in neurotropic and insulin-signaling pathways in SAMP8 mice. *J. Alzheimers. Dis.* **46,** 535–548 (2015).

412. Fiorini, A. *et al.* Antisense directed against PS-1 gene decreases brain oxidative markers in aged senescence accelerated mice (SAMP8) and reverses learning and memory impairment: a proteomics study. *Free Radic. Biol. Med.* **65,** 1–14 (2013).

413. Farr, S. A. *et al.* Antisense oligonucleotide against GSK-3β in brain of SAMP8 mice improves learning and memory and decreases oxidative stress: involvement of transcription factor Nrf2 and implications for Alzheimer disease. *Free Radic. Biol. Med.* **67,** 387–395 (2014).

414. McMahon, B. M. *et al.* Peptide nucleic acids targeted to the amyloid precursor protein. *J. Mol. Neurosci.* **20,** 261–265 (2003).

415. Boules, M., Williams, K., Gollatz, E., Fauq, A. & Richelson, E. Down-regulation of amyloid precursor protein by peptide nucleic acid in vivo. *J. Mol. Neurosci.* **24,** 123–128 (2004).

416. Koshkin, A. A. *et al.* LNA (Locked Nucleic Acids): synthesis of the adenine, cytosine, guanine, 5-methylcytosine, thymine and uracil bicyclonucleoside monomers, oligomerisation, and unprecedented nucleic acid recognition. *Tetrahedron* **54,** 3607–3630 (1998).

417. Kurreck, J., Wyszko, E., Gillen, C. & Erdmann, V. A. Design of antisense oligonucleotides stabilized by locked nucleic acids. *Nucleic Acids Res.* **30,** 1911–1918 (2002).

418. Wahlestedt, C. *et al.* Potent and nontoxic antisense oligonucleotides containing locked nucleic acids. *Proc. Natl. Acad. Sci. U. S. A.* **97,** 5633–5638 (2000).

419. Rapozzi, V. Antisense locked nucleic acids efficiently suppress BCR/ABL and induce cell growth decline and apoptosis in leukemic cells. *Mol. Cancer Ther.* **5,** 1683–1692 (2006).

420. Jeong, W. *et al.* Pilot trial of EZN-2968, an antisense oligonucleotide inhibitor of hypoxia-inducible factor-1 alpha (HIF-1α), in patients with refractory solid tumors. *Cancer Chemother. Pharmacol.* **73,** 343–348 (2014).

421. Dürig, J. *et al.* The novel antisense Bcl-2 inhibitor SPC2996 causes rapid leukemic cell clearance and immune activation in chronic lymphocytic leukemia. *Leukemia* **25,** 638–647 (2011).

422. Kao, S. C., Krichevsky, A. M., Kosik, K. S. & Tsai, L. H. BACE1 suppression by RNA interference in primary cortical neurons. *J. Biol. Chem.* **279,** 1942–1949 (2004).

423. Jabłkowski, M. *et al.* New type of BACE1 siRNA delivery to cells. *Med. Sci. Monit.* **20,** 2598–2606 (2014).

424. Sierant, M. *et al.* RNA interference in silencing of genes of Alzheimer's disease in cellular and rat brain models. *Nucleic Acids Symp. Ser.* 41–42 (2008).

425. Miller, V. M., Gouvion, C. M., Davidson, B. L. & Paulson, H. L. Targeting Alzheimer's disease genes with RNA interference: an efficient strategy for silencing mutant alleles. *Nucleic Acids Res.* **32,** 661–668 (2004).

426. Rodríguez-Lebrón, E., Gouvion, C. M., Moore, S. A., Davidson, B. L. & Paulson, H. L. Allele-specific RNAi mitigates phenotypic progression in a transgenic model of Alzheimer's disease. *Mol. Ther.* **17,** 1563–1573 (2009).

427. Krützfeldt, J. *et al.* Silencing of microRNAs in vivo with 'antagomirs'. *Nature* **438,** 685–689 (2005).

428. Krützfeldt, J. *et al.* Specificity, duplex degradation and subcellular localization of antagomirs. *Nucleic Acids Res.* **35,** 2885–2892 (2007).

429. Ebert, M. S., Neilson, J. R. & Sharp, P. A. MicroRNA sponges: competitive inhibitors of small RNAs in mammalian cells. *Nat. Methods* **4,** 721–726 (2007).

430. Lee, S. *et al.* miR-206 regulates brain-derived neurotrophic factor in Alzheimer disease model. *Ann. Neurol.* **72,** 269–277 (2012).

431. Zovoilis, A. *et al.* microRNA-34c is a novel target to treat dementias. *EMBO J.* **30,** 4299–4308 (2011).

432. Hickerson, R. P. *et al.* Stability study of unmodified siRNA and relevance to clinical use. *Oligonucleotides* **18,** 345–354 (2008).

433. Cho, I. S. *et al.* Improved serum stability and biophysical properties of siRNAs following chemical modifications. *Biotechnol. Lett.* **30,** 1901–1908 (2008).

434. Braasch, D. A. *et al.* RNA interference in mammalian cells by chemically-modified RNA. *Biochemistry* **42,** 7967–7975 (2003).

435. Van de Water, F. M. *et al.* Intravenously administered short interfering RNA accumulates in the kidney and selectively suppresses gene function in renal proximal tubules. *Drug Metab. Dispos.* **34,** 1393–1397 (2006).

436. Fedorov, Y. Off-target effects by siRNA can induce toxic phenotype. *RNA* **12,** 1188–1196 (2006).

437. Grimm, D. The dose can make the poison: lessons learned from adverse in vivo toxicities caused by RNAi overexpression. *Silence* **2,** 8 (2011).

438. Janzer, R. C. & Raff, M. C. Astrocytes induce blood-brain barrier properties in endothelial cells. *Nature* **325,** 253–257 (1987).

439. Armulik, A. *et al.* Pericytes regulate the blood-brain barrier. *Nature* **468,** 557–561 (2010).

440. Serlin, Y., Shelef, I., Knyazer, B. & Friedman, A. Anatomy and physiology of the blood–brain barrier. *Semin. Cell Dev. Biol.* **38,** 2–6 (2015).

441. Pardridge, W. M. Drug transport across the blood–brain barrier. *J. Cereb. Blood Flow Metab.* **32,** 1959–1972 (2012).

442. Bell, R. D. *et al.* Apolipoprotein E controls cerebrovascular integrity via cyclophilin A. *Nature* **485,** 512–516 (2012).

443. Popescu, B. O. *et al.* Blood-brain barrier alterations in ageing and dementia. *J. Neurol. Sci.* **283,** 99–106 (2009).

444. Semple, S. C. *et al.* Rational design of cationic lipids for siRNA delivery. *Nat. Biotechnol.* **28,** 172–176 (2010).

445. Zhang, S., Zhao, Y., Zhi, D. & Zhang, S. Non-viral vectors for the mediation of RNAi. *Bioorg. Chem.* **40,** 10–18 (2012).

446. Seow, Y. & Wood, M. J. Biological gene delivery vehicles: beyond viral vectors. *Mol. Ther.* **17,** 767–777 (2009).

447. Kanasty, R., Dorkin, J. R., Vegas, A. & Anderson, D. Delivery materials for siRNA therapeutics. *Nat. Mater.* **12,** 967–977 (2013).

448. Nguyen, J. & Szoka, F. C. Nucleic acid delivery: The missing pieces of the puzzle? *Acc. Chem. Res.* **45,** 1153–1162 (2012).

449. Zhang, Y., Wang, Z. & Gemeinhart, R. A. Progress in microRNA delivery. *J. Control. Release* **172,** 962–974 (2013).

450. Momen-Heravi, F., Bala, S., Bukong, T. & Szabo, G. Exosome-mediated delivery of functionally active miRNA-155 inhibitor to macrophages. *Nanomedicine Nanotechnology, Biol. Med.* **10,** 1517–1527 (2014).

451. Stoorvogel, W., Strous, G. J., Geuze, H. J., Oorschot, V. & Schwartz, A. L. Late endosomes derive from early endosomes by maturation. *Cell* **65,** 417–427 (1991).

452. Kowal, J., Tkach, M. & Théry, C. Biogenesis and secretion of exosomes. *Curr. Opin. Cell Biol.* **29C,** 116–125 (2014).

453. Ostrowski, M. *et al.* Rab27a and Rab27b control different steps of the exosome secretion pathway. *Nat. Cell Biol.* **12,** 19–30 (2010).

454. Savina, A., Fader, C. M., Damiani, M. T. & Colombo, M. I. Rab11 promotes docking and fusion of multivesicular bodies in a calcium-dependent manner. *Traffic* **6,** 131–143 (2005).

455. Hsu, C. *et al.* Regulation of exosome secretion by Rab35 and its GTPase-activating proteins TBC1D10A-C. *J. Cell Biol.* **189,** 223–232 (2010).

456. Fader, C. M., Savina, A., Sánchez, D. & Colombo, M. I. Exosome secretion and red cell maturation: exploring molecular components involved in the docking and fusion of multivesicular bodies in K562 cells. *Blood Cells. Mol. Dis.* **35,** 153–157 (2005).

457. Andreu, Z. & Yáñez-Mó, M. Tetraspanins in extracellular vesicle formation and function. *Front. Immunol.* **5,** 442 (2014).

458. Rana, S., Yue, S., Stadel, D. & Zöller, M. Toward tailored exosomes: the exosomal tetraspanin web contributes to target cell selection. *Int. J. Biochem. Cell Biol.* **44,** 1574–1584 (2012).

459. Rana, S. & Zöller, M. Exosome target cell selection and the importance of exosomal tetraspanins: a hypothesis. *Biochem. Soc. Trans.* **39,** 559–562 (2011).

460. Kim, D. *et al.* EVpedia: a community web portal for extracellular vesicles research. *Bioinformatics* **31,** 933–939 (2014).

461. Kalra, H. *et al.* Vesiclepedia: a compendium for extracellular vesicles with continuous community annotation. *PLoS Biol.* **10,** e1001450 (2012).

462. Villarroya-Beltri, C., Baixauli, F., Gutiérrez-Vázquez, C., Sánchez-Madrid, F. & Mittelbrunn, M. Sorting it out: regulation of exosome loading. *Semin. Cancer Biol.* **28,** 3–13 (2014).

463. Perez-Hernandez, D. *et al.* The intracellular interactome of tetraspanin-enriched microdomains reveals their function as sorting machineries toward exosomes. *J. Biol. Chem.* **288,** 11649–11661 (2013).

464. Van Niel, G. *et al.* The tetraspanin CD63 regulates ESCRT-independent and -dependent endosomal sorting during melanogenesis. *Dev. Cell* **21,** 708–721 (2011).

465. Trajkovic, K. *et al.* Ceramide triggers budding of exosome vesicles into multivesicular endosomes. *Science* **319,** 1244–1247 (2008).

466. Géminard, C., De Gassart, A., Blanc, L. & Vidal, M. Degradation of AP2 during reticulocyte maturation enhances binding of hsc70 and Alix to a common site on TFR for sorting into exosomes. *Traffic* **5,** 181–193 (2004).

467. Sahu, R. *et al.* Microautophagy of cytosolic proteins by late endosomes. *Dev. Cell* **20,** 131–139 (2011).

468. Zhang, Y. *et al.* Secreted monocytic miR-150 enhances targeted endothelial cell migration. *Mol. Cell* **39,** 133–144 (2010).

469. Collino, F. *et al.* Microvesicles derived from adult human bone marrow and tissue specific mesenchymal stem cells shuttle selected pattern of miRNAs. *PLoS One* **5,** e11803 (2010).

470. Li, L. *et al.* Argonaute 2 complexes selectively protect the circulating microRNAs in cell-secreted microvesicles. *PLoS One* **7,** 1–9 (2012).

471. Guduric-Fuchs, J. *et al.* Selective extracellular vesicle-mediated export of an overlapping set of microRNAs from multiple cell types. *BMC Genomics* **13,** 357 (2012).

472. Batagov, A. O., Kuznetsov, V. & Kurochkin, I. V. Identification of nucleotide patterns enriched in secreted RNAs as putative cis-acting elements targeting them to exosome nano-vesicles. *BMC Genomics* **12,** S18 (2011).

473. Bolukbasi, M. F. *et al.* miR-1289 and 'zipcode'-like sequence enrich mRNAs in microvesicles. *Mol. Ther. Nucleic Acids* **1,** e10 (2012).

474. Villarroya-Beltri, C. *et al.* Sumoylated hnRNPA2B1 controls the sorting of miRNAs into exosomes through binding to specific motifs. *Nat. Commun.* **4,** 2980 (2013).

475. Koppers-Lalic, D. *et al.* Nontemplated nucleotide additions distinguish the small RNA composition in cells from exosomes. *Cell Rep.* **8,** 1649–1658 (2014).

476. Squadrito, M. L. *et al.* Endogenous RNAs modulate microRNA sorting to exosomes and transfer to acceptor cells. *Cell Rep.* **8,** 1432–1446 (2014).

477. Hunter, M. P. *et al.* Detection of microRNA expression in human peripheral blood microvesicles. *PLoS One* **3,** e3694 (2008).

478. Mitchell, P. S. *et al.* Circulating microRNAs as stable blood-based markers for cancer detection. *Proc. Natl. Acad. Sci. U. S. A.* **105,** 10513–10518 (2008).

479. Lässer, C. *et al.* Human saliva, plasma and breast milk exosomes contain RNA: uptake by macrophages. *J. Transl. Med.* **9,** 9 (2011).

480. Keller, S., Ridinger, J., Rupp, A., Janssen, J. W. & Altevogt, P. Body fluid derived exosomes as a novel template for clinical diagnostics. *J. Transl. Med.* **9,** 86 (2011).

481. Miranda, K. C. *et al.* Nucleic acids within urinary exosomes/microvesicles are potential biomarkers for renal disease. *Kidney Int.* **78,** 191–199 (2010).

482. Hiemstra, T. F. *et al.* Human urinary exosomes as innate immune effectors. *J. Am. Soc. Nephrol.* **25,** 2017–2027 (2014).

483. Greening, D. W., Gopal, S. K., Xu, R., Simpson, R. J. & Chen, W. Exosomes and their roles in immune regulation and cancer. *Semin. Cell Dev. Biol.* **40,** 72–81 (2015).

484. Lachenal, G. *et al.* Release of exosomes from differentiated neurons and its regulation by synaptic glutamatergic activity. *Mol. Cell. Neurosci.* **46,** 409–418 (2011).

485. Chivet, M., Hemming, F., Pernet-Gallay, K., Fraboulet, S. & Sadoul, R. Emerging role of neuronal exosomes in the central nervous system. *Front. Physiol.* **3,** 145 (2012).

486. Melo, S. A. *et al.* Cancer exosomes perform cell-independent microRNA biogenesis and promote tumorigenesis. *Cancer Cell* **26,** 707–721 (2014).

487. Ratajczak, J. *et al.* Embryonic stem cell-derived microvesicles reprogram hematopoietic progenitors: evidence for horizontal transfer of mRNA and protein delivery. *Leukemia* **20,** 847–856 (2006).

488. Sobo-Vujanovic, A., Munich, S. & Vujanovic, N. L. Dendritic-cell exosomes cross-present Toll-like receptor-ligands and activate bystander dendritic cells. *Cell. Immunol.* **289,** 119–127 (2014).

489. Fevrier, B. *et al.* Cells release prions in association with exosomes. *Proc. Natl. Acad. Sci. U. S. A.* **101,** 9683–9688 (2004).

490. Vingtdeux, V., Sergeant, N. & Buée, L. Potential contribution of exosomes to the prion-like propagation of lesions in Alzheimer's disease. *Front. Physiol.* **3,** 229 (2012).

491. Rajendran, L. *et al.* Alzheimer's disease beta-amyloid peptides are released in association with exosomes. *Proc. Natl. Acad. Sci. U. S. A.* **103,** 11172–11177 (2006).

492. Baj-Krzyworzeka, M. *et al.* Tumour-derived microvesicles carry several surface determinants and mRNA of tumour cells and transfer some of these determinants to monocytes. *Cancer Immunol. Immunother.* **55,** 808–818 (2006).

493. Deregibus, M. C. *et al.* Endothelial progenitor cell derived microvesicles activate an angiogenic program in endothelial cells by a horizontal transfer of mRNA. *Blood* **110,** 2440–2448 (2007).

494. Valadi, H. *et al.* Exosome-mediated transfer of mRNAs and microRNAs is a novel mechanism of genetic exchange between cells. *Nat. Cell Biol.* **9,** 654–659 (2007).

495. Ekström, K. *et al.* Characterization of mRNA and microRNA in human mast cell-derived exosomes and their transfer to other mast cells and blood CD34 progenitor cells. *J. Extracell. Vesicles* **1,** 1–12 (2012).

496. Skog, J. *et al.* Glioblastoma microvesicles transport RNA and proteins that promote tumour growth and provide diagnostic biomarkers. *Nat. Cell Biol.* **10,** 1470–1476 (2008).

497. Mittelbrunn, M. *et al.* Unidirectional transfer of microRNA-loaded exosomes from T cells to antigen-presenting cells. *Nat. Commun.* **2,** 282 (2011).

498. Montecalvo, A. *et al.* Mechanism of transfer of functional microRNAs between mouse dendritic cells via exosomes. *Blood* **119,** 756–766 (2012).

499. Eldh, M. *et al.* Exosomes communicate protective messages during oxidative stress; possible role of exosomal shuttle RNA. *PLoS One* **5,** e15353 (2010).

500. Wang, K., Zhang, S., Weber, J., Baxter, D. & Galas, D. J. Export of microRNAs and microRNA-protective protein by mammalian cells. *Nucleic Acids Res.* **38,** 7248–7259 (2010).

501. Kuosmanen, S. M. *et al.* MicroRNA profiling of pericardial fluid samples from patients with heart failure. *PLoS One* **10,** e0119646 (2015).

502. Pegtel, D. M. *et al.* Functional delivery of viral miRNAs via exosomes. *Proc. Natl. Acad. Sci. U. S. A.* **107,** 6328–6333 (2010).

503. Cazzoli, R. *et al.* microRNAs derived from circulating exosomes as noninvasive biomarkers for screening and diagnosing lung cancer. *J. Thorac. Oncol.* **8,** 1156–1162 (2013).

504. Bellingham, S. A., Guo, B. B., Coleman, B. M. & Hill, A. F. Exosomes: vehicles for the transfer of toxic proteins associated with neurodegenerative diseases? *Front. Physiol.* **3,** 124 (2012).

505. Ailawadi, S., Wang, X., Gu, H. & Fan, G. Pathologic function and therapeutic potential of exosomes in cardiovascular disease. *Biochim. Biophys. Acta* **1852,** 1–11 (2014).

506. Kosaka, N. *et al.* Secretory mechanisms and intercellular transfer of microRNAs in living cells. *J. Biol. Chem.* **285,** 17442–17452 (2010).

507. Akao, Y. *et al.* Microvesicle-mediated RNA molecule delivery system using monocytes/macrophages. *Mol. Ther.* **19,** 395–399 (2011).

508. Alvarez-Erviti, L. *et al.* Delivery of siRNA to the mouse brain by systemic injection of targeted exosomes. *Nat. Biotechnol.* **29,** 341–345 (2011).

509. Flint, P. W., Li, Z. B., Lehar, M., Saito, K. & Pai, S. I. Laryngeal muscle surface receptors identified using random phage library. *Laryngoscope* **115,** 1930–1937 (2005).

510. Kumar, P. *et al.* Transvascular delivery of small interfering RNA to the central nervous system. *Nature* **448,** 39–43 (2007).

511. Wahlgren, J. *et al.* Plasma exosomes can deliver exogenous short interfering RNA to monocytes and lymphocytes. *Nucleic Acids Res.* **40,** 1–12 (2012).

512. Shtam, T. A. *et al.* Exosomes are natural carriers of exogenous siRNA to human cells in vitro. *Cell Commun. Signal.* **11,** 88 (2013).

513. Cooper, J. M. *et al.* Systemic exosomal siRNA delivery reduced alpha-synuclein aggregates in brains of transgenic mice. *Mov. Disord.* **29,** 1476–1485 (2014).

514. Lee, H. K. *et al.* Mesenchymal stem cells deliver synthetic microRNA mimics to glioma cells and glioma stem cells and inhibit their cell migration and self-renewal. *Oncotarget* **4,** 346–361 (2013).

515. Lee, H. K., Finniss, S., Cazacu, S., Xiang, C. & Brodie, C. Mesenchymal stem cells deliver exogenous miRNAs to neural cells and induce their differentiation and glutamate transporter expression. *Stem Cells Dev.* **23,** 2851–2861 (2014).

516. Sun, D. *et al.* A novel nanoparticle drug delivery system: the anti-inflammatory activity of curcumin is enhanced when encapsulated in exosomes. *Mol. Ther.* **18,** 1606–1614 (2010).

517. Zhuang, X. *et al.* Treatment of brain inflammatory diseases by delivering exosome encapsulated anti-inflammatory drugs from the nasal region to the brain. *Mol. Ther.* **19,** 1769–1779 (2011).

518. Haney, M. J. *et al.* Exosomes as drug delivery vehicles for Parkinson's disease therapy. *J. Control. Release* **207,** 18–30 (2015).

519. Maguire, C. A. *et al.* Microvesicle-associated AAV vector as a novel gene delivery system. *Mol. Ther.* **20,** 960–971 (2012).

520. Mizrak, A. *et al.* Genetically engineered microvesicles carrying suicide mRNA/protein inhibit schwannoma tumor growth. *Mol. Ther.* **21,** 101–108 (2013).

521. Ohno, S. *et al.* Systemically injected exosomes targeted to EGFR deliver antitumor microRNA to breast cancer cells. *Mol. Ther.* **21,** 185–191 (2013).

522. Pan, Q. *et al.* Hepatic cell-to-cell transmission of small silencing RNA can extend the therapeutic reach of RNA interference (RNAi). *Gut* **61,** 1330–1339 (2012).

523. Olson, S. D. *et al.* Examination of mesenchymal stem cell-mediated RNAi transfer to Huntington's disease affected neuronal cells for reduction of huntingtin. *Mol. Cell. Neurosci.* **49,** 271–281 (2012).

524. Lv, Z. *et al.* Argonaute 2 in cell-secreted microvesicles guides the function of secreted miRNAs in recipient cells. *PLoS One* **9,** e103599 (2014).

525. Banizs, A. B. *et al.* In vitro evaluation of endothelial exosomes as carriers for small interfering ribonucleic acid delivery. *Int. J. Nanomedicine* **9,** 4223–4230 (2014).

526. Wang, J. *et al.* Macrophage-secreted exosomes delivering miRNA-21 inhibitor can regulate BGC-823 cell proliferation. *Asian Pac. J. Cancer Prev.* **16,** 4203–4209 (2015).

527. Tian, Y. *et al.* A doxorubicin delivery platform using engineered natural membrane vesicle exosomes for targeted tumor therapy. *Biomaterials* **35,** 2383–2390 (2014).

528. Fuhrmann, G., Serio, A., Mazo, M., Nair, R. & Stevens, M. M. Active loading into extracellular vesicles significantly improves the cellular uptake and photodynamic effect of porphyrins. *J. Control. Release* **205,** 35–44 (2015).

529. Kim, S. *et al.* Exosomes derived from IL-10-treated dendritic cells can suppress inflammation and collagen-induced arthritis. *J. Immunol.* **174,** 6440–6448 (2005).

530. Kim, S. H. *et al.* Exosomes derived from genetically modified DC expressing FasL are anti-inflammatory and immunosuppressive. *Mol. Ther.* **13,** 289–300 (2006).

531. Bianco, N. R., Seon, H. K., Ruffner, M. A. & Robbins, P. D. Therapeutic effect of exosomes from indoleamine 2,3-dioxygenase-positive dendritic cells in collagen-induced arthritis and delayed-type hypersensitivity disease models. *Arthritis Rheum.* **60,** 380–389 (2009).

532. Kim, S. H., Bianco, N. R., Shufesky, W. J., Morelli, A. E. & Robbins, P. D. Effective treatment of inflammatory disease models with exosomes derived from dendritic cells genetically modified to express IL-4. *J. Immunol.* **179,** 2242–2249 (2007).

533. Akyurekli, C. *et al.* A systematic review of preclinical studies on the therapeutic potential of mesenchymal stromal cell-derived microvesicles. *Stem Cell Rev.* **11,** 150–160 (2015).

534. Timmers, L. *et al.* Reduction of myocardial infarct size by human mesenchymal stem cell conditioned medium. *Stem Cell Res.* **1,** 129–137 (2007).

535. Lai, R. C. *et al.* Exosome secreted by MSC reduces myocardial ischemia/reperfusion injury. *Stem Cell Res.* **4,** 214–222 (2010).

536. Xin, H. *et al.* Exosome-mediated transfer of miR-133b from multipotent mesenchymal stromal cells to neural cells contributes to neurite outgrowth. *Stem Cells* **30,** 1556–1564 (2012).

537. Kordelas, L. *et al.* MSC-derived exosomes: a novel tool to treat therapy-refractory graft-versus-host disease. *Leukemia* **28,** 970–973 (2014).

538. Zitvogel, L. *et al.* Eradication of established murine tumors using a novel cell-free vaccine: dendritic cell-derived exosomes. *Nat. Med.* **4,** 594–600 (1998).

539. Théry, C. *et al.* Indirect activation of naïve CD4+ T cells by dendritic cell-derived exosomes. *Nat. Immunol.* **3,** 1156–1162 (2002).

540. André, F. *et al.* Exosomes as potent cell-free peptide-based vaccine. I. Dendritic cell-derived exosomes transfer functional MHC class I/peptide complexes to dendritic cells. *J. Immunol.* **172,** 2126–2136 (2004).

541. Chaput, N. *et al.* Exosomes as potent cell-free peptide-based vaccine. II. Exosomes in CpG adjuvants efficiently prime naive Tc1 lymphocytes leading to tumor rejection. *J. Immunol.* **172,** 2137–2146 (2004).

542. Wolfers, J. *et al.* Tumor-derived exosomes are a source of shared tumor rejection antigens for CTL cross-priming. *Nat. Med.* **7,** 297–303 (2001).

543. Morse, M. A. *et al.* A phase I study of dexosome immunotherapy in patients with advanced non-small cell lung cancer. *J. Transl. Med.* **3,** 9 (2005).

544. Escudier, B. *et al.* Vaccination of metastatic melanoma patients with autologous dendritic cell (DC) derived-exosomes: results of the first phase I clinical trial. *J. Transl. Med.* **3,** 10 (2005).

545. Dai, S. *et al.* Phase I clinical trial of autologous ascites-derived exosomes combined with GM-CSF for colorectal cancer. *Mol. Ther.* **16,** 782–790 (2008).

546. Yang, Y. *et al.* Increased induction of antitumor response by exosomes derived from interleukin-2 gene-modified tumor cells. *J. Cancer Res. Clin. Oncol.* **133,** 389–399 (2007).

547. Zhang, Y. *et al.* Exosomes derived from IL-12-anchored renal cancer cells increase induction of specific antitumor response in vitro: a novel vaccine for renal cell carcinoma. *Int. J. Oncol.* **36,** 133–140 (2010).

548. Leung, A. K. L., Calabrese, J. M. & Sharp, P. A. Quantitative analysis of Argonaute protein reveals microRNA-dependent localization to stress granules. *Proc. Natl. Acad. Sci. U. S. A.* **103,** 18125–18130 (2006).

549. Kozomara, A. & Griffiths-Jones, S. miRBase: annotating high confidence microRNAs using deep sequencing data. *Nucleic Acids Res.* **42,** 68–73 (2014).

550. Flicek, P. *et al.* Ensembl 2014. *Nucleic Acids Res.* **42,** 749–755 (2014).

551. Untergasser, A. *et al.* Primer3-new capabilities and interfaces. *Nucleic Acids Res.* **40,** 1–12 (2012).

552. Bryksin, A. V. & Matsumura, I. Overlap extension PCR cloning: a simple and reliable way to create recombinant plasmids. *Biotechniques* **48,** 463–465 (2010).

553. Maurer-Stroh, S., Eisenhaber, B. & Eisenhaber, F. N-terminal N-myristoylation of proteins: refinement of the sequence motif and its taxon-specific differences. *J. Mol. Biol.* **317,** 523–540 (2002).

554. Zacharias, D. A., Violin, J. D., Newton, A. C. & Tsien, R. Y. Partitioning of lipid-modified monomeric GFPs into membrane microdomains of live cells. *Science* **296,** 913–916 (2002).

555. Fang, Y. *et al.* Higher-order oligomerization targets plasma membrane proteins and HIV gag to exosomes. *PLoS Biol.* **5,** e158 (2007).

556. Shen, B., Wu, N., Yang, M. & Gould, S. J. Protein targeting to exosomes/microvesicles by plasma membrane anchors. *J. Biol. Chem.* **286,** 14383–14395 (2011).

557. Gibson, D. G. *et al.* Enzymatic assembly of DNA molecules up to several hundred kilobases. *Nat. Methods* **6,** 343–345 (2009).

558. Eldh, M., Lötvall, J., Malmhäll, C. & Ekström, K. Importance of RNA isolation methods for analysis of exosomal RNA: Evaluation of different methods. *Mol. Immunol.* **50,** 278–286 (2012).

559. Feng, X., Zhao, P., He, Y. & Zuo, Z. Allele-specific silencing of Alzheimer's disease genes: the amyloid precursor protein genes with Swedish or London mutations. *Gene* **371,** 68–74 (2006).

560. Quah, B. J. C. & O'Neill, H. C. The immunogenicity of dendritic cell-derived exosomes. *Blood Cells, Mol. Dis.* **35,** 94–110 (2005).

561. Perez-Gonzalez, R., Gauthier, S. A., Kumar, A. & Levy, E. The exosome secretory pathway transports amyloid precursor protein carboxyl-terminal fragments from the cell into the brain extracellular space. *J. Biol. Chem.* **287,** 43108–43115 (2012).

562. Sharples, R. a *et al.* Inhibition of gamma-secretase causes increased secretion of amyloid precursor protein C-terminal fragments in association with exosomes. *FASEB J.* **22,** 1469–1478 (2008).

563. Joshi, P. *et al.* Microglia convert aggregated amyloid-β into neurotoxic forms through the shedding of microvesicles. *Cell Death Differ.* **21,** 582–593 (2014).

564. Saman, S. *et al.* Exosome-associated tau is secreted in tauopathy models and is selectively phosphorylated in cerebrospinal fluid in early Alzheimer disease. *J. Biol. Chem.* **287,** 3842–3849 (2012).

565. Saman, S. *et al.* Proteins recruited to exosomes by tau overexpression implicate novel cellular mechanisms linking tau secretion with Alzheimer's disease. *J. Alzheimers. Dis.* **40,** S47–70 (2014).

566. Kooijmans, S. A. A. *et al.* Electroporation-induced siRNA precipitation obscures the efficiency of siRNA loading into extracellular vesicles. *J. Control. Release* **172,** 229–238 (2013).

567. Stapulionis, R. Electric pulse-induced precipitation of biological macromolecules in electroporation. *Bioelectrochemistry Bioenerg.* **48,** 249–254 (1999).

568. Deun, J. Van *et al.* The impact of disparate isolation methods for extracellular vesicles on downstream RNA profiling. *Journal of Extracellular Vesicles* **3,** 24858 (2014).

569. Kannan, K. *et al.* Lysosome-associated membrane proteins h-LAMP1 (CD107a) and h-LAMP2 (CD107b) are activation-dependent cell surface glycoproteins in human peripheral blood mononuclear cells which mediate cell adhesion to vascular endothelium. *Cell. Immunol.* **171,** 10–19 (1996).

570. Vella, L. J. *et al.* Packaging of prions into exosomes is associated with a novel pathway of PrP processing. *J. Pathol.* **211,** 582–590 (2007).

571. Yuyama, K., Sun, H., Mitsutake, S. & Igarashi, Y. Sphingolipid-modulated exosome secretion promotes clearance of amyloid-beta by microglia. *J. Biol. Chem.* **287,** 10977–10989 (2012).

572. Yuyama, K. *et al.* Decreased amyloid-β pathologies by intracerebral loading of glycosphingolipid-enriched exosomes in Alzheimer model mice. *J. Biol. Chem.* **289,** 24488–24498 (2014).

573. Yuyama, K. *et al.* A potential function for neuronal exosomes: sequestering intracerebral amyloid-β peptide. *FEBS Lett.* **589,** 84–88 (2015).

574. Katsuda, T. *et al.* Human adipose tissue-derived mesenchymal stem cells secrete functional neprilysin-bound exosomes. *Sci. Rep.* **3,** 1197 (2013).

575. Arroyo, J. D. *et al.* Argonaute2 complexes carry a population of circulating microRNAs independent of vesicles in human plasma. *Proc. Natl. Acad. Sci. U. S. A.* **108,** 5003–5008 (2011).

576. Turchinovich, A., Weiz, L., Langheinz, A. & Burwinkel, B. Characterization of extracellular circulating microRNA. *Nucleic Acids Res.* **39,** 7223–7233 (2011).

577. Xu, J., Chen, Q., Zen, K., Zhang, C. & Zhang, Q. Synaptosomes secrete and uptake functionally active microRNAs via exocytosis and endocytosis pathways. *J. Neurochem.* **124,** 15–25 (2013).

578. Winter, J. & Diederichs, S. Argonaute proteins regulate microRNA stability: increased microRNA abundance by Argonaute proteins is due to microRNA stabilization. *RNA Biol.* **8,** 1149–1157 (2011).

579. Thomas, P. & Smart, T. G. HEK293 cell line: a vehicle for the expression of recombinant proteins. *J. Pharmacol. Toxicol. Methods* **51,** 187–200 (2005).

580. Li, J. *et al.* Serum-free culture alters the quantity and protein composition of neuroblastoma-derived extracellular vesicles. *Journal of Extracellular Vesicles* **4,** 26883 (2015).

581. Li, Y. Y. *et al.* Increased expression of miRNA-146a in Alzheimer's disease transgenic mouse models. *Neurosci. Lett.* **487,** 94–98 (2011).

582. Kim, J. *et al.* MiR-106b impairs cholesterol efflux and increases Aβ levels by repressing ABCA1 expression. *Exp. Neurol.* **235,** 476–483 (2012).

583. Chen, T. S. *et al.* Mesenchymal stem cell secretes microparticles enriched in pre-microRNAs. *Nucleic Acids Res.* **38,** 215–224 (2010).

584. Chendrimada, T. P. *et al.* TRBP recruits the Dicer complex to Ago2 for microRNA processing and gene silencing. *Nature* **436,** 740–744 (2005).

585. Gregory, R. I., Chendrimada, T. P., Cooch, N. & Shiekhattar, R. Human RISC couples microRNA biogenesis and posttranscriptional gene silencing. *Cell* **123,** 631–640 (2005).

586. Maniataki, E. & Mourelatos, Z. A human, ATP-independent, RISC assembly machine fueled by pre-miRNA. *Genes Dev.* **19,** 2979–2990 (2005).

587. Zhang, X., Graves, P. R. & Zeng, Y. Stable Argonaute2 overexpression differentially regulates microRNA production. *Biochim. Biophys. Acta - Gene Regul. Mech.* **1789,** 153–159 (2009).

588. Grimm, D. *et al.* Fatality in mice due to oversaturation of cellular microRNA/short hairpin RNA pathways. *Nature* **441,** 537–541 (2006).

589. Meier, J. *et al.* Genome-wide identification of translationally inhibited and degraded miR-155 targets using RNA-interacting protein-IP. *RNA Biol.* **10,** 1018–1029 (2013).

590. Mogilyansky, E. & Rigoutsos, I. The miR-17/92 cluster: a comprehensive update on its genomics, genetics, functions and increasingly important and numerous roles in health and disease. *Cell Death Differ.* **20,** 1603–1614 (2013).

591. Ivanovska, I. *et al.* MicroRNAs in the miR-106b family regulate p21/CDKN1A and promote cell cycle progression. *Mol. Cell. Biol.* **28,** 2167–2174 (2008).

592. Flores, O., Kennedy, E. M., Skalsky, R. L. & Cullen, B. R. Differential RISC association of endogenous human microRNAs predicts their inhibitory potential. *Nucleic Acids Res.* **42,** 4629–4639 (2014).

593. Nordin, J. Z. *et al.* Ultrafiltration with size-exclusion liquid chromatography for high yield isolation of extracellular vesicles preserving intact biophysical and functional properties. *Nanomedicine* **11,** 879–883 (2015).

594. Chow, V. W. *et al.* Modeling an anti-amyloid combination therapy for Alzheimer's disease. *Sci. Transl. Med.* **2,** 13ra1 (2010).

595. Perry, D. *et al.* Building a roadmap for developing combination therapies for Alzheimer's disease. *Expert Rev. Neurother.* **15,** 327–333 (2015).

596. Stephenson, D. *et al.* Charting a path toward combination therapy for Alzheimer's disease. *Expert Rev. Neurother.* **15,** 107–113 (2015).

597. Johnson, S. C. & Gerber, J. G. Advances in HIV/AIDS therapy. *Adv. Intern. Med.* **45,** 1–40 (2000).

598. Baxevanis, C. N., Perez, S. A. & Papamichail, M. Combinatorial treatments including vaccines, chemotherapy and monoclonal antibodies for cancer therapy. *Cancer Immunol. Immunother.* **58,** 317–324 (2009).

599. De Cates, A. N. *et al.* Fixed-dose combination therapy for the prevention of cardiovascular disease. *Cochrane database Syst. Rev.* **4,** CD009868 (2014).

600. Jacobsen, H. *et al.* Combined treatment with a BACE inhibitor and anti-Aβ antibody gantenerumab enhances amyloid reduction in APPLondon mice. *J. Neurosci.* **34,** 11621–11630 (2014).

601. Matchynski, J. J. *et al.* Combinatorial treatment of tart cherry extract and essential fatty acids reduces cognitive impairments and inflammation in the mu-p75 saporin-induced mouse model of Alzheimer's disease. *J. Med. Food* **16,** 288–295 (2013).

602. Chumakov, I. *et al.* Combining two repurposed drugs as a promising approach for Alzheimer's disease therapy. *Sci. Rep.* **5,** 7608 (2015).

603. Matsunaga, S., Kishi, T. & Iwata, N. Combination therapy with cholinesterase inhibitors and memantine for Alzheimer's disease: a systematic review and meta-analysis. *Int. J. Neuropsychopharmacol.* **18,** 115 (2015).

604. Rijpma, A., Meulenbroek, O. & Olde Rikkert, M. G. M. Cholinesterase inhibitors and add-on nutritional supplements in Alzheimer's disease: a systematic review of randomized controlled trials. *Ageing Res. Rev.* **16,** 105–112 (2014).

605. Zemek, F. *et al.* Outcomes of Alzheimer's disease therapy with acetylcholinesterase inhibitors and memantine. *Expert Opin. Drug Saf.* **13,** 759–774 (2014).

606. Strittmatter, W. J. *et al.* Apolipoprotein E: high-avidity binding to beta-amyloid and increased frequency of type 4 allele in late-onset familial Alzheimer disease. *Proc. Natl. Acad. Sci. U. S. A.* **90,** 1977–1981 (1993).

607. Ma, J., Yee, A., Brewer, H. B., Das, S. & Potter, H. Amyloid-associated proteins alpha 1-antichymotrypsin and apolipoprotein E promote assembly of Alzheimer beta-protein into filaments. *Nature* **372,** 92–94 (1994).

608. Namba, Y., Tomonaga, M., Kawasaki, H., Otomo, E. & Ikeda, K. Apolipoprotein E immunoreactivity in cerebral amyloid deposits and neurofibrillary tangles in Alzheimer's disease and kuru plaque amyloid in Creutzfeldt-Jakob disease. *Brain Res.* **541,** 163–166 (1991).

609. Vassar, R. *et al.* Beta-secretase cleavage of Alzheimer's amyloid precursor protein by the transmembrane aspartic protease BACE. *Science* **286,** 735–741 (1999).

610. Cruts, M., Theuns, J. & Van Broeckhoven, C. Locus-specific mutation databases for neurodegenerative brain diseases. *Hum. Mutat.* **33,** 1340–1344 (2012).

611. Yamada, K., Mizuno, M. & Nabeshima, T. Role for brain-derived neurotrophic factor in learning and memory. *Life Sci.* **70,** 735–744 (2002).

612. Lipovich, L. *et al.* Activity-dependent human brain coding/noncoding gene regulatory networks. *Genetics* **192,** 1133–1148 (2012).

613. Modarresi, F. *et al.* Inhibition of natural antisense transcripts in vivo results in gene-specific transcriptional upregulation. *Nat. Biotechnol.* **30,** 453–459 (2012).

614. Airavaara, M. *et al.* Identification of novel GDNF isoforms and cis-antisense GDNFOS gene and their regulation in human middle temporal gyrus of Alzheimer disease. *J. Biol. Chem.* **286,** 45093–45102 (2011).

615. Selkoe, D. J. *et al.* Beta-amyloid precursor protein of Alzheimer disease occurs as 110- to 135-kilodalton membrane-associated proteins in neural and nonneural tissues. *Proc. Natl. Acad. Sci. U. S. A.* **85,** 7341–7345 (1988).

616. Zhao, J. *et al.* Beta-site amyloid precursor protein cleaving enzyme 1 levels become elevated in neurons around amyloid plaques: implications for Alzheimer's disease pathogenesis. *J. Neurosci.* **27,** 3639–3649 (2007).

617. Holsinger, R. M. D., McLean, C. A., Beyreuther, K., Masters, C. L. & Evin, G. Increased expression of the amyloid precursor β-secretase in Alzheimer's disease. *Ann. Neurol.* **51,** 783–786 (2002).

618. Sankaranarayanan, S. *et al.* In vivo beta-secretase 1 inhibition leads to brain Abeta lowering and increased alpha-secretase processing of amyloid precursor protein without effect on neuregulin-1. *J. Pharmacol. Exp. Ther.* **324,** 957–969 (2008).

619. D'Amelio, M. *et al.* Caspase-3 triggers early synaptic dysfunction in a mouse model of Alzheimer's disease. *Nat. Neurosci.* **14,** 69–76 (2011).

620. Rissman, R. A. *et al.* Caspase-cleavage of tau is an early event in Alzheimer disease tangle pathology. *J. Clin. Invest.* **114,** 121–130 (2004).

621. Rohn, T. T. *et al.* Caspase-9 activation and caspase cleavage of tau in the Alzheimer's disease brain. *Neurobiol. Dis.* **11,** 341–354 (2002).

622. Tamayev, R., Akpan, N., Arancio, O., Troy, C. M. & D'Adamio, L. Caspase-9 mediates synaptic plasticity and memory deficits of Danish dementia knock-in mice: caspase-9 inhibition provides therapeutic protection. *Mol. Neurodegener.* **7,** 60 (2012).

623. Milton, N. G. Phosphorylation of amyloid-beta at the serine 26 residue by human cdc2 kinase. *Neuroreport* **12,** 3839–3844 (2001).

624. Milton, N. G. N. The amyloid-β peptide binds to cyclin B1 and increases human cyclin-dependent kinase-1 activity. *Neurosci. Lett.* **322,** 131–133 (2002).

625. Vincent, I., Jicha, G., Rosado, M. & Dickson, D. W. Aberrant expression of mitotic cdc2/cyclin B1 kinase in degenerating neurons of Alzheimer's disease brain. *J. Neurosci.* **17,** 3588–3598 (1997).

626. Patrick, G. N. *et al.* Conversion of p35 to p25 deregulates Cdk5 activity and promotes neurodegeneration. *Nature* **402,** 615–622 (1999).

627. Ko, J. *et al.* p35 and p39 are essential for cyclin-dependent kinase 5 function during neurodevelopment. *J. Neurosci.* **21,** 6758–6771 (2001).

628. Tseng, H., Zhou, Y., Shen, Y. & Tsai, L. A survey of Cdk5 activator p35 and p25 levels in Alzheimer's disease brains. *FEBS Lett.* **523,** 58–62 (2002).

629. Mateo, I. *et al.* Epistasis between tau phosphorylation regulating genes (CDK5R1 and GSK-3beta) and Alzheimer's disease risk. *Acta Neurol. Scand.* **120,** 130–133 (2009).

630. Okazawa, H. & Estus, S. The JNK/c-Jun cascade and Alzheimer's disease. *Am. J. Alzheimers. Dis. Other Demen.* **17,** 79–88 (2002).

631. Thakur, A. *et al.* c-Jun phosphorylation in Alzheimer disease. *J. Neurosci. Res.* **85,** 1668–1673 (2007).

632. Zhou, Q. *et al.* Inhibition of c-Jun N-terminal kinase activation reverses Alzheimer disease phenotypes in APPswe/PS1dE9 mice. *Ann. Neurol.* **77,** 637–654 (2015).

633. Carter, T. L. *et al.* Differential preservation of AMPA receptor subunits in the hippocampi of Alzheimer's disease patients according to Braak stage. *Exp. Neurol.* **187,** 299–309 (2004).

634. Yasuda, R. P. *et al.* Reduction of AMPA-selective glutamate receptor subunits in the entorhinal cortex of patients with Alzheimer's disease pathology: a biochemical study. *Brain Res.* **678,** 161–167 (1995).

635. Conejero-Goldberg, C. *et al.* Molecular signatures in post-mortem brain tissue of younger individuals at high risk for Alzheimer's disease as based on APOE genotype. *Mol. Psychiatry* **16,** 836–847 (2011).

636. Gaisler-Salomon, I. *et al.* Hippocampus-specific deficiency in RNA editing of GluA2 in Alzheimer's disease. *Neurobiol. Aging* **35,** 1785–1791 (2014).

637. Tackenberg, C. *et al.* NMDA receptor subunit composition determines beta-amyloid-induced neurodegeneration and synaptic loss. *Cell Death Dis.* **4,** e608 (2013).

638. Decker, H. *et al.* N-methyl-D-aspartate receptors are required for synaptic targeting of Alzheimer's toxic amyloid-β peptide oligomers. *J. Neurochem.* **115,** 1520–1529 (2010).

639. Jiang, H. & Jia, J. Association between NR2B subunit gene (GRIN2B) promoter polymorphisms and sporadic Alzheimer's disease in the North Chinese population. *Neurosci. Lett.* **450,** 356–360 (2009).

640. Andreoli, V. *et al.* Potential involvement of GRIN2B encoding the NMDA receptor subunit NR2B in the spectrum of Alzheimer's disease. *J. Neural Transm.* **121,** 533–542 (2014).

641. Bi, H. & Sze, C. I. N-methyl-D-aspartate receptor subunit NR2A and NR2B messenger RNA levels are altered in the hippocampus and entorhinal cortex in Alzheimer's disease. *J. Neurol. Sci.* **200,** 11–18 (2002).

642. Avrahami, L. *et al.* Inhibition of glycogen synthase kinase-3 ameliorates β-amyloid pathology and restores lysosomal acidification and mammalian target of rapamycin activity in the Alzheimer disease mouse model: in vivo and in vitro studies. *J. Biol. Chem.* **288,** 1295–1306 (2013).

643. Sperber, B. R., Leight, S., Goedert, M. & Lee, V. M. Glycogen synthase kinase-3β phosphorylates tau protein at multiple sites in intact cells. *Neurosci. Lett.* **197,** 149–153 (1995).

644. Georgievska, B. *et al.* AZD1080, a novel GSK3 inhibitor, rescues synaptic plasticity deficits in rodent brain and exhibits peripheral target engagement in humans. *J. Neurochem.* **125,** 446–456 (2013).

645. Ly, P. T. T. *et al.* Inhibition of GSK3β-mediated BACE1 expression reduces Alzheimer-associated phenotypes. *J. Clin. Invest.* **123,** 224–235 (2013).

646. Noh, M. *et al.* Newly developed glycogen synthase kinase-3 (GSK-3) inhibitors protect neuronal cells death in amyloid-beta induced cell model and in a transgenic mouse model of Alzheimer's disease. *Biochem. Biophys. Res. Commun.* **435,** 274–281 (2013).

647. Hu, S. *et al.* GSK3 inhibitors show benefits in an Alzheimer's disease (AD) model of neurodegeneration but adverse effects in control animals. *Neurobiol. Dis.* **33,** 193–206 (2009).

648. Sun, Y. *et al.* Differential activation of mTOR complex 1 signaling in human brain with mild to severe Alzheimer's disease. *J. Alzheimers. Dis.* **38,** 437–444 (2014).

649. Tang, Z. *et al.* Mammalian target of rapamycin (mTor) mediates tau protein dyshomeostasis: implication for Alzheimer disease. *J. Biol. Chem.* **288,** 15556–15570 (2013).

650. Caccamo, A. *et al.* mTOR regulates tau phosphorylation and degradation: implications for Alzheimer's disease and other tauopathies. *Aging Cell* **12,** 370–380 (2013).

651. Spilman, P. *et al.* Inhibition of mTOR by rapamycin abolishes cognitive deficits and reduces amyloid-beta levels in a mouse model of Alzheimer's disease. *PLoS One* **5,** e9979 (2010).

652. Caccamo, A., De Pinto, V., Messina, A., Branca, C. & Oddo, S. Genetic reduction of mammalian target of rapamycin ameliorates Alzheimer's disease-like cognitive and pathological deficits by restoring hippocampal gene expression signature. *J. Neurosci.* **34,** 7988–7998 (2014).

653. Caccamo, A., Majumder, S., Richardson, A., Strong, R. & Oddo, S. Molecular interplay between mammalian target of rapamycin (mTOR), amyloid-beta, and Tau: effects on cognitive impairments. *J. Biol. Chem.* **285,** 13107–13120 (2010).

654. Caccamo, A. *et al.* Naturally secreted amyloid-beta increases mammalian target of rapamycin (mTOR) activity via a PRAS40-mediated mechanism. *J. Biol. Chem.* **286,** 8924–8932 (2011).

655. Noh, K. M. & Koh, J. Y. Induction and activation by zinc of NADPH oxidase in cultured cortical neurons and astrocytes. *J. Neurosci.* **20,** RC111 (2000).

656. Kim, M. J. *et al.* Immunohistochemical study of p47Phox and gp91Phox distributions in rat brain. *Brain Res.* **1040,** 178–186 (2005).

657. Shimohama, S. *et al.* Activation of NADPH oxidase in Alzheimer's disease brains. *Biochem. Biophys. Res. Commun.* **273,** 5–9 (2000).

658. Bruce-Keller, A. J. *et al.* NOX activity is increased in mild cognitive impairment. *Antioxid. Redox Signal.* **12,** 1371–1382 (2010).

659. Ansari, M. a. & Scheff, S. W. NADPH-oxidase activation and cognition in Alzheimer disease progression. *Free Radic. Biol. Med.* **51,** 171–178 (2011).

660. Park, L. *et al.* Nox2-derived radicals contribute to neurovascular and behavioral dysfunction in mice overexpressing the amyloid precursor protein. *Proc. Natl. Acad. Sci. U. S. A.* **105,** 1347–1352 (2008).

661. Wilkinson, B. L. *et al.* Ibuprofen attenuates oxidative damage through NOX2 inhibition in Alzheimer's disease. *Neurobiol. Aging* **33,** e21–32 (2012).

662. Dikalov, S. I. *et al.* Distinct roles of Nox1 and Nox4 in basal and angiotensin II-stimulated superoxide and hydrogen peroxide production. *Free Radic. Biol. Med.* **45,** 1340–1351 (2008).

663. Bruce-Keller, A. J. *et al.* Cognitive impairment in humanized APP×PS1 mice is linked to Aβ(1-42) and NOX activation. *Neurobiol. Dis.* **44,** 317–326 (2011).

664. Flach, K. *et al.* Tau oligomers impair artificial membrane integrity and cellular viability. *J. Biol. Chem.* **287,** 43223–43233 (2012).

665. Huber, A. M. *et al.* Fyn inhibition rescues established memory and synapse loss in Alzheimer mice. *Arthritis Care Res. (Hoboken).* **66,** 732–740 (2014).

666. Manczak, M. & Reddy, P. H. RNA silencing of genes involved in Alzheimer's disease enhances mitochondrial function and synaptic activity. *Biochim. Biophys. Acta - Mol. Basis Dis.* **1832,** 2368–2378 (2013).

667. Mullan, M. *et al.* A pathogenic mutation for probable Alzheimer's disease in the APP gene at the N-terminus of beta-amyloid. *Nat. Genet.* **1,** 345–347 (1992).

668. Swayze, E. E. *et al.* Antisense oligonucleotides containing locked nucleic acid improve potency but cause significant hepatotoxicity in animals. *Nucleic Acids Res.* **35,** 687–700 (2007).

669. Seth, P. P. *et al.* Short antisense oligonucleotides with novel 2'-4' conformationaly restricted nucleoside analogues show improved potency without increased toxicity in animals. *J. Med. Chem.* **52,** 10–13 (2009).

670. Burdick, A. D. *et al.* Sequence motifs associated with hepatotoxicity of locked nucleic acid--modified antisense oligonucleotides. *Nucleic Acids Res.* **42,** 4882–4891 (2014).

671. Mukai, F., Ishiguro, K., Sano, Y. & Fujita, S. C. Alternative splicing isoform of tau protein kinase I/glycogen synthase kinase 3β. *J. Neurochem.* **81,** 1073–1083 (2002).

672. Wood-Kaczmar, A., Kraus, M., Ishiguro, K., Philpott, K. L. & Gordon-Weeks, P. R. An alternatively spliced form of glycogen synthase kinase-3beta is targeted to growing neurites and growth cones. *Mol. Cell. Neurosci.* **42,** 184–194 (2009).

673. Avila, J. *et al.* Tau phosphorylation by GSK3 in different conditions. *Int. J. Alzheimers. Dis.* **2012,** 578373 (2012).

674. Wang, S. *et al.* mTOR-mediated hyperphosphorylation of tau in the hippocampus is involved in cognitive deficits in streptozotocin-induced diabetic mice. *Metab. Brain Dis.* **29,** 729–736 (2014).

675. Chauhan, N. B. & Siegel, G. J. Antisense inhibition at the beta-secretase-site of beta-amyloid precursor protein reduces cerebral amyloid and acetyl cholinesterase activity in Tg2576. *Neuroscience* **146,** 143–151 (2007).

676. Sud, R., Geller, E. T. & Schellenberg, G. D. Antisense-mediated exon skipping decreases Tau protein expression: a potential therapy for tauopathies. *Mol. Ther. Nucleic Acids* **3,** e180 (2014).

677. Cerritelli, S. M. & Crouch, R. J. Ribonuclease H: the enzymes in eukaryotes. *FEBS J.* **276,** 1494–1505 (2009).

678. Zhang, Z. & Simpkins, J. W. Okadaic acid induces tau phosphorylation in SH-SY5Y cells in an estrogen-preventable manner. *Brain Res.* **1345,** 176–181 (2010).

679. Medina, M., Avila, J. & Villanueva, N. Use of okadaic acid to identify relevant phosphoepitopes in pathology: a focus on neurodegeneration. *Mar. Drugs* **11,** 1656–1668 (2013).

680. Gong, C. X. *et al.* Phosphorylation of microtubule-associated protein tau is regulated by protein phosphatase 2A in mammalian brain. Implications for neurofibrillary degeneration in Alzheimer's disease. *J. Biol. Chem.* **275,** 5535–5544 (2000).

681. Chen, Z. *et al.* Effects of PTEN inhibition on regulation of tau phosphorylation in an okadaic acid-induced neurodegeneration model. *Int. J. Dev. Neurosci.* **30,** 411–419 (2012).

682. Stanton, R. *et al.* Chemical modification study of antisense gapmers. *Nucleic Acid Ther.* **22,** 344–359 (2012).

683. Chauhan, N. B. Trafficking of intracerebroventricularly injected antisense oligonucleotides in the mouse brain. *Antisense Nucleic Acid Drug Dev.* **12,** 353–357 (2002).

684. Smith, R. A. *et al.* Antisense oligonucleotide therapy for neurodegenerative disease. *J. Clin. Invest.* **116,** 2290–2296 (2006).

685. Kordasiewicz, H. B. *et al.* Sustained therapeutic reversal of Huntington's disease by transient repression of huntingtin synthesis. *Neuron* **74,** 1031–1044 (2012).

686. Passini, M. A. *et al.* Antisense oligonucleotides delivered to the mouse CNS ameliorate symptoms of severe spinal muscular atrophy. *Sci. Transl. Med.* **3,** 72ra18 (2011).

687. Lee, H. J., Boado, R. J., Braasch, D. A., Corey, D. R. & Pardridge, W. M. Imaging gene expression in the brain in vivo in a transgenic mouse model of Huntington's disease with an antisense radiopharmaceutical and drug-targeting technology. *J. Nucl. Med.* **43,** 948–956 (2002).

688. Kozlu, S. *et al.* An aquaporin 4 antisense oligonucleotide loaded, brain targeted nanoparticulate system design. *Pharmazie* **69,** 340–345 (2014).

689. Du, L. *et al.* Arginine-rich cell-penetrating peptide dramatically enhances AMO-mediated ATM aberrant splicing correction and enables delivery to brain and cerebellum. *Hum. Mol. Genet.* **20,** 3151–3160 (2011).

690. Hua, Y. *et al.* Antisense correction of SMN2 splicing in the CNS rescues necrosis in a type III SMA mouse model. *Genes Dev.* **24,** 1634–1644 (2010).

691. Park, I. *et al.* Disease-specific induced pluripotent stem cells. *Cell* **134,** 877–886 (2008).

692. Li, Y., Liu, M. & Yang, S. Dendritic cells derived from pluripotent stem cells: potential of large scale production. *World J. Stem Cells* **6,** 1–10 (2014).

693. Pusic, A. D. & Kraig, R. P. Youth and environmental enrichment generate serum exosomes containing miR-219 that promote CNS myelination. *Glia* **62,** 284–299 (2014).

694. Chen, T. S. *et al.* Enabling a robust scalable manufacturing process for therapeutic exosomes through oncogenic immortalization of human ESC-derived MSCs. *J. Transl. Med.* **9,** 47 (2011).

695. Ju, S. *et al.* Grape exosome-like nanoparticles induce intestinal stem cells and protect mice from DSS-induced colitis. *Mol. Ther.* **21,** 1345–1357 (2013).

696. Nguyen, D. G., Booth, A., Gould, S. J. & Hildreth, J. E. K. Evidence that HIV budding in primary macrophages occurs through the exosome release pathway. *J. Biol. Chem.* **278,** 52347–52354 (2003).

697. Alvarez-Erviti, L. *et al.* Lysosomal dysfunction increases exosome-mediated alpha-synuclein release and transmission. *Neurobiol. Dis.* **42,** 360–367 (2011).

698. Skriner, K., Adolph, K., Jungblut, P. R. & Burmester, G. R. Association of citrullinated proteins with synovial exosomes. *Arthritis Rheum.* **54,** 3809–3814 (2006).

699. Grant, R. *et al.* A filtration-based protocol to isolate human plasma membrane-derived vesicles and exosomes from blood plasma. *J. Immunol. Methods* **371,** 143–151 (2011).

700. Chen, C. *et al.* Microfluidic isolation and transcriptome analysis of serum microvesicles. *Lab Chip* **10,** 505–511 (2010).

701. Tauro, B. J. *et al.* Comparison of ultracentrifugation, density gradient separation, and immunoaffinity capture methods for isolating human colon cancer cell line LIM1863-derived exosomes. *Methods* **56,** 293–304 (2012).

702. Tauro, B. J. *et al.* Two distinct populations of exosomes are released from LIM1863 colon carcinoma cell-derived organoids. *Mol. Cell. Proteomics* **12,** 587–598 (2013).

703. Clayton, A. *et al.* Adhesion and signaling by B cell-derived exosomes: the role of integrins. *FASEB J.* **18,** 977–979 (2004).

704. De La Peña, H. *et al.* Artificial exosomes as tools for basic and clinical immunology. *J. Immunol. Methods* **344,** 121–132 (2009).

705. Martinez-Lostao, L. *et al.* Liposome-bound APO2L/TRAIL is an effective treatment in a rabbit model of rheumatoid arthritis. *Arthritis Rheum.* **62,** 2272–2282 (2010).

706. De Miguel, D. *et al.* Liposomes decorated with Apo2L/TRAIL overcome chemoresistance of human hematologic tumor cells. *Mol. Pharm.* **10,** 893–904 (2013).

707. De Miguel, D., Gallego-Lleyda, A., Anel, A. & Martinez-Lostao, L. Liposome-bound TRAIL induces superior DR5 clustering and enhanced DISC recruitment in histiocytic lymphoma U937 cells. *Leuk. Res.* S0145–2126 (2015).

708. Properzi, F., Logozzi, M. & Fais, S. Exosomes: the future of biomarkers in medicine. *Biomark. Med.* **7,** 769–778 (2013).

709. Fiandaca, M. S. *et al.* Identification of preclinical Alzheimer's disease by a profile of pathogenic proteins in neurally derived blood exosomes: a case-control study. *Alzheimers. Dement.* **11,** 600–607 (2015).

710. Cheng, L. *et al.* Prognostic serum miRNA biomarkers associated with Alzheimer's disease shows concordance with neuropsychological and neuroimaging assessment. *Mol. Psychiatry* **20,** 1188–1196 (2015).

711. Goetzl, E. J. *et al.* Low neural exosomal levels of cellular survival factors in Alzheimer's disease. *Ann. Clin. Transl. Neurol.* **2,** 769–773 (2015).

712. Goetzl, E. J. *et al.* Altered lysosomal proteins in neural-derived plasma exosomes in preclinical Alzheimer disease. *Neurology* **85,** 40–47 (2015).

713. Kapogiannis, D. *et al.* Dysfunctionally phosphorylated type 1 insulin receptor substrate in neural-derived blood exosomes of preclinical Alzheimer's disease. *FASEB J.* **29,** 589–596 (2015).

714. Greenberger, L. M. *et al.* A RNA antagonist of hypoxia-inducible factor-1alpha, EZN-2968, inhibits tumor cell growth. *Mol. Cancer Ther.* **7,** 3598–3608 (2008).

715. Hildebrandt-Eriksen, E. S. *et al.* A locked nucleic acid oligonucleotide targeting microRNA-122 is well-tolerated in cynomolgus monkeys. *Nucleic Acid Ther.* **22,** 152–161 (2012).

716. Van der Ree, M. H. *et al.* Long-term safety and efficacy of microRNA-targeted therapy in chronic hepatitis C patients. *Antiviral Res.* **111,** 53–59 (2014).

717. Castro, D. & Iannaccone, S. T. Spinal muscular atrophy: therapeutic strategies. *Curr. Treat. Options Neurol.* **16,** 316 (2014).

718. Seth, P. P. *et al.* Design, synthesis and evaluation of constrained methoxyethyl (cMOE) and constrained ethyl (cEt) nucleoside analogs. *Nucleic Acids Symp. Ser. (Oxf).* 553–554 (2008).

719. Whitesell, L. *et al.* Stability, clearance, and disposition of intraventricularly administered oligodeoxynucleotides: implications for therapeutic application within the central nervous system. *Proc. Natl. Acad. Sci. U. S. A.* **90,** 4665–4669 (1993).

720. O'Loughlin, A. J., Woffindale, C. A. & Wood, M. J. A. Exosomes and the emerging field of exosome-based gene therapy. *Curr. Gene Ther.* **12,** 262–274 (2012).